NUREG/CR-6559
BNL-NUREG-52532

Large-Scale Vibration Tests of Main Steam and Feedwater Piping Systems With Conventional and Energy-Absorbing Supports

Evaluation of Test Results and Post-Test Analysis

Prepared by
Y. J. Park, G. DeGrassi, P. Bezler
C. H. Hofmayer

Brookhaven National Laboratory

Prepared for
U.S. Nuclear Regulatory Commission

AVAILABILITY NOTICE

Availability of Reference Materials Cited in NRC Publications

Most documents cited in NRC publications will be available from one of the following sources:

1. The NRC Public Document Room, 2120 L Street, NW., Lower Level, Washington, DC 20555-0001

2. The Superintendent of Documents, U.S. Government Printing Office, P. O. Box 37082, Washington, DC 20402-9328

3. The National Technical Information Service, Springfield, VA 22161-0002

Although the listing that follows represents the majority of documents cited in NRC publications, it is not intended to be exhaustive.

Referenced documents available for inspection and copying for a fee from the NRC Public Document Room include NRC correspondence and internal NRC memoranda; NRC bulletins, circulars, information notices, inspection and investigation notices; licensee event reports; vendor reports and correspondence; Commission papers; and applicant and licensee documents and correspondence.

The following documents in the NUREG series are available for purchase from the Government Printing Office: formal NRC staff and contractor reports, NRC-sponsored conference proceedings, international agreement reports, grantee reports, and NRC booklets and brochures. Also available are regulatory guides, NRC regulations in the *Code of Federal Regulations,* and *Nuclear Regulatory Commission Issuances.*

Documents available from the National Technical Information Service include NUREG-series reports and technical reports prepared by other Federal agencies and reports prepared by the Atomic Energy Commission, forerunner agency to the Nuclear Regulatory Commission.

Documents available from public and special technical libraries include all open literature items, such as books, journal articles, and transactions. *Federal Register* notices, Federal and State legislation, and congressional reports can usually be obtained from these libraries.

Documents such as theses, dissertations, foreign reports and translations, and non-NRC conference proceedings are available for purchase from the organization sponsoring the publication cited.

Single copies of NRC draft reports are available free, to the extent of supply, upon written request to the Office of Administration, Distribution and Mail Services Section, U.S. Nuclear Regulatory Commission, Washington, DC 20555-0001.

Copies of industry codes and standards used in a substantive manner in the NRC regulatory process are maintained at the NRC Library, Two White Flint North, 11545 Rockville Pike, Rockville, MD 20852-2738, for use by the public. Codes and standards are usually copyrighted and may be purchased from the originating organization or, if they are American National Standards, from the American National Standards Institute, 1430 Broadway, New York, NY 10018-3308.

DISCLAIMER NOTICE

This report was prepared under an international cooperative agreement for the exchange of technical information. Neither the United States Government nor any agency thereof, nor any of their employees, makes any warranty, expressed or implied, or assumes any legal liability or responsibility for any third party's use, or the results of such use, of any information, apparatus, product, or process disclosed in this report, or represents that its use by such third party would not infringe privately owned rights.

NUREG/CR-6559
BNL-NUREG-52532

Large-Scale Vibration Tests of Main Steam and Feedwater Piping Systems With Conventional and Energy-Absorbing Supports

Evaluation of Test Results and Post-Test Analysis

Manuscript Completed: April 1998
Date Published: August 1998

Prepared by
Y. J. Park, G. DeGrassi, P. Bezler
C. H. Hofmayer

Brookhaven National Laboratory
Upton, NY 11973-5000

N. C. Chokshi, NRC Project Manager

Prepared for
Division of Engineering Technology
Office of Nuclear Regulatory Research
U.S. Nuclear Regulatory Commission
Washington, DC 20555-0001
NRC Job Code W6081

NUREG/CR-6559 has been reproduced from the best available copy.

ABSTRACT

As part of collaborative efforts between the United States and Japan, the U.S. Nuclear Regulatory Commission (USNRC) and Brookhaven National Laboratory (BNL) participated in the Seismic Proving Test program of main steam and feedwater systems (MS) conducted by the Nuclear Power Engineering Corporation (NUPEC) for the Ministry of International Trade and Industry (MITI) of Japan. Scaled models of main steam piping for a typical PWR plant and feedwater piping for a BWR plant were fabricated by NUPEC and subjected to a large number of earthquake motions at NUPEC's Tadotsu Engineering Laboratory. Initially, the piping systems were supported by conventional snubbers and subjected to design level earthquakes as well as excitations beyond the design level. Then the snubbers were replaced by energy absorbing devices, and tests at various excitation levels up to the deformation limits of the energy absorbers were performed. This report describes the evaluation of the test results and BNL's post-test analyses.

CONTENTS

CONTENTS (Cont'd)

FIGURES

Page

FIGURES (Cont'd)

Page

FIGURES (Cont'd)

Page

FIGURES (Cont'd)

Page

FIGURES (Cont'd)

Page

TABLES

EXECUTIVE SUMMARY

As part of collaborative efforts between the United States and Japan, the U.S. Nuclear Regulatory Commission (USNRC) and Brookhaven National Laboratory (BNL) participated in the Seismic Proving Test program of main steam and feedwater systems (MS) conducted by the Nuclear Power Engineering Corporation (NUPEC) for the Ministry of International Trade and Industry (MITI) of Japan. Scaled models of main steam piping for a typical PWR plant and feedwater piping for a BWR plant were fabricated by NUPEC and subjected to a large number of earthquake motions at NUPEC's Tadotsu Engineering Laboratory. Initially, the piping systems were supported by conventional snubbers and subjected to design level earthquakes as well as excitations beyond the design level. Then the snubbers were replaced by energy absorbing devices, and tests at various excitation levels up to the deformation limits of the energy absorbers were performed.

BNL performed pre-and post-test analyses, and processed a large volume of recorded test results. This report describes the evaluation of the test results and BNL's post-test analyses. Two types of post-test analyses were performed, i.e., simulation analyses for correlation studies and design-based analyses. The objectives of the simulation analyses were to reproduce the recorded piping responses and to understand the mechanism producing the observed complex nonlinear behavior of the piping systems. In addition to conventional nonlinear time history analysis, equivalent linearization techniques were also used in this study. In the design-based analyses, the piping design analysis methods, used in the nuclear industry, were blindly applied to selected test runs of the conventional support cases. The objectives of the analyses were to evaluate the seismic design margins as well as to assess the adequacy of various analysis/design assumptions such as support modeling and damping assumptions.

A summary of major findings and conclusions, as well as engineering insights gained from the MS Test Program are presented in Chapter 7 of this report.

ACKNOWLEDGMENTS

This research program was performed as part of the collaborative efforts to promote the exchange of technical information between the Agency of Natural Resources and Energy of the Ministry of International Trade and Industry in Japan, and the U.S. Nuclear Regulatory Commission. Dr. Nilesh Chokshi was the NRC Project Manager, who contributed strong leadership and significant technical guidance throughout this program.

The authors wish to acknowledge the helpfulness and cooperation provided by the staffs of the Nuclear Power Engineering Corporation, Mitsubishi Heavy Industries and Hitachi Works for bringing this program to a successful conclusion. All of the test results included in this report were provided by NUPEC and are also included in their reports to MITI.

The authors also wish to thank S. Shteyngart and Y.K. Wang of Brookhaven National Laboratory for their analytical support and advice during the course of this program.

The authors would like to express special thanks to B. Roland, A. Melocoton and A. Costantini for their secretarial help throughout this program and dedication to the preparation of this report.

1 INTRODUCTION

In the seismic design of piping systems in nuclear power plants, pipe supports, such as snubbers, are idealized as simple springs and linear structural analyses are performed to quantify the pipe stresses and support forces. Past vibration tests of piping systems indicated that snubbers and other pipe support structures exhibit complex nonlinear behavior; and as a result, poor correlation between analysis and test results was observed in comparison studies. Further studies on the dynamic behavior of pipe supports are needed to improve analysis accuracy as well as to more accurately assess the seismic design margin of piping systems.

In addition to the conventional snubber supports, the use of mechanical energy absorbers as an alternative piping support has attracted a wide interest in the nuclear industry. The basic design concept of energy absorbers is to dissipate the vibration energy of a piping system through nonlinear hysteretic actions. Such devices may be used not only in new power plant design but also as part of the redesign of existing plants to reduce the number of snubbers.

As part of a collaborative effort between the United States and Japan, the U.S. Nuclear Regulatory Commission (USNRC) and Brookhaven National Laboratory (BNL) participated in the Seismic Proving Test program of main steam and feedwater systems (MS) conducted by the Nuclear Power Engineering Corporation (NUPEC) for the Ministry of International Trade and Industry (MITI) of Japan. Scaled models of main steam piping for a typical PWR plant and feedwater piping for a typical BWR plant were fabricated and subjected to a large number of earthquake motions at NUPEC's Tadotsu Engineering Laboratory. Initially, the piping systems were supported by conventional snubbers and subjected to the design level earthquakes as well as excitations beyond the design level. Then the snubbers were replaced by energy absorbing devices, and tests at various excitation levels up to the deformation limits of the energy absorbers were performed.

Two types of energy absorbing device were used in the MS Test Program, i.e., EAB (energy absorbing) supports for the feedwater piping and LED (lead extrusion damper) supports for the main steam piping. The EAB supports consist of X-shaped steel plates which absorb the vibration energy through out-of-plane bending of the plates into the plastic regime. The LED supports dissipate energy through the plastic deformation between an octagon-shaped rotor and the surrounding lead in a chamber. Prior to the shake table tests, component tests were conducted by NUPEC for these devices.

One unique feature of the MS Test Program was the use of a computer-controlled actuator system to generate independent support motions for the main steam piping. An actuator was mounted between the support structure and one nozzle of the main steam piping and shaken together with the test models. The independent support motions were generated based on a mathematical model of a steam generator, sensor readings of the table motions and actuator movements.

The overall objectives of this study were to gain insights of the dynamic behavior of nuclear piping systems based on large-scale vibration tests, to assess the current piping analysis methods, and to evaluate the performance of energy absorbing devices as an alternative piping support.

BNL performed pre- and post-test analyses, and processed a large volume of recorded test results. This report describes the evaluation of the test results and BNL's post-test analyses. Two types of post-test analyses were performed, i.e. simulation analyses for correlation studies and design-based analyses. The objectives of the simulation analyses were to reproduce the recorded piping responses and to understand the mechanisms producing the observed complex nonlinear behavior of the piping systems. In addition to conventional nonlinear time history analysis, equivalent linearization techniques were used in this study. In the design-based analyses, the piping design analysis methods, used in the nuclear industry, were blindly applied to selected test runs of the conventional support cases. The objectives of the analyses were to evaluate the seismic design margins as well as to assess the adequacy of various analysis/design assumptions such as support modeling and damping assumptions.

The recorded peak response values and time history plots for selected test runs are provided in Appendices of this report.

2 SUMMARY OF NUPEC'S TEST PLAN

NUPEC's test plan for the MS Test Program is described in detail in Appendix L of this report. This chapter summarizes their test plan. The dynamic tests were conducted in 1994 and 1995 using the large-scale shaking table at NUPEC's Tadotsu Engineering Laboratory.

As illustrated in Figure 2.1, the test model consists of the main steam line (M-line) of a typical PWR Plant and the feedwater line (F-line) of a typical BWR Plant. At the end of the M-line main pipe, a part of the steam supply pipe for the turbine driven auxiliary feedwater pump (which is called the M-line branch pipe in this report) is also included. The scale-down factors of the pipe models are 1/2.66 for the M-line and 1/2.3 for the F-line. Detailed information on the test models is given in Appendices A and C of this report. Both the M-line and F-line were filled with water at room temperature and were pressurized to a constant internal pressure during the tests.

For the M-line, the massive steam generator (SG) was not physically modeled. Instead, the SG was replaced by a computer-controlled actuator system which simulates the dynamic motions of the SG based on the mathematical model of the SG and sensor readings of the table motions, as illustrated in Figure 2.3.

The shaking table tests consisted of two phases: 1) the testing of piping systems with conventional snubber supports, and 2) the testing of the same piping systems with energy absorbing devices.

In the conventional support case, mechanical snubbers are the main seismic supports for both the M-line and the F-line. Other types of pipe supports, including hydraulic snubbers, hangers, guide (sliding) supports, and pin supports, are installed for both the M-line and F-line. Figure 2.2 illustrates the pipe supports for the F-line. The support denoted "FR1" is a guide support. All other supports for the F-line with conventional supports are mechanical snubbers or spring hangers. Figure 2.3 illustrates the pipe supports for the M-line. "MR8" is a pin support while "MR9/MR10" is a guide support or spring hanger.

In the energy absorbing (EA) support case, two types of EA's were used in the MS test program, i.e., EAB (energy absorbing) supports for the F-line and LED (lead extrusion damper) supports for the M-line. The energy absorbing mechanisms of these devices are described in detail in Appendix L of this report. Figures 2.4 and 2.5 illustrate the configurations of pipe supports for the F-line and the M-line. It should be noted that both EAB supports and mechanical snubbers are used for the F-line, while only LED supports are used in the M-line.

The instruments used during the MS test program include accelerometers, displacement transducers, strain gages, load cells and pressure gages. Their locations are shown in Appendix L of this report. Tables 2.1 through 2.4 list the selected measurement items used in the correlation studies described in the following chapters. The lists include the node and element numbers used in the analyses.

Table 2.5 summarizes the test runs, which consist of a total of about 200 dynamic tests performed at NUPEC's Tadotsu Laboratory during the MS Test Program. Appendix B of this report describes the details of all the major test runs.

The input table motions were developed from time history analyses of typical PWR and BWR power plants. According to the Japanese seismic design standards for nuclear power plants, two levels of earthquake motions, S_1 and S_2, are used for design analyses. In comparison with the design standards in the U.S., the S_1 motion is somewhat higher than the typical OBE level, and the S_2 motion is approximately equal to the typical SSE level. The PCCV wave (also denoted as C/V wave in this report) was obtained from the response of a prestressed concrete pressure vessel, and is used for multiple excitation tests of the M-line with conventional supports. For the energy absorbing support case, the following waves are used:

A-Wave S_1: PWR-S_1 motion,
A-Wave S_2: PWR-S_2 motion,
B-Wave S_1: A-Wave S_1 motion with time scale expanded by a factor of 2.72,
B-Wave S_2: A-Wave S_2 motion with time scale expanded by a factor of 2.72,
Tokachioki: Vertical component of the Hachinohe records from the 1968 Tokachioki earthquake,
C-Wave S_2: A-Wave S_2 motion with time scale varied for F-line test.

Figure 2.6 shows the response spectra for the A-Wave and B-Wave. It should be noted that all the above accelerograms are the "target waves," used as input to the shake table at Tadotsu Lab. The actual recorded table motions are slightly different than the target motions as described later in this report.

Table 2.1 Selected Measurement Items for M-line with Conventional Support

Instrumentation I.D.		ISSAC Node/Element No.	PSAFE2 Node Number
(Acceleration)			
AA1		N-10	1
MA1		N-50	6
MA2		N-90	10
MA3		N-130	12
MA4		N-150	15
MA5		N-165	42
MA6		N-180	16
MA8		N-200	19
MA10		N-250	21
(Displacement)	(Support load)		
AD1X, Y, Z		N-10	1
MD1a	MR1	101	10
MD2a	MR2	102	10
MD3b	MR3	103	11
MD4b	MR4	104	11
MD5	MR5	105	12
MD6	MR6	106	12
MD7	MR7	107	16
MD8X, Y, Z		N-150	15
MD9	MR11	109	212
MD10	MR12	110	222
MD11		112	261
(Stress)			
MS1		3	4
MS2'		5	5
MS2		7	31
MS3		9	8
MS4		14	33
MS5		17	14
MS6		46	42
MS8		23	18
MS9		25	36
MS10		30	22

Table 2.2 Selected Measurement Items for F-line with Conventional Support

Instrumentation I.D.		ISSAC Node/Element No.	PSAFE2 Node Number
(Acceleration)			
FA2		N-40	4
FA3		N-90	9
FA5		N-180	18
FA6		N-240	26
FA7		N-280	30
FA8		N-330	35
FA9		N-390	41
FA10		N-440	46
FA11		N-500	52
FA12		N-550	57
FA13		N-790	95
(Displacement)	(Support load)		
—	FR1	N-10	15
FD2b	FR2	201	22
FD3b	FR3	202	22
FD4b	FR4	203	28
FD5b	FR5	204	28
FD6b	FR6	205	38
FD7a, b	FR7	206	39
FD8a, b	FR8	207	39
FD9b	FR9	208	48
FD10b	FR10	209	48
(Stress)			
FS1		1	1
FS2		18	18/19
FS3		25	26/27
FS4		30/55	30
FS5		39	39
FS6		41/80	41
FS7		41	44
FS8		50	50
FS9		51/105	52
FS10		57	55/56
FS11		60	57/58
FS12		64	60
FS13		66	62/63
FS14		68	64
FS15		80	73
FS16		85	78
FS17		90	80/81
FS18		92	92
FS19		105	91
FS20		112	95
FS21		115	98/99
FS22		117	100

Note: For ISSAC models, N- indicates a node number and all other numbers represent element numbers.

Table 2.3 Selected Measurement Items for M-line with EA Support

Instrument I.D.		ISSAC Node/Element Number	PSAFE2 Node Number
(Acceleration)			
AA1		N-10	1
MA1		N-50	6
MA16		N-90	10
MA17		N-130	12
MA4		N-150	15
MA5		N-165	35
MA6		N-180	16
MA8		N-200	19
MA10		N-250	21
(Displacement)	(Support force)		
AD1X, Y, Z		N-10	1
MD9	MR11	110	212
MD10	MR12	111	222
MD11		112	261
MD12 (X)		N-90	10
MD13 (Y)		N-90	10
MD14	MR8	106	16
MD15	MR15	LED-1	12
MD16	MR16	LED-2	12
MD17	MR17	LED-3	50
MD18X, Y, Z		N-150	15
(Stress)			
MS1		3	4
MS2		7	31
MS3		9	8
MS4		14	12
MS5		17	14
MS6		47	35
MS10		30	22

Table 2.4 Selected Measurement Items for F-line with EA Support

Instrumentation I.D.		ISSAC Node/Element No.	PSAFE2 Node/Number
(Acceleration)			
FA3		N-90	6
FA5		N-180	13
FA6		N-240	18
FA7		N-280	21
FA8		N-330	108
FA9		N-390	30
FA10		N-440	111
FA11		N-500	38
FA12		N-550	44
FA13		N-790	119
(Displacement)	(Support load)		
	FR1	N-10	10
FD6b	FR6	205	27
FD11b	FR11	401 (EAB-1)	16
FD12b	FR12	402 (EAB-2)	28
FD13b	FR13	207	28
FD14b	FR14	403 (EAB-3)	112
FD15b	FR15	208	112
(Stress)			
FS1		1	1A
FS2		18	14
FS3		25	19
FS4		30	21
FS5		39	29
FS6		41	30
FS7		43-1	32
FS8		50	113
FS9		51	38
FS10		57	43
FS11		60	45
FS12		64	114
FS13		66	49
FS14		68	50N
FS15		80	51
FS16		86	54N
FS17		90	56
FS18		92	58N
FS19		105	59
FS20		112	119
FS21		115	65
FS22		117	66N

Note: For ISSAC models, N- indicates a node number and all other numbers represent element numbers

Table 2.5 Summary of Test Runs

Pipe Support	Test Item	Table Motions
Conventional Support Case	Preliminary Test (PC)	• Sinusoidal waves • Random waves
	Seismic Proving Test (VC)	• Design motions S_1 and S_2
	Design Method Confirmation Test (DC)	• Design motion S_2 • C/V wave
	Marginal Test (MC)	• Amplified S_2 motion
Energy Absorbing Support Case	Preliminary Test (PE)	• Sinusoidal waves • Random waves
	Design Method Confirmation Test-I (DE1)	• A-wave and B-wave • Actuator for M-line operated
	Design Method Confirmation Test-II (DE2)	• A-wave • Actuator for M-line not operated (fixed)
	Marginal Test (ME)	• A-wave and B-wave with varied amplitude and time scale • Tokachi-oki wave

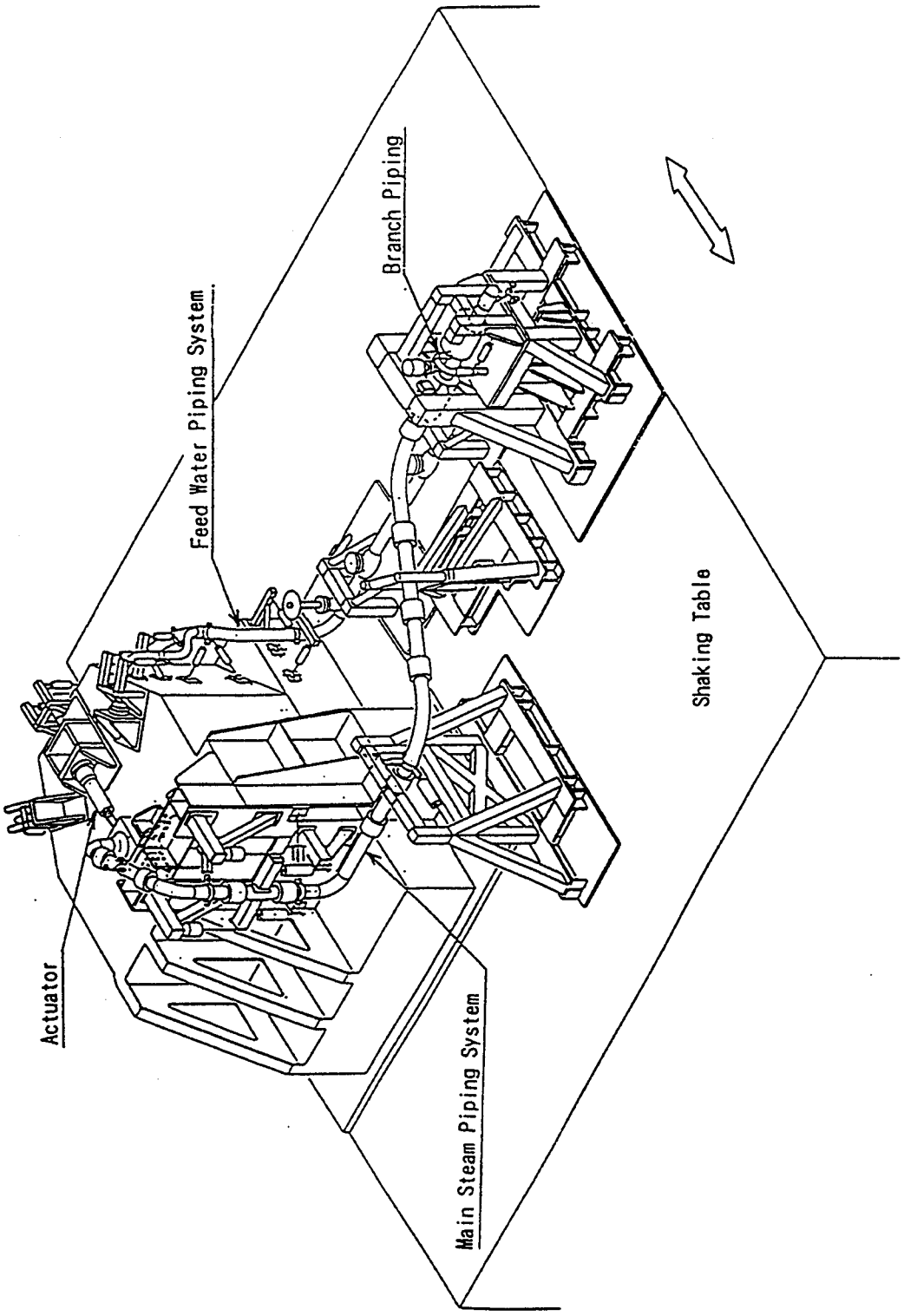

Figure 2.1 MS Seismic Proving Test Model

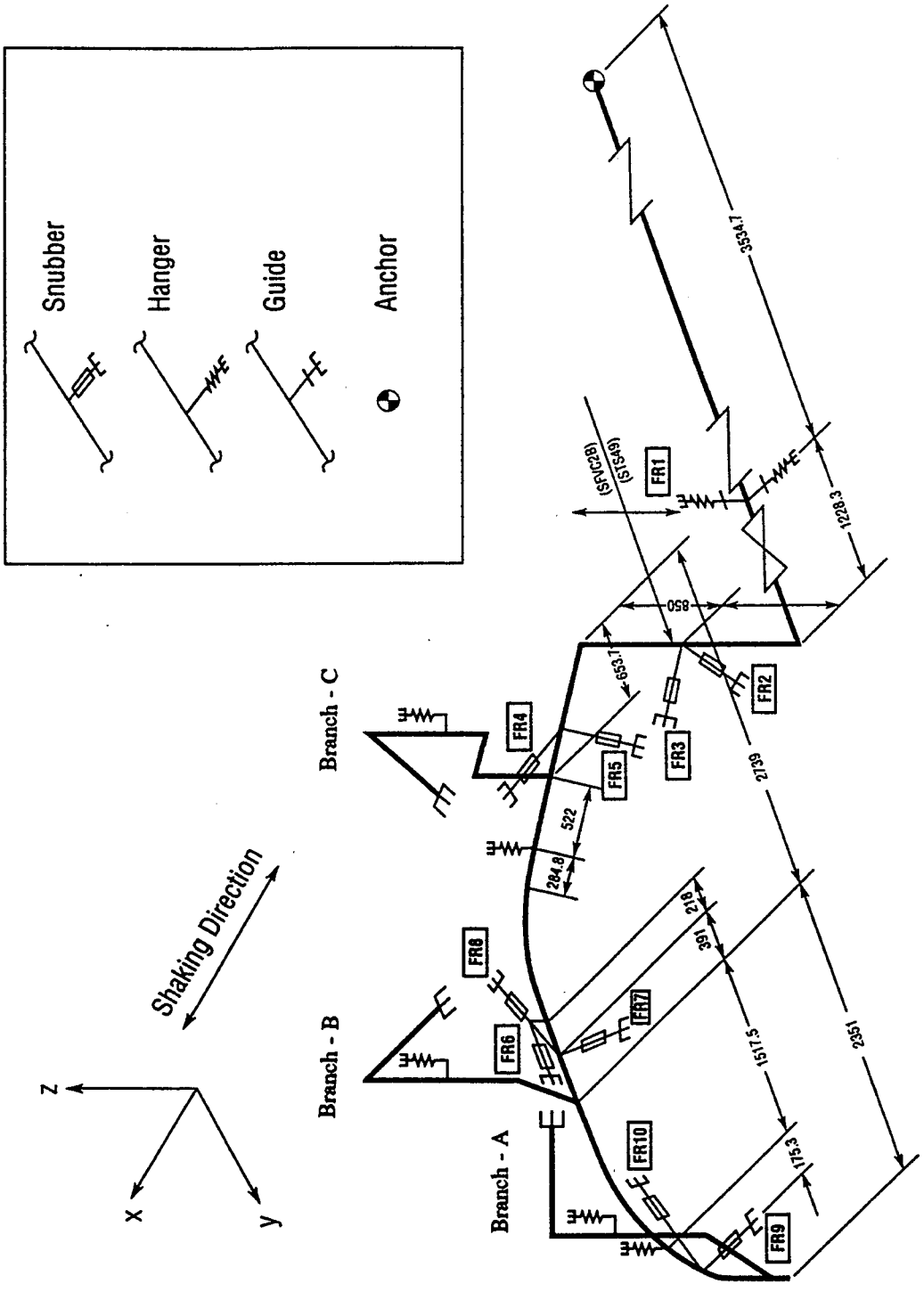

Figure 2.2 Pipe Supports of F-line, Conventional Support Case

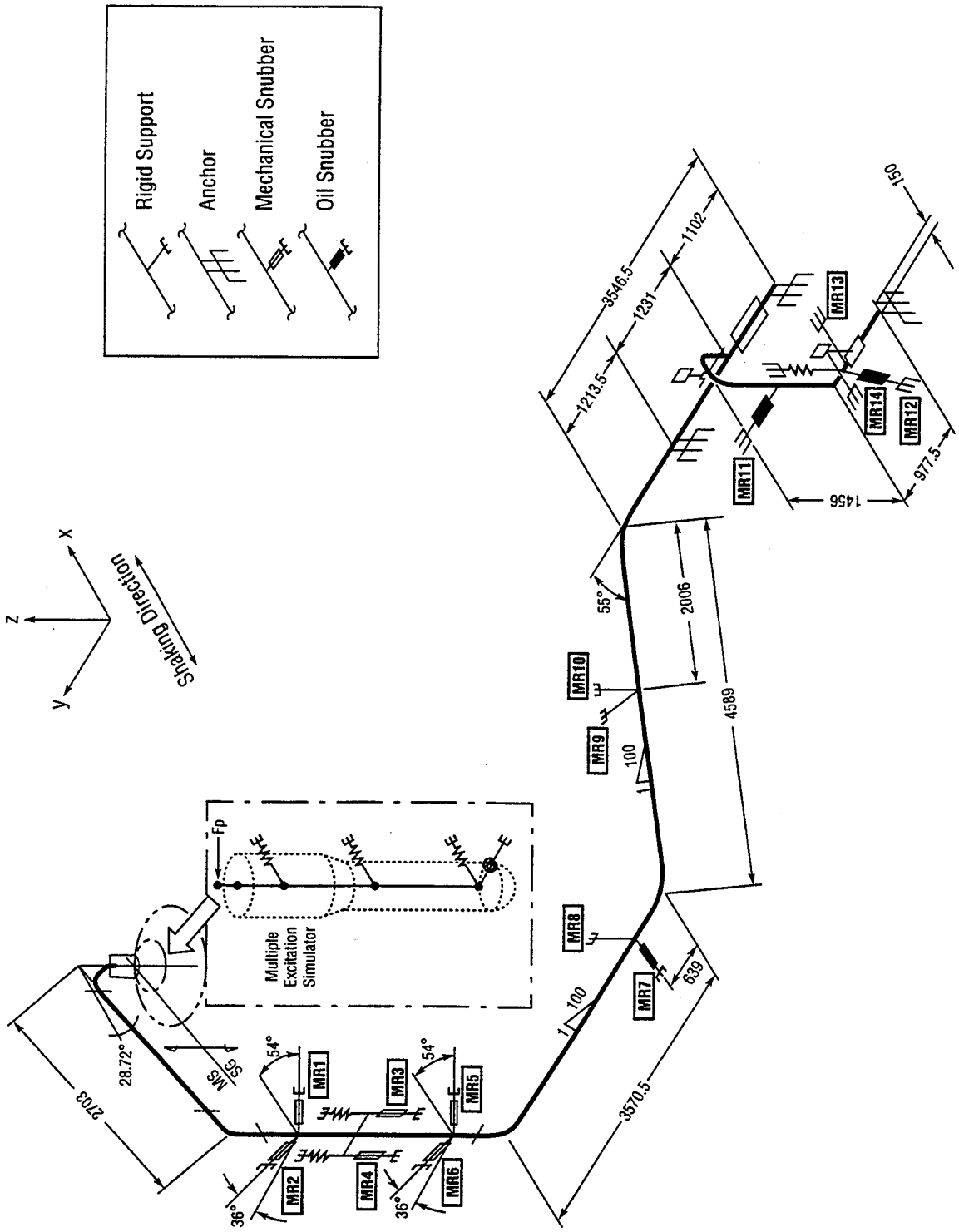

Figure 2.3 Pipe Supports of M-line, Conventional Support Case

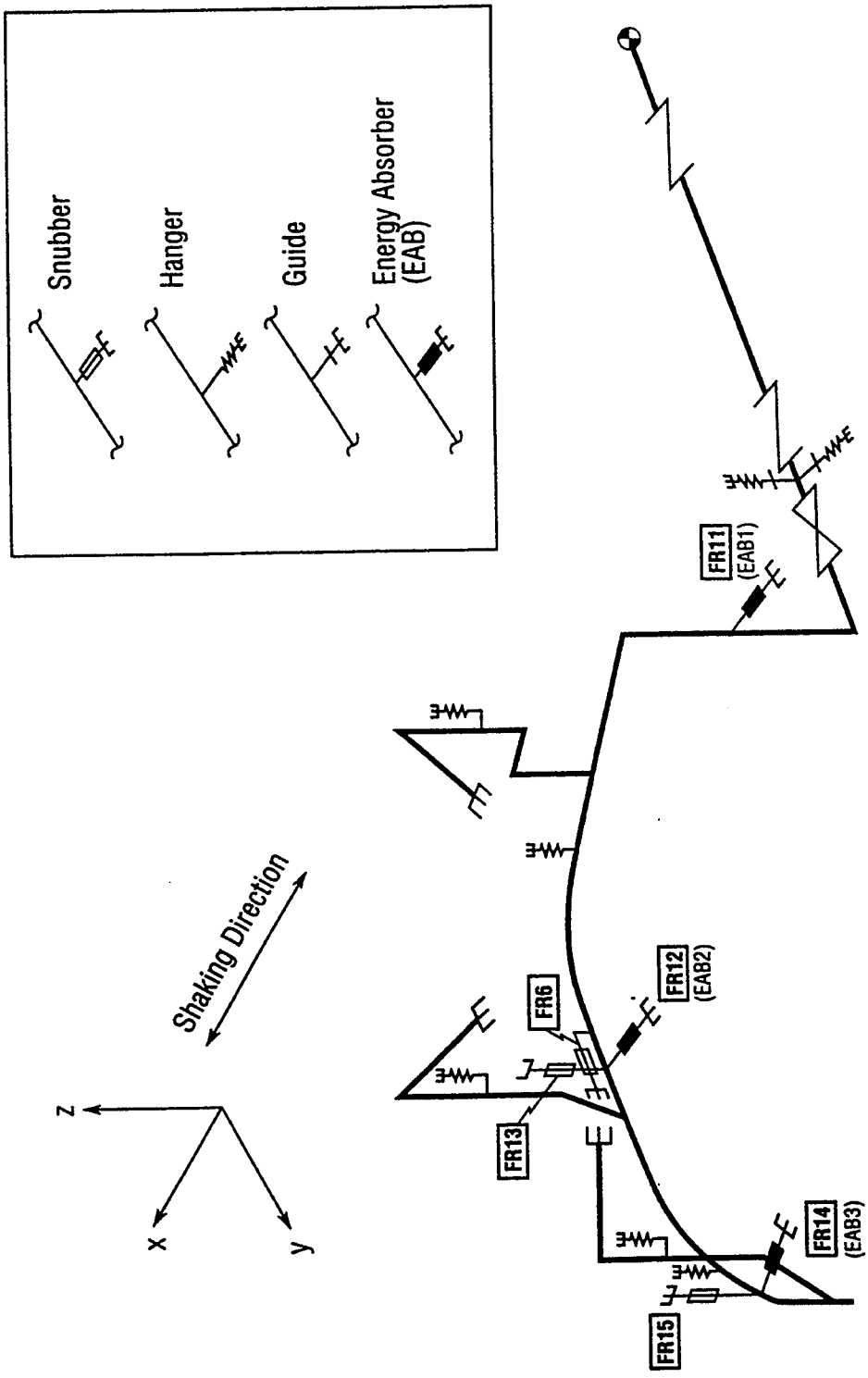

Figure 2.4 Pipe Supports of F-line, EA Support Case

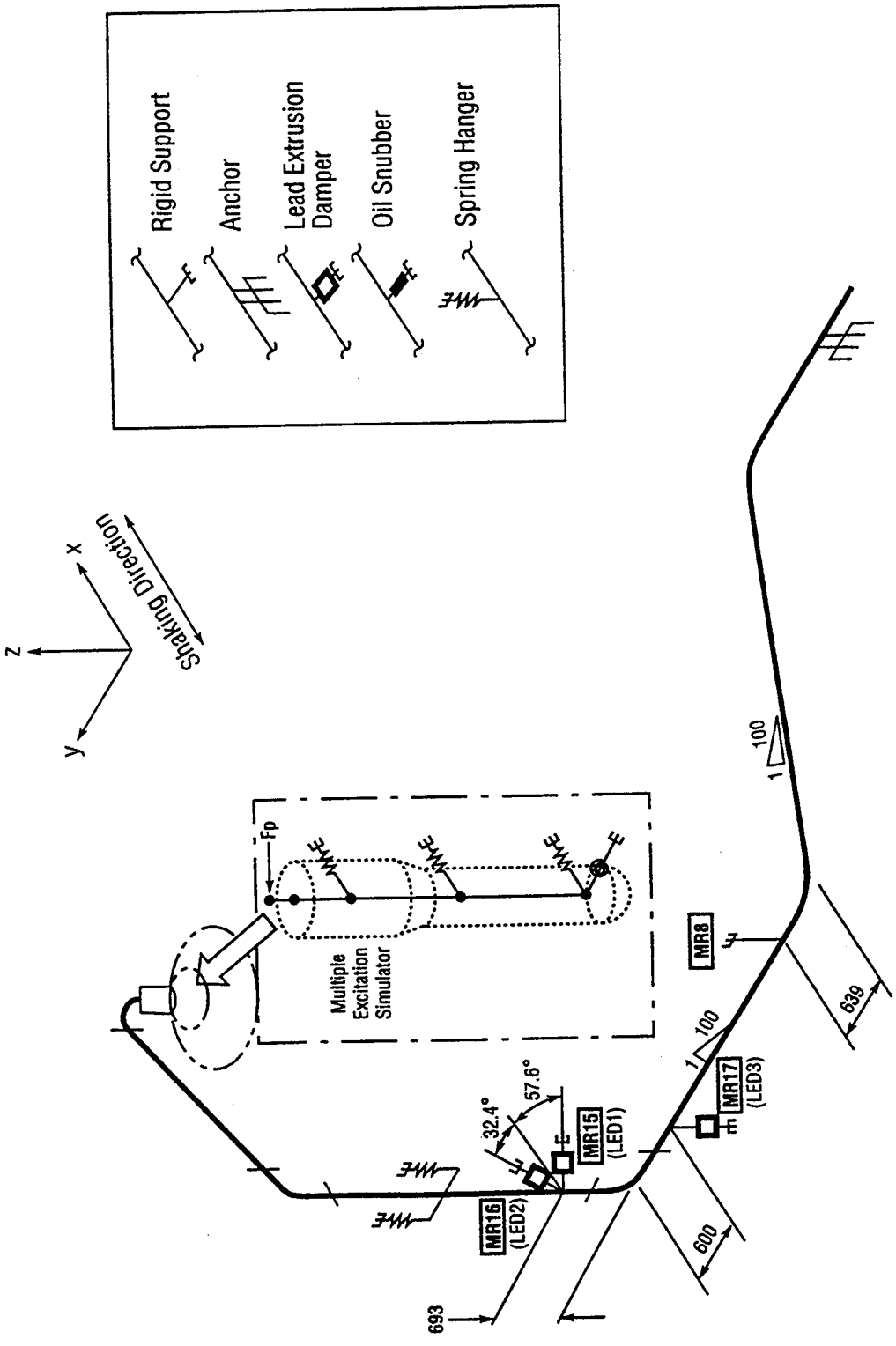

Figure 2.5 Pipe Supports of M-line, EA Support Case

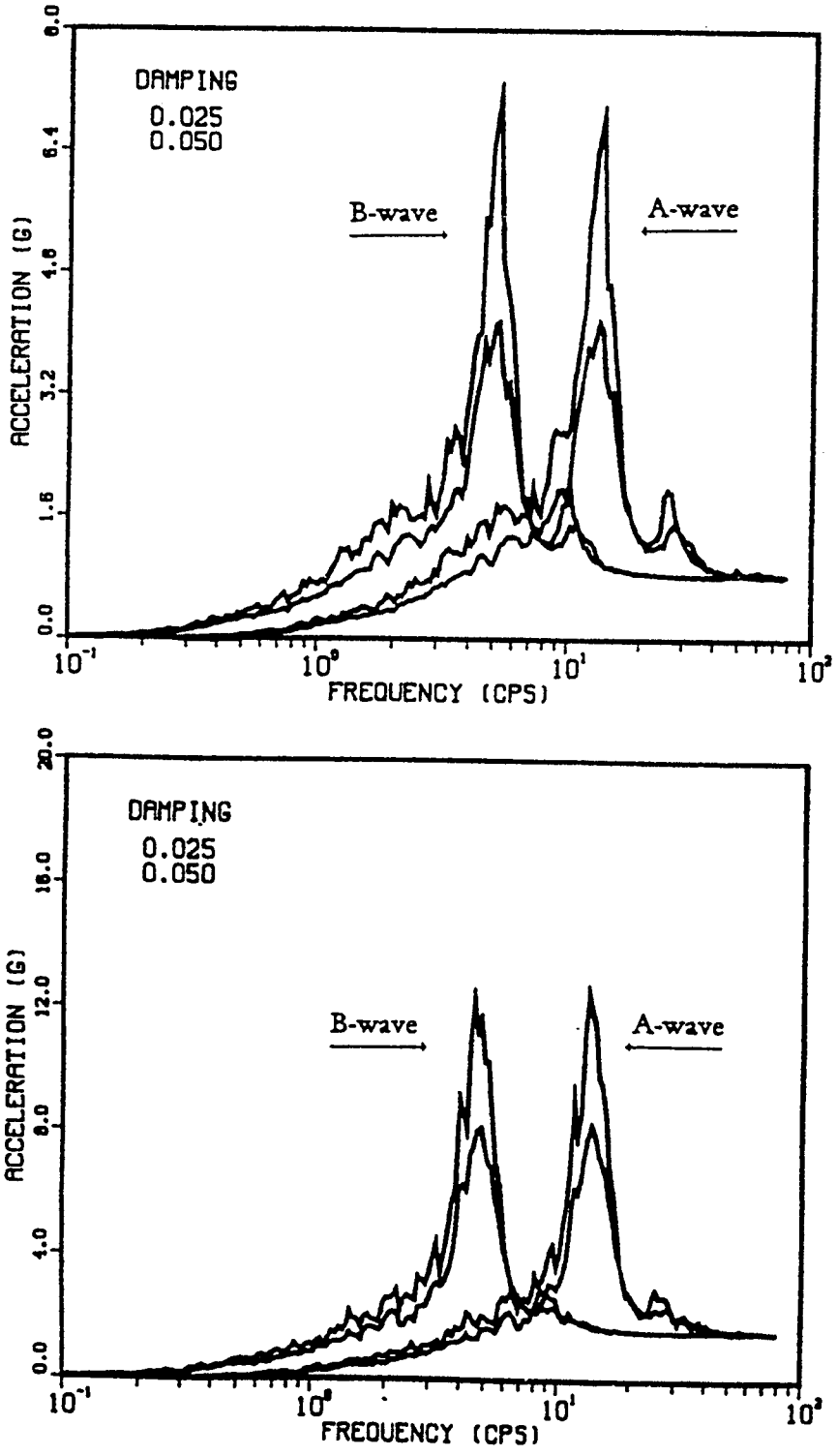

(a) S_1 Motion

(b) S_2 Motion

Figure 2.6 Response Spectra of A-Wave and B-Wave

3 SUMMARY OF NUPEC'S TEST RESULTS

3.1 Introduction

The test results of the MS Test Program are described in detail in Appendix M of this report. Listings of recorded peak responses and plots of selected channels for six test runs are also provided in Appendices E through J. This chapter briefly outlines the observed piping responses for both the conventional support case and the EA support case, and summarizes major findings from the MS Test Program.

3.2 Conventional Support Case

Figure 3.1 shows the hysteretic responses of mechanical snubbers of the M-line with conventional supports for the 1.0 S2(M) test run. The observed complex nonlinearity in the snubber behavior was considered to be mainly caused by the mechanical gaps in both snubbers and the connection to pipes (i.e., pipe clamps) as well as by the orthogonal (to the snubber axis) forces. The irregularity in the hysteretic behavior seems to be more pronounced for the snubbers with lower applied forces, i.e., the snubbers MR3 and MR4. Table 3.1 lists the measured peak responses. The recorded support forces were higher than the values estimated during planning due to the gap nonlinearity of the snubbers. However, the pipe stresses were much lower than the yield stress of 25 Kg/mm^2, and not significantly affected by the high-frequency vibrations caused by the mechanical gaps.

As indicated in Table 3.1, the peak relative displacement applied by the independent actuator at the SG-joint (AD1) was 2.46 mm for this test run. A different combination of the table motion and the independent actuator motion was used in the multiple excitation test to study the effects of the independent support motion on the piping responses (see Appendix M for a more detailed description of the test results). In that test, the amplitude of the table motion was reduced to 1/3 of the foregoing 1.0 S2(M) test run, but the peak relative displacement of the independent actuator was increased from 2.46 mm to 3.54 mm. As a result, higher support forces and pipe stresses were measured at several locations, indicating the significance of the independent support motions on the piping responses.

Figure 3.2 shows the hysteretic responses of mechanical snubbers of the F-line with conventional supports for the 1.0 S2(F) test run. Table 3.2 lists the recorded peak responses. Again, highly irregular hysteretic responses are observed for snubbers with lower applied forces, e.g., FR2, FR3, FR4 and FR5. In the test series where only the table motion amplitude was varied, it was observed that almost all the measured peak responses were not proportional to the table motion amplitude. The response amplification factors at higher excitations tend to be reduced, particularly for the pipe stresses and the support forces.

3.3 Energy Absorbing Support Case

As illustrated in Figure 2.5, the mechanical snubbers of the M-line were replaced with three LED supports in the main piping and a large number of test runs were conducted. The test results from the 1.0 S2(A) test run are given in Table 3.3 and Figure 3.3. The response of the LED supports shown in Figure 3.3 indicate stable hysteresis loops of the newly proposed energy absorbing device. In test series with varied table motion amplitudes, it was observed that both the support forces and the pipe stresses tended to level off in higher amplitude tests, indicating the effectiveness of the LED supports. Since only three LED supports were installed on the test model, the measured pipe stresses were much higher than those measured in the test cases with conventional supports.

After the independent support motion (ISM) tests described above, the SG-joint was fixed to the common support structures and a large number of uniform motion tests were performed mainly for assessing the seismic margin of the

LED supports. The most severe test was conducted at the end of the MS Test Program using the Tokachi-Oki earthquake wave (see Appendix J of the report).

As illustrated in Figure 2.4, three mechanical snubbers and three EAB supports were installed on the F-line. The test results for the 1.0 S2(A) wave test run are summarized in Table 3.4 and Figure 3.4. The observed hysteretic responses of the mechanical snubbers indicate a highly irregular nonlinearity. The responses of the EAB supports, on the other hand, seem predictable. The most severe test wave for the F-line was the 1.2 S2(C) wave (see Appendix H of this report). During this test run, the peak displacement response of EAB-3 exceeded the displacement limit of 15 mm, which is the movable length of pins within the slots (see Appendix L of this report for the details of the EAB mechanism). Also, the peak support force of 10.74 tons for mechanical snubber FR15 is about 2.4 times higher than the design capacity of 4.5 tons.

3.4 Major Findings from the MS Test Program

An enormous amount of test data were generated for the dynamic responses of piping systems with various support configurations from a total of more than 200 test runs. This report, in fact, describes only a small portion of the obtained test results. The test results were studied further and analyzed as part of the simulation studies, which are described in Chapter 5 of this report. Based on the observation of the test results describes above, the following conclusions can be drawn.

- During the MS Test Program, the accuracy of the shaking table control was excellent, and the predicted floor responses of a reactor building were successfully reproduced.

- The great quantity of test results on earthquake response of piping with various support conditions, including the ISM tests, can be used to verify existing computer codes.

- The scaled piping specimens of the main steam line and the feedwater line properly modeled actual piping systems in typical PWR and BWR nuclear power plants, particularly the pipe support conditions. The recorded piping responses, however, did not exactly reproduce the piping responses predicted by the pre-test analyses due to various nonlinearities and flexibilities in the pipe supports. This complexity, however, may also exist in piping systems of actual power plants.

- The tested piping systems, even those with conventional supports, are complex nonlinear structures. Various mechanical gaps in pipe support systems were a main factor of the observed nonlinearities that were not considered in the pre-test analyses.

- Under the design earthquake loadings, the measured pipe stresses were much lower than the yield stresses for both the conventional and E.A. support cases.

- Due to the nonlinearities in support systems, the measured responses were not proportional to the excitation amplitude levels. In almost all the test cases, the ratios of the measured responses to the excitation amplitude levels tend to be reduced at higher excitation levels.

- Mechanical snubbers contribute to a spring hardening characteristic to the piping systems, i.e., the vibration frequencies tend to be increased at higher excitation levels. On the other hand, the E.A. support systems contribute a soft spring softening characteristic, i.e., the vibration frequencies tend to be reduced at higher excitation levels.

- The structural as well as functional integrities of conventional snubbers were confirmed up to a support force 2.4 times higher than the rated design load.

- Rate-dependent characteristics were observed in the response of LED supports. The behavior of the EAB supports was more predictable, and rate-dependency was not observed.

- Both the LED and EAB support systems sustained a large number of earthquake loadings that were much higher than the design load levels without losing structural or functional integrity. During a few tests with highest table motions, pipe stresses slightly exceeded the yield stress level at a few locations. However, the piping remained elastic, and no structural damage was observed during detailed inspections after the MS program.

- The observation of the test results implied an advantage of the E.A. supports over conventional snubbers because piping systems can be designed more flexible using much fewer numbers of pipe supports. The larger pipe deflection; and, therefore, higher pipe stresses, in a more flexible piping system can be compensated for by large energy absorbing capabilities of E.A. supports as well as by the inherent large seismic margin in piping. This will enhance the seismic reliability of nuclear piping systems during a large earthquake event, particularly against large differential support motions. Also, the dynamic responses appeared to be more predictable than those of conventional snubbers.

- The test series of the M-line with the independent actuator clearly demonstrated the significance of the independent support motion (ISM). In the conventional support case, the magnitude of the peak differential displacement had a much larger impact on the measured pipe stresses and the support forces than the level of acceleration input, as illustrated by the comparison between the 1.0 S2(M) test (Table M.6) and the ⅓ S2(M) Multiple Excitation test (Table M.7). In the E.A. support case, this tendency was much less obvious as the flexibility of the E.A. supports tends to reduce a local stress concentration and leads to a more uniform strain distribution.

Table 3.1 Measured Peak Responses of M-line with Conventional Supports, 1.0 S2(M) Test Run

Acceleration (g)			Displacement (mm)			Support Forces (ton)		Pipe Stress (kg/mm^2)	
Instrument	**Direction**	**Values**	**Instrument**	**Direction**	**Values**	**Instrument**	**Values**	**Instrument**	**Values**
AA1	X Y Z	5.04 0.27 0.40	AD1	X Y Z	2.46 0.06 0.19	MR1	5.22	MS1	1.86
MA1	X Y Z	6.04 4.07 1.72	MD1a		1.35	MR2	6.81	MS2[1]	0.97
MA2	X Y Z	4.83 2.47 2.11	MD2a		1.56	MR3	1.46	MS2	1.63
MA3	X Y Z	3.80 1.40 1.65	MD3b		0.88	MR4	1.41	MS3	2.30
MA4	X Y Z	3.15 1.24 1.47	MD4b		0.94	MR5	2.51	MS4	1.37
MA5	X Y	3.05 1.19	MD5a (5b)		0.77 (0.76)	MR6	3.27	MS5	1.02
MA6	X Y	2.02 1.14	MD6a (6b)		0.85 (0.64)	MR7	1.55	MS6	1.52
MA8	X Y Z	2.15 1.31 1.83	MD7a (7b)		0.67 (0.31)	MR9	1.10	MS8	0.80
MA10	X Y Z	2.38 0.34 0.95	MD8	X Y Z	1.28 0.54 0.93	MR10	0.97	MS9	0.63

Table 3.2 Measured Peak Responses of F-line with Conventional Supports, 1.0 S2(F) Test Run

Acceleration (g)			Displacement (mm)		Support Forces (ton)		Pipe Stress (kg/mm²)	
Instrument	**Direction**	**Values**	**Instrument**	**Values**	**Instrument**	**Values**	**Instrument**	**Values**
FA2	X Y Z	2.09 0.62 0.93	FD2b	0.32	FR2	0.88	FS1	2.9
							FS2	1.3
FA3	X Y Z	2.63 0.17 1.36	FD3b	0.68	FR3	1.39	FS3	1.0
							FS4	1.3
FA5	X Y Z	2.08 0.28 1.09	FD4b	0.46	FR4	0.96	FS5	1.6
							FS6	1.4
FA6	X Y Z	2.07 1.45 1.51	FD5b	0.71	FR5	1.42	FS7	1.6
							FS8	0.4
FA7	X Y Z	3.38 1.24 1.19	FD6b	0.79	FR6	2.45	FS9	1.6
							FS10	0.9
FA8	X Y Z	3.07 1.28 1.64	FD7a, b	0.88 (0.39)	FR7	3.52	FS11	1.7
							FS12	1.4
FA9	X Y Z	2.69 1.24 1.24	FD8a, b	0.63 (0.33)	FR8	2.42	FS13	1.4
							FS14	2.9
FA10	X Y Z	2.78 1.11 1.13	FD9b	0.49	FR9	2.73	FS15	1.2
							FS19	1.6
FA11	X Y Z	3.11 1.90 1.19	FD10b	0.56	FR10	1.85	FS20	2.1
							FS21	1.8
FA12	X Y Z	3.10 1.95 1.30					FS22	2.8
FA13	X Y Z	3.18 1.36 1.26						

Table 3.3 Measured Peak Responses of M-line with LED Supports, 1.0 S2(A) Test Run

Acceleration (g)			Displacement (mm)			Support Forces (ton)		Pipe Stress (kg/mm^2)	
Instrument	**Direction**	**Values**	**Instrument**	**Direction**	**Values**	**Instrument**	**Values**	**Instrument**	**Values**
AA1	X Y Z	4.42 0.33 0.45	AD1	X Y Z	2.95 0.25 0.19	MR8	5.91	MS1	9.1
MA1	X Y Z	3.80 5.60 2.02	MD15/ LED-1		2.6	MR15/ LED-1	1.60	MS2'	4.7
MA16	X Y Z	3.37 7.44 2.22	MD16/ LED-2		5.2	MR16/ LED-2	1.81	MS2	1.8
MA17	X Y Z	4.74 2.25 1.97	MD17/ LED-3		4.5	MR17/ LED-3	1.01	MS3	5.5
MA4	X Y Z	3.38 2.78 2.06	MD18	X Y Z	5.5 4.8 4.6			MS4	3.0
MA5	X Y	2.70 2.85						MS5	4.3
MA6	X Y	2.18 2.98						MS6	4.1
MA8	X Y Z	2.29 2.75 4.99						MS8	2.0
MA10	X Y Z	2.06 1.39 5.61						MS9	3.7
								MS10	2.2

Table 3.4 Measured Peak Responses of F-line with EAB Supports, 1.0 S2(A) Test Run

Acceleration (g)			Displacement (mm)		Support Forces (ton)		Pipe Stress (kg/mm^2)	
Instrument	Direction	Values	Instrument	Values	Instrument	Values	Instrument	Values
FA3	X Y Z	3.08 0.41 1.80	FD6b	1.05	FR6b	1.66	FS1	4.3
							FS2	4.5
FA5	X Y Z	2.98 0.62 2.28	FD11b/ EAB-1	5.42	FR11b/ EAB-1	0.71	FS3	6.9
							FS4	9.5
FA6	X Y Z	4.94 3.28 3.30	FD12b/ EAB-2	7.20	FR12b/ EAB-2	1.43	FS5	2.4
							FS6	5.0
FA7	X Y Z	5.20 1.98 2.22	FD13b	1.25	FR13b	4.89	FS7	3.5
							FS8	1.2
FA8	X Y Z	4.97 1.28 2.96	FD14b/ EAB-3	8.50	FR14b/ EAB-3	1.45	FS9	8.5
							FS10	5.7
FA9	X Y Z	3.04 1.57 2.43	FD15b	0.82	FR15b	4.37	FS11	5.9
							FS12	3.6
FA10	X Y Z	3.29 1.52 2.84					FS13	7.1
							FS14	8.8
FA11	X Y Z	4.07 3.75 3.06					FS15	6.0
							FS19	8.3
FA12	X Y Z	5.56 2.48 2.14					FS20	3.7
							FS21	10.7
FA13	X Y Z	3.68 1.90 3.31					FS22	8.1

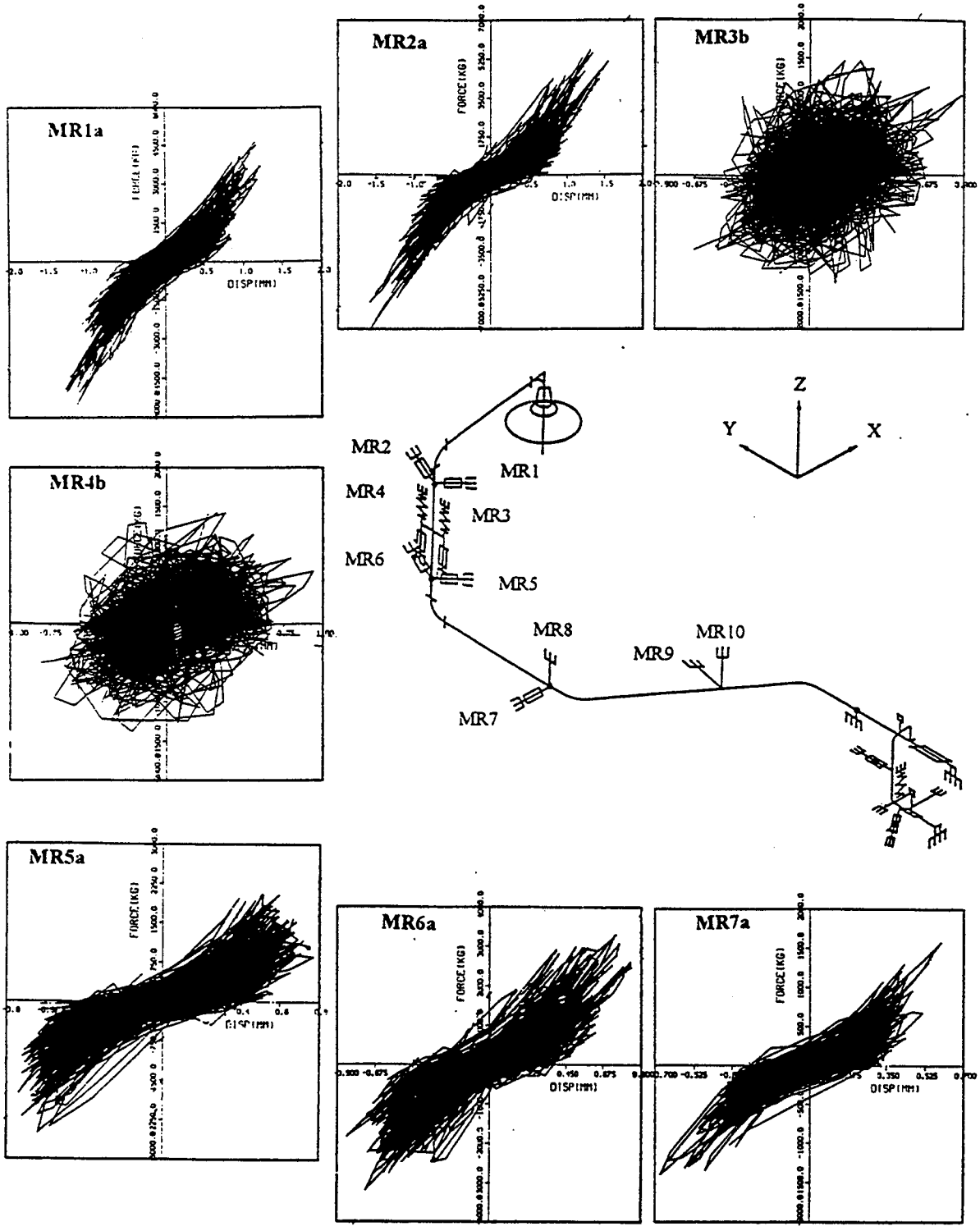

Figure 3.1 Hysteretic Responses of Snubbers of M-line with Conventional Supports, 1.0 S2(M) Test Run

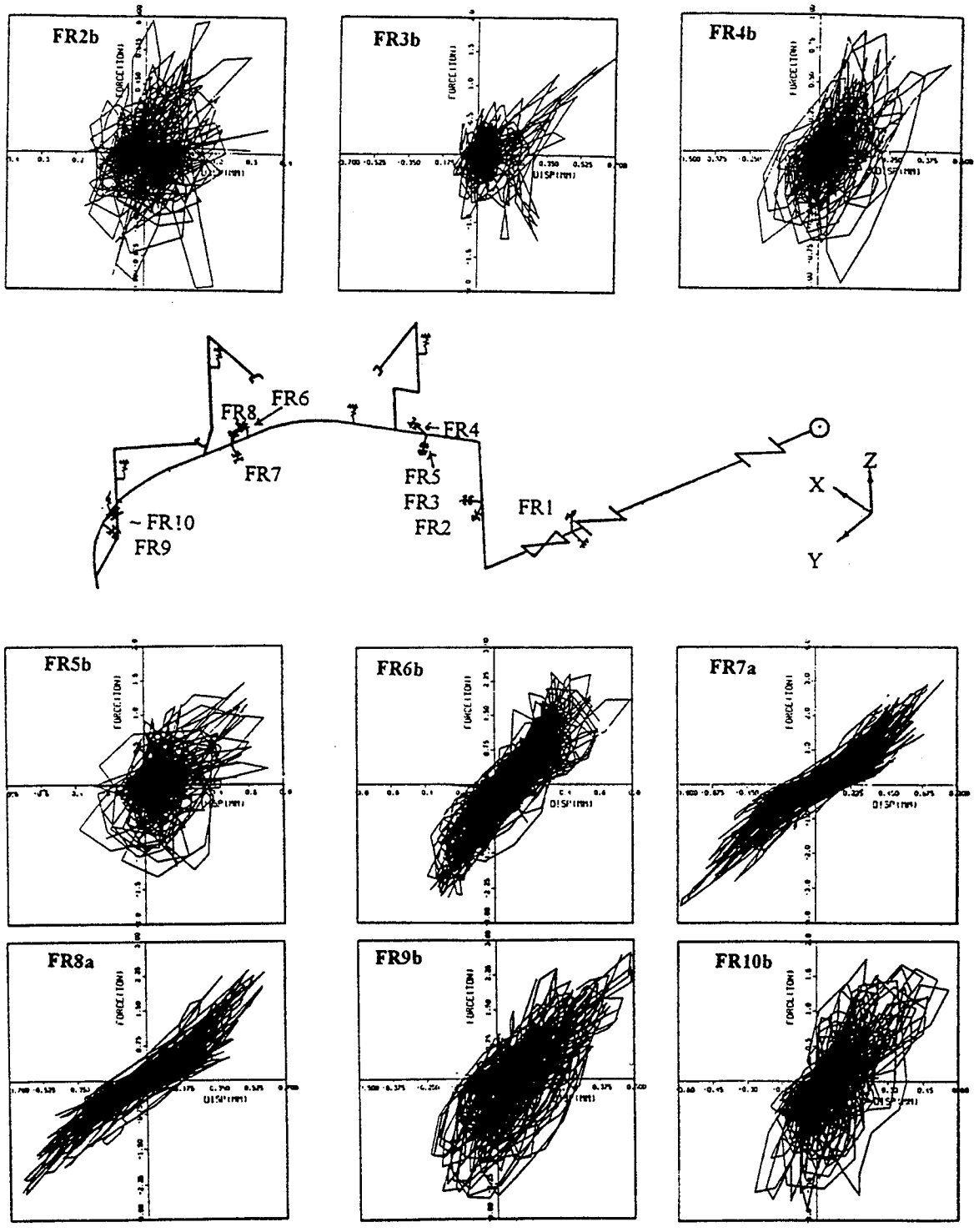

Figure 3.2 Hysteretic Response of Snubbers of F-line with Conventional Supports, 1.0 S2(F) Test Run

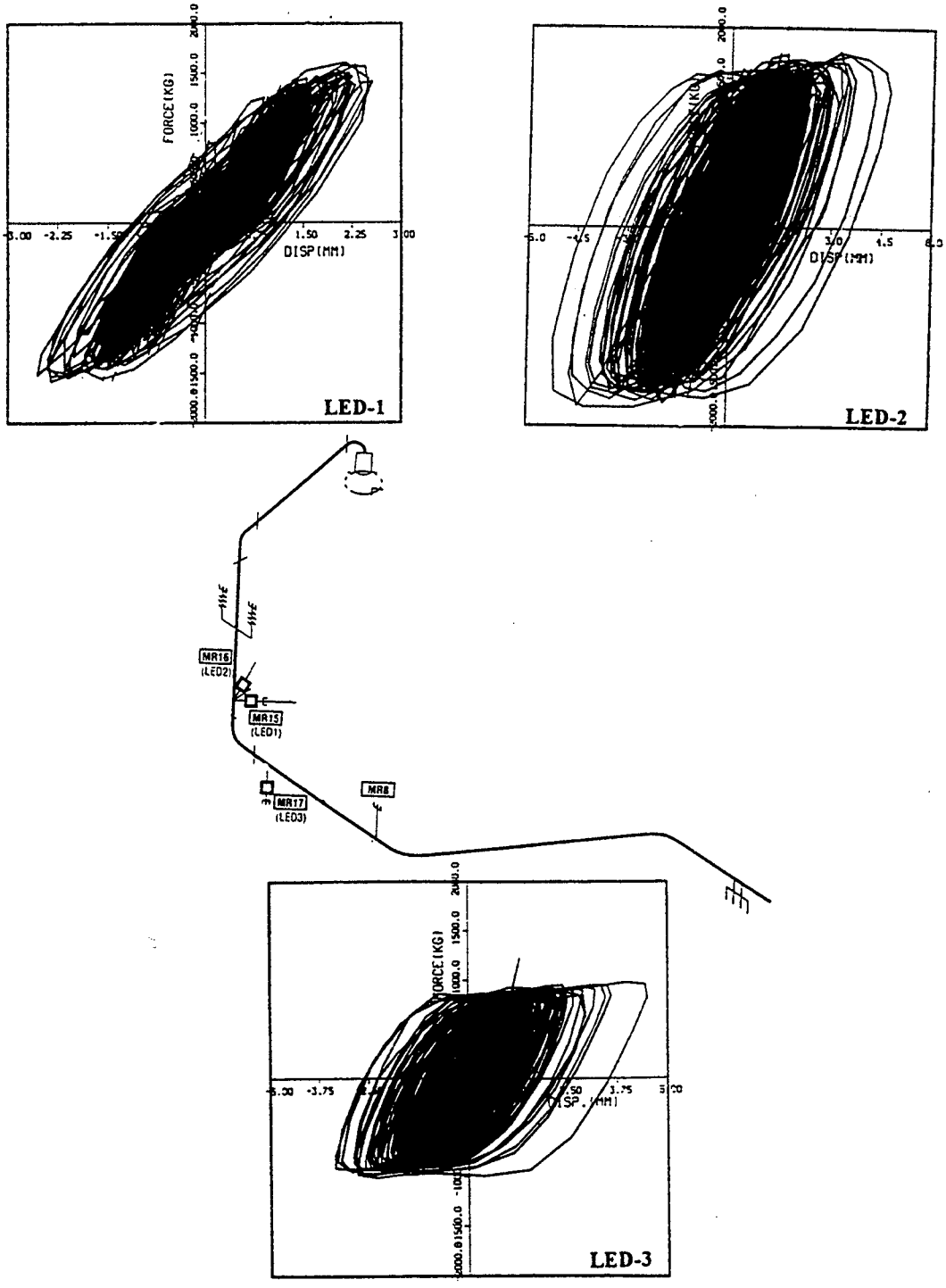

Figure 3.3 Hysteretic Responses of M-line with LED Supports, 1.0 S2(A) Test Run

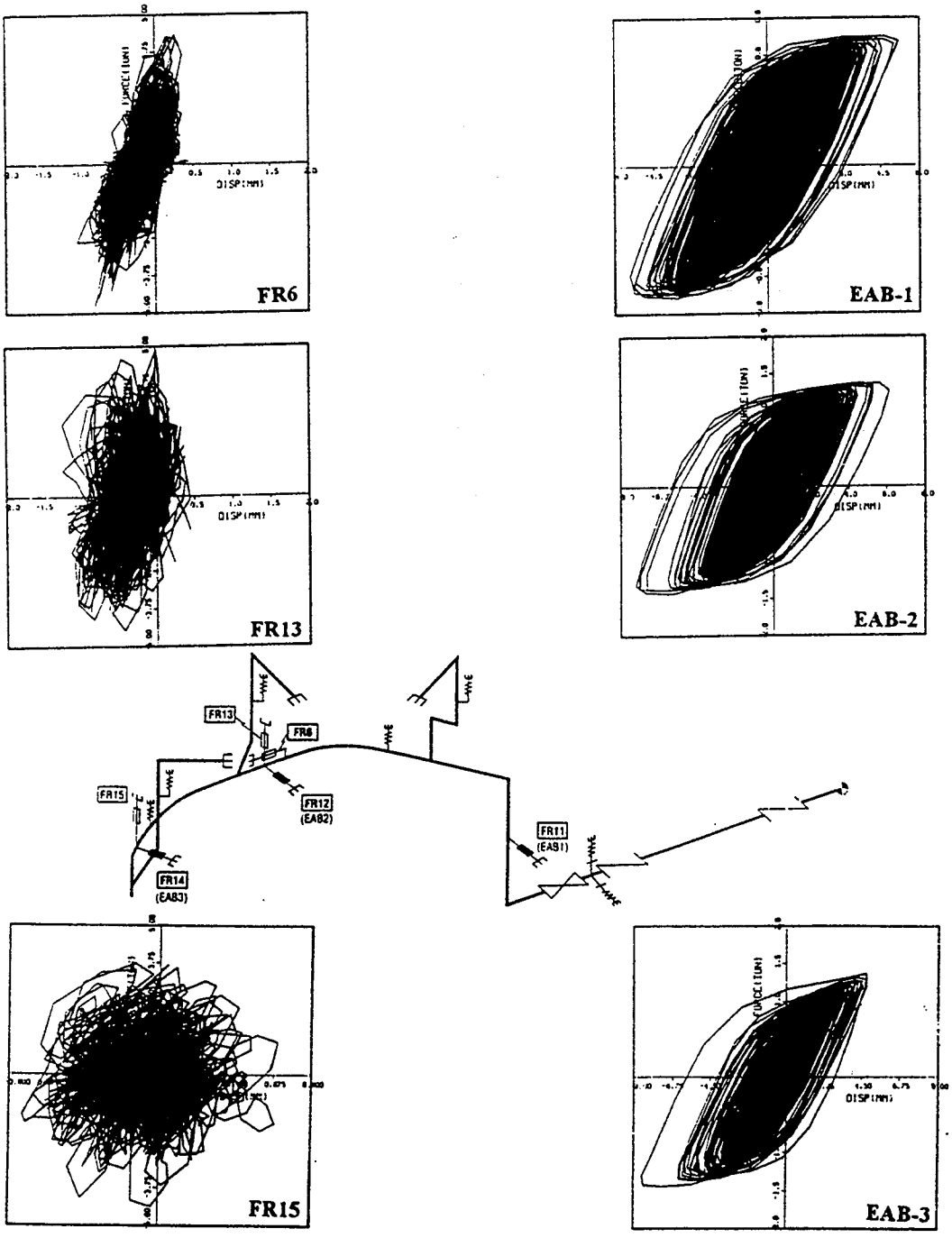

Figure 3.4 Hysteretic Responses of F-line with EAB Supports, 1.0 S2(A) Test Run

4 ANALYSIS PLAN

4.1 Analysis Objectives

Two types of post-test analyses were performed for selected test runs, i.e., simulation analyses for the correlation studies described in Chapter 5, and design-based analyses described in Chapter 6. The objectives of the simulation analyses were to reproduce the recorded piping responses and to understand the mechanism of the observed complex nonlinear behavior of the piping systems described in the preceding chapter. Factors that were considered to be critical in simulation analyses included the modeling of the nonlinearity of support structures, consideration of seismic anchor motions, damping assumption, and detuning effects of nonlinear piping systems. In addition to conventional direct time integration analyses, equivalent linearization techniques were also used in this study. Existing equivalent linearization analysis techniques were reviewed, modified and refined for a better correlation with the observed nonlinear piping responses.

In the design-based analyses, the piping design analysis methods, currently used in the nuclear industry, were blindly applied to selected test runs of the conventional support cases. The objectives of these analyses were to evaluate the seismic design margins for support forces and pipe stresses, as well as to assess the adequacy of various analysis/design assumptions, including modeling of support structures, damping assumptions, and independent support motion (ISM) consideration.

4.2 Review of Piping Analysis Methods

4.2.1 Design Analysis Methods in Nuclear Industry

The seismic design of piping in nuclear power plants is based on ASME Design Codes and the US NRC Standard Review Plant (SRP) and Regulatory Guides (e.g., R.G. 1.61 for damping values, R.G. 1.92 for modal combination rules, and R.G. 1.122 for development of floor spectra). The response spectrum approach using the SRSS combination rule and broadened spectra (by ±15%) is predominantly used in design calculations. Time history analysis, which is more time consuming, is rarely used for piping design. To avoid excessive conservatism, the peak shifting approach is used as an alternative to broadened response spectra. System modal responses at frequencies up to the ZPA range are combined using the SRSS rule. When two frequencies are close, i.e., two frequencies differ from each other by 10% or less of the lower frequency, the coupling effect of vibration modes are considered by using the double sum method or grouping method. In the rigid frequency range, the responses may be underestimated due to the foregoing modal cutoff. The missing mass correction may be necessary when this effect is considered to be significant. The response spectrum analysis is performed for three earthquake components separately, and the calculated responses, including support forces and pipe stresses, are then combined using the SRSS rule.

While the seismic inertia forces are quantified using the response spectrum approach, a separate static analysis is normally performed for the seismic anchor motions (SAM), and combined with the inertia part. When more than one SAM is involved in a piping system, the worst combination of the peak relative displacements is considered to give the maximum stresses in the pipe.

In the structural analyses of piping systems, various pipe supports are usually modeled as uniaxial springs. The supports are modeled using their actual stiffness values or rigid stiffness values. When rigid stiffness values are used, sufficiently large values should be assumed to ensure that the stiffness of the supports do not affect the calculated vibration frequencies.

4.2.2 Analysis Methods for Nonlinear Piping Systems

The main objective of the MS Test Program is to study the dynamic behavior of conventional as well as energy absorbing (E.A.) pipe supports. The test results described in the foregoing Chapter 3 indicate a complex nonlinear characteristic of conventional mechanical snubbers, whereas the hysteretic behavior of the E.A. supports is considered to be more predictable. According to the studies for the HDR-VKL piping system (Ref. 2) in which a full-scale piping system with snubbers and E.A. supports was subjected to high-level vibrations and the test results were compared with linear as well as nonlinear analyses, a relatively poor correlation was observed between the measured responses and the analysis predictions particularly for support forces and acceleration responses. The high-frequency components caused by gaps in snubbers and other support structures were considered to be a main cause of the analysis errors.

In the past a large number of studies were performed to simulate the nonlinear dynamic behavior of various pipe supports. The nonlinear time history (NTH) analysis method was mainly used to study the effects of gap nonlinearities (e.g., Refs. 3 and 4). An equivalent linearization approach method (ELA) was also applied to account for the gap nonlinearity in seismic stop piping supports (Ref. 5). In that analysis formulation, the equivalent stiffness for the gap nonlinearity was evaluated using Caughey's Method (Ref. 6), and the responses were obtained by the iterative response spectral method.

Similar ELA analyses were applied to snubber supports (e.g., Ref. 7), as well as to various E.A. supports (e.g., Refs. 8 and 9). In most of the past studies on the application of the ELA to nonlinear piping systems, the equivalent stiffnesses and damping were evaluated as a function of pipe support deflections, and an iterative response spectral method was used to obtain the responses of piping systems. Comparisons to NTH analysis generally indicate that the ELA provides a conservative result (e.g., Ref. 8).

4.3 Analysis Methods

4.3.1 Modeling of Pipes

In the simulation analyses described in Chapter 5, straight and circular curved beam elements are used to model the piping. In to the ISSAC code (Ref. 10), the basic flexibility matrix (6x6) of the circular curved beam is formulated as follows.

$$F_{11} = \frac{R}{EA}\left(\phi + \frac{1}{2}\sin 2\phi\right) + \frac{RK_Z}{GA}\left(\phi - \frac{1}{2}\sin 2\phi\right) + \frac{R^3}{\mu EI_Z}(\phi + 2\cdot\phi\cdot\cos^2\phi - 1.5\sin 2\phi)$$

$$f_{12} = f_{21} = \frac{R^3}{\mu EI_Z}(2\sin^2\phi - \phi\cdot\sin 2\phi)$$

$$f_{16} = f_{61} = \frac{R^3}{\mu EI_Z}(2\phi\cdot\cos\phi - 2\sin\phi)$$

$$f_{22} = \frac{R}{EA}\left(\phi - \frac{1}{2}\sin 2\phi\right) + \frac{RK_Z}{GA}\left(\phi + \frac{1}{2}\sin 2\phi\right) + \frac{R^3}{\mu EI_Z}\left(\phi + 2\phi\sin^2\phi - \frac{1}{2}\sin 2\phi\right)$$

$$f_{26} = f_{62} = -\frac{R^2}{\mu EI_Z}(2\phi \cdot \sin\phi)$$

$$f_{33} = \frac{K_y \cdot R}{GA}\cdot(2\phi) + \frac{R^3}{EI_y}\left(\phi - \frac{1}{4}\sin 4\phi\right) + \frac{R^3}{GK_t}\left(3\phi - 2\sin 2\phi + \frac{1}{4}\sin 4\phi\right)$$

$$f_{66} = \frac{R}{\mu EI_Z}(2\phi) \qquad (4.1)$$

$$f_{34} = f_{43} = -\frac{R^2}{EI_y}\left(\phi\cos\phi - \frac{1}{2}\cos\phi\cdot\sin 2\phi\right) + \frac{R^2}{GK_t}\left\{2\sin\phi - \cos\phi\left(\phi + \frac{1}{2}\sin 2\phi\right)\right\}$$

$$f_{35} = f_{53} = \frac{R^2}{EI_y}\left(\phi\sin\phi + \frac{1}{2}\sin\phi\cdot\sin 2\phi\right) + \frac{R^2}{GK_t}\left(\phi\sin\phi - \frac{1}{2}\sin\phi\sin 2\phi\right)$$

$$f_{44} = \frac{R}{EI_y}\left(\phi - \frac{1}{2}\sin 2\phi\right) + \frac{R}{GK_t}\left(\phi + \frac{1}{2}\sin 2\phi\right)$$

$$f_{55} = \frac{R}{EI_y}\left(\phi + \frac{1}{2}\sin 2\phi\right) + \frac{R}{GK_t}\left(\phi - \frac{1}{2}\sin 2\phi\right)$$

where:

R = elbow radius
ϕ = half of elbow angle;
E = modulus of elasticity;
A = cross-sectional area;
I_Z = moment of inertia for in-plane bending;
I_y = moment of inertia for out-of-plane bending;

K_z = shape factor for in-plane shear;
K_y = shape factor for out-of-plane shear;
μ = flexibility factor;
G = shear modulus;
K_t = St. Venant torsion constant.

The above flexibility factor, μ, as well as the stress intensification factor, i, are evaluated based on the ASME codes (Ref. 11).

For elbows. . . . .

$$\mu = \frac{1.65}{h}, \qquad i = \frac{0.9}{h^{2/3}}, \qquad h = \frac{tR}{r^2} \tag{4.2}$$

where, t = pipe thickness,
R = elbow radius at the center of pipe section
r = radius of pipe at the middle of thickness

For tee joint. . . . .

$$\mu = 1.0, \qquad i = \frac{0.9}{h^{2/3}}, \qquad h = \frac{4.4t}{r} \tag{4.3}$$

where, t = pipe thickness of the main line
r = pipe radius of main line at the middle of thickness

4.3.2 Modeling of Pipe Supports

The gap nonlinearity of mechanical snubbers is illustrated in Figure L.12. The nonlinear model used in the ISSAC code is shown in Figure 4.1, which is a non-hysteretic bilinear model. The initial stiffness factor, α, is assumed to be zero in the analyses. The parameters to define the nonlinearity, Δ and K, are listed in Tables L.3 and L.4. In the analyses, a different gap value, Δ, and a different stiffness, K, are used between the compression side and tension side.

To model the E.A. supports, the so-called Bouc-Wen model was used (Ref. 12). According to Wen (1980), the nonlinear restoring force, q, is expressed as,

$$q = \alpha k u + (1 - \alpha) kZ \tag{4.4}$$

$$\dot{Z} = \dot{u} - \beta \cdot \dot{u}|Z|^n - \gamma\ |\dot{u}|Z|Z|^{n-1} \tag{4.5}$$

in which, u and $\dot{u}$ = the relative displacement and velocity; K = the initial stiffness; α = the postyield stiffness ratio; and Z = hysteretic component with the unit of displacement; and n= a parameter to characterize hysteresis loops.

The above hysteretic parameters, K, α, β, γ and n, were determined by curve-fitting the available component test data

for the EAB supports and the MS test results for the LED supports. The results are shown in Figures 4.2 through 4.5. It seems that a better curve-fit is observed for the EAB supports than the LED supports.

4.3.3 Nonlinear Time History Analysis

In the ISSAC code (Ref. 10), the equations of motion for nonlinear time history analyses are expressed in the following incremental form:

$$\begin{bmatrix} m_1 & o \\ o & m_2 \end{bmatrix} \begin{Bmatrix} \ddot{u}_1 \\ \ddot{u}_2 \end{Bmatrix} + \begin{bmatrix} c_1 & o \\ o & c_2 \end{bmatrix} \begin{Bmatrix} \dot{u} \\ \dot{u}_2 \end{Bmatrix} + \{R\} + \begin{bmatrix} k_1 & k_2 \\ k_2^T & k_3 \end{bmatrix} \begin{Bmatrix} du_1 \\ du_2 \end{Bmatrix} = \begin{Bmatrix} o \\ P \end{Bmatrix} \tag{4.6}$$

in which, u_1 = free (non-constrained) absolute displacements; u_2 = forced (constrained) absolute displacements; R= restoring forces; and P = reaction forces. The conventional Newmark's β-method is used to solve the above equations by assuming the following Rayleigh damping;

$$[c] = \alpha\,[M] + \beta[K] \tag{4.7}$$

According to the above formulation, any number of independent support motions can be applied directly to the analysis model.

4.3.4 Equivalent Linearization Approach

The detailed analysis formulations for the ELA are given in Appendix K of this report. The analysis methods are briefly summarized in this section. Two types of ELA are used in this study, i.e.,

ELA/RS. . . . . Response spectral approach using SRSS approximation.

ELA/LRV. . . . .Linear random vibration approach using power density spectra for input.

ELA/RS Method. . .According to the classical study by Caughey (1963), the equivalent stiffness, k_{eq}, of a hysteretic system is obtained based on the slowly-varying assumption on the nonlinear oscillation, as

$$K_{eq} = \frac{1}{\pi U} \int_0^{2\pi} F(u) \cdot \cos\theta \; d\theta, \quad u = U \cdot \cos\theta \tag{4.8}$$

in which, U is the peak displacement amplitude; and F(u) is the nonlinear restoring force for the largest hysteresis loop as a function of displacement, u.

In the gap nonlinearity shown in Figure 4.1, the equivalent stiffness is expressed as,

$$k_{eq} = \alpha K + \frac{2K}{\pi}(1-\alpha)\left\{\cos^{-1}\left(\frac{1}{\mu}\right) - \left(\frac{1}{\mu}\right)\sqrt{1-\frac{1}{\mu^2}}\right\} \tag{4.9}$$

For the equivalent modal damping, h_{eq}, the formulation proposed by Tansirikongkol and Pecknold (Ref.14) is used in this study.

$$h_{eq,r} = h_{o,r}\frac{\omega_r}{\omega_{eq,r}} + \frac{\sum_i \epsilon_{ir}^2 \cdot S_i}{2M_r \cdot \omega_{eq,r}^2} \tag{4.10}$$

$h_{o,r}$ = elastic modal damping
ω_r = frequency for r-th mode
$\omega_{eq,r}$ = equivalent frequency
M_r = modal mass
ϵ_{ir} = modal strain of component-I
S_i = normalized hysteresis area of component-I

$$= \frac{A}{\pi U^2} \cdot \frac{4}{\pi} K_e (1-\alpha)\left(\frac{\mu-1}{\mu^2}\right) \quad \textit{.....for binlinear system}$$

The SRSS approximation is used in the iterative solution scheme, in which the above k_{eq} and h_{eq} are updated, followed by a new eigenvalue analysis of the equivalent linear system.

ELA/LRV Method

This method is based on linear random vibration theory and a modified Kryloff-Bogoliubov equivalent linearization approach. A displacement component, u_i, in a piping system is expressed as,

$$u_i = \sum_r \phi_{ir} q_r + \sum_m \phi_{im} X_m \tag{4.11}$$

in which, q_r is the r-th normal mode response; ϕ_{ir} is the eigenvector of the fixed-based system; X_m is the differential displacement at the m-th fixed degree of freedom; and ϕ_{im} is the displacement mode due to the m-th differential displacement. Assuming stationality of responses, the covariance for a pair of displacements, u_i and u_j, are obtained as,

$$R_{u_i u_j}(o) = \sum_r \sum_s \phi_{ir}\phi_{is}R_{rs} + \sum_m \sum_n \varphi_{im}\varphi_{jm} \cdot \bar{R}_{mn} \tag{4.12}$$

in which, R_{rs} is the covariance for the r-th and s-th normal mode responses; and $\bar{R}_{mn}$ is the covariance for the m-th and n-th differential displacements.

$$R_{rs} = \sum_{k} \sum_{l} C_{kl} \cdot \beta_{rk} \beta_{sl} \int_{-\infty}^{\infty} H_r(\omega) \cdot H_s(\omega) \sqrt{S_k(\omega) \cdot S_l(\omega)} d\omega \tag{4.13}$$

$$\bar{R}_{mn} = C_{mn} \int_{-\infty}^{\infty} H_r(\omega) \cdot H_s(\omega) \sqrt{S_k(\omega) \cdot S_l(\omega)}\, d\omega \tag{4.14}$$

in which, C_{kl} is the correlation coefficient for the k-th and l-th excitations; β_{rk} is the r-th participation factor for the k-th excitation; $H_r(\omega)$ is the transfer function for the r-th mode; and $S_k(\omega)$ is the k-th PSD function.

The equivalent component stiffness k_{eq}, and modal damping, h_{eq}, can be defined using the peak distribution functions, $p_1(u, \sigma_\epsilon)$ and $p_2(u, \sigma_\epsilon)$, as,

$$\begin{aligned} K_{eq} &= \int_0^{\infty} K_{eq}(u) \cdot p_1(u,\sigma_\epsilon)\, du \\ h_{eq} &= \int_0^{\infty} h_{eq}(u) \cdot p_2(u,\sigma_\epsilon)\, du \end{aligned} \tag{4.15}$$

in which, σ_ϵ is the standard deviation of the strain response. The details of the above peak distribution functions can be found in Appendix K. The foregoing eqs. (4.8) and (4.10) can be used for the peak response dependent stiffness and damping, K_{eq} (u) and h_{eq} (u).

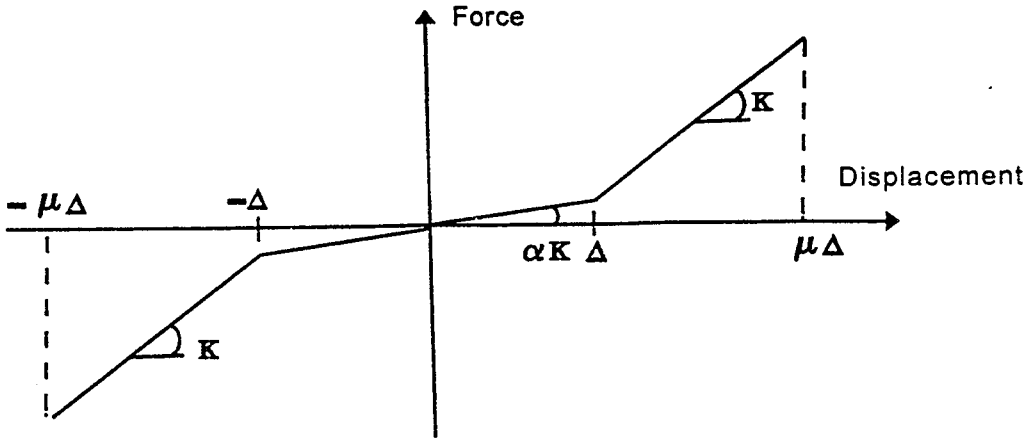

Figure 4.1 Modeling of Gap Nonlinearity for Mechanical Snubbers

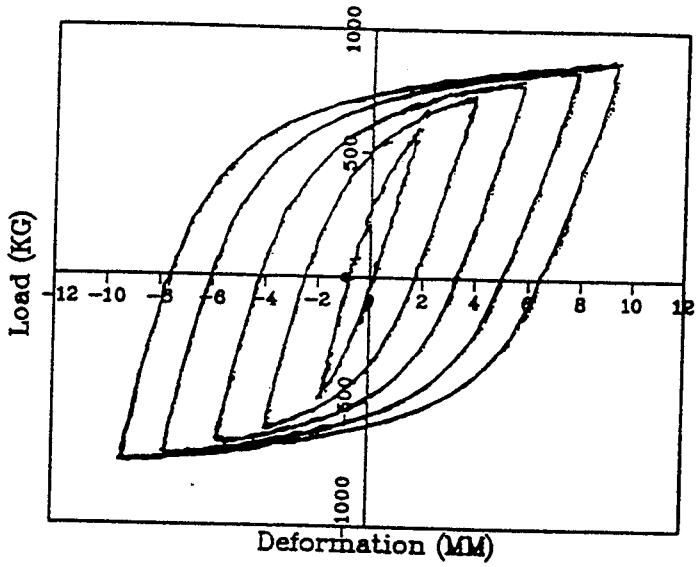

(a) Component Test Result

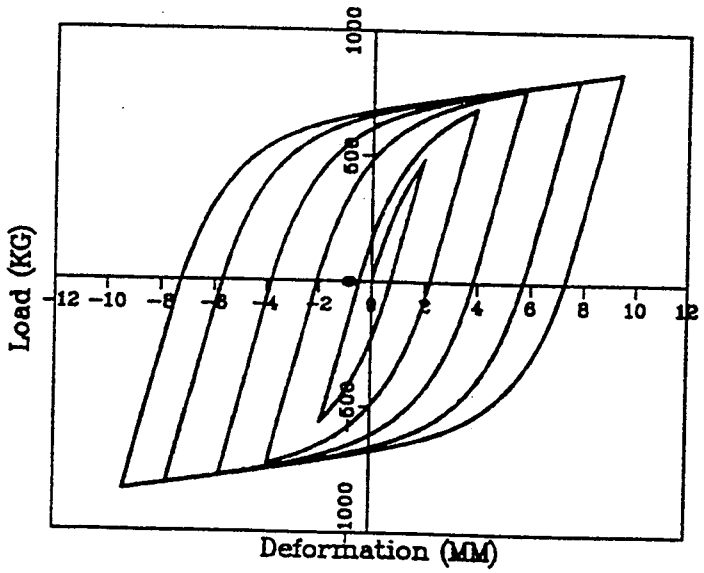

(b) Bouc-Wen Model

Parameters: k_e **=400 kg/mm,** α **= 0.04,** $\beta = \gamma$ **= 0.28, n = 1.**

Figure 4.2 Modeling of 0.5 Ton EAB Support

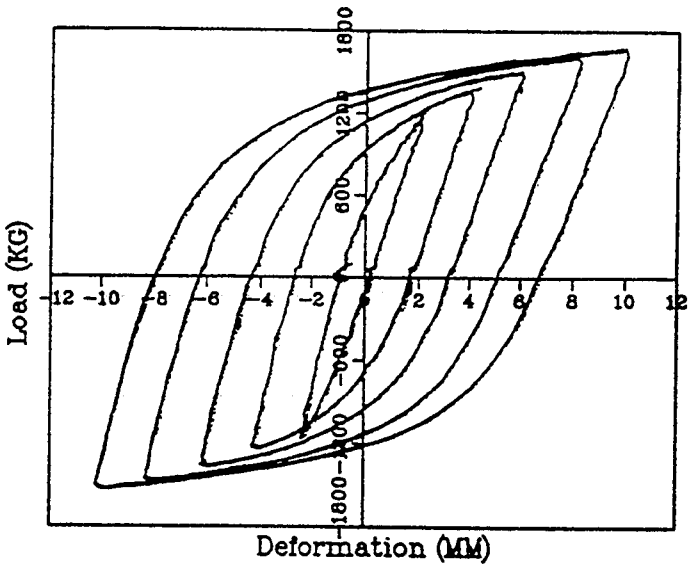

(a) Component Test Result

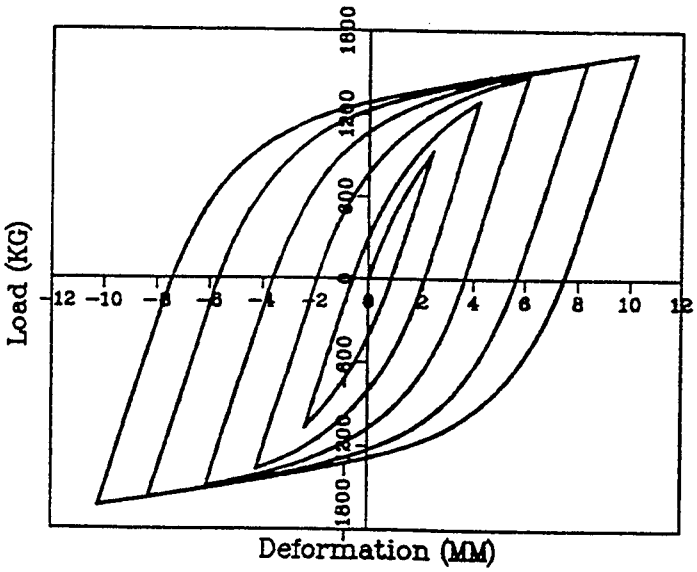

(b) Bouc-Wen Model

Parameters: $k_e = 600$ kg/mm, $\alpha = 0.05$, $\beta = \gamma = 0.214$, $n = 1$.

Figure 4.3 Modeling of 1.0 Ton EAB Support

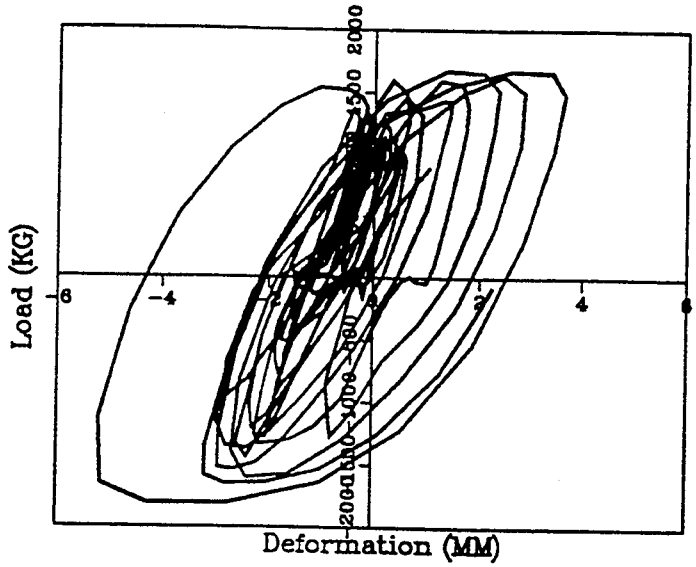

(a) Test Result from S_2-A Run

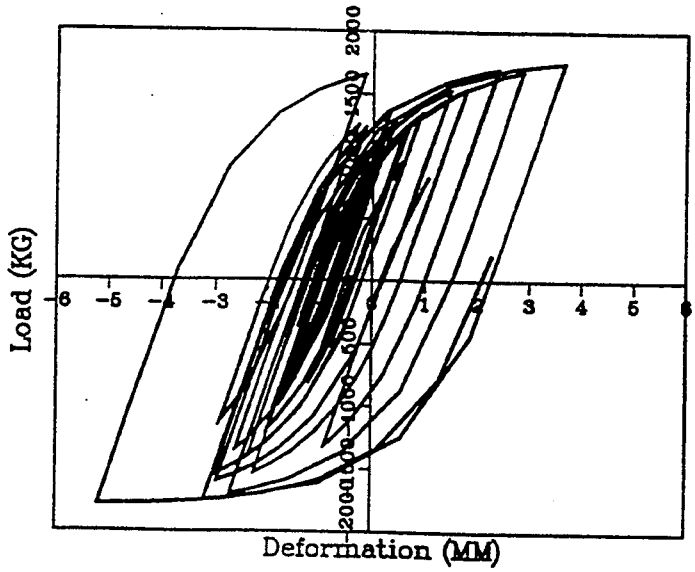

(b) Bouc-Wen Model

Parameters: $k_e = 1250$ kg/mm, $\alpha = 0$, $\beta = \gamma = 0.347$, $n = 1$.

Figure 4.4 Modeling of LED-2 Support

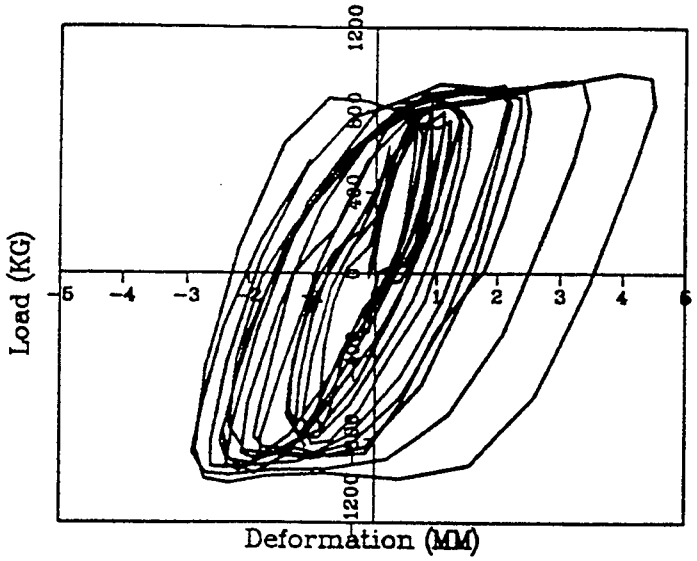

(a) Test Result from S_2-A Run

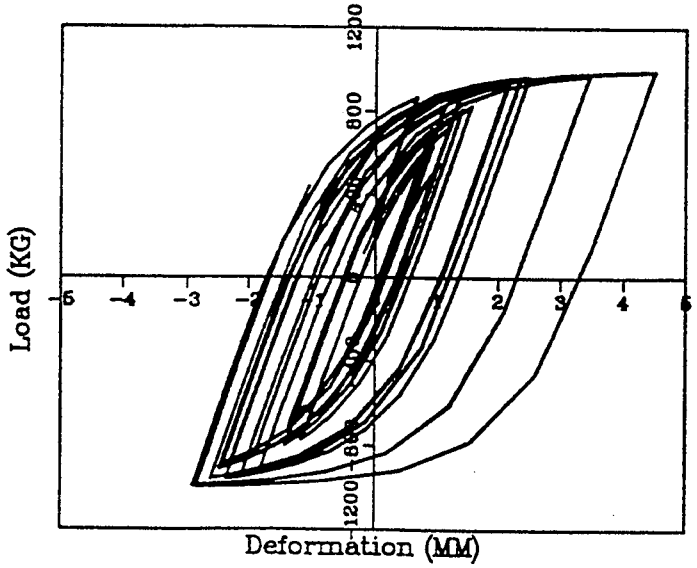

(b) Bouc-Wen Model

Parameters: $k_e = 850$ kg/mm, $\alpha = 0$, $\beta = \gamma = 0.425$, $n = 1$.

Figure 4.5 Modeling of LED-3 Support

5 CORRELATION ANALYSES

5.1 Summary of Analyses

A total of 17 test cases were selected for this correlation study as listed in Table 5.1. For the M-line with conventional supports, two test runs, VC-6 and MC-6, were selected in which the SG-model shown in Figure L.7 was used for the independent actuator motion. In addition, one test run, DC-3, was selected from the multiple excitation test series in which the 2 DOF model shown in Figure L.8 was used to reproduce the PCCV waves for the independent actuator motions.

For the F-line with conventional supports, two test runs, VC-3 and MC-3, were selected. In these tests, the S2(F) waves (BWR waves) were used with amplitude scale factors of 1.0 and 1.3, respectively.

A larger number of test runs were selected for the energy absorbing support case. For the M-line with actuator, three test runs using S2(A) waves, DE1-1, DE1-3 and DE1-9, were selected in which the amplitude scale factor was the only parameter varied during the tests. Among the test series for the M-line with the SG-joint fixed to the support structure (without actuator), three test runs, DE2-13, DE2-15, and ME-9, were selected as listed in Table 5.1. All the test runs used the S2(A) waves with amplitude scale factors of ⅓, 1.0 and 2.5. In addition, a Tokachi-Oki wave test, ZT-2, was analyzed. This test run produced the highest responses of the M-line piping system.

For the F-line with EAB supports, four (4) S2(A) wave tests, DE1-1', DE1-3', DE1-9 and ME-9, were selected in which the amplitude scale factors were ⅓, 1.0, 1.3 and 2.5. In addition, the most severe test run, ZT-1, was also analyzed as listed in Table 5.1.

Table 5.2 summarizes the types of analyses performed for the correlation studies. Three (3) types of analyses, i.e., nonlinear time history analysis (NTH), the equivalent linearization approach (ELA) based on the SRSS modal superposition (ELA/RS) and the ELA based on the linear random vibration theory (ELA/LRV) were performed. Since the ELA/RS approach cannot account for the multiple excitation motions, only the NTH and ELA/LRV were used for the M-line when the independent actuator was operated.

The BNL's in-house code, ISSAC, was mainly used in this correlation study. The commercially available ANSYS code was also used for the M-line with LED supports to cross-check the adequacy of the analysis methods. Since the gap nonlinearity of snubbers (see Figure 4.1) cannot be properly modeled with the ANSYS code, for the nonlinear dynamic analyses, the ANSYS analysis was limited to the M-line with LED supports (without actuator) case. During the planning stage of the MS Test Program, the commercial code, ABAQUS, was also used to confirm the pre-test analyses by the ISSAC code. The calculated results are summarized at the end of this chapter.

5.2 Analysis Models

Figures 5.1 through 5.4 show the analysis models for the ISSAC code. The types of elements used for the models are listed in Table 5.3. Straight and circular curved elastic beam elements are used to model the piping. As described in previous chapters, the Bouc-Wen model is used to characterize the hysteretic behavior of the E.A. supports while the gap nonlinearity, shown in Fig. 4.1, is used for snubbers.

5.3 Input Table Motions

For all the analysis cases described in this chapter, the table motions recorded during the tests were used as the input to the analysis models. The acceleration records of XOXB, YD2-E, and ZOXB were used to represent the table motions in the X, Y and Z-directions, respectively. Figures 5.5 through 5.8 show the recorded accelerograms. It should be noted that the input motion, S2(M), is the same as the A-wave, S2(A).

5.4 M-Line With Conventional Supports

As shown in Figure 5.5, table motions XOXB, and ZOXB were used as the basic input motions in the X and Z-directions, respectively. The independent actuator motion is applied at the SG-joint, which is Node-10 in Figure 5.1 (see Figure 2.3 also). The recorded accelerogram AA1-X corresponds to the independent support motion as shown in Figure 5.9-(a) and Figure 5.10(a) from 1.0 S2(M) test run. Due to the low-frequency components introduced by the low-pass filter used in Tadotsu's data acquisition system, a significant drift (or displacement) was observed in the recorded accelerogram, AA1-X. Since the amount of the drift was found to be so large (more than 10 meters), the application of a conventional baseline correction scheme was considered to be inappropriate since it would distort the original recorded motions. To alleviate this problem, the independent actuator motion, AA1-X, was newly generated using the recorded relative actuator displacement, AD1-X. The following numerical procedure was used for this purpose:

1. Numerically differentiate the recorded relative displacement, AD1-X, twice to obtain the relative acceleration of the actuator motion;
2. Eliminate the numerical errors in the calculated acceleration, which were evaluated by integrating twice to reproduce the relative displacement, and then compare with the original displacement record. An iterative procedure was used to minimize the numerical errors caused by the numerical differentiations;
3. Baseline correct the calculated relative acceleration;
4. Add the relative acceleration of the actuator motion to the base table motion, XOXB, to obtain the absolute acceleration for AA1-X.

The generated actuator motion is shown in Figure 5.9-(b). In comparison with the recorded motion, the errors in the spectral value (shown in Figure 5.10) are considered to be small.

For the simulation study, S2(M) test runs and the Multiple Excitation test run were selected as listed in the foregoing Table 5.1. Two types of analyses, i.e., nonlinear time history (NTH) and equivalent linearization approach based on linear random vibration theory (ELA/LRV), were used. In the ELA/LRV analyses, a viscous damping value of 5.0% was assumed for all the modes, and the cutoff frequency was 100Hz. The correlation between input motions was considered to exist only between the independent actuator motion (AA1-X) and the X-direction table motion (XOXB). All other motions were considered to be uncorrelated (statistically independent). In the NTH analyses, internal damping was considered in the form of Rayleigh damping. The assumed damping value was 5.0% at 20Hz. Table 5.4 compares the calculated vibration frequencies from ELA/LRV with those measured during sine sweep tests. In general, vibration frequencies tend to increase as the excitation level increases due to the hard spring nature of the snubbers. More detailed comparisons between measured and calculated responses are described below for the three test runs.

1.0 S2(M) Test run. . . . .The calculated and measured peak response values are tabulated in Table 5.5. It is observed that some of the calculated acceleration values in Table 5.5 (a) and support forces in Table 5.5 (c) overestimate the measured peak values. The low-pass filter, that was used to process the measured data, seems to affect the recorded

peak values significantly. To simulate the effects of filtering on the recorded responses, the analysis results were filtered in the time domain using the averaging method. A cutoff frequency of the low-pass filter was set at 200Hz. The filtered analysis results are tabulated in Table 5.5 (a) and (c). Displacements and pipe stresses were not filtered since they were much less affected by a low-pass filter. The effect of filtering on acceleration responses is illustrated in Figure 5.13. At the measuring location, MA3-X, the low-pass filter reduced the peak value by 62% (11.73g to 4.43g), and the calculated accelerogram correlates better with the measured one. Figures 5.14 through 5.16 illustrate the effects of filtering on the hysteretic behavior of mechanical snubbers. It can be observed that the filtering introduces an artificial hysteretic damping in the calculated snubber responses, which somewhat resembles the recorded hysteresis in Figures 5.15 and 5.16 for MR5 and MR6. The unique nonlinearity found in MR3 (Figure 5.14), which was caused primarily by the lateral movements of snubbers, was not reproduced in the filtered analysis results.

Figures 5.17 through 5.21 show comparisons of peak response values. It can be observed that after filtering the NTH analysis results correlate well with the measured responses. The results from the ELA/LRV generally follow those of the NTH for all responses.

1.5 S2(M) Test Run. . . . .All peak response values are tabulated in Table 5.6, and those of the X-direction accelerations and support forces are plotted in figures 5.22 and 5.23. It can be observed that the tendencies of the results are very similar to those of the foregoing 1.0 S2(M) test case.

Multiple Excitation Run. . . . .All peak response values are tabulated in Table 5.7, and those of the X-direction accelerations and support forces are plotted in Figures 5.24 and 5.25. In comparison with the foregoing 1.0 S2(M) test run, the acceleration responses are much lower but the support forces are somewhat higher. This is due to the fact that the differential displacement of the independent actuator motion of 3.54 mm (see AD1-X in Table 5.7 (b)) is larger than 2.46 mm in the 1.0 S2(M) test case (see AD1-X in Table 5.5 (b)).

5.5 F-line With Conventional Supports

Two test runs, 1.0 S2(F) and 1.3 S2(F), were used for the correlation studies of the F-line with conventional supports. The input table motions are shown in Figure 5.6 for the 1.0 S2(F) test run. The table motions for the 1.3 S2(F) case are 30% higher than those shown in Figure 5.6. A sharp spectral peak at 14.5Hz in the X-direction motion (see Figure 5.6 (a)) dominates the table motions in these test runs. The same damping assumption used for the M-line was used in these analyses. In the NTH analyses, Rayleigh damping was assumed to be 5% at 16.4Hz. Two types of equivalent linearization analyses, i.e., ELA/RS and ELA/LRV, were performed for these cases. A cutoff frequency of 80Hz was assumed in both the ELA methods. Table 5.8 compares the calculated vibration frequencies from the equivalent linearization analyses with those measured during sine sweep tests. It should be noted that due to the very steep slope near the spectral peak at 14.5Hz, a slight difference in the calculated frequency values tends to affect the responses significantly.

1.0 S2(F) Test Run. . . . .All response values are tabulated in Table 5.9. These values are also plotted in Figures 5.30 through 5.34. The same low-pass filter was applied to the NTH analysis results (for accelerations and support forces). It can be observed that most of the recorded peak values fall between the non-filtered original analysis results (NTH-A in Table 5.9) and the filtered analysis (NTH-B in Table 5.9) results. An additional NTH analysis was performed for this test run (NTH-C in Table 5.9) to study the effects of changing the snubber stiffnesses. All the snubber stiffnesses were reduced by 50% in this additional analysis, and the results were compared with the measured and original analysis results. No significant improvement was made by changing the snubber stiffnesses. Figures 5.26 and 5.27 show comparisons of the acceleration time histories. A better correlation can be found in the filtered analysis results. Figures 5.28 and 5.29 show examples of the hysteretic responses of snubbers. In general, the filtered analysis results show better correlation. However, a highly irregular nonlinearity observed in some of the snubber responses, e.g.,

snubber FR3 in Figure 5.28, was not reproduced in the analyses. Figures 5.30 through 5.32 show plots of the peak acceleration responses tabulated in Table 5.9 (a). Although it is difficult to draw a clear conclusion, the observed analysis errors are greater than that of the foregoing analyses for the M-line, and the ELA/LRV results correlate better than those by ELA/RS. The peak responses of support forces are shown in Figure 5.33. The analysis results, particularly the filtered NTH results, correlate well with the measured peak values. Again, the ELA/LRV results correlate with the NTH results better than the ELA/RS. The correlation of pipe stresses are tabulated in Table 5.9 (d) and plotted in Figure 5.34. The analyses tend to over-predict the measured peak stresses, particularly where stress intensification factors are used to multiply the stress values from the analyses. It seems that the stress intensification factors listed in Table 5.9 (d) are in general conservative. A similar trend was observed in the foregoing M-line analyses (see Figure 5.21).

1.3 S2(F) Test Run. . . . .The peak response values are tabulated in Table 5.10, and those of the X-direction accelerations and support forces are plotted in Figures 5.35 and 5.36. The analysis correlation for this higher-excitation run is better than that of the foregoing 1.0 S2(F) test. Again, the ELA/LRV results correlate better than the ELA/RS. It seems the effects of gaps in mechanical snubbers have a larger impact on responses in lower-amplitude test runs.

5.6 M-line With LED Supports and With Independent Actuator Motion

As illustrated in Figure 5.3, the snubber supports were replaced with three (3) Lead Extrusion Dampers (LED) for this test series. The arrangement of the independent actuator remained the same. In this correlation study, test runs using S2(A) waves were analyzed. The S2(A) waves are identical with the foregoing S2(M) waves shown in Figure 5.5. Three (3) test runs, i.e., ⅓ S2(A), 1.0 S2(A) and 1.3 S2(A), were selected. The only parameter varied during these test runs was the excitation amplification factor, i.e., ⅓, 1.0 and 1.3.

Two types of analyses, i.e., NTH and ELA/LRV, were performed for this test series. In the ELA/LRV analyses, a viscous damping value of 2.5% was assumed for all the modes, and the cutoff frequency was 100Hz. The assumption regarding the correlation between the table motions is the same as in Section 5.4, i.e., only the correlation between the independent actuator motion (AA1-X) and the X-direction table motion (XOXB) was considered. In the NTH analyses, the Rayleigh damping was assumed to be 2.5% at 10Hz (first linear mode).

1.0 S2(A) Test Run. . . . .The peak response values are tabulated in Table 5.11, and plotted in Figures 5.37 through 5.40. Some comparisons of acceleration time histories and the hysteretic responses of the LED supports are shown in Figures 5.41 and 5.42. Overall, the NTH analysis results correlate well with the measured responses except for the acceleration responses near the SG-joint (e.g., MA1) and the response of LED-3 (see Figure 5.42 (c)). The former problem may be caused, at least partially, by the complex responses of the support frame -- shake table system, as well as the low-pass filter used during the MS test runs as described before. In this analysis, a numerical filter was not applied to the calculated responses. The latter problem was caused by the complex nonlinear behavior of a pin-support at MR8 (see Figure A.14 in Appendix-A for details of the pin-support). In the analysis, MR8 is modeled using a linear spring element.

⅓ S2(A) Test Run. . . . .For this test run, the peak accelerations in the X-direction are plotted in Figure 5.43 and the hysteretic responses of the LED supports are shown in Figure 5.45. Although the acceleration responses agree well with the test results, the displacements of the LED supports are underestimated. At a lower response range, the observed hysteresis loops of the LED supports exhibit a pinching characteristic caused by a mechanical gap (see Figure 5.45). As the response level increases, however, this pinching effects become negligible.

1.3 S2(A) Test Run. . . . .The peak acceleration responses are plotted in Figure 5.44, and the hysteretic responses of the LED supports are shown in Figure 5.46. The trends are similar to the foregoing 1.0 S2(A) case, i.e., some discrepancies of acceleration responses near the SG-joint, and the response of LED-3 is underestimated.

Overall Correlation. . . . .Figure 5.47 summarizes the comparison of the displacement responses of the LED supports. The NTH analysis results correlate well with the measured responses for LED-1 and LED-2, but the responses of LED-3 are consistently underestimated. Tables 5.12 and 5.13 list the calculated equivalent vibration frequencies and the equivalent damping values obtained from the ELA/LRV analyses. Figures 5.48 through 5.51 show the calculated transfer functions (ratio of power spectral density functions) of acceleration responses. As the response level increases, most of the lower vibration modes shift to lower frequencies, and the damping values increase significantly.

5.7 M-line With LED Supports and Without Independent Actuator Motion

A series of tests were conducted for the M-line with LED supports and with the SG-joint as fixed condition. Since independent motion was not applied at the SG-joint, the piping system was subjected to uniform motions. The primary objective of this test series was to introduce large plastic responses in the LED supports as part of the margin tests. For this test series, in addition to the NTH analysis, two types of equivalent linearization analyses, i.e., ELA/LRV and ELA/RS, were performed. The same analysis assumptions/conditions as described in Section 5.6 were used for these cases, except for the damping value assumption which is described below.

2.5 S2(A) Test Run. . . . .The peak responses are tabulated in Table 5.14, and plotted in Figures 5.52 through 5.56. Initially, a damping value of 2.5% was assumed in the NTH analysis, which is marked "NTH-A" in Table 5.14. Since most of the analysis results for this case underestimated the measured responses, the damping value was reduced to 1% of critical, which is marked "NTH-B" in Table 5.14. In the equivalent linearization analyses, a damping value of 1.0% was assumed for all modes. The comparisons shown in Figures 5.52 through 5.56 indicates that the NTH analysis results for a lower damping value agree with the measured responses. It seems that the independent actuator attached at the SG-joint may have contributed to the damping of the M-line. This may explain the appropriateness of lower damping in this test series as the actuator was not operated during the tests. The comparisons of acceleration time histories in Figure 5.57 and the hysteretic responses of the LED supports in Figure 5.58 suggest that the NTH analysis with 1% damping generally captured the nonlinear response. A significant discrepancy between the test and analyses can be found in the vertical accelerations near the anchor, i.e., MA8 and MA10 in Figure 5.54. Large vertical accelerations found in the measured responses may have been caused by an additional deflection of the anchor; whereas in the analysis, the anchor was assumed to be fixed.

Tokachi-Oki Test Run. . . . .The input table motions for this test run can be found in Figure 5.7. A sharp spectral peak at around 5Hz dominates the table motion in the X-direction as shown in Figure 5.7. This Table motion was prepared to produce a significant plastic deformation in the LED supports, and this test run was the most severe on the M-line. The peak responses are tabulated in Table 5.15 and plotted in Figures 5.59 through 5.63. It was found that the NTH analysis, which is marked "NTH-A" in Table 5.15, (1% damping assumption) underestimates the recorded responses, particularly those of the LED supports [see Table 5.15 (b)]. As the piping system was subjected to a large number of cyclic loading reversals, degradation of the support systems may have occurred, and affected the responses of this test run, which was conducted at the very end of the MS Test Program. To account for the effects of possible degradation, the initial stiffnesses of LED-2 and LED-3 were reduced by 20%, and the stiffnesses of the pin-support, MR8, by 50%. The stiffness of LED-1, which was not subjected to large deformations, was not changed in this analysis marked "NTH-B" in Table 5.15. The comparisons of acceleration time histories in Figure 5.64, and the hysteretic responses of the LED supports in Figure 5.65 indicate the NTH-B analysis results generally correlate well with the recorded responses. The ELA/LRV method produced similar responses as the NTH analysis, but the ELA/RS

analysis tends to overshoot the measured responses. It seems that this test, in which significant inelastic responses were developed, is beyond the applicable range of the equivalent linearization approaches.

⅓ S2(A) Test Run. . . . .The comparisons of the hysteretic responses of the LED supports are shown in Figure 5.66 for this low-level test run. The NTH analysis correlates well with the measured responses (see Figure 5.45 for the case in which the independent actuator was activated).

1.0 S2(A) Test Run. . . . .The comparisons of the hysteretic responses of the LED supports are shown in Figure 5.67. The NTH analysis seems to correlate well with the measured responses.

Overall Correlation. . . . .The comparison of analysis versus test results is summarized in Figure 5.68 for the S2(A) test series. Most of the response values from NTH and ELA analyses seem to correlate well with the measured responses, except for pipe stress values at MS1 and MS5. The ELA/LRV analysis results seem to correlate with the NTH analysis for most response quantities. The calculated equivalent vibration frequencies and the equivalent damping values are listed in Tables 5.16 and 5.17. It seems the ELA/RS method tends to underpredict the frequency drift in comparison with the ELA/LRV method, particularly for higher excitation runs.

5.8 F-line With EAB Supports

The analysis model is illustrated in Figure 5.4. It should be noted that both EAB supports and mechanical snubbers were attached to the piping during this test series. Three types of analyses were performed for this test series, i.e., NTH, ELA/RS and ELA/LRV. For the equivalent linearization analyses, a linear damping value of 1.0% was assumed for all the modes. The cutoff frequency was assumed to be 80Hz.

S2(A) Test Run. . . . .The peak response values are tabulated in Table 5.18 and plotted in Figures 5.69 through 5.73. The NTH analysis results correlate well with the measured peak values, except for pipe stresses which are overestimated and the response of EAB-3 which is underestimated. Between the two ELA analyses, the ELA/LRV again gives better correlations than the ELA/RS. Acceleration time histories are shown in Figure 5.74, and the hysteretic responses of the EAB supports and mechanical snubbers are plotted in Figures 5.75 and 5.76. As indicated in Figure 5.76, the responses of the mechanical snubbers exhibited a highly irregular nonlinear behavior, which was not reproduced in the NTH analysis.

2.5 S2(A) Test Run. . . . .The calculated results are given in Table 5.19 and Figures 5.77 through 5.84. Tendencies similar to the above case can be observed, i.e., the pipe stresses are overestimated and the response of EAB-3 is underestimated. The complex nonlinearity of snubber response, shown in Figure 5.84, is probably the main cause of the discrepancies between the analysis and test results.

1.2 S2(C) Test Run. . . . .For this test run, the time scale of the S2(A) wave was extended by a factor of 1.6. The spectral peak of the X-direction motion, therefore, was shifted to around 9Hz as shown in Figure 5.8 (a). This motion was the most severe on to the F-line, and the test was conducted at the very end of the MS Test Program. The calculated results are given in Table 5.20 and Figures 5.85 through 5.92.

Overall Correlation. . . . .The NTH analysis results for test case 1.3 S2(A) are shown in Figures 5.93 and 5.94. Some results for the test series using the S2(A) wave are summarized in Figure 5.95. The highly irregular nonlinear behavior of the mechanical snubbers (see Figures 5.76, 5.84, 5.92 and 5.94) is believed to be the main cause of the observed discrepancies between calculated and measured responses.

5.9 Additional Analyses Using Commercial Codes

During the planning stage of the MS Test Program, the commercial FEM code, ABAQUS, was used to confirm the prediction analyses by the ISSAC code. However, for this application, this commercial code has a serious limitation since it cannot properly model the gap nonlinearity in snubbers (see Figure L.12). Also, due to a numerical inefficiency, a large displacement drift was artificially introduced in results for the independent support motion (ISM) analysis. Table 5.21 summarizes the peak response values for the M-line with LED supports with independent actuator motions. In these analyses, the independent motion at the SG-joint was considered by including the fictitious SG model as part of the analysis model (see Figure L.10). Bilinear hysteretic models were used in the ABAQUS analyses, whereas the Bouc-Wen model was used in the ISSAC analyses. The direct comparison with the foregoing post-test analyses, given in Table 5.11 for S2(A) wave, could not be made because a significant difference existed between the planned and achieved table motions, particularly for the independent actuator motions. Also, the low-pass filter used to process the MS test data significantly altered the measured peak values. Comparison results in Table 5.21 indicate that the two analyses, although there exist several differences in modeling such as the hysteretic model of LED supports and the formulation of elbow elements, agree well for almost all the responses quantities.

An attempt was made to use the ANSYS code as part of the post-test analysis efforts. Use of the gap element in the ANSYS code for modeling the snubbers was not successful because of numerical problems. Also, the ISM analysis was not possible due to an inefficient numerical algorithm as described above. Therefore, the test runs for the M-line with LED supports and without independent actuator motion were the only cases suitable for the ANSYS code. Again, equivalent bilinear models were used for the LED supports. Table 5.22 summarizes the peak displacement responses, while the hysteretic responses of the LED supports are given in Figure 5.96. Although a very small time increment of 0.0002 sec. was used in the direct time integration analyses, the ANSYS results significantly overshoot the measured responses. A comparison of acceleration responses was not possible since the ANSYS code does not provide the acceleration response results.

5.10 Major Findings From Correlation Studies

In performing the correlation studies, various technical difficulties were encountered including:

- The recorded response results show a highly irregular and complex nonlinearity in the mechanical snubber responses. This phenomenon was caused by various factors, including clearance gaps in both the snubbers and pipe clamps, the effects of orthogonal (to the snubber axes) forces on the snubbers, and rate-dependent characteristics of snubbers.

- In the MS test program, in addition to snubber and E.A. supports, various other pipe supports were used as part of the test models, including guides, pin-supports and anchors. Due to gaps and additional flexibilities, these pipe support structures also exhibited nonlinear characteristics, which were not properly modeled in the analyses.

- A low-pass filter used to process the MS test records affected the high-frequency components of the acceleration and support force responses.

- All of the main (X-direction) table motions were characterized by a sharp spectral peak. Due to the steep slopes near the spectral peak, minor analysis errors, particularly in the equivalent linearization analyses, were magnified.

Because of the above technical difficulties, various analysis discrepancies as described above were encountered. Based on the comparison between the predicted and measured response for a large number of test cases, the following conclusions may be drawn.

- The piping systems, even with conventional snubber supports, are highly complex nonlinear structures. Further efforts are needed to improve analysis accuracy to achieve better correlation with measured results.

- At the beginning of the correlation study, the significance of the linear damping assumption in nonlinear analysis was underestimated. Depending on the type and number of pipe supports, the damping values varied in both the M-line and F-line, a fact which had to be properly accounted for in the nonlinear analysis for better correlation.

- The proposed E.A. supports can be properly modeled using the Bouc-Wen hysteretic model.

- Two types of equivalent linearization analyses were performed, i.e., ELA/RS and ELA/LRV. In almost all the analysis cases, the ELA/LRV analyses consistently gave a better correlation with the NTH analyses than the ELA/RS approach. The major cause of the observed analysis errors in ELA/RS analysis may be the SRSS mode combination procedure used in the analysis formulations.

- The analysis example for the M-line using the Tokachi-Oki wave indicates that a minor change in the stiffness of pipe supports significantly affects the calculated responses.

- Commercially available FEM codes had only a limited applicability in this test program due to the lack of a suitable nonlinear model for snubbers.

- The evaluation of seismic margin of piping systems needs to be performed by a nonlinear analysis because of large analysis errors in conventional linear analysis.

Table 5.1 Test Runs Selected for Correlation Studies

Piping System	Support	Input Motion	Test No. (Serial No.)	Peak Acceleration	
				H (gal)	V (gal)
M-line with Actuator	Conventional	1.0 S_2 (M) 1.5 S_2 (M) 1/3 S_2 (M) *1	VC-6 (94120505) MC-6 (94120905) DC-3 (94120702)	1.52 2.28 0.51	0.35 0.52 0
F-line	Conventional	1.0 S_2 (F) 1.3 S_2 (F)	VC-3 (95011107) MC-3 (95011805)	1.11 1.45	0.19 0.24
M-line with Actuator	LED	1/3 S_2 (A) 1.0 S_2 (A) 1.3 S_2 (A)	DE1-1 (95041903) DE1-3 (95041909) DE1-9 (95042407)	0.51 1.52 1.98	0.12 0.35 0.45
M-line without Actuator	LED	1/3 S_2 (A) 1.0 S_2 (A) 2.5 S_2 (A) Tokachi-oki	DE2-13 (95060506) DE2-15 (95060206) ME-9 (95070502) ZT-2 (95071403)	0.51 1.52 3.80 2.57	0.12 0.35 0.87 0
F-line	EAB	1/3 S_2 (A) 1.0 S_2 (A) 1.3 S_2 (A) 2.5 S_2 (A) 1.2 S_2 (C)	DE1-1' (95051504) DE1-3' (95051202) DE1-9 (95042407) ME-9 (95070502) ZT-1 (95071402)	0.51 1.52 1.98 3.80 1.82	0.12 0.35 0.45 0.87 0.42

Note (*1) : Multiple excitation Test with 2DOF SG model

Table 5.2 Types of Analyses Performed for Correlation Studies

Piping System	Support	Analysis Types		
		Time History (NTH)	Response Spectra (RS)	Linear Random Vibration (LRV
M-line with Actuator	Conventional	0		0
F-line	Conventional	0	0	0
M-line with Actuator	LED	0		0
M-line without Actuator	LED	0	0	0
F-Line	EAB	0	0	0

Table 5.3 List of Elements in Analysis Models

Component	Type of Element	Material Model
Straight Pipes	Straight 3-D beam	Elastic
Elbows	Circular curved beam	Elastic
Snubbers	Uniaxial Spring	Gap (*1)
EAB & LED	Uniaxial Spring	Bouc-Wen Model
Guide	Uniaxial Spring	Elastic

Note (*1): See Figure 4.1

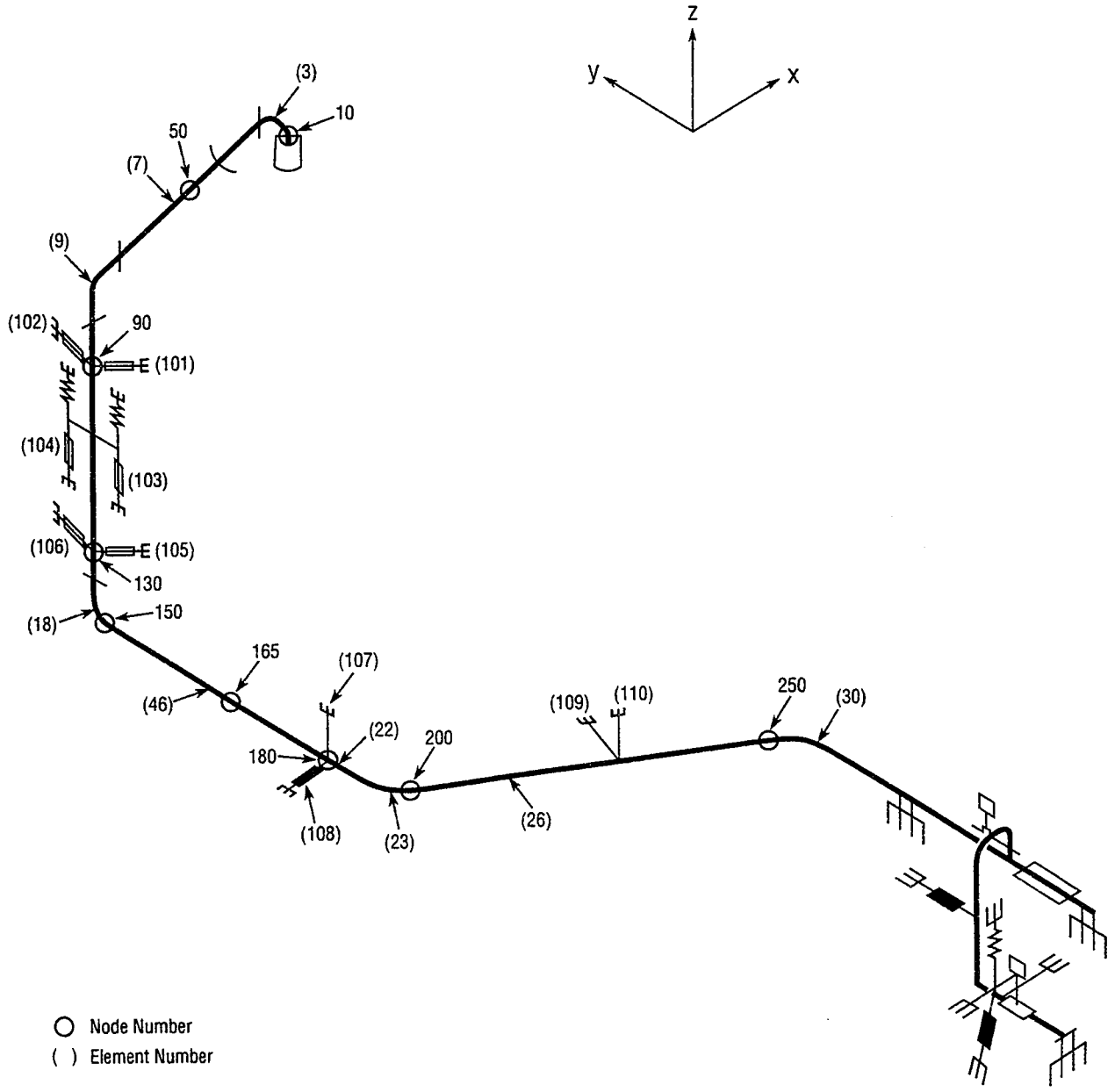

Figure 5.1 ISSAC Model for M-line with Conventional Supports

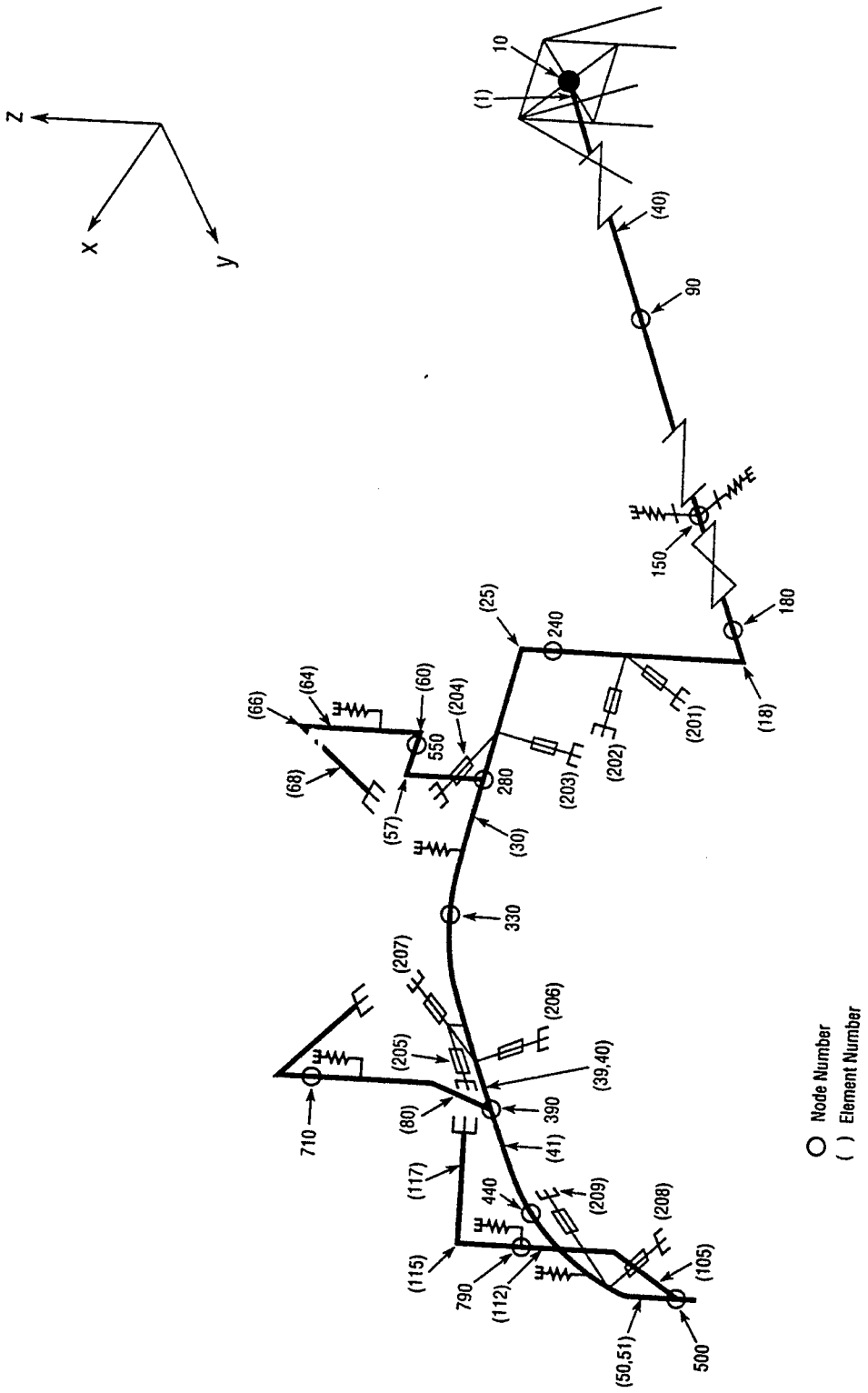

Figure 5.2 ISSAC Model for F-line with Conventional Supports

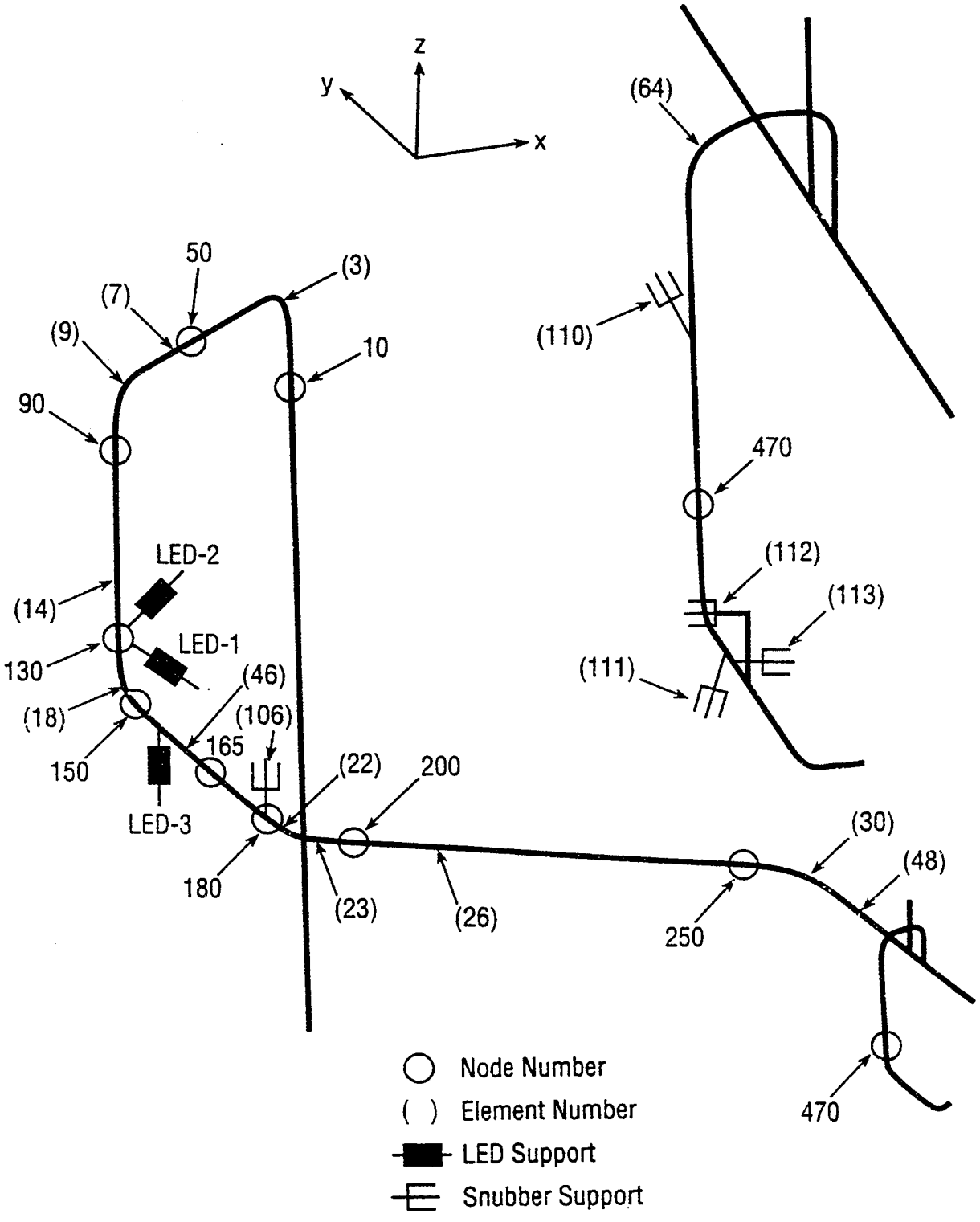

Figure 5.3 ISAAC Model for M-line with LED Supports

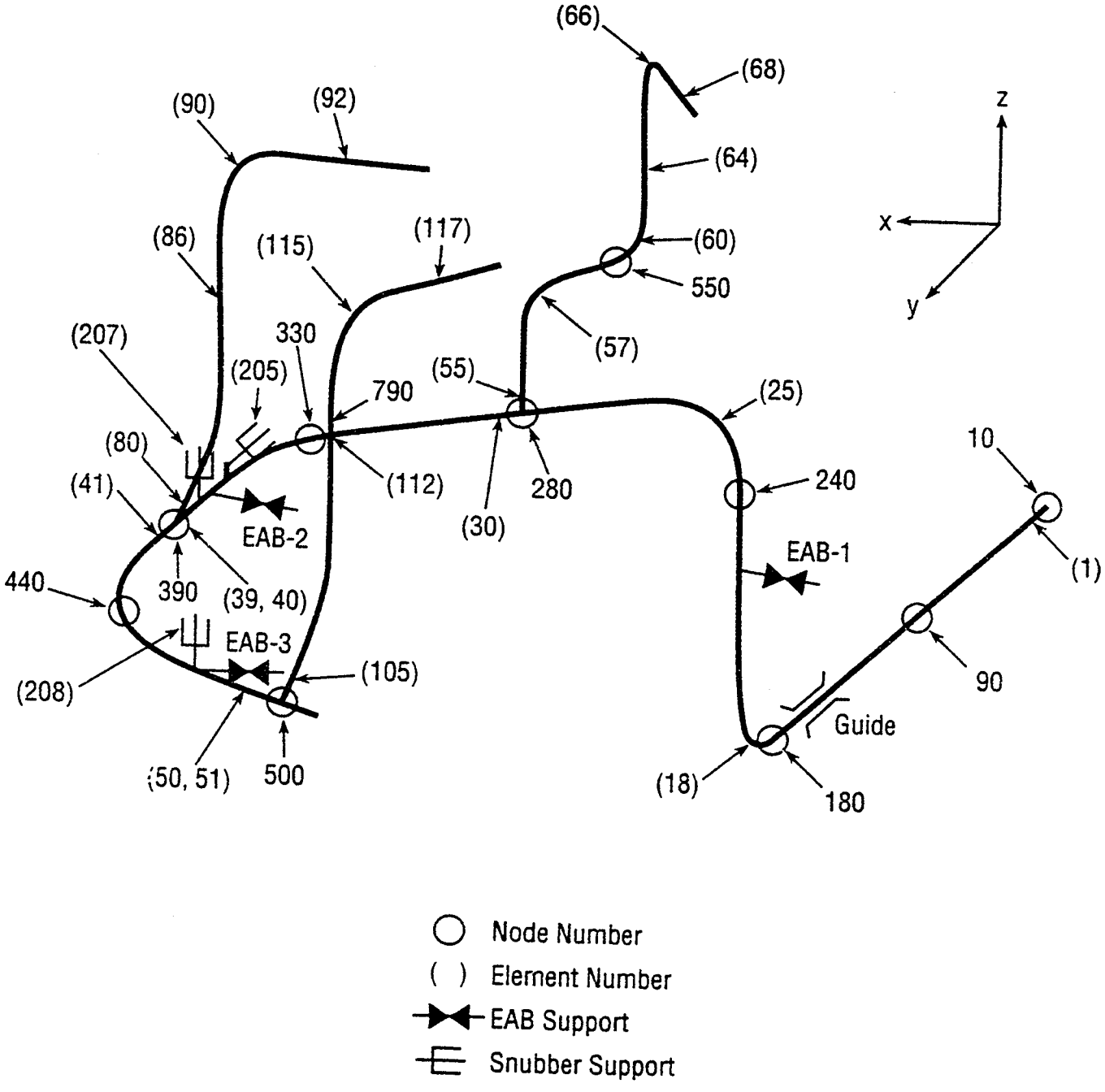

Figure 5.4 ISAAC Model for F-line with EAB Supports

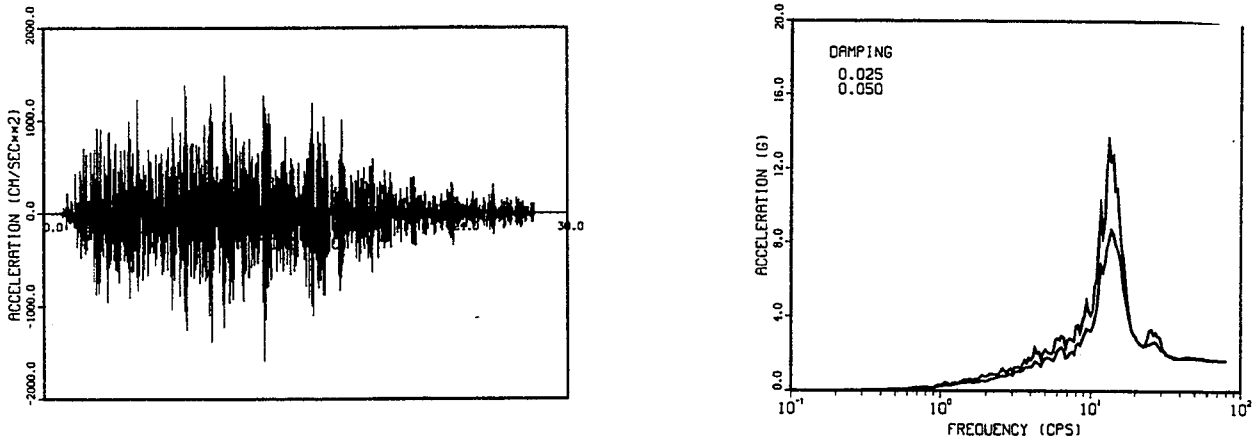

(a) Table Motion in X-direction

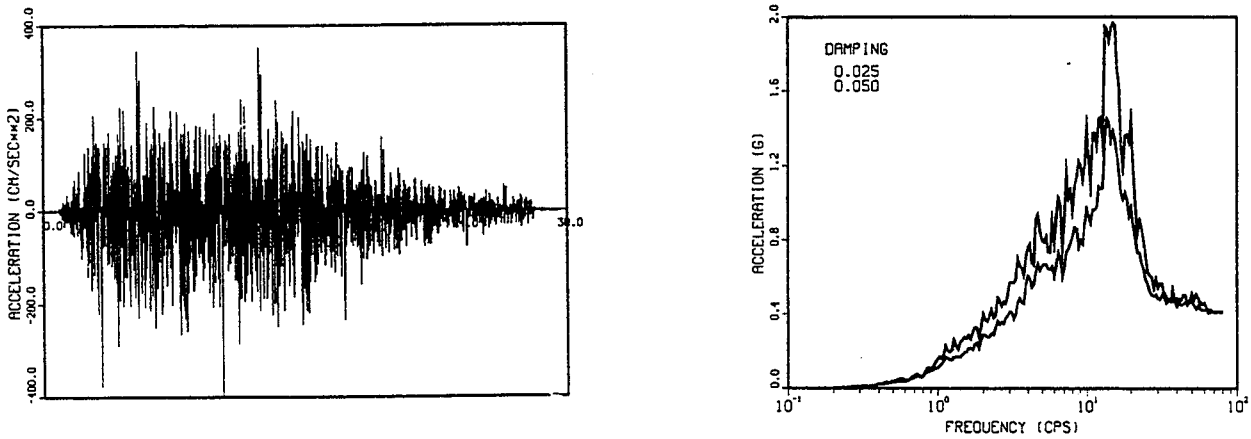

(b) Table Motion in Z-direction

Figure 5.5 Table Motions S2 (A) Test

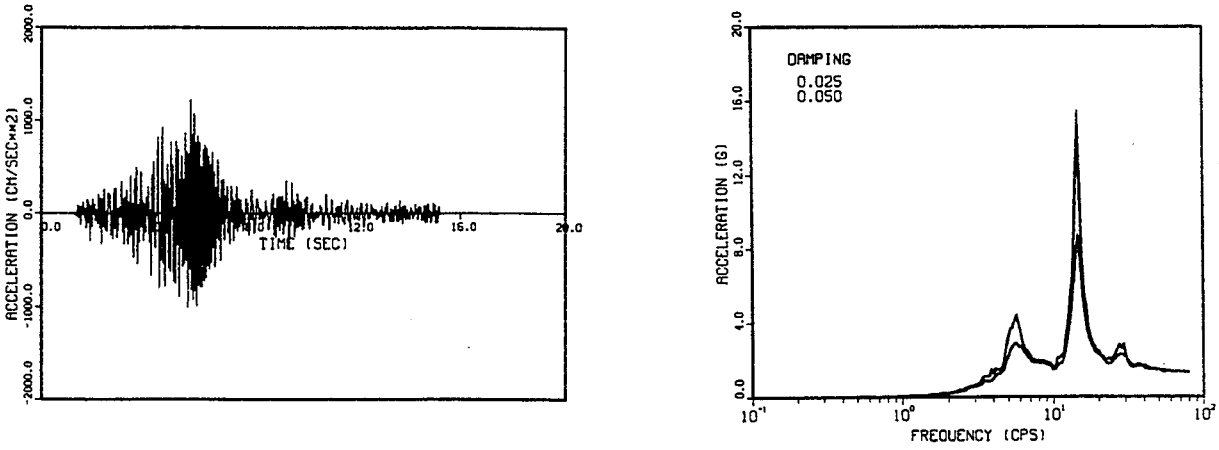

(a) Table Motion in X-direction

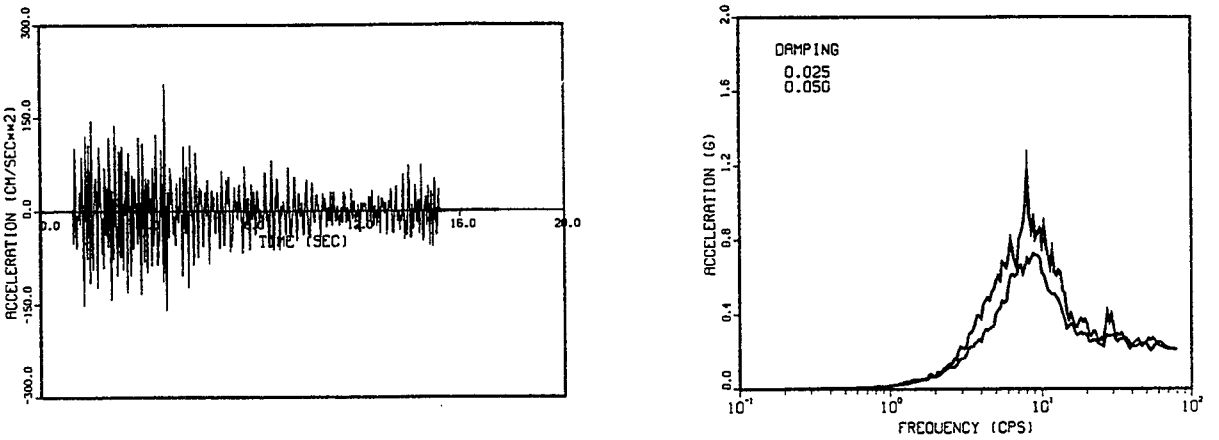

(b) Table Motion in Z-direction

Figure 5.6 Table Motions S2 (F) Test

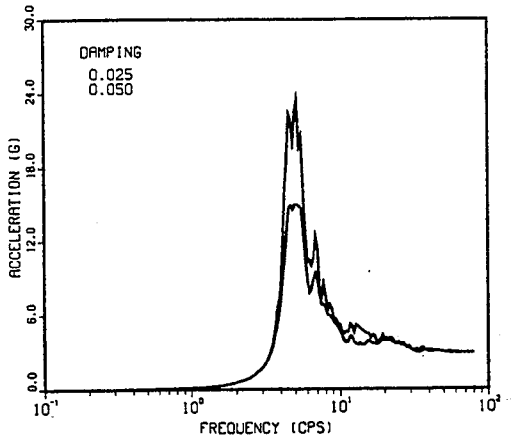

Figure 5.7 Table Motion, Tokachi-oki Wave, X-direction

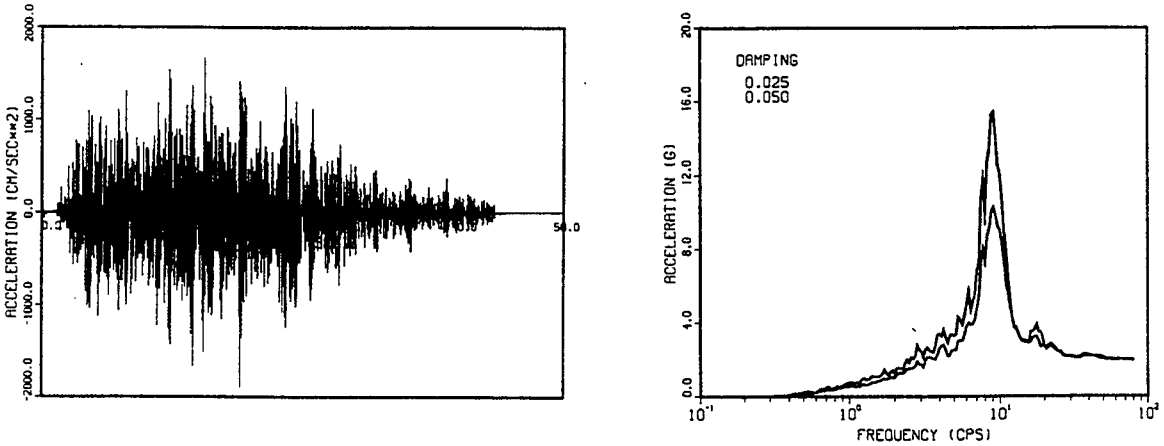

(a) Table Motion in X-direction

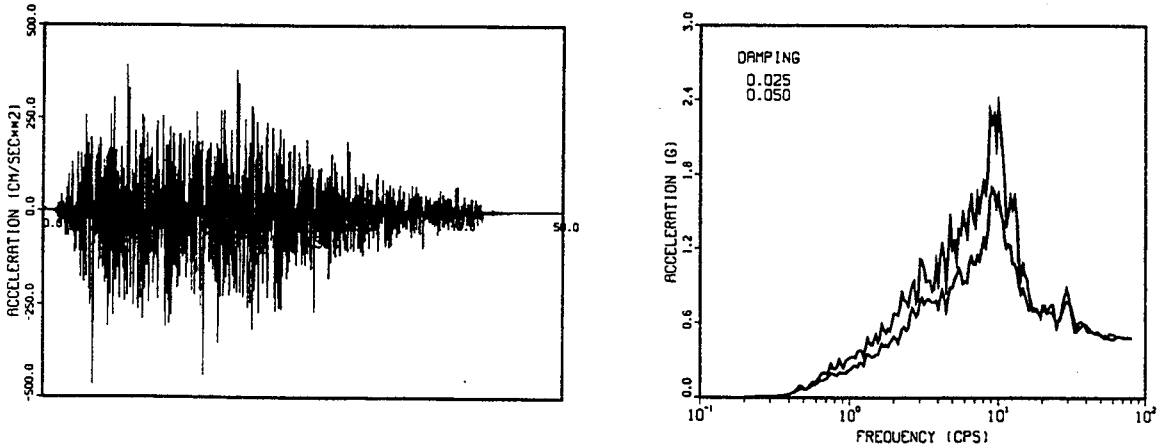

(b) Table Motion in Z-direction

Figure 5.8 Table Motions, 1.2 S2 (C) Test

Table 5.4 Comparison of Vibration Frequencies Obtained from Equivalent Linearization Analysis for S2 (M) Tests

Mode	Test (*1)	Analyses (Hz)			
		1/3 S2M	2/3 S2M	1.0 S2M	1.5 S2M
1	20.6(*2)				
2	20.8	20.42	21.97	22.23	22.51
3	22.6	24.18	25.34	22.99	23.88
4	23.2	27.86	29.56	29.76	30.11

Note (*1)Evaluated from sine sweep test. (Horizontal 200 gal and vertical 130 gal)
Note (*2) First SG-mode (not vibration mode of piping)

Table 5.5 Comparison of Peak Response Values for 1.0 S2 (M) Test Run

(a) Accelerations (g)

Instrument/Node	Direction	Test	NTH		LRV
			Original	Filtered	
AA 1/10	X	5.04	5.33	5.33	5.57
	Y	0.27	0.12	0.12	0.13
	Z	0.40	0.39	0.39	0.39
MA 1/50	X	6.04	5.46	5.45	4.82
	Y	4.07	4.48	4.47	1.84
	Z	1.72	4.91	1.22	1.66
MA 2/90	X	4.83	10.31	3.95	3.88
	Y	2.47	12.45	2.10	1.86
	Z	2.11	2.16	1.41	1.66
MA 3/130	X	3.80	11.73	4.43	3.70
	Y	1.40	13.06	1.50	1.65
	Z	1.65	2.22	1.39	1.66
MA 4/150	X	3.15	9.23	4.06	3.58
	Y	1.24	1.86	1.01	1.08
	Z	1.47	4.07	1.29	1.73
MA 5/165	X	3.05	3.93	3.20	3.32
	Y	1.19	1.95	1.00	1.09
MA 6/180	X	2.02	6.66	2.30	2.39
	Y	1.14	1.87	1.10	1.09
MA 8/200	X	2.15	3.05	2.21	2.06
	Y	1.31	1.83	1.33	1.06
	Z	1.83	0.91	0.68	0.70
MA10/250	X	2.38	3.64	2.58	1.83
	Y	0.34	2.41	0.46	0.21
	Z	0.95	0.81	0.46	0.51

Table 5.5 Comparison of Peak Response Values for 1.0 S2 (M) Test Run (Cont'd)

(b) Displacement (mm)

Instrument	Direction	Test	NTH	LRV
AD 1/N-10	X Y Z	2.46 0.06 0.19	2.42 0 0	2.51 0 0
MD1a/101		1.35	0.98	0.84
MD2a/102		1.56	1.01	1.31
MD3b/103		0.88	0.80	0.83
MD4b/104		0.94	0.94	0.81
MD5a(5b)/105		0.77 (0.76)	0.64	0.52
MD6a(6b)/106		0.85 (0.64)	0.76	1.23
MD7a(7b)/107		0.67 (0.31)	1.14	1.12
MD8/N-150	X Y Z	1.28 0.54 0.93	1.70 0.70 0.88	1.68 0.84 0.88

(c) Support Forces (ton)

Instrument/ Element	Test	NTH		LRV
		Original	Filtered	
MR 1/101	5.22	5.40	4.57	4.45
MR2/102	6.81	6.19	5.84	8.49
MR3/103	1.46	1.03	0.94	1.24
MR4/104	1.41	1.19	1.07	1.21
MR5/105	2.51	3.79	3.31	2.44
MR6/106	3.27	5.11	4.65	10.32
MR7/107	1.55	2.96	2.59	2.67
MR9/109	1.10	4.99	4.86	2.11
MR10/110	0.97	2.90	2.86	0.45

Table 5.5 Comparison of Peak Response Values for 1.0 S2 (M) Test Run (Cont'd)

(d) Pipe Stress (kg/mm^2)

Instrument/Element	Stress Intensification Factor	Test	NTH	LRV
MS1/3	2.0	1.86	1.51	1.87
MS2'/5	1.0	0.97	0.99	1.72
MS2/7	1.0	1.63	2.07	2.20
MS3/9	2.0	2.30	1.67	2.72
MS4/14	1.0	1.37	1.59	1.28
MS5/17	2.0	1.02	1.45	0.84
MS6/46	1.0	1.52	2.59	1.94
MS8/23	1.0	0.80	1.05	0.73
MS9/25	1.0	0.63	1.09	0.68
MS10/30	1.0	0.61	0.54	0.31

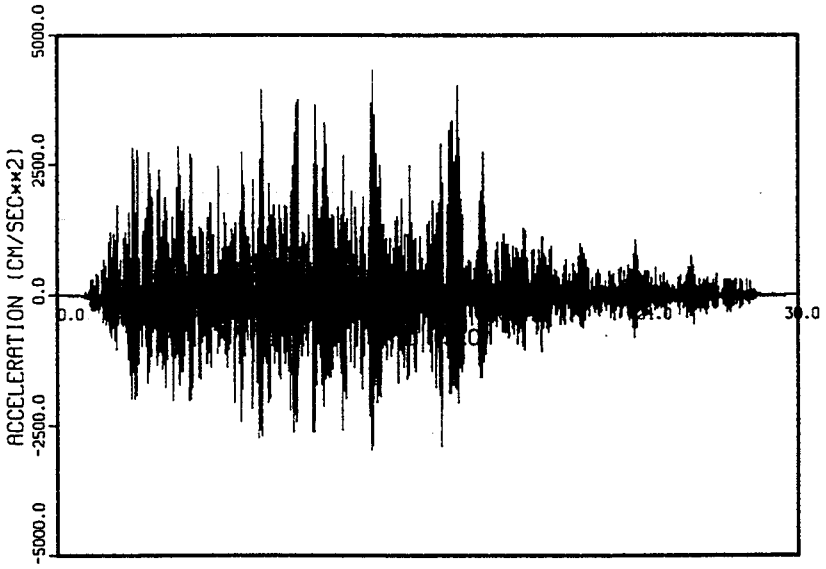

(a) Recorded Accelerogram (Peak = 4.42g)

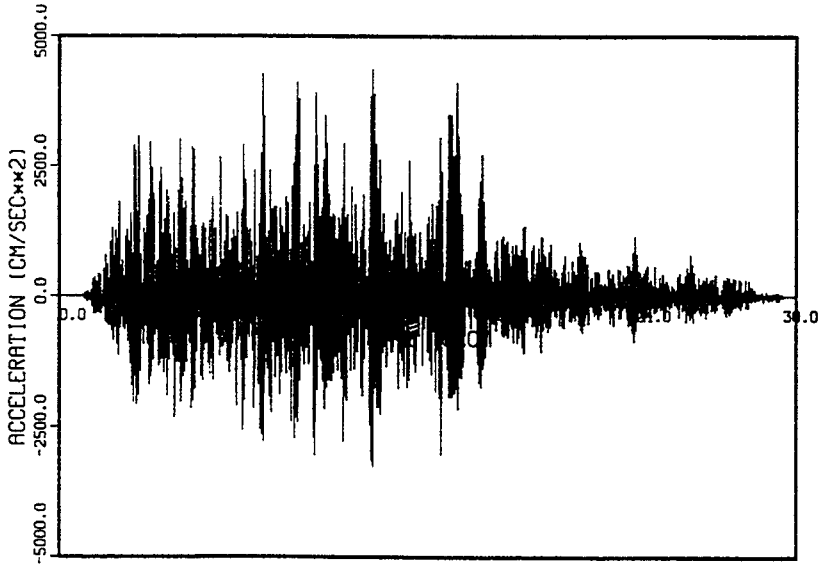

(b) Generated Acceleragram (Peak - 4.46g)

Figure 5.9 Generated Accelerogram for AA1-X

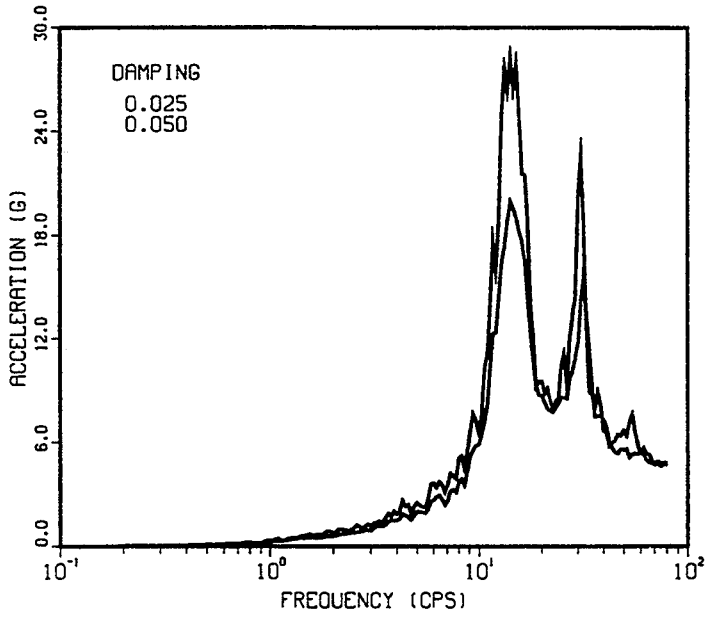

(a) Recorded Motion

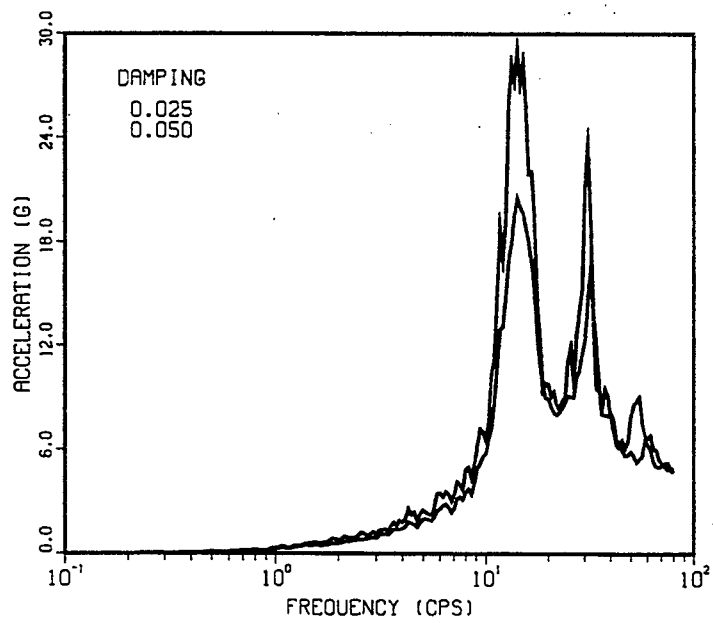

(b) Generated Motion

Figure 5.10 Comparison of Response Spectra for AA1-X

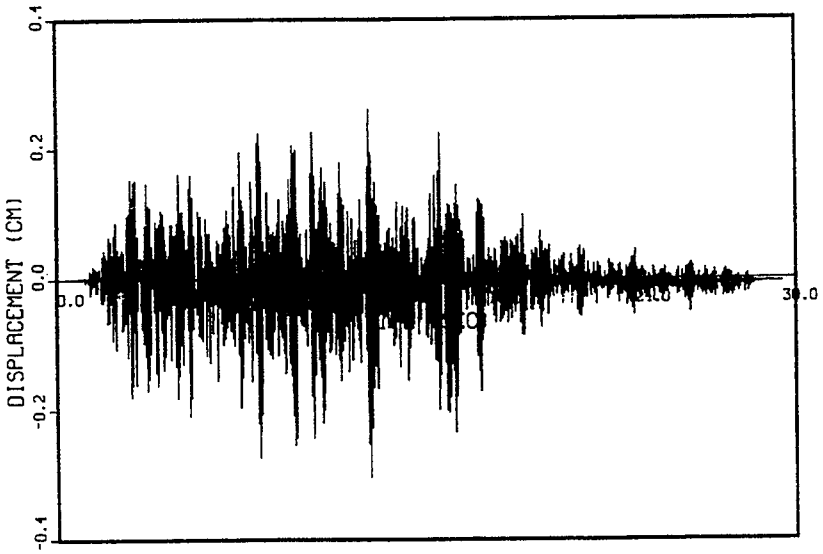

Generated Actuator Motion (Peak = 3.05 mm)

Figure 5.11 Relative Displacement of Actuator Motion, AD1-X

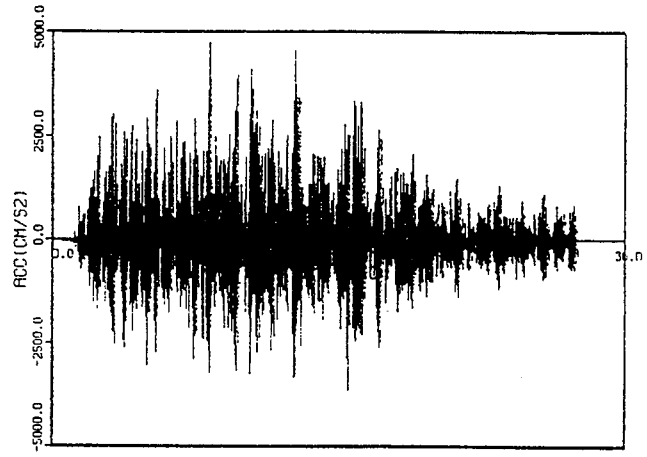

(a) Recorded
(Peak : Ax = 4.83g)

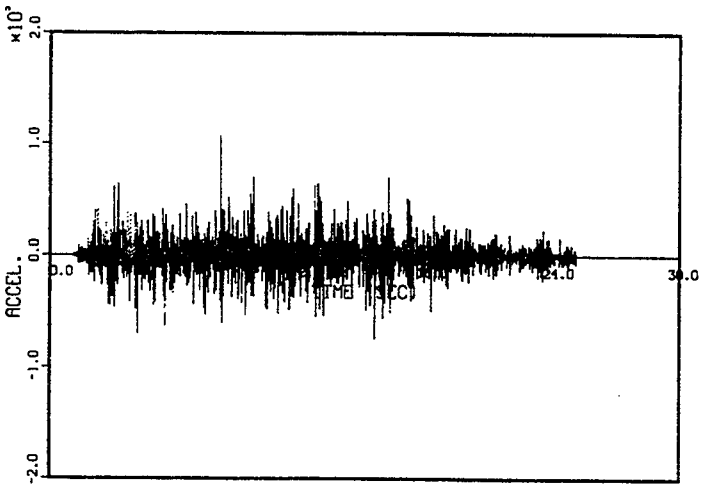

(b) Original Analysis
(Peak: Ax = 10.31g)

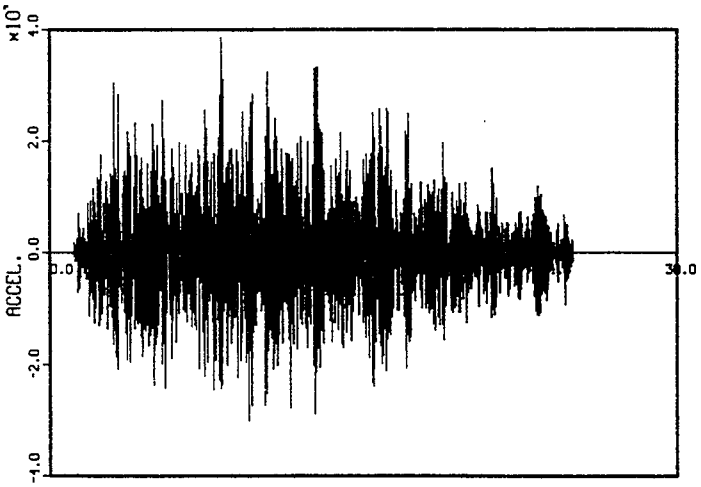

(c) Filtered Analysis Result
(Peak: Ax = 3.95g)

Figure 5.12 Comparison of Acceleration Time History, MA2-X, from Test Run 1.0S2 (M)

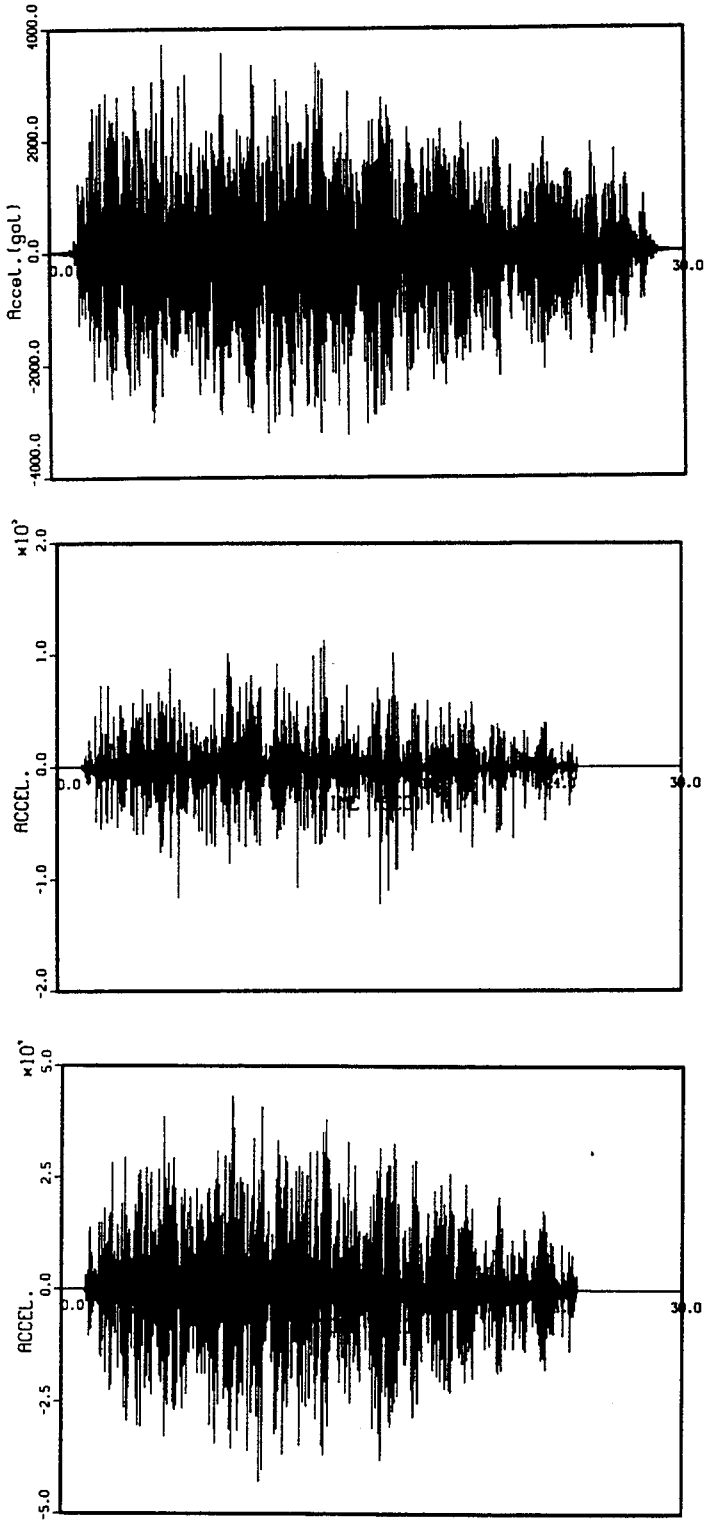

(a) Recorded
(Peak: Ax = 3.80 g)

(b) Original Analysis
(Peak: Ax = 11.73 g)

(c) Filtered Analysis Result
(Peak: Ax = 4.43 g)

Figure 5.13 Comparison of Acceleration Time History, MA3-X, from Test Run 1.0 S2 (M)

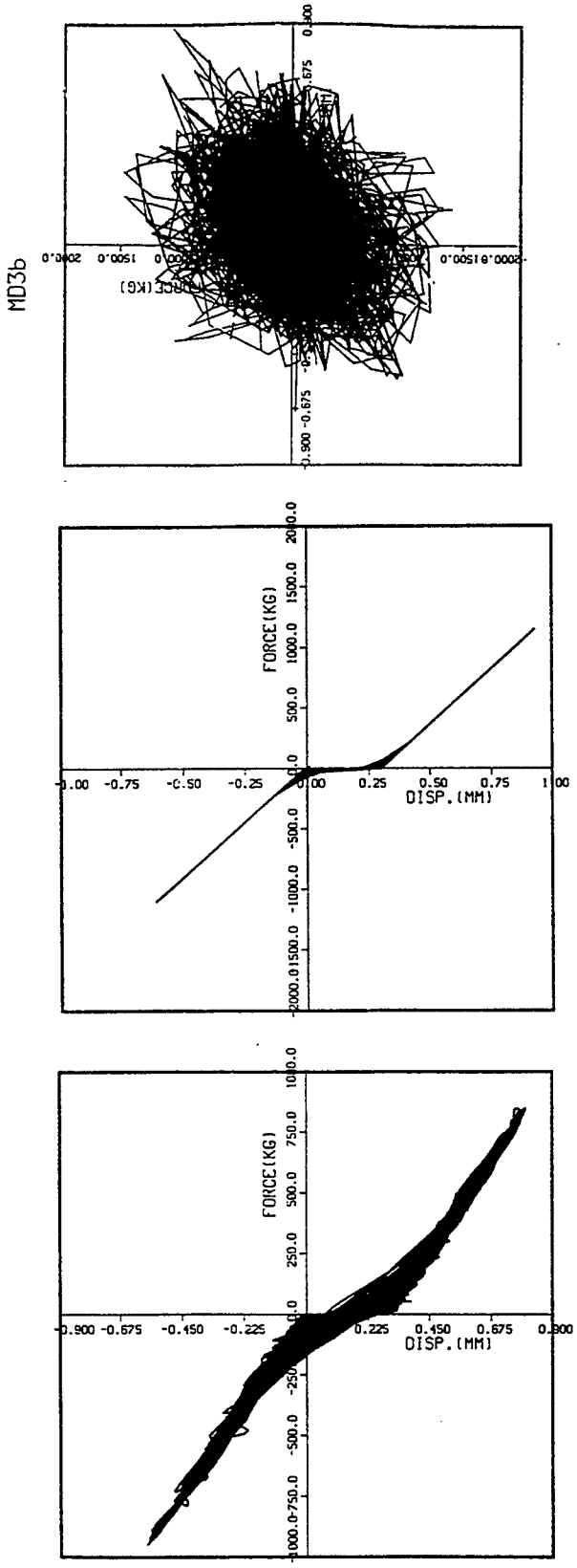

(a) Recorded
Peak: U = 0.88 mm
f = 1.46 ton

(b) Original Analysis
Peak: U = 0.80 mm
f = 1.19 ton

(c) Filtered Analysis Results
Peak : U = 0.80 mm
f = 1.07 ton

Figure 5.14 Comparison of Force-Deformation Relationship of Snubber, MR3, from Test Run 1.0 S2 (M)

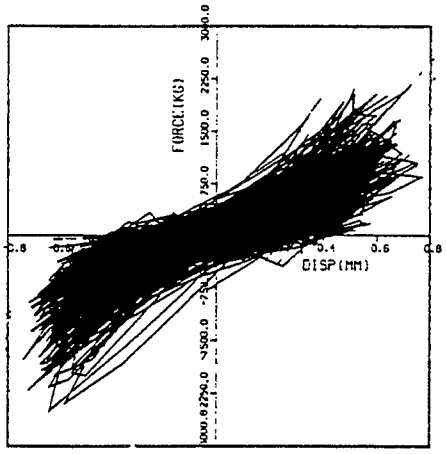

(a) Recorded
Peak: U = 0.77 mm
f = 2.51 ton

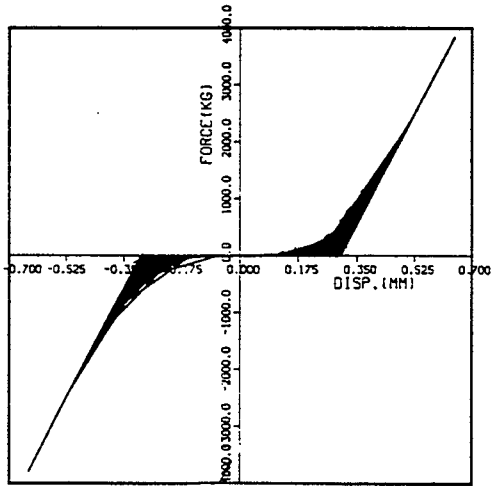

(b) Original Analysis
Peak: U = 0.64 mm
f = 3.79 ton

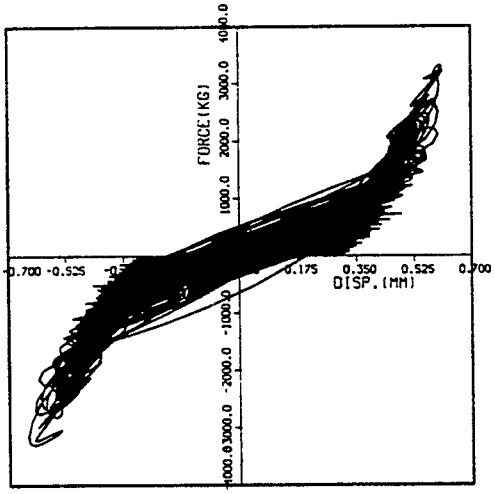

(c) Filtered Analysis Result
Peak: U = 0.64 mm
f = 3.31 ton

Figure 5.15 Comparison of Force Deformation Relationship of Snubber, MR5 from Test Run 1.0 S2 (M)

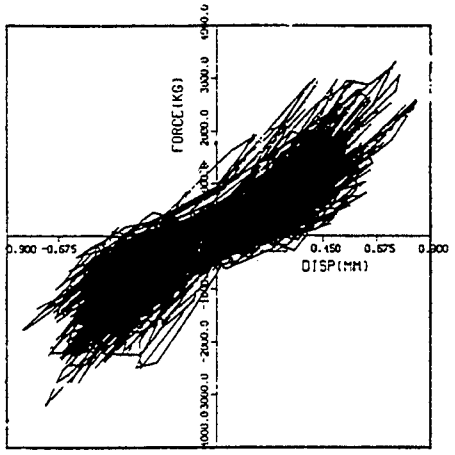

(a) Recorded
Peak: U = 0.85 mm
f = 3.27 ton

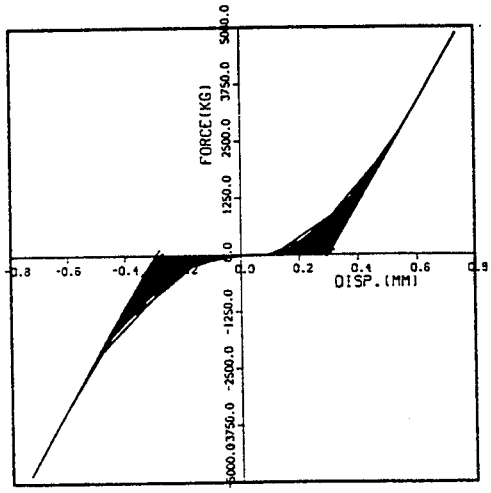

(b) Original Analysis
Peak: U = 0.76
f = 5.11 ton

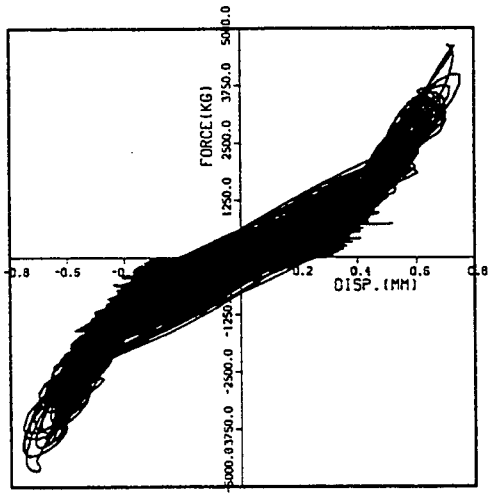

(c) Filtered Analysis Result
Peak : U = 0.76 mm
f = 4.65 ton

Figure 5.16 Comparison of Force Deformation Relationship of Snubber, MR6, from Test Run 1.0 S2 (M)

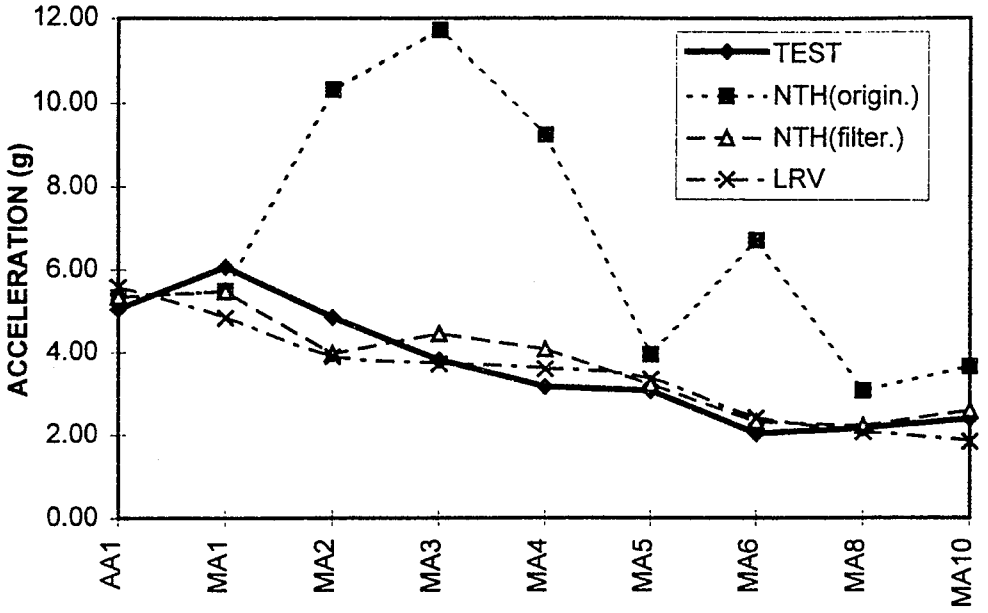

Figure 5.17 Comparison of Responses of M-line for S2(M) Test Run, X-Direction Accelerations

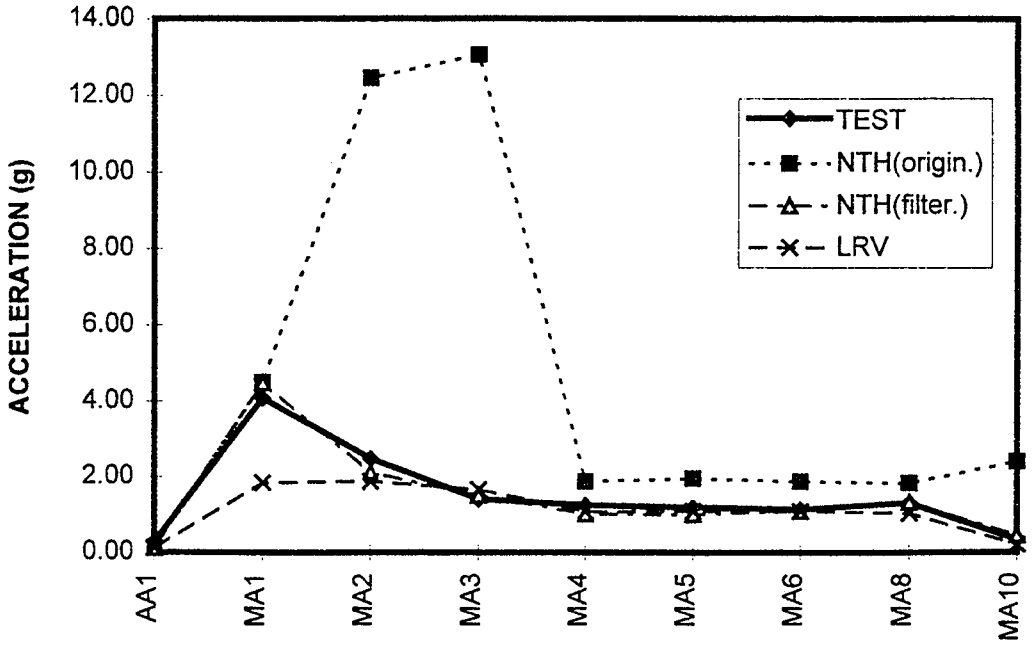

Figure 5.18 Comparison of Responses of M-line for S2 (M) Test Run, Y-Direction Acceleration

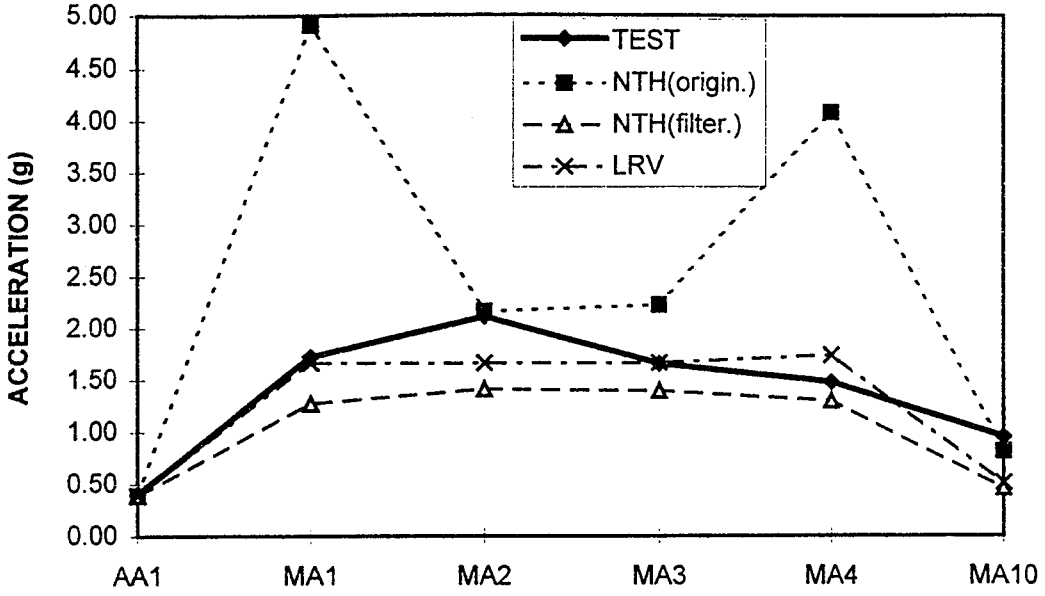

Figure 5.19 Comparison of Responses of M-line for S2(M) Test Run, Z-Direction Acceleration

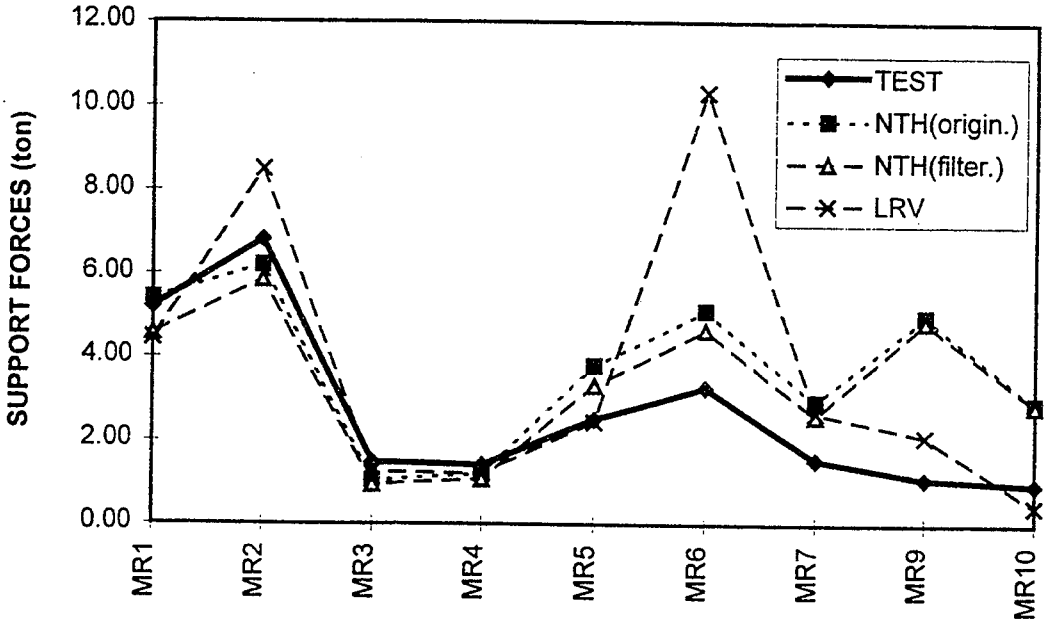

Figure 5.20 Comparison of Response of M-line for S2 (M) Test Run, Support Forces

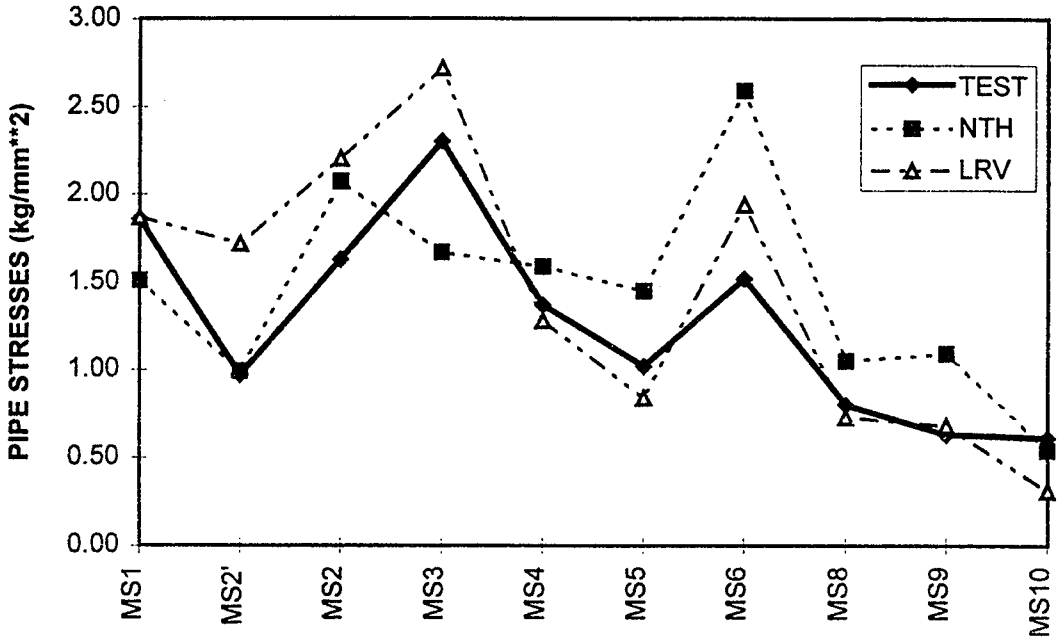

Figure 5.21 Comparison of Responses of M-line for S2 (M) Test Run, Pipe Stresses

Table 5.6 Comparison of Peak Response Values for 1.52 S2(M) Test Run

(a) Acceleration (g)

Instrument/Node	Direction	Test	NTH		LRV
			Original	Filtered	
AA1/10	X	7.00	7.27	7.27	7.55
	Y	0.29	0.17	0.17	0.18
	Z	0.59	0.60	0.60	0.60
MA1/50	X	7.64	8.33	8.33	6.49
	Y	4.70	5.85	5.85	3.90
	Z	2.16	6.43	1.59	2.46
MA2/90	X	6.49	15.00	4.80	4.93
	Y	3.34	15.61	2.41	2.96
	Z	3.06	2.77	1.84	1.71
MA3/130	X	4.68	16.53	5.08	4.33
	Y	1.79	13.78	1.63	1.53
	Z	2.64	2.77	1.83	1.86
MA4/150	X	4.58	13.77	5.22	5.18
	Y	1.47	2.60	1.29	2.20
	Z	2.38	5.04	1.77	1.60
MA5/165	X	4.08	5.49	4.48	5.33
	Y	1.60	2.66	1.28	1.21
MA6/180	X	3.04	10.41	3.78	3.40
	Y	1.53	2.66	1.40	2.24
MA8/200	X	3.02	4.11	3.07	2.98
	Y	1.62	2.60	1.52	2.30
	Z	1.85	1.47	1.15	1.03
MA10/250	X	3.21	4.97	3.43	2.86
	Y	0.49	3.27	0.56	0.39
	Z	1.21	1.10	0.62	0.79

Table 5.6 Comparison of Peak Response Values for 1.52 S2(M) Test Run (Cont'd)

(b) Displacement (mm)

Instrument/Element	Direction	Test	NTH	LRV
ADl/N-10	X Y Z	3.79 0.08 0.28	3.78 0 0	3.11 0 0
MD1a/101		1.59	1.25	1.11
MD2a/102		2.25	1.35	1.82
MD3b/103		1.15	1.06	1.28
MD4b/104		1.08	1.13	1.37
MD5a(5b)/105		1.02(0.91)	0.76	0.72
MD6a(6b)106		1.07(0.96)	0.90	0.87
MD7a(7b)107		1.10(0.54)	1.55	1.28
MD8/N-150	X Y Z	1.98 0.70 1.13	2.12 0.74 1.10	2.58 1.08 1.33

Table 5.6 Comparison of Peak Response Values for 1.52 S2(M) Test Run (Cont'd)

(c) Support Forces (ton)

Instrument/Element	Test	NTH		LRV
		Original	Filtered	
MR1/101	7.62	7.28	6.45	6.32
MR2/102	10.58	8.82	8.50	12.39
MR3/103	2.39	1.39	1.29	2.07
MR4/104	2.29	1.51	1.39	2.23
MR5/105	3.78	5.15	4.98	4.66
MR6/106	4.20	6.65	6.55	6.33
MR7/107	2.59	4.05	3.83	3.19
MR9/109	1.86	7.00	6.80	3.11
MR10/110	0.95	4.41	4.32	0.86

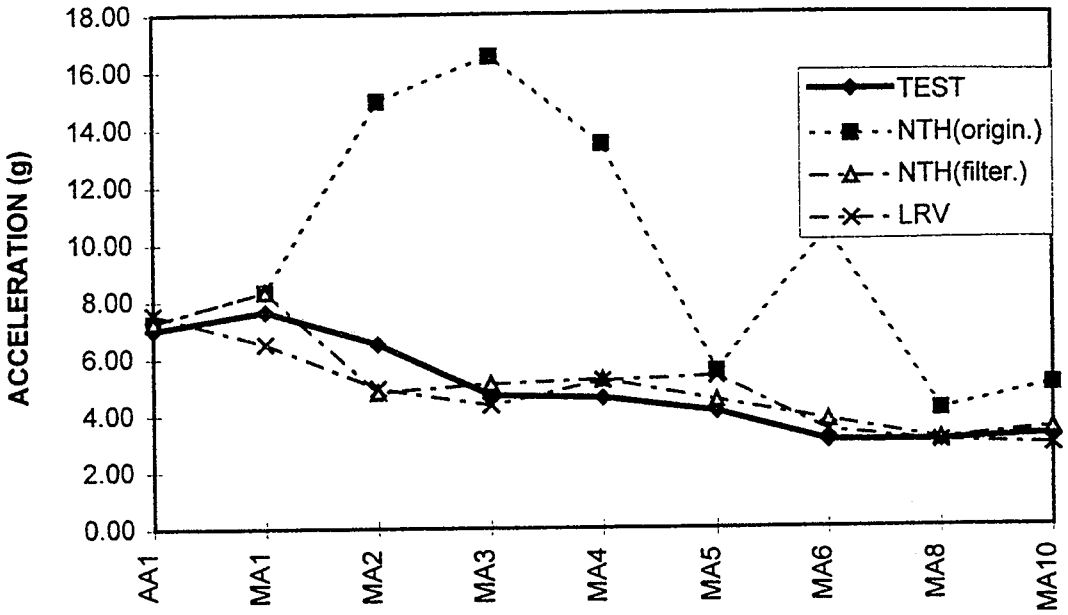

Figure 5.22 Comparison of Responses of M-line for 1.5 S2(M) Test Run, X-Direction Accelerations

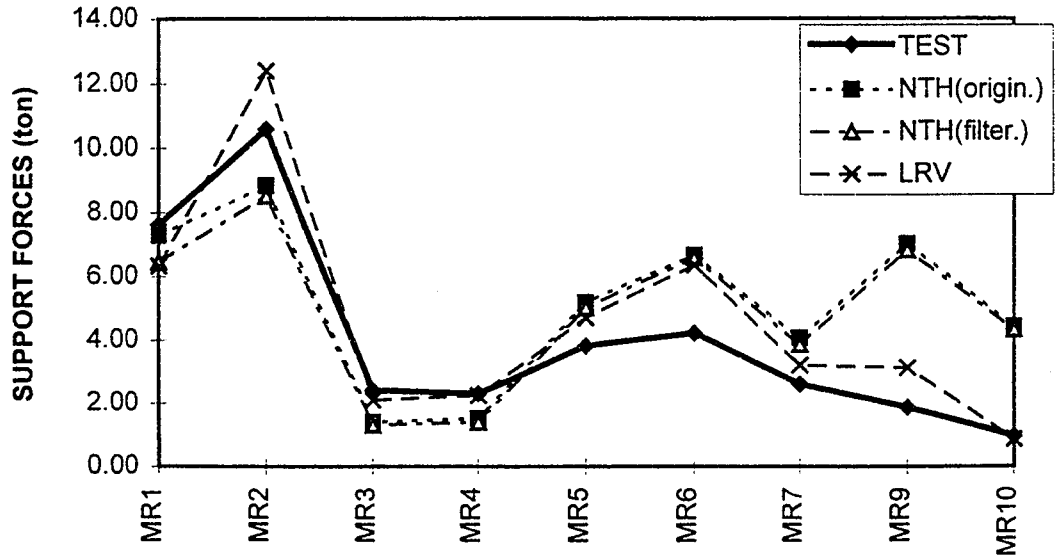

Figure 5.23 Comparison of Responses of M-line for 1.5 S2 (M) Test Run, Support Forces

Table 5.7 Comparison of Peak Response Values for Multiple Excitation Test (DC-3)

(a) Acceleration (g)

Instrument/Node	Direction	Test	NTH		LRV
			Original	Filtered	
AA1/10	X	2.23	2.27	2.27	2.40
	Y	0.18	0.05	0.05	0.05
	Z	0.19	0.01	0.01	0.02
MA1/50	X	2.43	3.44	3.44	2.03
	Y	2.66	2.97	2.97	2.68
	Z	1.06	4.66	0.79	0.60
MA2/90	X	2.01	5.30	1.61	1.65
	Y	2.49	6.98	1.60	1.53
	Z	1.15	1.58	0.72	0.73
MA3/130	X	2.95	12.55	2.87	3.02
	Y	1.38	7.87	1.34	1.42
	Z	1.03	1.56	0.71	0.73
MA4/150	X	3.25	9.07	2.66	2.06
	Y	0.77	1.58	0.89	0.53
	Z	0.64	2.32	0.69	0.48
MA5/165	X	2.01	3.49	2.74	2.36
	Y	0.73	1.57	0.89	0.52
MA6/180	X	1.47	3.60	1.91	1.38
	Y	0.74	1.55	0.97	0.82
MA8/200	X	1.06	1.48	1.07	1.09
	Y	0.88	1.38	1.05	1.01
	Z	1.37	0.80	0.62	0.55
MA10/250	X	1.02	1.62	1.04	1.32
	Y	0.22	1.01	0.26	0.38
	Z	0.60	0.28	0.22	0.18

Table 5.7 Comparison of Peak Response Values for Multiple Excitation Test (DC-3) (Cont'd)

(b) Displacement (mm)

Instrument/Element	Direction	Test	NTH	LRV
AD1/N-10	X Y Z	3.54 0.08 0.27	3.29 0 0	3.51 0 0
MD1a/101		1.33	0.76	1.01
MD2a/102		1.73	1.11	1.23
MD3b/103		0.51	0.65	0.71
MD4b/104		0.55	0.47	0.42
MD5a(5b)/105		1.01 (0.60)	0.54	0.55
MD6a(6b)/106		0.85 (0.48)	0.66	0.70
MD7a(7b)/107		0.51 (0.23)	0.82	0.75
MD8/N-150	X Y Z	2.00 0.26 0.45	1.75 0.59 0.55	1.61 0.62 0.65

(c) Support Forces (ton)

Instrument/Element	Test	NTH		LRV
		Original	Filtered	
MR1/101	6.05	3.92	3.69	5.63
MR 2/102	7.39	6.94	6.71	7.88
MR 3/103	0.94	0.65	0.53	1.02
MR 4/104	0.67	0.37	0.34	0.49
MR 5/105	2.60	2.61	1.93	2.78
MR6/106	2.66	4.02	3.32	4.44
MR7/107	1.37	1.69	1.53	1.46
MR9/109	0.50	2.04	1.85	1.91
MR10/110	0.71	0.53	0.44	0.51

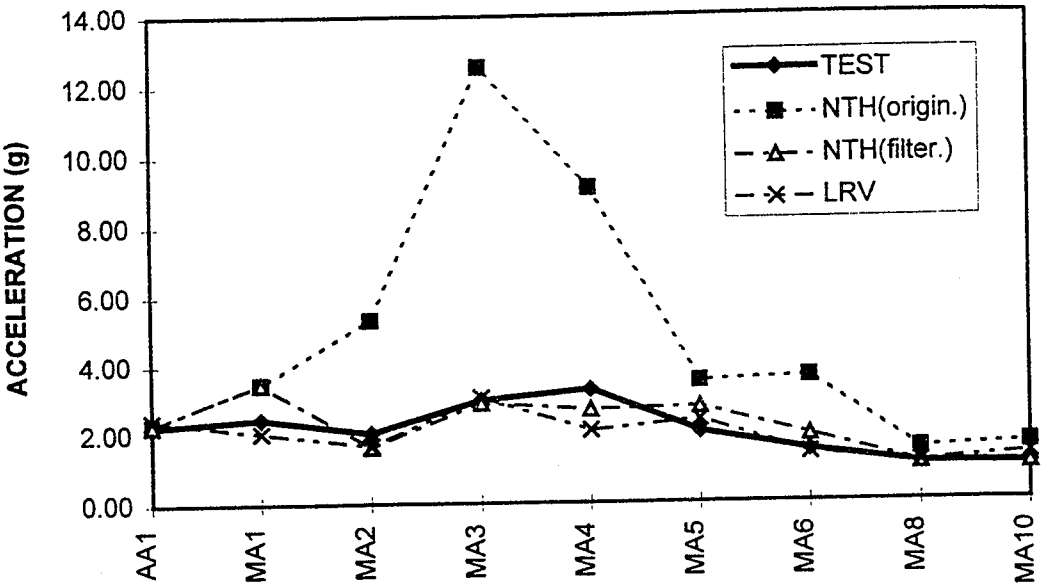

Figure 5.24 Comparison of Responses of M-line for Multiple Excitation Test Run, X-Direction Accelerations

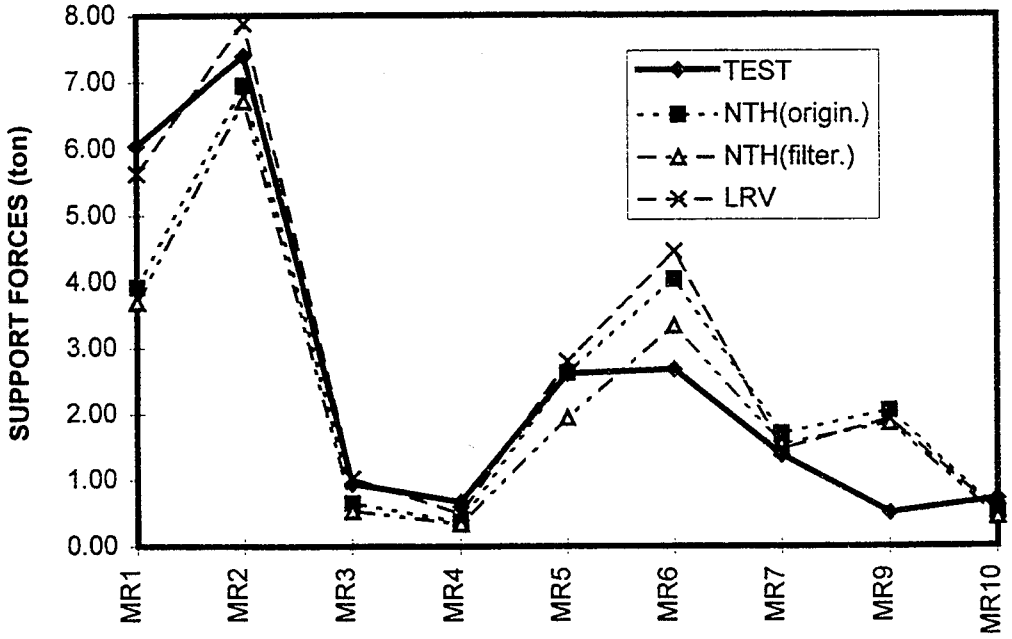

Figure 5.25 Comparison of Responses of M-line for Multiple Excitation Test Run, Support Forces

Table 5.8 Comparison of Vibration Frequencies of F-line with Conventional Supports

Mode	Test(*1)	1.0 S2(F)		1.3 S2(F)	
		RS/ELA(*2)	LRV/ELA(*3)	RS/ELA	LRV/ELA
1	16.4 Hz	15.54Hz	16.64 Hz	16.88 Hz	16.71 Hz
2	21.0	18.30	18.01	18.71	18.06
3	22.4	19.03	19.46	19.69	19.58
4	23.4	20.46	21.18	21.12	21.12
5	25.8	23.70	24.48	24.37	24.61
6	27.4	25.92	28.17	27.34	28.39
7	28.0	27.28	29.19	28.89	29.26

Note: (*1) Evaluated from the horizontal sine sweep tests at 150 gal.
(*2) Equivalent Linearization analysis based on Response Spectrum Method
(*3) Equivalent Linearization analysis based on Linear Random Vibration Method

Table 5.9 Response of F-line with Conventional Supports for S2(F) Test Run

(a) Acceleration (g)

Instrument/Node	Direction	Test	NTH (*1)			ELA (*2)	
			A	B	C	RS	LRV
FA2/40	X	2.09	2.40	2.18	2.14	2.41	2.36
	Y	0.62	0.37	0.30	0.23	0.23	0.22
	Z	0.93	1.20	1.09	0.77	1.72	1.35
FA3/90	X	2.63	2.53	2.36	2.07	2.61	2.91
	Y	0.17	0.40	0.32	0.24	0.24	0.23
	Z	1.36	1.21	0.99	0.77	1.88	1.46
FA5/180	X	2.08	2.68	1.55	1.36	1.93	2.39
	Y	.28	0.44	0.33	0.24	0.26	0.24
	Z	1.09`	0.86	0.54	0.63	1.04	0.69
FA6/240	X	2.07	3.14	1.90	1.76	1.59	1.69
	Y	1.45	2.24	1.20	1.50	0.78	1.71
	Z	1.51	0.93	0.80	0.77	1.39	0.98
FA7/280	X	3.38	2.97	2.23	2.11	2.04	2.29
	Y	1.24	1.73	0.93	1.53	0.68	1.58
	Z	1.19	1.34	0.84	0.75	1.29	1.42
FA8/330	X	3.07	2.82	2.39	2.05	2.21	2.55
	Y	1.28	1.51	1.20	1.55	0.77	1.25
	Z	1.64	1.63	1.35	1.20	2.10	1.80
FA9/390	X	2.69	3.29	2.36	3.79	1.63	1.94
	Y	1.24	1.44	1.13	1.62	0.79	0.70
	Z	1.24	2.57	0.64	1.48	0.58	0.72
FA10/440	X	2.78	3.35	3.07	4.16	2.15	2.52
	Y	1.11	1.45	1.08	1.52	0.74	0.85
	Z	1.13	1.46	1.02	0.89	0.92	0.73
FA11/500	X	3.11	4.01	3.56	4.98	2.42	2.99
	Y	1.90	2.38	1.11	1.42	0.70	1.24
	Z	1.19	1.85	1.09	0.93	0.72	0.78
FA12/550	X	3.10	3.30	2.85	2.07	2.96	3.15
	Y	1.95	1.73	1.24	1.48	2.22	1.76
	Z	1.30	1.07	0.68	0.59	1.35	1.11
FA13/790	X	3.18	2.83		3.09	1.91	2.29
	Y	1.36	1.19		0.70	0.66	0.69
	Z	1.26	1.51		0.89	0.74	0.74

Note: (1) Nonlinear time history analysis (A = original model; B= filtered results; C=snubber stiffnesses are reduced)

(2) Equivalent Linearization Analyses (RS = response spectrum approach; LRV = linear random vibration approach)

Table 5.9 Response of F-line with Conventional Supports for S2(F) Test Run (Cont'd)

b) Displacement (mm)

Instrument/Element	Test(*1)	NTH		ELA	
		A	C	RS	LRV
FD2b/201	0.32	0.26	0.27	0.18	0.25
FD3b/202	0.68	0.35	0.46	0.30	0.33
FD4b/203	0.46	0.32	0.40	0.46	0.36
FD5b/204	0.71	0.37	0.36	0.36	0.39
FD6b/205	0.79	0.56	1.43	0.43	0.51
FD7a,b/206	0.39 (0.88)	0.63	1.17	0.27	0.56
FD8a,b/207	0.33 (0.63)	0.47	0.77	0.30	0.45
FD9b/208	0.49	0.70	1.40	0.35	0.67
FD10b/209	0.56	0.54	0.87	0.31	0.38

(*1) Recorded displacements are b-measurements, and ( ) indicates a-measurements.

c) Support Forces (ton)

Instrument/Element	Test 95011107	NTH			ELA	
		A	B	C	RS	LRV
FR2/201	0.88	0.82	0.45	0.45	0.22	0.73
FR3/202	1.39	1.47	1.24	1.15	1.15	1.38
FR4/203	0.96	1.12	0.95	0.77	1.96	1.38
FR5/204	1.42	1.09	0.91	0.52	1.09	1.22
FR6/205	2.45	3.32	2.98	5.31	2.32	2.98
FR7/206	3.52	2.97	2.70	3.47	0.50	2.56
FR8/207	2.42	2.13	1.97	2.07	1.03	2.07
FR9/208	2.73	3.38	3.06	4.07	1.28	3.33
FR10/209	1.85	2.77	2.48	2.83	0.89	1.46

Table 5.9 Response of F-line with Conventional Supports for S2(F) Test Run (Cont'd)

d) Pipe Stresses (kg/mm^2)

Instrument/ Element	Stress Intensification	Test	NTH		ELA	
			A	C	RS	LRV
FS1/1	1.0	2.9	1.6	1.4	1.5	2.8
FS2/18	2.63	1.3	2.3	2.0	2.1	1.8
FS3/25	2.63	1.0	0.8	0.7	0.9	1.0
FS4/30-55	2.54	1.3	1.9	1.6	2.2	2.3
FS5/39	1.0	1.6	3.5	4.3	1.8	3.4
FS6/41-80	2.54	1.4	2.8	3.8	2.7	3.4
FS7/41	1.0	1.6	1.7	1.8	1.0	1.3
FS8/50	1.0	0.4	0.4	0.5	0.3	0.6
FS9/51-105	2.54	1.6	1.1	1.5	2.1	2.7
FS10/57	2.27	0.9	0.8	0.7	1.0	1.2
FS11/60	2.75	1.7	2.3	2.3	3.3	3.1
FS12/64	1.0	1.4	1.4	1.1	1.5	1.8
FS13/66	2.27	1.4	1.2	1.6	1.2	1.4
FS14/68	1.0	2.9	2.2	2.2	2.5	2.8
FS15/80	1.0	1.2	1.5	2.0	0.8	1.4
FS19/105	1.0	1.6	1.4	2.7	0.8	1.3
FS20/112	1.0	2.1	1.4	1.9	0.9	1.4
FS21/115	2.27	1.8	1.9	4.0	1.1	1.8
FS22/117	1.0	2.8	2.5	4.3	1.6	2.7

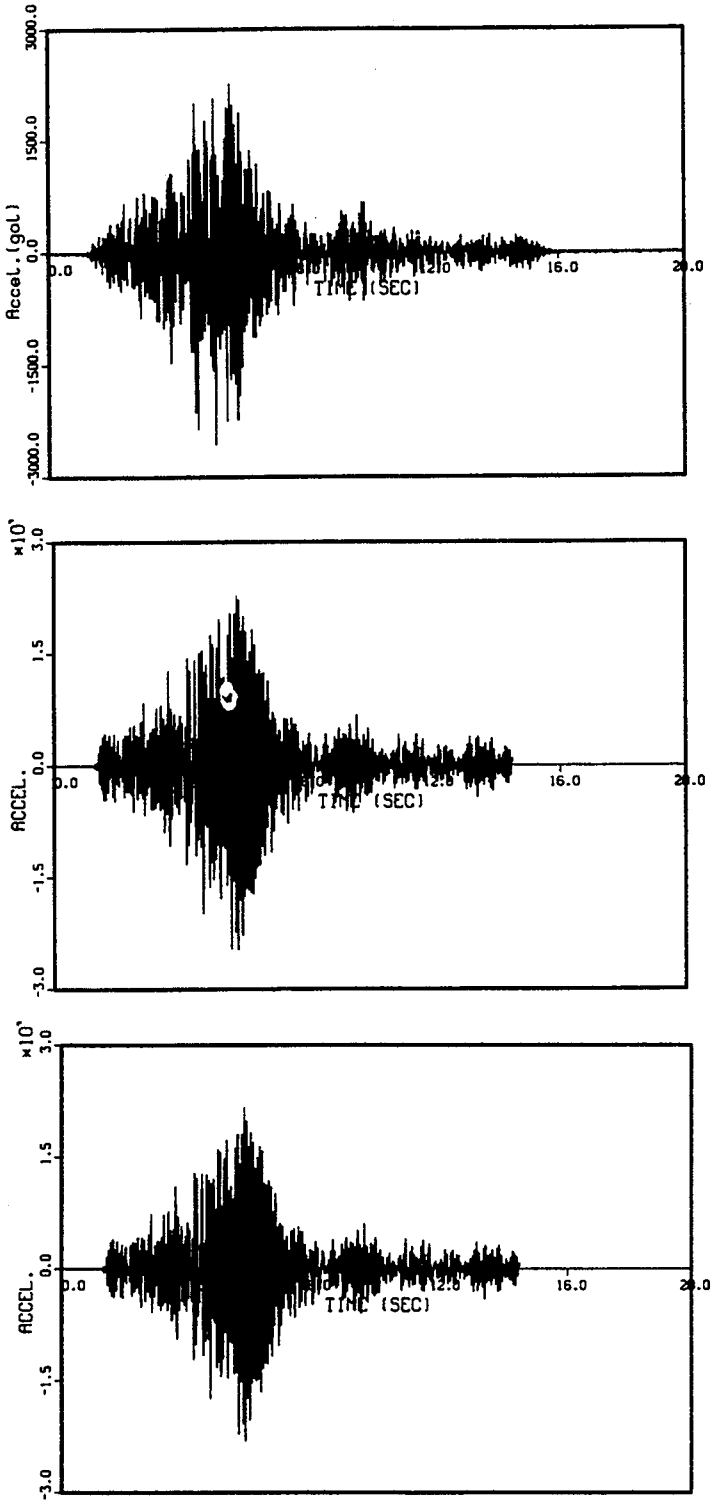

a) Recorded
(Peak: Ax=2.63 g)

(b) Original Analysis
(Peak: Ax=2.53 g)

(c) Filtered Analysis Result
(Peak: Ax=2.36 g)

Figure 5.26 Comparison of Acceleration Time Histories, FA3-X, for Test Run 1.0 S2(F)

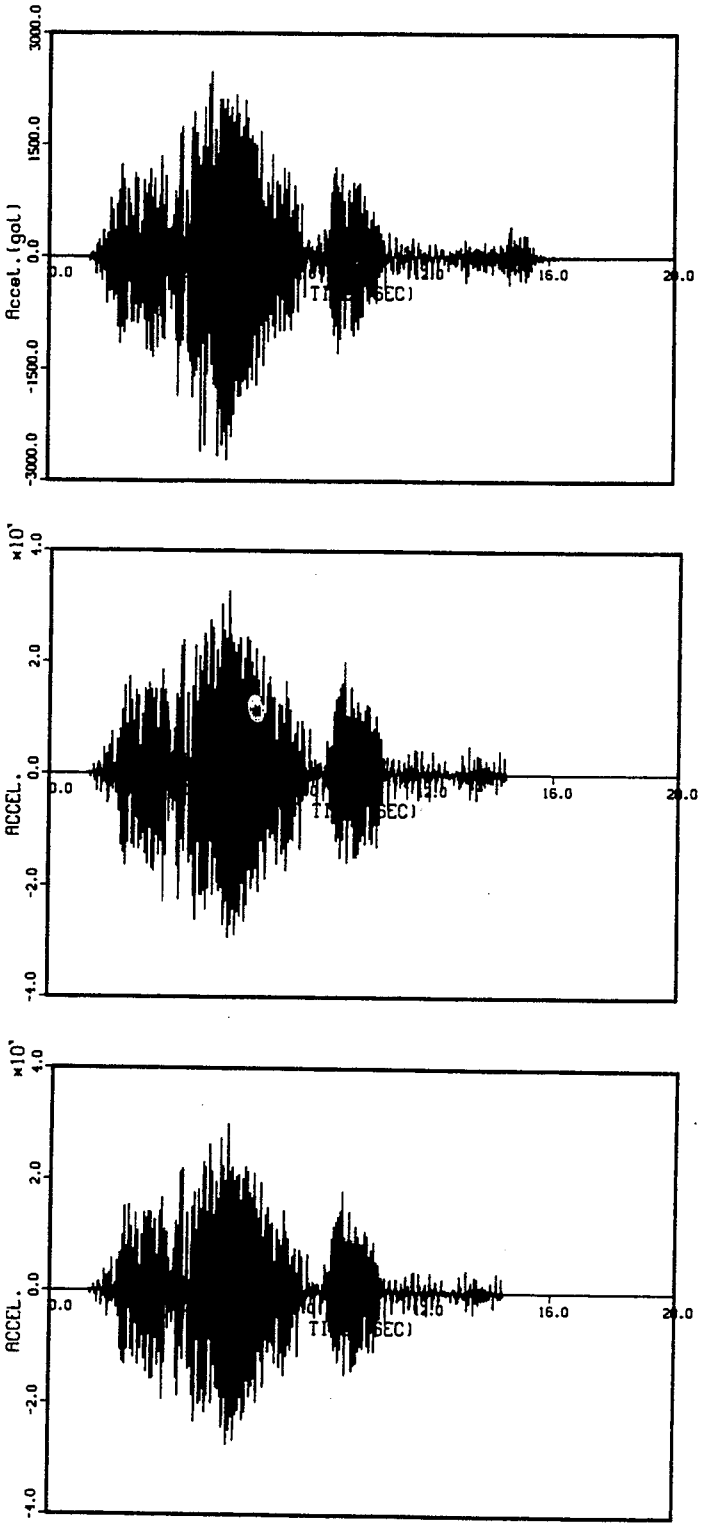

a) Recorded
(Peak: Ax=2.78 g)

(b) Original Analysis
(Peak: Ax=3.35 g)

Filtered Analysis Result
(Peak: Ax=3.07 g)

Figure 5.27 Comparison of Acceleration Time Histories, FA10-X, for Test Run 1.0 S2(F)

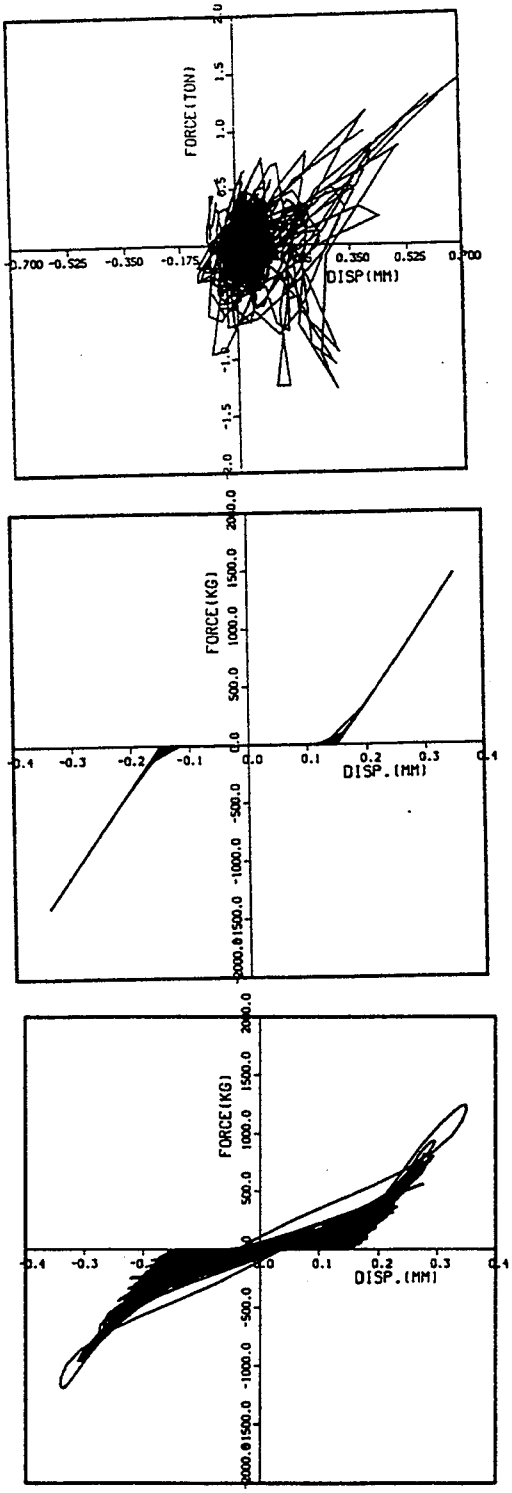

a) Recorded
(Peak: U=0.68 mm
f=1.39 ton)

(b) Original Analysis
(Peak: U=0.35 mm
f=1.47 ton)

(c) Filtered Analysis Result
(Peak: U=0.35 mm
f=1.24 ton)

Figure 5.28 Comparison of Force-Deformation Relationships of Snubber, FR3, for Test Run 1.0 S2(F)

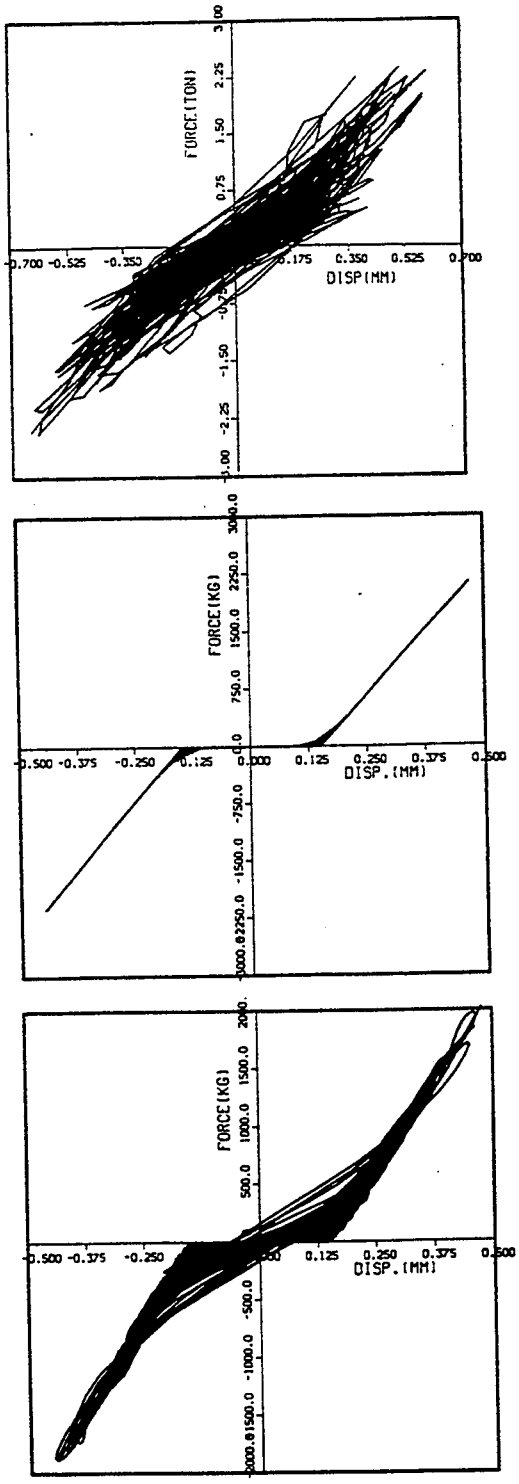

(a) Recorded
(Peak: U=0.63 mm
f=2.42 ton)

(b) Original Analysis
(Peak: U=0.47 mm
f=3.38 ton)

(c) Filtered Analysis Result
(Peak: U=0.47 mm
f=3.06 ton)

Figure 5.29 Comparison of Force-Deformation Relationships of Snubber, FR8, for Test Run 1.0 S2(F)

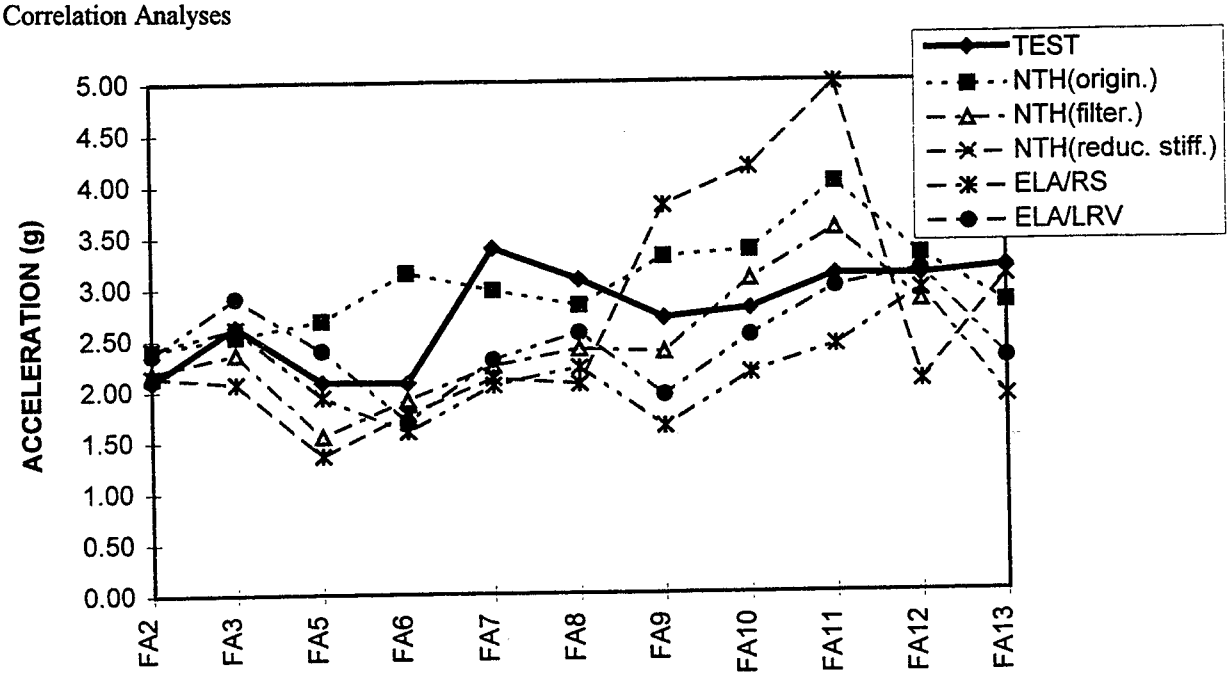

Figure 5.30 Comparison of Responses of F-line for S2(F) Test Run, X-Direction Acceleration

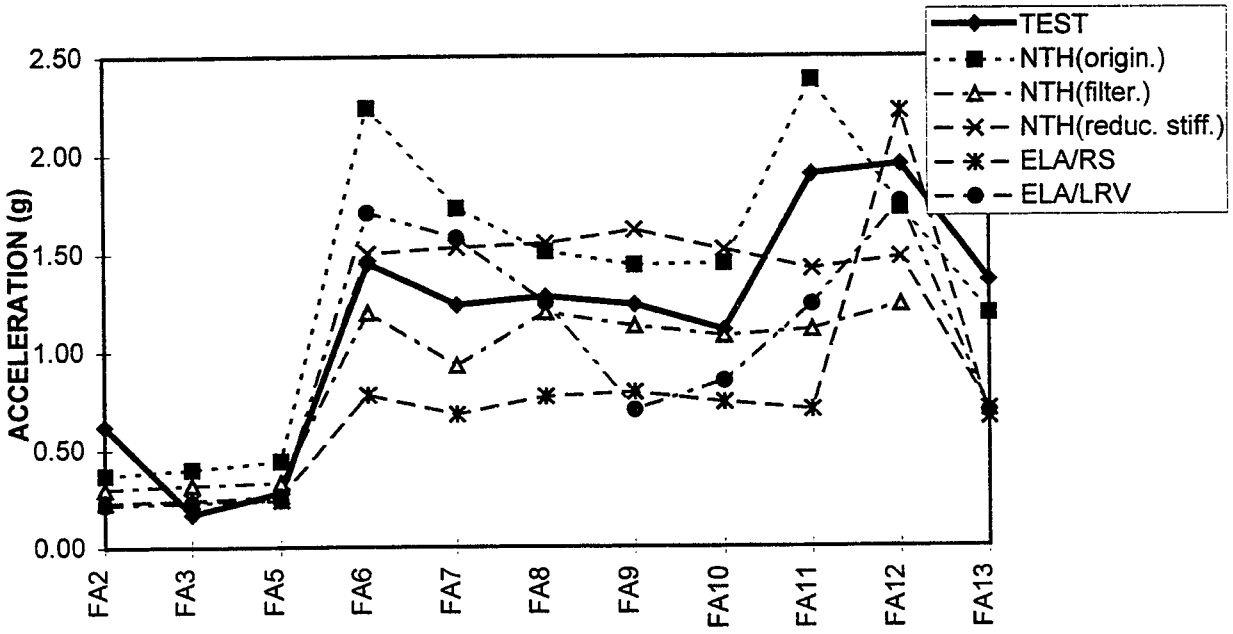

Figure 5.31 Comparison of Responses of F-line for S2(F) Test Run, Y-Direction Acceleration

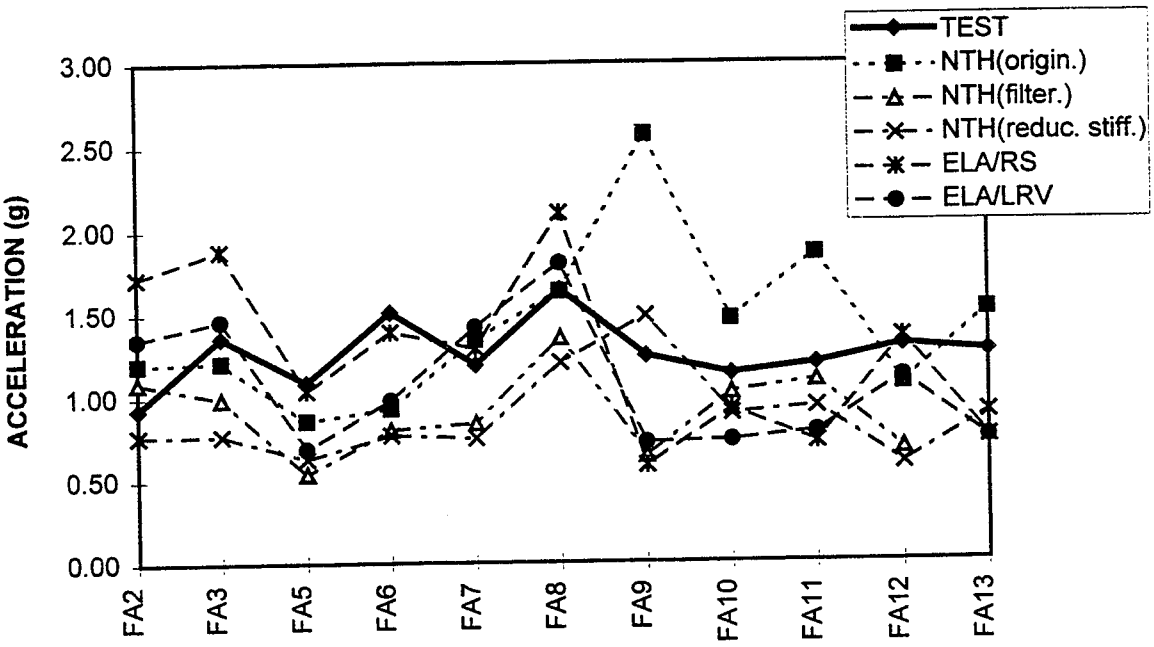

Figure 5.32 Comparison of Responses of F-line for S2(F) Test Run, Z-Direction Acceleration

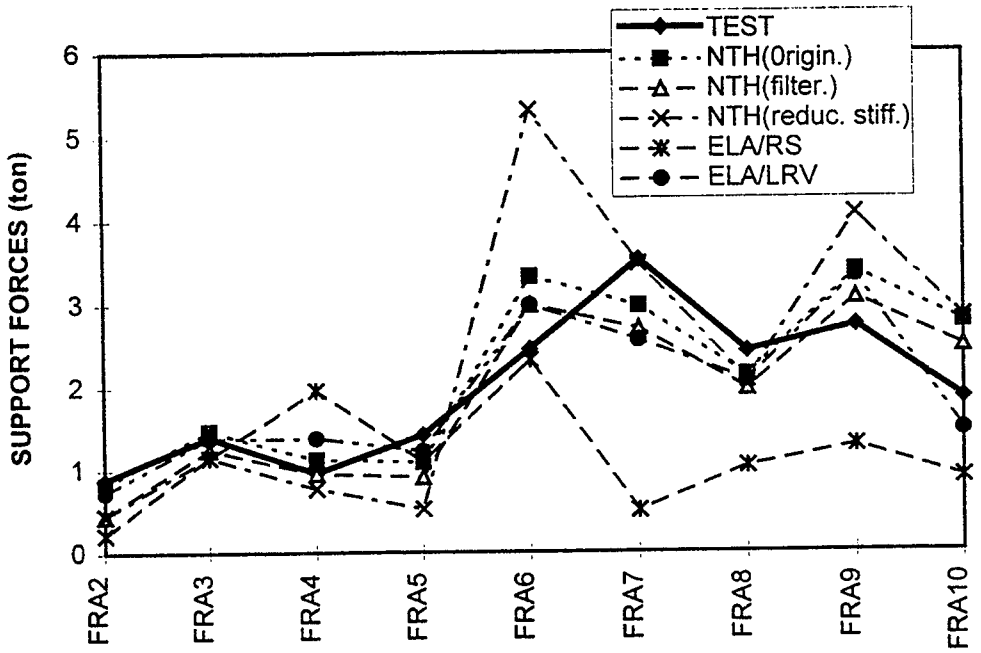

Figure 5.33 Comparison of Responses of F-line for S2(F) Test Run, Support Forces

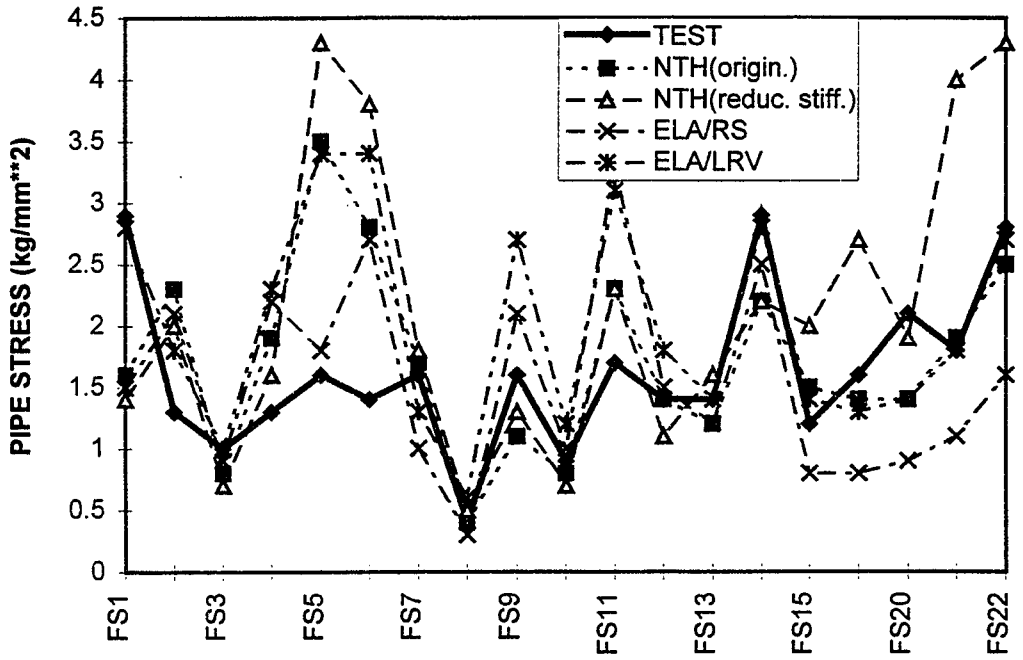

Figure 5.34 Comparison of Responses of F-line for S2(F) Test Run, Pipe Stresses

Table 5.10 Response of F-line with Conventional Supports for 1.3 S2 (F) Test Run

(a) Acceleration (g)

Insturment Node	Direction	Test	NTH(*1)		ELA (*2)	
			A	B	RS	LRV
FA2/40	X	2.58	3.04	2.77	3.60	3.67
	Y	0.71	0.43	0.32	0.36	0.29
	Z	1.00	1.42	1.28	1.39	1.32
FA3/90	X	3.21	3.52	3.09	3.96	4.10
	Y	0.23	0.46	0.34	0.39	0.30
	Z	1.63	1.38	1.14	1.39	1.86
FA5/180	X	1.66	2.64	1.78	2.68	1.78
	Y	0.29	0.49	0.35	0.41	0.32
	Z	0.32	1.16	0.74	0.83	0.98
FA6/240	X	2.86	3.34	2.66	2.03	3.21
	Y	1.76	2.78	1.39	0.87	1.92
	Z	1.81	1.10	0.87	1.17	1.27
FA7/280	X	3.67	3.57	2.74	2.85	2.99
	Y	1.30	1.93	1.12	0.65	1.69
	Z	1.46	2.59	1.37	1.78	1.85
FA8/330	X	3.54	3.23	2.83	3.15	3.36
	Y	1.31	2.05	1.39	0.83	0.83
	Z	1.96	2.24	1.94	3.18	2.70
FA9/390	X	3.41	4.26	2.76	2.16	2.56
	Y	1.42	1.87	1.41	0.84	0.86
	Z	1.17	3.35	0.87	0.59	0.84
FA10/440	X	3.75	4.14	3.67	2.73	3.37
	Y	1.14	1.95	1.41	0.79	0.80
	Z	1.20	2.20	1.01	1.18	1.04
FA11/500	X	3.76	4.66	4.25	2.99	3.84
	Y	2.09	2.56	1.27	1.30	1.90
	Z	1.42	2.41	1.12	1.00	0.71
FA12/550	X	4.35	3.94	3.43	4.24	4.18
	Y	2.58	1.94	1.52	2.63	2.20
	Z	1.46	1.21	0.83	1.23	1.38
FA13/790	X	3.09	3.47		2.29	2.95
	Y	1.21	1.43		0.92	1.58
	Z	1.43	1.77		1.11	1.35

*Note: (*1) Nonlinear time history analyses (A = original analysis; B = filtered results)
(*2) Equivalent Linearization Analyses (RS = response spectrum approach; LRV = linear random vibration approach

Table 5.10 Response of F-line with Conventional Supports for 1.3 S2 (F) Test Run (Cont'd)

(b) Displacement (mm)

Instrument Element	Test	NTH	ELA	
			RS	LRV
FD2b/201	0.41	0.29	0.24	0.31
FD3b/202	0.69	0.40	0.40	0.43
FD4b/203	0.62	0.36	0.24	0.45
FD5b/204	0.73	0.43	0.36	0.47
FD6b/205	0.91	0.64	0.44	0.63
FD7a,b/206	0.51(1.02)	0.70	0.38	0.71
FD8a,b/207	0.45 (0.88)	0.58	0.38	0.60
FD9b/208	0.73	0.79	0.45	0.75
FD10b/209	0.76	0.58	0.28	0.55

(1*) Recorded displacements are b-measurement, and ( ) indicates a-measurements

(c) Support Forces (ton)

Instrument Element	Test	NTH		ELA	
		A	B	RS	LRV
FR2/201	1.13	1.03	0.61	0.66	1.17
FR3/202	1.70	1.83	1.52	1.92	2.15
FR4/203	1.18	1.41	1.29	0.74	1.86
FR5/204	2.06	1.33	1.13	1.09	1.55
FR6/205	3.64	3.82	3.59	2.40	3.98
FR7/206	4.13	3.70	3.43	1.28	3.63
FR8/207	3.40	2.86	2.74	1.58	3.10
FR9/208	3.25	3.97	3.64	1.92	3.84
FR10/209	2.31	3.23	2.92	0.65	2.84

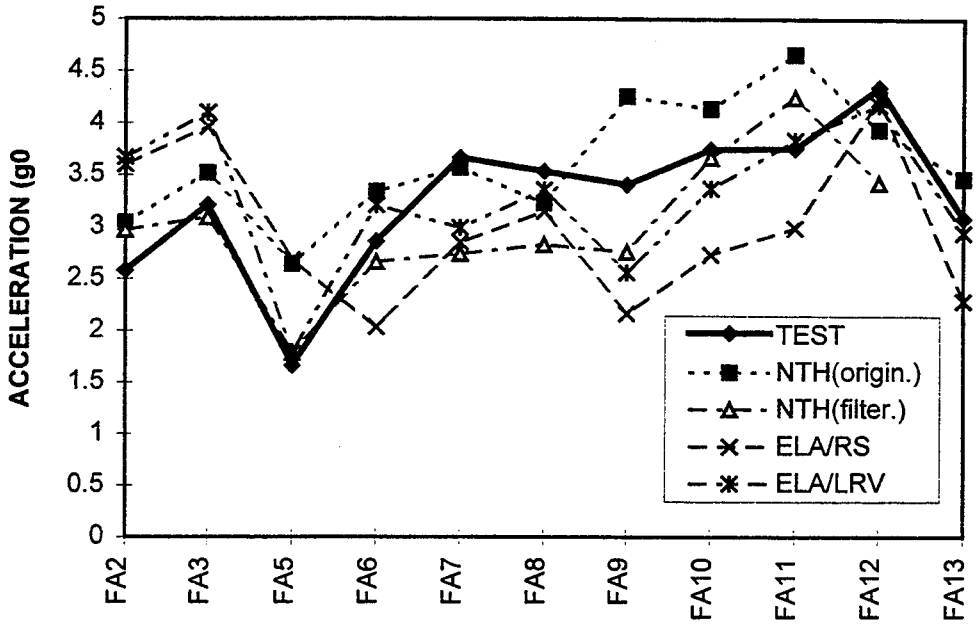

Figure 5.35 Comparison of Responses of F-line for 1.3 S2(F) Test Run, X-Direction

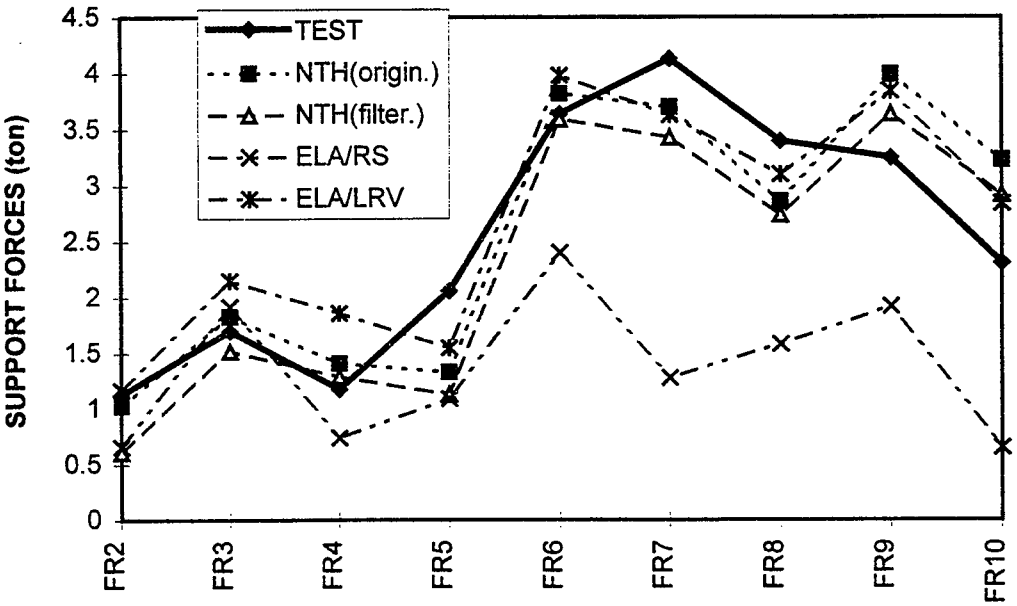

Figure 5.36 Comparison of Responses of F-line for 1.3 S2(F) Test Run, Support Forces

Table 5.11 Response of M-line with LED Supports and Actuator for S2(A) Test Run

(a) Acceleration (g)

Instrument	Direction	Test	NTH	LRV
AA1/10	X Y Z	4.42 0.33 0.45	4.46 0.11 0.40	4.55 0.11 0.40
MA1/50	X Y Z	3.80 5.60 2.02	5.53 3.79 6.09	4.32 3.36 4.68
MA16/90	X Y Z	3.37 7.44 2.22	4.39 4.79 2.22	3.57 4.90 1.34
MA17/130	X Y Z	4.74 2.25 1.97	5.16 1.71 2.60	5.54 1.46 2.36
MA4/150	X Y Z	3.38 2.78 2.06	3.94 2.37 1.98	3.70 2.26 1.89
MA5/165	X Y	2.70 2.85	2.76 2.33	2.89 2.27
MA6/180	X Y	2.18 2.98	2.31 2.16	2.00 2.26
MA8/200	X Y Z	2.29 2.75 4.99	1.88 2.41 1.76	1.89 1.99 2.05
MA10/250	X Y Z	2.06 1.39 5.61	3.42 2.37 2.71	3.44 2.08 2.19

(b) Displacement (mm)

Instrument/Element	Direction	Test	NTH	LRV
AD1/N-10	X Y Z	2.95 0.25 0.19	3.02 0 0	3.12 0 0
MD15/LED-1 MD16/LED-2 MD17/LED-3		2.6 5.2 4.5	2.92 5.10 2.72	2.44 4.11 2.27
MD18/N-150	X Y Z	5.5 4.8 4.6	5.17 5.32 3.04	4.37 4.58 2.46

Table 5.11 Response of M-line with LED Supports and Actuator for S2(A) Test Run (Cont'd)

(c) Support Forces (ton)

Instrument/Element	Test	NTH	LRV
MR8/106	5.91	4.15	---
MRI5/LED-1	1.60	1.64	---
MR16/LED-2	1.81	1.77	---
MR17/LED-3	1.01	0.94	---

(d) Pipe Stress (kg/mm^2)

Instrument/Element	Stress Intensification Factor	Test	NTH	LRV
MS1/3	2.0	9.1	7.38	6.97
MS2'/5	1.0	4.7	3.58	3.36
MS2/7	1.0	1.8	1.72	2.81
MS3/9	2.0	5.5	3.20	3.97
MS4/14	1.0	3.0	1.44	2.02
MS5/17	2.0	4.3	4.74	4.08
MS6/46	1.0	4.1	2.38	3.61
MS8/23	1.0	2.0	2.33	2.14
MS9/25	1.0	3.7	2.72	3.34
MS10/30	1.0	2.2	1.58	1.53

Table 5.12 Comparison of Vibration Frequencies of M-line with Actuator Obtained from Equivalent Linearization Analyses for S2(A) Test

Mode	Linear	1/3 S2(A)	1.0 S2(A)	1.3 S2(A)
2	10.08	9.21	8.59	8.20
3	12.44	10.53	10.18	9.94
4	14.74	14.08	12.5	12.07
5	16.20	15.08	14.74	14.75

Table 5.13 Comparison of Equivalent Modal Damping Obtained from Equivalent Linearization Analyses for S2(A) Tests

Mode	Analyses (%)			
	Linear	1/3 S2(A)	1.0 S2(A)	1.3 S2(A)
2	2.5	6.1	9.8	13.5
3	2.5	6.9	7.0	6.7
4	2.5	4.4	12.1	14.8
5	2.5	3.7	2.8	2.7

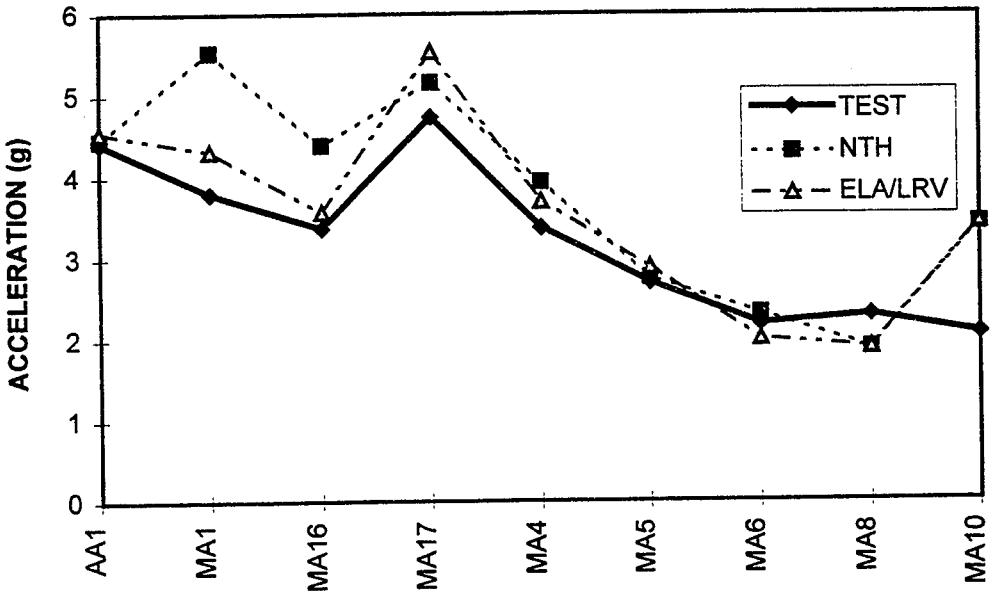

Figure 5.37 Comparison of Responses of M-line with LED Supports for S2(A) Test Run, X-Direction Acceleration

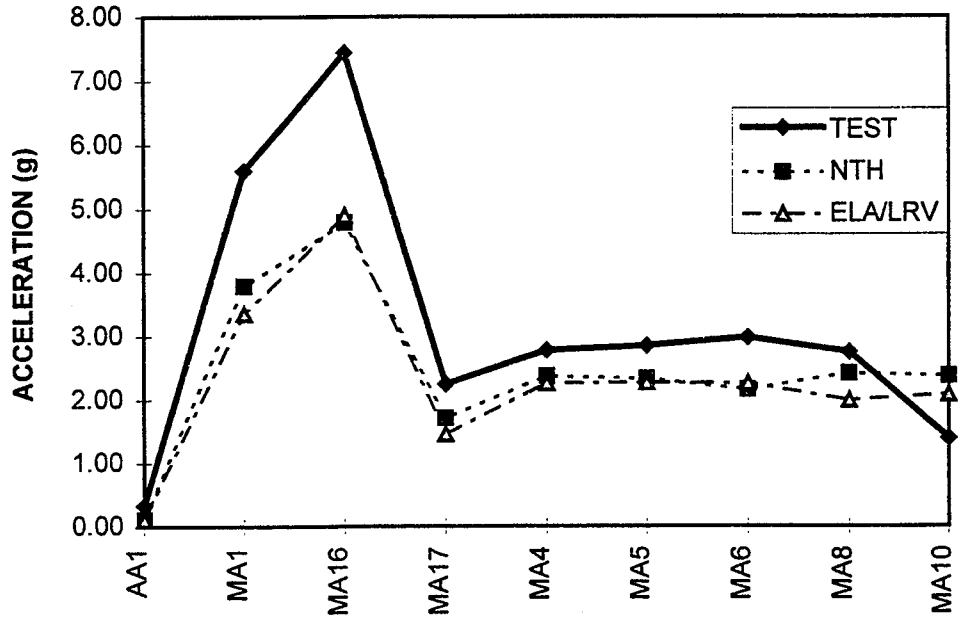

Figure 5.38 Comparison of Responses of M-line with LED Supports for S2(A) Test Run, Y-Direction Acceleration

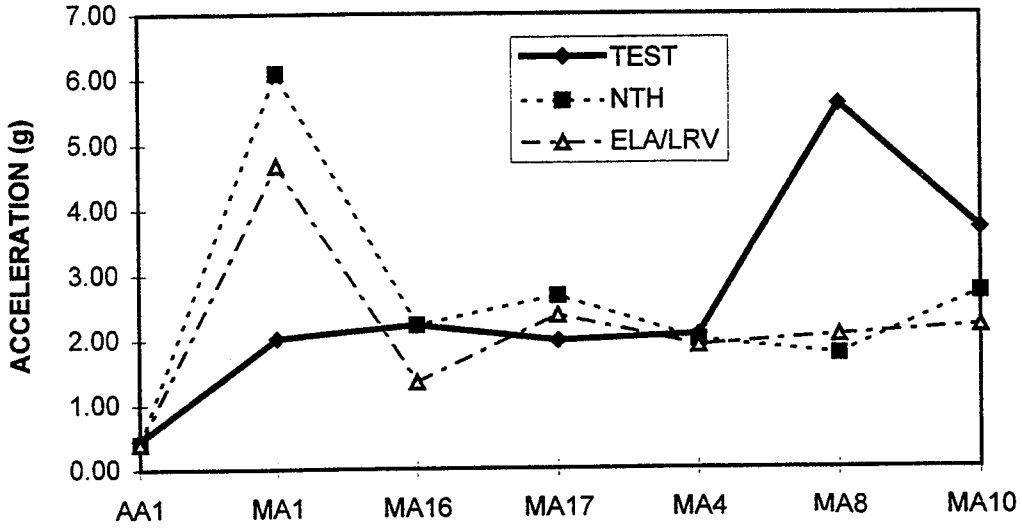

Figure 5.39 Comparison of Responses of M-line with LED Supports for S2(A) Test Run, Z-Direction Acceleration

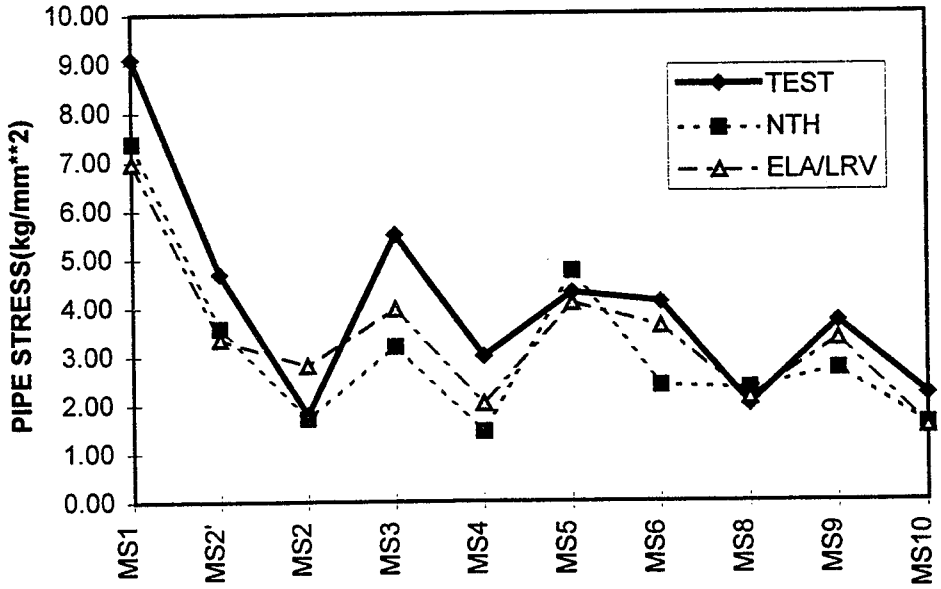

Figure 5.40 Comparison of Responses of M-line with LED Supports for S2(A) Test Run, Pipe Stresses

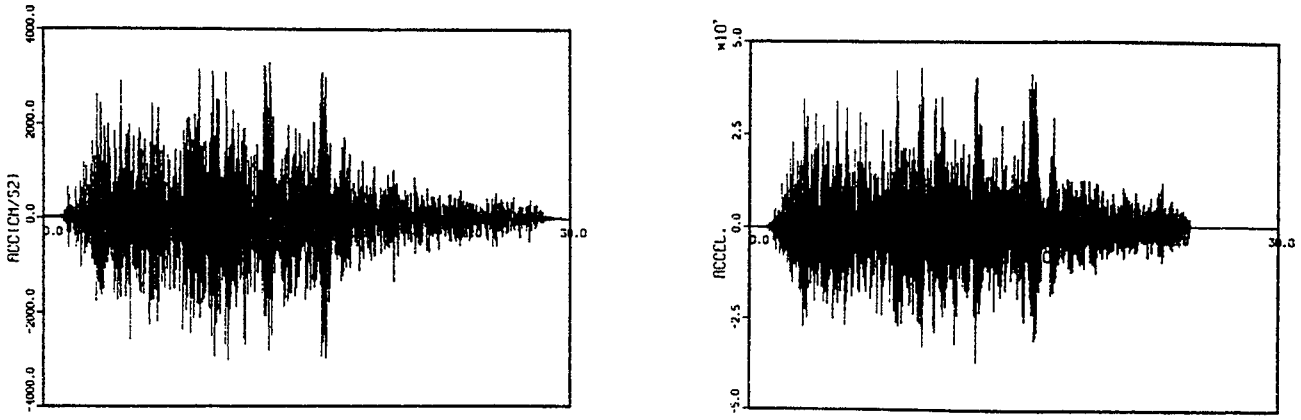

Recorded
(Peak: Ax=3.37g)

Analysis
(Peak: Ax=4.39g)

(a) MA16-X

Figure 5.41 Comparison of Acceleration Time Histories of M-line with LED Support for S2 (A) Test Run

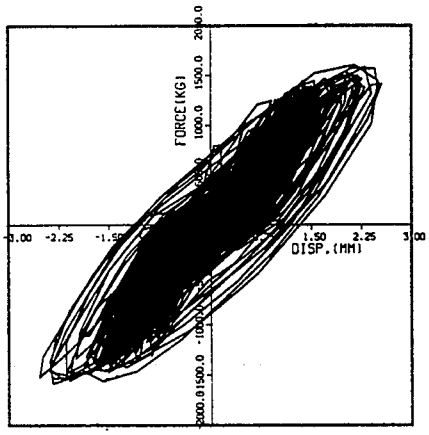

Recorded
(Peak: U=2.6 mm)

(a) LED-1

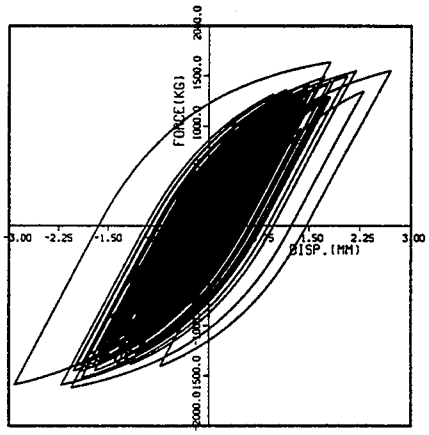

Analysis
(Peak: U=2.92 mm)

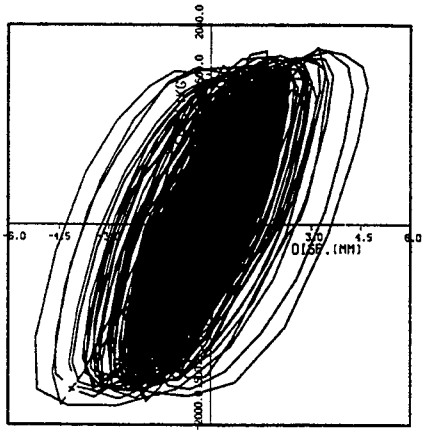

Recorded
(Peak: U=5.2 mm)

(b) LED-2

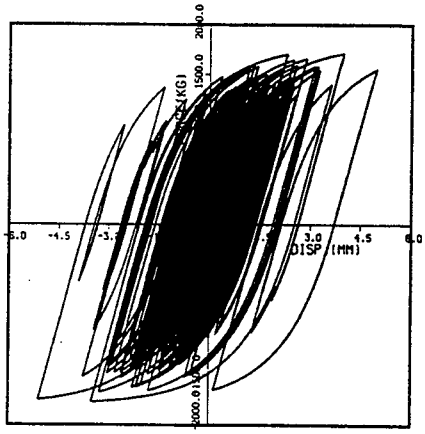

Analysis
(Peak: U=5.10 mm)

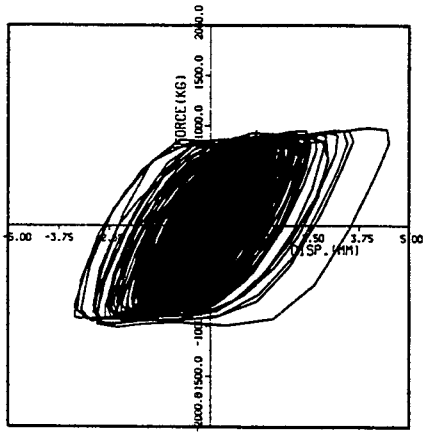

Recorded
(Peak: U=4.5 mm)

(c) LED-3

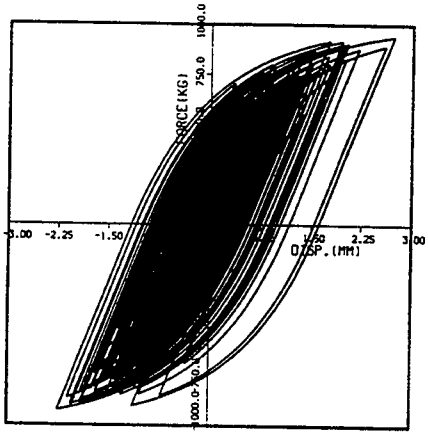

Analysis
(Peak: U=2.72 mm)

Figure 5.42 Comparisons of Force-Deformation Relationships of LED Supports of M-line for S2(A) Test Run

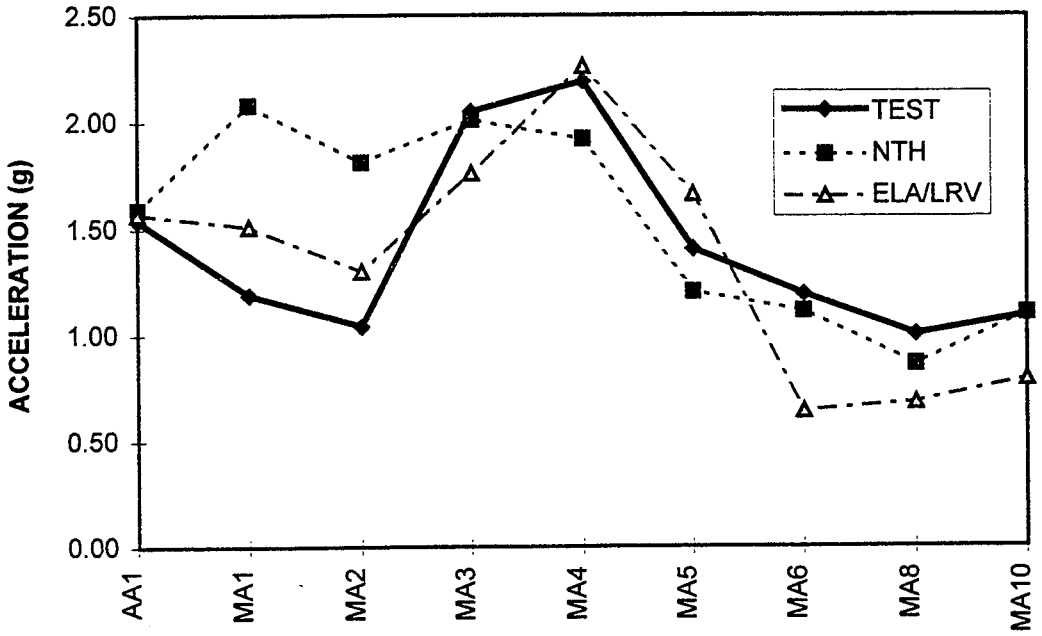

Figure 5.43 Comparison of Responses of M-line with LED Supports for 1/3 S2(A) Test Run, X-Direction Acceleration

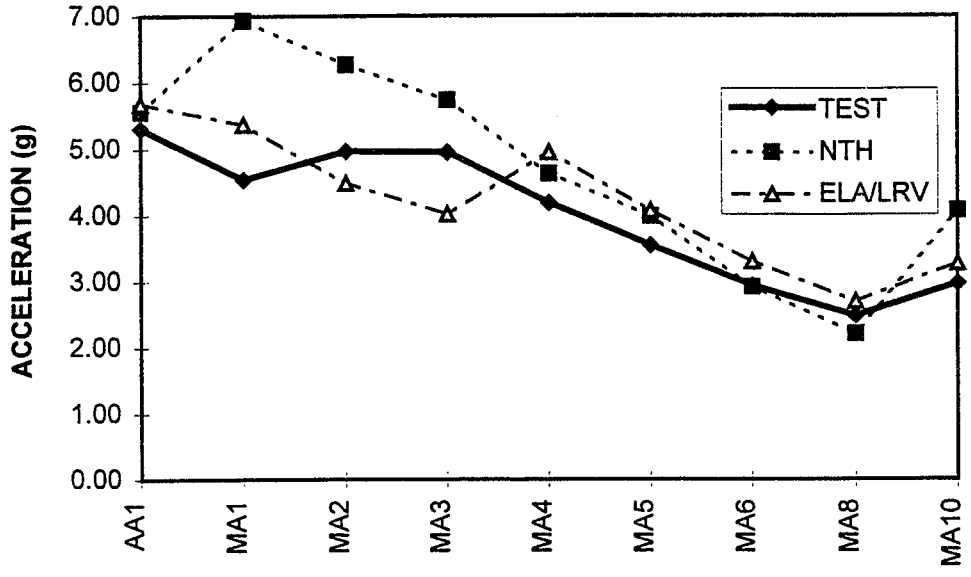

Figure 5.44 Comparison of Responses of M-line with LED Supports for 1.3 S2(A) Test Run, X-Direction Acceleration

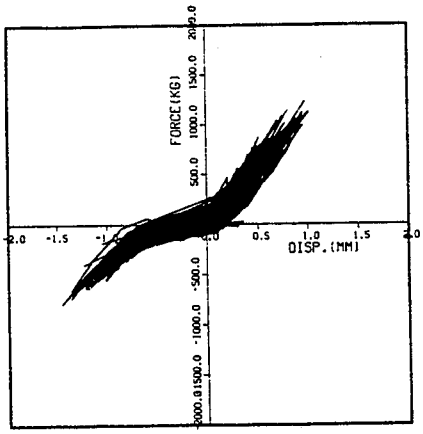

Recorded
(Peak: U=1.40 mm)

(a) LED-1

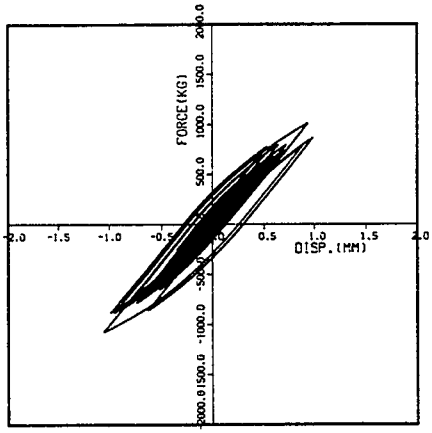

Analysis
(Peak: U=1.06 mm)

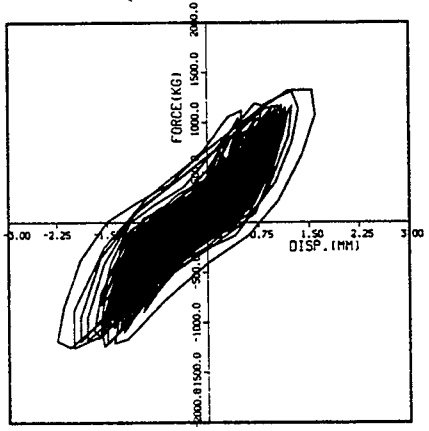

Recorded
(Peak: U=2.25 mm)

(b) LED-2

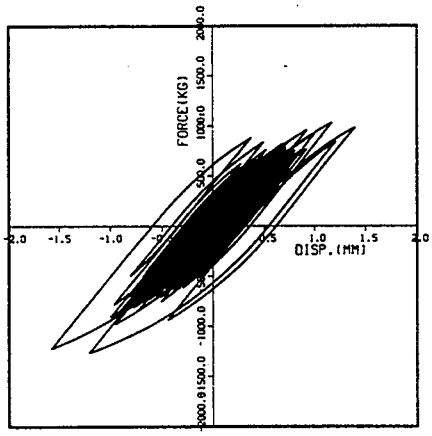

Analysis
(Peak: U=1.58 mm)

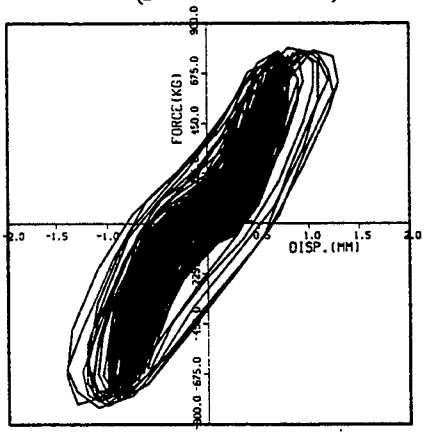

Recorded
(Peak: U=1.40 mm)

(c) LED-3

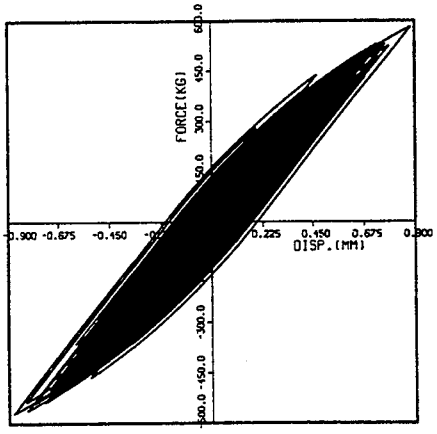

Analysis
(Peak: U=0.88 mm)

Figure 5.45 Comparisons of Force-Deformation Relationships of LED Supports of M-line for 1/3 S2(A) Test Run

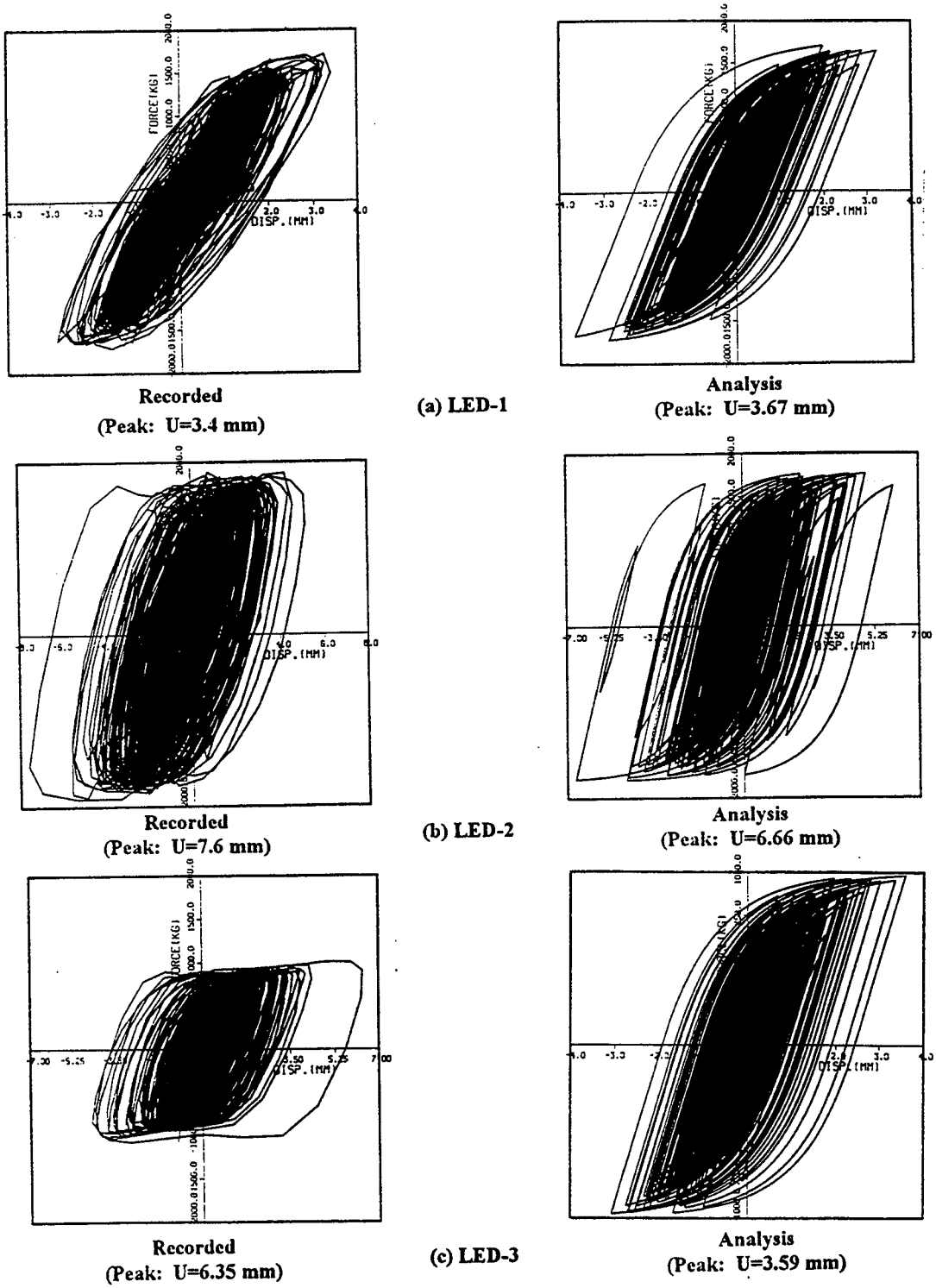

Recorded
(Peak: U=3.4 mm)

(a) LED-1

Analysis
(Peak: U=3.67 mm)

Recorded
(Peak: U=7.6 mm)

(b) LED-2

Analysis
(Peak: U=6.66 mm)

Recorded
(Peak: U=6.35 mm)

(c) LED-3

Analysis
(Peak: U=3.59 mm)

Figure 5.46 Comparison of Force-Deformation Relationships for LED Supports of M-line for 1.3 S2(A) Test Run

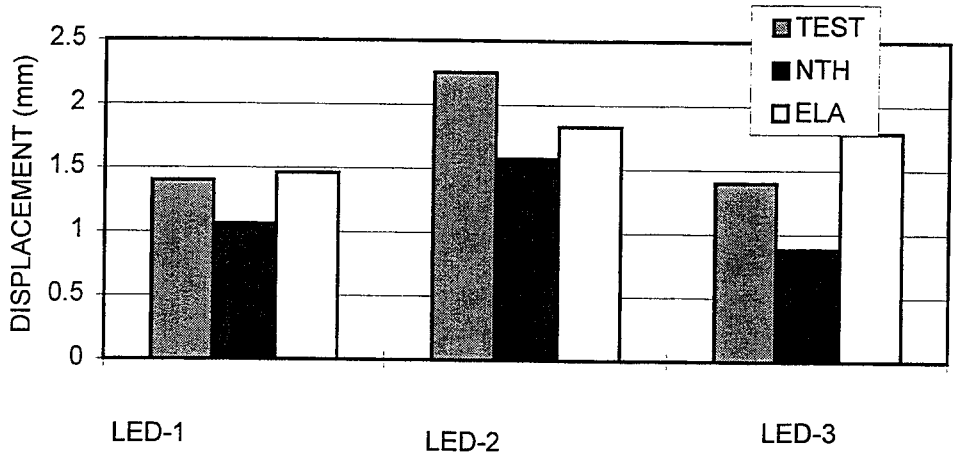

(a) 1/3 S2(A)

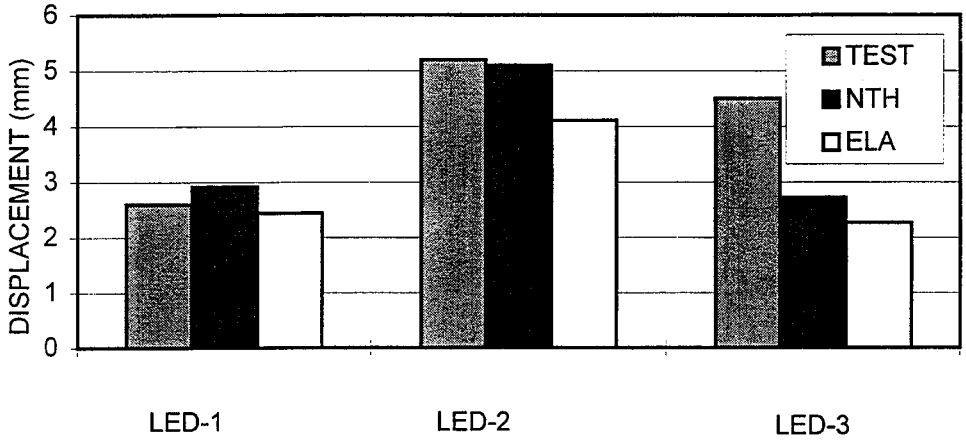

(b) 1.0 S2(A)

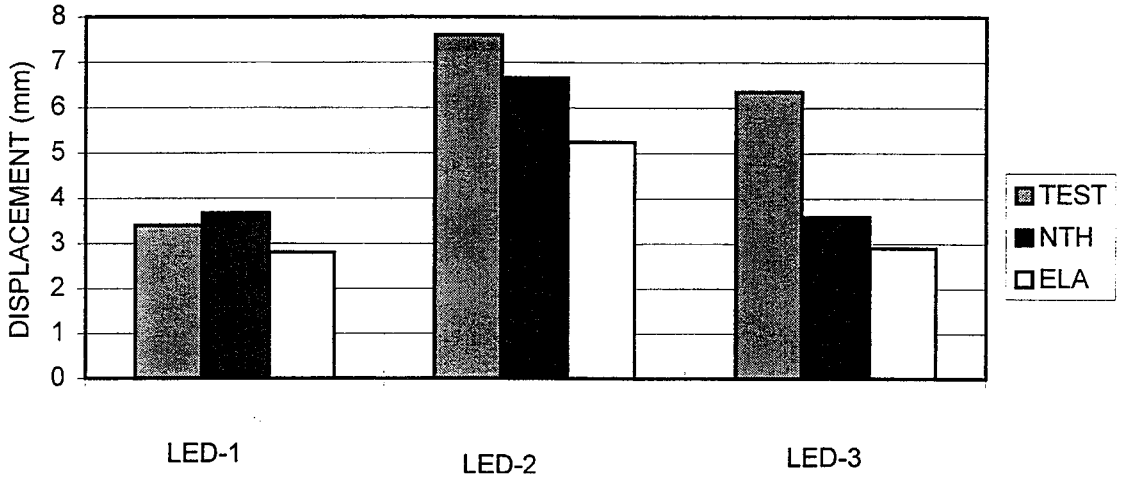

(c) 1.3 S2(A)

Figure 5.47 Comparison of Peak Displacements of LED Supports for M-line with Actuator

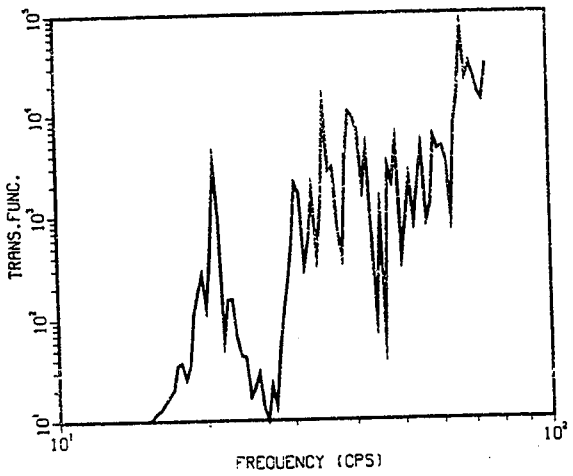

(a) 1/3 S2(A)

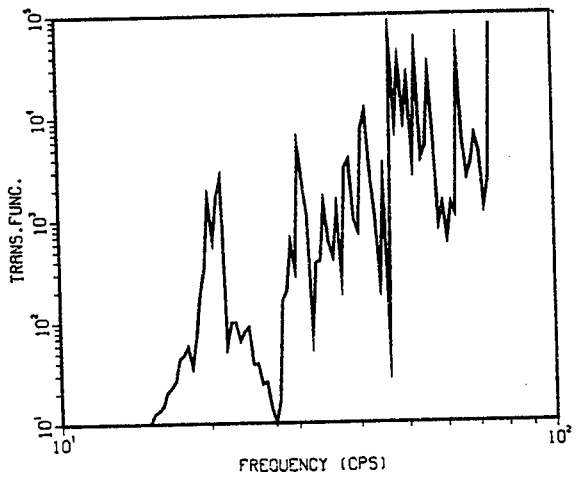

(b) 1.0 S2(A)

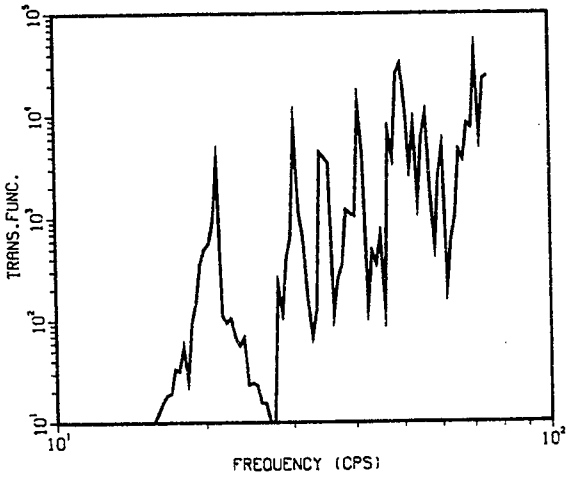

(c) 1.3 S2(A)

Figure 5.48 Transfer Functions of X-Direction Acceleration for M-line with LED Supports for AA1-X

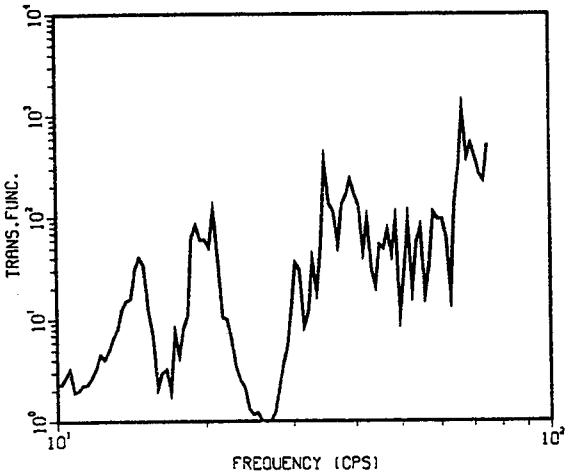

(a) 1/3 S2(A)

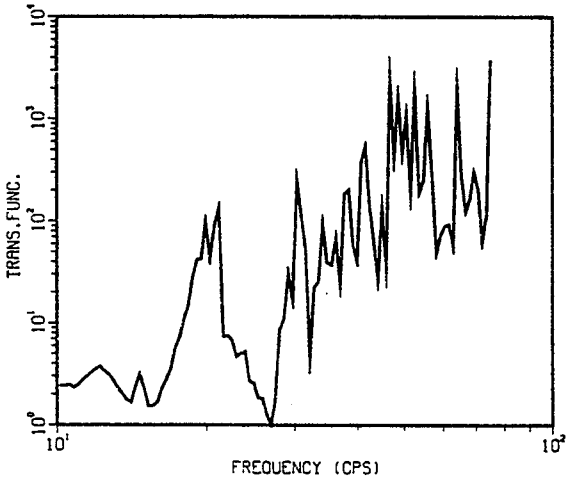

(b) 1.0 S2(A)

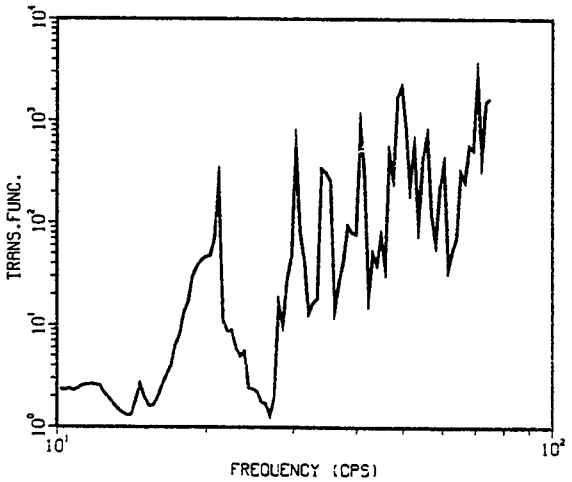

(c) 1.3 S2(A)

Figure 5.49 Transfer Functions of X-Direction Acceleration for M-line with LED Supports for MA17-X

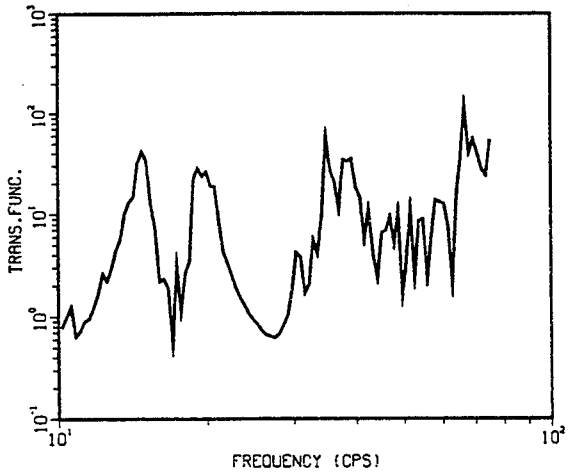

(a) 1/3 S2(A)

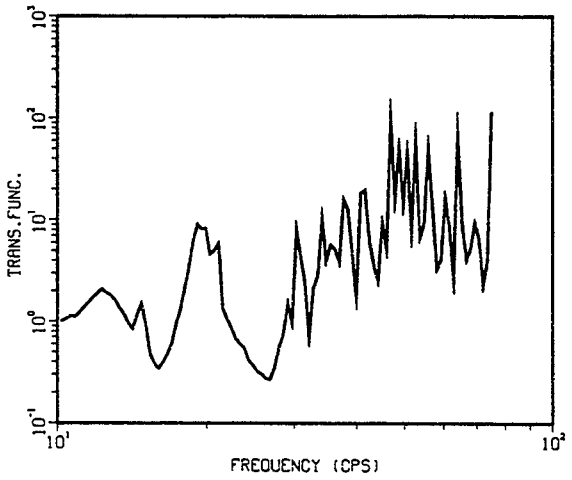

(b) 1.0 S2 (A)

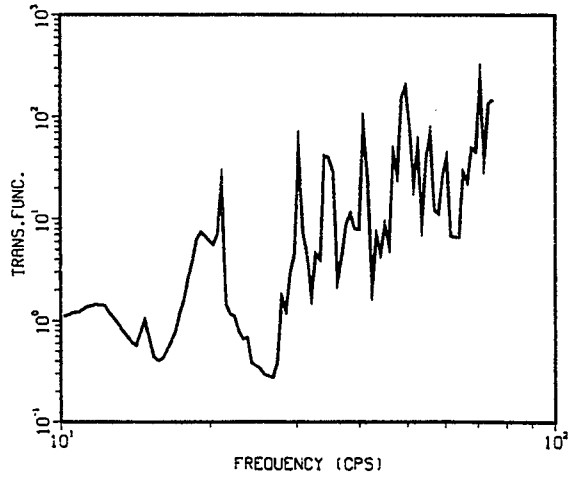

(c) 1.3 S2(A)

Figure 5.50 Transfer Functions of X-Direction Acceleration for M-line with LED Supports for MA5-X

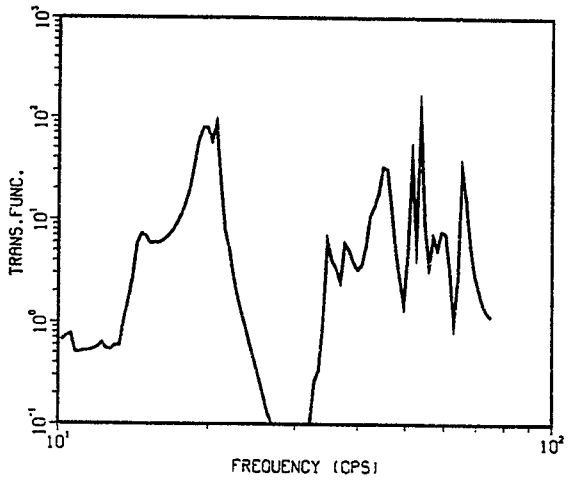

(a) 1/3 S2(A)

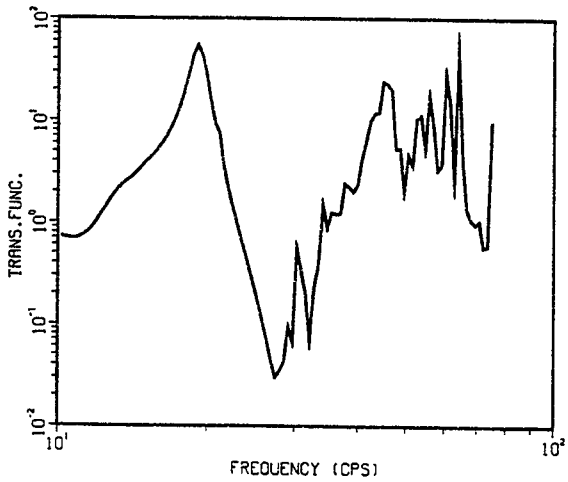

(b) 1.0 S2(A)

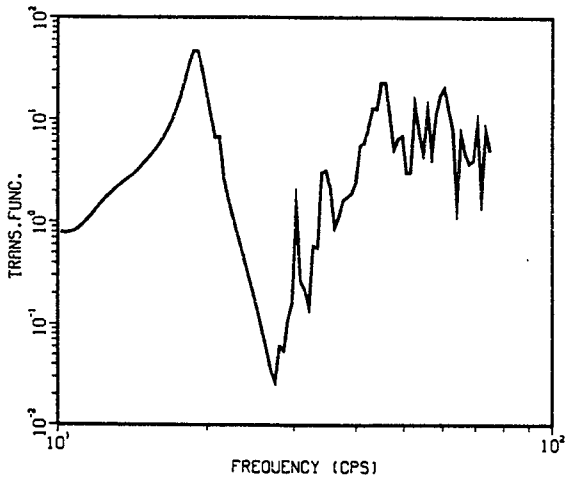

(c) 1.3 S2(A)

Figure 5.51 Transfer Functions of X-Direction Acceleration for M-line with LED Supports for MA10-X

Table 5.14 Responses of M-line with LED Supports for Margin Test, 2.5 S2(A)

(a) Acceleration (g)

Instrument/Node Num.	Direction	Test	NTH(*1)		ELA	
			A	B	RS	LRV
MA1/50	X	5.65	3.24	3.69	4.05	3.94
	Y	9.17	3.38	6.50	4.02	5.21
	Z	3.01	2.10	2.99	2.82	2.79
MA16/90	X	6.05	3.85	5.10	5.47	5.58
	Y	12.11	4.42	8.36	5.33	6.32
	Z	3.55	2.60	4.93	4.44	3.21
MA17/130	X	6.27	6.02	6.49	6.83	5.79
	Y	4.21	3.45	3.07	3.66	3.10
	Z	3.84	2.60	4.93	4.45	3.21
MA4/150	X	5.14	5.56	5.86	7.84	5.37
	Y	4.72	4.84	5.95	4.70	5.28
	Z	3.74	2.37	4.61	3.99	2.76
MA5/165	X	4.06	3.78	5.42	5.44	3.92
	Y	4.92	4.88	6.01	4.71	5.30
MA6/180	X	4.23	2.78	4.28	5.04	3.92
	Y	5.25	4.86	6.01	4.68	5.28
MA8/200	X	4.31	2.92	3.54	5.18	3.45
	Y	4.73	3.95	5.18	4.03	4.59
	Z	12.00	1.68	3.52	2.55	2.76
MA10/250	X	5.17	5.37	4.62	6.18	5.16
	Y	2.63	1.02	1.00	1.67	1.83
	Z	10.47	4.09	8.32	5.73	6.86

Note (*1): Nonlinear time history analyses (A: 2.5% damping; B: 1% damping).

Table 5.14 Responses of M-line with LED Supports for Margin Test, 2.5 S2(A)

(b) Displacement (mm)

Instrument/Element Num.		Test	NTH		ELA	
			A	B	RS	LRV
MD12, 13/N-90	(X)	21.1	20.7	24.1	16.0	16.6
	(Y)	4.2	12.2	12.9	9.2	10.3
MD15/LED-1		4.7	6.0	6.0	8.6	6.2
MD16/LED-2		10.8	10.7	10.3	8.9	9.5
MD17/LED-3		7.5	8.6	8.9	8.6	6.1
MD18/N-150	(X)	10.2	11.6	14.9	12.2	10.9
	(Y)	9.6	13.3	9.75	9.1	10.9
	(Z)	7.4	9.4	10.2	9.5	6.9

(c) Pipe Stress (kg/mm^2)

Instrument/Element	Stress Intensification Factor	Test	NTH		ELA	
			A	B	RS	LRV
MS1/3	2.0	23.2	10.6	27.2	23.4	19.9
MS2'/5	1.0	11.7	6.9	11.2	9.6	7.8
MS2/7	1.0	3.1	4.0	11.4	7.4	8.1
MS3/9	2.0	8.8	8.0	13.7	8.6	9.3
MS4/14	1.0	6.2	3.2	7.1	5.6	8.1
MS5/17	2.0	9.0	15.6	16.8	23.0	18.6
MS6/46	1.0	5.9	4.5	10.6	6.6	7.4
MS8/23	1.0	4.7	6.1	7.2	8.2	6.2
MS9/25	1.0	6.8	5.6	8.6	7.7	6.1
MS10/30	1.0	4.4	5.1	9.2	6.7	4.8

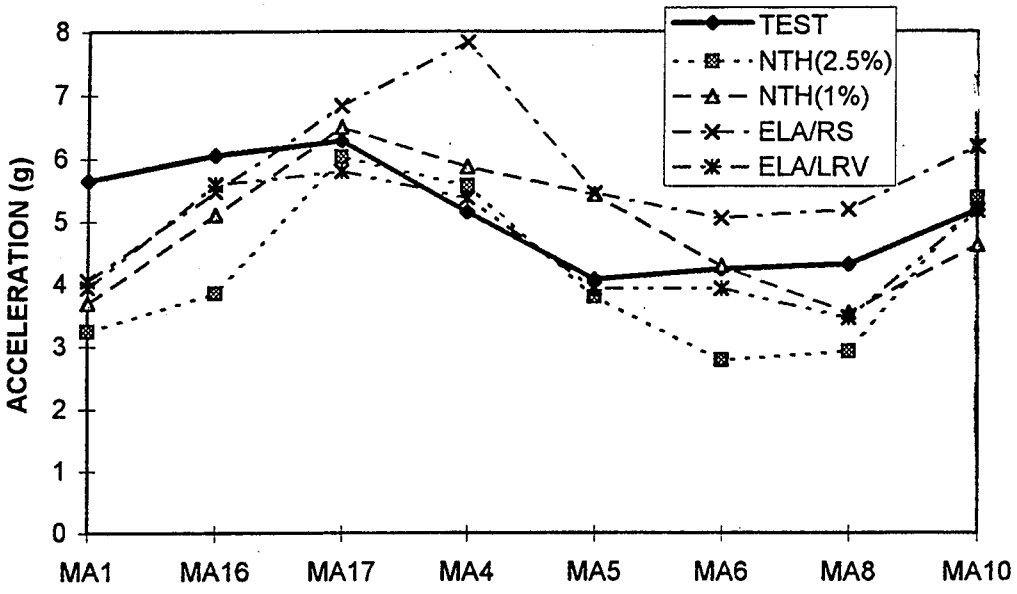

Figure 5.52 Comparison of Responses of M-line with LED Supports Without Actuator for 2.5 S2(A) Test Run, X-Direction Accelerations

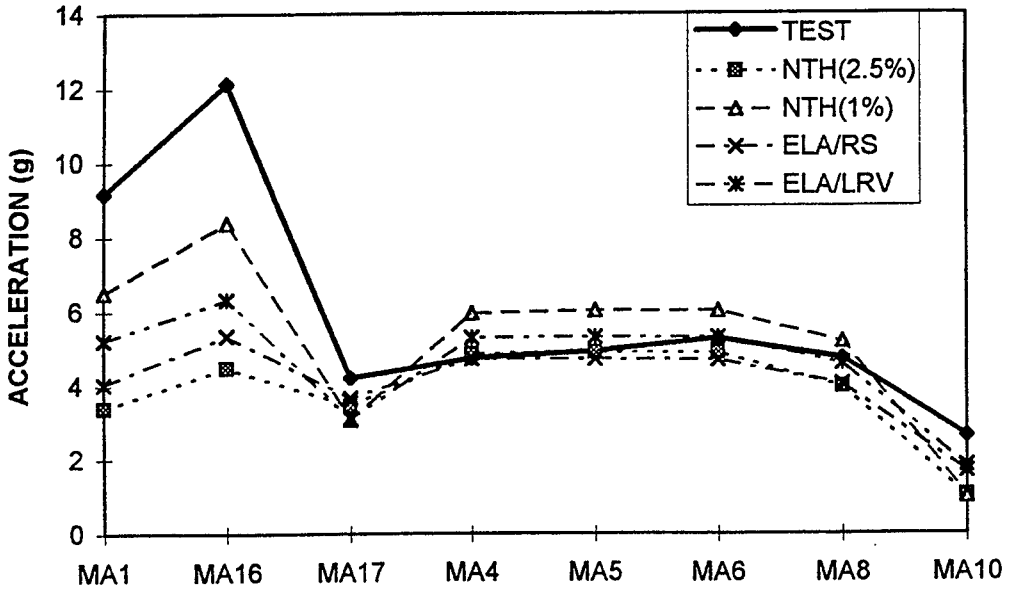

Figure 5.53 Comparison of Responses of M-line with LED Supports Without Actuator for 2.5 S2(A) Test Run, Y-Direction Accelerations

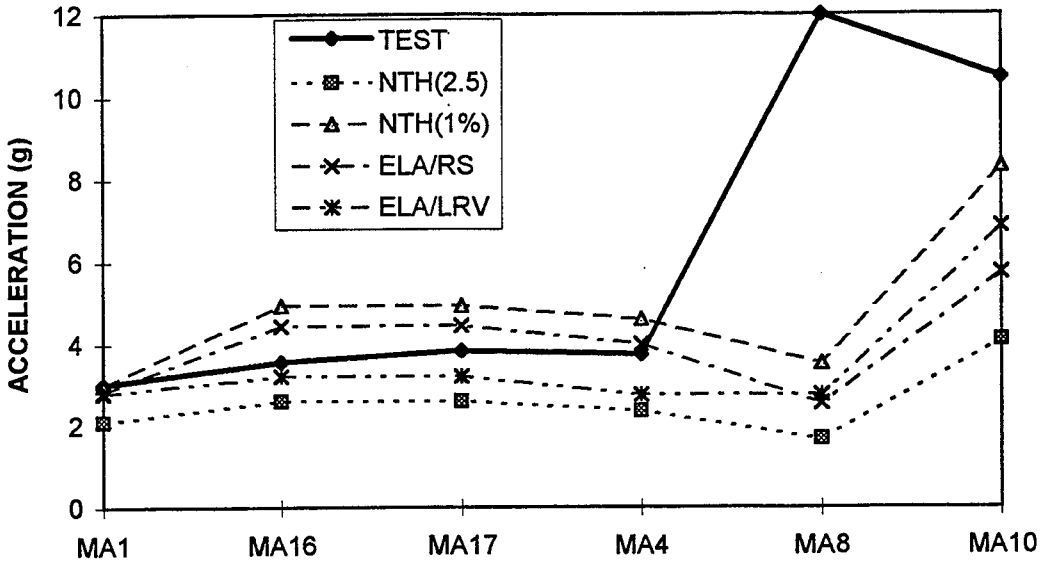

Figure 5.54 Comparison of Responses of M-line with LED Supports Without Actuator for 2.5 S2(A) Test Run, Z-Direction Accelerations

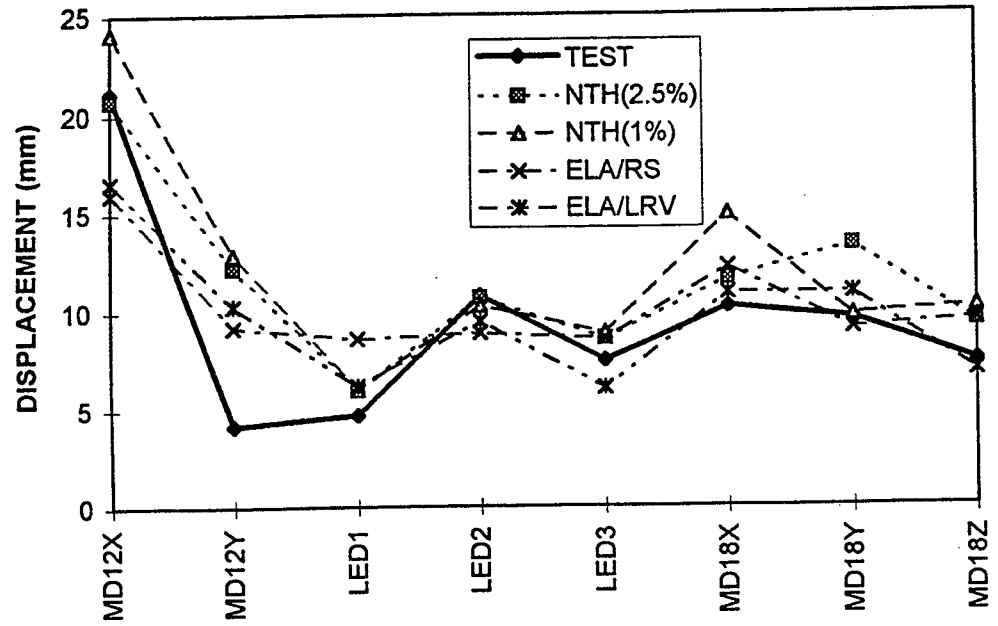

Figure 5.55 Comparison of Responses of M-line with LED Supports Without Actuator for 2.5 S2(A) Test Run, Displacement

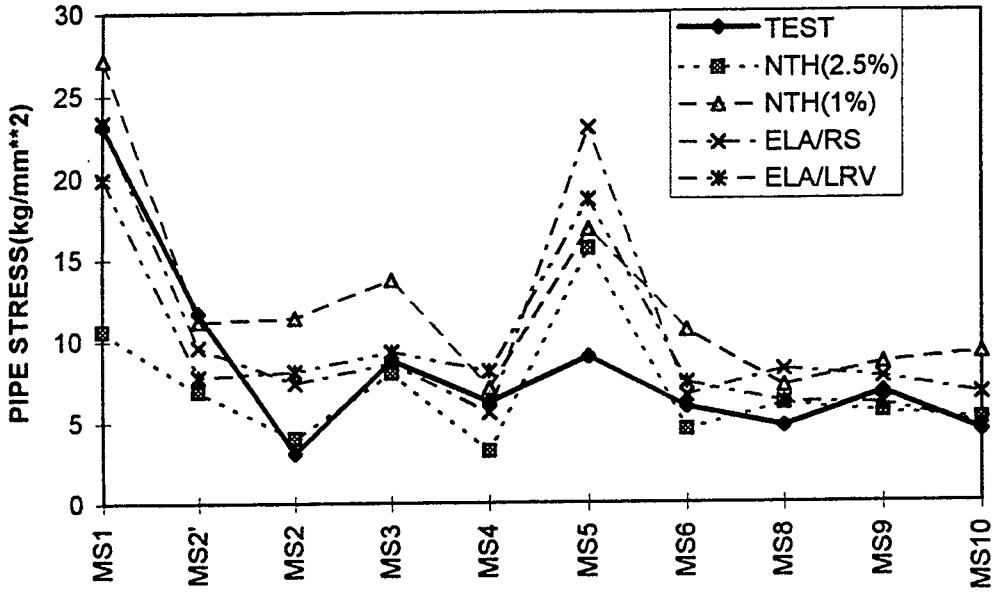

Figure 5.56 Comparison of Responses of M-line with LED Supports Without Actuator for 2.5 S2(A) Test Run, Pipe Stresses

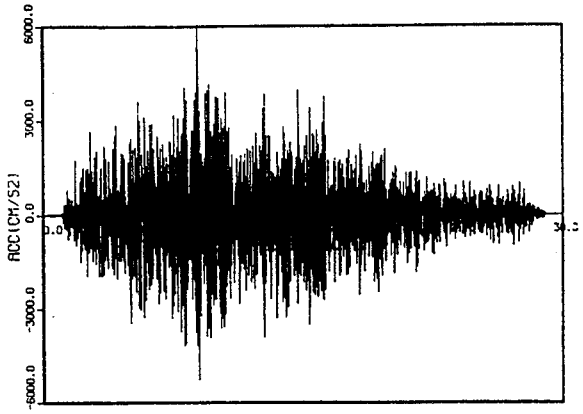

Recorded
(Peak: Ax=6.05g)

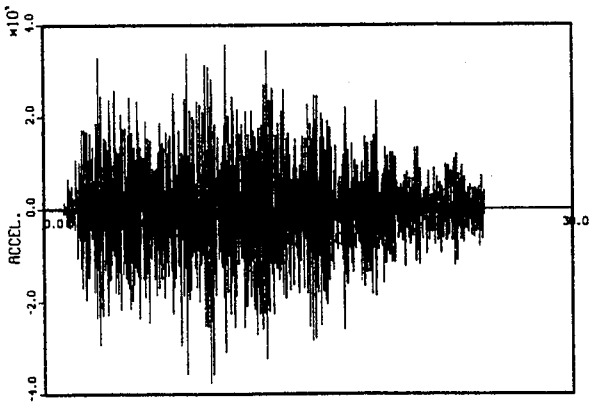

Analysis
(Peak: Ax=3.85g)

Figure 5.57 Comparison of Acceleration Time Histories of M-line with LED Supports for 2.5 S2(A) Test Run

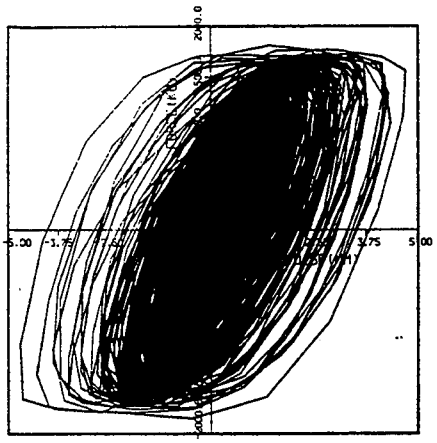

Recorded
(Peak: U=4.7 mm)

(a) LED-1

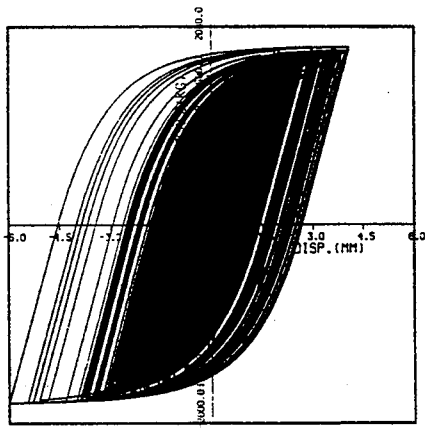

Analysis
(Peak: U=6.0 mm)

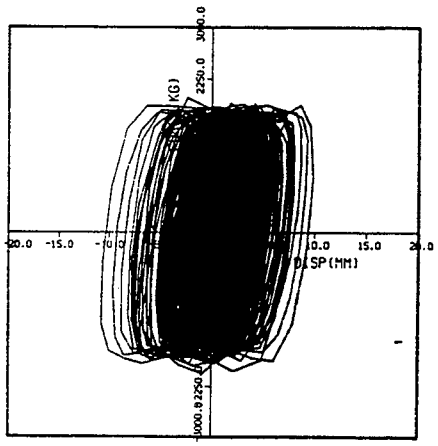

Recorded
(Peak: U=10.8 mm)

(b) LED-2

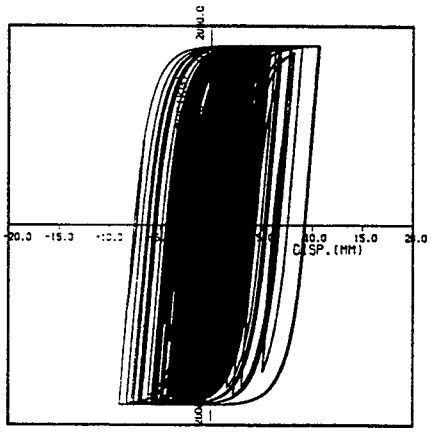

Analysis
(Peak: U=10.7 mm)

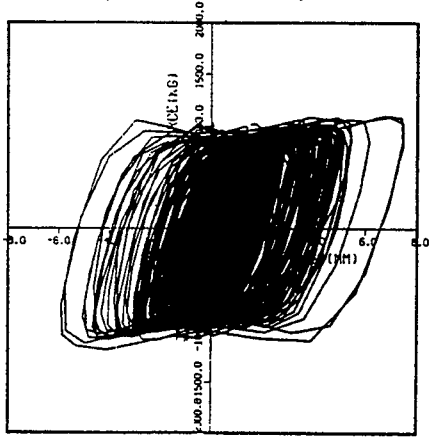

Recorded
(Peak: U=7.5 mm)

(c) LED-3

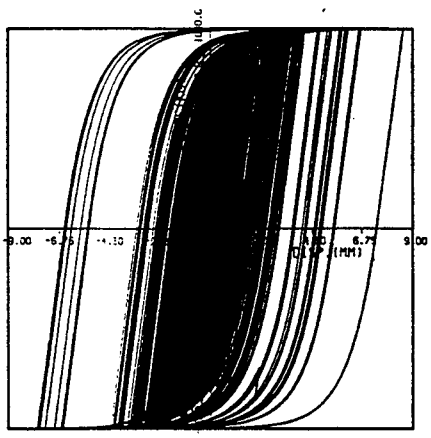

Analysis
(Peak: U=8.6 mm)

Figure 5.58 Comparisons of Force-Deformation Relationships of LED Supports of M-line for 2.5 S2 (A) Test Run

Table 5.15 Responses of M-line with LED Supports for Margin Test, Tokachi-Oki

(a) Acceleration (g)

Instrument/ Node Num.	Direction	Test	NTH(*1)		ELA	
			A	B	RS	LRV
MA1/50	X	6.16	4.19	3.30	3.33	3.20
	Y	5.43	3.61	1.89	2.44	1.94
	Z	2.54	2.19	1.30	1.67	1.76
MA16/90	X	4.51	5.22	5.05	3.77	3.79
	Y	6.29	4.82	3.89	5.77	3.49
	Z	3.76	3.67	2.86	3.86	2.17
MA17/130	X	6.00	4.55	8.16	8.48	4.23
	Y	5.98	2.05	3.48	7.84	3.23
	Z	3.83	3.67	2.84	3.85	2.18
MA4/150	X	6.04	4.28	7.95	11.22	4.72
	Y	4.25	3.28	3.53	8.26	3.38
	Z	2.58	3.28	2.19	3.83	2.28
MA5/165	X	6.13	3.63	7.12	9.94	6.42
	Y	4.27	3.29	3.50	8.24	3.38
MA6/180	X	5.16	3.81	5.97	8.49	5.13
	Y	4.40	3.29	3.49	8.21	3.38
MA8/200	X	5.33	3.55	4.23	7.11	3.92
	Y	3.83	3.20	3.31	7.36	3.12
	Z	7.58	1.02	1.45	1.94	1.39
MA10/250	X	4.10	3.83	4.12	4.16	3.44
	Y	2.14	0.63	0.57	1.13	0.43
	Z	7.95	1.62	2.99	3.06	2.67

Note: (*1): Nonlinear time history analyses (A = original model; B = properties of LED-2, LED-3 and MR8 were changed to account for the effects of degradation).

(b) Displacement (mm)

Instrument/Element Num.		Test	NTH		ELA	
			A	B	RS	LRV
MD12, 13/N-90	(X)	17.3	42.0	16.4	40.4	10.4
	(Y)	10.2	21.2	3.9	29.9	3.4
MD15/LED-1		4.7	7.1	4.5	11.8	2.9
MD16/LED-2		54.9	27.2	43.4	92.9	25.3
MD17/LED-3		15.3	19.0	13.0	29.2	6.5
MD18/N-150	(X)	50.9	28.2	43.9	89.7	25.3
	(Y)	36.0	21.2	30.2	70.1	18.9
	(Z)	15.3	21.2	13.3	30.0	6.6

Table 5.15 Responses of M-line with LED Supports for Margin Test, Tokachi-Oki (Cont'd)

(c) Pipe Stress (kg/mm^2)

Instrument/ Element	Stress Intensification Factor	Test	NTH		ELA	
			A	B	RS	LRV
MS1/3	2.0	15.8	16.0	19.0	41.6	13.8
MS2'/5	1.0	9.1	6.3	10.6	25.6	7.3
MS2/7	1.0	11.3	7.7	18.2	39.8	12.2
MS3/9	2.0	26.9	17.8	39.0	76.8	24.2
MS4/14	1.0	7.7	6.1	9.5	24.0	5.9
MS5/17	2.0	13.8	19.3	18.9	78.4	22.8
MS6/46	1.0	4.8	6.1	7.4	11.9	3.9
MS8/23	1.0	9.4	6.7	9.5	20.2	4.7
MS9/25	1.0	8.3	6.7	9.4	20.5	5.1
MS10/30	1.0	9.3	5.6	10.9	24.1	6.9

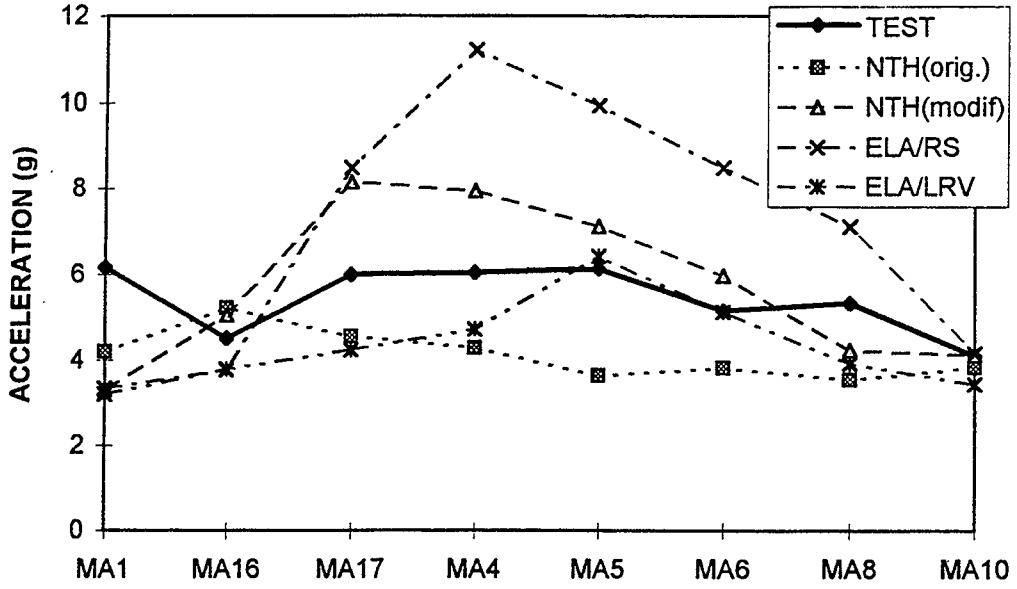

Figure 5.59 Comparison of Responses of M-line with LED Supports Without Actuator for Tokachi-Oki Wave Test Run, X-Direction Accelerations

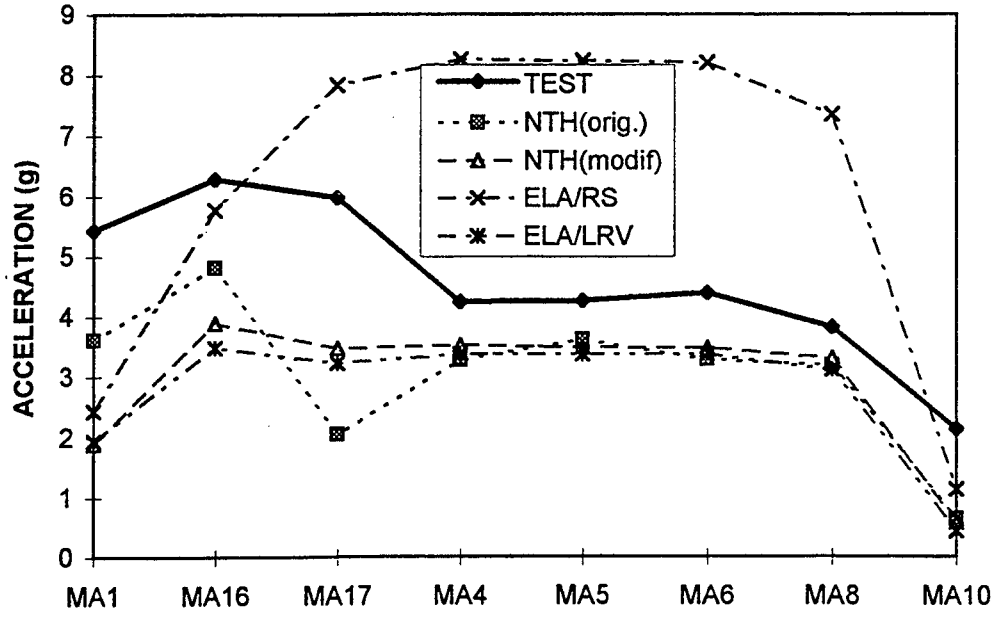

Figure 5.60 Comparison of Responses of M-line with LED Supports Without Actuator for Tokachi-Oki Wave Test Run, Y-Direction Accelerations

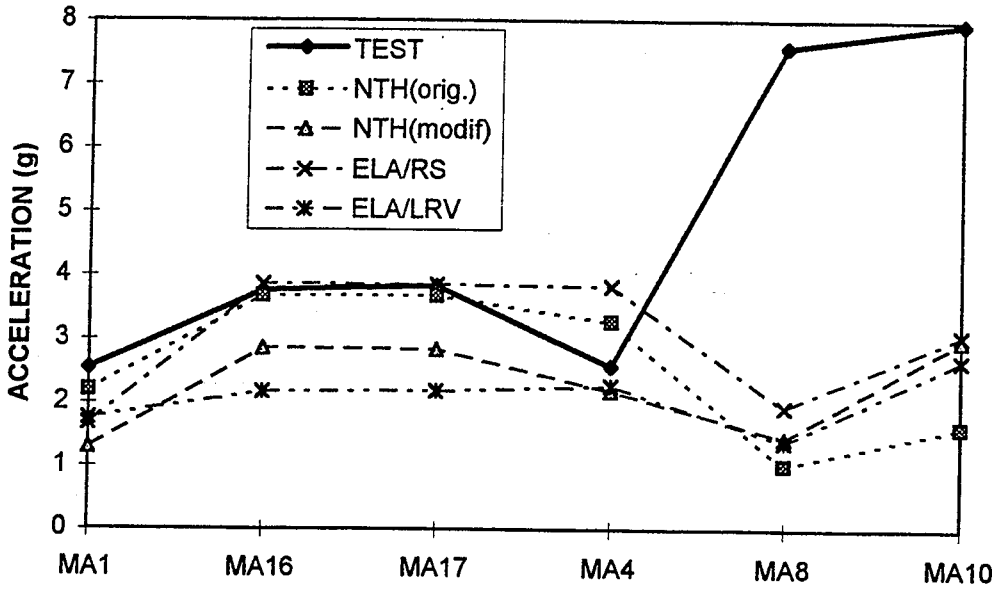

Figure 5.61 Comparison of Responses of M-line with LED Supports Without Actuator for Tokachi-Oki Wave Test Run, Z-Direction Accelerations

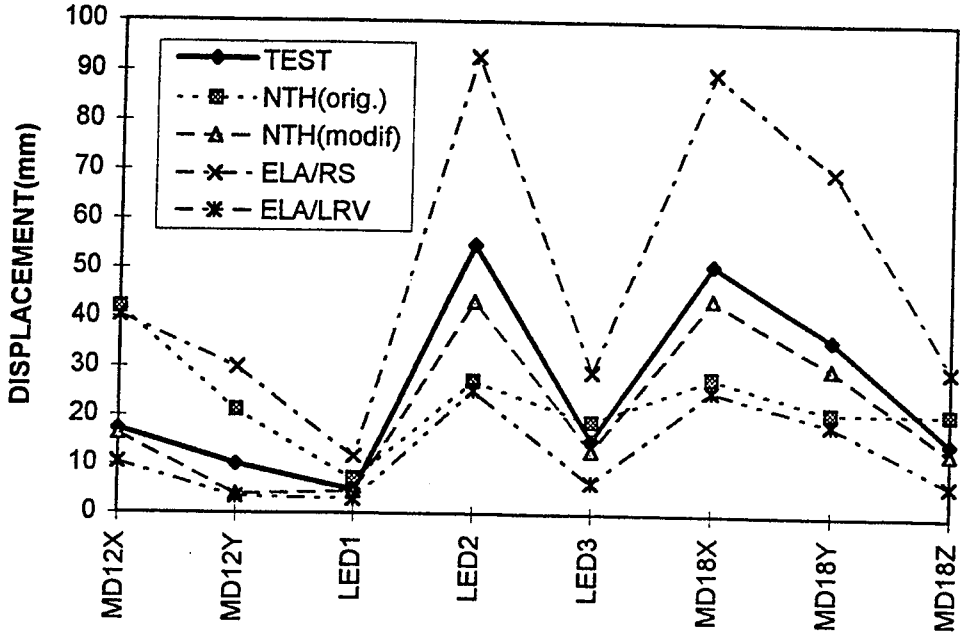

Figure 5.62 Comparison of Responses of M-line with LED Supports Without Actuator for Tokachi-Oki Wave Test Run, Displacements

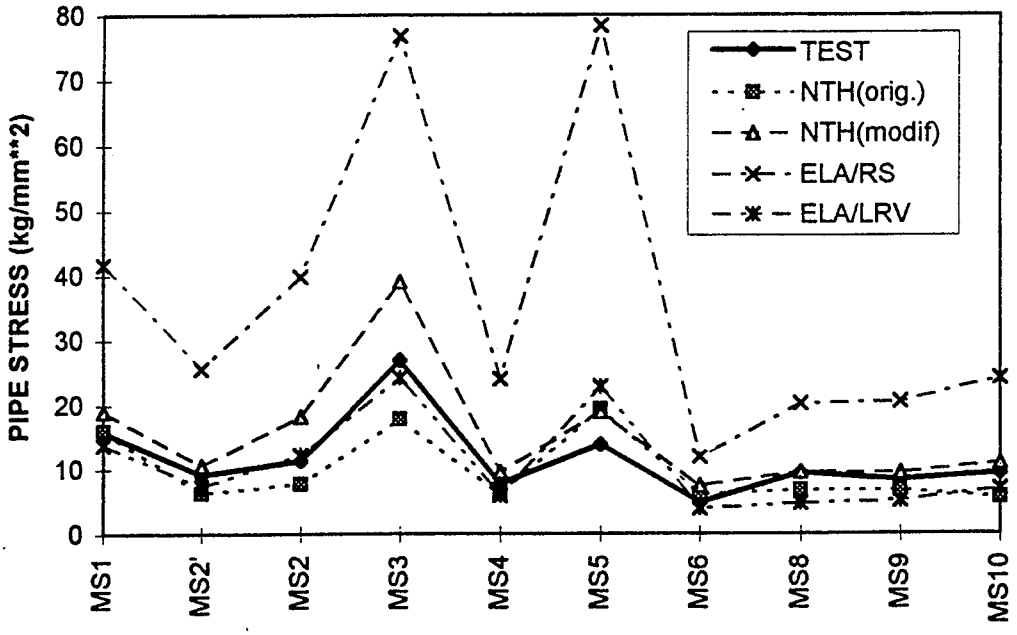

Figure 5.63 Comparison of Responses of M-line with LED Supports Without Actuator for Tokachi-Oki Wave Test Run, Pipe Stresses

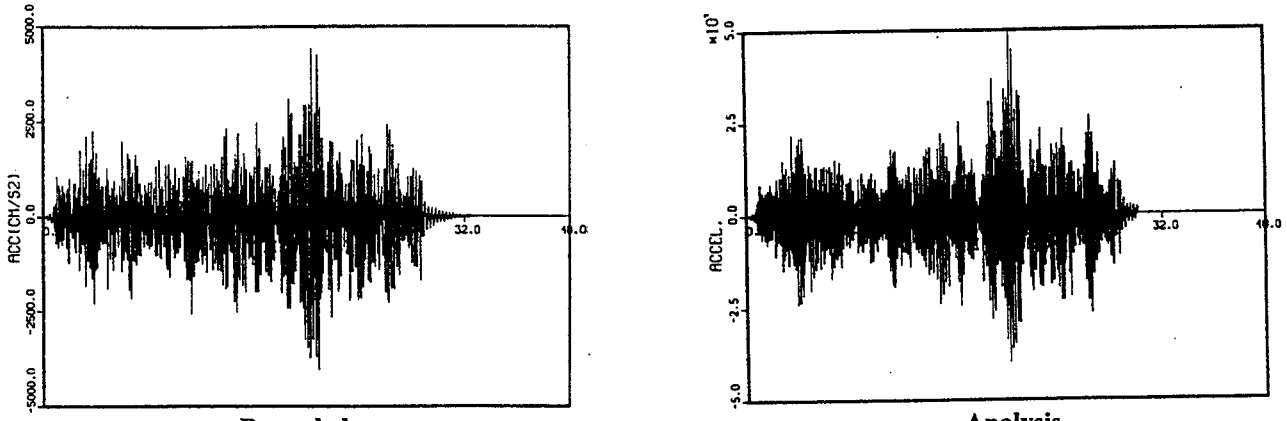

Recorded
(Peak: Ax=4.51g)

Analysis
(Peak: Ax=5.05g)

(a) MA16-X

Figure 5.64 Comparison of Acceleration Time Histories of M-line with LED Supports for Tokachi-Oki Test Run

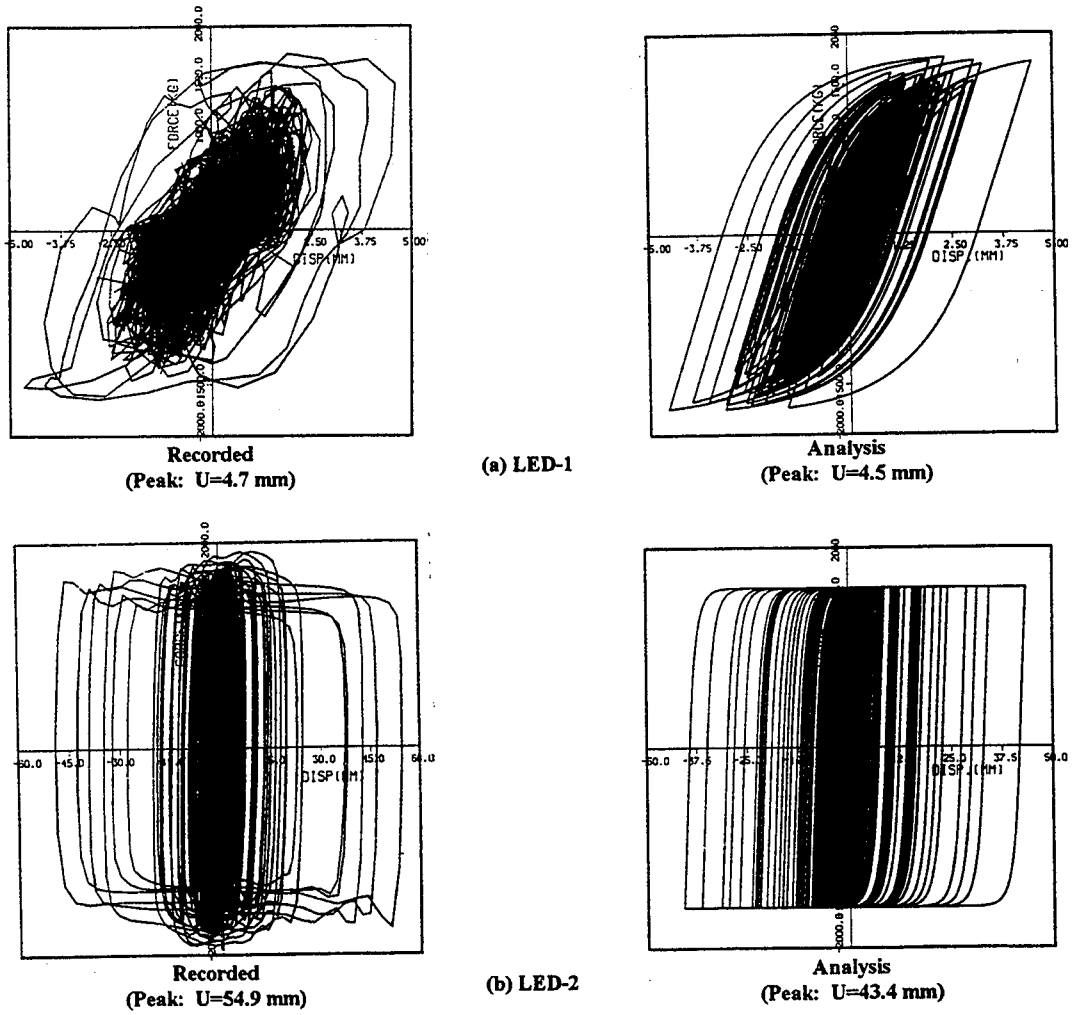

Figure 5.65 Comparison of Force-Deformation Relationships of LED Supports of M-line for Tokachi-Oki Wave Test Run

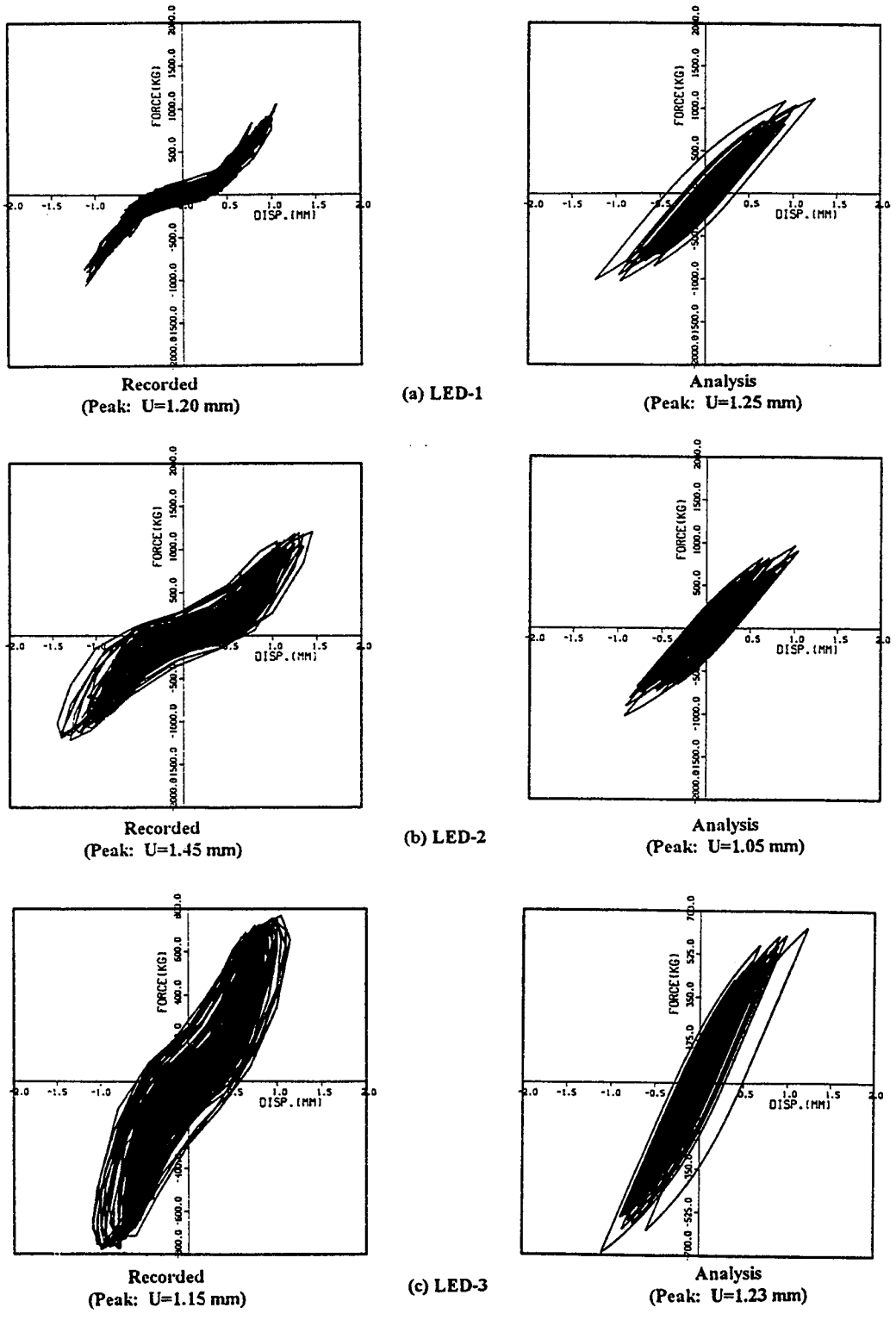

Recorded
(Peak: U=1.20 mm)

(a) LED-1

Analysis
(Peak: U=1.25 mm)

Recorded
(Peak: U=1.45 mm)

(b) LED-2

Analysis
(Peak: U=1.05 mm)

Recorded
(Peak: U=1.15 mm)

(c) LED-3

Analysis
(Peak: U=1.23 mm)

Figure 5.66 Comparisons of Force-Deformation Relationships of LED Supports of M-line Without Actuator for 1/3 S2(A) Test Run

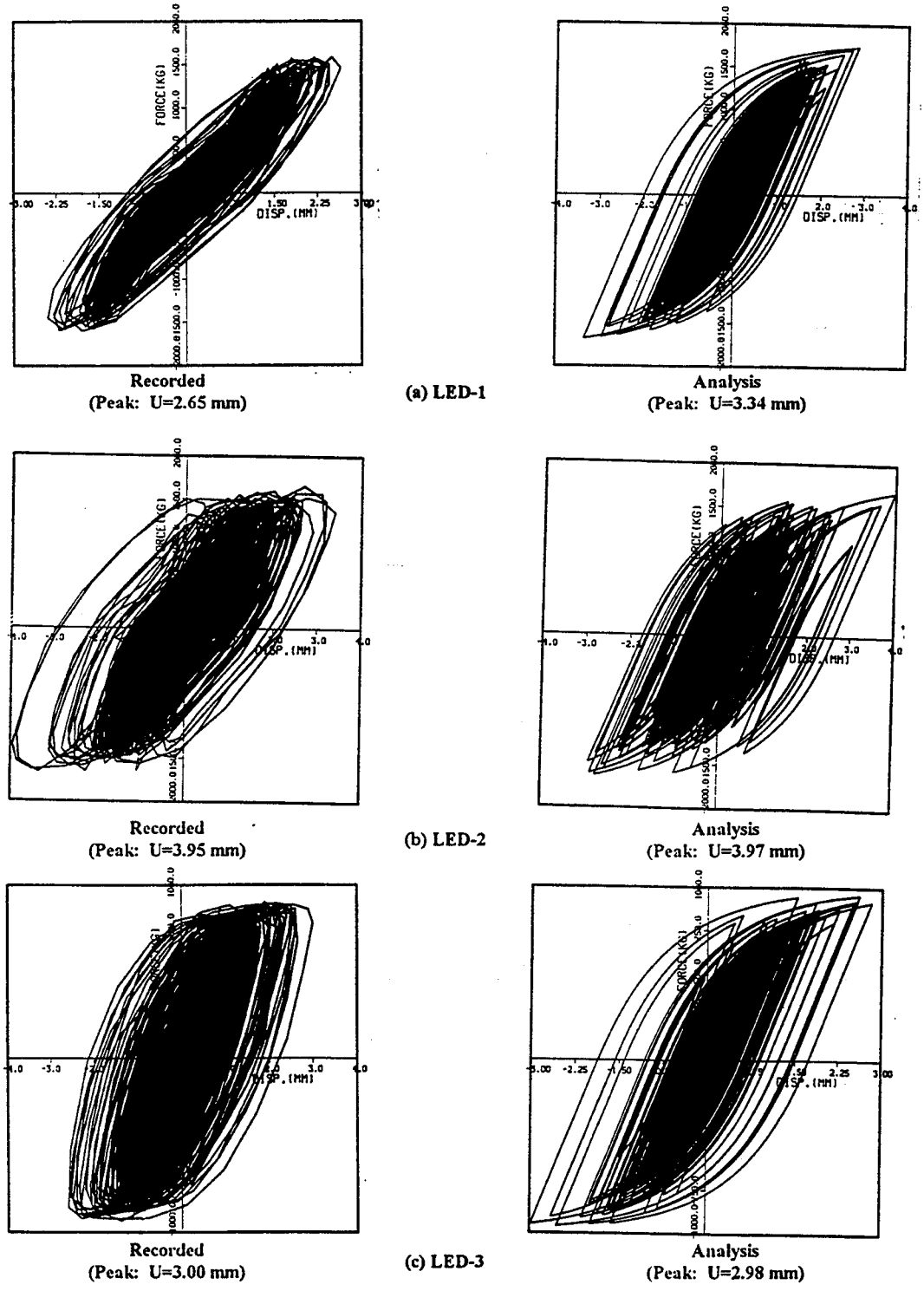

Recorded
(Peak: U=2.65 mm)

(a) LED-1

Analysis
(Peak: U=3.34 mm)

Recorded
(Peak: U=3.95 mm)

(b) LED-2

Analysis
(Peak: U=3.97 mm)

Recorded
(Peak: U=3.00 mm)

(c) LED-3

Analysis
(Peak: U=2.98 mm)

Figure 5.67 Comparison of Force-Deformation Relationships of LED Supports of M-line Without Actuator for 1.0 S2(A) Test Run

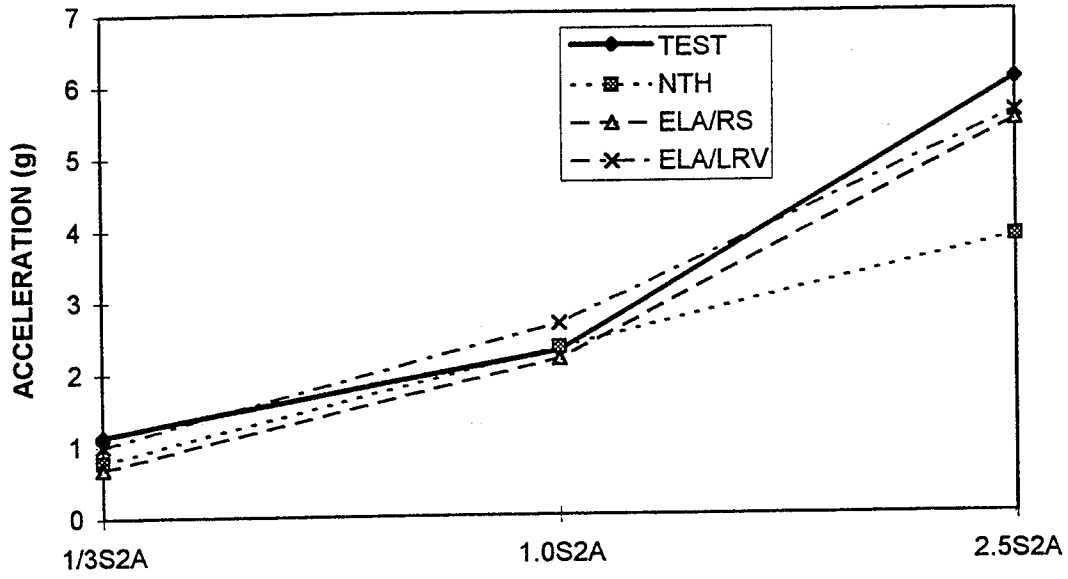

(a) MA16-X

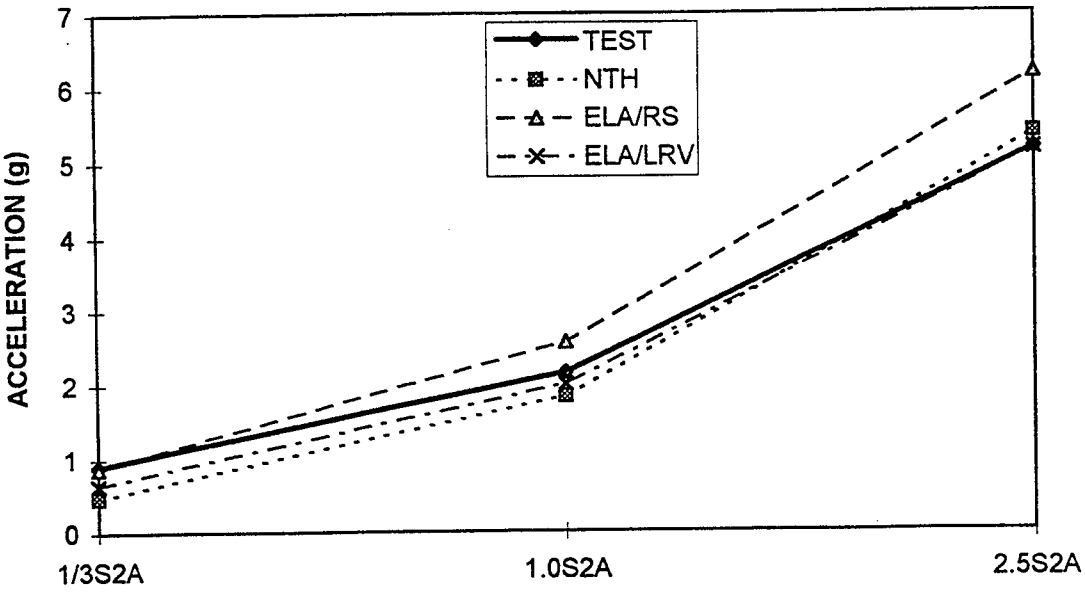

(b) MA10-X

Figure 5.68 Comparison of Peak Responses for M-line with LED Supports Without Actuator

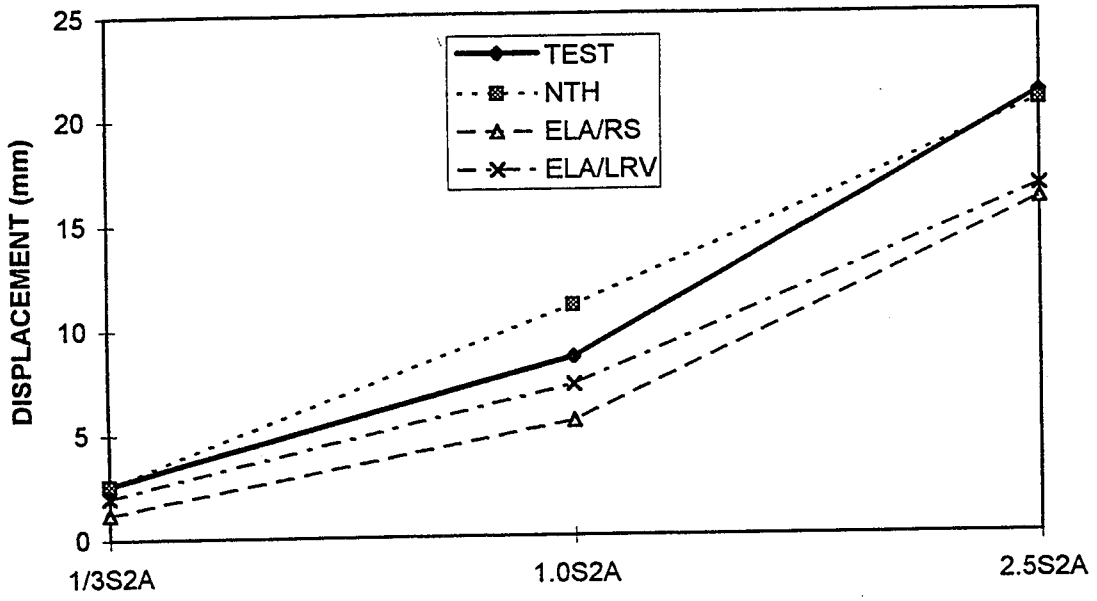

(c) MD12-X

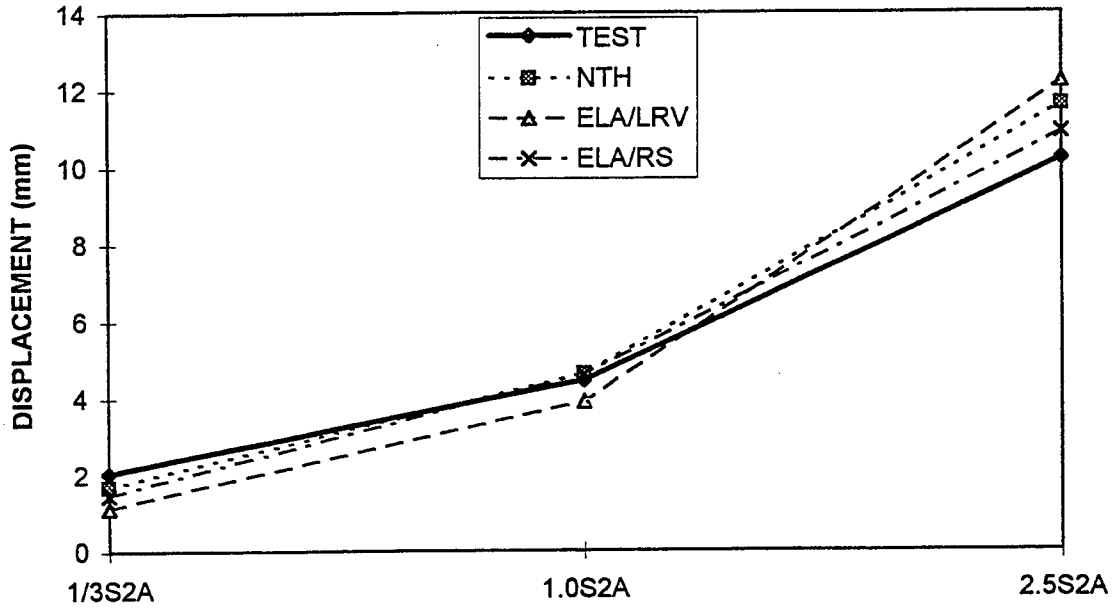

(d) MD18-X

Figure 5.68 Comparison of Peak Responses for M-line with LED Supports Without Actuator (Cont'd)

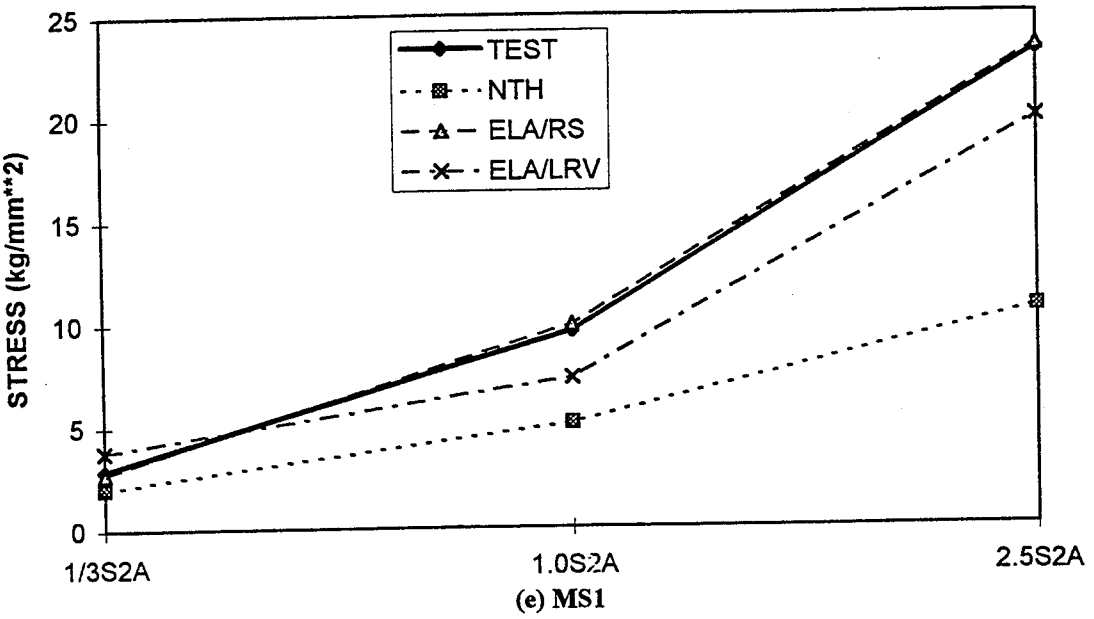

(e) MS1

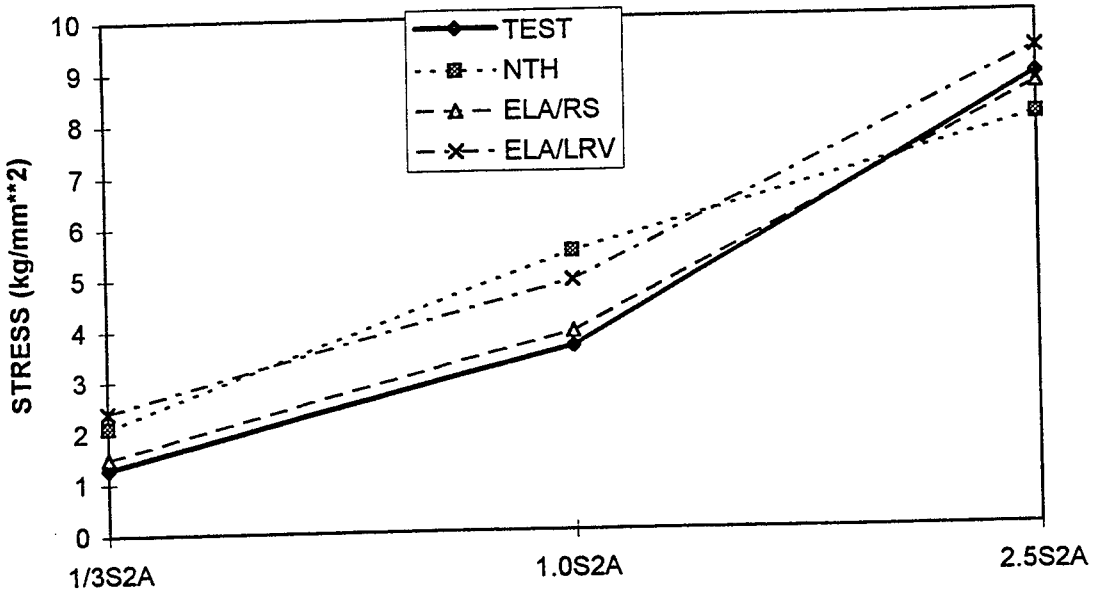

(f) MS3

Figure 5.68 Comparison of Peak Responses for M-line with LED Supports Without Actuator (Cont'd)

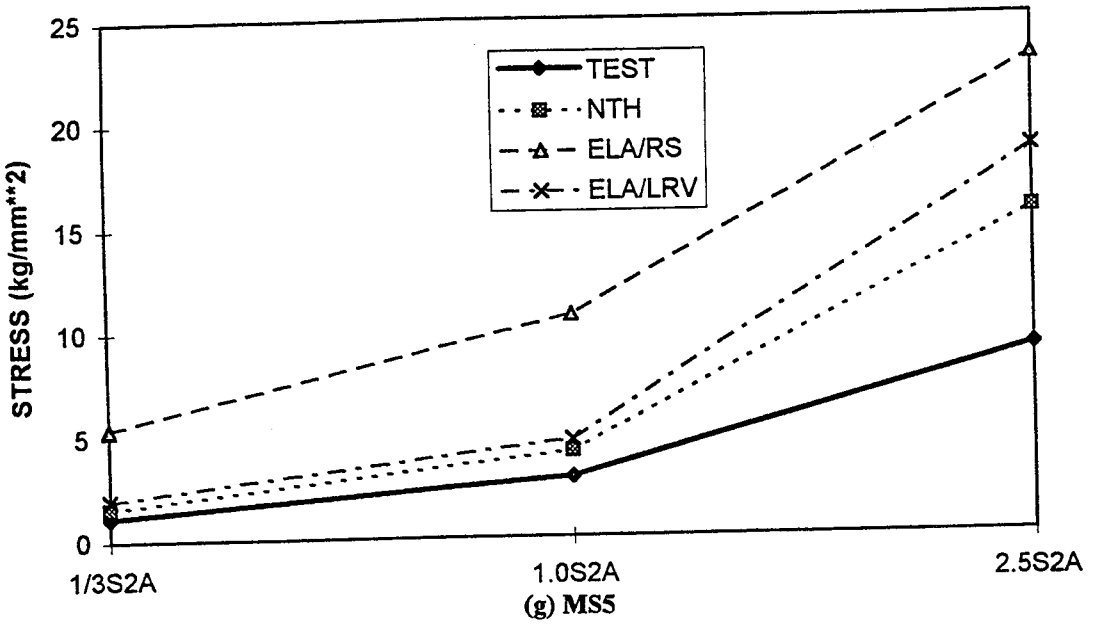

(g) MS5

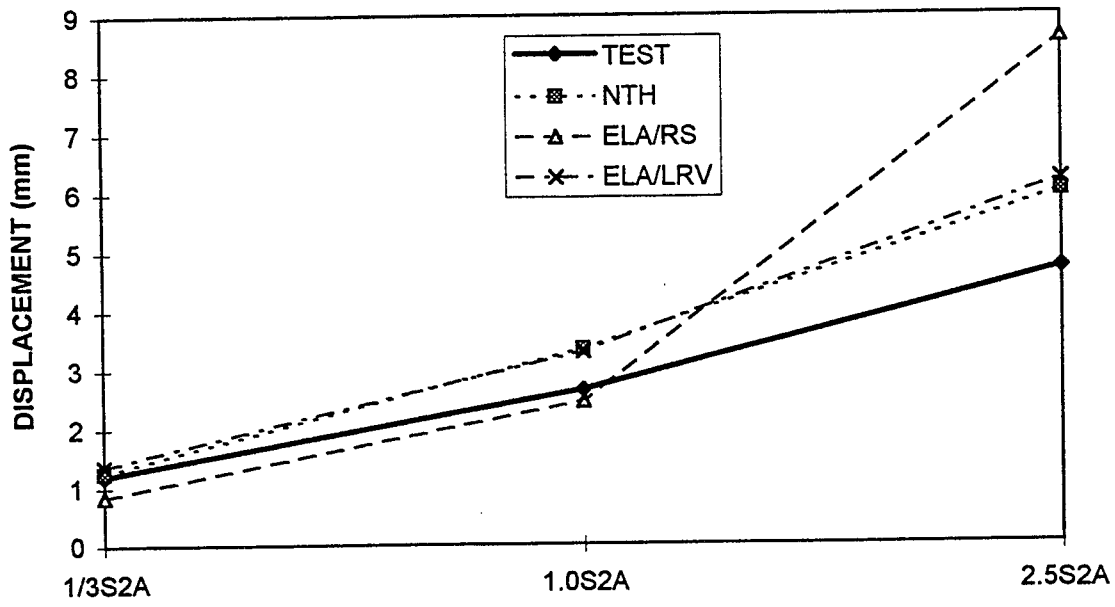

(h) LED-1

Figure 5.68 Comparison of Peak Responses for M-line with LED Supports Without Actuator (Cont'd)

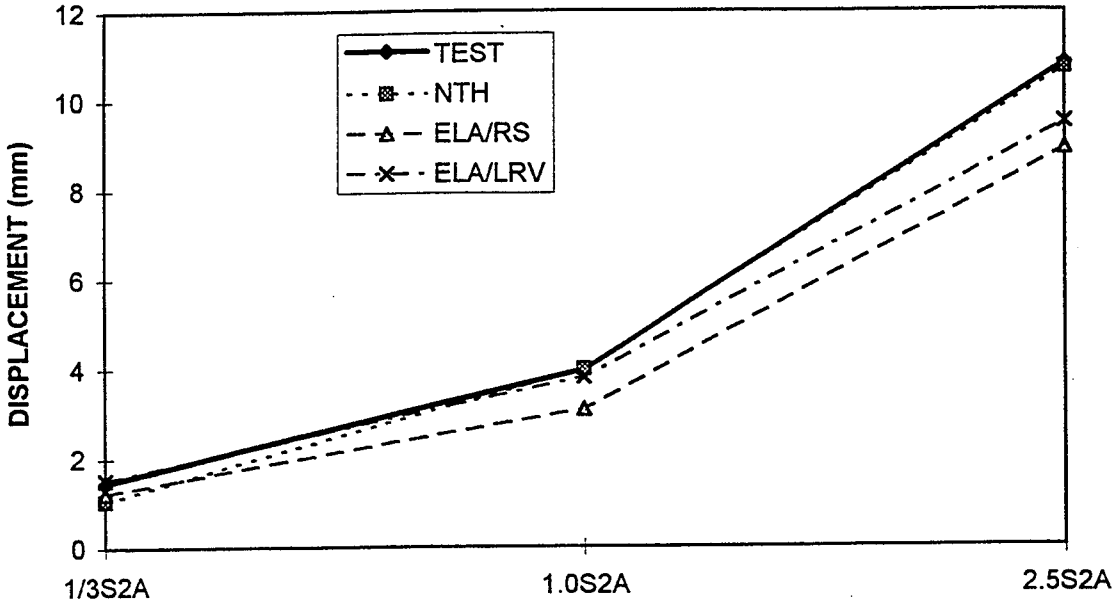

(i) LED-2

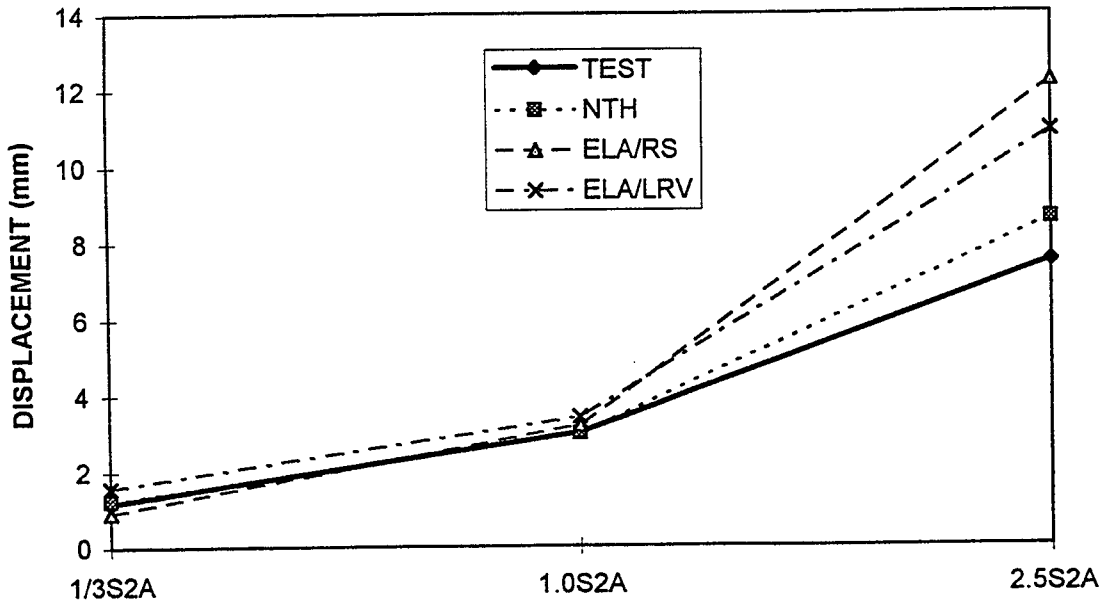

(j) LED-3

Figure 5.68 Comparison of Peak Responses for M-line with LED Supports Without Actuator (Cont'd)

Table 5.16 Comparison of Vibration Frequencies of M-line with LED Supports without Actuator Obtained From Equivalent Linearization Analyses

Mode	Linear	⅓ S2(A)		1.0 S2(A)		2.5 S2(A)	
		RS	LRV	RS	LRV	RS	LRV
1	8.27Hz	8.27	8.02	7.21	6.83	5.60	5.53
2	9.38	9.12	8.88	8.43	8.54	8.42	8.51
3	9.60	9.52	9.92	9.28	9.78	9.21	9.23
4	15.24	14.41	13.51	12.31	11.96	10.69	10.85
5	16.64	15.91	15.50	14.51	13.86	12.68	12.88

Table 5.17 Comparison of Equivalent Modal Damping of M-line with LED Supports without Actuator Obtained From Equivalent Linearization Analyses

Mode	Linear	⅓ S2(A)		1.0 S2(A)		2.5 S2(A)	
		RS	LRV	RS	LRV	RS	LRV
1	1.0%	2.7	3.3	15.0	14.9	23.4	36.6
2	1.0%	3.4	2.5	4.1	2.7	3.5	3.8
3	1.0%	2.1	1.3	1.8	1.7	4.3	4.9
4	1.0%	6.4	4.9	12.5	10.7	11.6	15.8
5	1.0%	5.0	3.4	10.2	8.4	9.0	11.2

Table 5.18 Responses of F-line with EAB Supports for S2(A) Test Run

(a) Acceleration (g)

Instrument/Node Num.	Direction	Test	NTH	ELA	
				RS	LRV
FA3/90	X	3.08	4.31	3.26	3.95
	Y	0.41	0.74	0.39	0.24
	Z	1.80	2.00	2.33	2.20
FA5/180	X	2.98	2.51	2.44	2.19
	Y	0.62	0.77	0.42	0.14
	Z	2.28	1.95	1.69	1.61
FA6/240	X	4.94	3.39	3.54	4.63
	Y	3.28	2.38	2.19	1.89
	Z	3.30	2.93	2.51	2.20
FA7/280	X	5.20	3.31	3.68	5.05
	Y	1.98	1.84	1.50	2.05
	Z	2.22	2.40	1.67	2.01
FA8/330	X	4.97	3.32	3.45	4.62
	Y	1.28	1.53	0.80	1.37
	Z	2.96	2.55	1.35	2.02
FA9/390	X	3.04	3.85	3.28	3.24
	Y	1.57	1.69	0.86	1.29
	Z	2.43	2.53	0.78	0.80
FA10/440	X	3.29	3.87	3.87	3.54
	Y	1.52	1.64	0.92	1.29
	Z	2.84	3.22	1.35	1.26
FA11/500	X	4.07	4.15	4.65	3.51
	Y	3.75	2.57	3.52	2.73
	Z	3.06	3.36	1.44	0.96
FA12/550	X	5.56	4.10	3.35	4.28
	Y	2.48	2.55	1.77	2.14
	Z	2.14	1.90	1.35	1.24
FA13/790	X	3.68	2.51	2.68	1.71
	Y	1.90	2.78	1.48	1.32
	Z	3.31	2.13	1.27	0.84

Table 5.18 Responses of F-line with EAB Supports for S2(A) Test Run (Cont'd)

(b) Displacement (mm)

Instrument/Element Num.	Test	NTH	ELA	
			RS	LRV
FD6b/205	1.05	0.83	0.61	0.67
FD11b/EAB-1	5.42	4.51	4.29	6.60
FD12b/EAB-2	7.20	6.34	4.95	6.84
FD13b/207	1.25	0.92	0.68	0.87
FD14b/EAB-3	8.50	5.01	6.02	5.77
FD15b/208	0.82	0.72	0.71	0.68

(c) Support Forces (ton)

Instrument/Element Num.	Test	NTH	ELA	
			RS	LRV
FR6b/205	1.66	5.30	3.27	---
FR11b/EAB-1	0.71	0.71	0.69	---
FR12b/EAB-2	1.43	1.54	1.35	---
FR13b/207	4.89	5.50	3.40	---
FR14b/EAB-3	1.45	1.45	1.37	---
FR15b/208	4.37	3.98	3.71	---

Table 5.18 Responses of F-line with EAB Supports for S2(A) Test Run (Cont'd)

(d) Pipe Stress (kg/mm^2)

Instrument/Element	Stress Intensification Factor	Test	NTH	ELA	
				RS	LRV
FS1/1	1.0	4.3	4.9	3.6	5.2
FS2/18	2.63	4.5	8.3	5.4	7.4
FS3/25	2.63	6.9	7.4	8.8	6.9
FS4/30-55	2.54	9.5	8.1	15.9	8.2
FS5/39	1.0	2.4	5.2	3.0	4.9
FS6/41-80	2.54	5.0	16.7	6.2	14.0
FS7/41	1.0	3.5	2.7	2.6	3.0
FS8/50	1.0	1.2	1.3	1.4	1.5
FS9/51-105	2.54	8.5	16.7	18.3	18.8
FS10/57	2.27	5.7	7.1	6.1	6.0
FS11/60	2.75	5.9	12.7	10.1	11.4
FS12/64	1.0	3.6	4.6	4.2	5.2
FS13/66	2.27	7.1	5.8	5.9	9.6
FS14/68	1.0	8.8	10.8	9.9	9.3
FS15/80	1.0	6.0	6.3	5.3	7.3
FS19/105	1.0	8.3	6.6	7.2	7.4
FS20/112	1.0	3.7	5.9	4.8	5.2
FS21/115	2.27	10.7	10.1	14.1	11.1
FS22/117	1.0	8.1	8.7	6.8	7.0

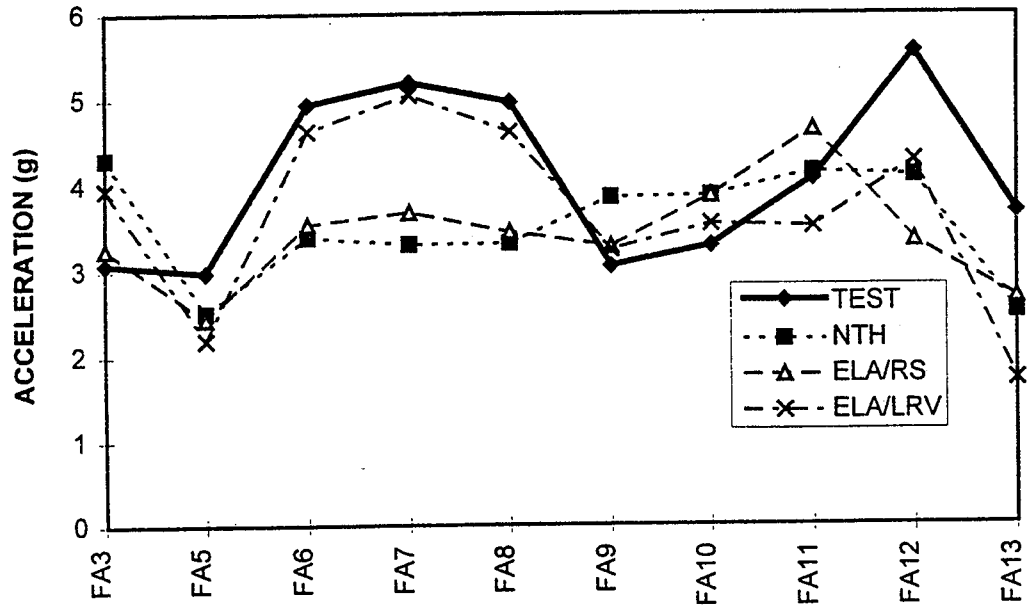

Figure 5.69 Comparison of Responses of F-line with EAB Supports for 1.0 S2(A) Test Run, X-Direction Accelerations

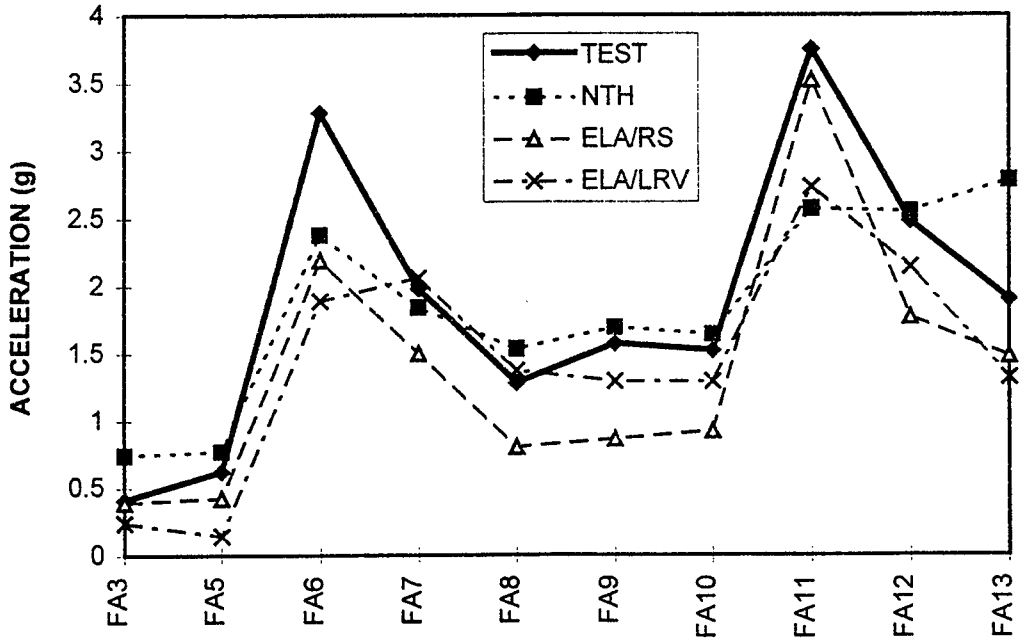

Figure 5.70 Comparison of Responses of F-line with EAB Supports for 1.0 S2(A) Test Run, Y-Direction Accelerations

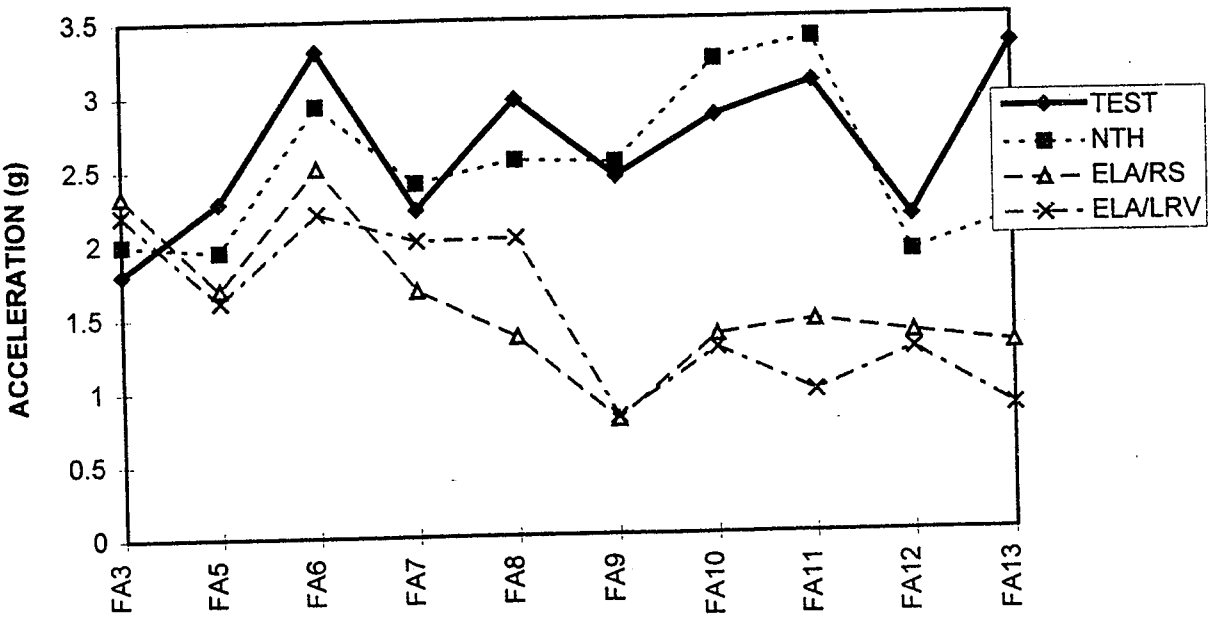

Figure 5.71 Comparison of Responses of F-line with EAB Supports for 1.0 S2(A) Test Run, Z-Direction Acceleration

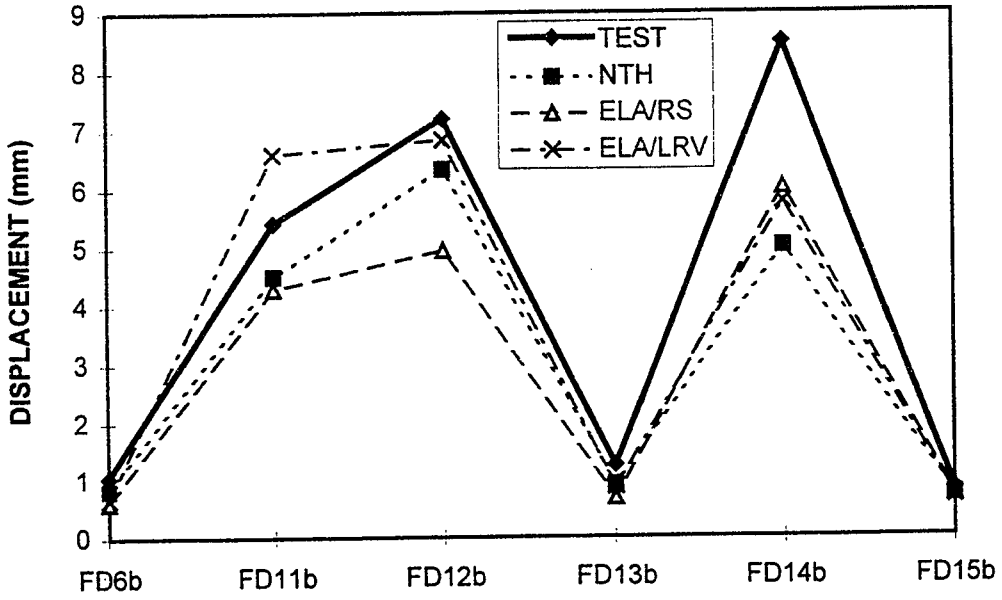

Figure 5.72 Comparison of Responses of F-line with EAB Supports for 1.0 S2(A) Test Run, Displacement

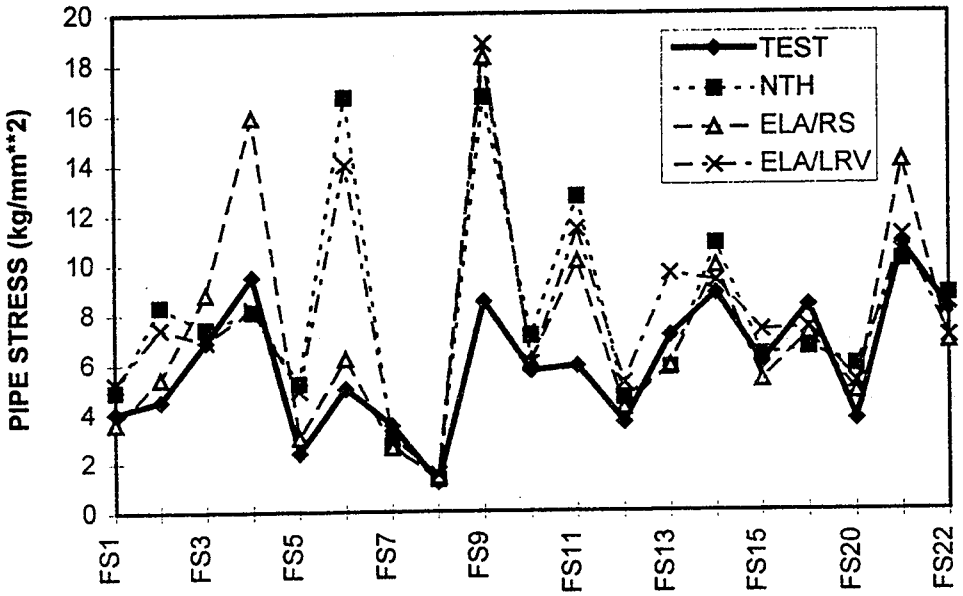

Figure 5.73 Comparison of Responses of F-line with EAB Supports for 1.0 S2(A) Test Run, Pipe Stresses

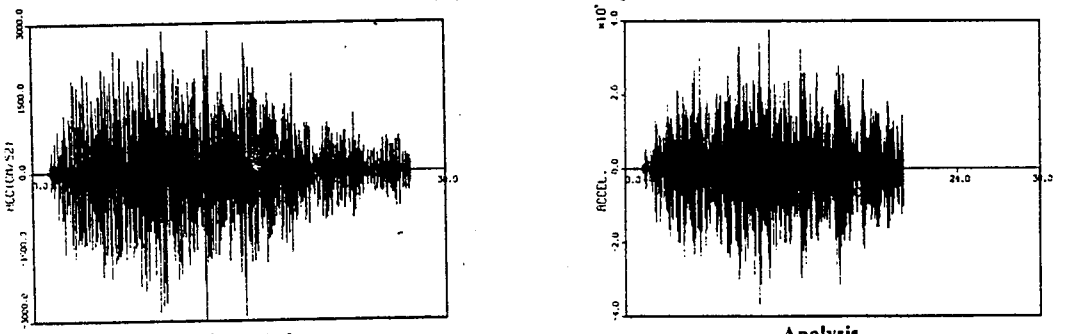

(a) FA9-X

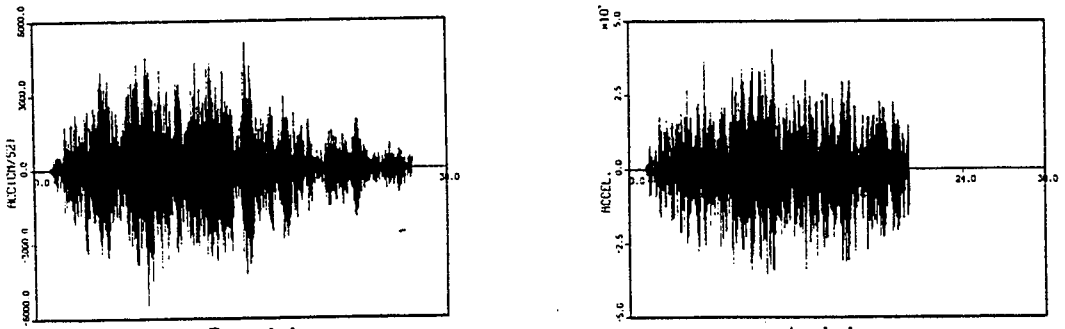

(b) FA12-X

Figure 5.74 Comparison of Acceleration Time Histories of F-line with EAB Supports for 1.0 S2(A) Test Run

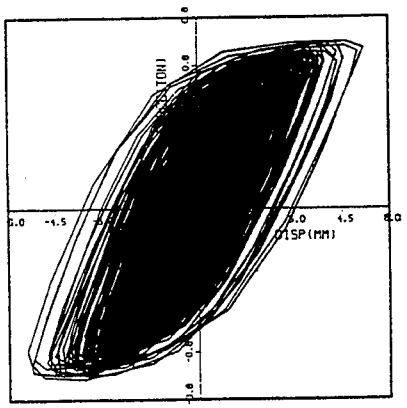

Recorded
(Peak: U=5.42 mm)

(a) EAB-1

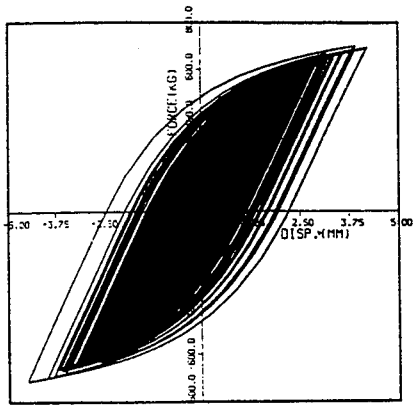

Analysis
(Peak: U=4.51 mm)

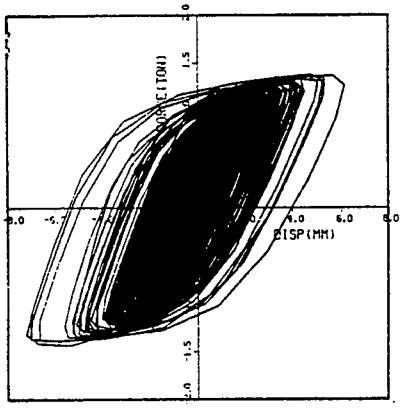

Recorded
(Peak: U=7.20 mm)

(b) EAB-2

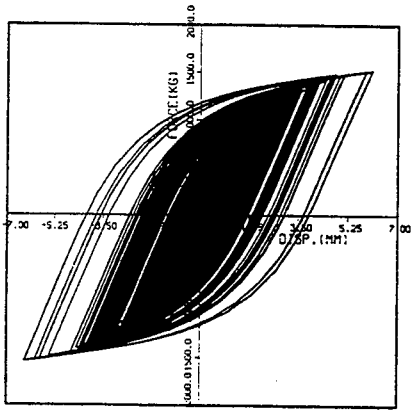

Analysis
(Peak: U=6.34 mm)

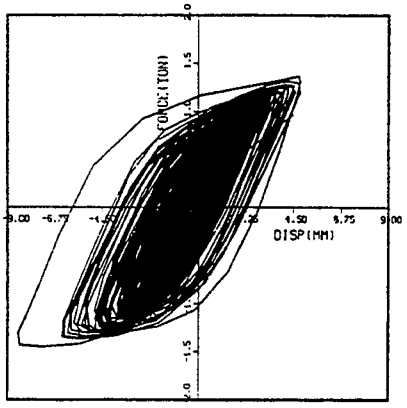

Recorded
(Peak: U=8.50 mm)

(c) EAB-3

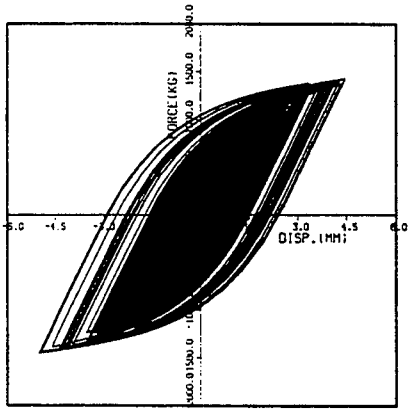

Analysis
(Peak: U=5.01 mm)

Figure 5.75 Comparison of Force-Deformation Relationship of EAB Supports of F-line for 1.0 S2(A) Test Run

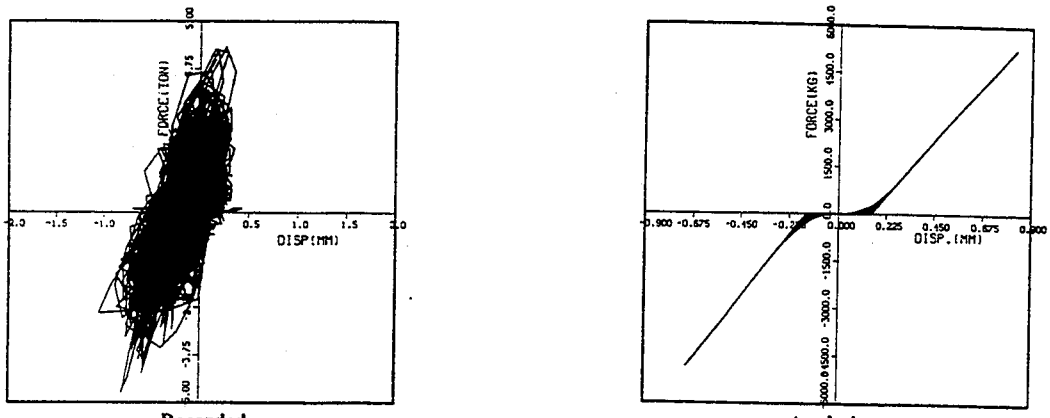

Recorded
(Peak: U=1.05 mm)

(a) FR6

Analysis
(Peak: U=0.83 mm)

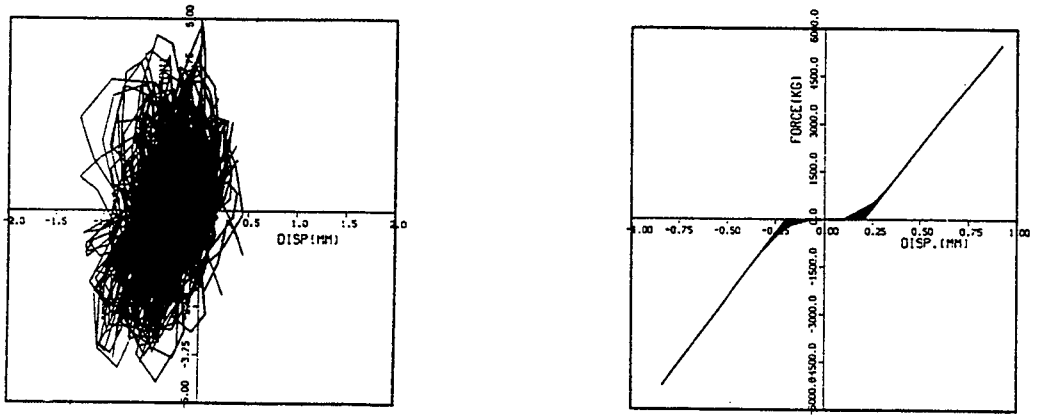

Recorded
(Peak: U=1.25 mm)

(b) FR13

Analysis
(Peak: U=0.92 mm)

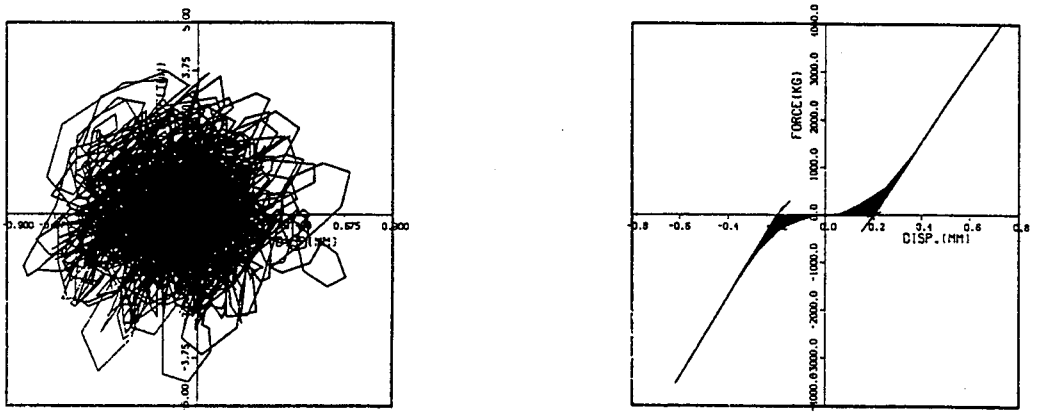

Recorded
(Peak: U=0.82 mm)

(c) FR15

Analysis
(Peak: U=0.72 mm)

Figure 5.76 Comparison of Force-Deformation Relationships of Mechanical Snubbers of F-line with EAB Supports for 1.0 S2 (A) Test Run

Table 5.19 Responses of F-line with EAB Supports for 2.5 S2(A) Test Run

(a) Acceleration (g)

Instrument/Node Num.	Direction	Test	NTH	ELA	
				RS	LRV
FA3/90	X	8.25	10.20	8.19	8.92
	Y	0.71	1.09	0.89	0.30
	Z	3.56	3.87	5.55	4.38
FA5/180	X	5.01	4.51	6.11	4.41
	Y	0.85	1.18	0.95	0.31
	Z	3.16	3.34	3.62	2.93
FA6/240	X	7.35	6.68	9.39	8.43
	Y	5.54	4.58	4.65	3.76
	Z	4.64	4.90	5.24	3.86
FA7/280	X	9.74	5.84	9.66	9.32
	Y	3.53	3.24	3.57	3.83
	Z	3.92	3.77	3.74	3.85
FA8/330	X	9.22	6.10	8.95	8.93
	Y	2.20	2.26	1.58	2.50
	Z	6.01	4.19	3.11	4.06
FA9/390	X	6.79	6.32	8.41	6.51
	Y	2.67	2.29	1.55	2.42
	Z	4.57	3.43	1.76	1.62
FA10/440	X	5.49	7.63	9.84	6.60
	Y	2.84	2.39	1.81	2.42
	Z	5.47	3.78	3.02	2.38
FA11/500	X	7.40	7.73	11.94	6.33
	Y	7.04	5.77	8.60	6.10
	Z	4.72	4.20	3.40	2.13
FA12/550	X	8.27	6.41	8.47	8.00
	Y	4.16	4.77	3.74	4.69
	Z	3.66	2.83	2.84	2.52
FA13/790	X	5.77	3.92	6.59	3.83
	Y	2.92	4.12	3.46	2.97
	Z	5.25	3.12	2.89	2.00

Table 5.19 Responses of F-line with EAB Supports for 2.5 S2(A) Test Run (Cont'd)

(b) Displacement (mm)

Instrument/Element Num.	Test	NTH	ELA	
			RS	LRV
FD6b/205	1.7	1.2	1.1	1.2
FD11b/EAB-1	11.3	10.1	13.1	13.1
FD12b/EAB-2	16.0	13.6	16.2	14.9
FD13b/207	2.4	1.7	1.7	1.7
FD14b/EAB-3	17.7	11.9	20.2	12.1
FD15b/208	2.5	1.2	1.9	1.2

(c) Support Forces (ton)

Instrument/Element Num.	Test	NTH	ELA	
			RS	LRV
FD6b/205	8.11	7.72	7.25	---
FD11b/EAB-1	0.82	0.81	0.65	---
FD12b/EAB-2	1.72	1.73	1.36	---
FD13b/207	9.92	12.00	11.8	---
FD14b/EAB-3	1.78	1.68	1.40	---
FD15b/208	8.90	8.18	13.0	---

Table 5.19 Responses of F-line with EAB Supports for 2.5 S2(A) Test Run (Cont'd)

(d) Pipe Stresses (kg/mm^2)

Instrument/Element	Stress Intensification Factor	Test	NTH	ELA	
				RS	LRV
FS1/1	1.0	10.3	9.4	11.4	11.3
FS2/18	2.63	9.1	18.2	16.7	16.5
FS3/25	2.63	12.9	17.4	24.6	23.8
FS4/30-55	2.54	16.0	27.7	26.4	25.3
FS5/39	1.0	5.6	11.0	9.5	10.6
FS6/41-80	2.54	8.9	22.7	29.5	25.8
FS7/41	1.0	7.7	6.4	9.9	6.5
FS8/50	1.0	2.5	3.6	5.8	3.5
FS9/51-105	2.54	17.1	39.1	61.7	39.8
FS10/57	2.27	8.7	14.4	17.0	12.4
FS11/60	2.75	11.3	25.0	26.3	26.0
FS12/64	1.0	6.2	9.1	10.8	11.4
FS13/66	2.27	13.5	13.4	18.3	19.5
FS14/68	1.0	16.2	19.6	22.0	19.0
FS15/80	1.0	11.2	14.5	18.5	16.0
FS19/105	1.0	16.8	15.4	24.3	15.7
FS20/112	1.0	7.7	11.6	17.1	11.8
FS21/115	2.27	21.8	21.9	36.5	23.1
FS22/117	1.0	16.6	15.9	21.8	16.7

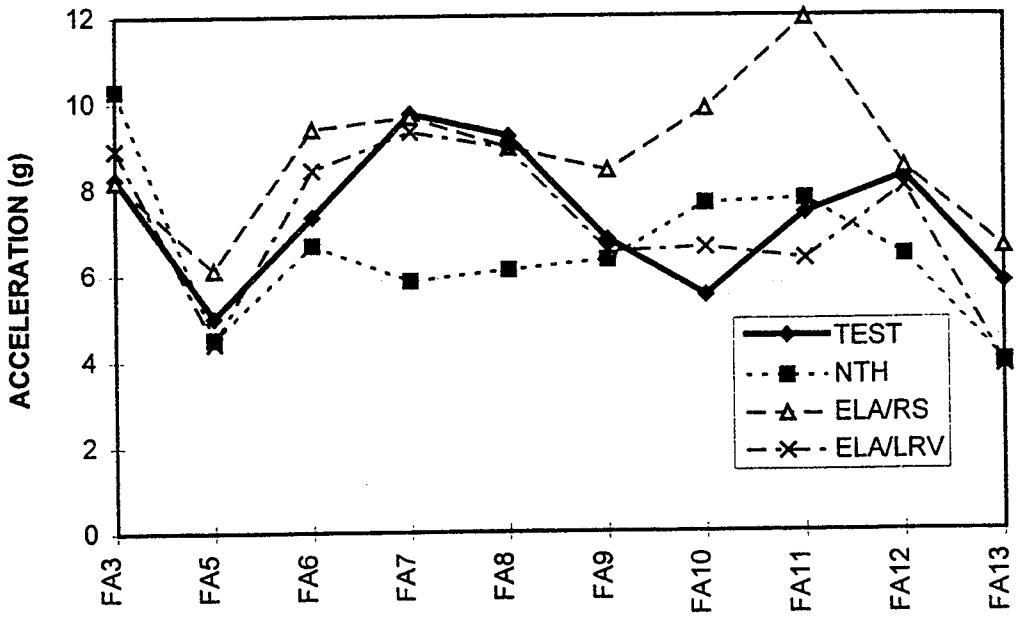

Figure 5.77 Comparison of Responses of F-line with EAB Supports for 2.5 S2(A) Test Run, X-Direction Accelerations

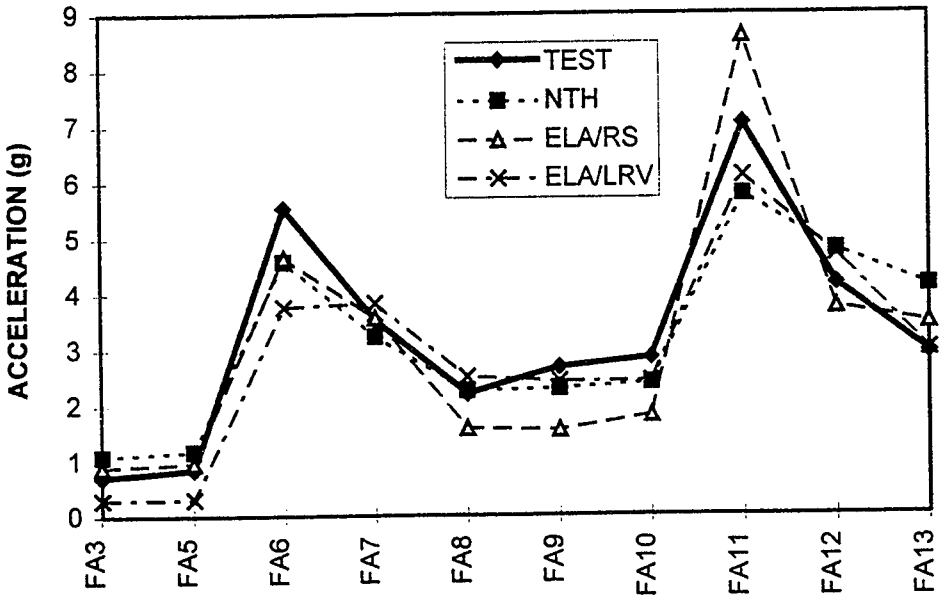

Figure 5.78 Comparison of Responses of F-line with EAB Supports for 2.5 S2(A) Test Run, Y-Direction Accelerations

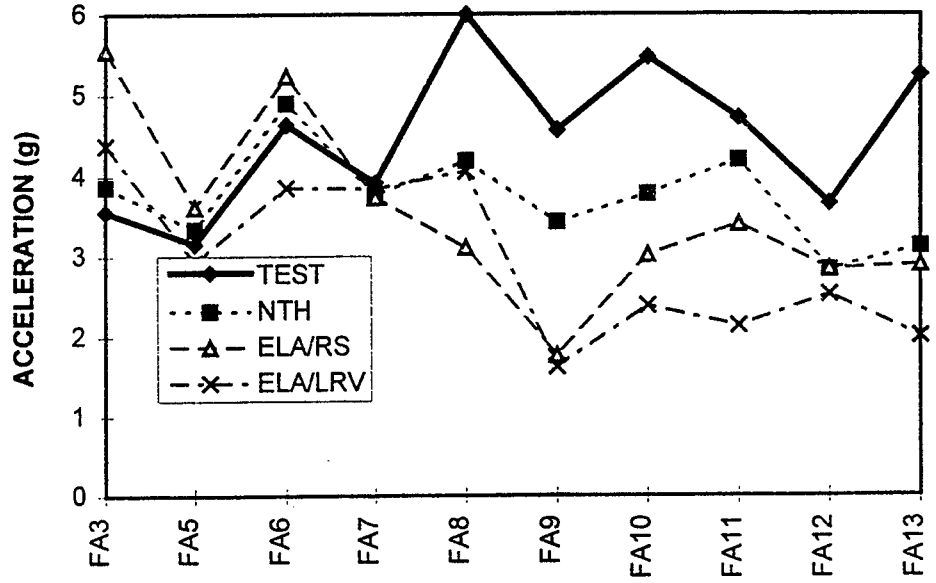

Figure 5.79 Comparison of Responses of F-line with EAB Supports for 2.5 S2(A) Test Run, Z-Direction Accelerations

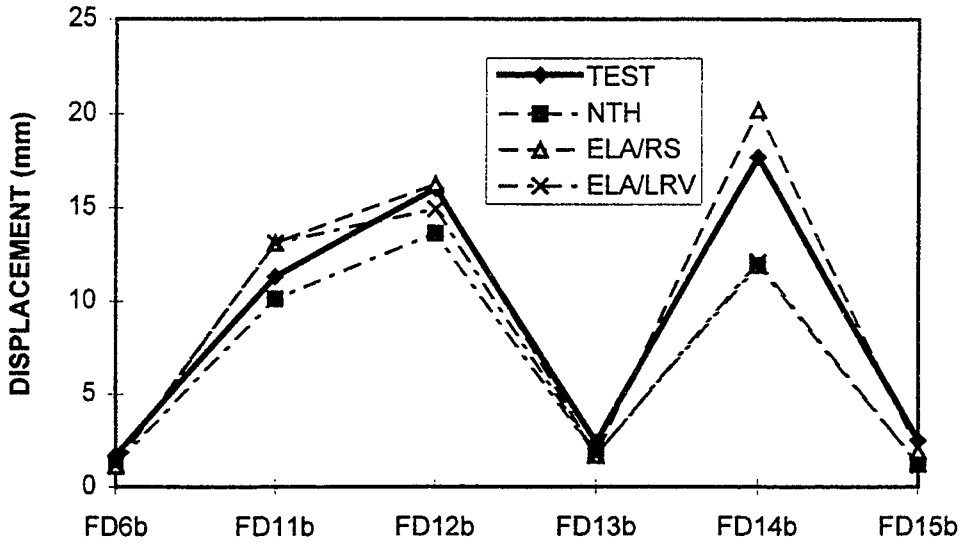

Figure 5.80 Comparison of Responses of F-line with EAB Supports for 2.5 S2(A) Test Run, Displacements

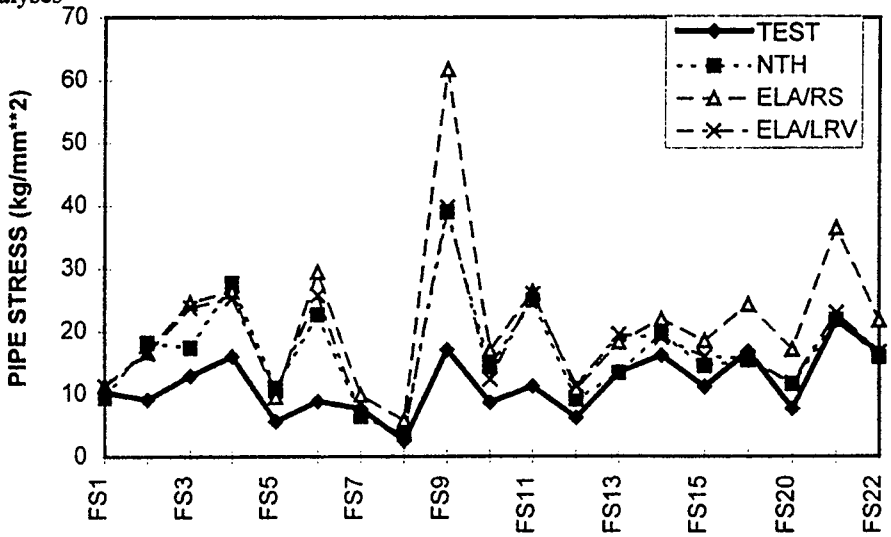

Figure 5.81 Comparison of Responses of F-line with EAB Supports for 2.5 S2(A) Test Run, Pipe Stresses

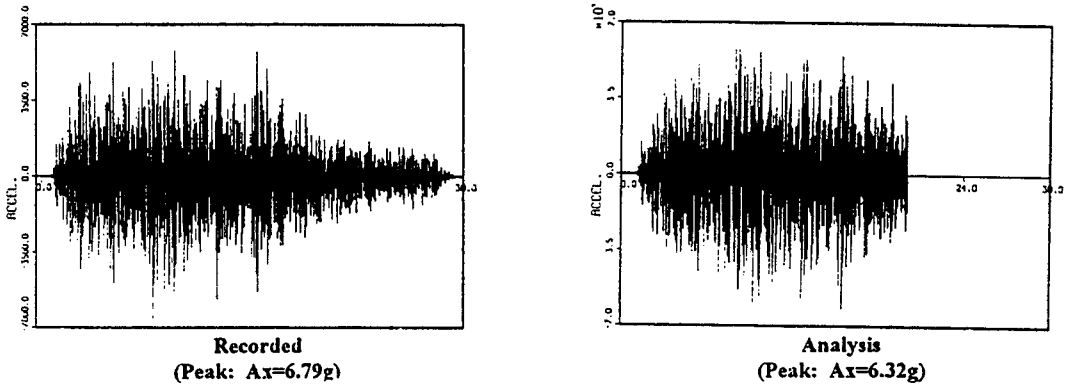

Recorded
(Peak: Ax=6.79g)

Analysis
(Peak: Ax=6.32g)

(a) FA9-X

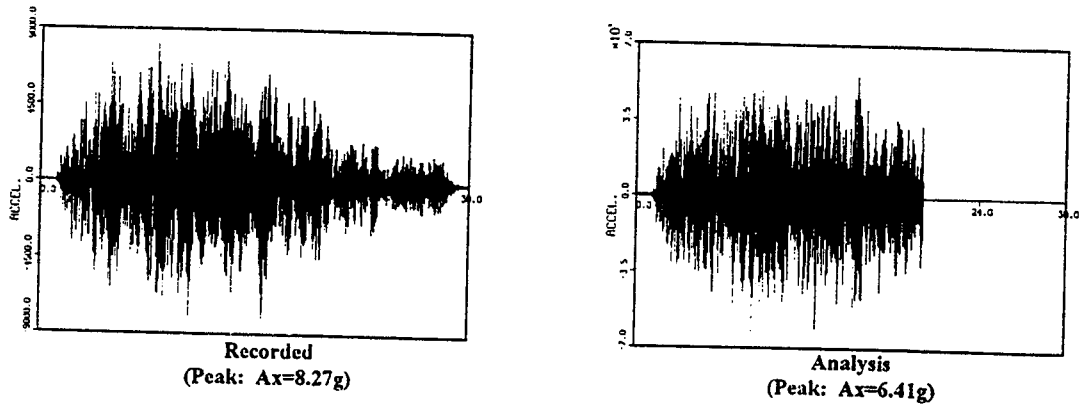

Recorded
(Peak: Ax=8.27g)

Analysis
(Peak: Ax=6.41g)

(b) FA12-X

Figure 5.82 Comparison of Acceleration Time Histories of F-line with EAB Supports for 2.5 S2(A) Test Run

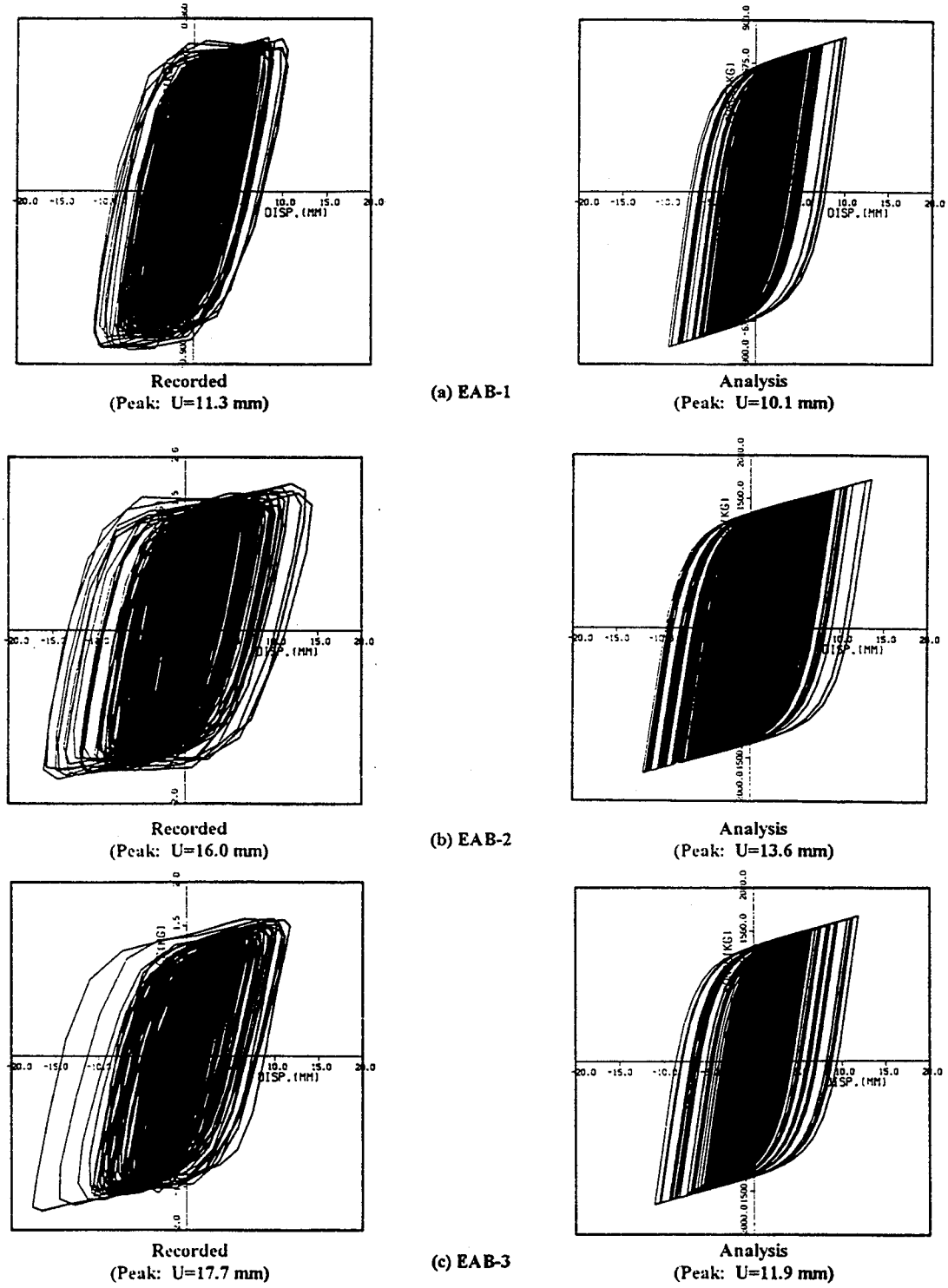

Recorded (Peak: U=11.3 mm) — (a) EAB-1 — Analysis (Peak: U=10.1 mm)

Recorded (Peak: U=16.0 mm) — (b) EAB-2 — Analysis (Peak: U=13.6 mm)

Recorded (Peak: U=17.7 mm) — (c) EAB-3 — Analysis (Peak: U=11.9 mm)

Figure 5.83 Comparison of Force-Deformation Relationship of EAB Supports of F-line for 2.5 S2(A) Test Run

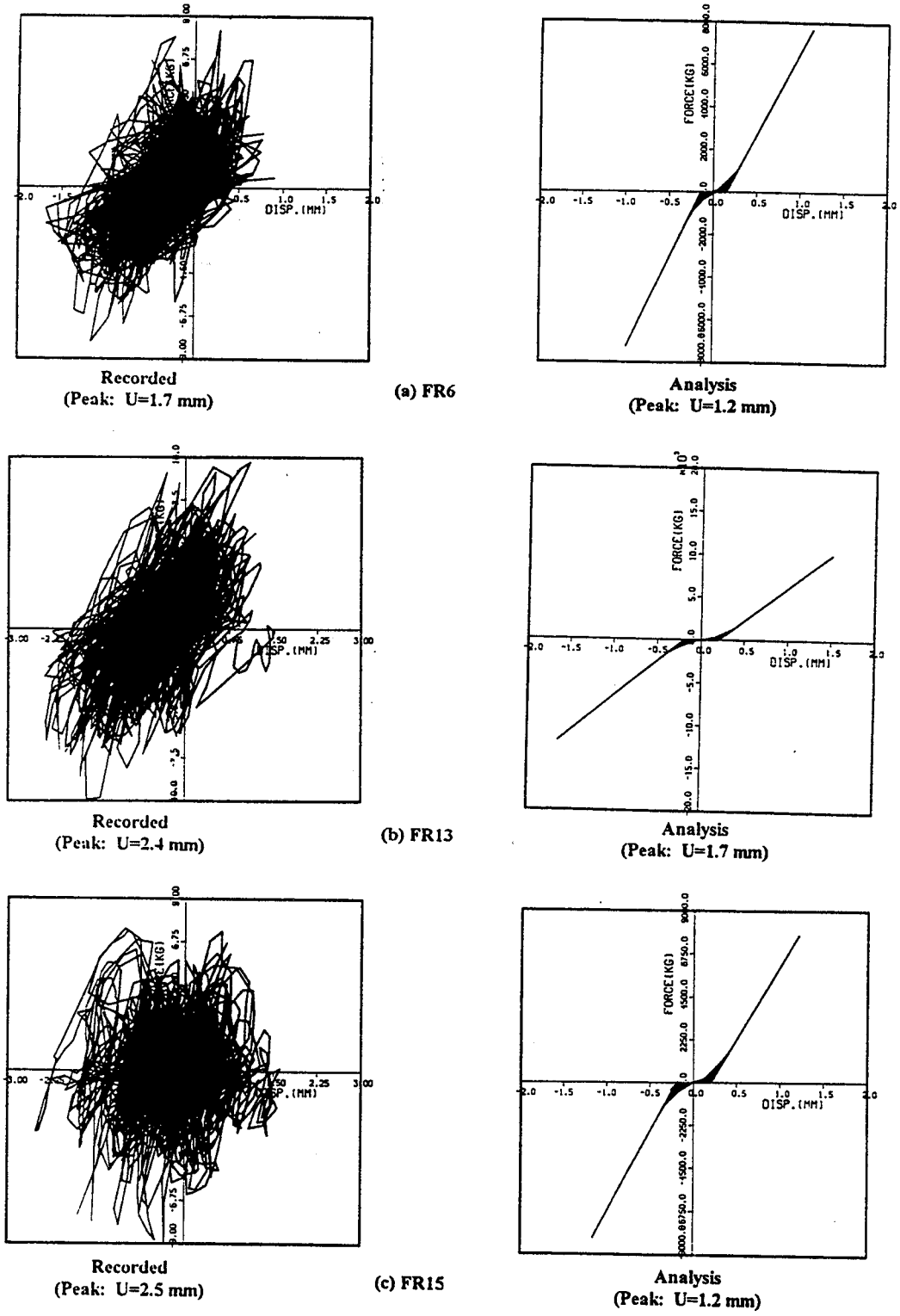

Figure 5.84 Comparison of Force-Deformation Relationships of Mechanical Snubbers of F-line with EAB Supports for 2.5 S2(A) Test Run

Table 5.20 Responses of F-line with EAB Supports for 1.2 S2(C) Test Run

(a) Acceleration

Instrument/Node Num.	Direction	Test	NTH	ELA	
				RS	LRV
FA3/90	X	2.99	2.65	3.40	2.17
	Y	0.27	0.48	0.40	0.10
	Z	1.27	1.17	1.96	0.74
FA5/180	X	3.13	2.56	2.41	2.32
	Y	0.42	0.50	0.43	0.20
	Z	1.34	1.02	1.10	0.68
FA6/240	X	3.75	3.10	3.63	3.24
	Y	3.62	2.60	2.85	1.35
	Z	1.76	1.66	1.58	0.88
FA7/280	X	3.19	3.27	4.01	3.47
	Y	1.80	1.80	2.22	1.09
	Z	1.95	1.73	1.16	0.82
FA8/330	X	3.41	3.58	5.00	3.80
	Y	1.21	1.26	0.61	0.68
	Z	2.75	2.52	1.07	0.82
FA9/390	X	5.03	5.04	9.99	5.70
	Y	1.20	1.27	0.71	0.96
	Z	3.49	2.89	1.34	2.82
FA10/440	X	7.73	6.69	14.39	7.67
	Y	0.99	1.27	0.66	0.95
	Z	5.80	2.69	1.80	2.01
FA11/500	X	10.09	6.93	15.61	8.10
	Y	4.06	2.18	2.97	1.83
	Z	3.76	2.69	1.68	1.81
FA12/550	X	3.70	3.40	3.43	3.14
	Y	2.23	2.39	2.60	1.30
	Z	2.03	1.37	1.28	0.76
FA13/790	X	3.93	4.13	6.54	3.82
	Y	1.79	2.48	1.91	1.84
	Z	4.14	1.61	1.21	1.58

Table 5.20 Responses of F-line with EAB Supports for 1.2 S2(C) Test Run (Cont'd)

(b) Displacement (mm)

Instrument/Element Num.	Test	NTH	ELA	
			RS	LRV
FD6b/205	1.4	0.84	1.32	0.81
FD11b/EAB-1	4.2	3.79	6.63	4.62
FD12b/EAB-2	13.4	10.3	24.5	13.1
FD13b/207	2.0	1.06	2.39	1.36
FD14b/EAB-3	19.2	12.4	32.4	16.2
FD15b/208	2.2	1.23	2.89	1.53

(c) Support Forces (ton)

Instrument/Element Num.	Test	NTH	ELA	
			RS	LRV
FD6b/205	6.39	5.44	9.33	---
FD11b/EAB-1	0.71	0.69	0.67	---
FD12b/EAB-2	1.71	1.63	1.41	---
FD13b/207	7.88	6.94	16.9	---
FD14b/EAB-3	3.59	1.69	1.56	---
FD15b/208	10.74	8.37	21.2	---

Table 5.20 Responses of F-line with EAB Supports for 1.2 S2(C) Test Run (Cont'd)

(d) Pipe Stresses (kg/mm2)

Instrument/Element	Stress Intensification Factor	Test	NTH	ELA	
				RS	LRV
FS1/1	1.0	3.4	6.2	13.3	7.2
FS2/18	2.63	6.1	7.7	10.3	9.4
FS3/25	2.63	5.8	4.6	6.9	6.5
FS4/30-55	2.54	8.0	8.4	14.4	12.0
FS5/39	1.0	3.5	4.9	11.2	5.0
FS6/41-80	2.54	10.5	20.1	46.7	25.4
FS7/41	1.0	3.9	5.6	15.2	8.5
FS8/50	1.0	2.5	2.8	9.1	4.4
FS9/51-105	2.54	22.1	38.1	103.6	53.3
FS10/57	2.27	8.4	9.5	26.1	8.5
FS11/60	2.75	8.9	9.7	32.7	18.2
FS12/64	1.0	3.8	5.5	10.5	6.6
FS13/66	2.27	5.8	7.6	13.4	9.2
FS14/68	1.0	17.5	12.6	28.0	14.6
FS15/80	1.0	12.8	12.5	30.0	16.1
FS19/105	1.0	21.5	15.0	40.8	21.0
FS20/112	1.0	9.2	9.8	28.5	14.3
FS21/115	2.27	27.8	21.9	60.4	31.1
FS22/117	1.0	17.8	17.0	34.9	18.1

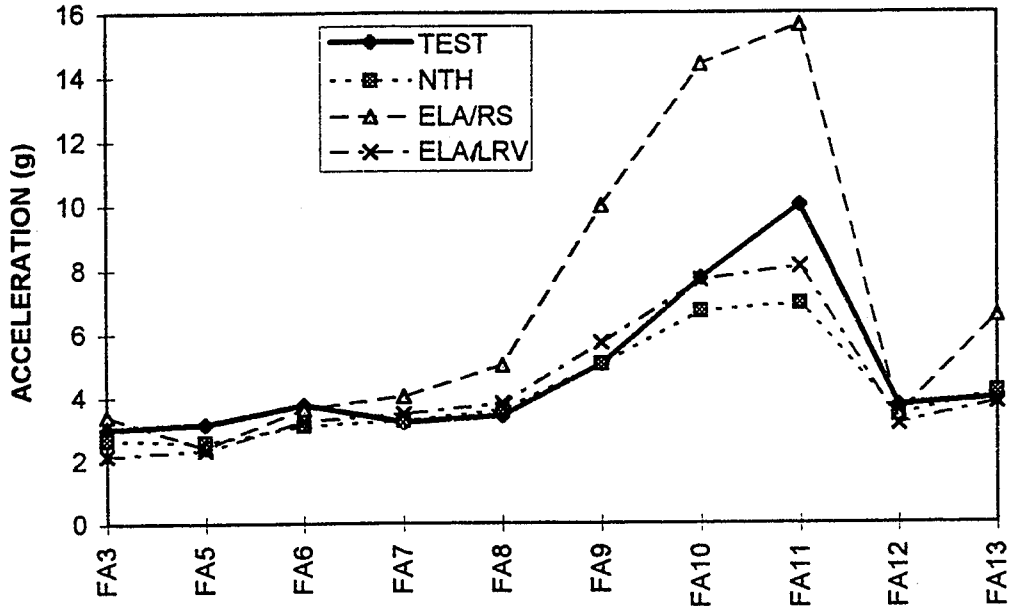

Figure 5.85 Comparison of Responses of F-line with EAB Supports for 1.2 S2(C) Test Run, X-Direction Accelerations

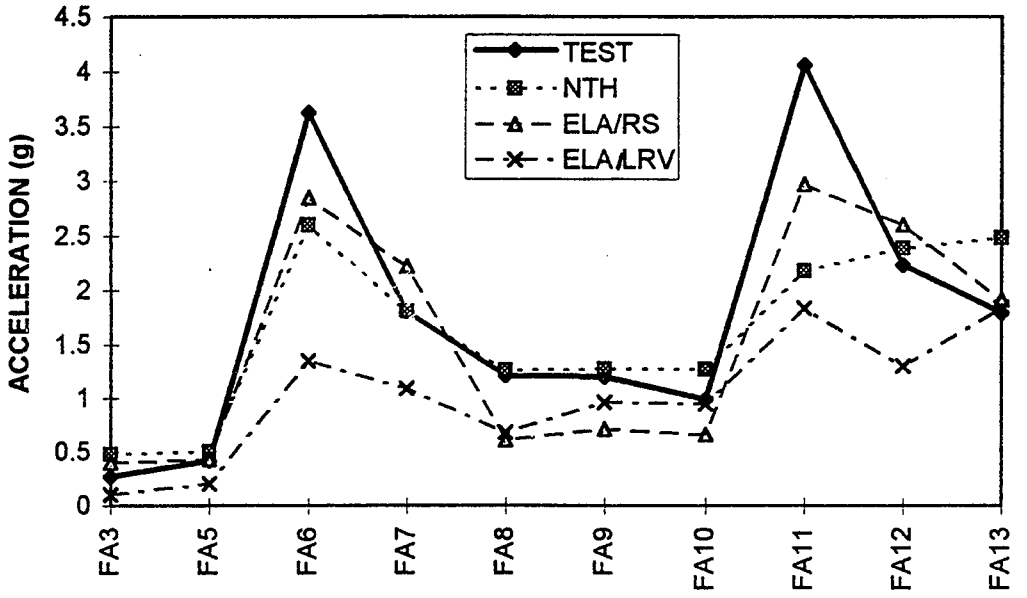

Figure 5.86 Comparison of Responses of F-line with EAB Supports for 1.2 S2(C) Test Run, Y-Direction Accelerations

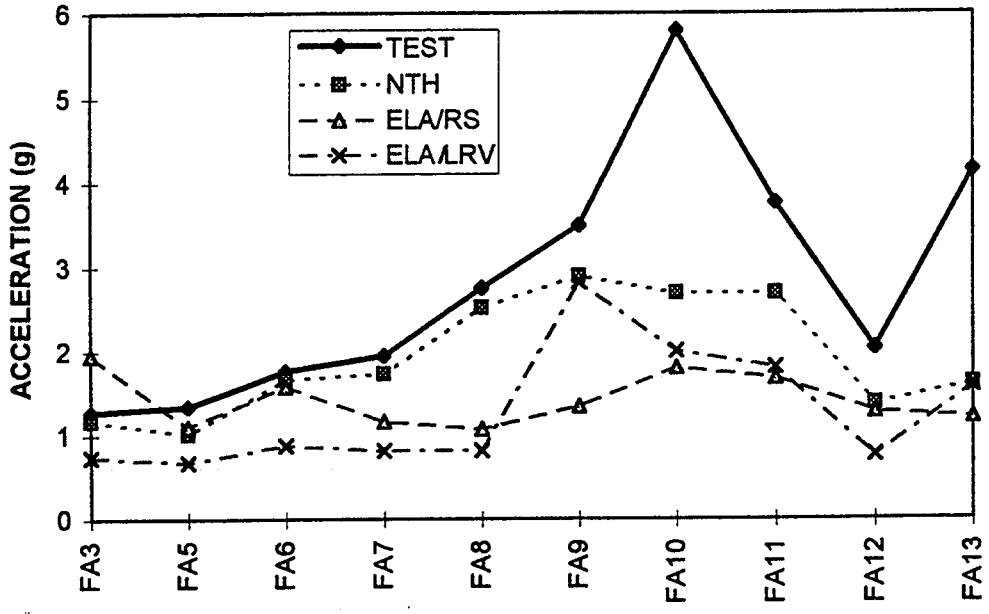

Figure 5.87 Comparison of Responses of F-line with EAB Supports for 1.2 S2(C) Test Run, Z-Direction Accelerations

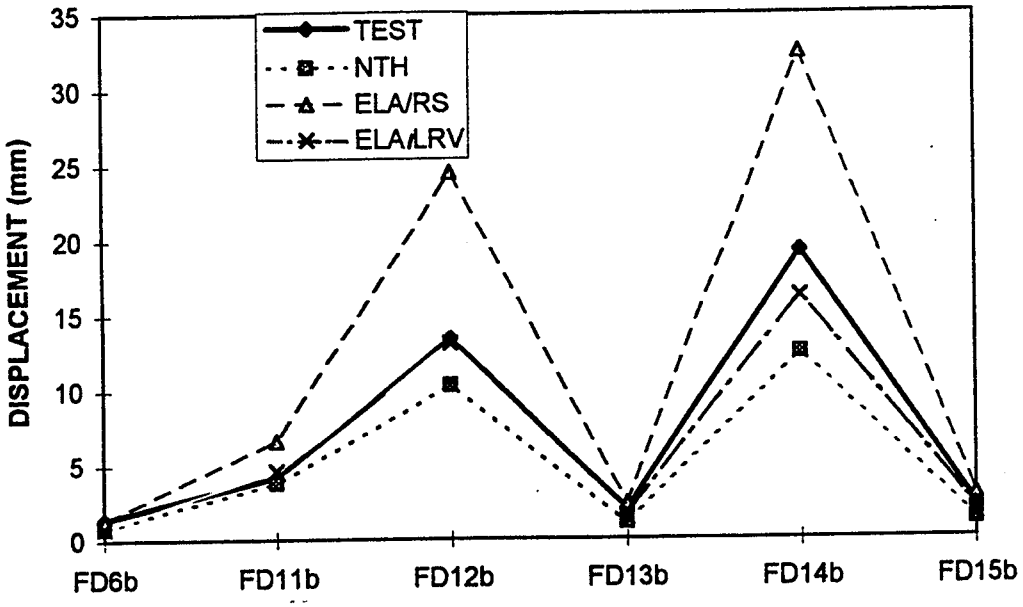

Figure 5.88 Comparison of Responses of F-line with EAB Supports for 1.2 S2(C) Test Run, Displacements

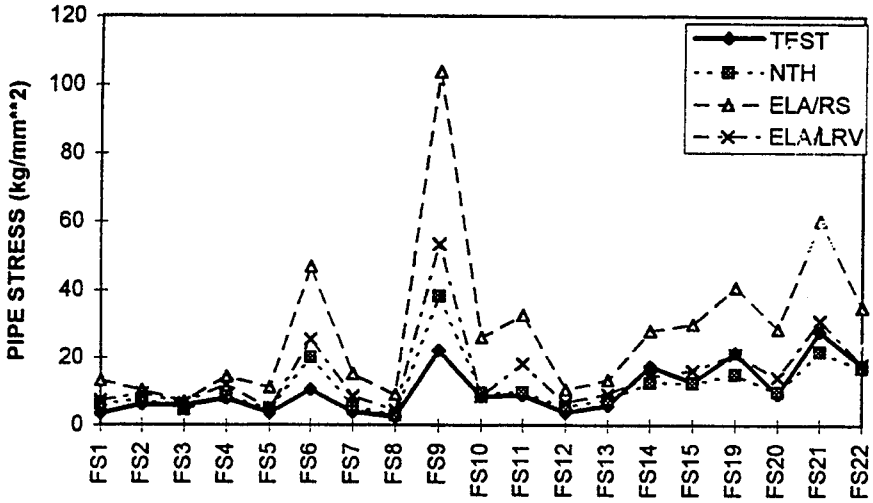

Figure 5.89 Comparison of Responses of F-line with EAB Supports for1.2 S2(C) Test Run, Pipe Stresses

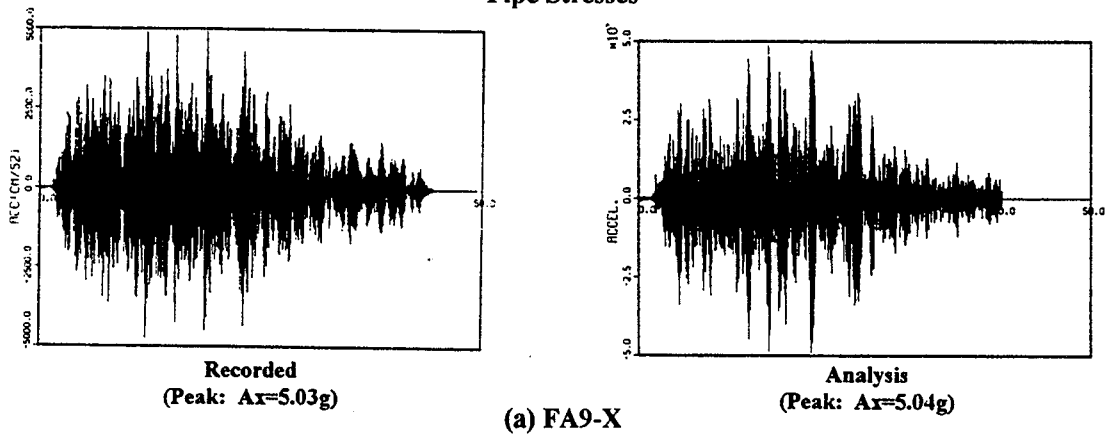

Recorded
(Peak: Ax=5.03g)

Analysis
(Peak: Ax=5.04g)

(a) FA9-X

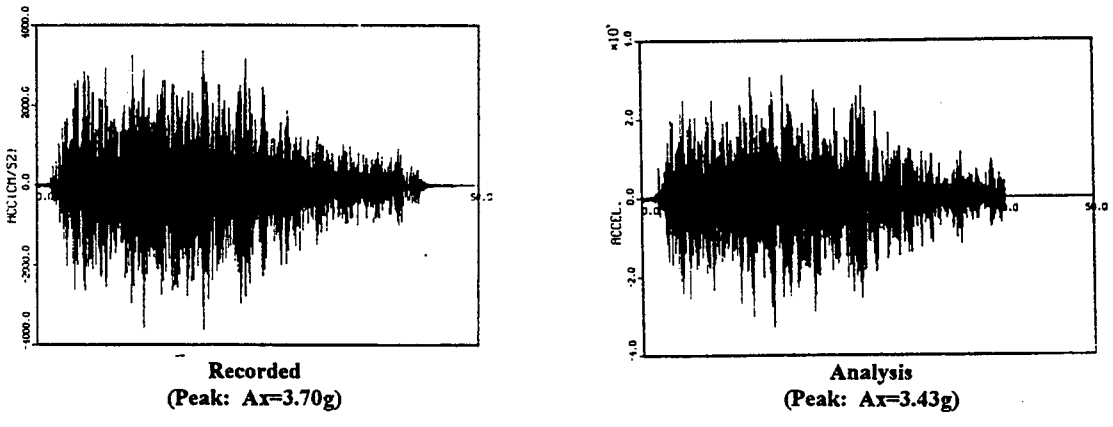

Recorded
(Peak: Ax=3.70g)

Analysis
(Peak: Ax=3.43g)

(b) FA12-X

Figure 5.90 Comparison of Acceleration Time Histories of F-line with EAB Supports for 1.2 S2(C) Test Run

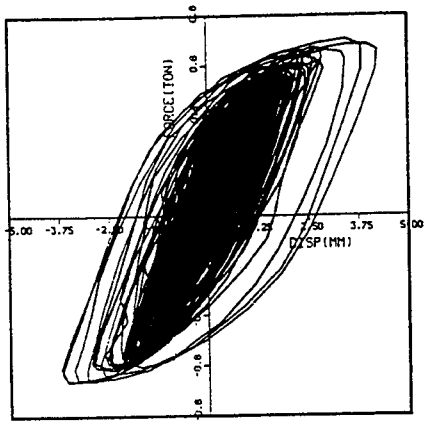

Recorded
(Peak: U=4.2 mm)

(a) EAB-1

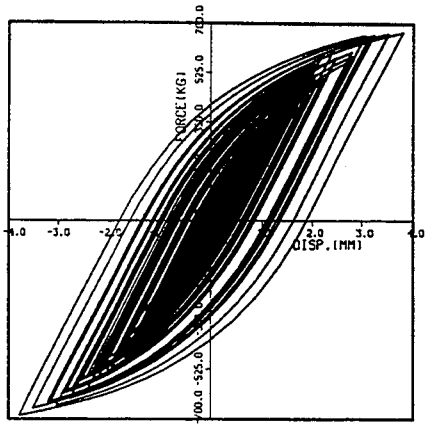

Analysis
(Peak: U=3.79 mm)

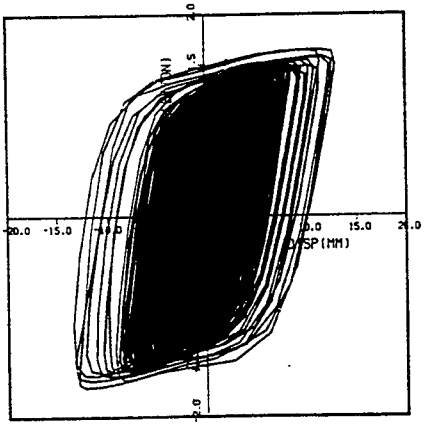

Recorded
(Peak: U=13.4 mm)

(b) EAB-2

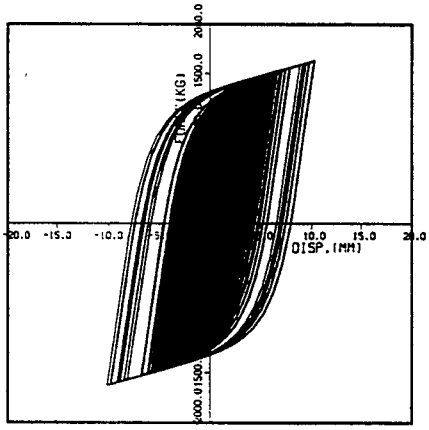

Analysis
(Peak: U=10.3 mm)

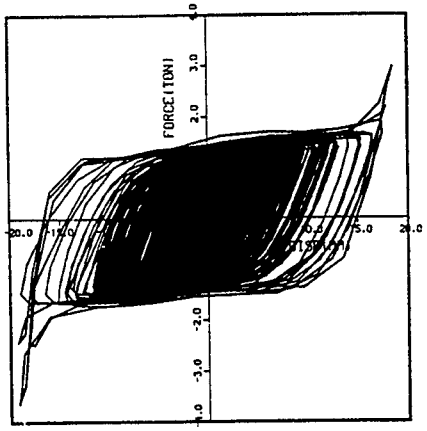

Recorded
(Peak: U=19.2 mm)

(c) EAB-3

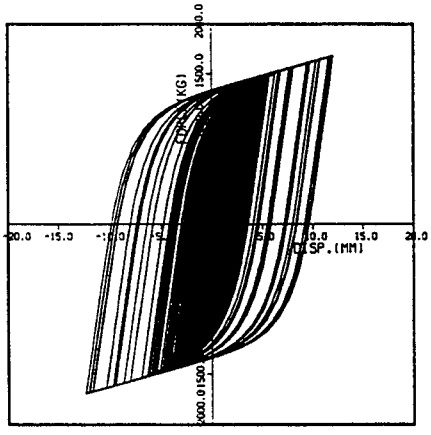

Analysis
(Peak: U=12.4 mm)

Figure 5.91 Comparisons of Force-Deformation Relationship of EAB Supports of F-line for 1.2 S2(C) Test Run

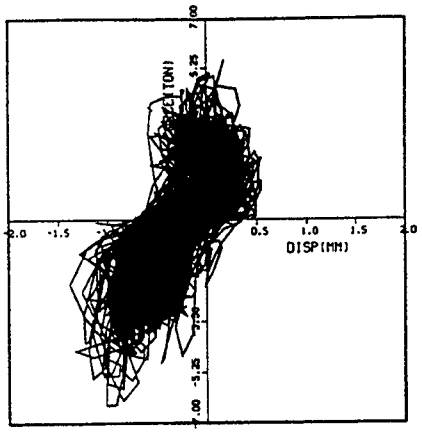

Recorded
(Peak: U=1.4 mm)

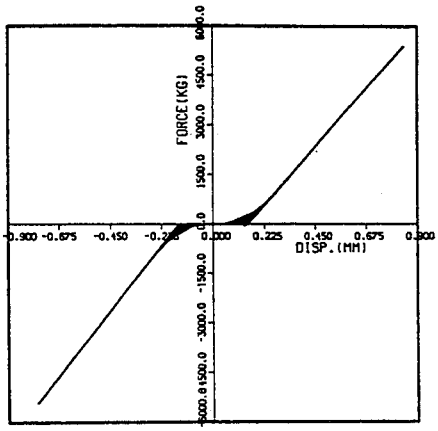

Analysis
(Peak: U=0.84 mm)

(a) FR6

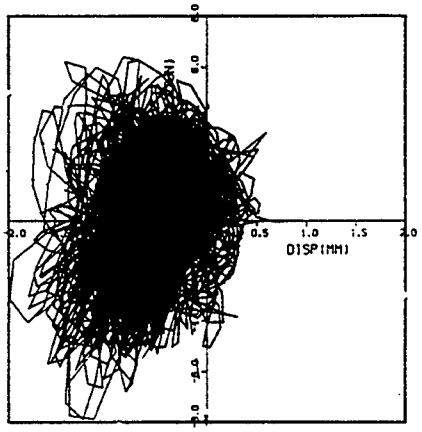

Recorded
(Peak: U=2.0 mm)

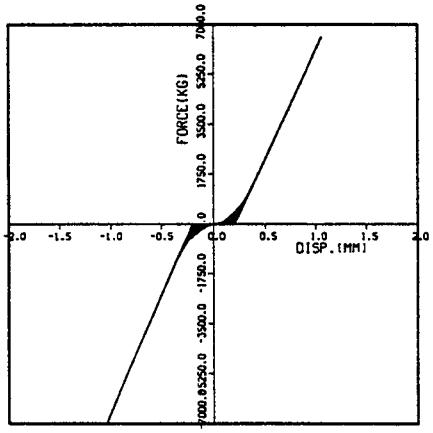

Analysis
(Peak: U=1.06 mm)

(b) FR13

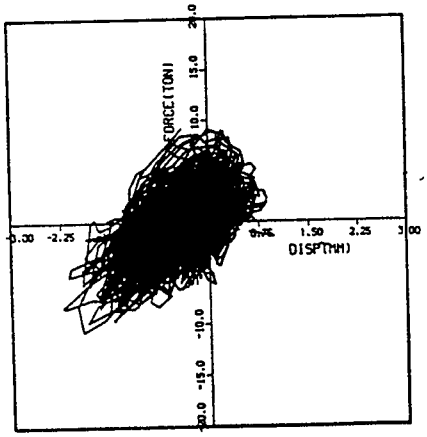

Recorded
(Peak: U=2.2 mm)

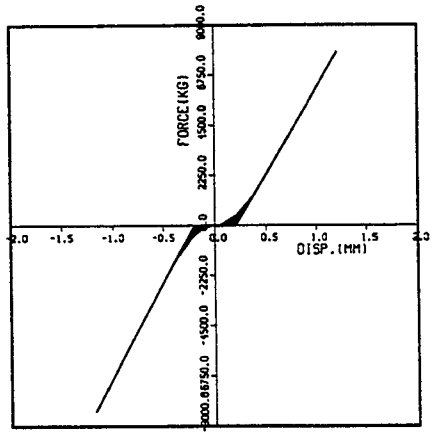

Analysis
(Peak: U=1.23 mm)

(c) FR15

Figure 5.92 Comparisons of Force-Deformation Relationships of Mechanical Snubbers of F-line with EAB Supports for 1.2 S2(C) Test Run

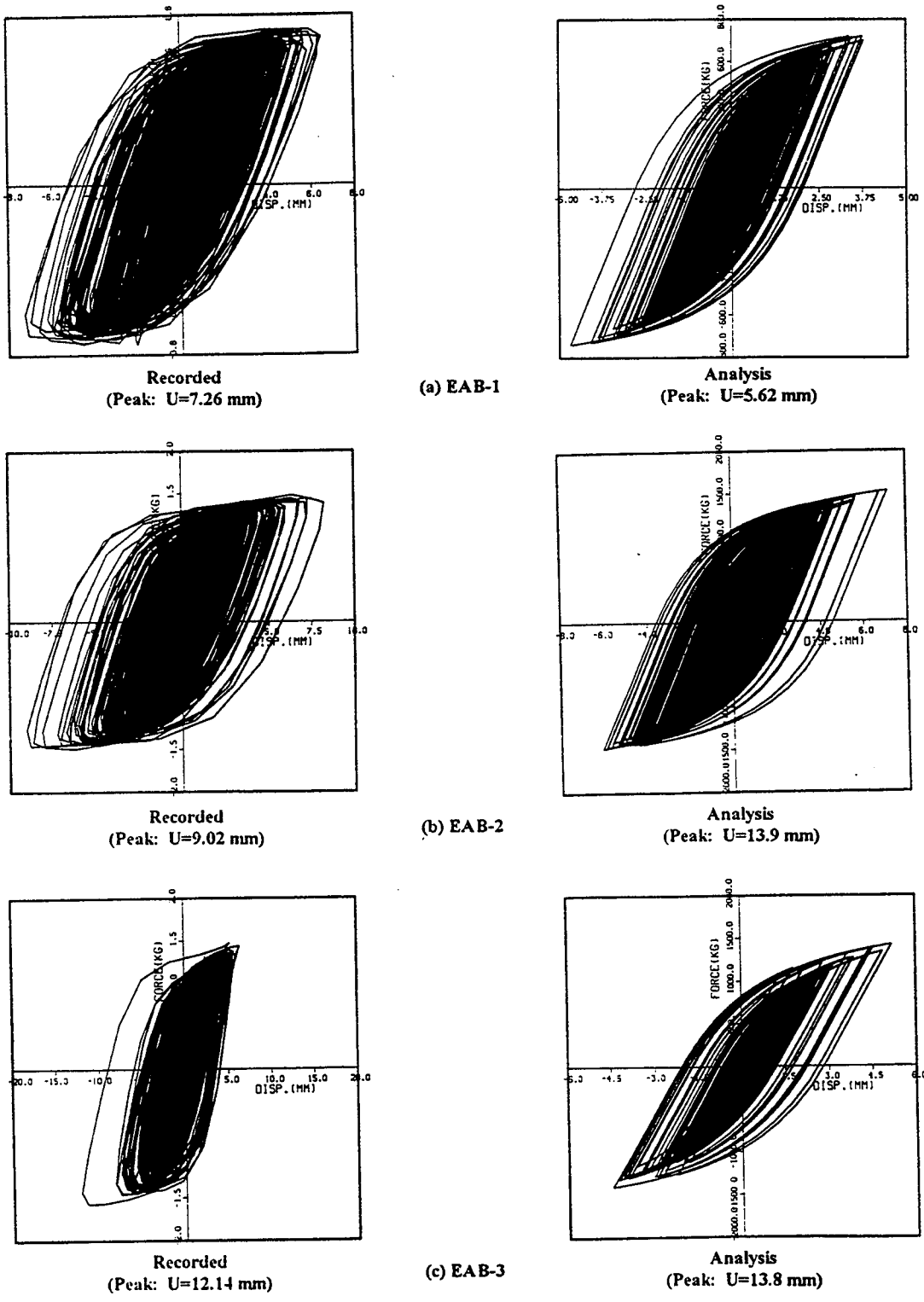

Recorded
(Peak: U=7.26 mm)

(a) EAB-1

Analysis
(Peak: U=5.62 mm)

Recorded
(Peak: U=9.02 mm)

(b) EAB-2

Analysis
(Peak: U=13.9 mm)

Recorded
(Peak: U=12.14 mm)

(c) EAB-3

Analysis
(Peak: U=13.8 mm)

Figure 5.93 Comparisons of Force-Deformation Relationship of EAB Supports of F-line for 1.3 S2(A) Test Run

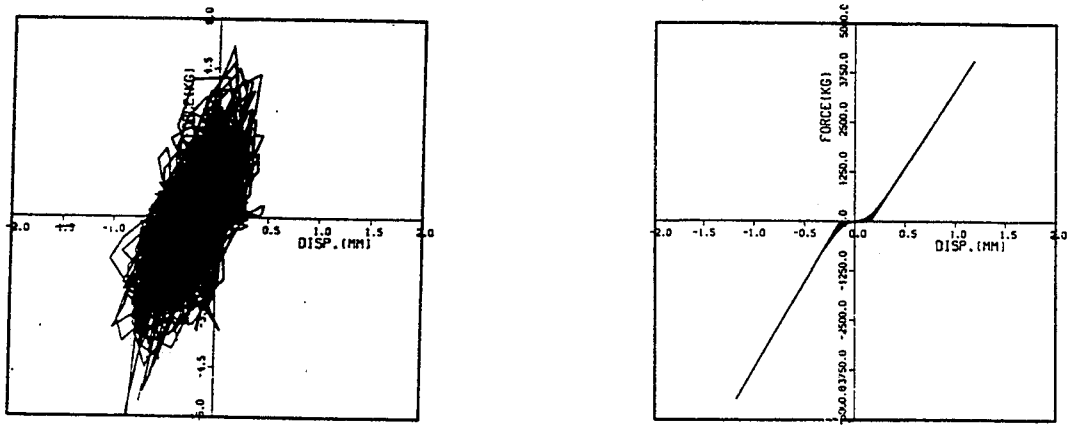

Recorded
(Peak: U=1.03 mm)

(a) FR6

Analysis
(Peak: U=1.2 mm)

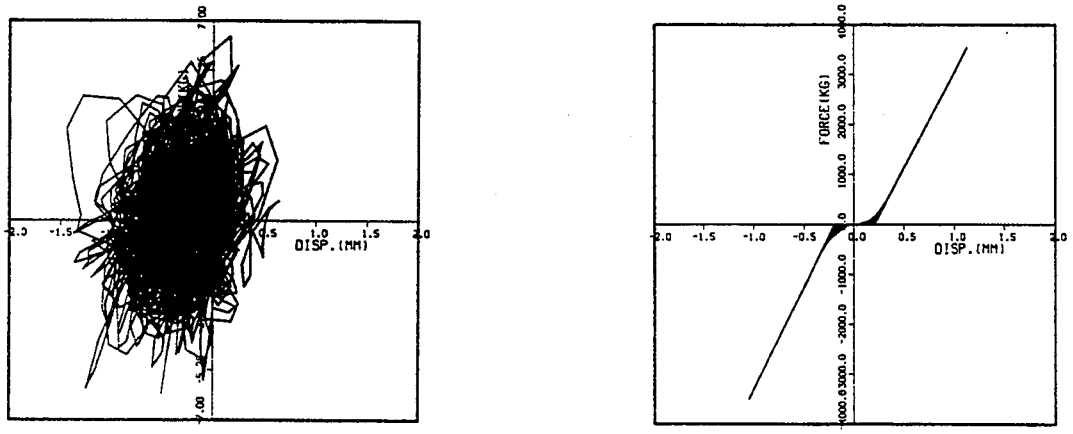

Recorded
(Peak: U=1.44 mm)

(b) FR13

Analysis
(Peak: U=1.7 mm)

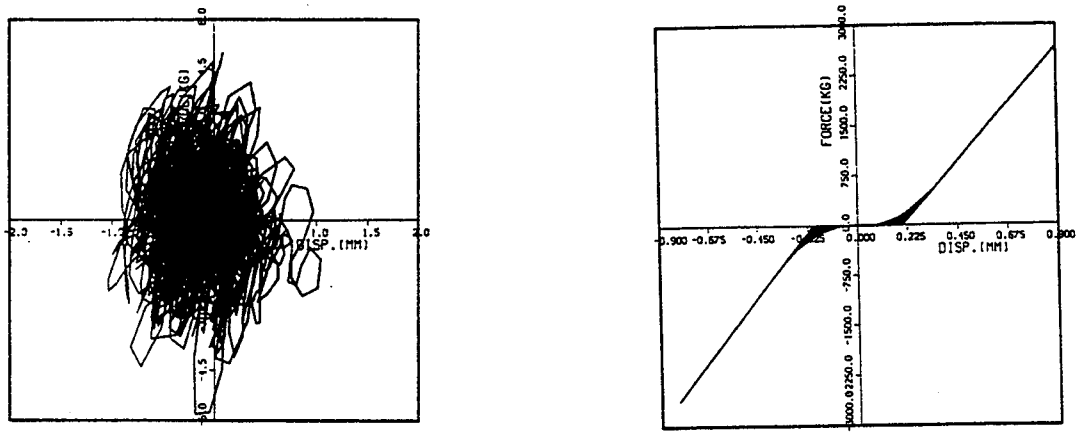

Recorded
(Peak: U=1.04 mm)

(c) FR15

Analysis
(Peak: U=1.8 mm)

Figure 5.94 Comparisons of Force-Deformation Relationships of Mechanical Snubbers of F-line with EAB Supports for 1.3 S2(A) Test Run

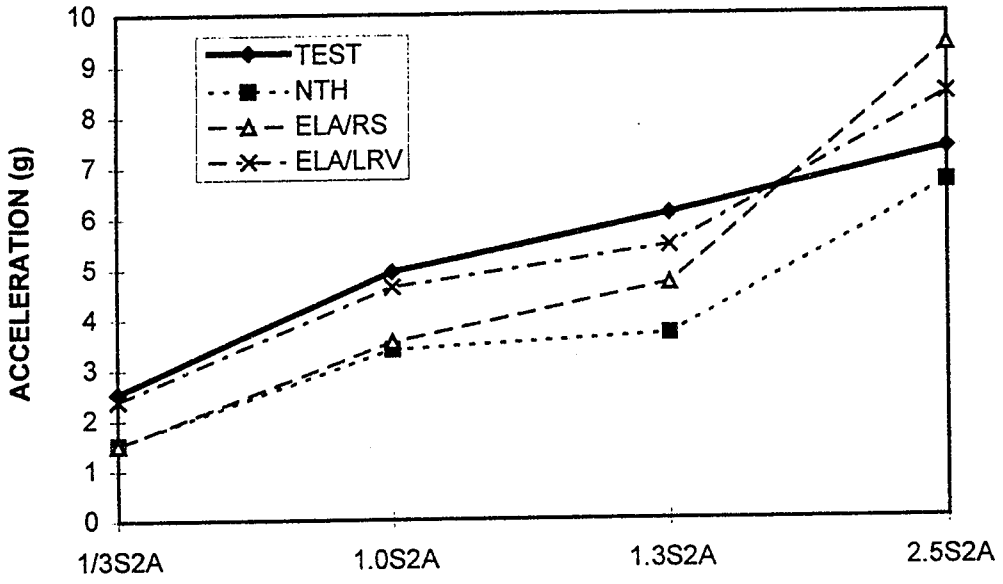

(a) FA6-X

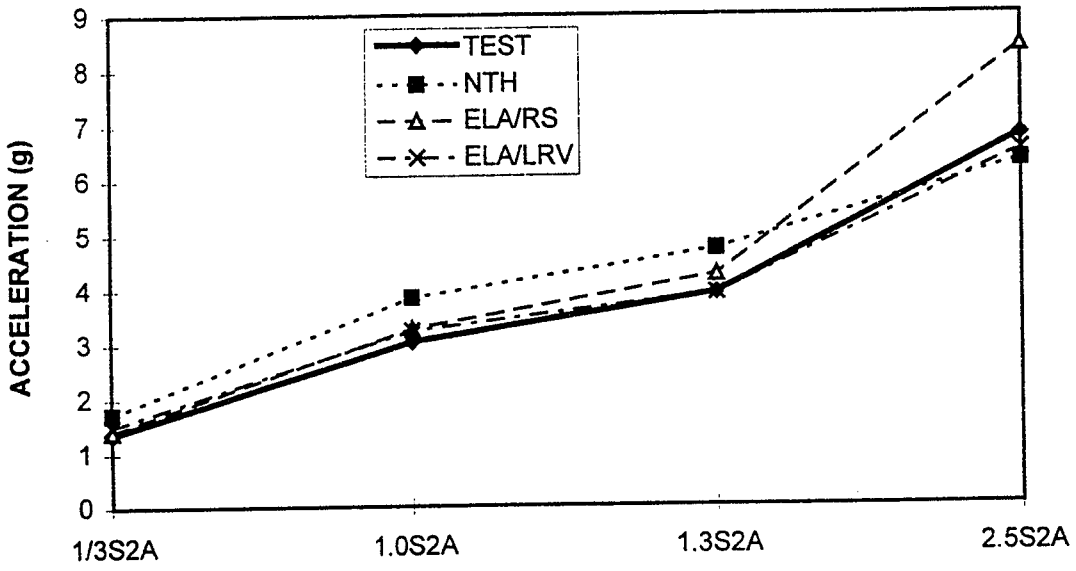

(b) FA9-X

Figure 5.95 Comparison of Peak Responses for F-line with EAB Supports

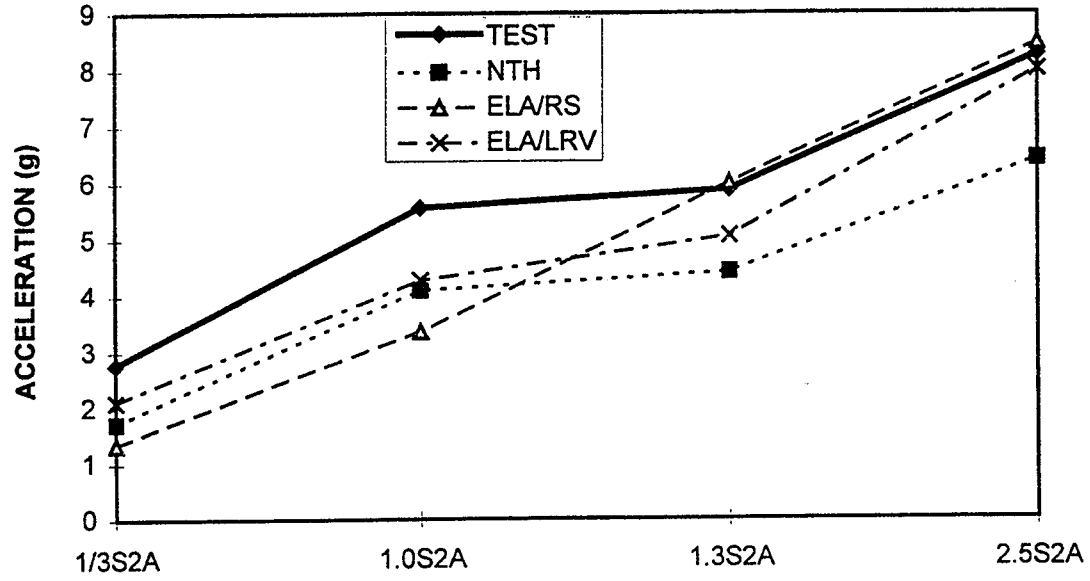

(c) FA12-X

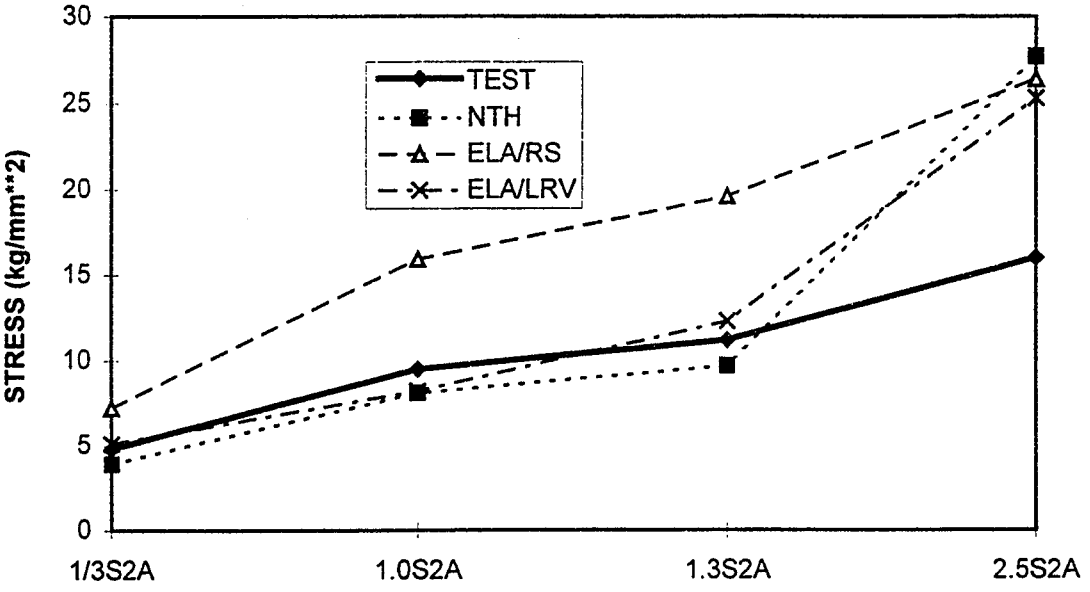

(d) FS4

Figure 5.95 Comparison of Peak Responses for F-line with EAB Supports (Cont'd)

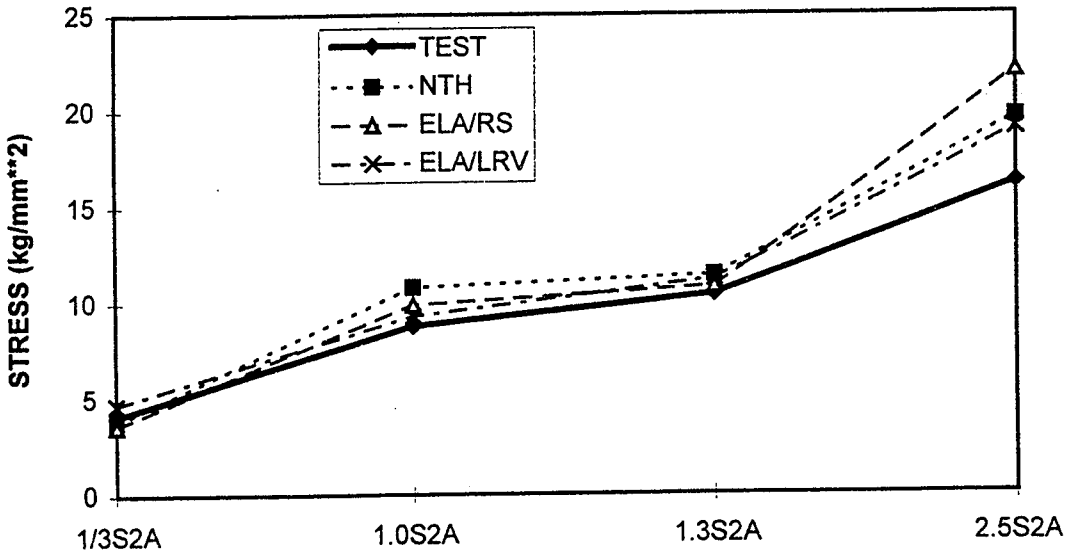

(e) FS14

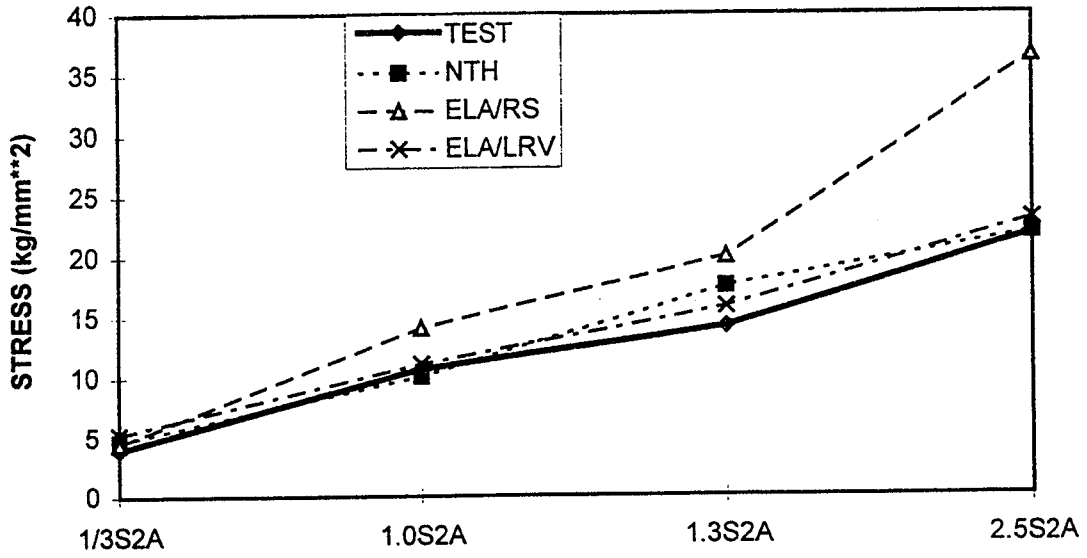

(f) FS21

Figure 5.95 Comparison of Peak Responses for F-line with EAB Supports (Cont'd)

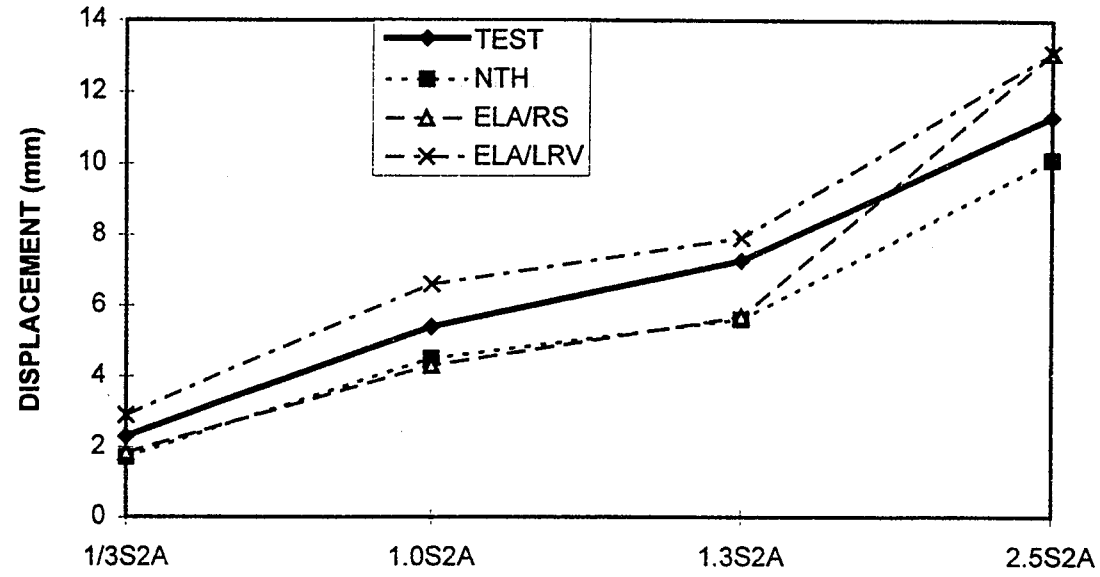

(g) EAB-1

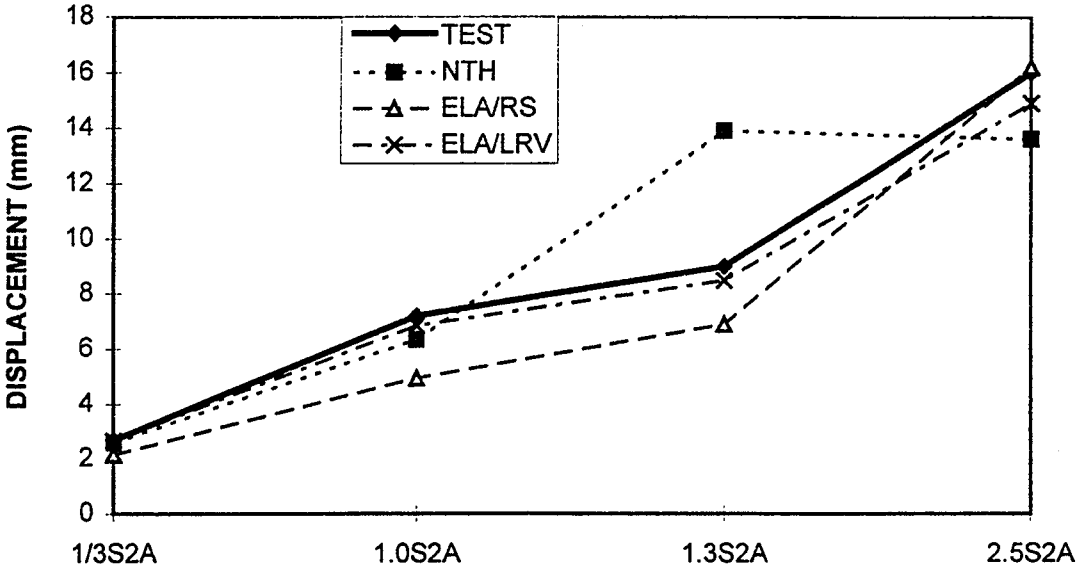

(h) EAB-2

Figure 5.95 Comparison of Peak Responses for F-line with EAB Supports (Cont'd)

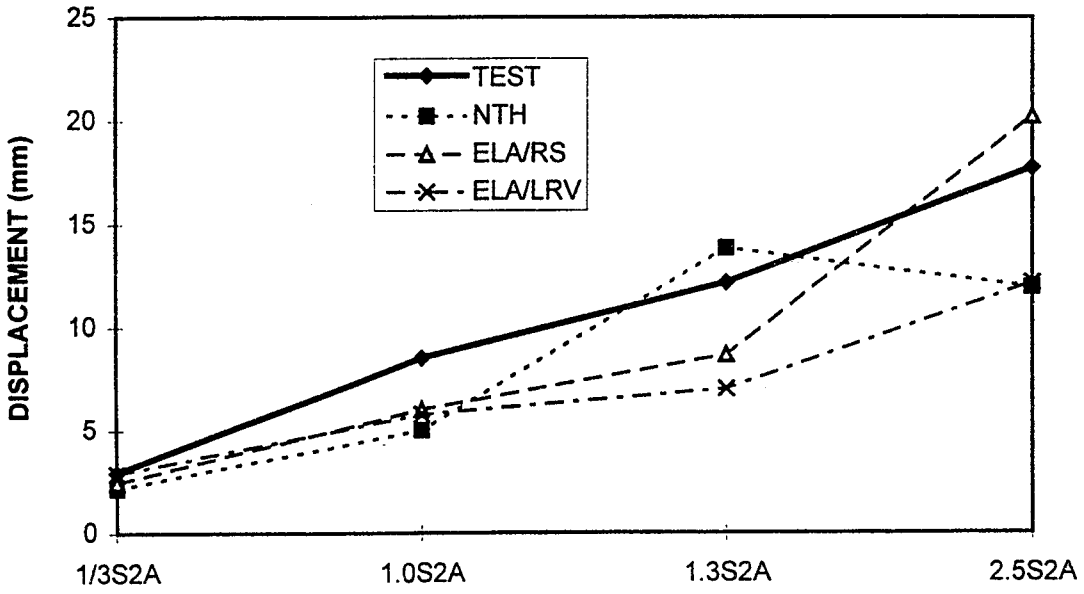

(i) EAB-3

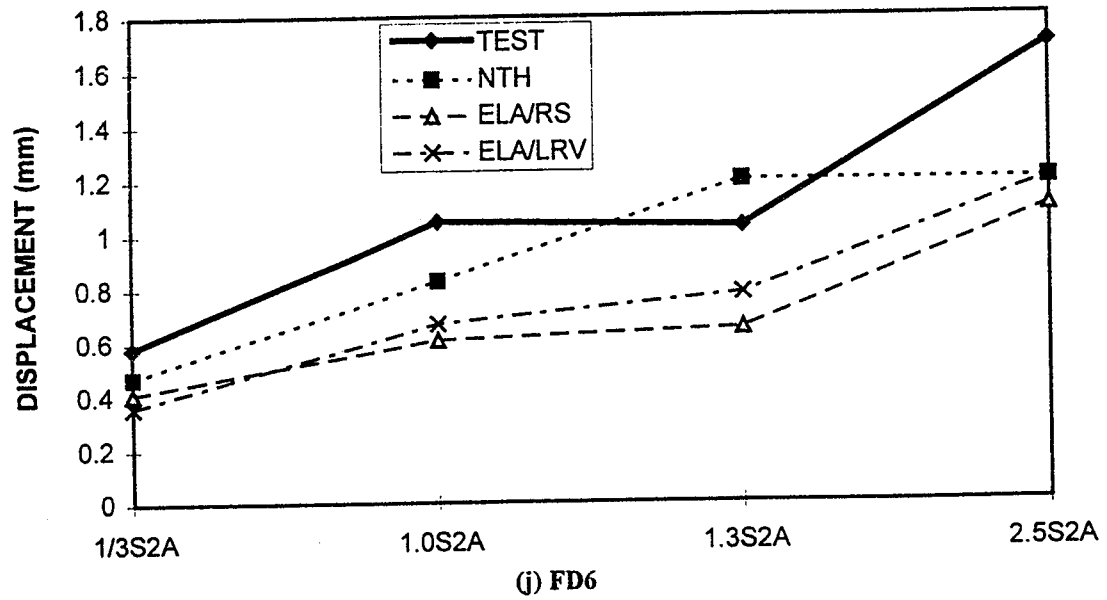

(j) FD6

Figure 5.95 Comparison of Peak Responses for F-line with EAB Supports (Cont'd)

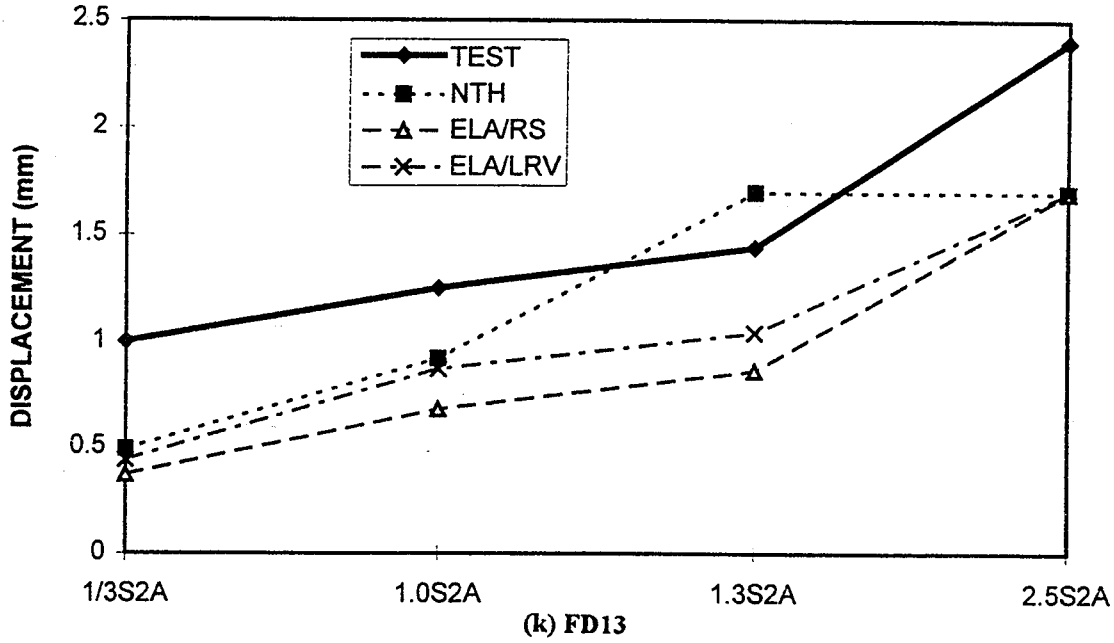

(k) FD13

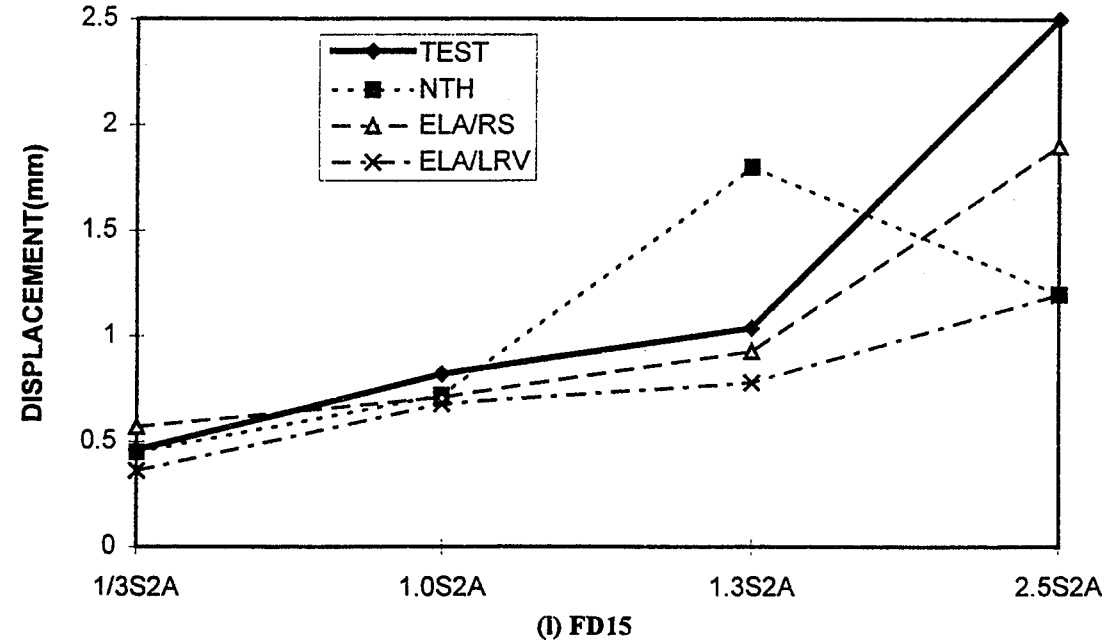

(l) FD15

Figure 5.95 Comparison of Peak Responses for F-line with EAB Supports (Cont'd)

Table 5.21 Pre-test Analyses of M-line with LED Supports for A-wave Motions Using ABAQUS and ISSAC Codes

(a) Acceleration (g)

Instrument/Node Num.	Direction	S_1 MOTION		S_2 MOTION	
		ABAQUS	ISSAC	ABAQUS	ISSAC
AA1/10	Y	1.82	1.76	3.66	3.14
	X	0	0	0	0
	Z	0.20	0.20	0.38	0.38
MA1/50	Y	1.80	1.47	3.33	2.58
	X	1.20	1.08	2.57	2.11
	Z	0.66	0.54	1.05	0.79
MA16/90	Y	1.66	1.29	2.67	2.10
	X	1.80	1.66	4.15	3.65
	Z	1.08	0.93	1.58	1.43
MA17/130	Y	1.89	1.77	3.28	2.81
	X	0.61	0.58	1.11	0.84
	Z	1.08	0.93	1.58	1.43
MA4/150	Y	2.24	1.95	3.25	3.09
	X	1.43	1.23	2.32	1.95
	Z	0.94	0.80	1.40	1.17
MA5/165	Y	1.87	1.41	2.56	2.18
	X	1.44	1.23	2.35	1.96
MA6/180	Y	1.17	0.83	1.78	1.32
	X	1.44	1.23	2.35	1.95
MA8/200	Y	1.06	0.87	1.40	1.27
	X	1.49	1.21	2.23	1.79
	Z	0.90	0.76	1.49	1.32
MA10/250	Y	1.03	0.84	2.10	1.83
	X	0.34	0.24	0.44	0.33
	Z	0.99	0.85	1.71	1.37

Table 5.21 Pre-test Analyses of M-line with LED Supports for A-wave Motions Using ABAQUS and ISSAC Codes (Cont'd)

(b) Displacement (mm)

Instrument/Node Num.		S_1 MOTION		S_2 MOTION	
		ABAQUS	ISSAC	ABAQUS	ISSAC
AD1/N-10	(X)	1.37	1.29	2.64	2.37
	(Y)	0	0	0	0.0
	(Z)	0.02	0.02	0.03	0.03
MD12, 13/N-90	(X)	3.04	1.87	4.34	2.61
	(Y)	4.92	3.51	9.10	6.27
MD15/LED-1		1.62	1.77	2.63	2.61
MD16/LED-2		3.37	2.37	4.18	4.98
MD17/LED-3		2.28	2.00	2.90	2.43
MD18/N-150	(X)	3.40	2.43	4.97	5.42
	(Y)	4.60	3.16	6.15	5.26
	(Z)	2.58	2.25	3.33	2.75

(c) Support Forces (ton)

Instrument/Node Num.	S_1 MOTION		S_2 MOTION	
	ABAQUS	ISSAC	ABAQUS	ISSAC
MR8/106	1.52	1.21	2.76	2.23
MR15/LED-1	1.51	1.34	1.56	1.50
MD16LED-2	1.58	1.41	1.62	1.64
MD17/LED-3	1.05	0.93	1.04	0.98

Table 5.21 Pre-test Analyses of M-line with LED Supports for A-wave Motions Using ABAQUS and ISSAC Codes (Cont'd)

(d) Pipe Stress σ (kg/mm^2)

Instrument/Node Num.		S_1 MOTION		S_2 MOTION	
		ABAQUS	ISSAC	ABAQUS	ISSAC
MS1/3	(2.0)[1]	4.10	4.16	6.64	6.66
MS2/7	(1.0)	0.80	0.93	1.04	1.37
MS3/9	(2.0)	2.50	2.02	3.54	3.38
MS4/14	(1.0)	0.81	0.88	1.16	1.36
MS5/17	(2.0)	3.90	3.42	6.54	5.12
MS6/46	(1.0)	1.82	1.52	2.88	2.44
MS10/30	(1.0)	1.60	1.31	2.41	1.60

[1]Value in ( ) is stress intensification factor.

Table 5.22 Displacement Responses of M-line With LED Supports and Without Actuator for 2.5 S2(A) Test Run Using ANSYS and ISSAC Codes

Instrument/Element Num.		Test	ANSYS	ISSAC
MD12, 13/N-90	(X)	21.1	23.9	20.7
	(Y)	4.2	11.2	12.2
MD15/LED-1		4.7	11.9	6.0
MD16/LED-2		10.8	30.5	10.7
MD17/LED-3		7.5	8.8	8.6
MD18/N-150	(X)	10.2	24.4	11.6
	(Y)	9.6	18.2	13.3
	(Z)	7.4	9.8	9.4

*Note: Damping was assumed to be 2.5%.

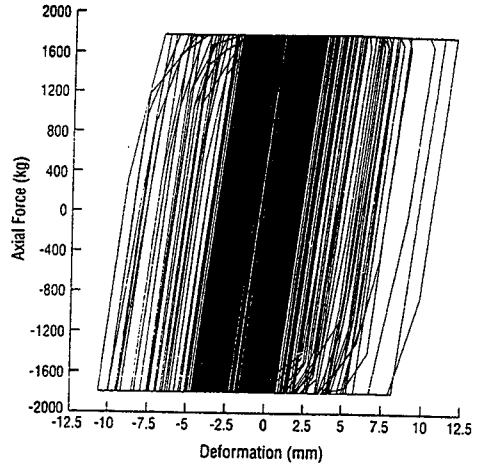

(a) LED-1
(Peak: U=11.9 mm)

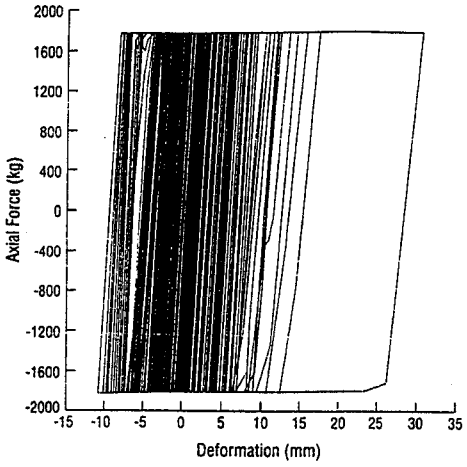

(b) LED-2
(Peak: U=30.5 mm)

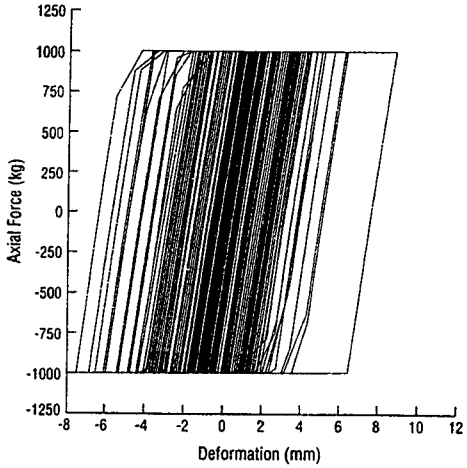

(c) LED-3
(Peak: U=8.8 mm)

Figure 5.96 Hysteretic Responses of LED Supports for M-line without Independent Actuator for 2.5 S2(A) Test Run, by ANSYS Code

6 DESIGN ANALYSIS

6.1 Analysis Summary

A series of seismic analyses were performed to predict the responses of the F-line and the M-line with conventional supports using piping design analysis methods and procedures that are currently applied in the nuclear industry. The objective of these studies was to investigate the degree of conservatism associated with current piping design analysis methods by direct comparison of analysis results to test results. For each piping system, a baseline analysis case was defined using representative modeling methods and design parameters. Each baseline analysis case was analyzed using the S_2 earthquake level test input motion. Additional studies were performed to investigate the effects of specific variations in modeling methods, analysis parameters and seismic input level on the results.

The BNL in-house piping analysis computer program, PSAFE2, was used to perform the design analyses. For additional verification of the analysis results, the ANSYS program was also applied in selected cases. Consistent with design practice, linear elastic finite element models of the two piping systems were formulated using the information on piping layout geometry, cross-sectional properties, material properties, support locations, and added masses given in the design drawings and design specifications. Straight and curved elastic pipe elements were used to represent the piping and linear spring elements were used to represent the pipe supports.

Consistent with design practice, the response spectrum method of analysis was used. The seismic response spectra were developed from recorded acceleration versus time measurements taken during the test. The F-line analysis assumed uniform table motion at all supports. Three sets of broadened response spectra corresponding to the three orthogonal directions of table motion were generated. The M-line analysis considered uniform table motion and independent actuator motion. The analysis was based on the independent support motion analysis method using two support groups. For the M-line, three sets of broadened table motion spectra and three sets of broadened independent actuator motion spectra were generated.

The studies investigated two critical design responses: pipe stresses and support loads. The analytically predicted values of these responses were compared to the peak test values recorded at the instrumented locations. At each location, the ratio of analysis response to test response was calculated to assess the conservatism associated with the baseline analysis methods. Additional analyses were performed to investigate the effects of parameter variations on these ratios. For both the F-line and the M-line, additional analyses were performed to investigate the effects of variations in snubber stiffnesses, damping, response spectrum broadening and seismic input level. For the M-line, additional variations associated with the independent support motion analysis method were studied. Specific details of the design parameters and methods applied in the baseline analyses and in the additional analyses are given and discussed below.

6.2 F-line Design Analysis

6.2.1 Baseline Model and Analysis Parameters

The PSAFE2 baseline analysis model of the F-line is similar to the ISSAC model shown in Figure 5.2 except for the frame support at the end which is replaced by a rigid anchor. The geometric and material properties of the piping are given in Table L.1. The piping system is supported by mechanical snubbers, hangers, guides and anchors as shown in Figure 2.2. Preliminary analyses had shown snubber modeling to be a critical parameter in predicting piping system response. Test results had shown the snubbers to exhibit complex nonlinear behavior. However, in design analyses, snubbers are modeled as linear springs with spring constants supplied by the snubber vendors based on test data. For the F-line baseline analysis, the spring constants were calculated based on component test data provided by NUPEC.

Figure L.12 illustrates the idealized force versus displacement characteristics based on component tests and the equivalent linear stiffness used in the baseline design analysis model. Table 6.1 lists the stiffness values used in this analysis. The effects of variations in the snubber linear stiffness assumptions were further investigated and are discussed below.

In piping design analysis, the response spectrum analysis method is generally applied to predict seismic response. For the F-line, the table input motion was assumed to be uniform at all supports. Response spectra in three directions were calculated from the table motion acceleration time histories measured at instrument locations XO(XB), ZO(XB), and YD2-E. Test run VC-3 with S_2(F) level input motion was selected for the baseline analysis case. The three response spectra were broadened by $\pm$15 percent in accordance with NRC Regulatory Guide 1.122 as shown in Figure 6.1. Since the size of the piping is less than 12 inches in diameter, two percent damping was used based on NRC Regulatory Guide 1.61. Using the PSAFE2 computer program, modal responses of the piping system were calculated up to a cutoff frequency of 50 Hz. Modal responses were combined in accordance with the NRC Regulatory Guide 1.92 Grouping Method. This method specifies that maximum responses of closely spaced groups of modes within a frequency range of ten percent be combined by absolute sum. The total response is then obtained by combining these closely spaced group responses and the responses of all non-closely spaced modes by the square root of the sum of the squares (SRSS) method. The three directional responses were combined by the SRSS method as specified in NRC Regulatory Guide 1.92.

6.2.2 Additional Analyses

Additional design analyses were performed to investigate the effects of variations in design modeling and analysis parameters on the analysis to test ratios. Preliminary analyses had shown snubber stiffness to be a critical modeling parameter. The common current design practice is to model piping system snubbers using vendor supplied equivalent linear stiffness values determined by test for each specific snubber category, size and capacity. Another design practice is the use of a single representative design value for all snubbers. In earlier design analyses, a common practice was to assume that all supports including snubbers are rigid. Therefore, additional analyses were performed to determine piping system response using these two modeling variations. Design stiffness values of 4348 kg/mm provided by NUPEC were used in the first case and very large stiffness values (10^{11} kg/mm) were used to represent rigid stiffness in the second case. All other modeling and design parameters were the same as the baseline case. The results of these analyses are discussed in the next section.

Three additional analyses were performed for the F-line to investigate the effects of variations in damping, response spectrum broadening and seismic input. The damping values specified in NRC R.G. 1.61 are generally believed to be very conservative. The current ASME Code allows the use of 5 percent damping for response spectrum analysis. Therefore this value was selected for further investigation. The response spectra corresponding to table input motions were regenerated using 5 percent damping and the baseline analysis model was reanalyzed using this input.

Response spectrum broadening in a design analysis introduces conservatism to account for uncertainties in material properties and modeling techniques. Peak broadening by $\pm$15 percent is an upper limit which is generally used in lieu of performing specific studies to quantify the frequency variations associated with significant parameter variations as specified in NRC R.G. 1.122. In order to quantify the degree of conservatism that may be introduced by this peak broadening, an additional analysis of the baseline model was performed using the unbroadened table motion response spectra.

A final additional F-line analysis was performed to investigate the responses and margin (analysis/test ratio) at a higher level of seismic input. The table input motion from test run MC-3 which corresponded to a 1.3S_2(F) level earthquake

input was used to generate the broadened response spectra at two percent damping. The baseline model was analyzed to predict the seismic responses for comparison to test measurements at this higher input level.

6.2.3 Analysis Results

The critical design responses investigated in this study were pipe stress and support force. In the analyses, maximum pipe stresses were calculated in accordance with the ASME Code methodology. Using this procedure, the three directional components of moment at a cross section are combined by SRSS to determine the resultant moment. The pipe stress is computed by dividing the resultant moment by the section modulus and multiplying by the appropriate stress index. Pipe stresses from the test were determined from strain gage measurements. Figure L.21(d) shows the locations of the strain gages on the F-line. Each location contained either two or four gages around the pipe circumference. The maximum test pipe stresses were calculated by multiplying the largest strain measurement at each cross sectional location by Young's modulus. Maximum support forces at each support location were calculated in the analysis and were directly compared with the peak test values obtained at the load cell locations shown in Figure L.21(c).

6.2.3.1 Baseline Analysis

The results of the F-line baseline analysis are presented in tabular form in Tables 6.3(a) and 6.3(b). The tables list the maximum recorded test response (stress or support force), the corresponding analysis response, and the analysis to test ratio at each instrumented location. Table 6.7 summarizes the average, the maximum, and the minimum analysis to test ratios for all locations for the baseline analysis and the other design analyses discussed below. The results are also presented in graphical form in Figures 6.2 and 6.3. The figures show a direct comparison of the analysis versus test response and the computed analysis to test ratio at each location. The results show that the baseline analysis over predicts the pipe stress at most locations. The average analysis to test ratio for pipe stress is 2.07, varying from a low of 0.55 to a high of 4.56. On the other hand, the support forces predicted by analysis show smaller deviations from test results. The average analysis to test ratio is 1.15, varying from 0.68 to 1.64.

6.2.3.2 Snubber Stiffness Variations

The results of the analyses which involved variations in snubber stiffnesses are shown in Figures 6.4 and 6.5. A comparison of the frequencies of the three models to the frequencies determined in the test is shown in Table 6.5. Both the equivalent linear snubber baseline model frequencies and the design snubber stiffness model frequencies compare reasonable well to the test frequencies. However, the rigid snubber model frequencies are significantly higher. The stress results show the design snubber model to provide the most conservative results with an average analysis to test ratio of 3.17 and with no ratio less than one. The rigid snubber model gave the least conservative stress results with an average ratio of 1.4 and a number of locations where stress was under predicted. The same trend was observed in the support force results. The design snubber model over predicted support forces at all locations except one while the rigid snubber model under predicted at all locations but one.

6.2.3.3 Damping Variation

The comparison of results between the baseline analysis which assumed 2 percent damping and the analysis which assumed 5 percent damping are shown in Figures 6.6 and 6.7. As expected, the higher damping analysis predicted lower responses. The average analysis to test ratios for both stresses and support forces were reduced by almost 25 percent. The average stress ratio was 1.57 while the average support force ratio was 0.89 with most support forces under predicted.

6.2.3.4 Unbroadened Response Spectrum

The comparison of results between the baseline analysis which used a 15 percent broadened response spectrum and the analysis which used the unbroadened response spectrum are shown in Figures 6.8 and 6.9. The unbroadened response spectrum analysis results gave average analysis to test ratios which were approximately 30 percent lower than the baseline analysis. Most support forces were under predicted with an average ratio of 0.79. The average stress ratio was reduced to 1.50.

6.2.3.5 Higher Input Level

The results of the $1.3S_2(F)$ level earthquake analysis and comparisons to the corresponding test results are shown in Figures 6.10 and 6.11. Comparisons of the analysis to test ratios between this case and the baseline analysis shows the higher input level case ratios to be slightly more conservative at nearly every location. The average stress ratio is 2.39 versus 2.07 for the baseline case. The average support force ratio is 1.19 versus 1.15 for the baseline case.

6.3 M-line Design Analysis

6.3.1 Baseline Model and Analysis Parameters

The PSAFE2 baseline analysis model of the M-line is similar to the ISSAC model shown in Figure 5.1 except that a single linear spring element is used to represent snubbers MR3 and MR4. The geometric and material properties of the piping are given in Table L.1. The piping system is supported by mechanical snubbers, a hydraulic snubber, hangers, guides and anchors as shown in Figure 2.3. Preliminary analyses had shown snubber modeling to be a critical parameter in predicting piping system response. Although the snubbers exhibit complex nonlinear behavior, in design analyses, they are modeled as linear springs. In the same manner as the F-line design analysis, the M-line snubbers were modeled as linear springs with equivalent linear spring constants calculated as shown in Figure L.12. Table 6.2 lists the stiffness values used in the baseline design analysis model. Variations in the snubber stiffness assumptions were also investigated as discussed in the next section.

The M-line tests utilized an independent actuator to simulate the motion of the steam generator at one end of the piping system. Since the pipe was subjected to two distinctly different support input motions, the independent support motion (ISM) response spectrum method of analysis was applied as the baseline design analysis method. For analysis purposes, the M-line supports were divided into two support groups. The first group consisted solely of the anchor at the steam generator nozzle end of the system. The input motion was based on the recorded test motion of the actuator at instrument locations designated AA1-X, AA1-Y, and AA1-Z. The second group consisted of all other supports with input motion based on the table motion recorded at instrument locations XO(XB), ZO(XB) and YD2-E. Test run VC-6 with $S_2(M)$ level input motion was selected as the baseline analysis case. All response spectra were generated from the recorded acceleration time history data at the instrument locations noted above and broadened by $\pm$15 percent in accordance with NRC R.G. 1.122 as shown in Figure 6.12. Since the piping is less than 12 inches in diameter, two percent damping was used based on NRC R.G. 1.61. Due to the higher frequency peaks in the response spectra, modal responses were calculated up to a cutoff frequency of 100 Hz. Both modal responses and directional responses were combined by the SRSS method as recommended in NUREG-1061. In addition, since an ISM response spectrum analysis generates a set of responses for each support group, an additional level of combination is required. For the M-line baseline analysis, the two support group responses were combined by the NRC-accepted absolute sum method as recommended in NUREG-1061. Finally an additional set of static analyses is needed to determine the responses induced by the relative support displacements (seismic anchor motions). For the M-line, three static seismic anchor motion (SAM) analyses were performed for each direction of displacement. The peak actuator relative displacements in each direction recorded by instruments AD1-X, AD1-Y, and AD1-Z were applied in separate analyses

and the responses were combined by the SRSS method. The total piping system responses were obtained by combining the SAM responses with the inertial responses from the response spectrum analysis by SRSS as recommended in NUREG-1061.

6.3.2 Additional Analyses

Additional design analyses were performed to investigate the effects of variations in design modeling and analysis parameters on the design margins. A number of the modeling and analysis parameter variations were investigated for the M-line for the same reasons as for the F-line as discussed in Section 6.2.2 above. Modeling variations included the use of a single design value for snubber stiffness (3760 kg/mm as provided by NUPEC), and the use of rigid snubber stiffness. Parameter variations included 5 percent versus 2 percent damping and unbroadened versus broadened spectra.

Additional M-line design analyses were performed to study variations associated with the independent support motion analysis method. An analysis was performed to investigate the support group response combination method. The absolute sum method provides the most conservative response and has been recommended by NRC. However, the SRSS combination method has been applied in some cases. In order to investigate the potential differences, the baseline model was reanalyzed using the SRSS support group combination method. Another analysis was performed to investigate the inertia and SAM response combination. The SRSS method has been recommended in NUREG-1061 but the absolute sum method would provide more conservative results. An additional design analysis using this method was performed to assess the differences.

An additional M-line analysis was performed to investigate the differences between the ISM response spectrum method and the enveloped response spectrum method. Using the baseline model and analysis parameters, an envelope of the actuator response spectrum and the table response spectrum was developed for each direction of motion. A uniform motion response spectrum analysis was performed and the results were compared to the ISM analysis results and the test results.

Finally, two additional analyses was performed to investigate the responses and margins for a higher level $1.5S_2(M)$ test run MC-6 and for the multiple excitation test with modified actuator motion simulating the CV wave (test run DC-3: 1/3 $S_2(M)$ + CV).

6.3.3 Analysis Results

The critical design responses investigated in this study were pipe stress and support force. Maximum pipe stresses predicted by analysis were calculated in accordance with ASME Code methodology and compared against test stresses which were determined from strain gage measurements as described in Section 6.2.3. Figure L.20(c) shows the locations of the strain gages on the M-line. Maximum support forces at each support location were calculated in the analysis and directly compared with the maximum test values obtained at the load cell locations shown in Figure L.20(b).

6.3.3.1 Baseline Analysis

The results of the M-line baseline analysis are presented in Tables 6.4(a) and 6.4(b), and in Figures 6.13 and 6.14. The tables and figures present the peak test response, the corresponding analysis response, and the analysis to test ratio at each instrumented location. Table 6.8 gives the average, the maximum, and the minimum analysis to test ratios for all locations for the baseline analysis and the other design analyses discussed below. The results of the baseline analysis show that the analysis predicts conservative values of stress at all locations. The average analysis to test ratio

for pipe stress is 1.87, varying from 1.21 to 2.79. The support forces predicted by analysis are less conservative. On the average, the support forces are over predicted with an average ratio of 1.66, varying from 0.70 to 4.76. It was noted that support forces were under predicted in the supports closest to the independent actuator.

6.3.3.2 Snubber Stiffness Variations

The results of the analyses with variations in snubber stiffnesses are shown in Figures 6.15 and 6.16. A comparison of the piping model frequencies and test frequencies is shown in Table 6.6. All three models overestimated the frequencies determined by test. The design snubber stiffness model frequencies were closest to the test frequencies. The rigid snubber model frequencies were highest. Figure 6.15 shows that all three models gave conservative pipe stress results with no under prediction of stress. The design stiffness model gave the largest analysis to test stress ratio of 2.13 while the rigid model gave the lowest average ratio of 1.78. Support forces showed the same trend on average ratios with an average ratio of 1.85 for the design snubber model and 1.39 for the rigid snubber model. However, all three models under predicted support forces at some locations. It was noted that the rigid model was the only one that over predicted support forces at supports MR1 and MR2 which are closest to the actuator.

6.3.3.3 Damping Variation

The comparison of results between the baseline analysis with 2 percent damping and the analysis with 5 percent damping are shown in Figures 6.17 and 6.18. In the higher damping analysis, both the stresses and support forces were lower as expected. The average analysis to test ratios were reduced by nearly 20 percent. The average stress ratio was 1.53 while the average support force ratio was 1.35. Stresses ratios were still greater than one at each location. Support forces, however, were under predicted in five of the nine locations.

6.3.3.4 Unbroadened Response Spectrum

The comparison of results between the baseline design analysis which used a 15 percent broadened response spectrum and the analysis with the unbroadened response spectrum are shown in Figures 6.19 and 6.20. Average stress ratios are almost 15 percent lower and average support load ratios are almost 20 percent lower than the baseline case. The average stress ratio is 1.63 and is greater than one at all locations. The average support force ratio is 1.36 but, as in the baseline case, the support forces are under predicted at the supports closest to the actuator.

6.3.3.5 SRSS Support Group Response Combination Method

The comparison of results between the baseline design analysis which combined the two support group responses by the absolute sum method and the analysis which combined support group responses by SRSS are shown in Figures 6.21 and 6.22. As expected, the average ratios for the SRSS combination case were lower. Both the average stress ratio and the average support force ratio were reduced by about 15 percent. The average stress ratio is 1.58 and is greater than one in all locations. The average support force ratio is 1.43 but is less than one at four locations.

6.3.3.6 Absolute Sum Inertia and SAM Combination

The comparison of results between the baseline design analysis which combined the inertia and seismic anchor motion (SAM) responses by the SRSS method and the analysis which combined these responses by the absolute sum method are shown in Figures 6.23 and 6.24. The average stress ratio for the absolute sum case was nearly 20 percent higher (2.20) and the average support force ratio was almost ten percent higher (1.79) than the baseline analysis case. As in the baseline case, the stress ratio exceeded one at all locations. Support forces predicted near the actuator were closer to the test values but were still under predicted at the MR2, MR3 and MR4 locations.

6.3.3.7 Enveloped Response Spectrum Method

The comparison of results between the baseline analysis which applied the independent support motion response spectrum analysis method and the analysis which utilized the enveloped response spectrum analysis method are shown in Figures 6.25 and 6.26. As anticipated, the stress and support force ratios are much higher when the enveloped method is used. Average stress ratio is 5.12 and greater than one at all locations. Average support force ratio is 5.82 although the support force at one location (MR2) is still underpredicted.

6.3.3.8 Higher Level Input

The results of the $1.5S_2(M)$ level earthquake analysis and comparisons to the corresponding test results are shown in Figures 6.27 and 6.28. Stress ratios for this case are comparable to the baseline case with an average stress ratio of 1.90 compared to 1.87 for the baseline case and with no stress ratios less than one. Support force ratios are slightly lower with an average ratio of 1.54 compared with the baseline average value of 1.66. As in the baseline case, support forces are underpredicted at the same locations near the actuator.

6.3.3.9 Multiple Excitation Test Input

The results of the $1/3S_2(M)$ + CV multiple excitation test input analysis and comparisons to its corresponding test results are shown in Figures 6.29 and 6.30. Stress ratios for this case are significantly lower than for the baseline case. The average stress ratio is 1.20 with stresses underpredicted at three locations. Support force ratios are also lower with an average value of 1.42. The support forces are underpredicted at the supports closest to the actuator as well as at a number of other locations.

6.4 Conclusions

The comparisons of design analysis to test results presented above demonstrate the overall conservatism of the baseline design analysis methods. For both piping systems, the pipe stress results were generally more conservative than the support force results. On an average basis, the design analyses provided adequate margins for both pipe stresses and support forces. However, the analysis to test result ratios varied significantly from one location to another. M-line stresses predicted by the baseline analysis exceeded the test measurements at all locations. F-line design analysis stresses were underpredicted at a few locations although the stresses at those locations were low. M-line support forces were underpredicted at locations near the independent actuator. F-line support forces were underpredicted at several locations.

The analyses involving snubber stiffness variations showed the importance of proper support stiffness representation in a piping analysis. For both piping systems, the equivalent linear stiffness snubber model and the design stiffness snubber model provided reasonably conservative results. The rigid snubber model gave unrealistically high piping system frequencies and the lowest analysis to test margins. This was especially evident for F-line support forces.

The analyses which involved higher level test input ($1.3S_2(F)$ and $1.5S_2(M)$) provided margins which were fairly consistent with the baseline S_2 level analyses. The additional analyses which investigated other variations in analysis parameters and methods (damping, response spectrum broadening, support group combination, etc.) provided useful information on how these variations may reduce or increase the conservatism in the design margins for representative piping systems.

Table 6.1 F-line Equivalent Linear Snubber Stiffnesses Used in Baseline Design Analysis

Snubber	Ke (Kg/mm)
FR2	3492
FR3	5366
FR4	2958
FR5	3464
FR6	6861
FR7	4824
FR8	5124
FR9	4848
FR10	5270

Table 6.2 M-line Equivalent Linear Snubber Stiffnesses Used in Baseline Design Analysis

Snubber	Ke (Kg/mm)
MR1	5639
MR2	6094
MR3/MR4	3875
MR5	8301
MR6	8301
MR7	5000

Table 6.3 F-line Baseline Analysis vs. Test Results

(a) Pipe Stresses

Location	Test (kg/mm2)	Analysis (kg/mm2)	Analysis/Test Ratio
FS1	2.87	8.73	3.04
FS2	1.32	3.22	2.44
FS3	0.99	3.20	3.23
FS4	1.25	5.67	4.54
FS5	1.58	3.15	1.99
FS6	1.42	6.48	4.56
FS7	1.6	2.57	1.61
FS8	0.44	0.33	0.75
FS9	1.61	0.88	0.55
FS10	0.9	2.52	2.80
FS11	1.71	5.62	3.29
FS12	1.42	2.16	1.52
FS13	1.43	3.06	2.14
FS14	2.87	3.85	1.34
FS15	1.23	1.21	0.98
FS19	1.56	1.45	0.93
FS20	2.06	1.72	0.83
FS21	1.78	2.73	1.54
FS22	2.8	3.61	1.29

Table 6.3 F-line Baseline Analysis vs. Test Results (Cont'd)

(b) Support Forces

Location	Test (kg)	Analysis (kg)	Analysis/TestRatio
FR2	884	831	0.94
FR3	1394	2045	1.47
FR4	960	1012	1.05
FR5	1423	2187	1.54
FR6	2453	4027	1.64
FR7	3518	2409	0.68
FR8	2423	2244	0.93
FR9	2732	2573	0.94
FR10	1853	2128	1.15

Table 6.4 M-line Baseline Analysis vs. Test Results

(a) Pipe Stresses

Location	Test (Kg/mm2)	Analysis (Kg/mm2)	Analysis/Test Ratio
MS1	1.86	3.82	2.05
MS2'	0.97	1.17	1.21
MS2	1.63	2.49	1.53
MS3	2.30	3.21	1.40
MS4	1.37	2.32	1.69
MS5	1.02	1.83	1.80
MS6	1.52	3.63	2.39
MS8	0.80	1.96	2.44
MS9	0.63	1.76	2.79
MS10	0.61	0.85	1.40

(b) Support Forces

Location	Test (kg)	Analysis (kg)	Analysis/Test Ratio
MR1	5220	3760	0.72
MR2	6810	4774	0.70
MR3,MR4	2870	2129	0.74
MR5	2510	3070	1.22
MR6	3270	3625	1.11
MR7	1550	3168	2.04
MR8	430	2048	4.76
MR9	1100	2486	2.26
MR10	970	1349	1.39

Table 6.5 F-line Piping Frequencies Test vs. Analysis

Test (Hz)	Analysis (Hz)		
	Baseline Model Equivalent Linear Stiffnesses	Design Snubber Stiffnesses	Rigid Snubber Stiffnesses
16.4	18.9	17.1	23.0
21.0	21.8	21.6	25.2
22.4	22.5	22.4	26.1
23.4	24.0	24.1	29.5
25.8	25.8	26.1	30.2
27.4	27.9	27.8	32.5
28.0	29.6	29.5	35.2

Table 6.6 M-line Piping Frequencies Test vs Analysis

Test (Hz)	Analysis (Hz)		
	Baseline Model Equivalent Linear Stiffnesses	Design Snubber Stiffnesses	Rigid Snubber Stiffnesses
20.8	23.9	21.5	27.9
22.6	25.4	22.4	32.6
23.2	25.8	27.5	34.9

Table 6.7 Summary of F-line Design Analysis to Test Ratios

Analysis Case	Analysis/Test: Stresses			Analysis/Test: Support Forces		
	Average	Maximum	Minimum	Average	Maximum	Minimum
Baseline	2.07	4.56	0.55	1.15	1.64	0.68
Design Snubbers	3.17	5.20	1.25	2.04	5.11	0.84
Rigid Snubbers	1.40	2.95	0.60	0.69	1.23	0.39
5% Damping	1.57	3.44	0.43	0.89	1.27	0.52
Unbroadened Spectra	1.50	3.75	0.34	0.79	1.21	0.52
1.3 S_2(F)	2.39	6.22	0.77	1.19	1.66	0.80

Table 6.8 Summary of M-line Design Analysis to Test Ratios

Analysis Case	Analysis/Test: Stresses			Analysis/Test: Support Forces		
	Average	Maximum	Minimum	Average	Maximum	Minimum
Baseline	1.87	2.79	1.21	1.66	4.76	0.70
Design Snubbers	2.13	3.80	1.19	1.85	6.04	0.53
Rigid Snubbers	1.78	3.05	1.06	1.39	2.79	0.67
5% Damping	1.53	2.21	1.16	1.35	3.81	0.56
Unbroadened Spectra	1.63	2.28	1.07	1.36	3.40	0.54
SRSS Supp. Grp. Comb.	1.58	2.40	1.11	1.43	4.10	0.60
Abs. Inertia + SAM Comb.	2.20	2.87	1.44	1.79	4.86	0.82
Enveloped RS	5.12	13.7	1.76	5.82	21.3	0.79
1.5 S_2(M)	1 90	2 .73	1.19	1.54	3.48	0.67
1/3 S_2(M) + CV	1.20	1.80	0.75	1.42	4.97	0.55

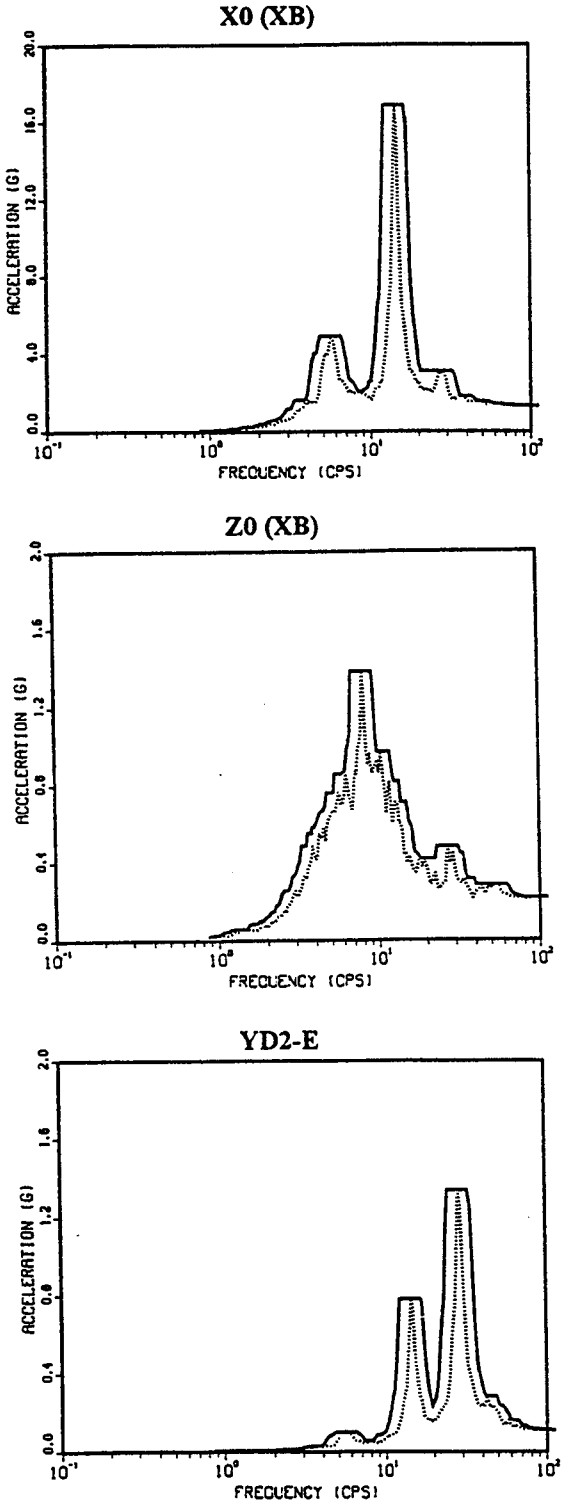

Figure 6.1 F-line Baseline Analysis Response Spectra $S_2(F)$ - 2% Damping

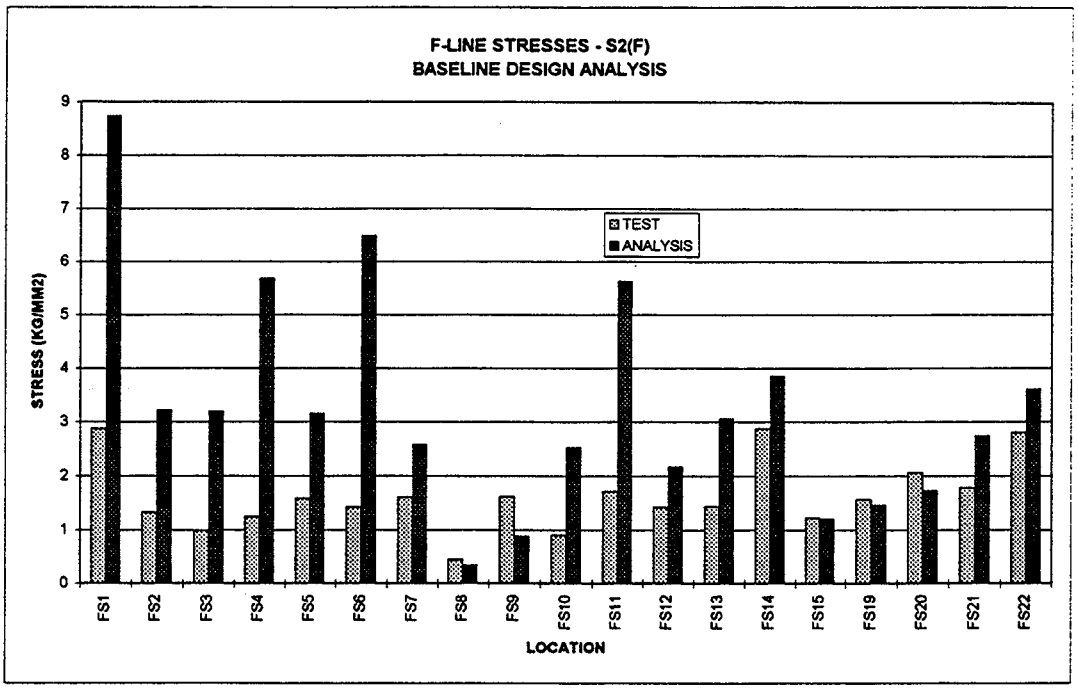

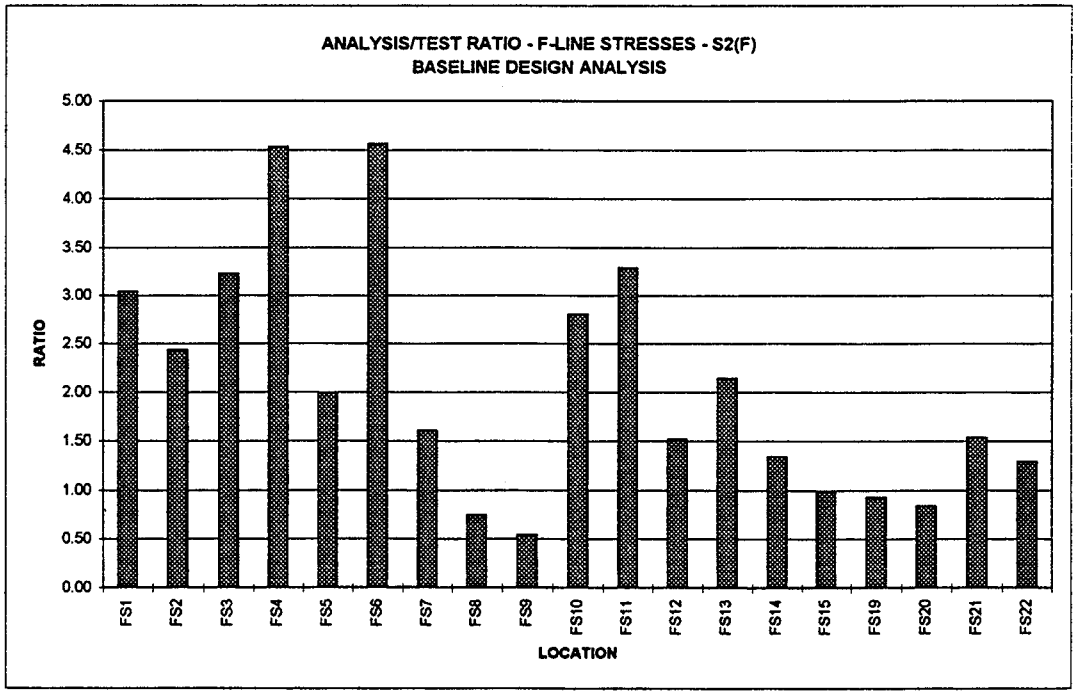

Figure 6.2 Comparison of Peak Stresses for F-line Baseline Design Analysis vs. Test

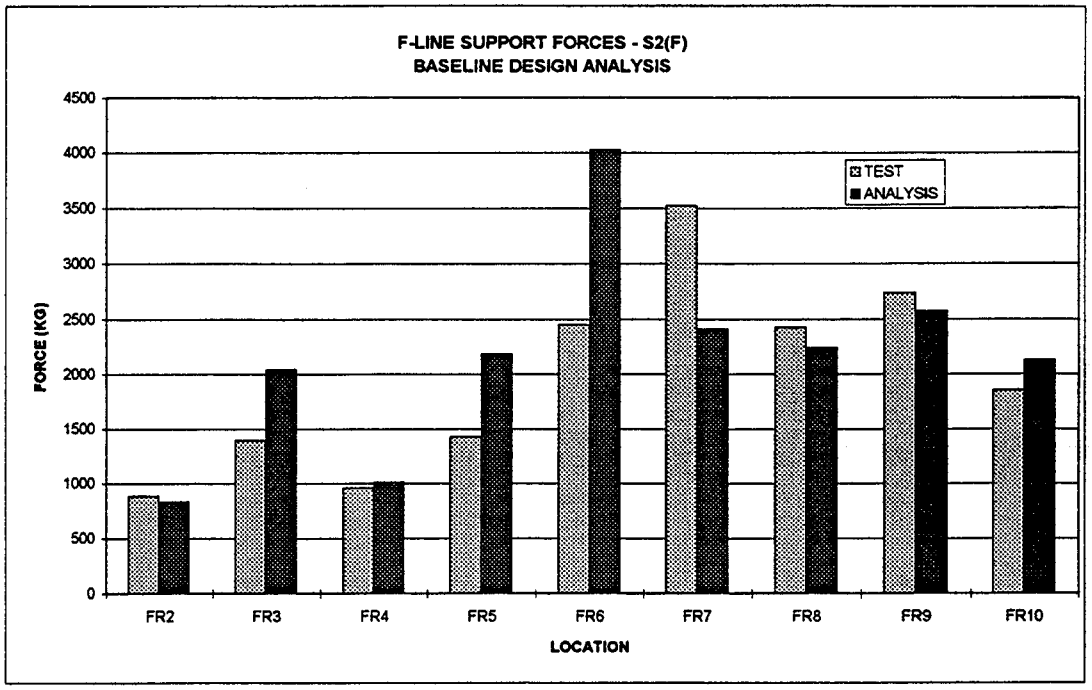

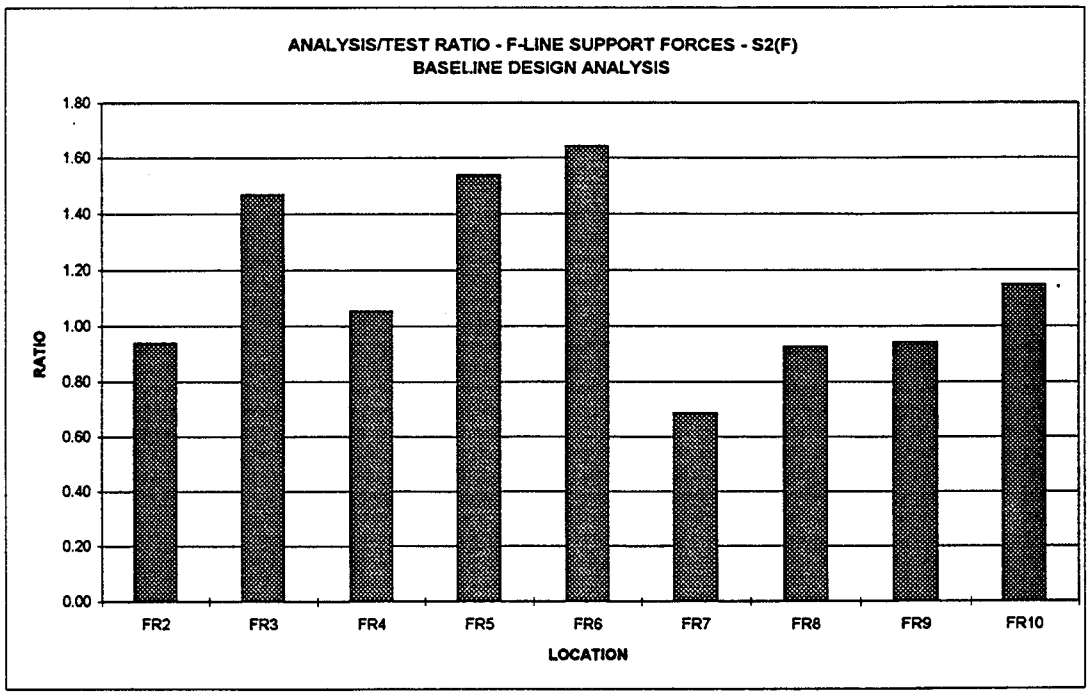

Figure 6.3 Comparison of Peak Support Forces for F-line Baseline Design Analysis vs. Test

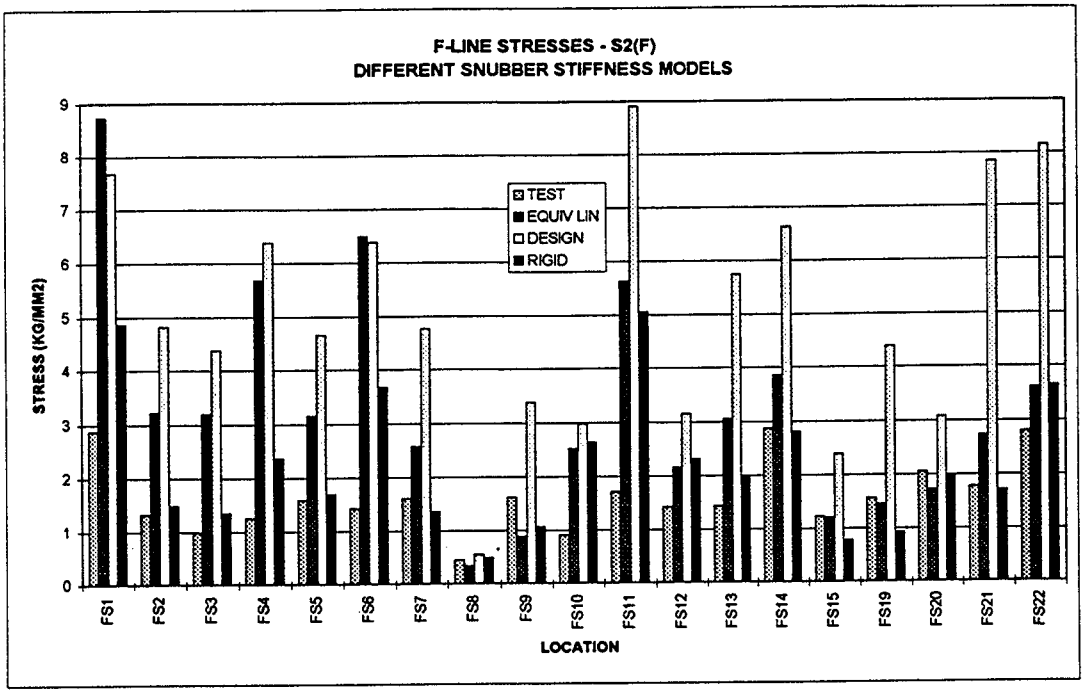

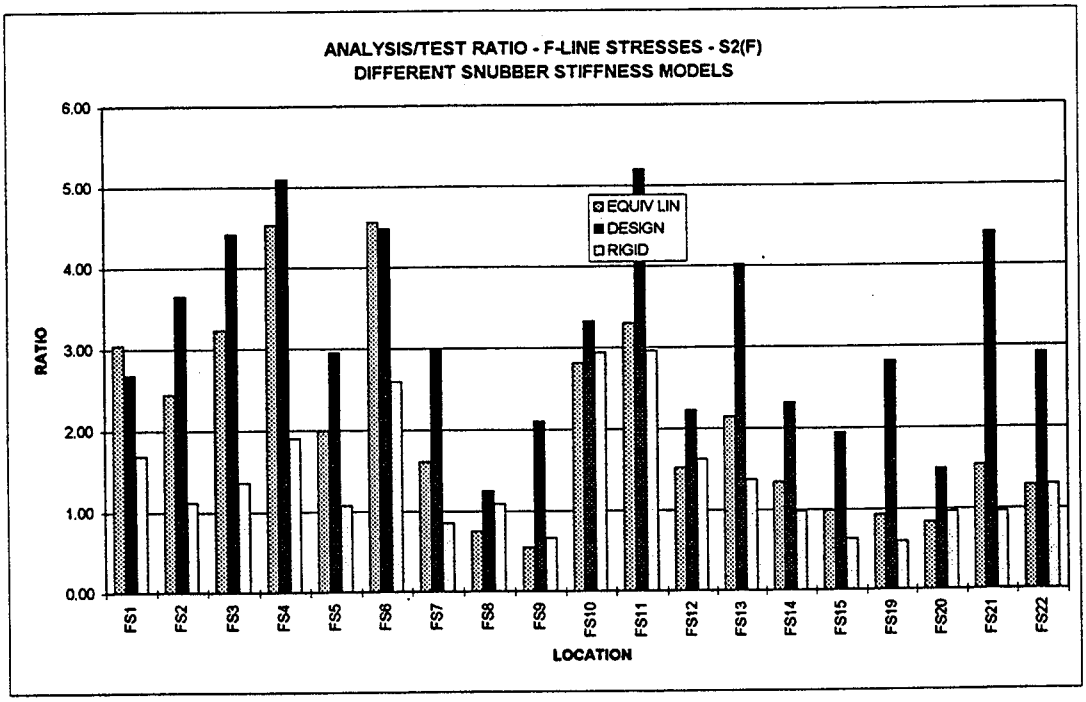

Figure 6.4 Comparison of Peak Stresses for F-line Design Analyses with Different Snubber Stiffness Models

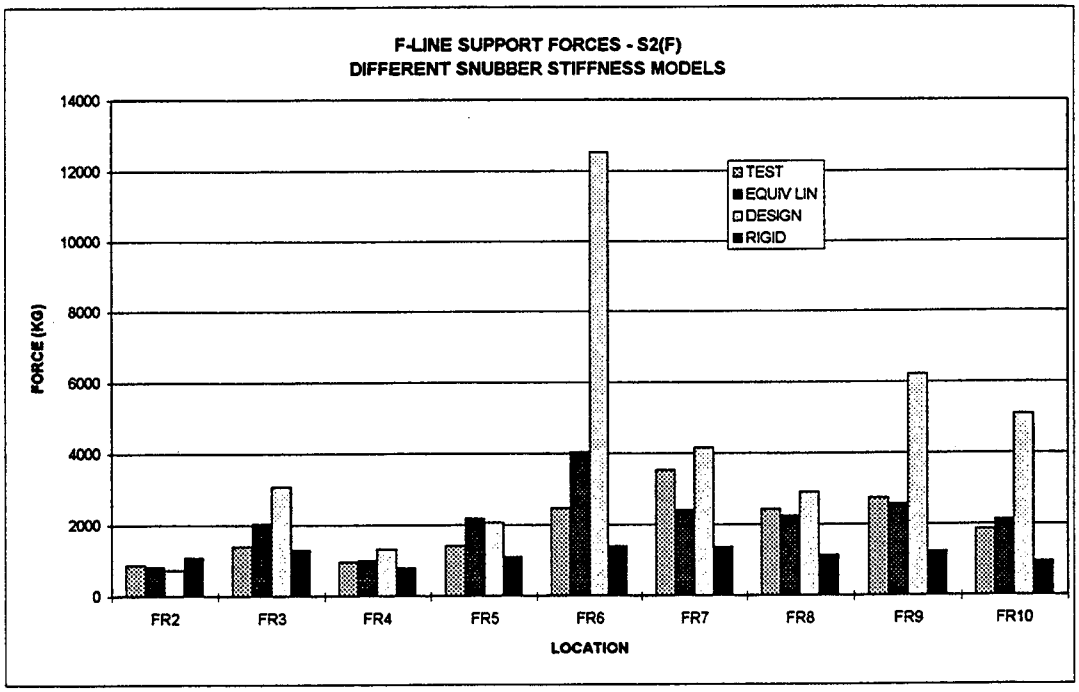

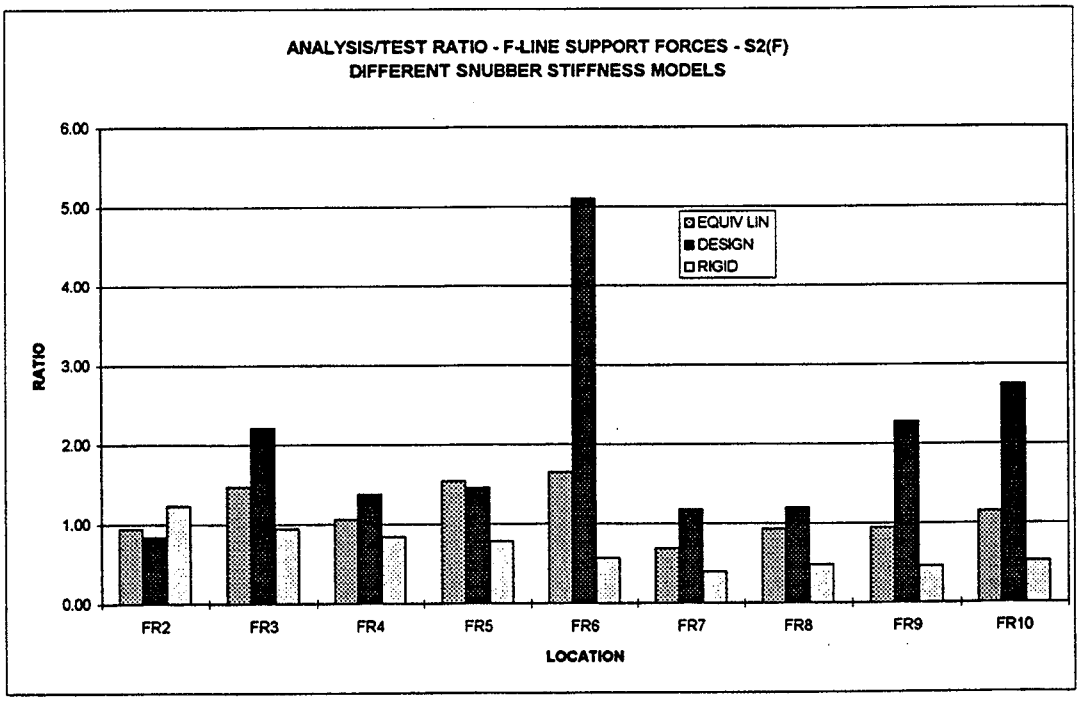

Figure 6.5 Comparison of Peak Support Forces for F-line Design Analyses with Different Snubber Stiffness Models

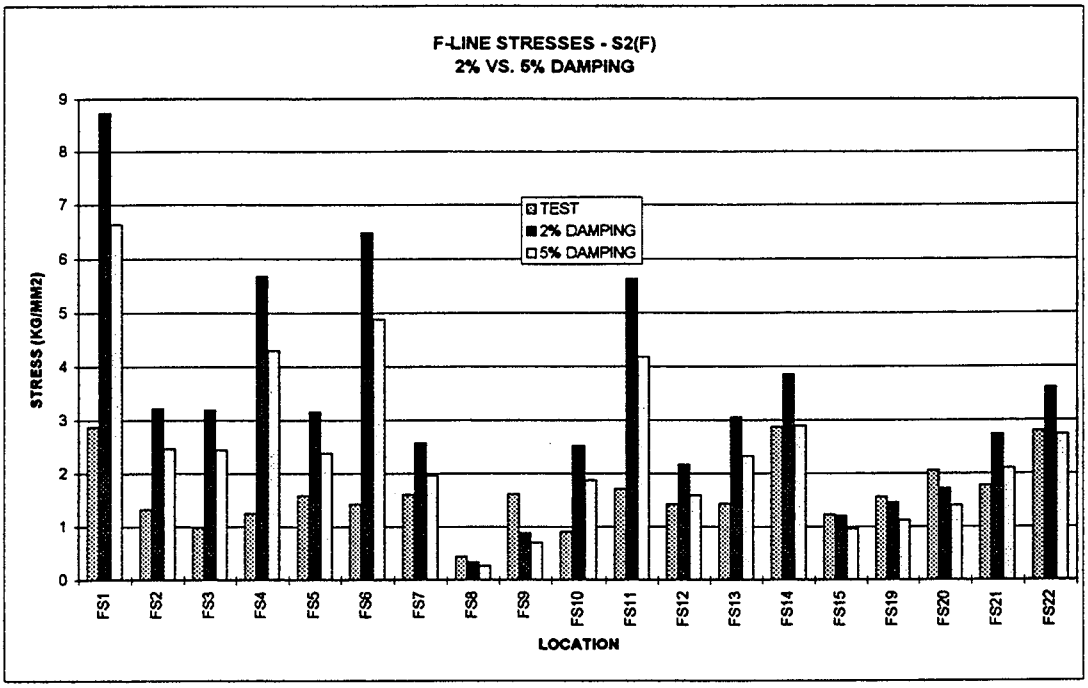

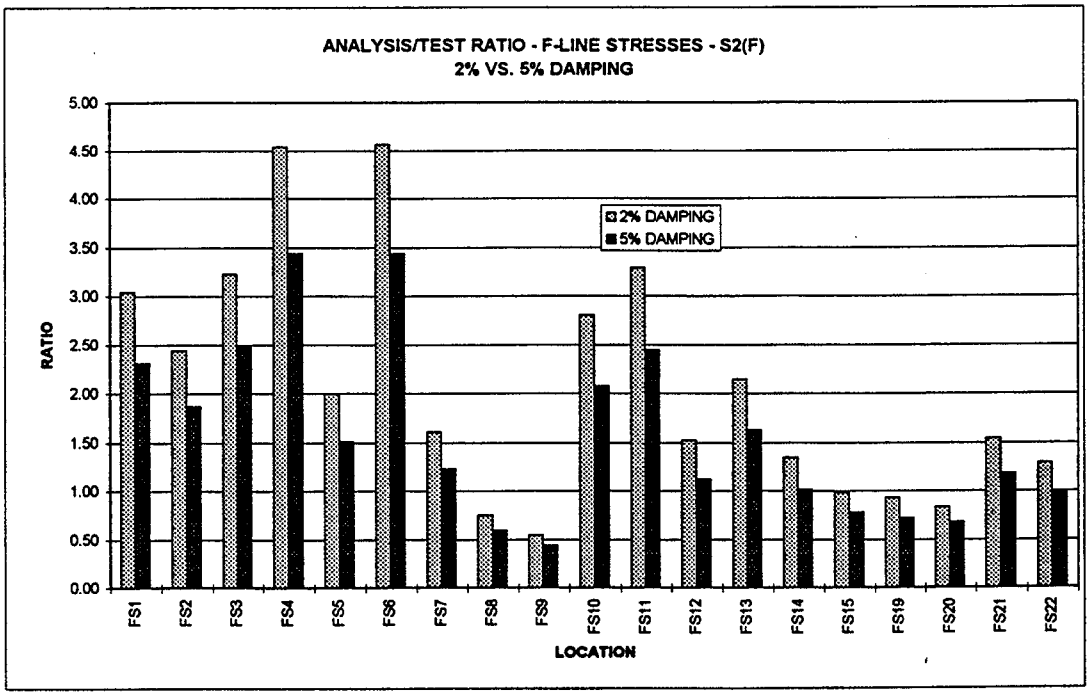

Figure 6.6 Comparison of Peak Stresses for F-line Design Analysis with 2% vs. 5% Damping

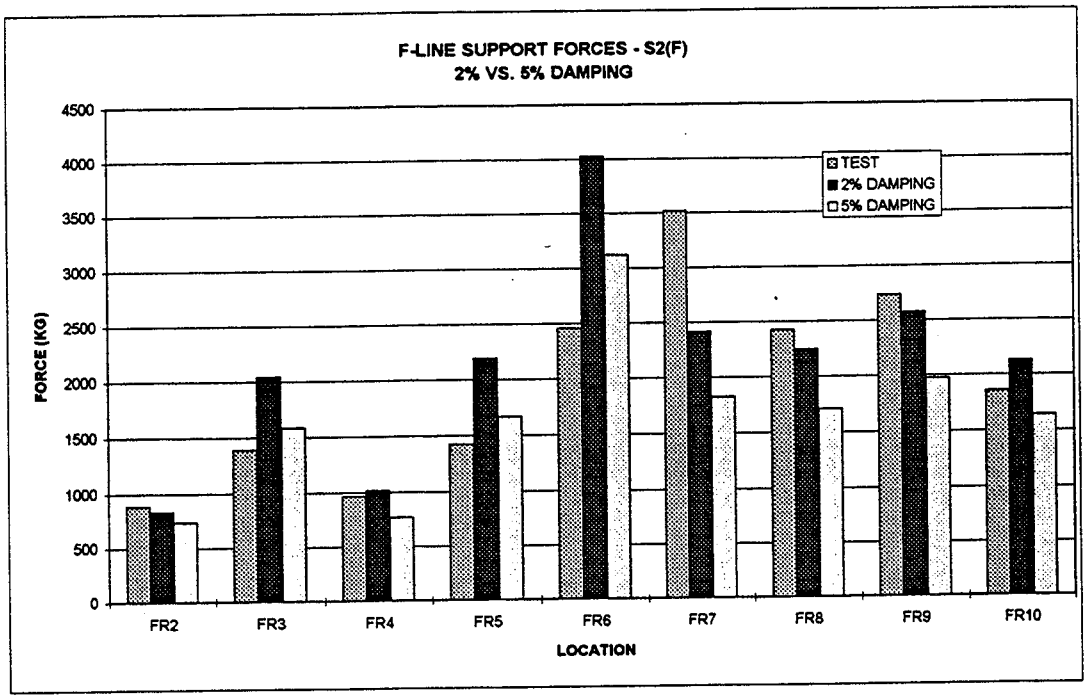

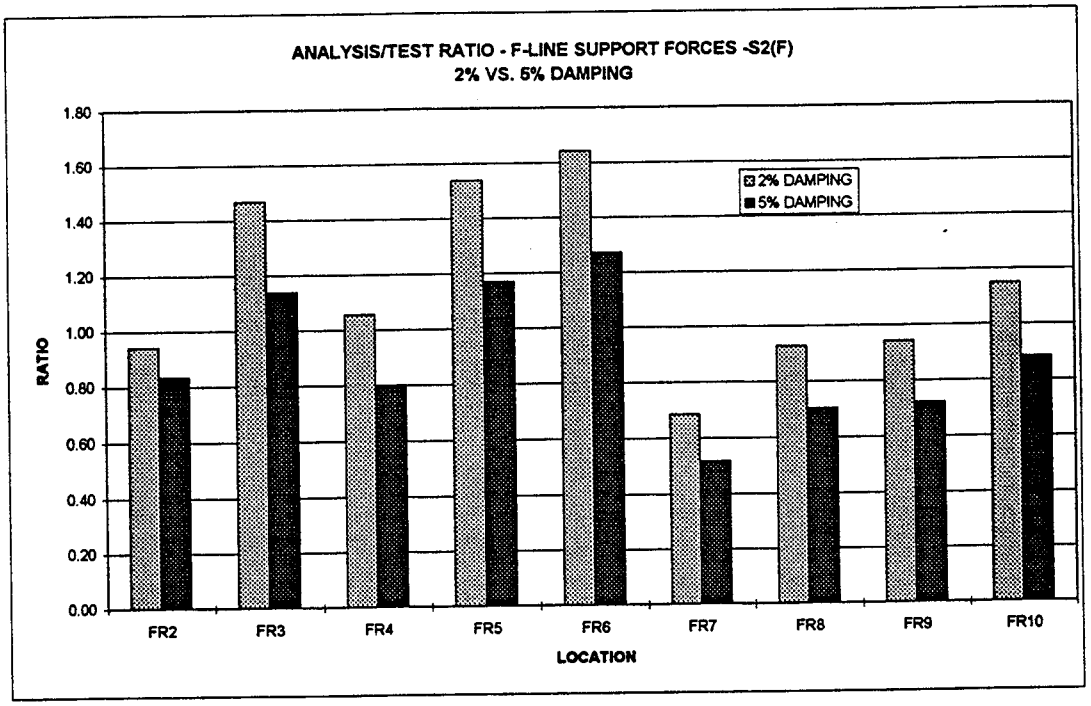

Figure 6.7 Comparison of Peak Support Forces for F-line Design Analyses with 2% vs. 5% Damping

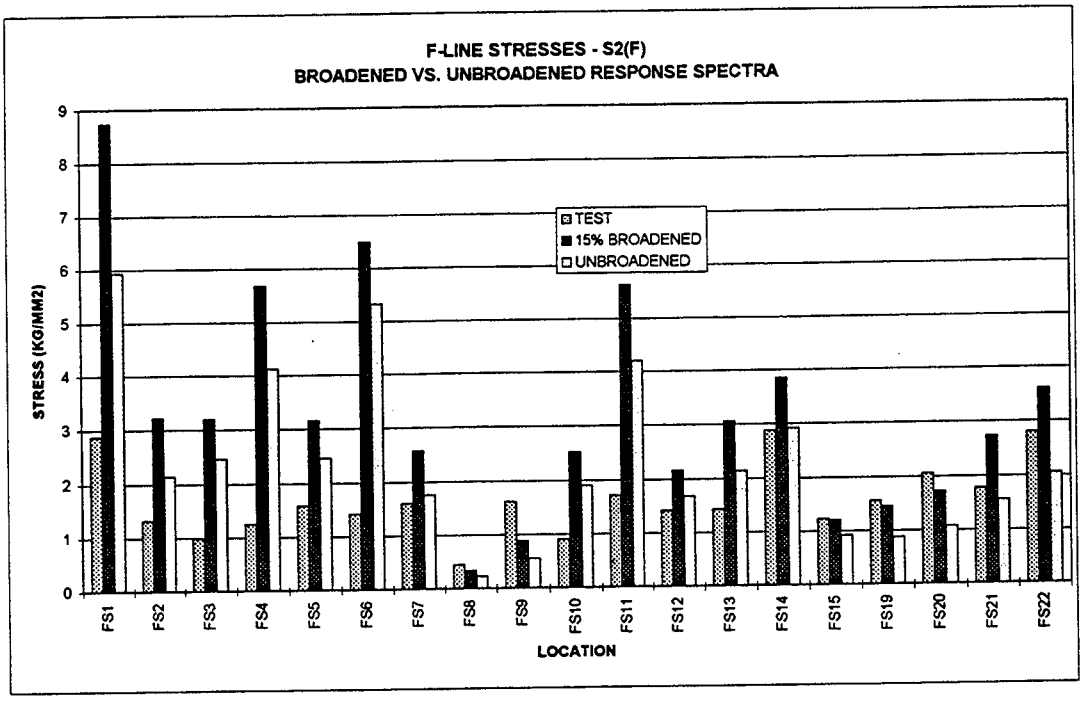

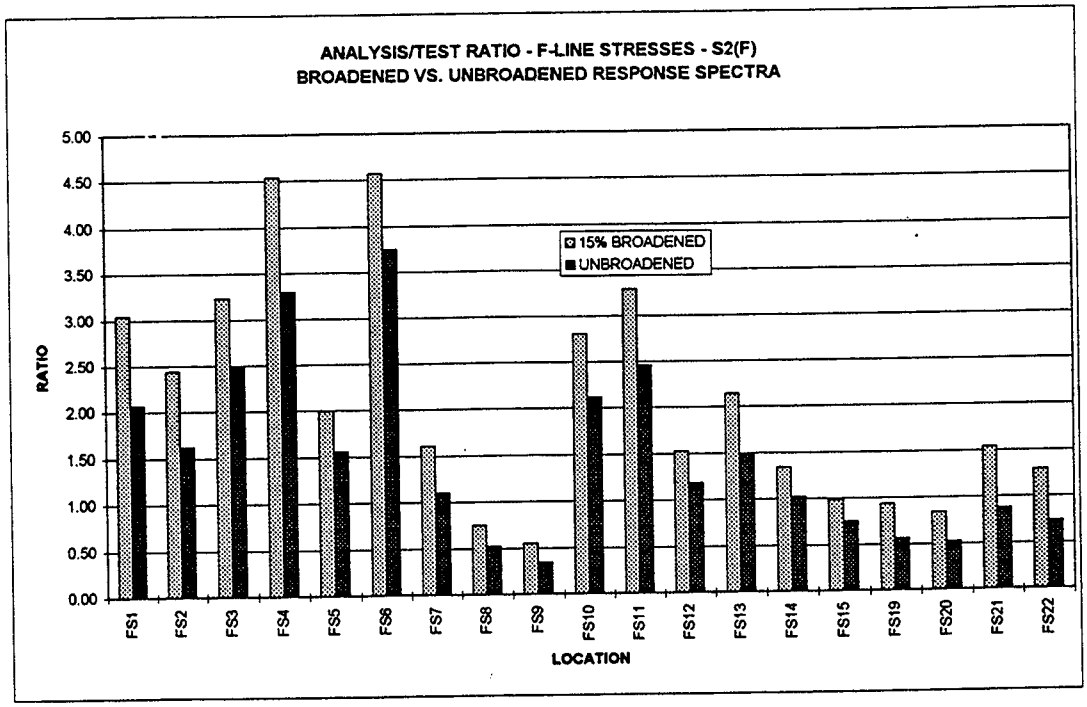

Figure 6.8 Comparison of Peak Stresses for F-line Design Analyses Using Broadened vs. Unbroadened Response Spectra

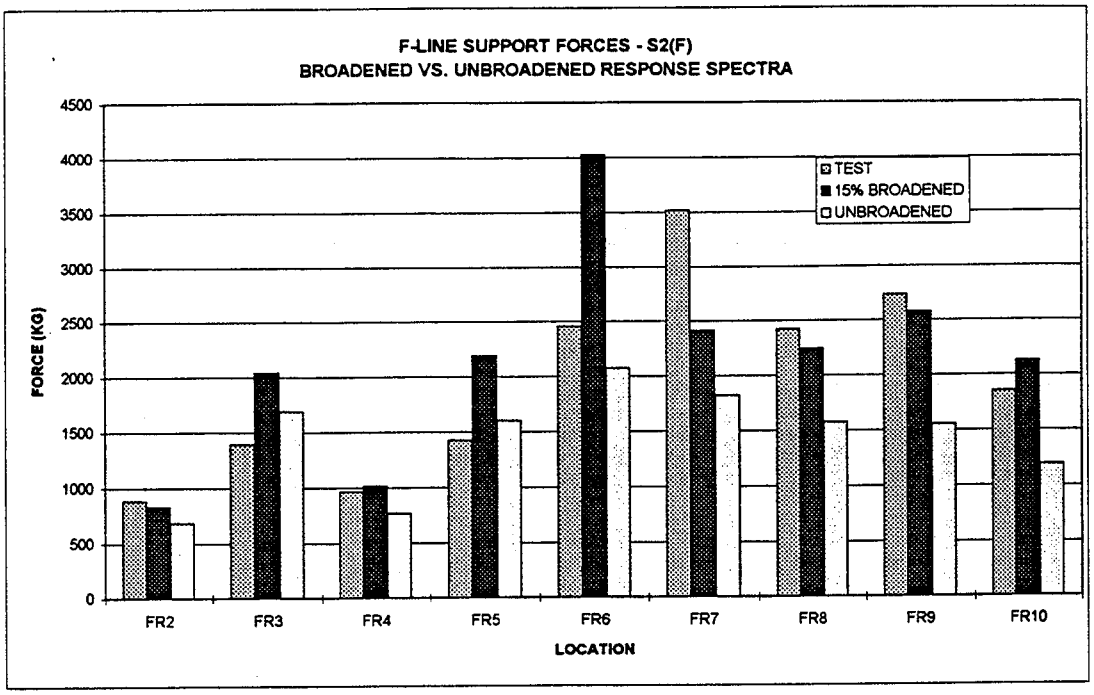

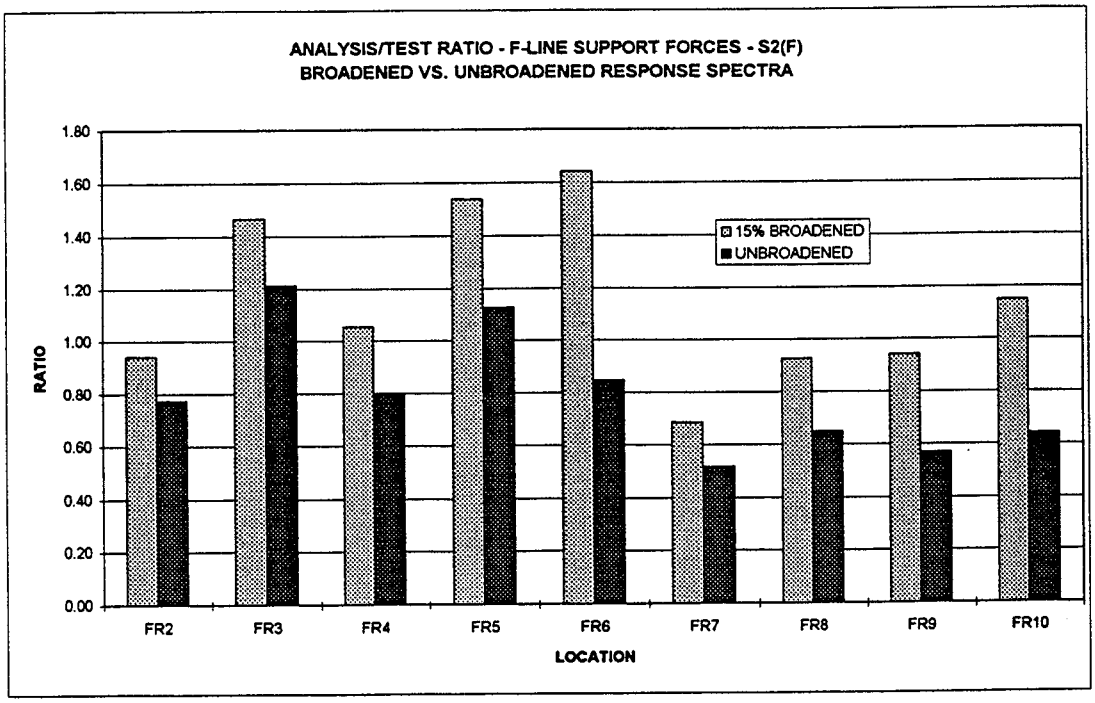

Figure 6.9 Comparison of Peak Support Forces for F-line Design Analyses Using Broadened vs. Unbroadened Response Spectra

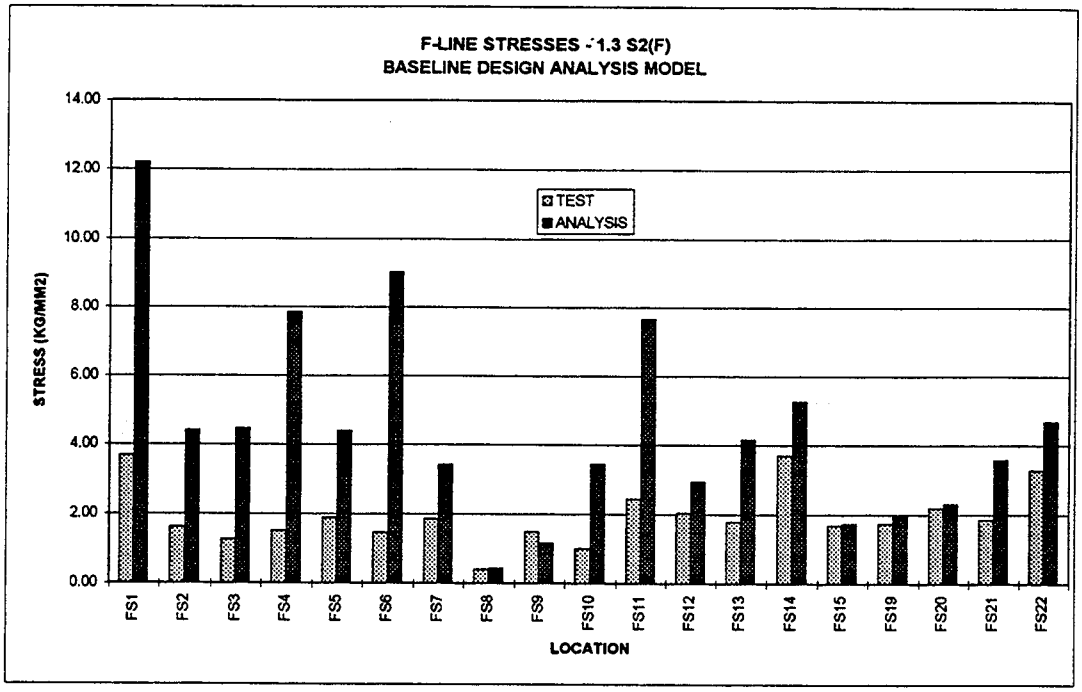

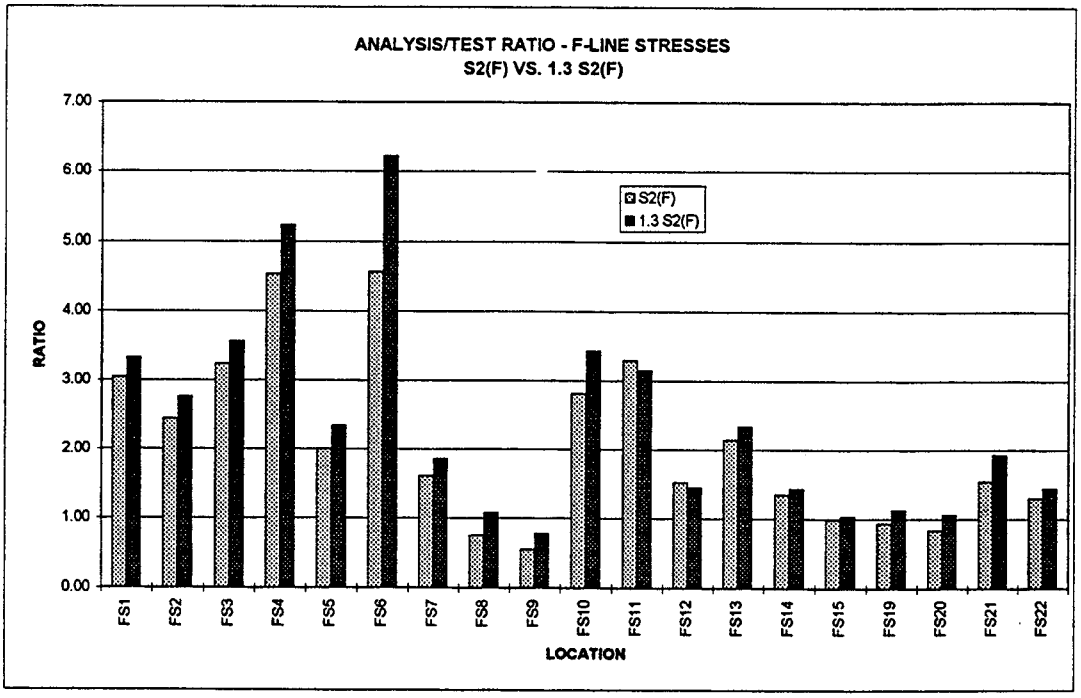

Figure 6.10 Comparison of Peak Stresses for F-line Design Analysis vs. Test Results for 1.3 S2(F) and 1.0 S2(F) Input Motion

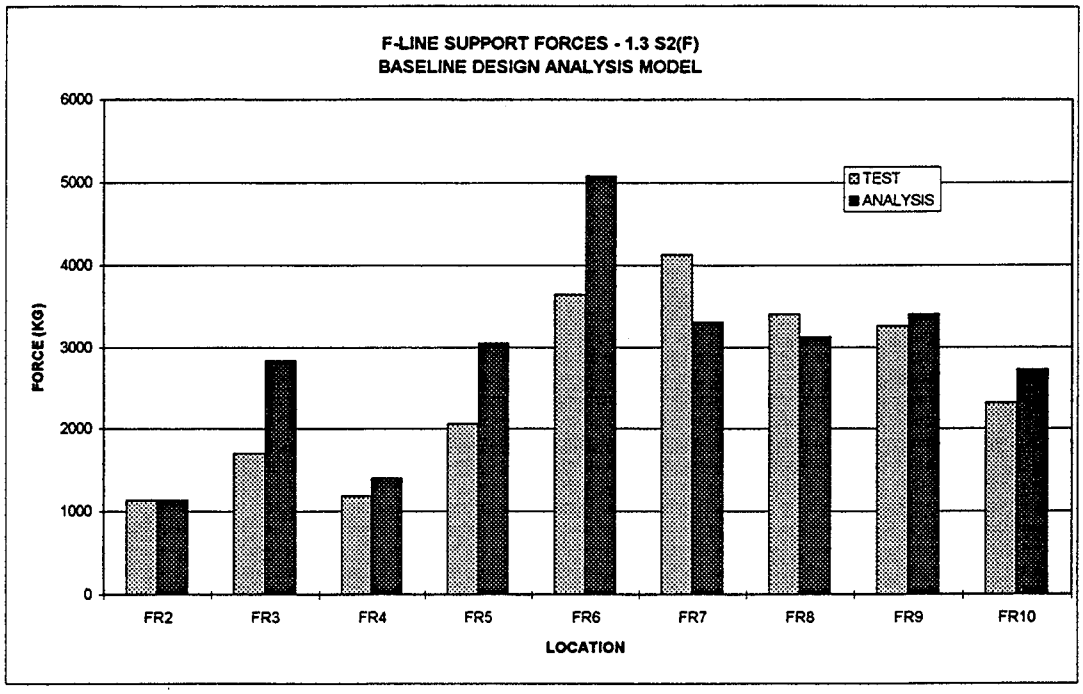

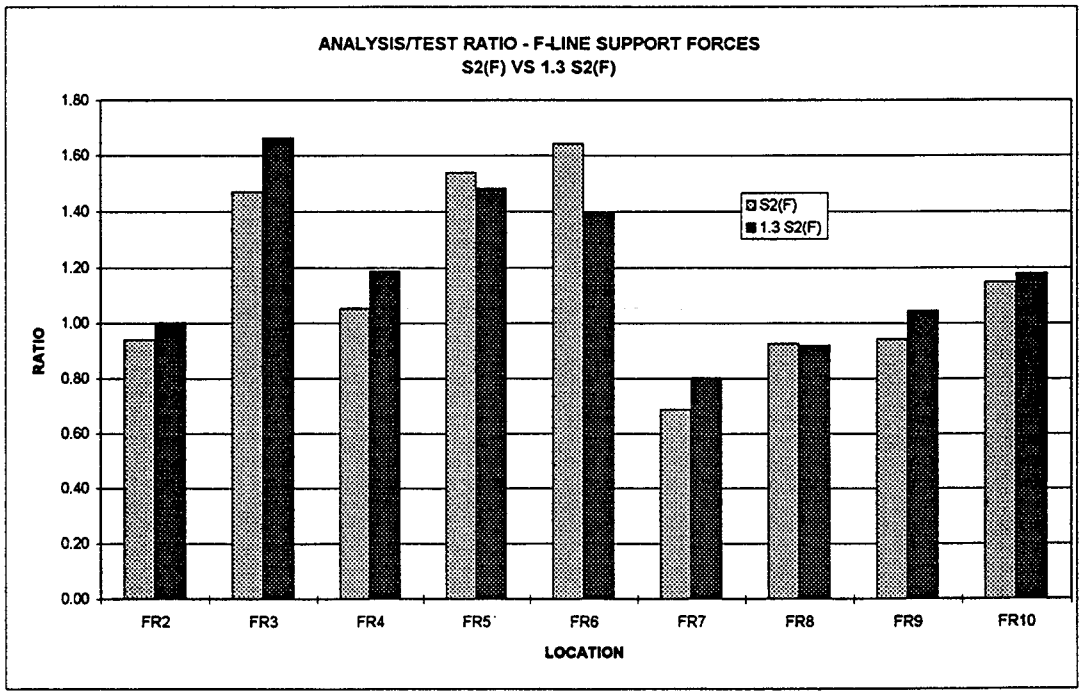

Figure 6.11 Comparison of Peak Support Forces for F-line Design Analysis vs. Test Results for 1.3 S2(F) and 1.0 S2(F) Input Motion

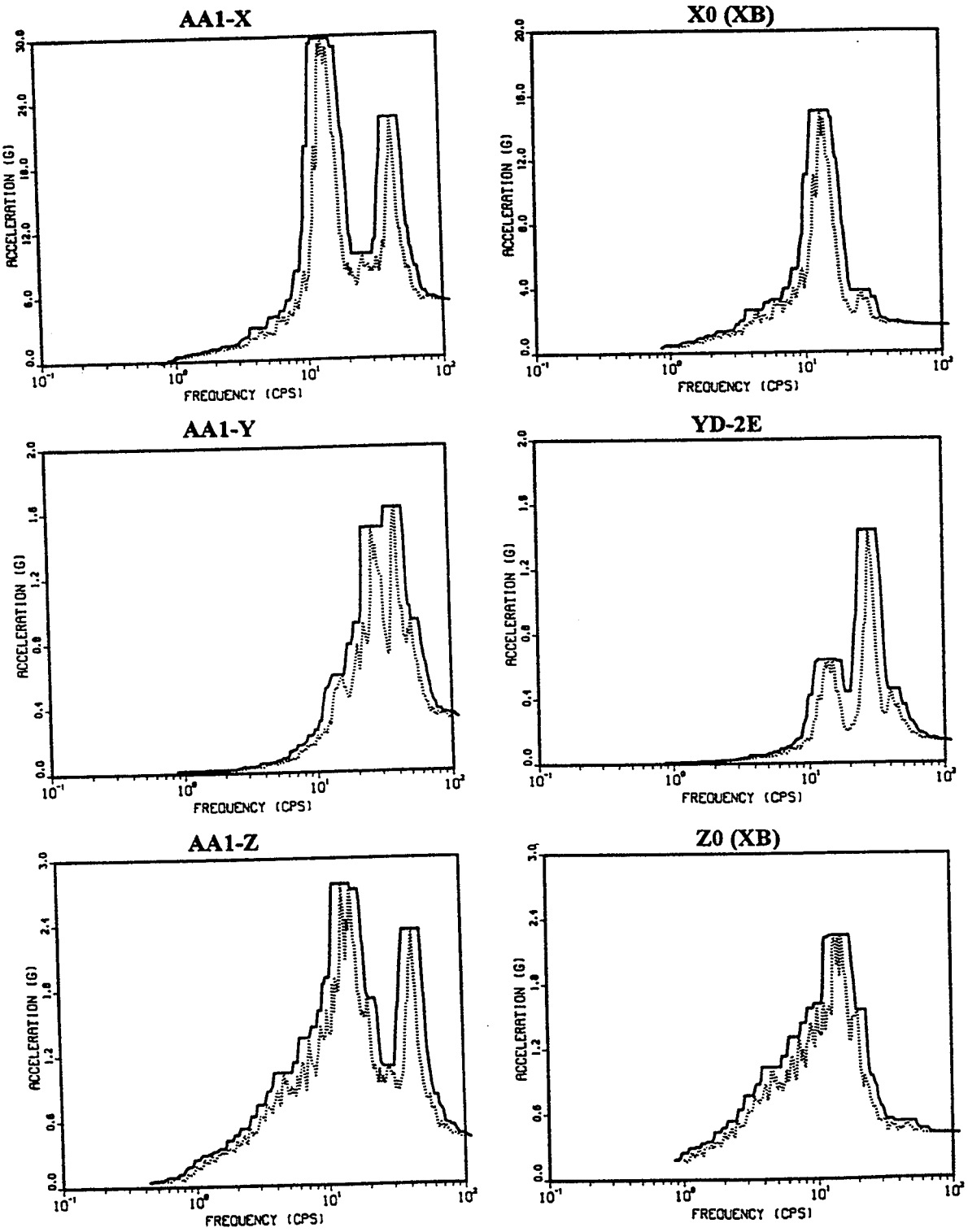

Figure 6.12 M-line Baseline Analysis Response Spectra
S2(M) - 2% Damping

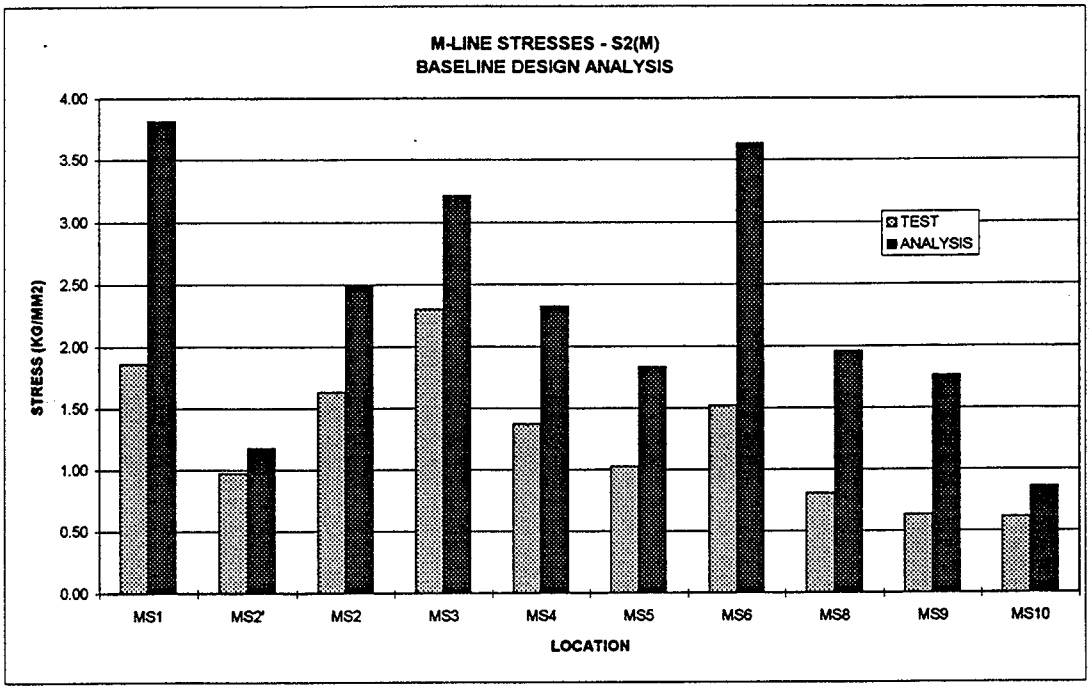

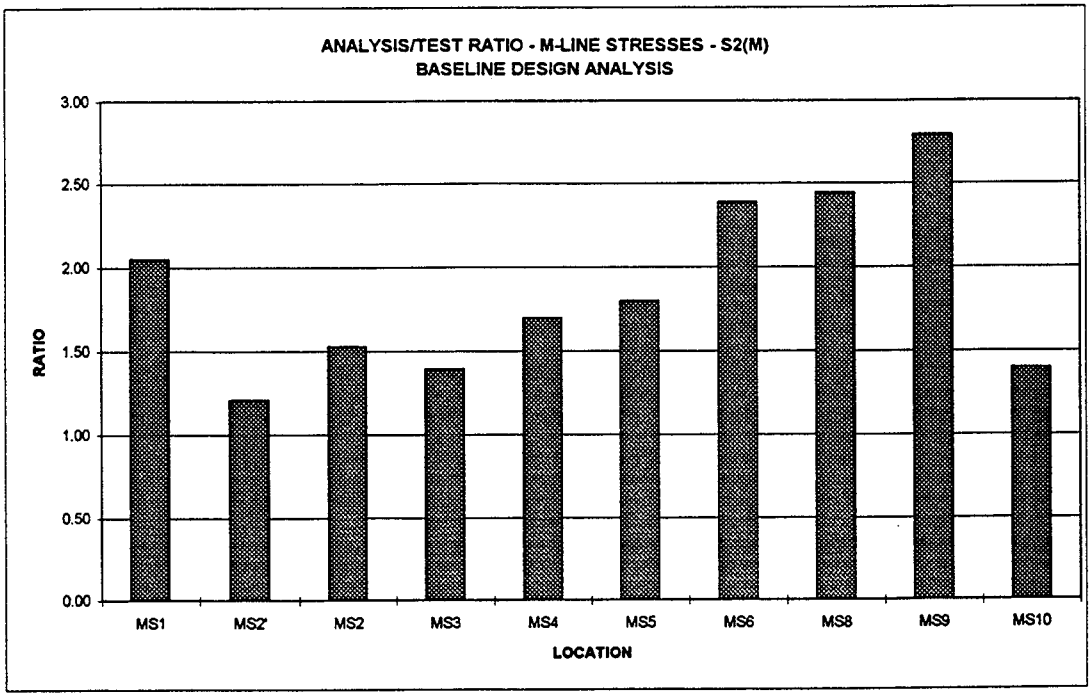

Figure 6.13 Comparison of Peak Stresses for M-line Baseline Design Analysis vs. Test

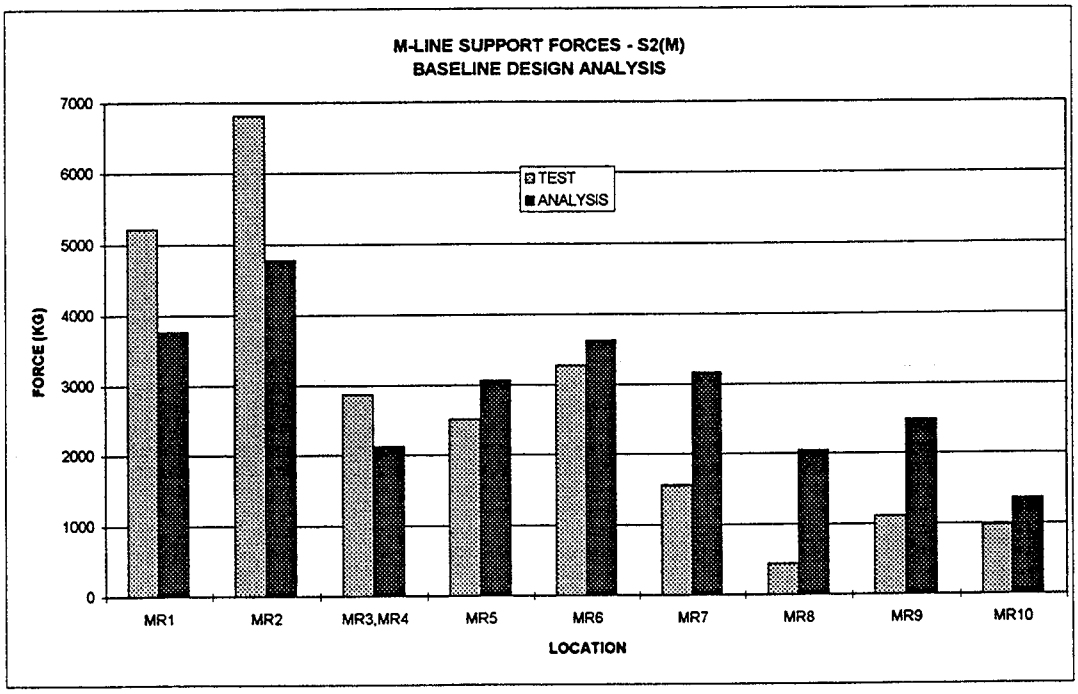

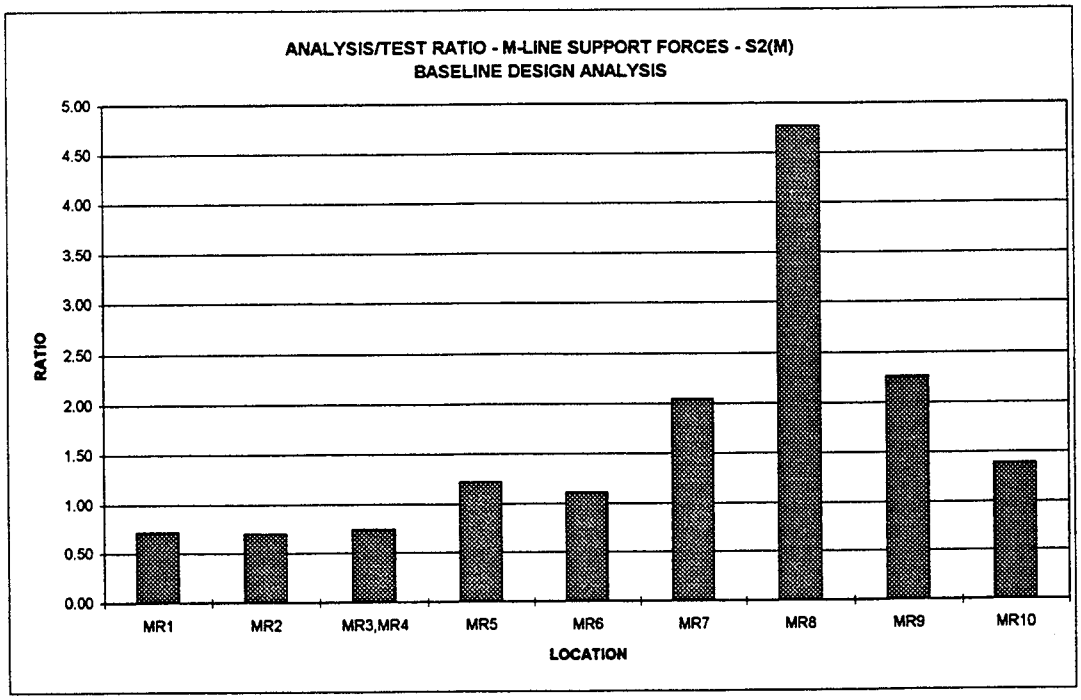

Figure 6.14 Comparison of Peak Support Forces for M-line Baseline Design Analysis vs. Test

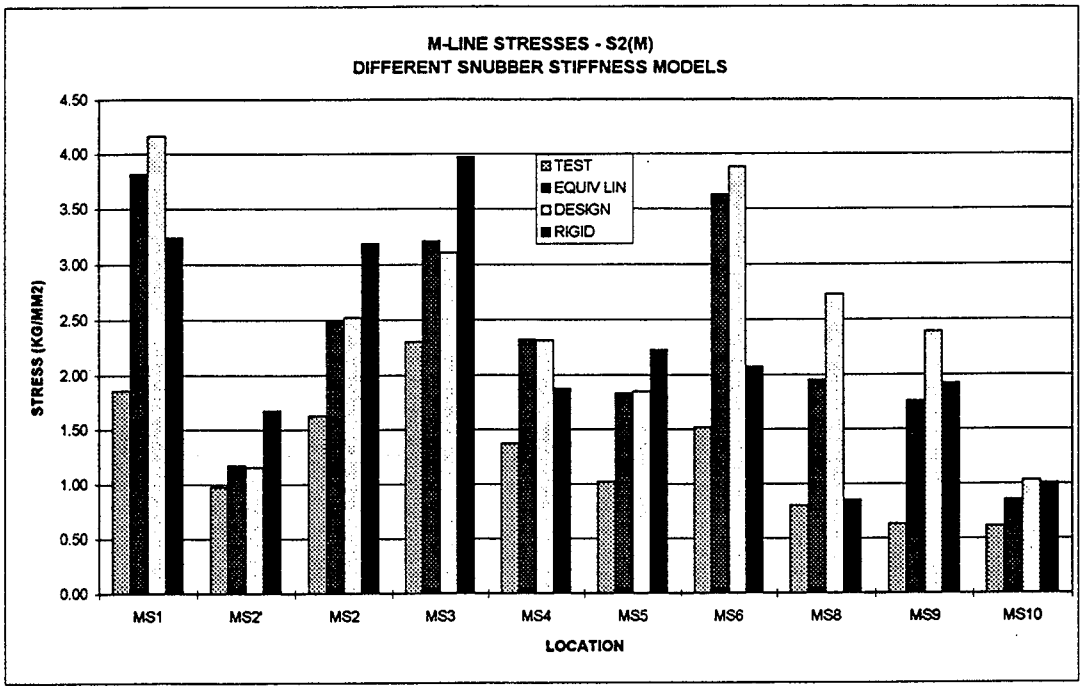

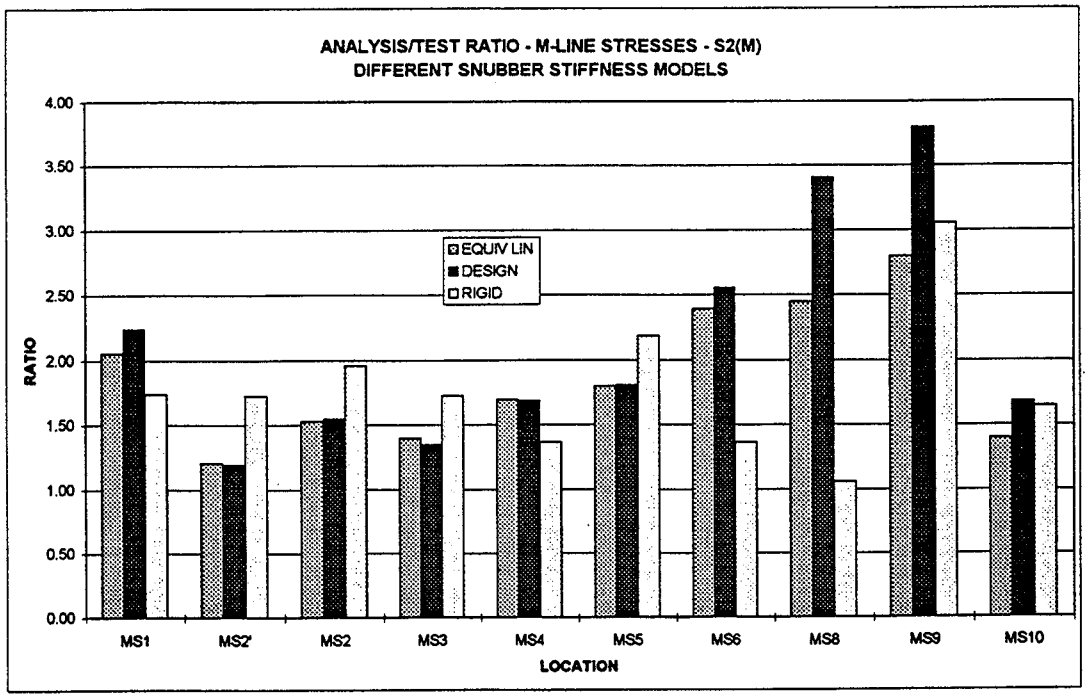

Figure 6.15 Comparison of Peak Stresses for M-line Design Analysis with Different Snubber Stiffness Models

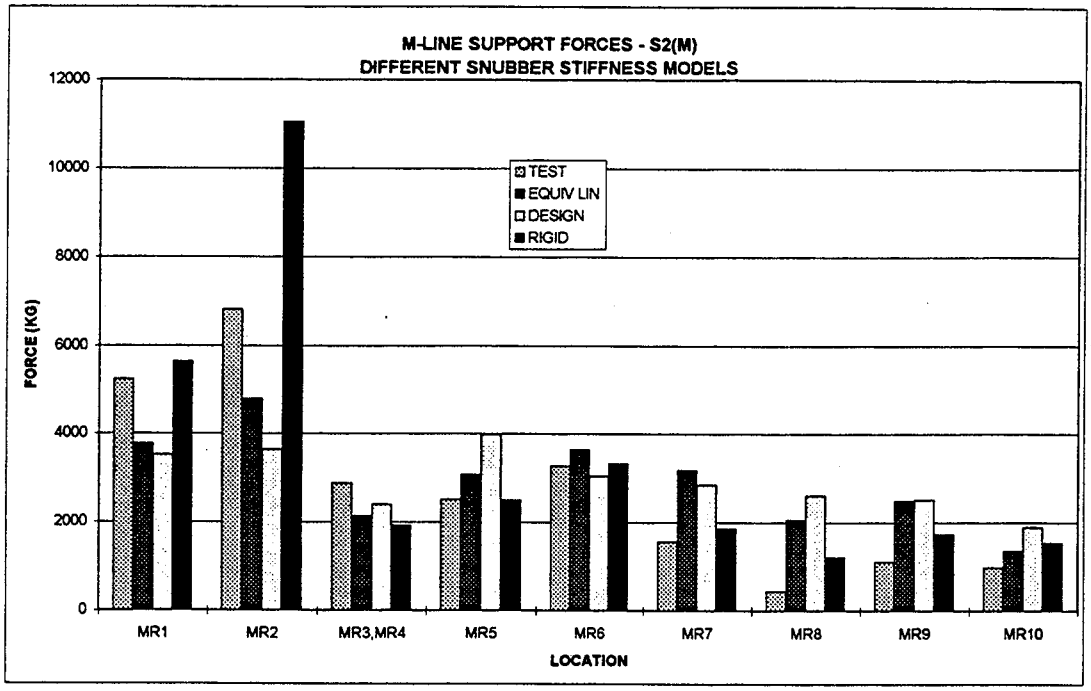

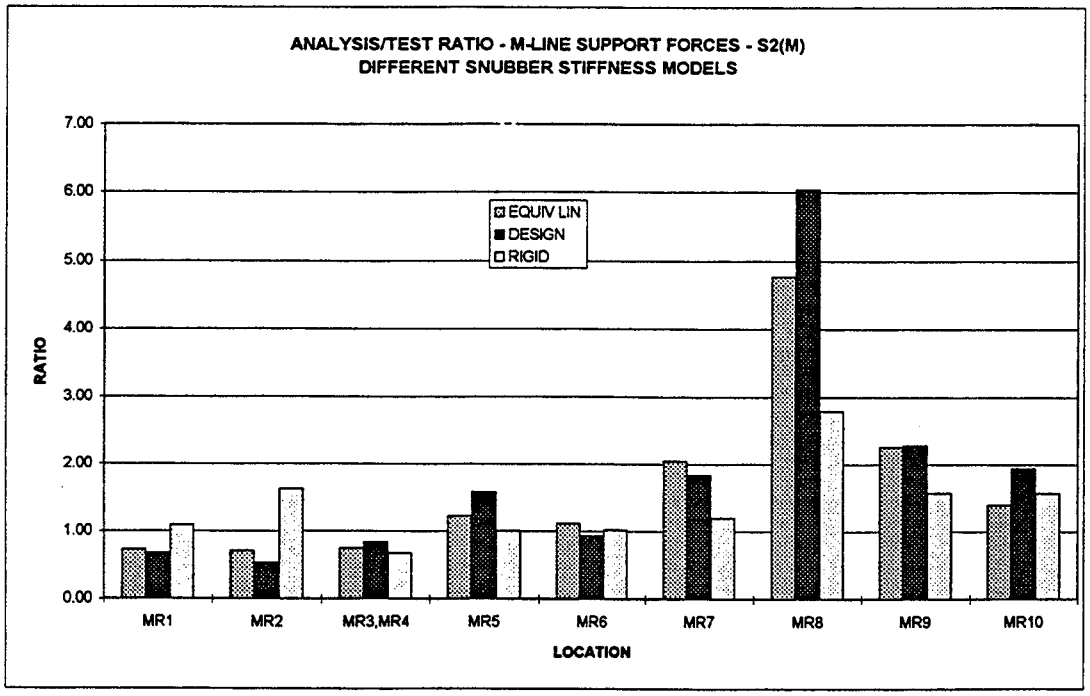

Figure 6.16 Comparison of Peak Support Forces for M-line Design Analysis with Different Snubber Stiffness Models

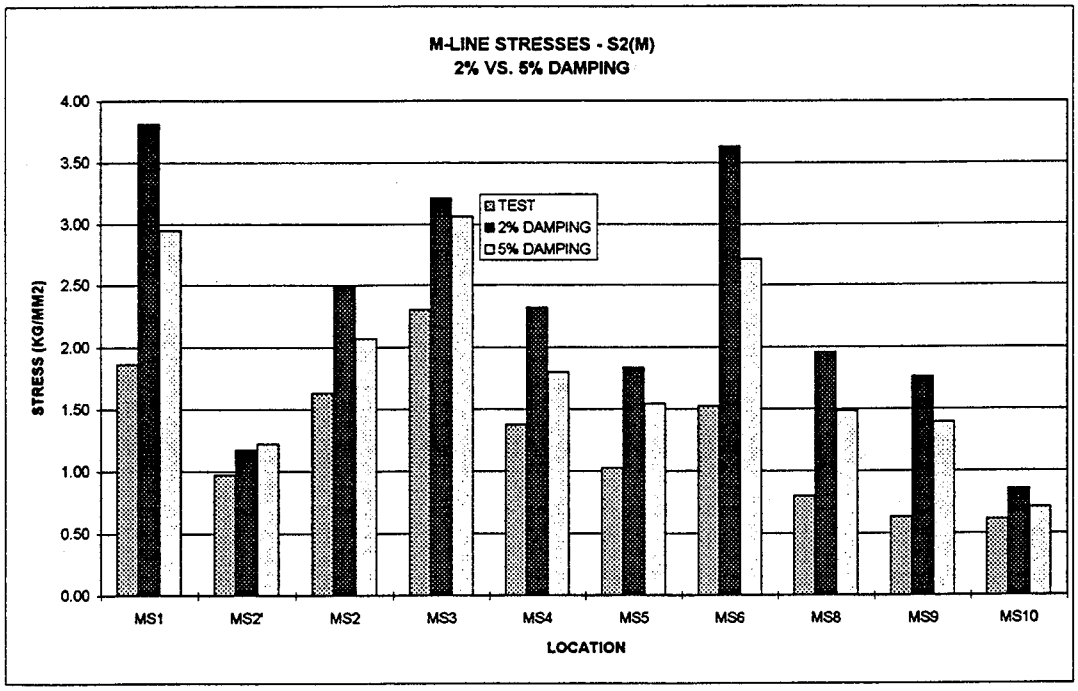

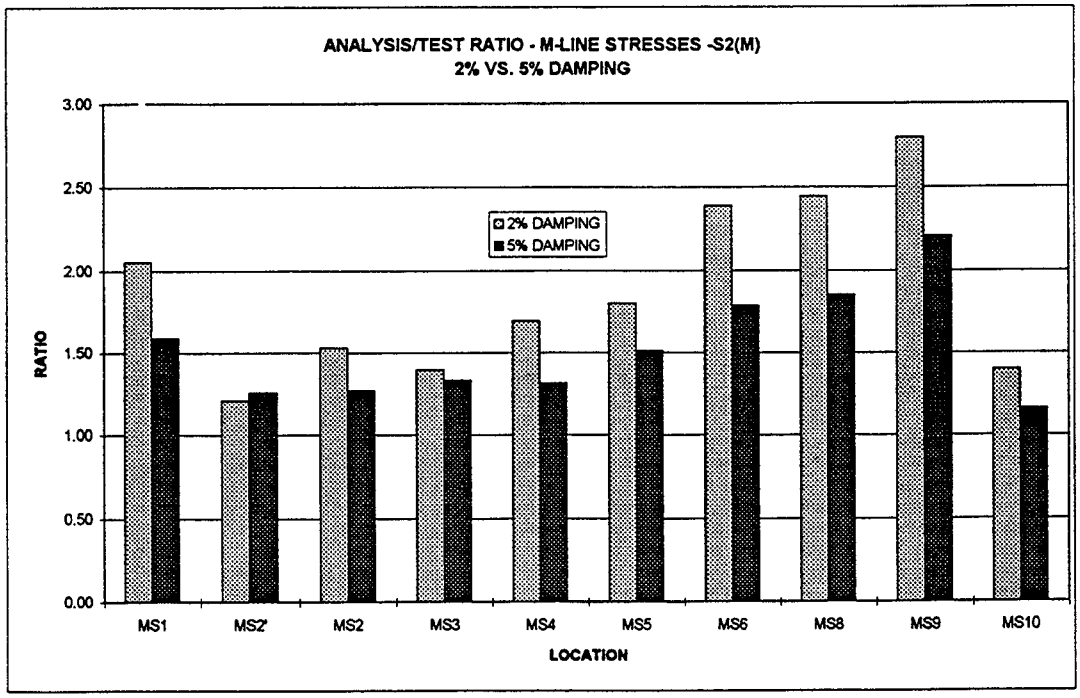

Figure 6.17 Comparison of Peak Stresses for M-line Design Analyses with 2% vs. 5% Damping

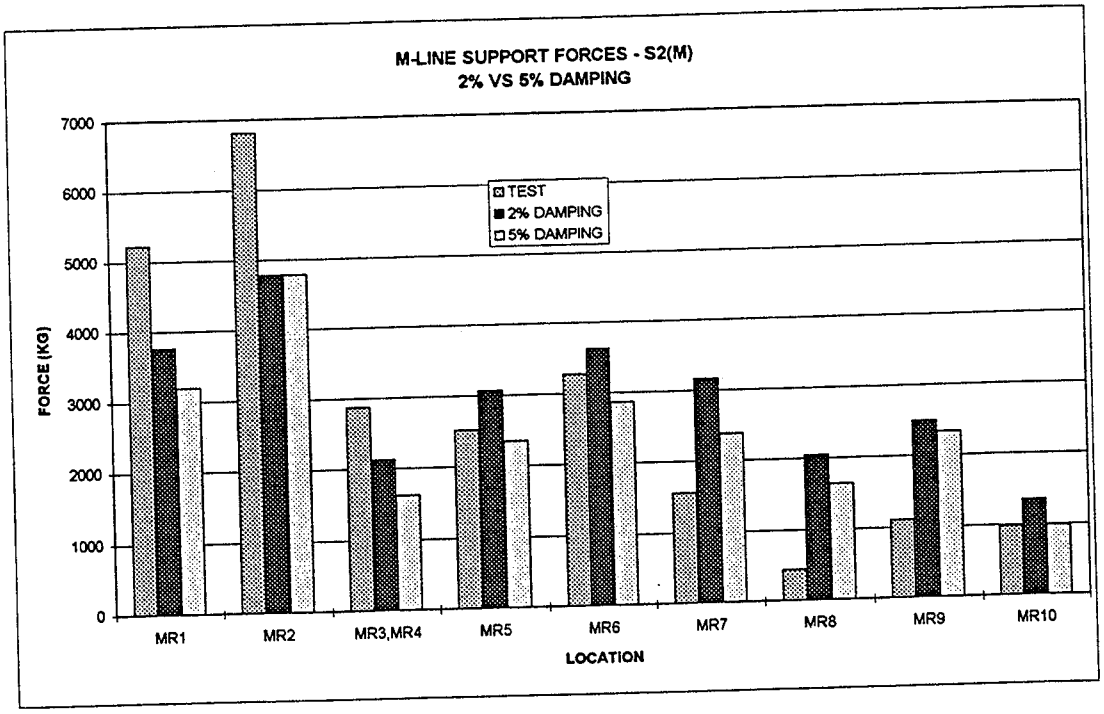

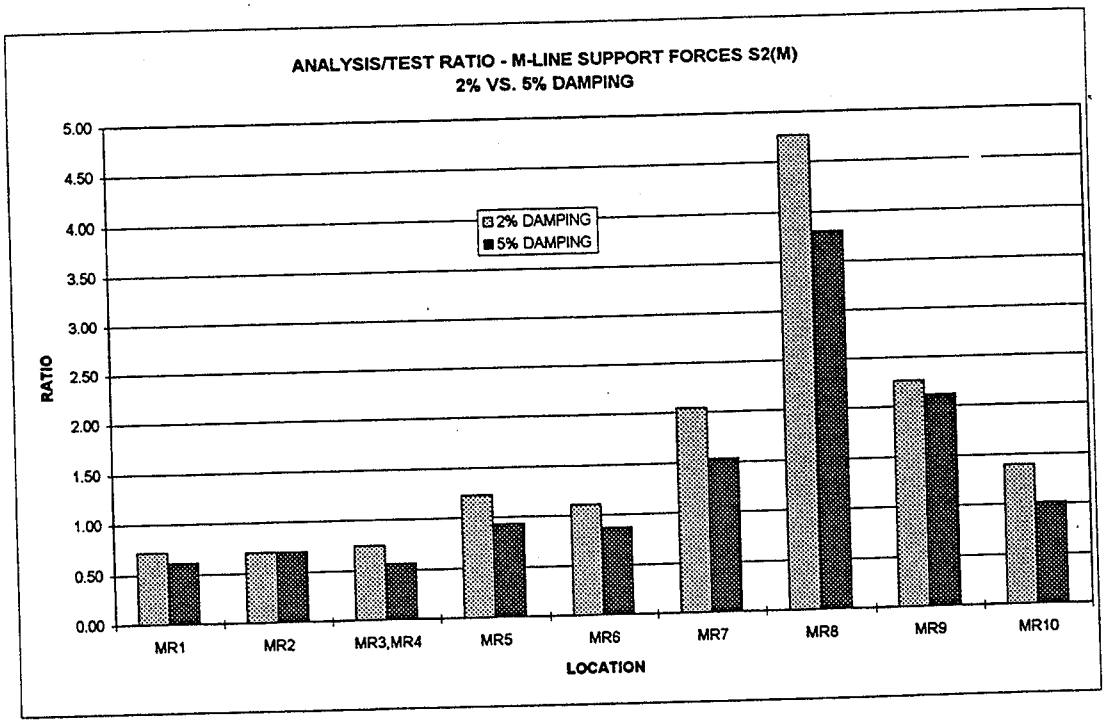

Figure 6.18 Comparison of Peak Support Forces for M-line Design Analysis with 2% vs. 5% Damping

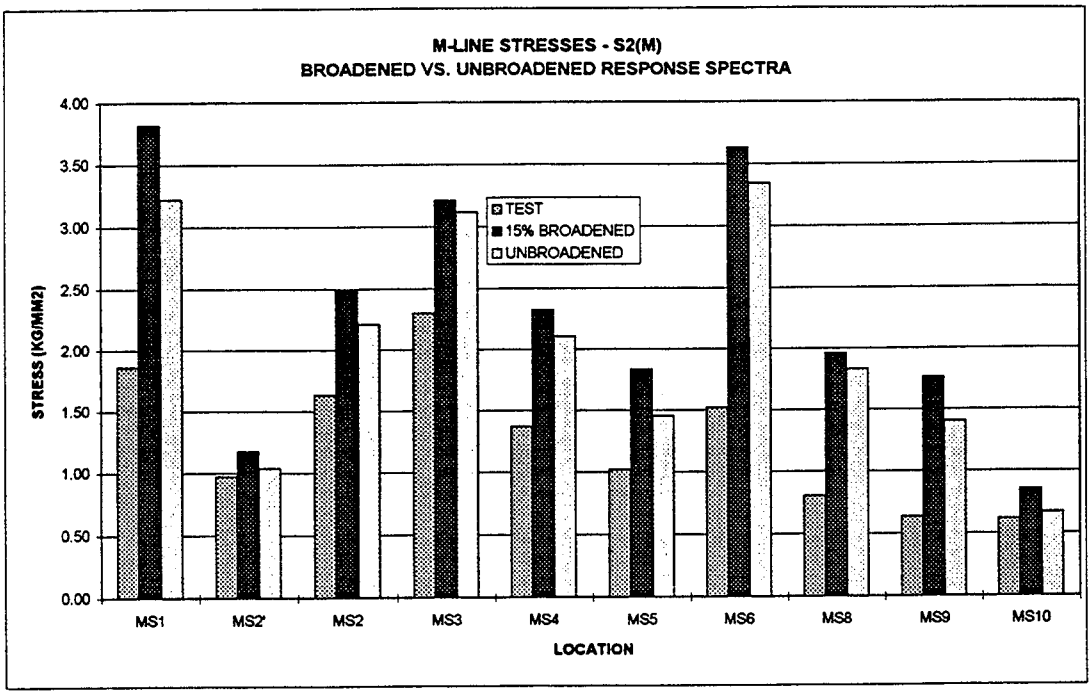

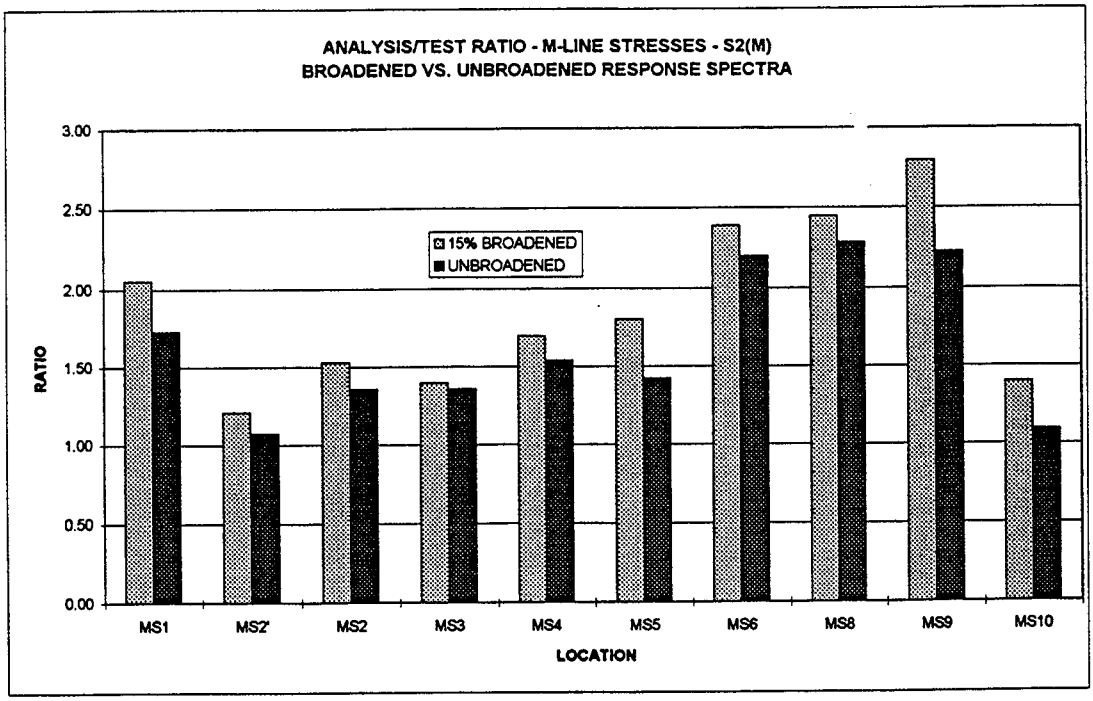

Figure 6.19 Comparison of Peak Stresses for M-line Design Analyses Using Broadened vs. Unbroadened Response Spectra

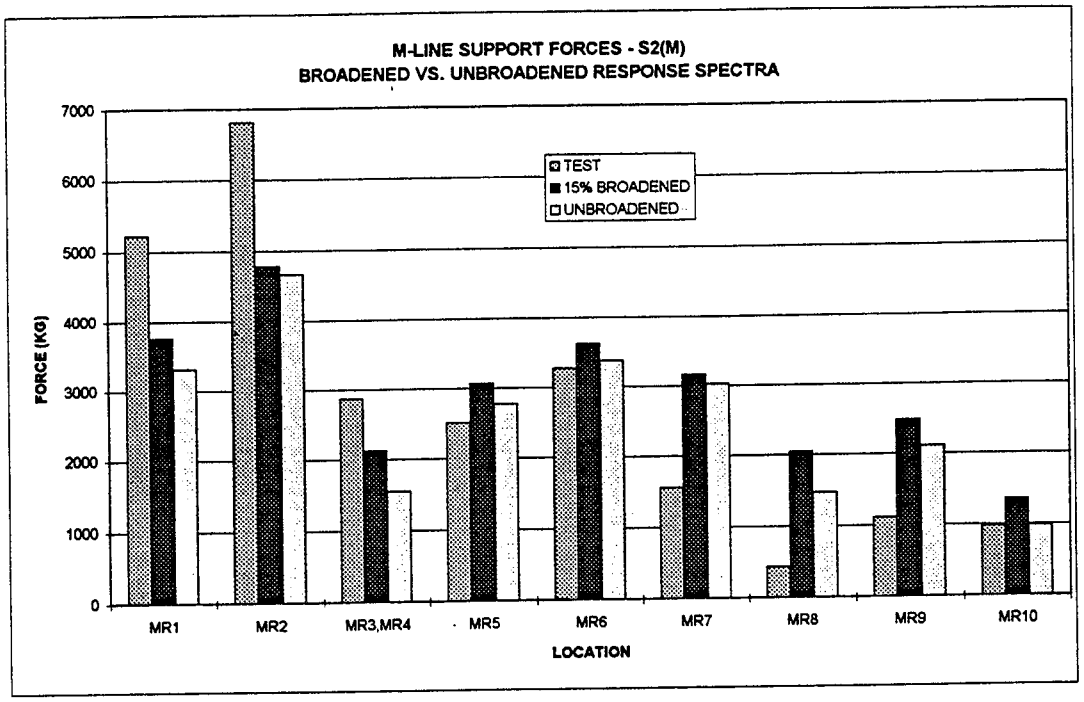

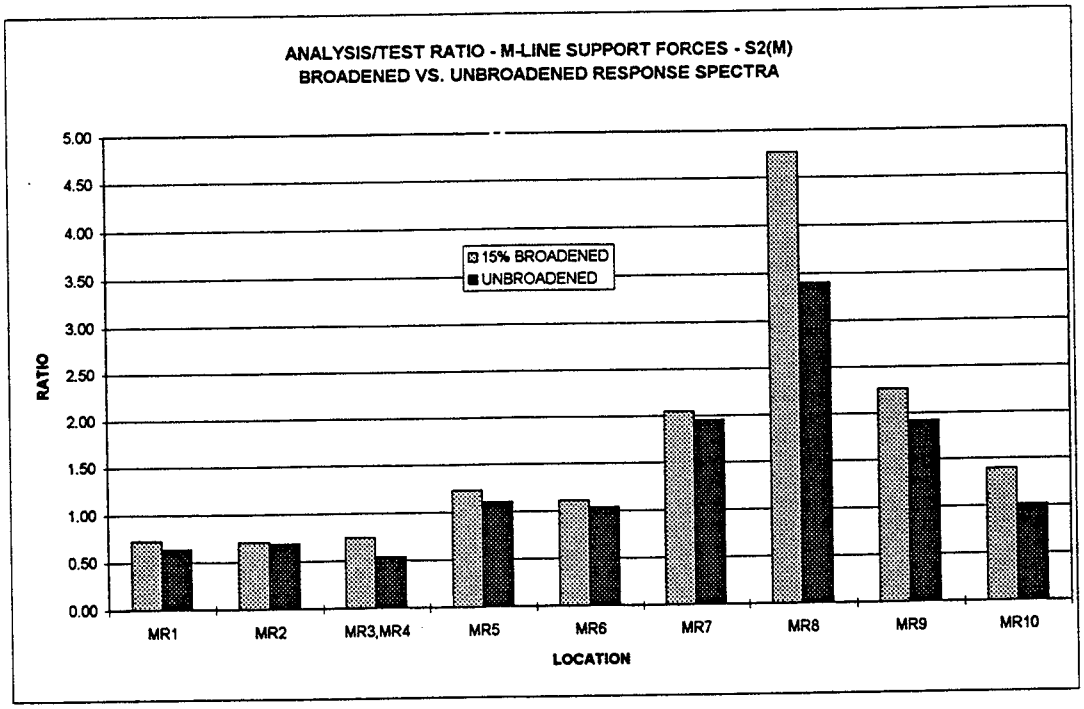

Figure 6.20 Comparison of Peak Support Forces for M-line Design Analyses Using Broadened vs. Unbroadened Response Spectra

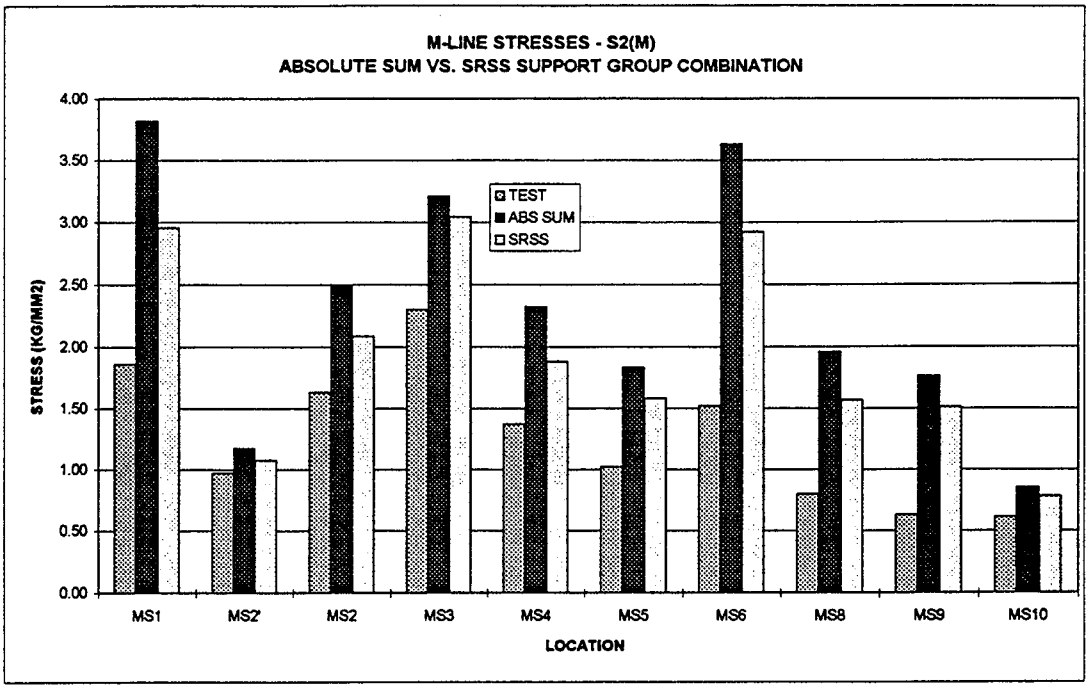

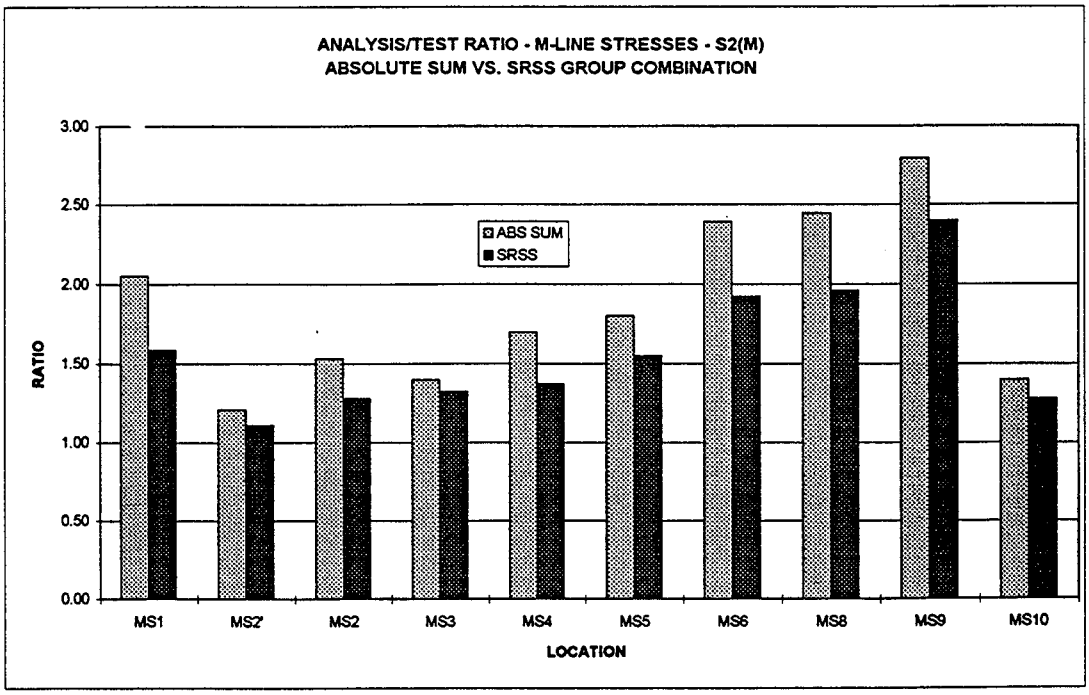

Figure 6.21 Comparison of Peak Stresses for M-line Design Analyses Using Absolute Sum vs. SRSS Support Group Combination Methods

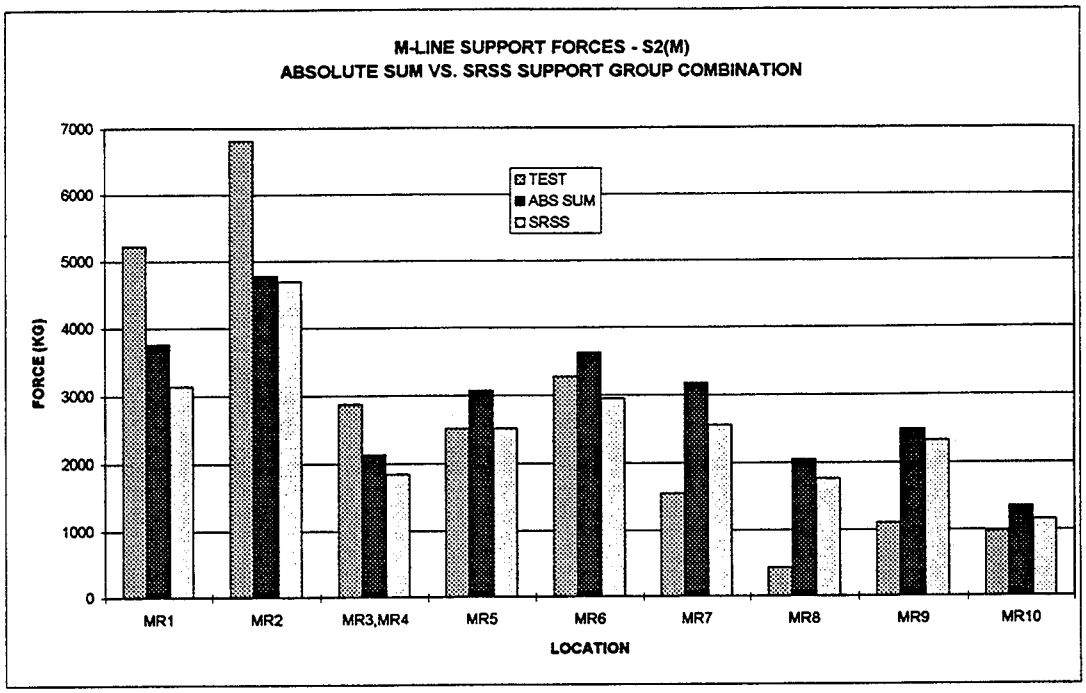

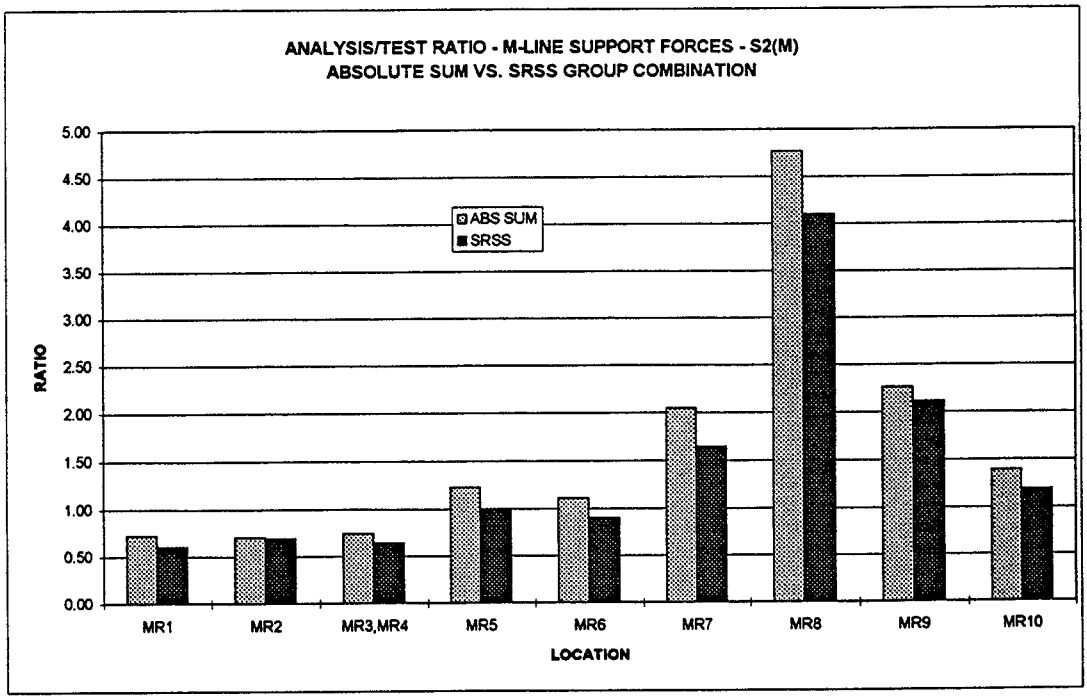

Figure 6.22 Comparison of Peak Support Forces for M-line Design Analyses Using Absolute Sum vs. SRSS Support Group Combination Methods

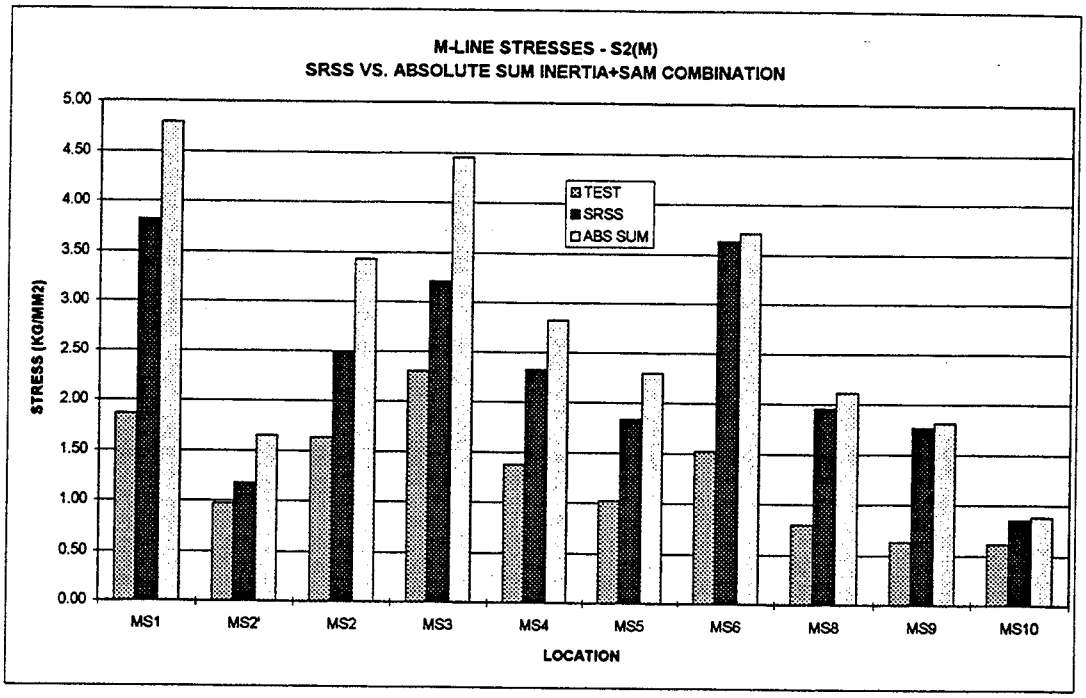

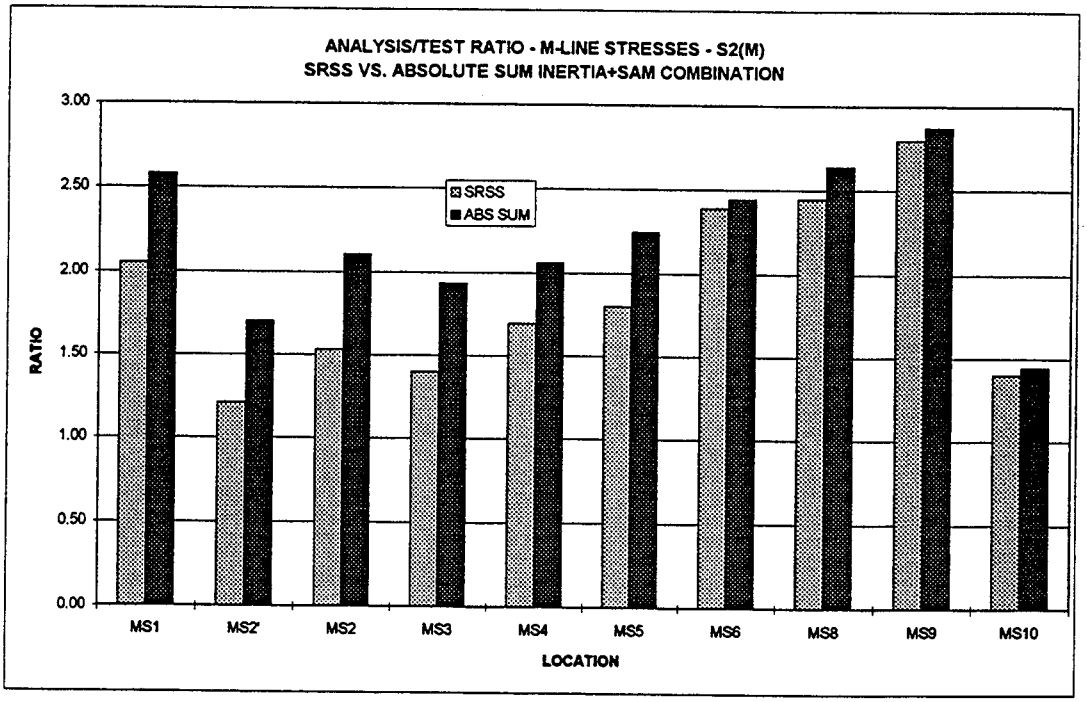

Figure 6.23 Comparison of Peak Stresses for M-line Design Analyses Using SRSS vs. Absolute Sum Inertia + SAM Combination Method

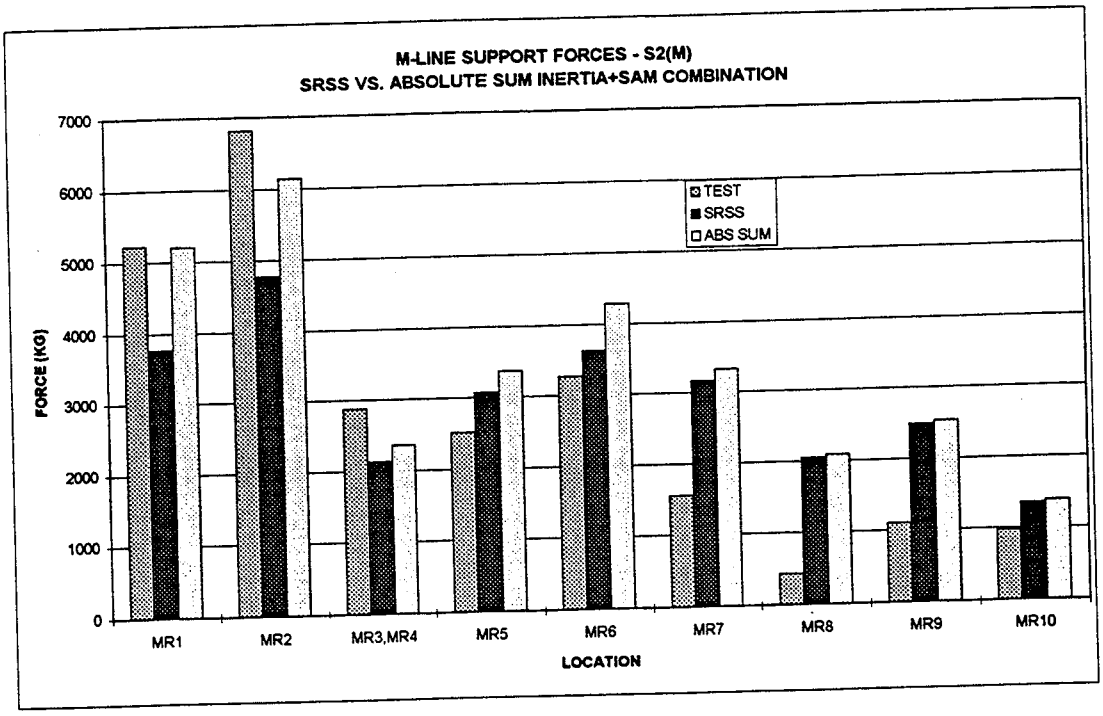

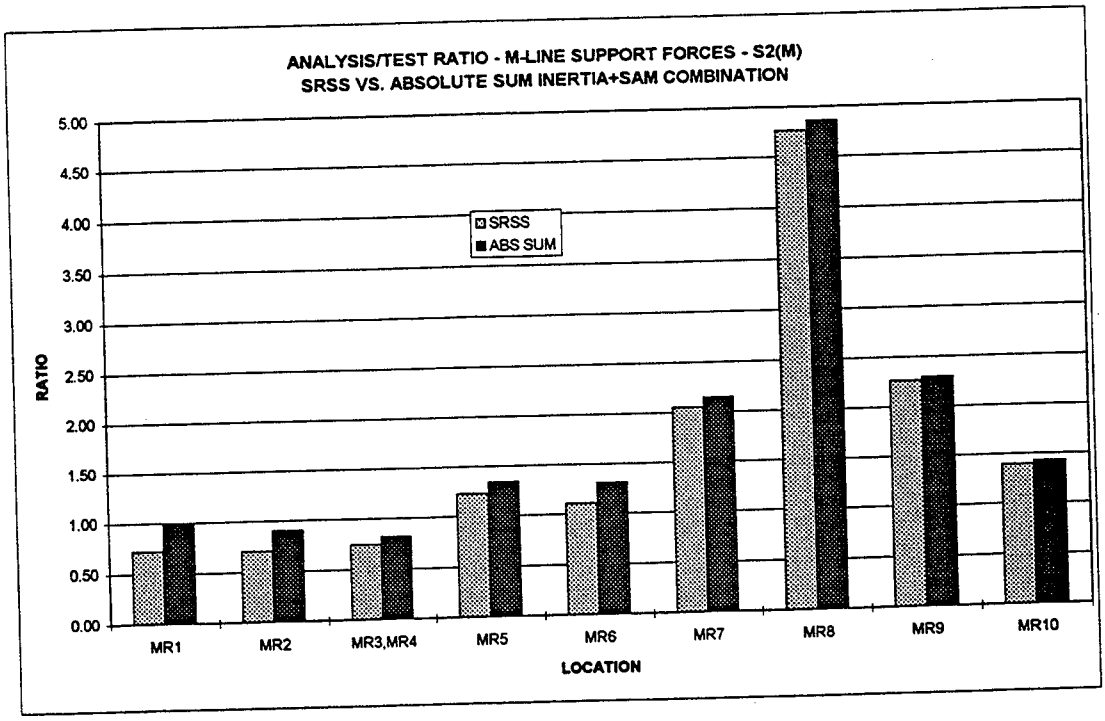

Figure 6.24 Comparison of Peak Support Forces for M-line Design Analyses Using SRSS vs. Absolute Sum Inertia + SAM Combination Method

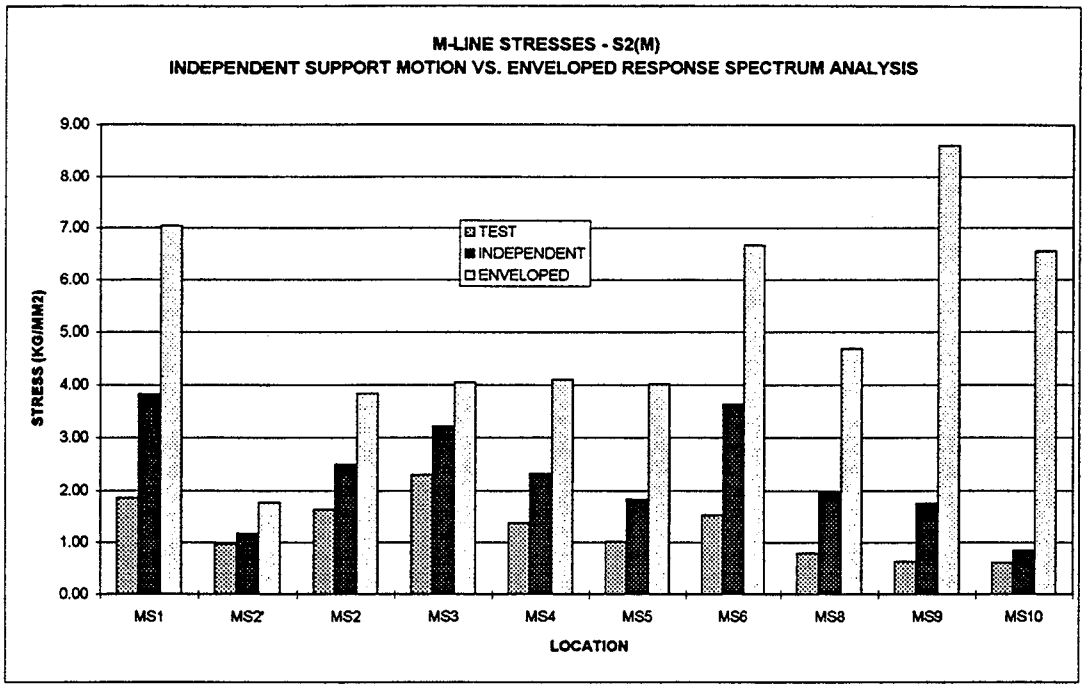

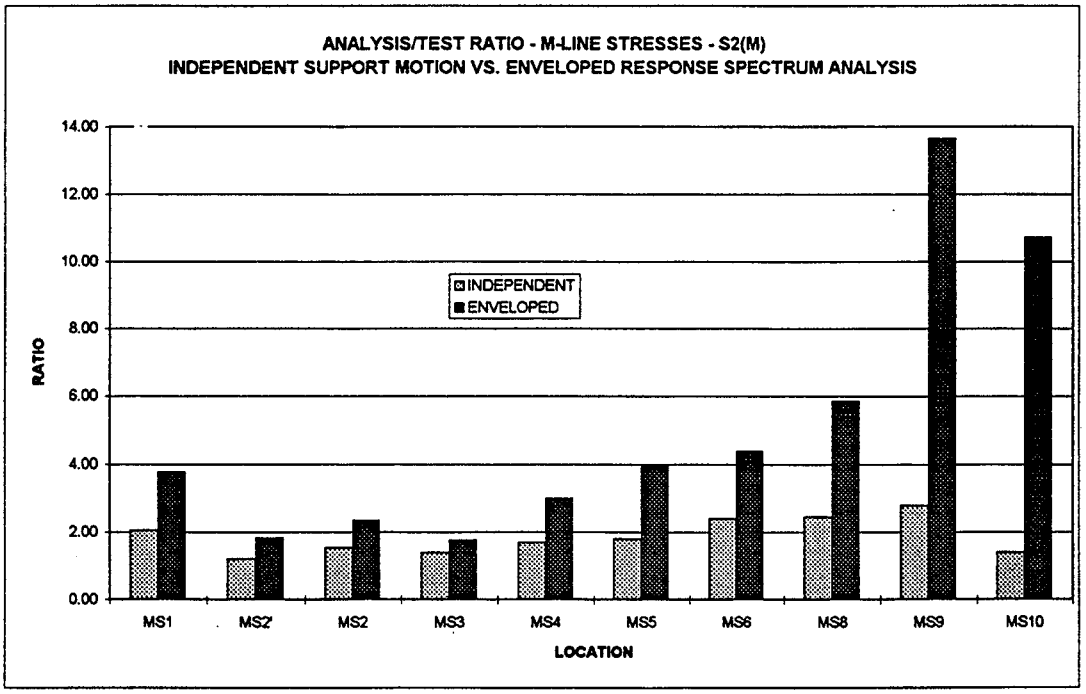

Figure 6.25 Comparison of Peak Stresses for M-line Design Analyses Using Independent Support Motion vs. Enveloped Response Spectrum Analysis Methods

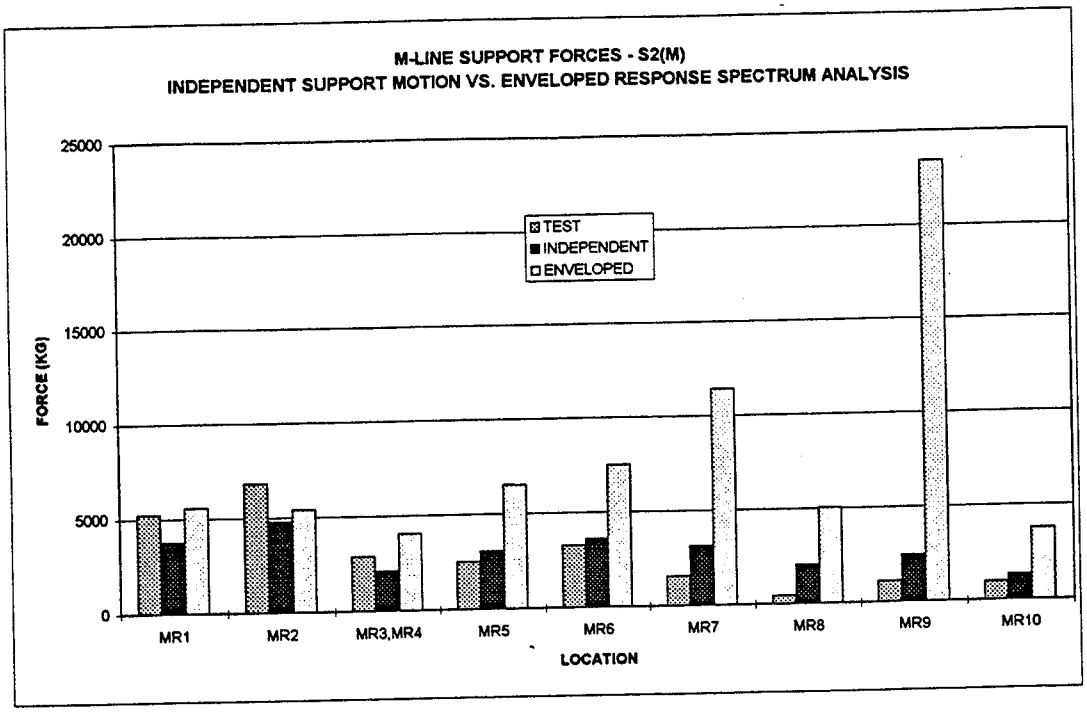

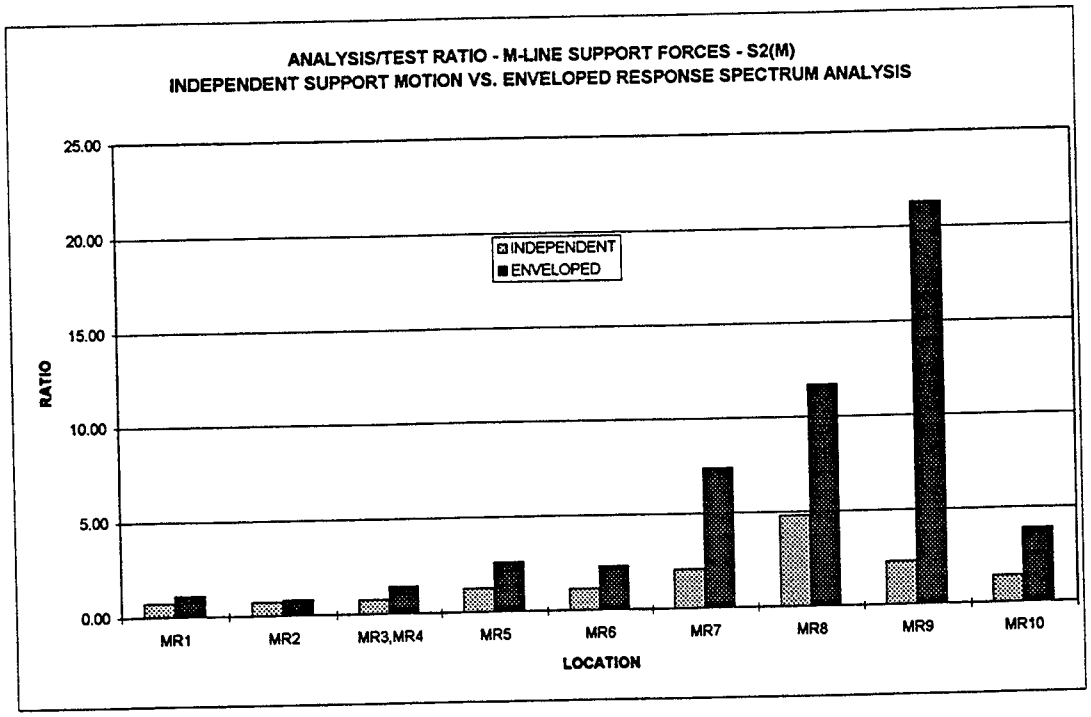

Figure 6.26 Comparison of Peak Support Forces for M-line Design Analyses Using Independent Support Motion vs. Enveloped Response Spectrum Analysis Methods

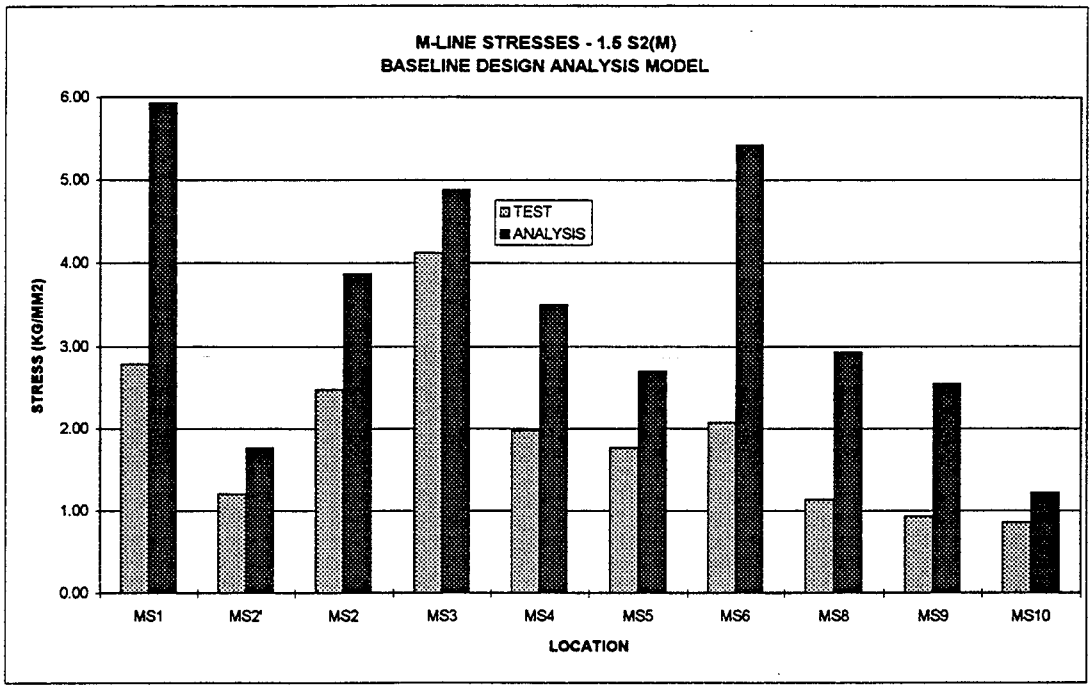

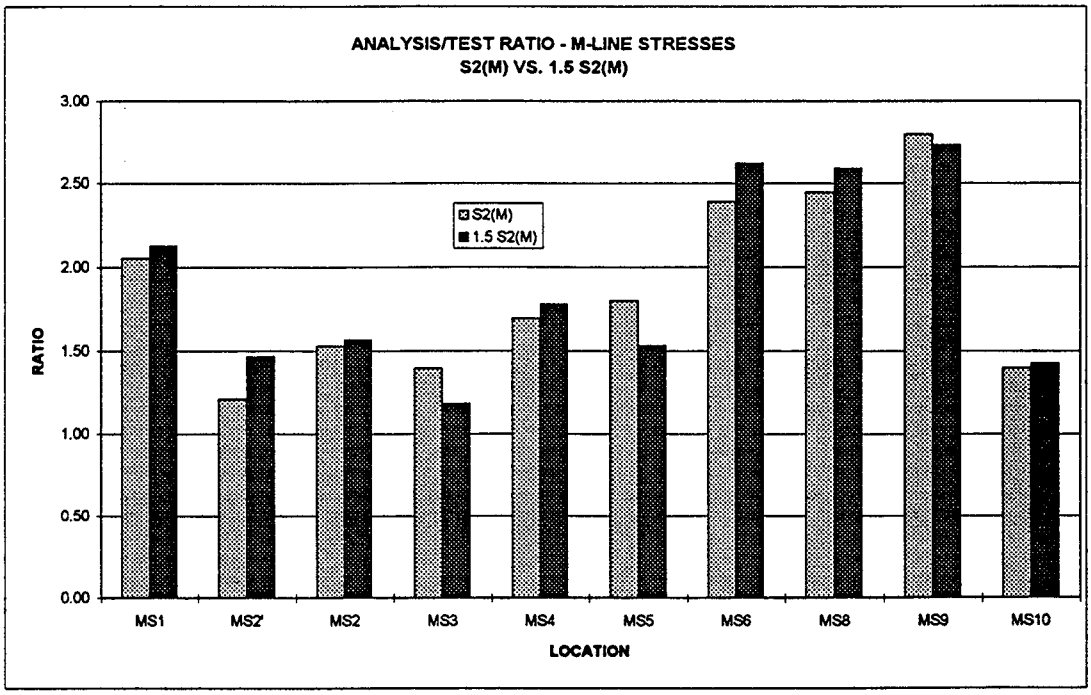

Figure 6.27 Comparison of Peak Stresses for M-line Design Analyses vs. Test Results for 1.5 S2(M) and 1.0 S2(M) Input Motion

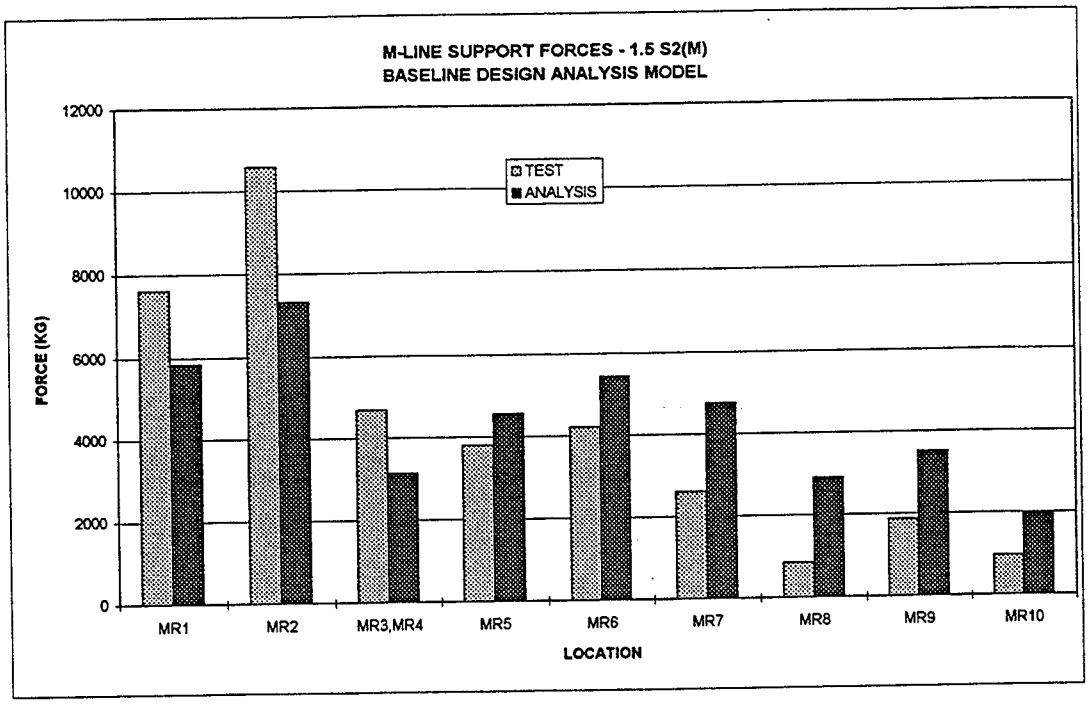

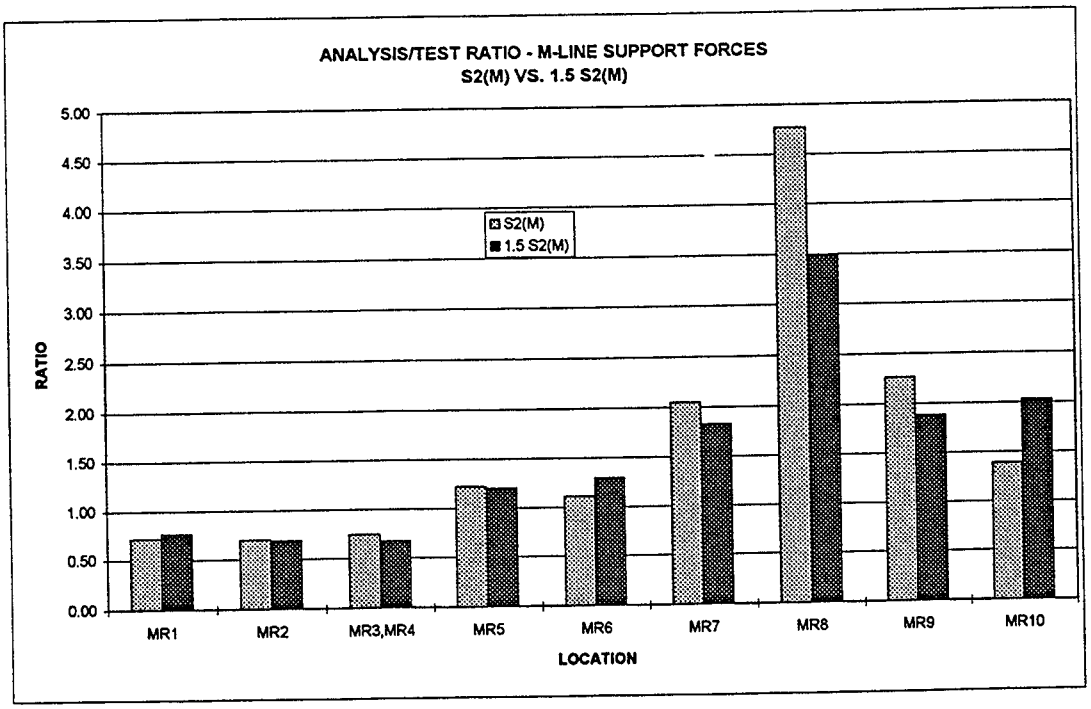

Figure 6.28 Comparison of Peak Support Forces for M-line Design Analyses vs. Test Results for 1.5 S2(M) and 1.0 S2(M) Input Motion

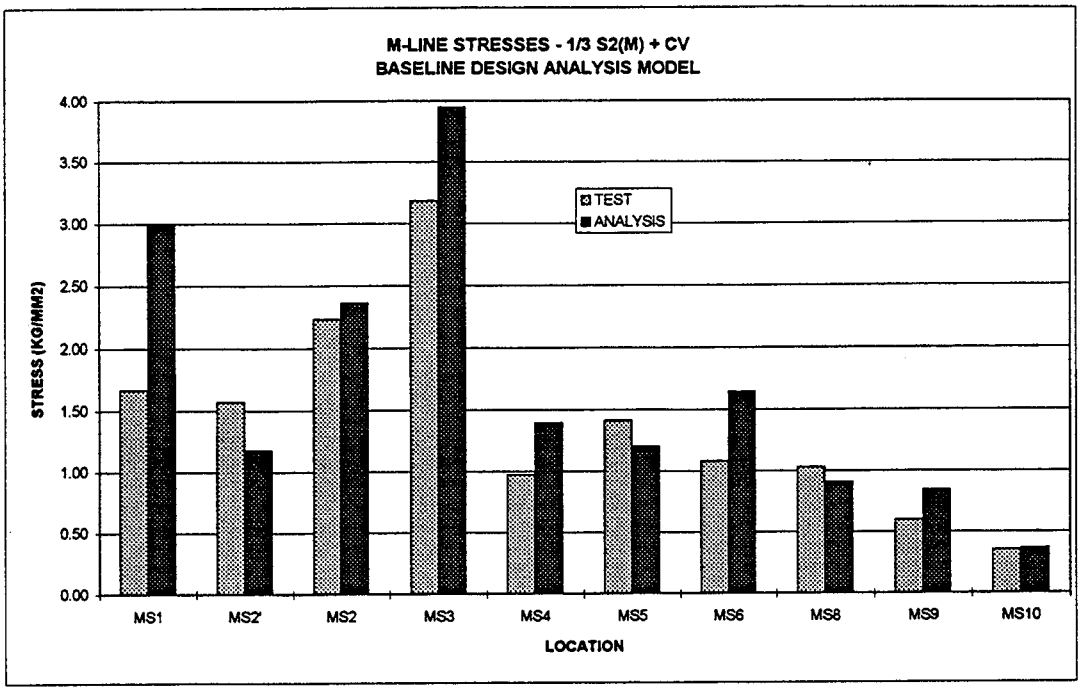

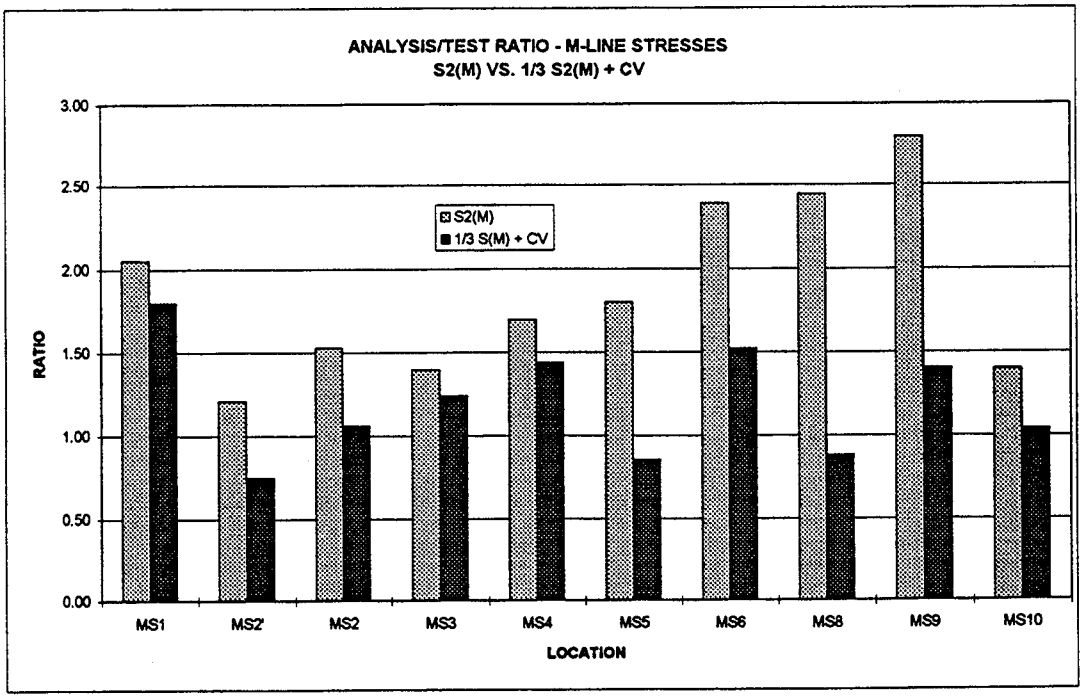

Figure 6.29 Comparison of Peak Stresses for M-line Design Analyses vs. Test Results for 1/3 S2(M) + CV and 1.0 S2(M) Input Motion

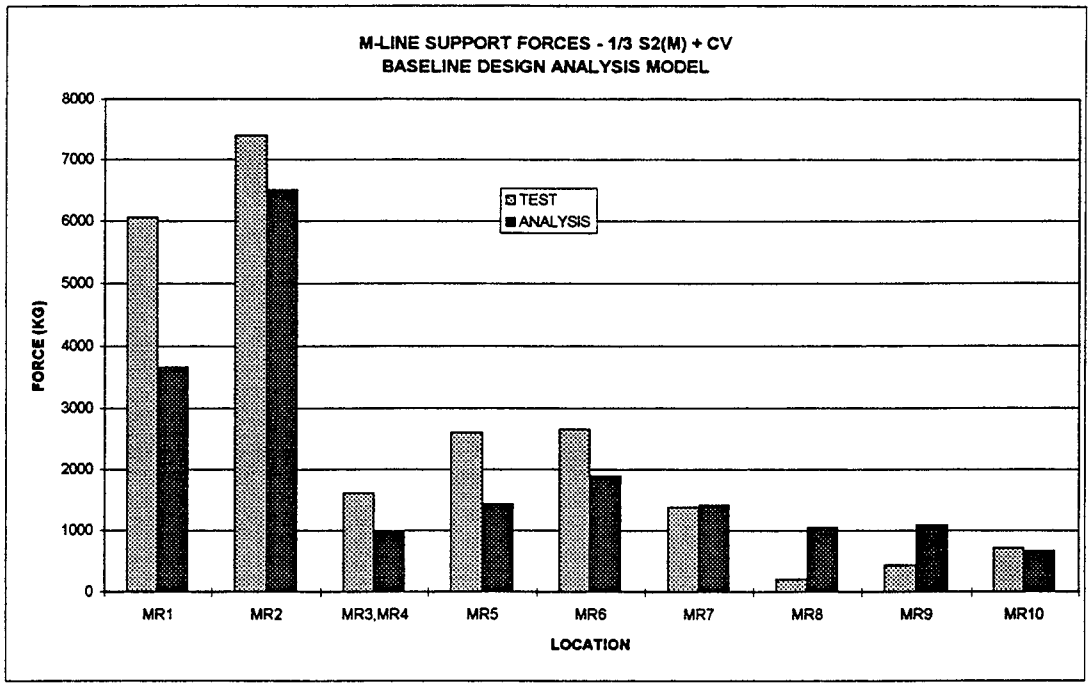

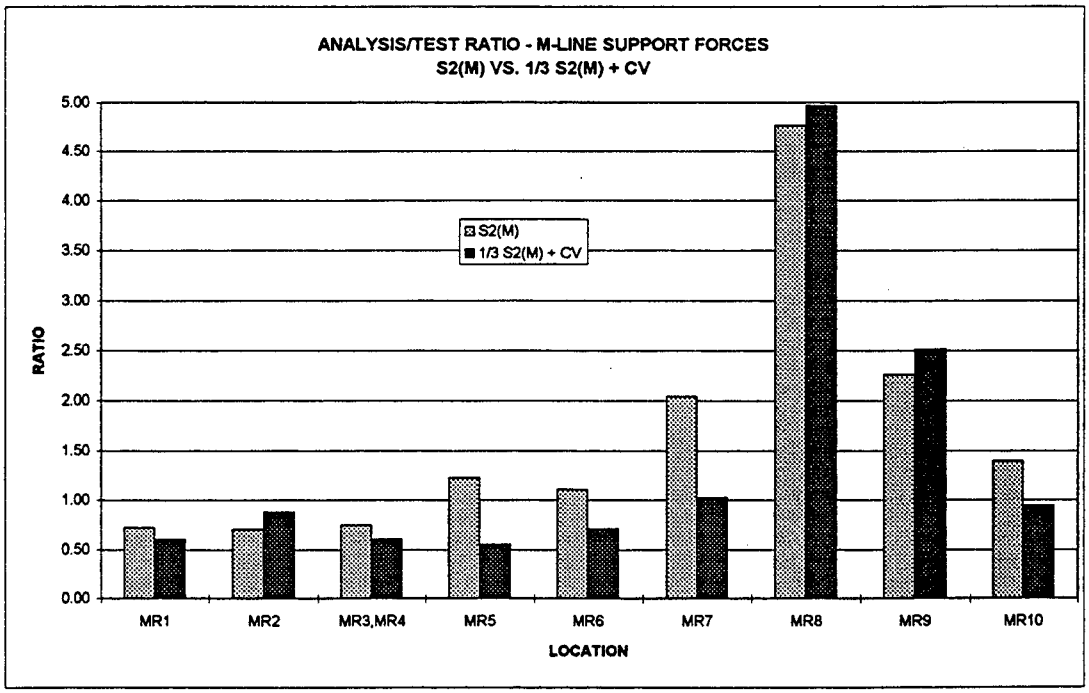

Figure 6.30 Comparison of Peak Support Forces for M-line Design Analyses vs. Test Results for 1/3 S2(M) + CV and 1.0 S2(M) Input Motion

7 CONCLUSIONS

The overall objectives of this study were to gain insights into the dynamic behavior of nuclear piping systems based on large-scale vibration tests, to assess the current piping analysis methods, and to evaluate the performance of energy absorbing devices as an alternative piping support. These objectives have been accomplished as described in detail in the previous chapters. This chapter provides a summary of major findings and conclusions, as well as engineering insights gained from the MS Test Program.

7.1 Test Results

A total of more than 200 vibration tests were conducted and an enormous amount of test data was obtained for piping systems with various support conditions. The data obtained can be utilized in future efforts to verify structural analysis computer codes.

Both the fabrication of the test specimens and the shaking table control were considered adequate to reproduce the dynamic responses of actual piping systems in a nuclear power plant under severe earthquake shaking.

The observed responses of snubber supports revealed highly complex nonlinear hysteretic characteristics. The main causes of the observed nonlinearities are considered to be various mechanical gaps both inside the snubbers and at the pipe clamps, rate-dependent characteristics of snubbers, and the effects of orthogonal (to the snubber axis) forces on the snubbers. The last factor, i.e., the effects of orthogonal forces, has never been identified as a critical factor in snubber behavior in past studies. During the MS Test Program, the structural as well as functional integrity of mechanical snubbers was confirmed up to support forces 3.6 times the rated design load. The measured pipe stresses under the design earthquakes were much lower than the yield stress level.

In the second phase of the test program, the conventional snubbers were replaced with E.A. supports and the systems were tested under design earthquakes, as well as at higher excitations up to the deformation limits of the E.A. supports. The large number of vibration tests revealed a significant energy absorbing capability of the E.A. devices, and the observed hysteretic behavior was considered to be more predictable than that of the conventional snubbers. Under the design earthquake, the measured pipe stresses were higher than those with the conventional snubbers but still much lower than the yield stress level. Both the LED and EAB support systems sustained a large number of earthquake loadings at much higher than the design load levels without losing structural or functional integrity. During a few tests with the highest table motions, pipe stresses slightly exceeded the yield stress level at a few locations. However, the piping remained essentially elastic, and no structural damage was observed during the detailed inspections after the MS test program.

The comparison of piping response between the conventional support case and the E.A. support case has shown distinctively different dynamic characteristics. Mechanical snubbers contribute a spring hardening type vibration characteristic to the piping systems, i.e., the vibration frequencies tend to increase at higher excitation levels. On the other hand, the E.A. supports contribute a spring softening type characteristic, i.e., the vibration frequencies tend to reduce at higher excitation levels. In both the cases, the measured response quantities were not proportional to the excitation level. The ratios of almost all measured response quantities to the excitation level tend to reduce at a higher table motion amplitude.

7.2 Post-test Analyses

As part of the post-test analysis efforts, two types of analyses were performed, i.e., simulation analyses to reproduce the observed responses described in Chapter 5, and design-based analyses to assess various design/analysis assumptions described in Chapter 6.

For the simulation analyses, in addition to conventional NTH analyses, two types of ELA analyses were also applied. For the conventional support case, it was found that the low-pass filter used to process the test records during testing altered the measured peak values of acceleration and support forces. The discrepancies between analyses and tests have been reduced significantly by applying a similar low-pass filter to the calculated nonlinear response results. The observed irregular nonlinearity of mechanical snubbers was not reproduced in the analyses, and was considered to be a main cause of the observed analysis discrepancies.

In the simulation analyses for the E.A. support case, the Bouc-Wen hysteretic model properly reproduced the observed nonlinear behavior of the E.A. supports. However, in addition to the problems associated with the mechanical snubbers, other types of pipe supports such as pin supports and sliding guides also contributed nonlinear characteristics to piping systems due to mechanical gaps in their support structures. In general, the observed analysis errors are less for higher excitation test runs as the effects of mechanical gaps in pipe supports become less significant.

Two types of equivalent linearization analyses were performed, i.e., ELA/RS and ELA/LRV. In almost all the analysis cases, the ELA/LRV analyses gave consistently better correlation with the NTH analyses than the ELA/RS approach. Since both the ELA methods are much less time consuming than NTH analyses, the methods may prove to be acceptable alternatives for piping design when the effects of nonlinearities in pipe supports are considered.

In the design-based analyses described in Chapter 6, a set of analysis assumptions were made according to current piping design practice in the nuclear industry, and this analysis case was called "the baseline case". The selected analysis assumptions included the use of the response spectrum approach, broadened (±15%) spectra, a 2% damping value, the SRSS combination rule and a static analysis for SAM (see Section 4.2.1.). The design margins were evaluated in terms of the ratios of the calculated pipe stresses and support forces to the recorded response values. Only the conventional support cases were analyzed. The comparisons of design analysis to test results demonstrated the overall conservatism of the baseline design analysis methods. For both piping systems, the pipe stress results were generally more conservative than the support force results. On an average basis, the design analyses provided adequate margins for both pipe stresses and support forces. However, the analysis to test result ratios varied significantly from one location to another. M-line stresses predicted by the baseline analysis exceeded the test measurements at all locations. F-line design analysis stresses were underpredicted at a few locations although the stresses at those locations were low. M-line support forces were underpredicted at locations near the independent actuator. F-line support forces were underpredicted at several locations.

A series of parametric studies were also performed by varying the major analysis assumptions. When the snubbers were modeled as rigid supports, a large analysis error in the calculated frequencies was observed, and the average support forces were underpredicted. It was concluded that the snubber stiffness assumption was a critical factor, and the design snubber stiffness model provided the best frequency match and the largest average margins. As expected, the analysis cases with 5% damping and unbroadened spectra gave lower margins, both underpredicting the average support forces. For the M-line analysis, the use of the enveloped response spectrum method gave much higher margins than the baseline case analyses, which used the Independent Support Motion (ISM) response spectrum method.

8 REFERENCES

1. NUPEC, "Proving Tests on The Seismic Reliability for Nuclear Power Plant, MS Seismic Proving Test," Nuclear Power Engineering Corporation, 1992-1996.

2. D.G. Schrammel, "Comparison of Measurements and Calculations for the High-Level Seismic Tests of Piping at the HDR (Test Group SHAM)," SMiRT 11, Vol. K, Tokyo, Japan, August 1991, pp. 445-450.

3. R. Gerard, et. al., "Comparison of Modal Spectral and Non-linear Time History Analysis of A Piping System," SMiRT 9, Vol. K, Lausanne, August 1987, pp. 911-916.

4. H. Kobayashi, et. al., "Dynamic Response of the Piping System on the Rack Structure with Gap and Frictions," SMiRT 9, Vol. K2, Lausanne, August 1987, pp. 995-1000.

5. Cloud, R.L., Anderson, P.H., and Leung, J.S.M., "Seismic Stops vs. Snubbers: A Reliable Alternative," Nuclear Engineering and Design, 107, 1988, pp. 205-213.

6. Caughey, T.K., "Equivalent Linearization Techniques," Journal of the Acoustical Society of America, Vol. 35, No. 11, 1963, pp. 1706-1711.

7. L.K. Severud, "Simplified Analytical Methods and Experimental Correlation of Damping in Piping During High-Level Inelastic Response," SMiRT 9, Vol. K2, Lausanne, August 1987, pp. 989-994.

8. C.W. Lin and A.D. Romanko, "Simplified Piping Analysis Methods for Piping with Inelastic Supports," SMIRT 9, Vol. K2, Lausanne, August 1987, pp. 929-937.

9. T. Igusa, et. al., "Methods of Analysis of Piping Systems with Nonlinear Vibration Absorbers," SMiRT 11, Vol. K2, Tokyo, Japan, August 1991, pp. 511-516.

10. Y.J. Park, "ISSAC. . .User's Manual," informal technical report, Brookhaven National Laboratory, January 1997.

11. ASME Boiler and Pressure Vessel Code, Section III, Division 1-NC, 1992.

12. Y.K. Wen, "Equivalent Linearization Hysteretic Systems Under Random Excitation," Journal of Applied Mechanics, Vol. 47, No. 1, 1980, pp. 150-154.

13. Y.J. Park and C.H. Hofmayer, "Practical Application of Equivalent Linearization Approaches to Nonlinear Piping Systems," PVP/ASME Conference, Honolulu, Hawaii, 1989.

14. Tansirikongkol, V. and Pecknold, D.A., "Approximate Modal Analysis of Bilinear MDF Systems," Journal of Engineering Division, ASCE, Vol. 106, No. EM2, April 1980, pp. 361-375.

APPENDIX A

COLLECTION OF PHOTOGRAPHS OF MS TEST MODEL

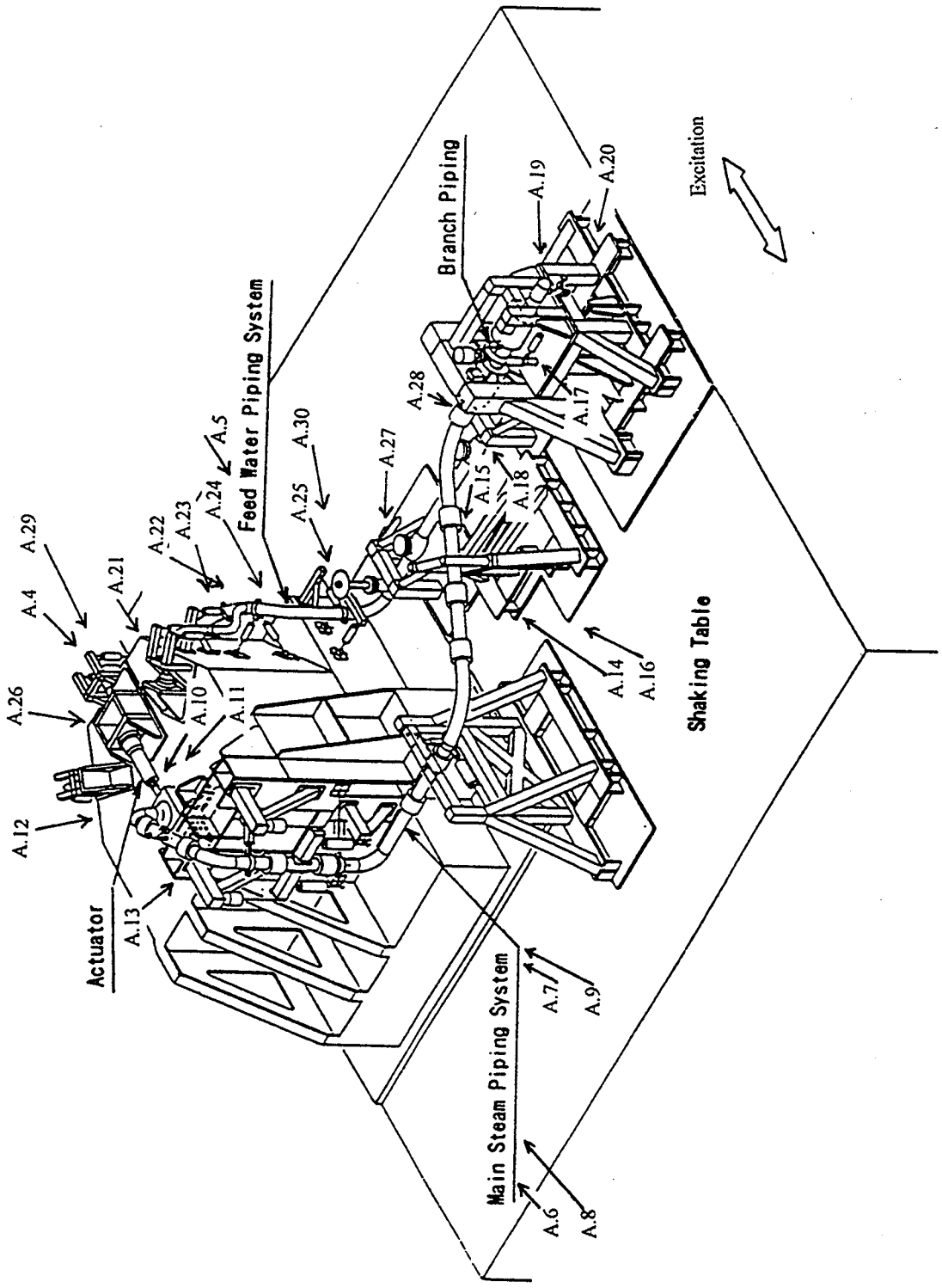

Figure A.1 Locations of Photographs on MS Test Model

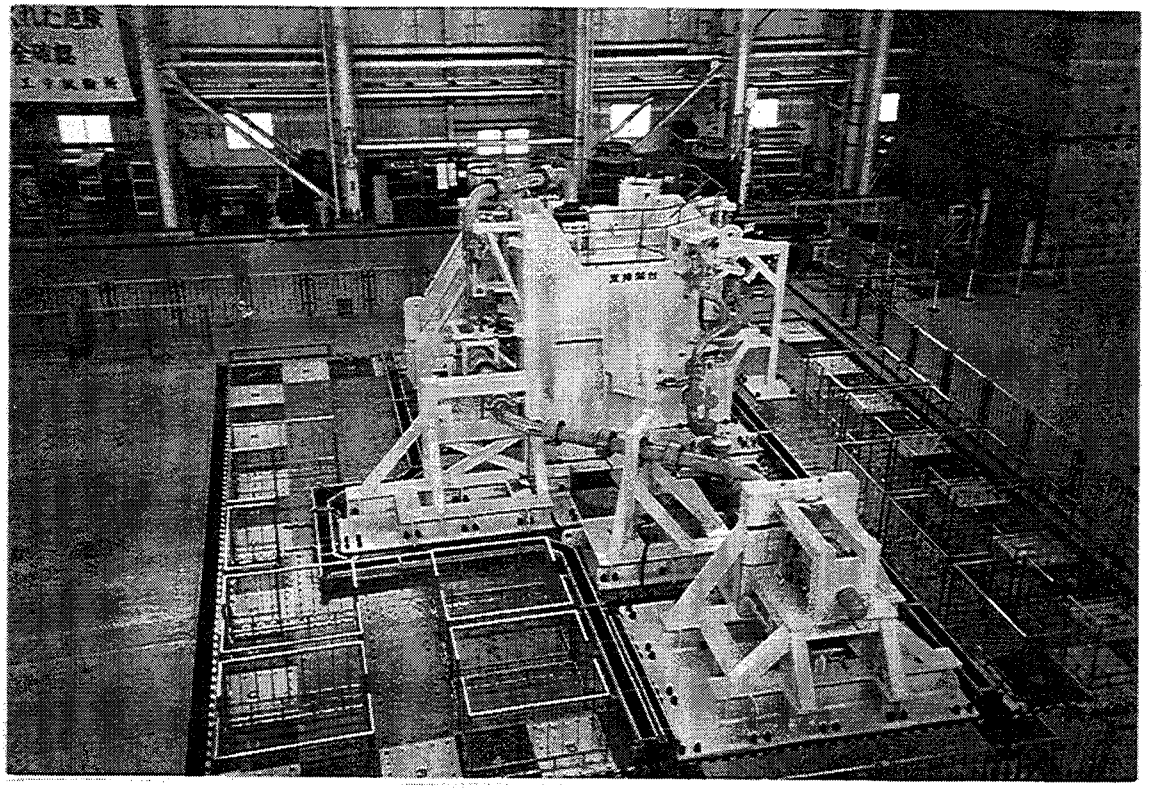

Figure A.2 MS Proving Test Model (M-line left, F-line right)

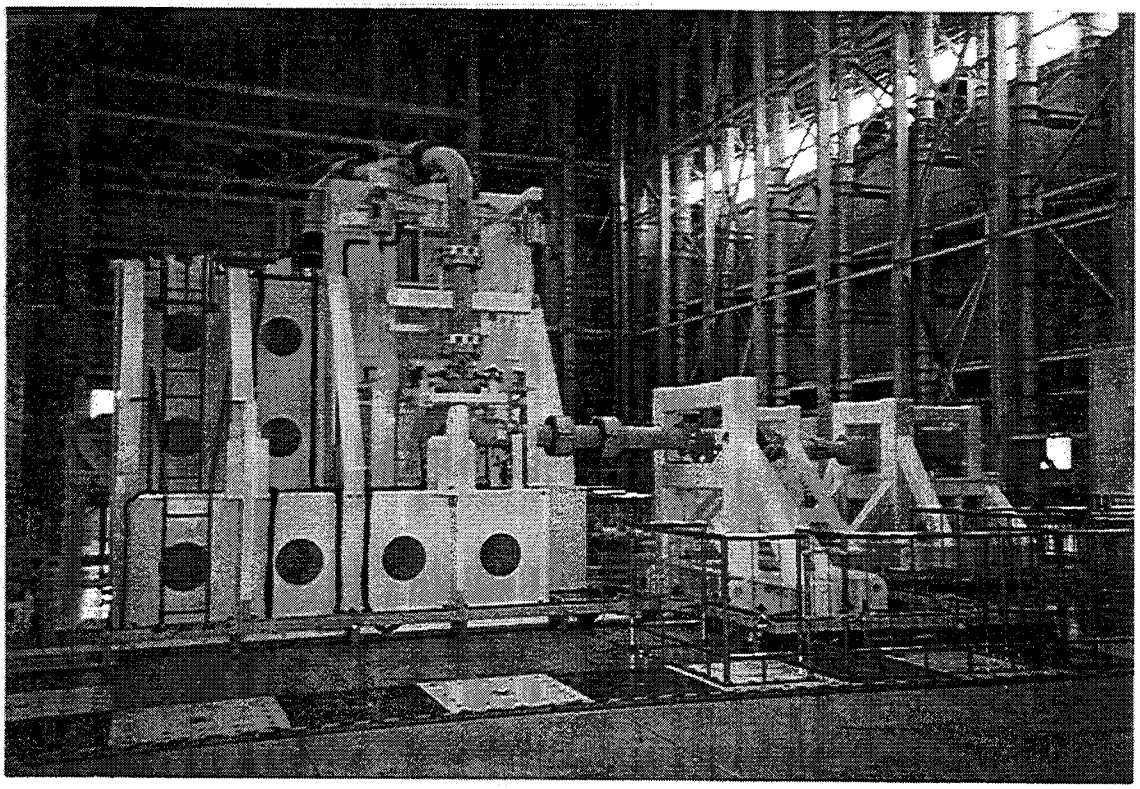

Figure A.3 M-line (LED support)

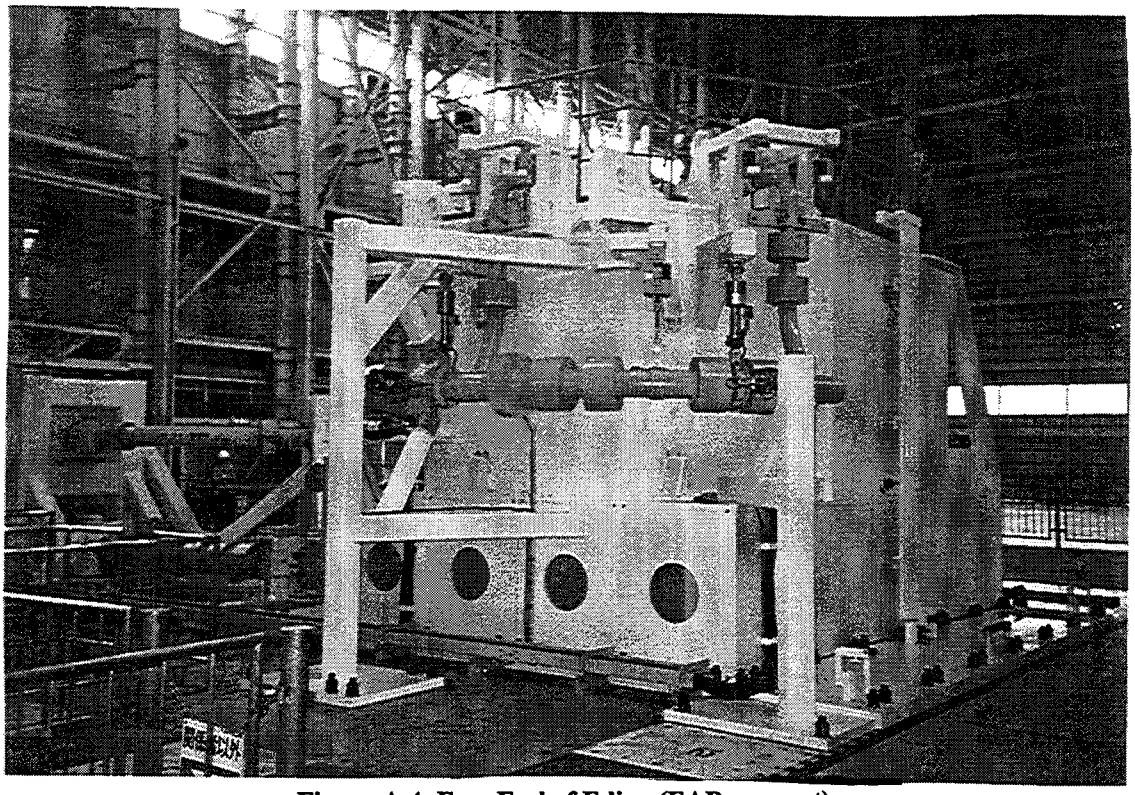

Figure A.4 Free End of F-line (EAB support)

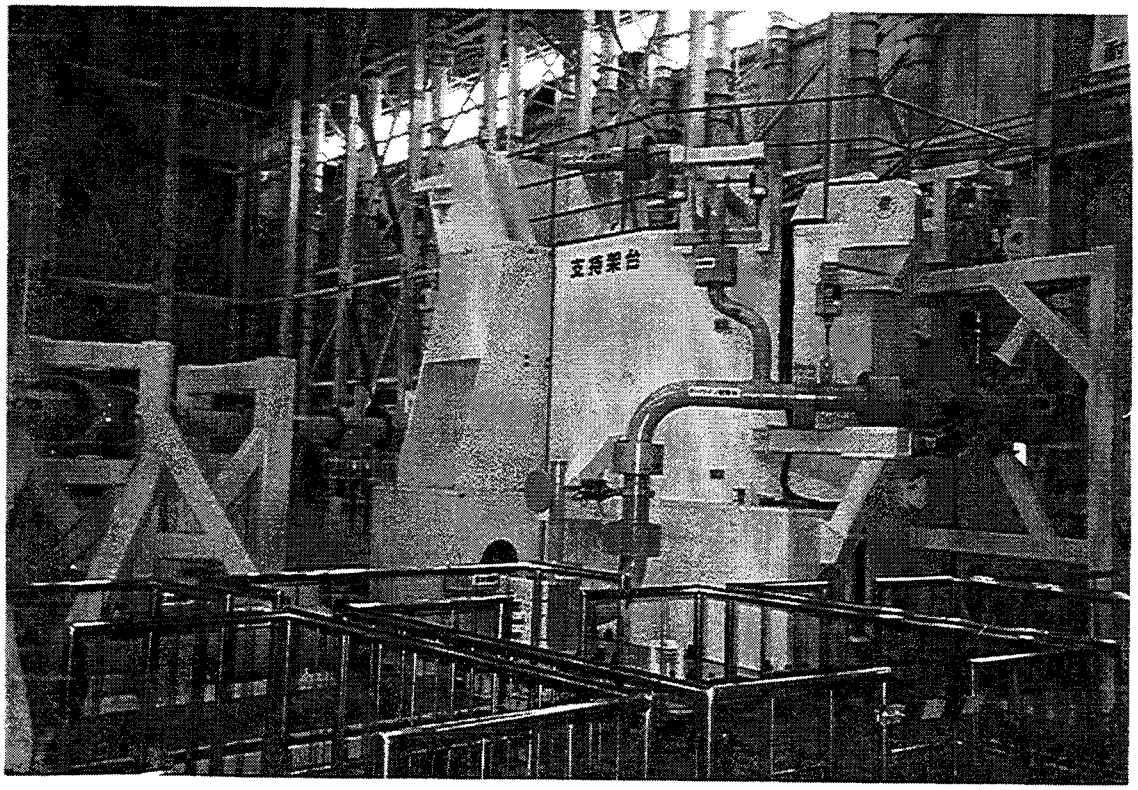

Figure A.5 F-line (EAB support)

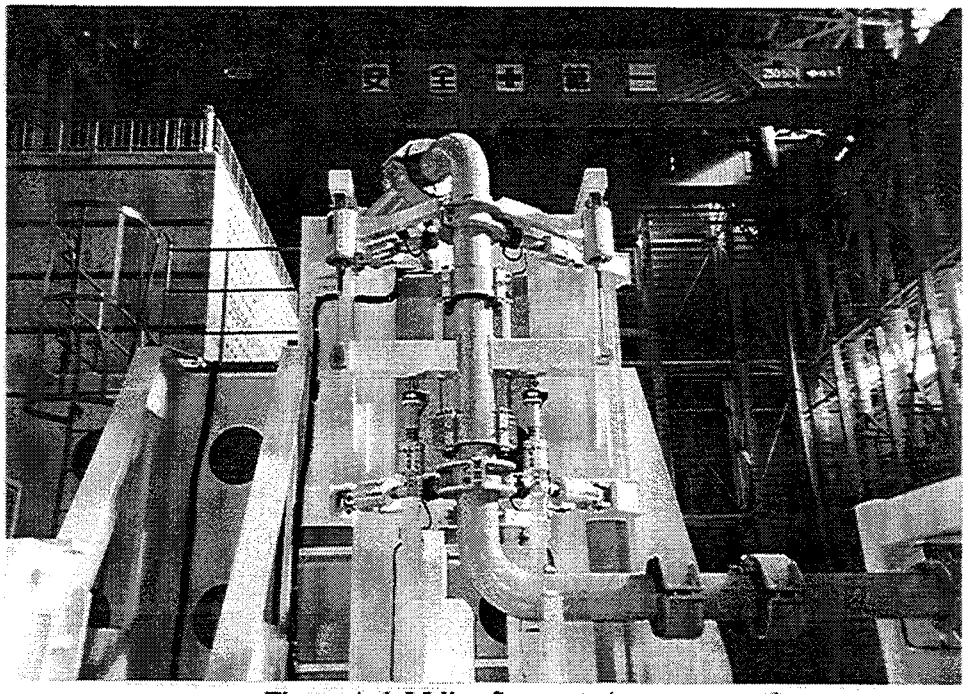

Figure A.6 M-line Supports (conv. support)

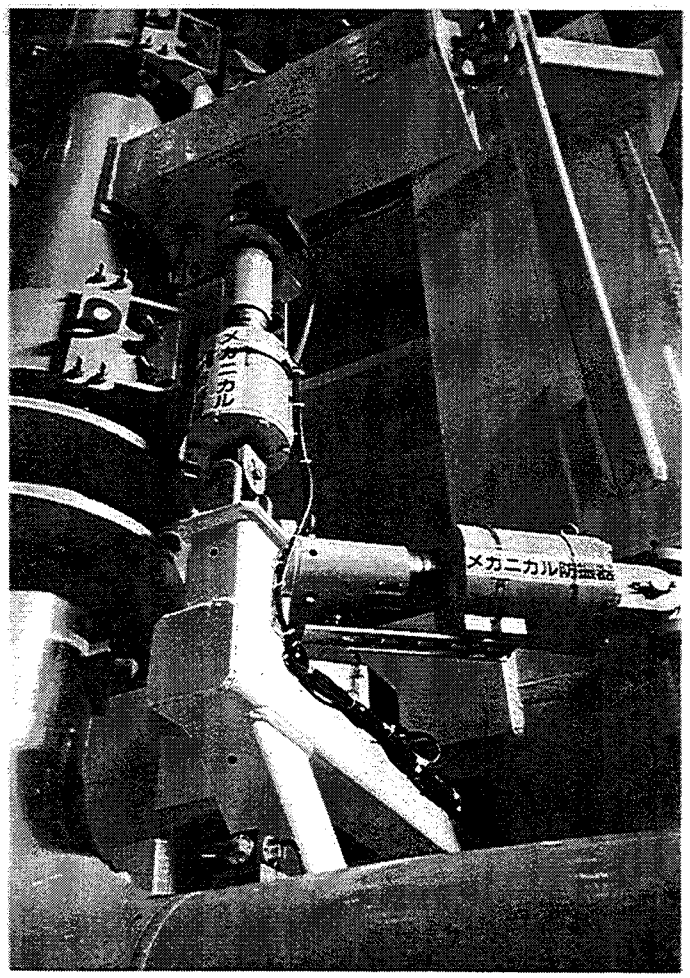

Figure A.7 Mechanical Snubbers of M-line (MR3-vertical and MR5-horizontal)

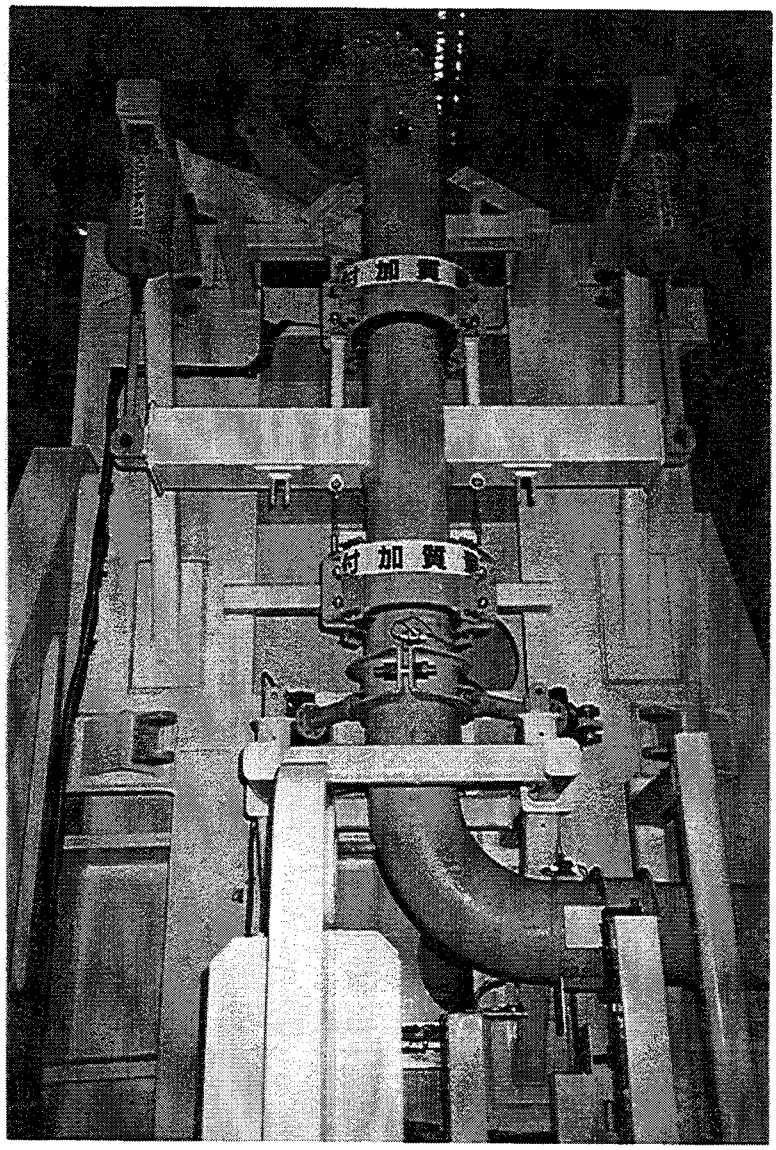

Figure A.8 LED Supports of M-line (MR15 and MR16)

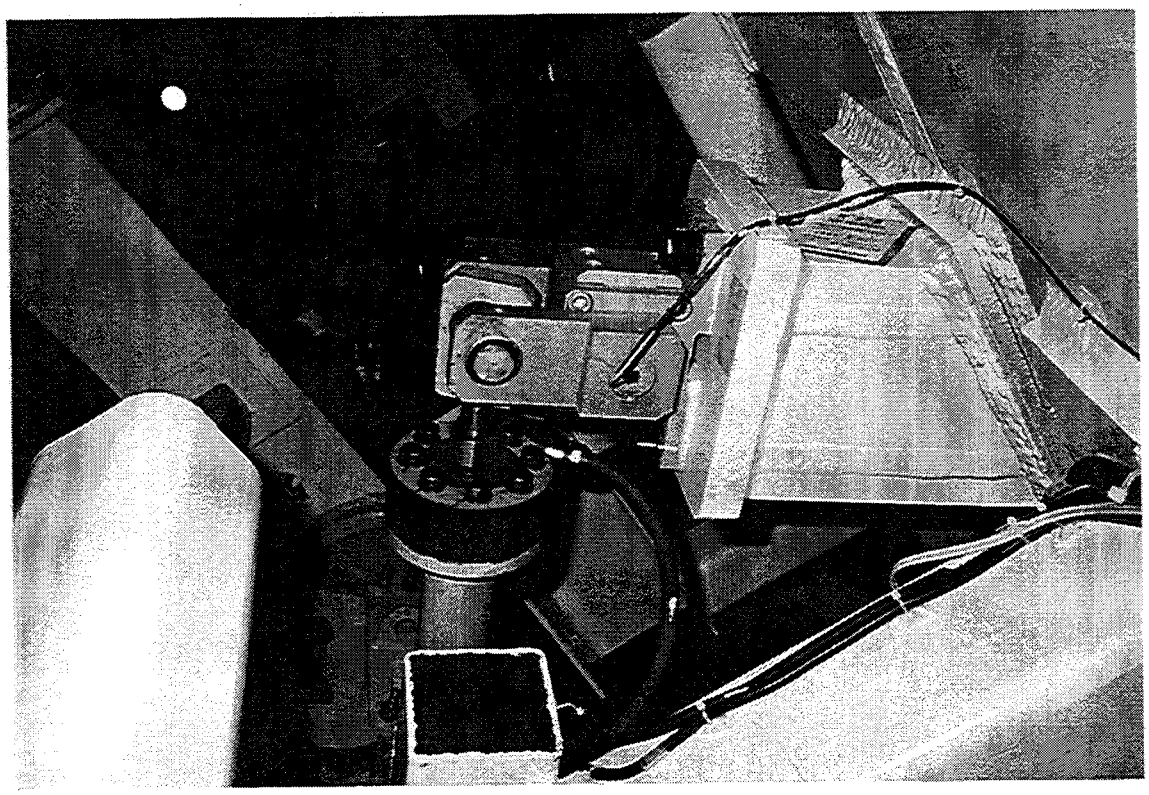

Figure A.9 Close-up of LED Support of M-line (MR15)

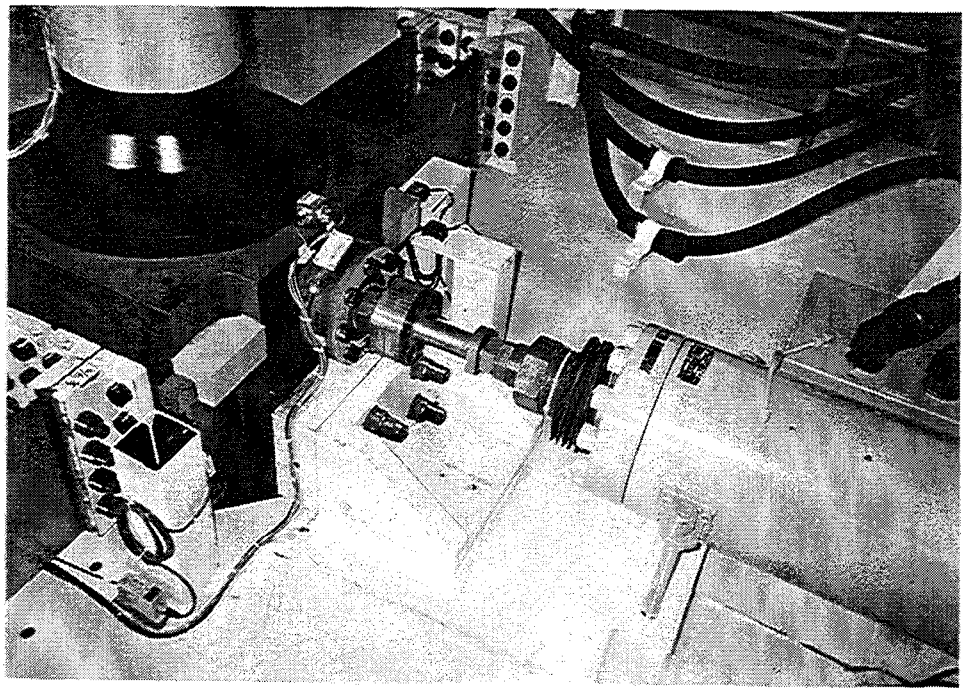

Figure A.10 Independent Actuator of M-line

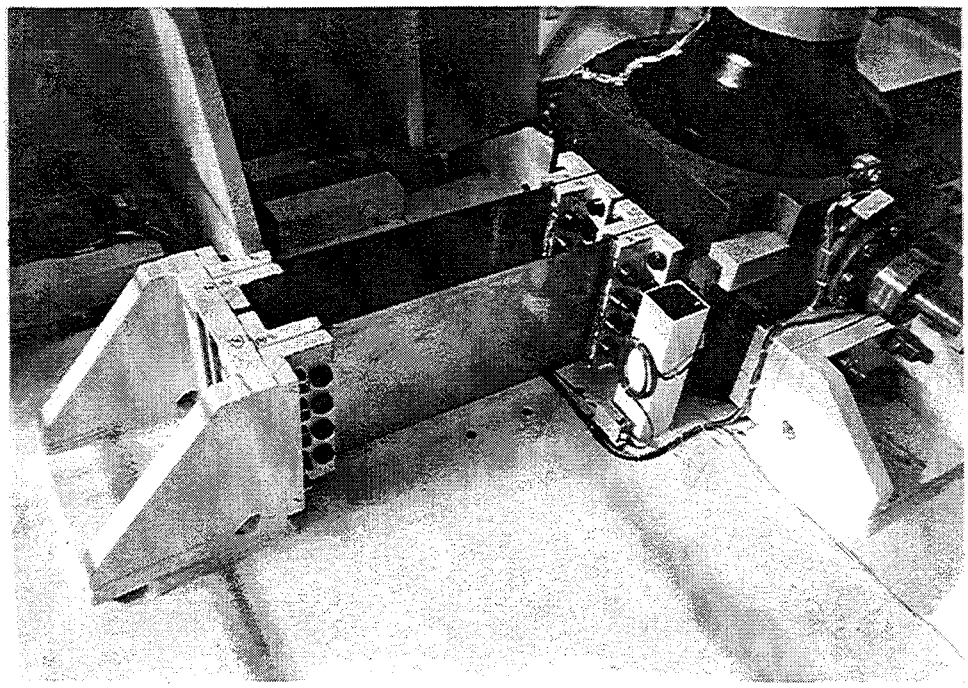

Figure A.11 Parallel Springs at Top of SG joint

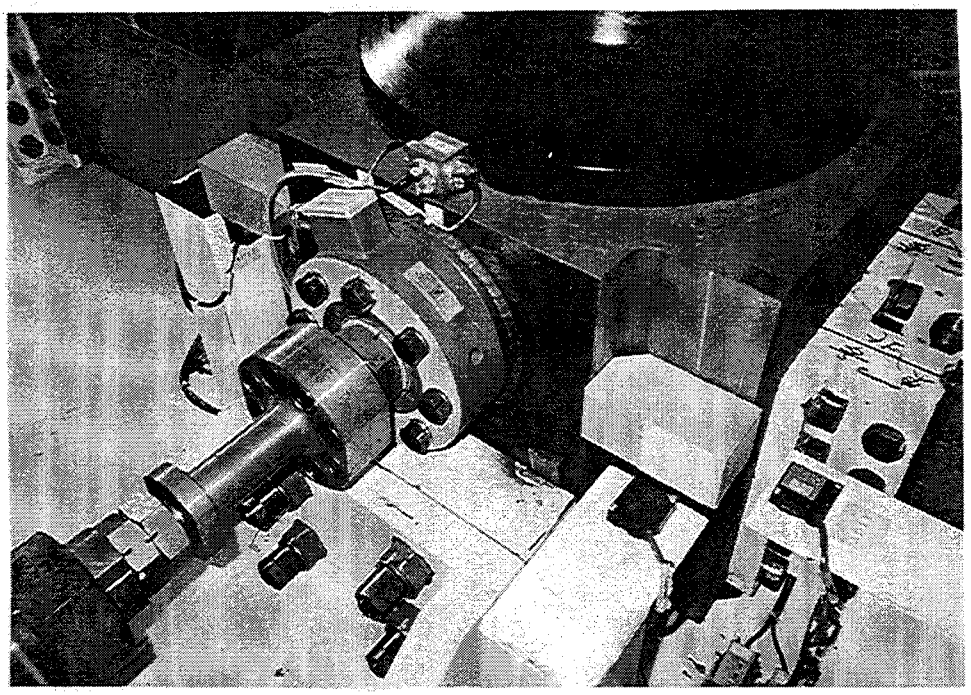

Figure A.12 Shims for Gap at SG Joint

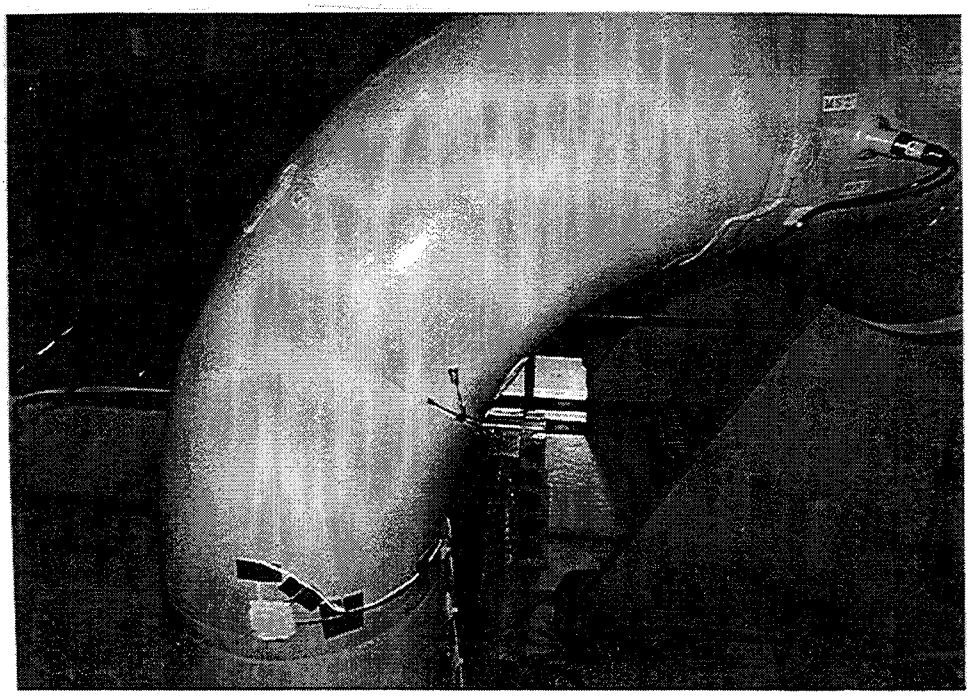

Figure A.13 Strain Gauges on M-line Elbow

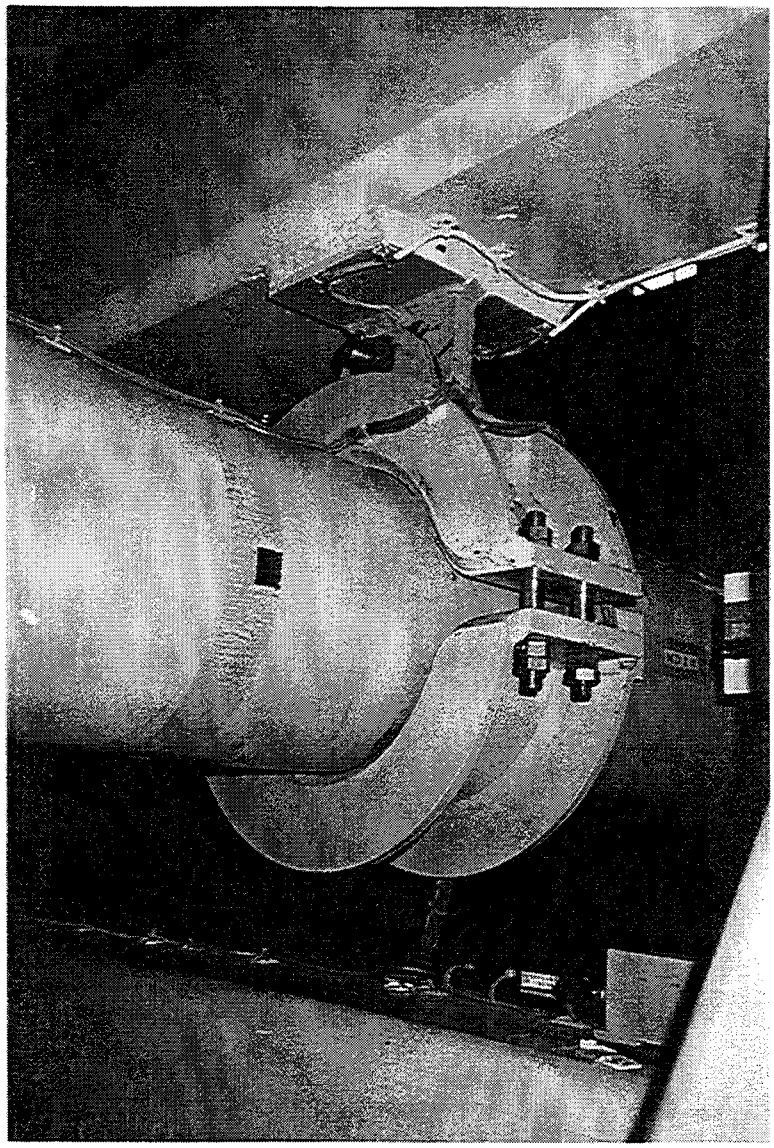

Figure A.14 Pin-Support of M-line (MR8)

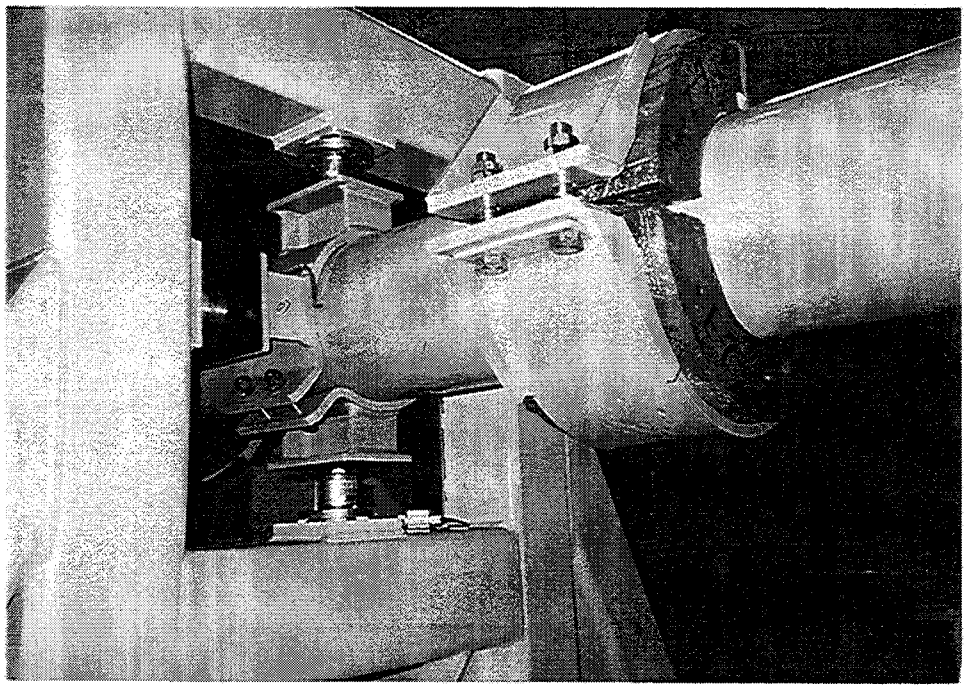

Figure A.15 Sliding Supports of M-line (MR9 and MR10)

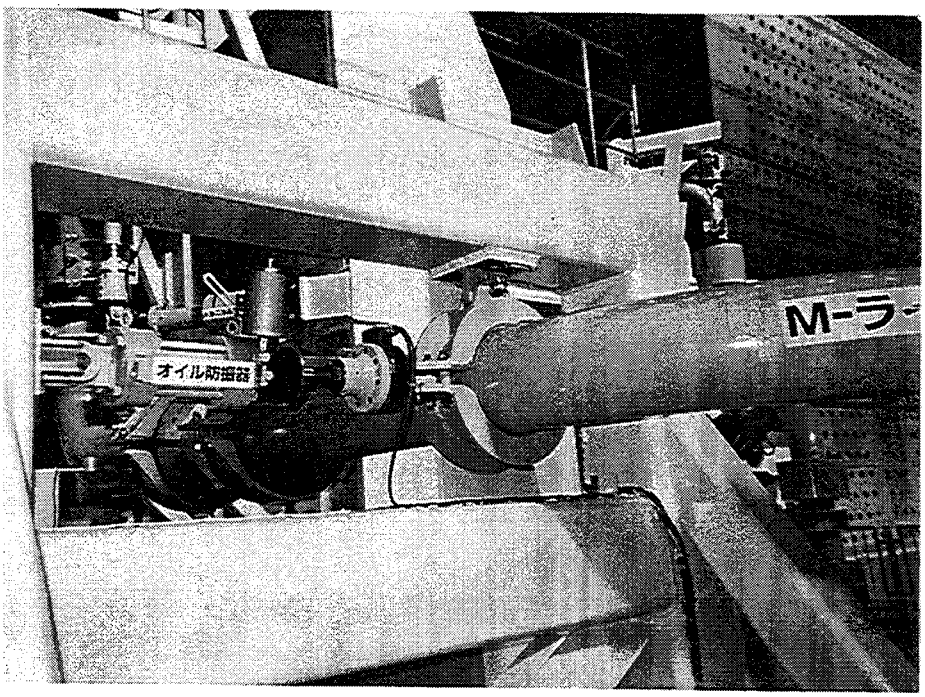

Figure A.16 Oil Snubber of M-line with Conventional Support (MR7)

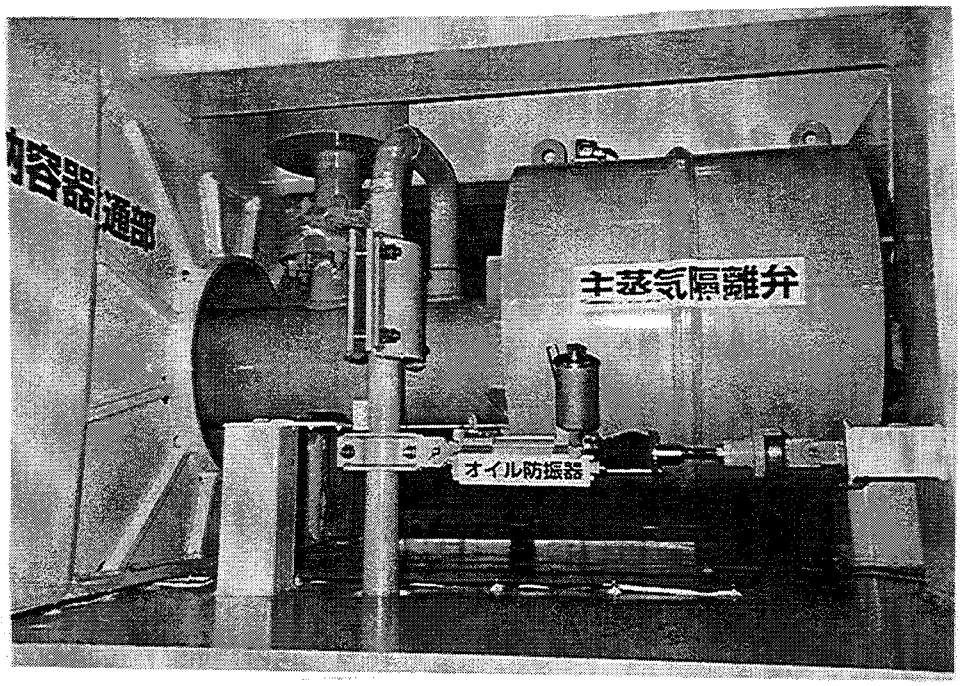

Figure A.17 Main Steam Separation Valve and Branch Line with Horizontal Oil Snubber of M-line (MR11)

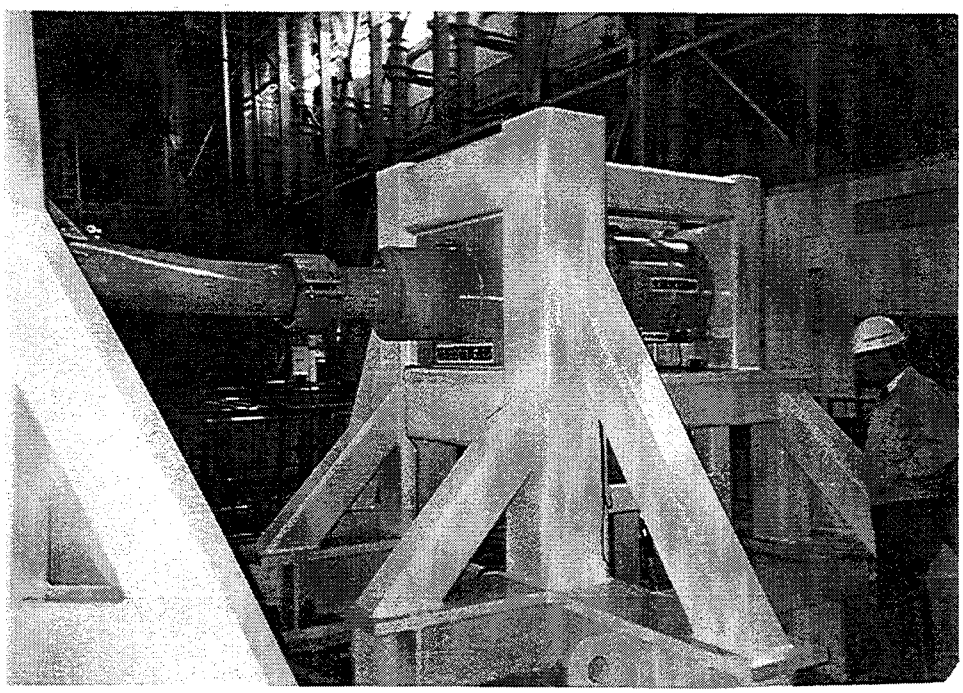

Figure A.18 Anchor at Penetration Part of M-line

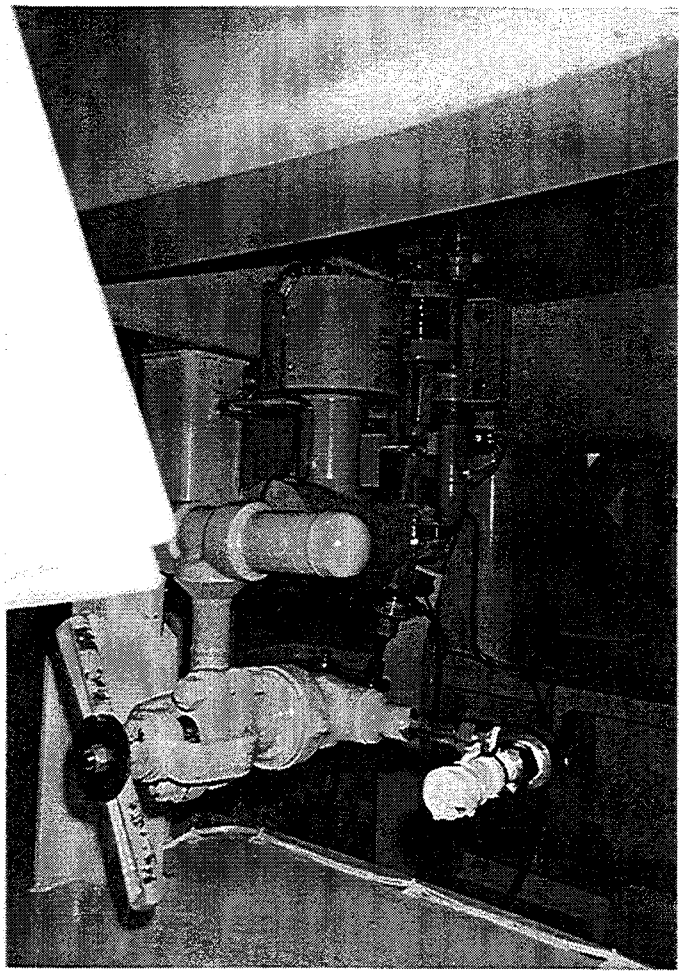

Figire A.19 End of Branch Line of M-line

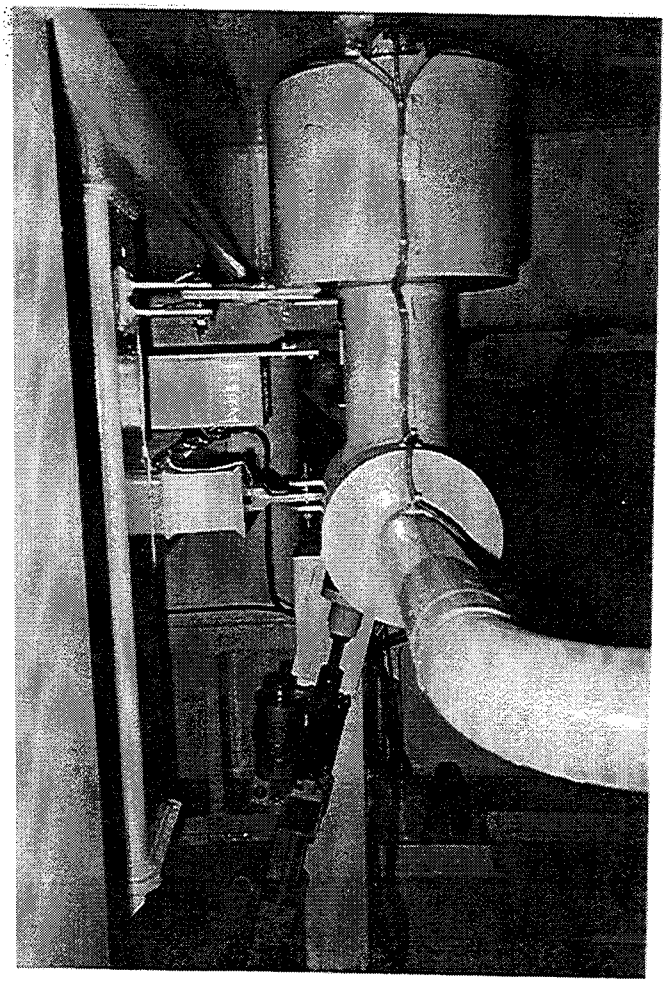

Figure A.20 End of Branch Line, with Oil Snubber, M-line (MR12)

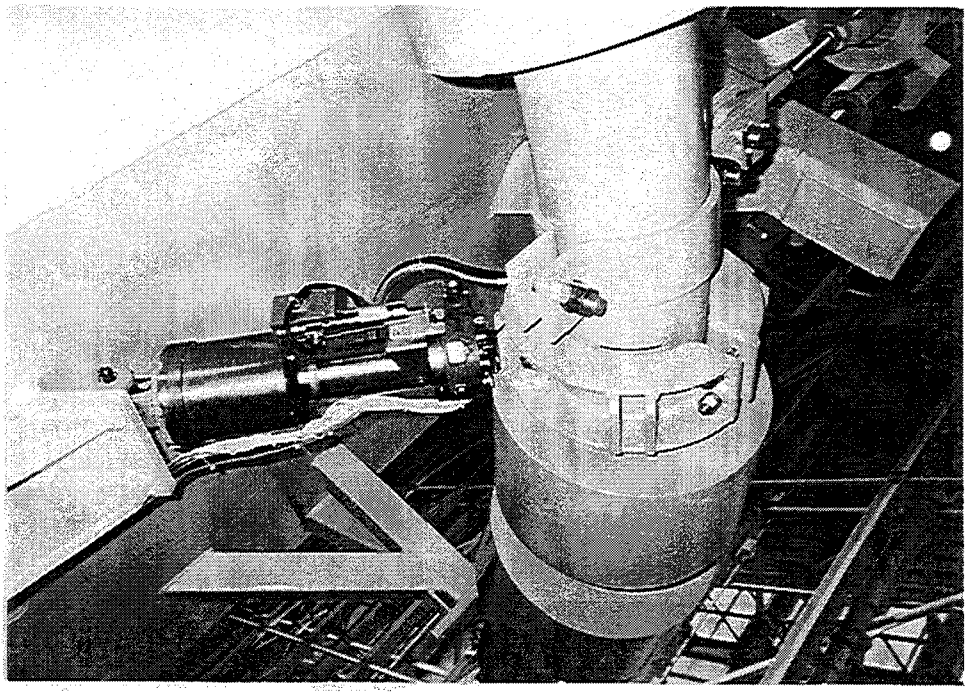

Figure A.21 Upward View of End of F-line with Conventional Support and Mechanical Snubber (FR9)

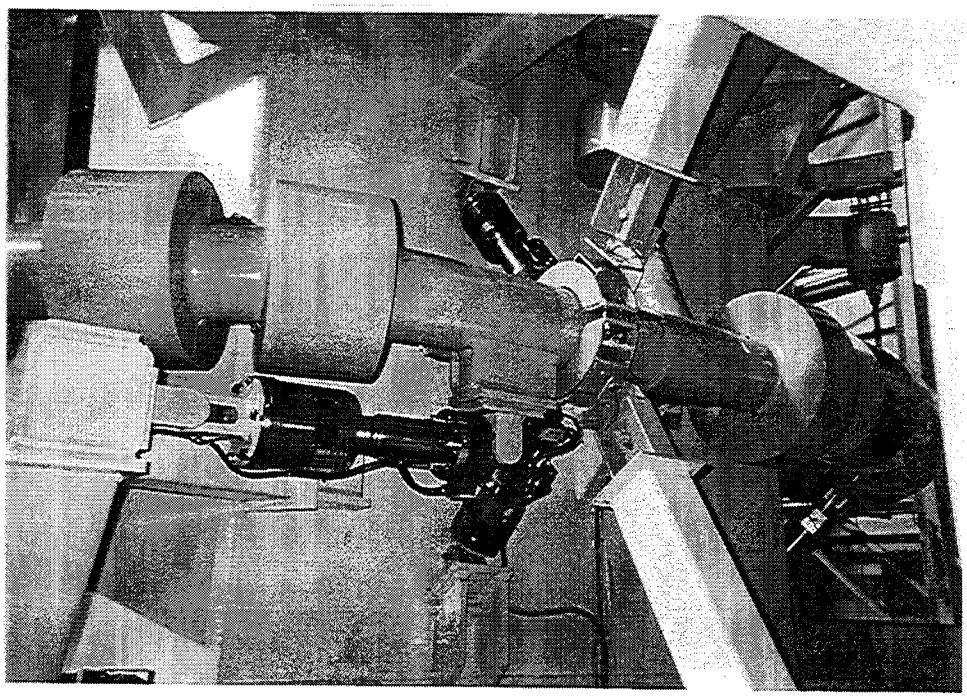

Figure A.22 Three Mechanical Snubbers of F-line (FR6-horizontal, FR7-downward, FR8-upward)

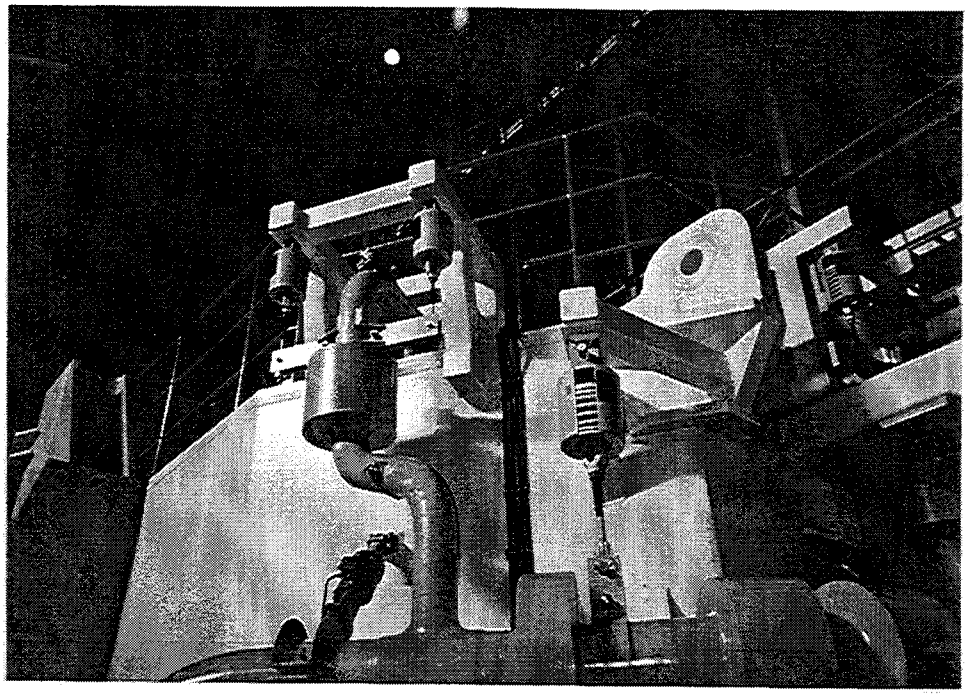

Figure A.23 Branch-A and Mechanical Snubber of F-line (FR4)

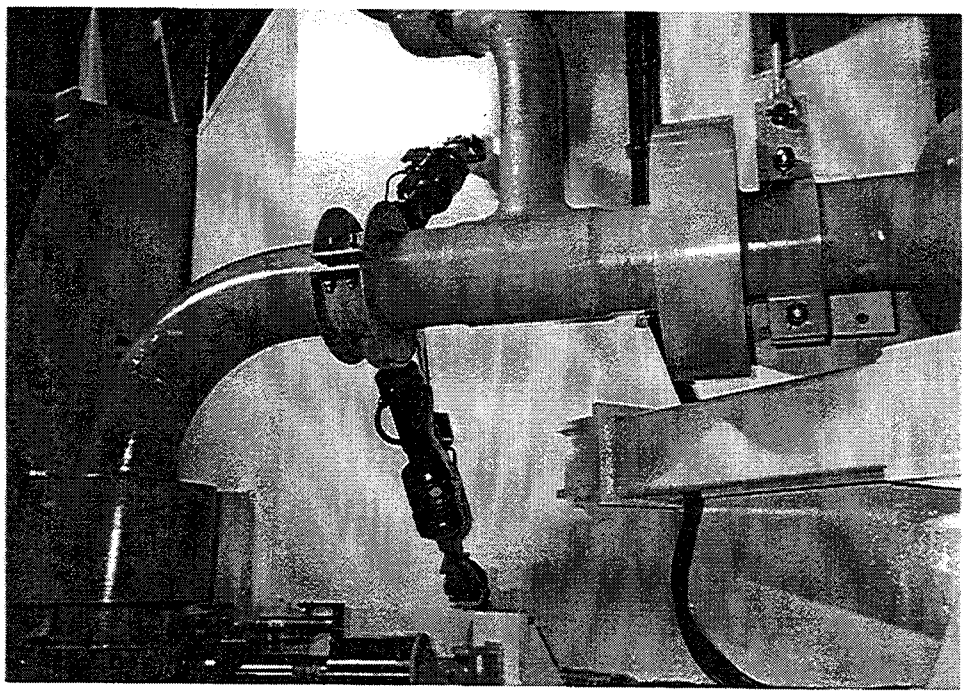

Figure A.24 Mechanical Snubbers of F-line (FR5-downward, FR4-upward)

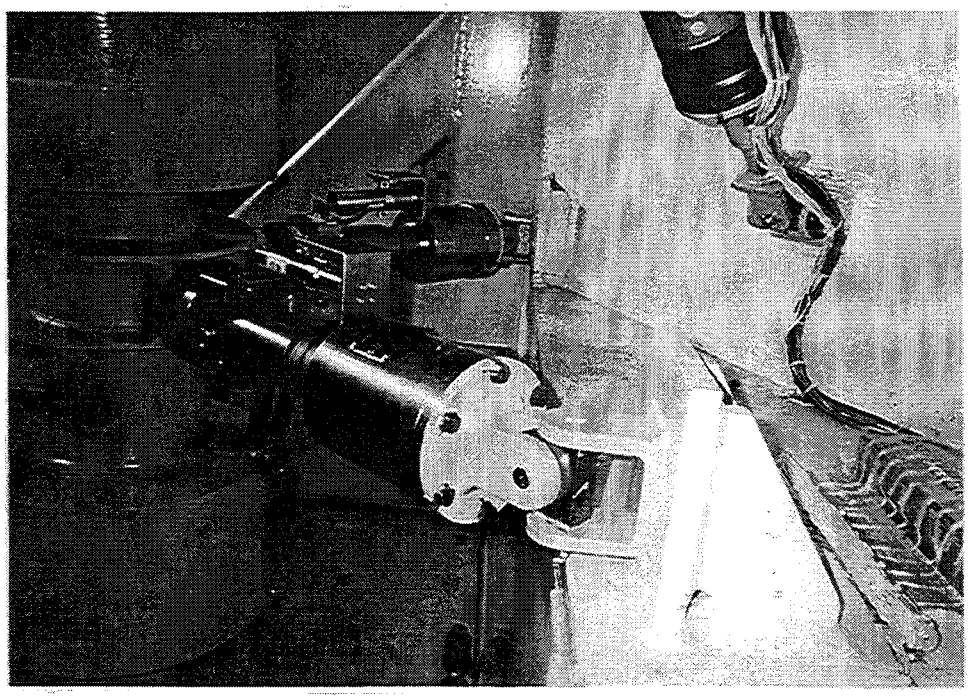

Figure A.25 Two Horizontal Mechanical Snubbers of F-line (FR3-near Side, FR2-far Side)

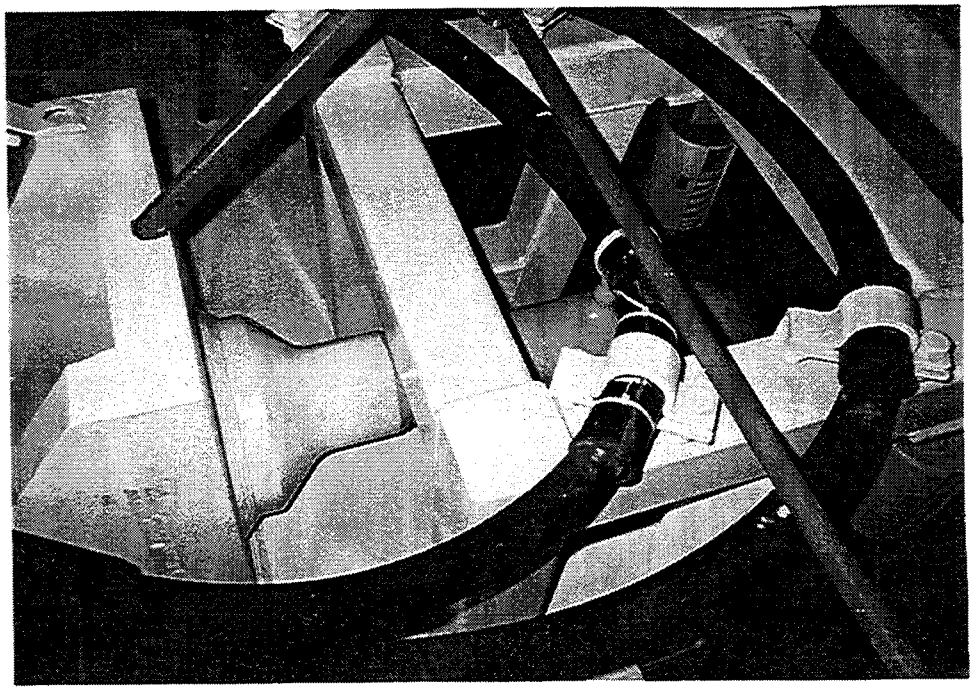

Figure A.26 Anchor of Branch Line-C of F-line

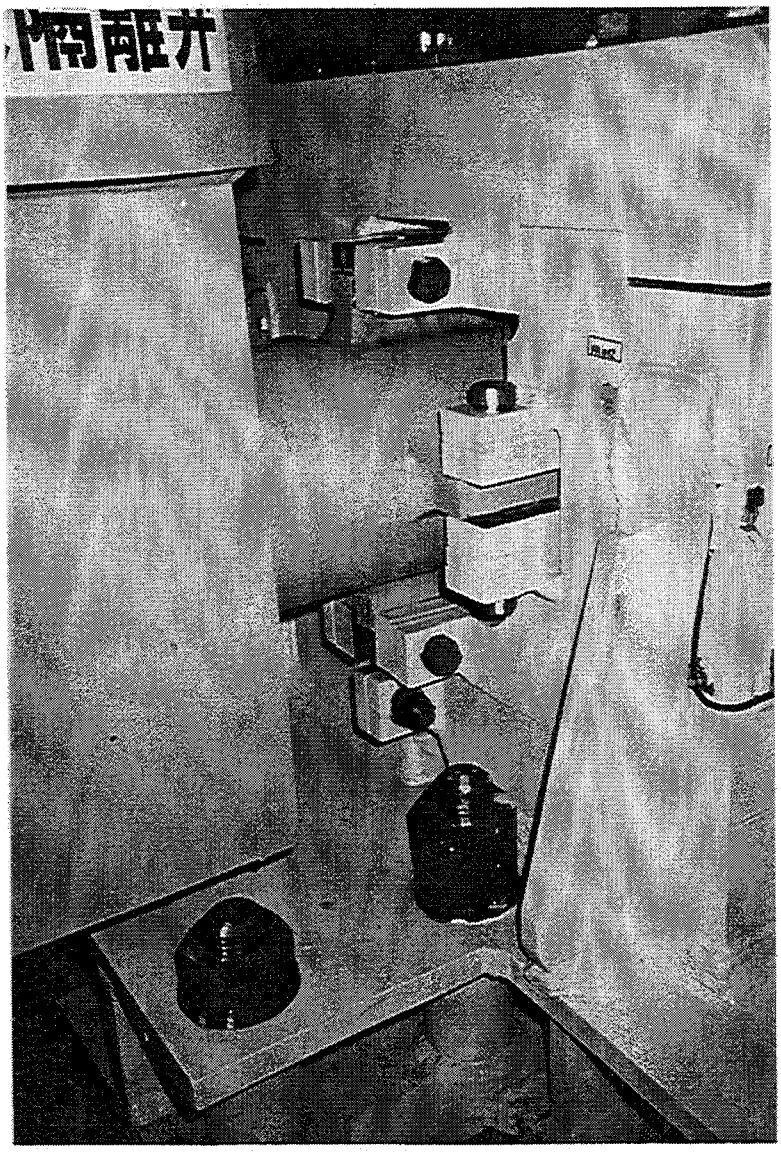

Figure A.27 Sliding Support of F-line (FR1)

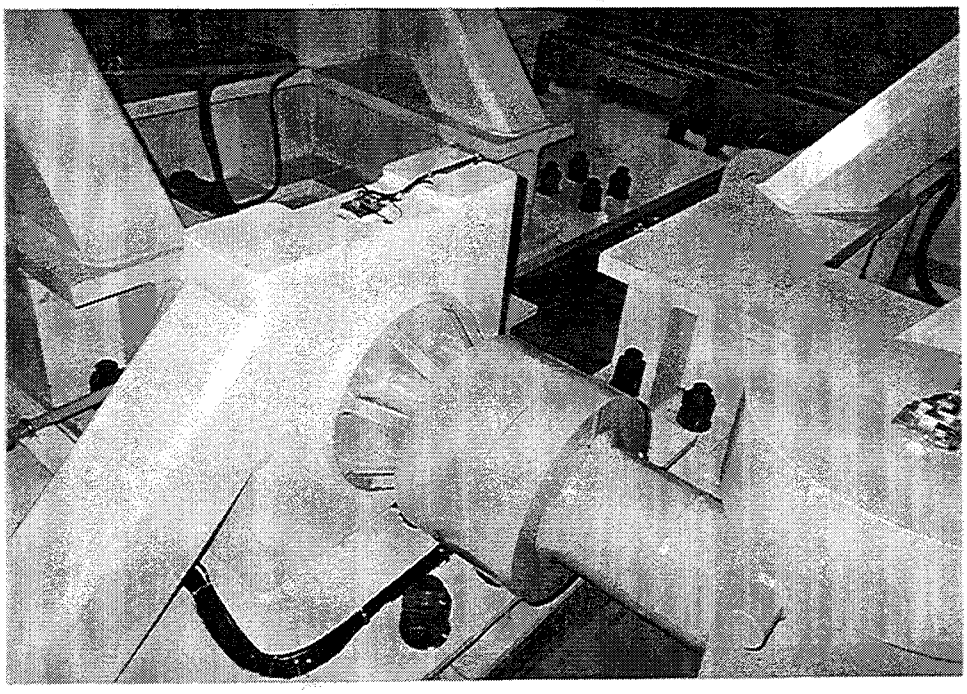

Figure A.28 Anchor of Main F-line

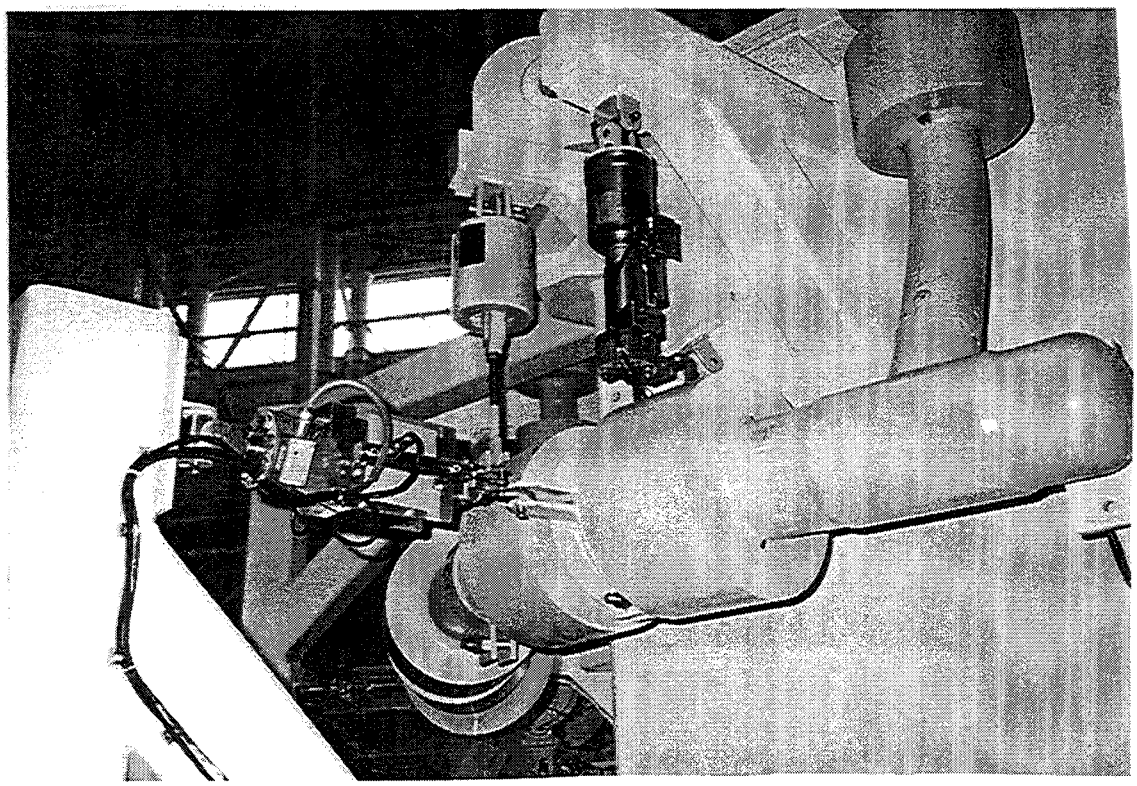

Figure A.29 Free-end of F-line with EAB Support

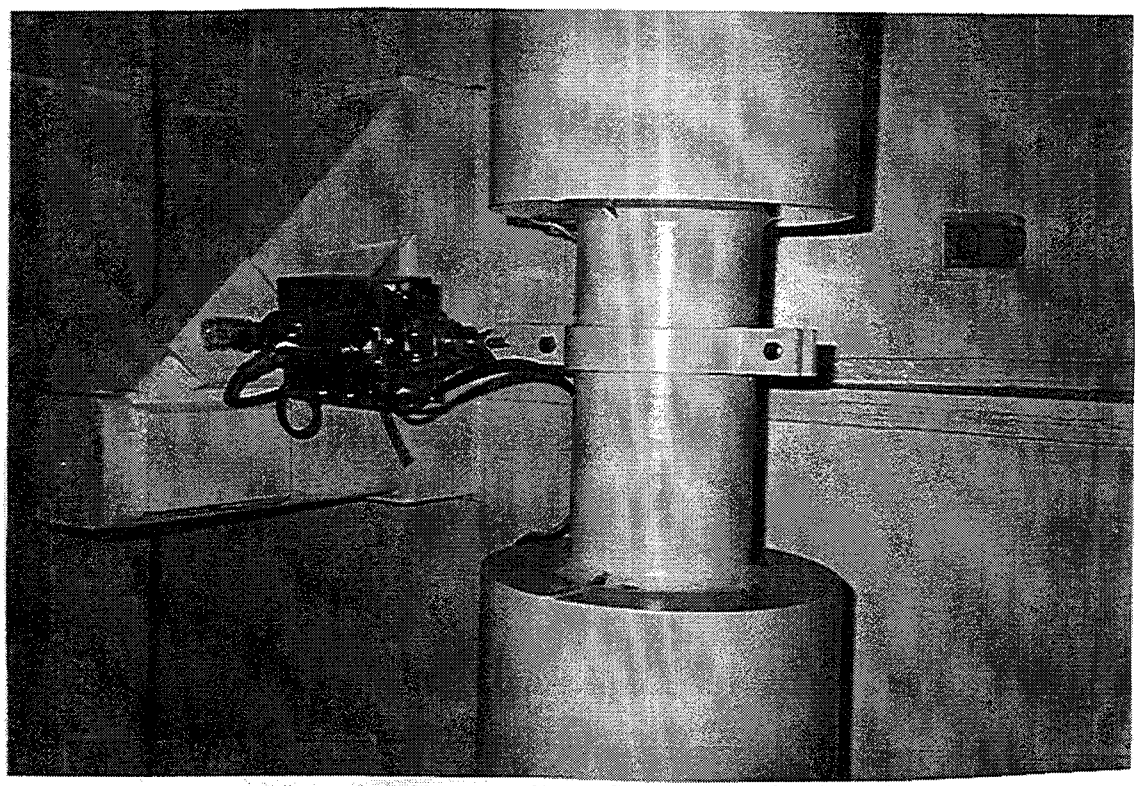

Figure A.30 Close-up of EAB Support of F-line (FR11)

Figure A.31 Mechanical Snubber

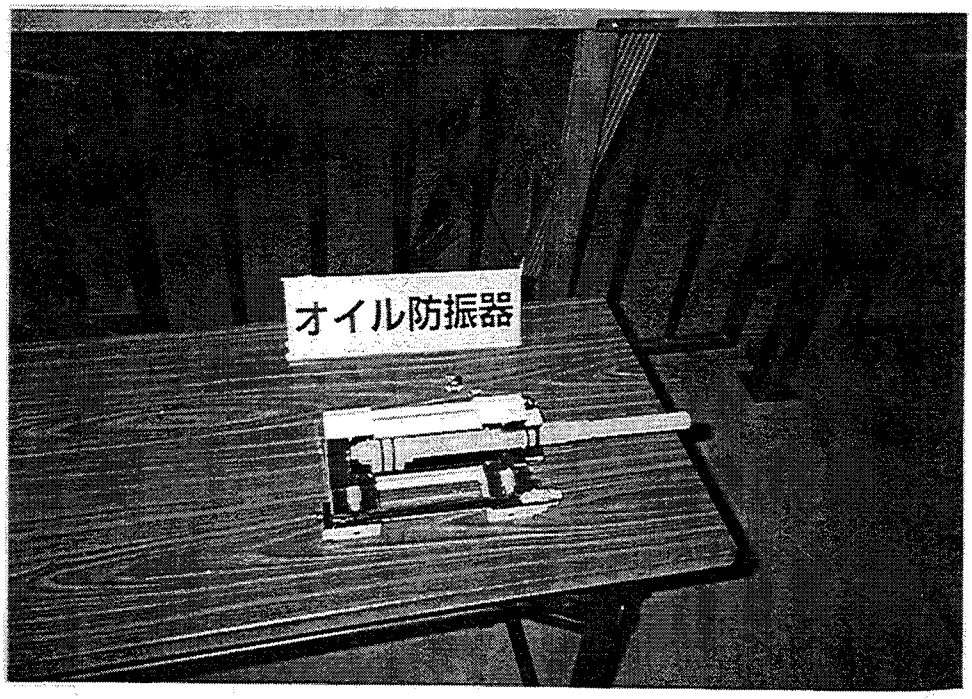

Figure A.32 Oil Snubber

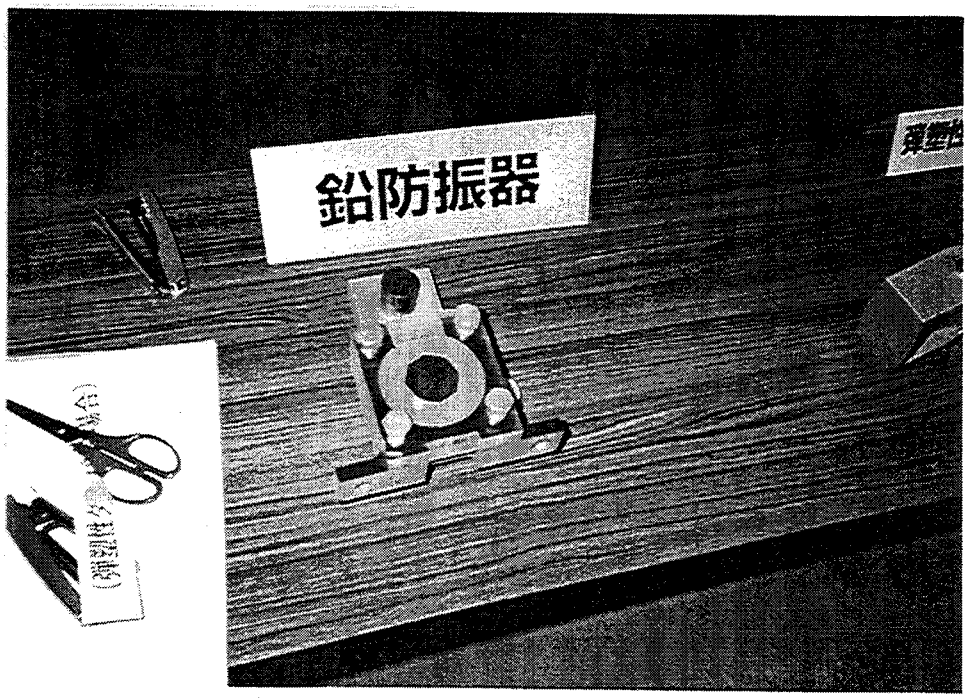

Figure A.33 LED Support of M-line

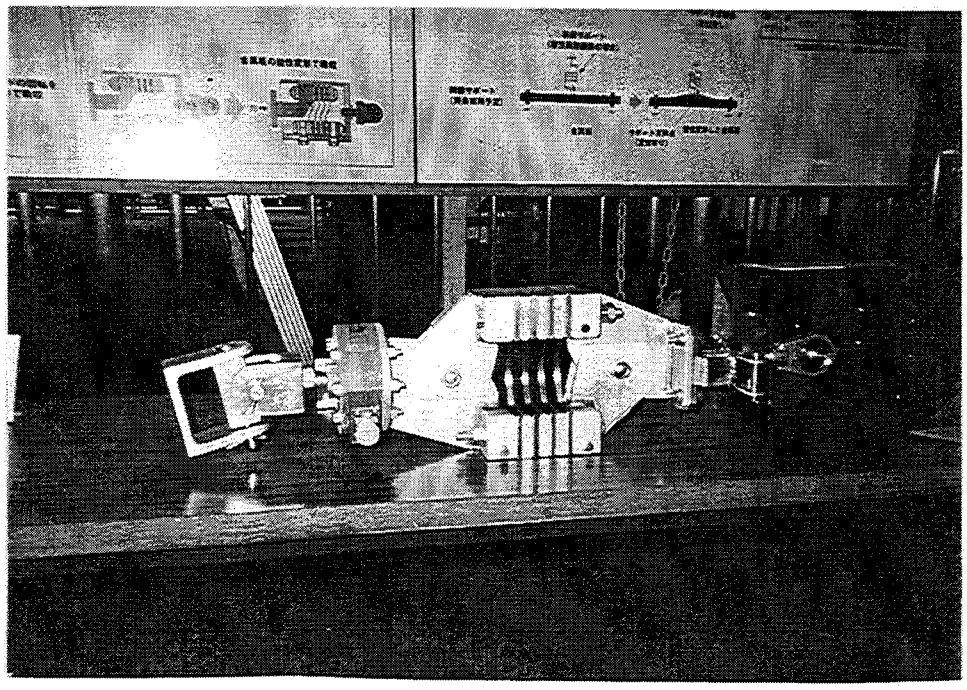

Figure A.34 EAB Support of F-line

APPENDIX B

LIST OF MS TEST RUNS

Table B.1 List of MS Test Runs for Conventional Support

Test	Line	Test No	Table Motion			I.D. Number	Test Condition
			Accel. (gal)		Type		
			H	V			
Preliminary test	M	PC-58	500	---	Random Waves		Actuator operated. Pink noise input
		PC-59	---	150			
		PC-60	600	---			
		PC-61	---	250			
	F	PC-62	250	---			
		PC-63	---	150			
		PC-64	500	---			
		PC-65	---	250			
Verification test for S_2 motion	F	VC-1	363.3	61.3	1/3S2(F)	95011103	BWR S_2 wave
		VC-2	726.7	122.7	2/3S2(F)	95011105	
		VC-3	1090	184	3/3S2(F)	95011107	
	M	VC-4	496.7	113.3	1/3S2(M)	94120203	PWR S_2 wave. Actuator operated
		VC-5	993.3	226.7	2/3S2(M)	94120207	
		VC-6	1490	340	3/3S2(M)	94120505	
		VC-7	1490	340	3/3S2(M)	94120601	Actuator not operated

Table B.1 List of MS Test Runs for Conventional Support

Test	Line	Test No	Table Motion			I.D. Number	Test Condition
			Accel. (gal)		Type		
			H	V			
Verification test for S_1 motion	F	VC-8	237	48	1/3S1(F)	95011203	BWR S_1 wave
		VC-9	474	96	2/3S1(F)	95011206	
		VC-10	711	144	3/3S1(F)	95011209	
	M	VC-11	271.7	63.7	1/3S1(M)	94120603	PWR S_1 wave Actuator operated
		VC-12	543.3	126.7	2/3S1(M)	94120605	
		VC-13	815	190	3/3S1(M)	94120609	
Multiple excitation test	M	DC-1	249	---	1/6S2(M)	94120706	Table: S_2 wave Actuator: C/V wave SG Model: 2DOF Model
		DC-2	373	---	1/4S2(M)	94120704	
		DC-3	496.7	---	1/3S2(M)	94120702	
C/V wave test	M	DC-4	459	113.3	1/3S2CV	94120708	Table: C/V wave SG Mode: Original SG model
		DV-5	918	226.7	2/3S2CV	94120710	
		DV-6	1377	340	3/3S2CV	94120802	
Marginal test	F	MC-1	1199	202.4	1.1S2(F)	95011803	
		MC-2	1308	220.8	1.2S2(F)	95011804	
		MC-3	1417	239.2	1.3S2(F)	95011805	
	M	MC-4	1788	408	1.2S2(M)	94120902	Actuator operated
		MC-5	1937	442	1.3S2(M)	94120904	
		MC-6	2235	510	1.5S2(M)	94120905	

Table B.1 List of MS Test Runs for Conventional Support

Test	Line	Test No	Table Motion			I.D. Number	Test Condition
			Accel. (gal)		Type		
			H	V			
Public test		DT-1	818	332	Kobe		
		DT-2	1490	340	3/3S2(M)		
		DT-3	818	332	Kobe		
		DT-4	1490	340	3/3S2(M)		

Table B.2 List of MS Test Runs for EA Supports Preliminary Tests

Test	Test No	Table Motion			I.D. Number	Test Condition
		Accel. (gal)		Type		
		H	V			
Table control conpensation	PE-1	400	---	PSD (H)		Dynamic characteristics of table with actuator operated
	PE-2	---	200	PSD (V)		
	PE-3	---	200	PSD (P)		
Adjustment of independent actuator	PE-4	200	---	Random wave		• Independent actuator control • Linear S/G model
	PE-5	300	---			
	PE-6	400	---			
	PE-7	200	---			• Independnet actuator control • Nonlinear S/G model
	PE-8	300	---			
	PE-9	400	---			
	PE-10	496.4	113.4	1/3 S_2 (A)		• Actuator control for seismic motion • Nonlinear S/G model
	PE-11	992.9	226.8	2/3 S_2 (A)		
	PE-12	1489.3	340.2	3/3 S_2 (A)		
Random wave tests	PE-13	500	---	Random wave		• Actuator operated • Dynamic characteristics of model for random wave
	PE-14	700	---			
	PE-15	900	---			
	PE-16	1100	---			
	PE-17	---	250			
	PE-18	---	500			
	PE-19	---	700			
Sine sweep tests	PE-20	50	---	Sine waves		• Actuator operated • 4~30 Hz, $\Delta f = 0.2$ Hz
	PE-21	100	---			
	PE-22	150	---			
	PE-23	200	---			
	PE-24	---	30			
	PE-25	---	60			
	PE-26	---	90			
	PE-27	---	120			

Table B.3 List of MS test runs for EA Supports Design Method Confirmation Tests (Case -I)

Test	Test No	Table Motion			I.D. Number	Test Condition
		Accel. (gal)		Type		
		H	V			
A-wave test	DE1-1	496.4	113.4	1/3S_2 (A)	95041903	• M-line only • Actuator operated
	DE1-2	992.9	226.8	2/3S_2 (A)	95041906	
	DE1-3	1489.3	340.2	3/3S_2 (A)	95041909	
	DE1-1′	496.4	113.4	1/3S_2 (A)	95051504	• F-line only
	DE1-2′	992.9	226.8	2/3S_2 (A)	95051502	
	DE1-3′	1489.3	340.2	3/3S_2 (A)	95051202	
	DE1-4	271.5	63.4	1/3S_1 (A)	95042504	• F & M -lines • Acturator operated
	DE1-5	543.0	126.8	2/3S_1 (A)	95042103	
	DE1-6	814.4	190.1	3/3S_1 (A)	95042106	
Repeatability tests for A-wave	DE1-10	1489.3	340.2	3/3S_2 (A)		• DE1-10 for repeatability (three times)
	DE1-11	1489.3	---	3/3S_2 (A)		
	DE1-12	---	340.2	3/3S_2 (A)		
Effects of vertical motion tests for A-wave	DE1-13	1489.3	442.3	1.3S_2 (A)		• Actuator operated • Only vertical motions varied
	DE1-14	1489.3	510.3	1.5S_2 (A)		
	DE1-15	1489.3	680.4	2.0S_2 (A)		
	DE1-16	1489.3	850.5	2.5S_2 (A)		
	DE1-17	1489.3	1020.6	3.0S_2 (A)		
B-wave test	DE1-18	496.4	113.4	1/3S_2 (B)	95042705	• F & M-lines • Actuator operated
	DE1-19	992.9	226.8	2/3S_2 (B)	95042708	
	DE1-20	1489.3	340.2	3/3S_2 (B)	95042804	
	DE1-21	271.5	63.4	1/3S_1 (B)	95050804	
	DE1-22	543.0	126.8	2/3S_1 (B)	95050807	
	DE1-23	814.4	190.1	3/3S_1 (B)	95050903	
Repeatability tests for B-wave	DE1-27	1489.3	340.2	3/3S_2 (B)		• DE1-27 for repeatability (three times)
	DE1-28	1489.3	---	3/3S_2 (B)		
	DE1-29	---	340.2	3/3S_2 (B)		
Effects of vertical motion tests for B-wave	DE1-30	1489.3	442.3	1.3S_2 (B)		• Actuator operated • Only vertical motions varied
	DE1-31	1489.3	510.3	1.5S_2 (B)		
	DE1-32	1489.3	680.4	2.0S_2 (B)		

Table B.4 List of MS Test Runs for EA Supports Design Method Confirmation Tests (Case-II)

Test	Test No.	Table Motion			I.D. Number	Test Condition
		Accel. (gal)		Type		
		H	V			
Random wave tests without gap	DE2-1	500	---	Random wave		• Actuator fixed • No gap in M-line
	DE2-2	700	---			
	DE2-3	900	---			
	DE2-4	---	250			
	DE2-5	---	500			
	DE2-6	---	700			
Sine sweep tests without gap	DE2-7	100	---	Sine wave		• Actuator fixed • No gap for M-line
	DE2-8	150	---			
	DE2-9	200	---			
	DE2-10	---	60			
	DE2-11		90			
	DE2-12		120			
A-wave tests without gap	DE2-13	496.4	113.4	1/3 S_2 (A)	95060506	• Actuator fixed • No gap for M-line
	DE2-14	992.9	226.8	2/3 S_2 (A)	95060503	
	DE2-15	1489.3	340.2	3/3 S_2 (A)	95060206	
Random wave tests with gap	DE2-16	500	---	Random wave		• Actuator fixed • Gap for M-line
	DE2-17	700	---			
	DE2-18	900	---			
	DE2-19	---	250			
	DE2-20	---	500			
	DE2-21	---	700			
Sine sweep tests with gap	DE2-22	100	---	Sine wave		• Actuator fixed • Gap for M-line
	DE2-23	150	---			
	DE2-24	200	---			
	DE2-25	---	60			
	DE2-26	---	90			
	DE2-27	---	120			

Table B.4 List of MS Test Runs for EA Supports Design Method Confirmation Tests (Case-II)

Test	Test No.	Table Motion			I.D. Number	Test Condition
		Accel. (gal)		Type		
		H	V			
A-wave tests with gap	DE2-28	496.4	113.4	1/3 S_2 (A)	95061602	• Actuator fixed • Gap for M-line
	DE2-29	992.9	226.8	2/3 S_2 (A)	95061604	
	DE2-30	1489.3	340.2	3/3 S_2 (A)	95061606	
Public tests	DT-1	864	322	H-wave		• Not recorded • H-wave is BWR-S_2
	DT-2	818	332	Kobe		

Table B.5 List of MS Test Runs for EA Supports Margin Tests

Test	Test No.	Table Motion			I.D. Number	Test Condition
		Accel. (gal)		Type		
		H	V			
Sine sweep tests	ME-1	250	---	Sine wave		• Actuator fixed • No gap for M-line
	ME-2	300	---			
A-wave margin tests	DE1-7	1638.2	374.2	1.1 S_2 (A)	95042404	• F & M-lines • Actuator operated
	DE1-8	1787.2	408.2	1.2 S_2 (A)	95042406	
	DE1-9	1936.1	442.3	1.3 S_2 (A)	95042407	
B-wave margin tests	DE1-24	1638.2	374.2	1.1 S_2 (B)	95051002	• F & M-lines • Actuator operated
	DE1-25	1787.2	408.2	1.2 S_2 (B)	95051003	
	DE1-26	1936.1	442.3	1.3 S_2 (B)	95051004	
Higher A-wave margin tests	ME-3	1936.1	442.3	1.3 S_2 (A)		• Actuator fixed • No gap for M-line
	ME-4	2234.0	510.3	1.5 S_2 (A)		
	ME-5	2531.8	578.3	1.7 S_2 (A)		
	ME-6	2829.7	646.4	1.9 S_2 (A)		
	ME-7	3127.5	714.4	2.1 S_2 (A)		
	ME-8	3425.4	782.5	2.3 S_2 (A)		
	ME-9	3723.3	850.5	2.5 S_2 (A)	95070502	
Tokachioki-wave tests	ME-10	1128.0	---	15TOKACHI	t = 1.0	• Actuator fixed • No gap for M-line • Time scale varied • Mainly for M-line
	ME-11	1128.0	---	15TOKACHI	t = 0.9	
	ME-12	1128.0	---	15TOKACHI	t = 1.1	
	ME-13	1128.0	---	15TOKACHI	t = 0.8	
	ME-14	1128.0	---	15TOKACHI	t = 0.7	
	ME-15	1504.0	---	20TOKACHI	t = 0.75	
	ME-16	1504.0	---	20TOKACHI	t = 0.8	
	ME-17	1504.0	---	20TOKACHI	t = 0.7	
	ME-18	1128.0	---	15TOKACHI	t = 0.6	
	ME-19	1128.0	---	15TOKACHI	t = 0.5	
	ME-20	1880.0	---	25TOKACHI	t = 0.8	
	ME-21	2256.0	---	30TOKACHI	t = 0.8	
	ME-22	2444.0	---		t = 0.8	
	ME-23	2481.6	---	33TOKACHI	t = 0.8	

Table B.5 List of MS Test Runs for EA Supports Margin Tests

Test	Test No.	Table Motion		Type	I.D. Number	Test Condition
		Accel. (gal)				
		H	V			
C-wave margin tests	ME-24	992.9	226.8	2/3 S_2 (C)t = 1.4		• Actuator fixed • No gap for M-line • Mainly for F-line
	ME-25	992.9	226.8	2/3 S_2 (C) t = 1.45		
	ME-26	1489.3	340.2	3/3 S_2 (C) t = 1.4		
	ME-27	1787.2	408.2	1.2 S_2 (C) t = 1.4		
	ME-28	2085.0	476.3	1.4 S_2 (C) t = 1.4		
	ME-29	2234.0	510.3	1.5 S_2 (C) t = 1.4		
	ME-30	2531.8	578.3	1.7 S_2 (C) t = 1.4		
	ME-31	2829.7	646.4	1.9 S_2 (C) t = 1.4	95071304	
Examinatio n tests	ZT-1	1787.2	408.2	1.2 S_2 (C) t= 1.6	95071402	• Actuator fixed • No gap for M-line
	ZT-2	2519.2	---	33.5 TOKACHI (25∗1.34) t = 0.8	95071403	

APPENDIX C

ADDITIONAL DRAWINGS OF MS TEST MODEL

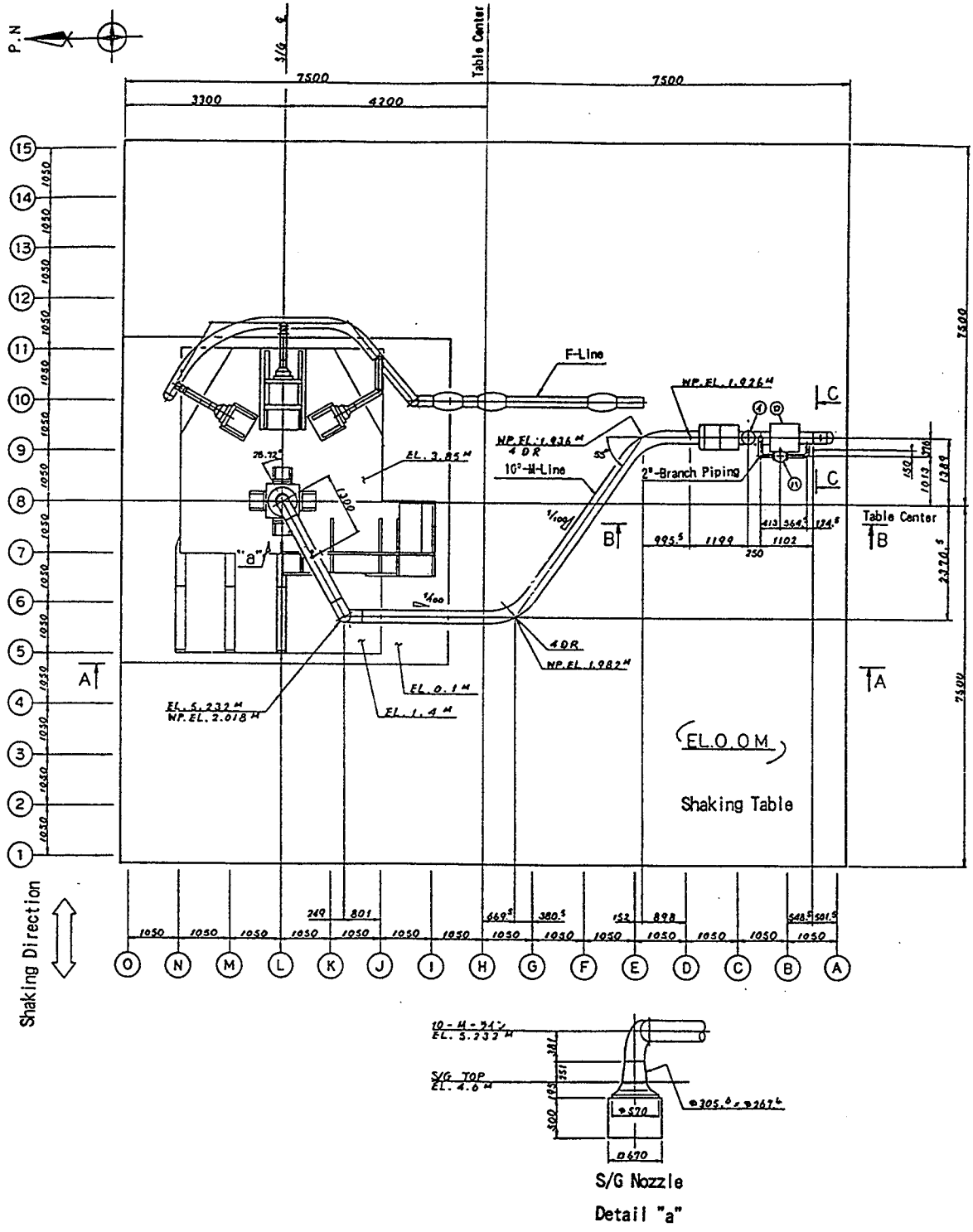

Figure C.1 Layout of Piping System Models

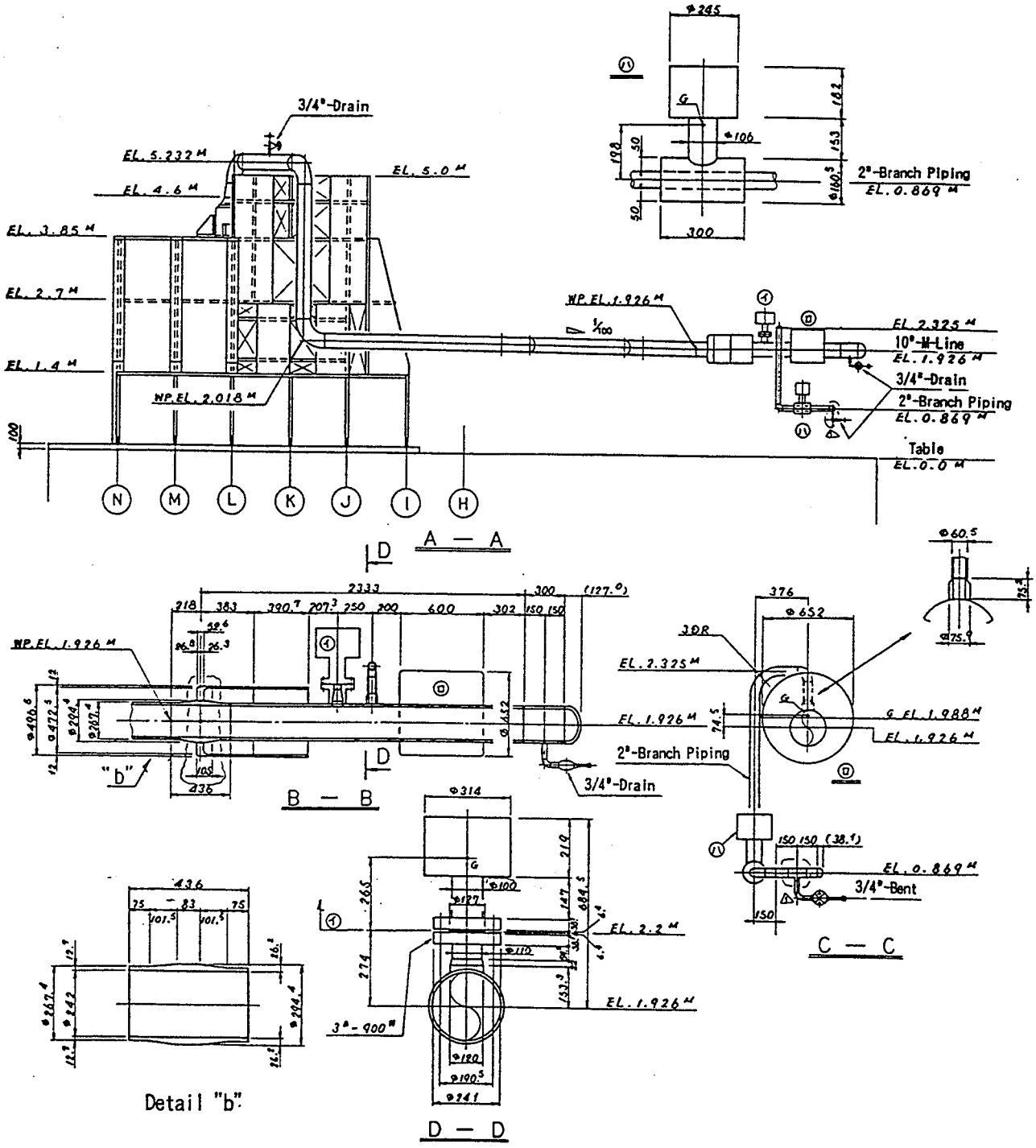

Figure C.2 Cross-sections of Figure C.1

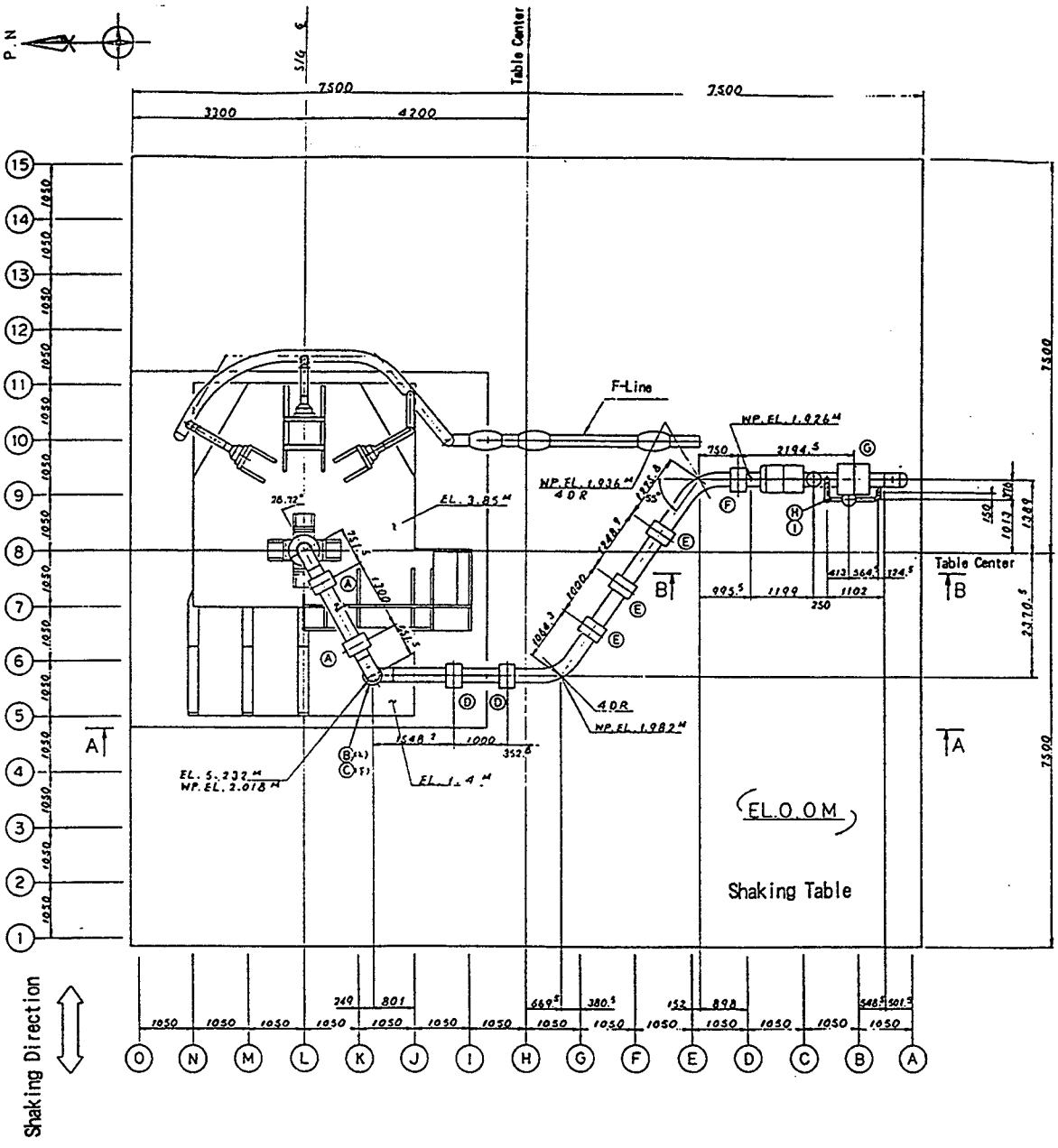

Figure C.3 Layout of Additional Masses

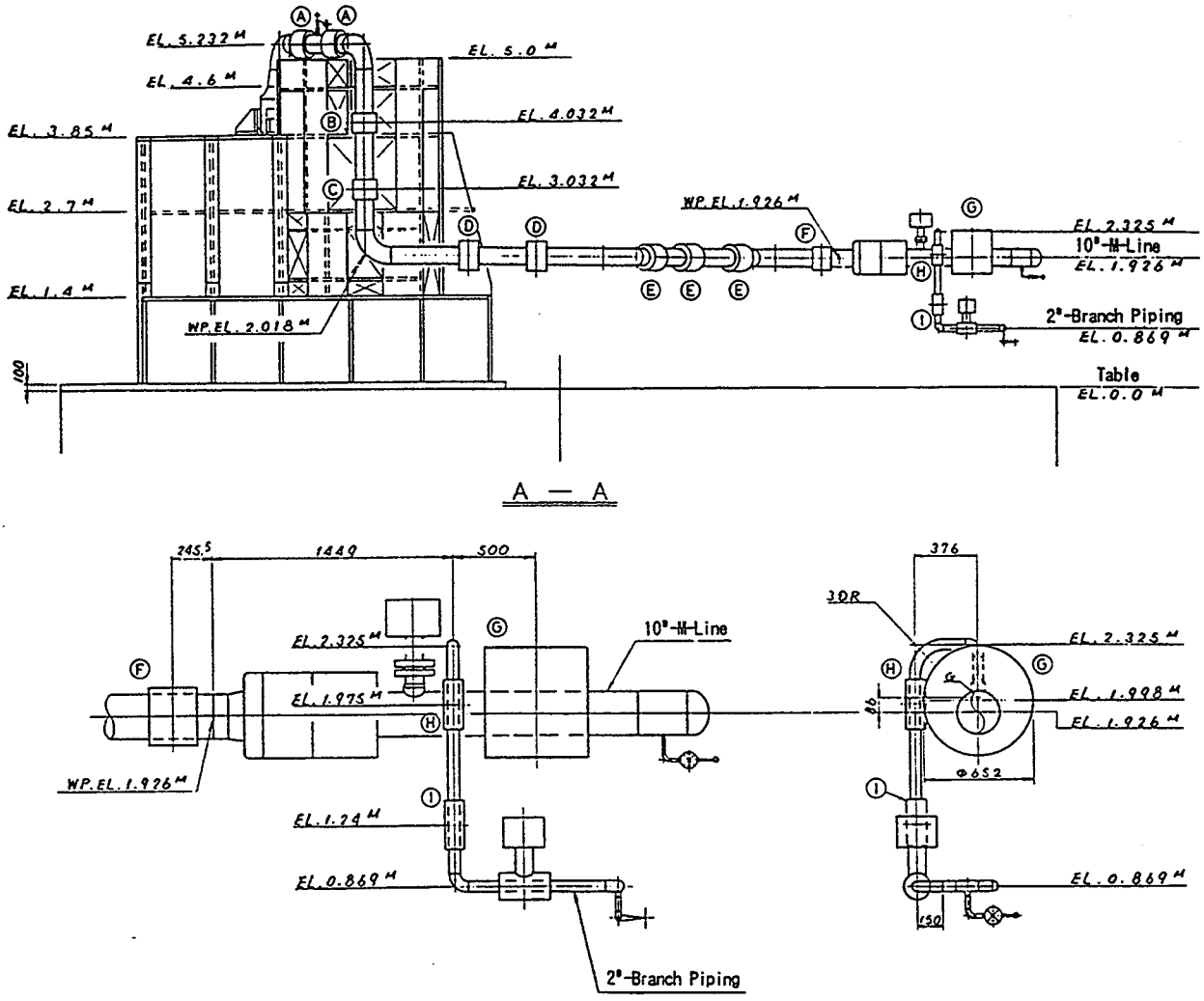

	Length	Weight	Diameter(Thickness)		Length	Weight	Diameter(Thickness)
	長さ(mm)	重量(kg)	直径及び(厚さ)mm		長さ(mm)	重量(kg)	直径及び(厚さ)mm
Ⓐ	300	358.9	459.9 (96.3)	Ⓗ	300	24.0	114.1 (26.8)
Ⓑ	300	131.2	350.2 (41.4)	Ⓘ	300	21.5	109.8 (24.6)
Ⓒ	300	105.9	335.9 (34.3)				
Ⓓ	300	395.1	445.3 (89.0)				
Ⓔ	300	339.1	451.4 (92.0)				
Ⓕ	300	114.8	341.0 (36.8)				
Ⓖ	600	1813.0	652.0 (肉厚)				

Figure C.4 Detail of Additional Masses

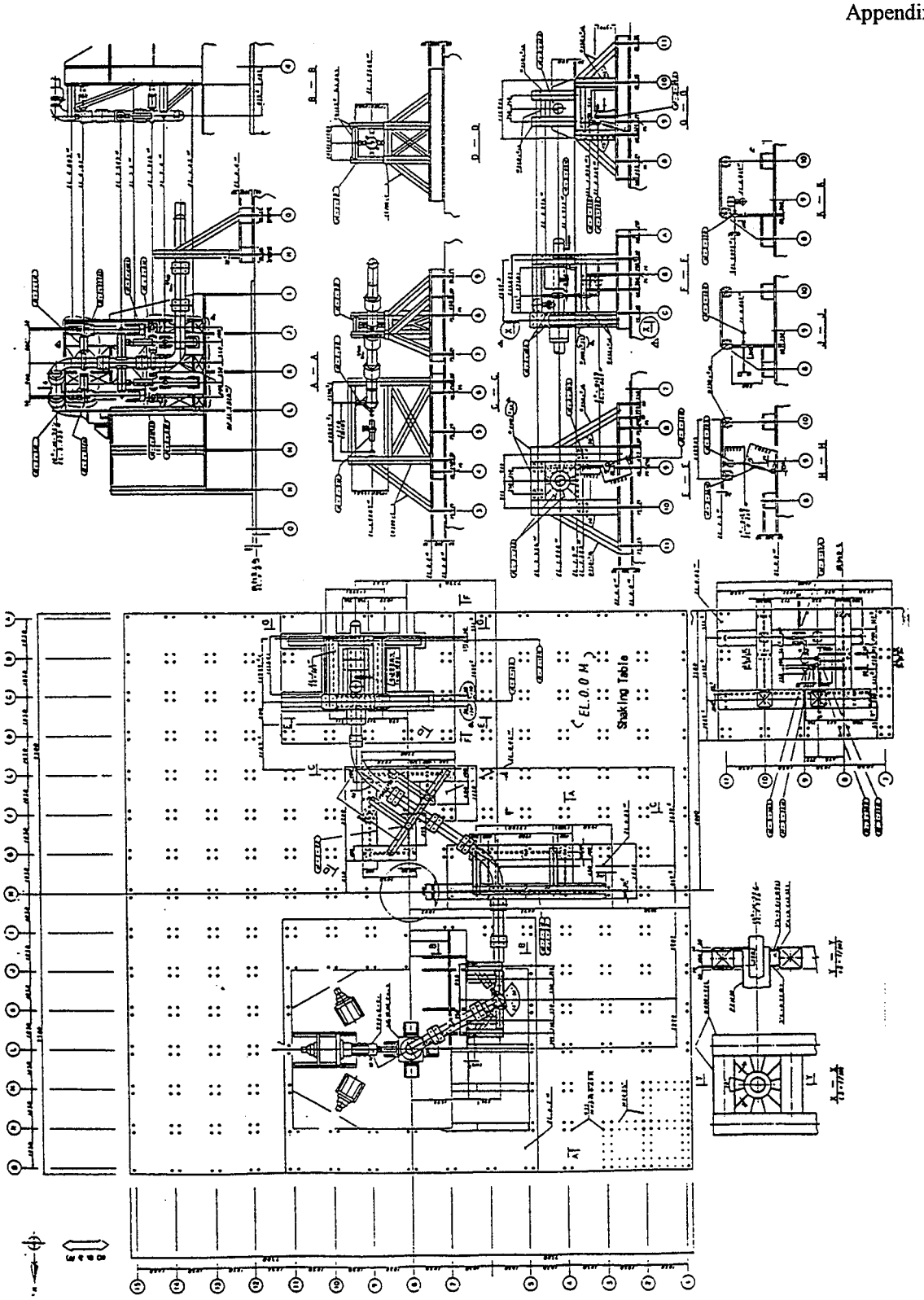

Figure C.5 Schematic Drawing of Support Structures

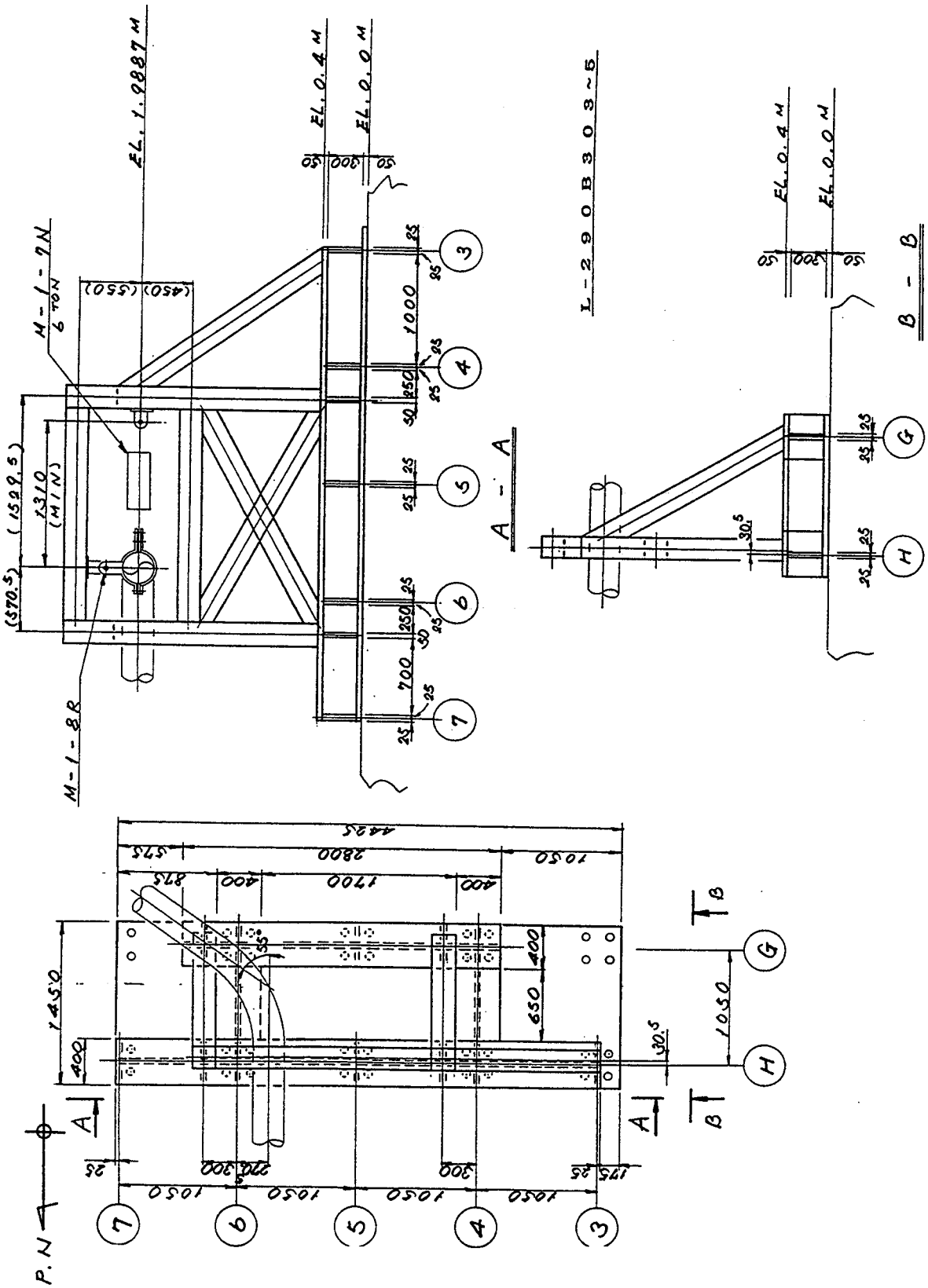

Figure C.6 Schematic Drawing of Support Structure (M-line middle support, Part 1)

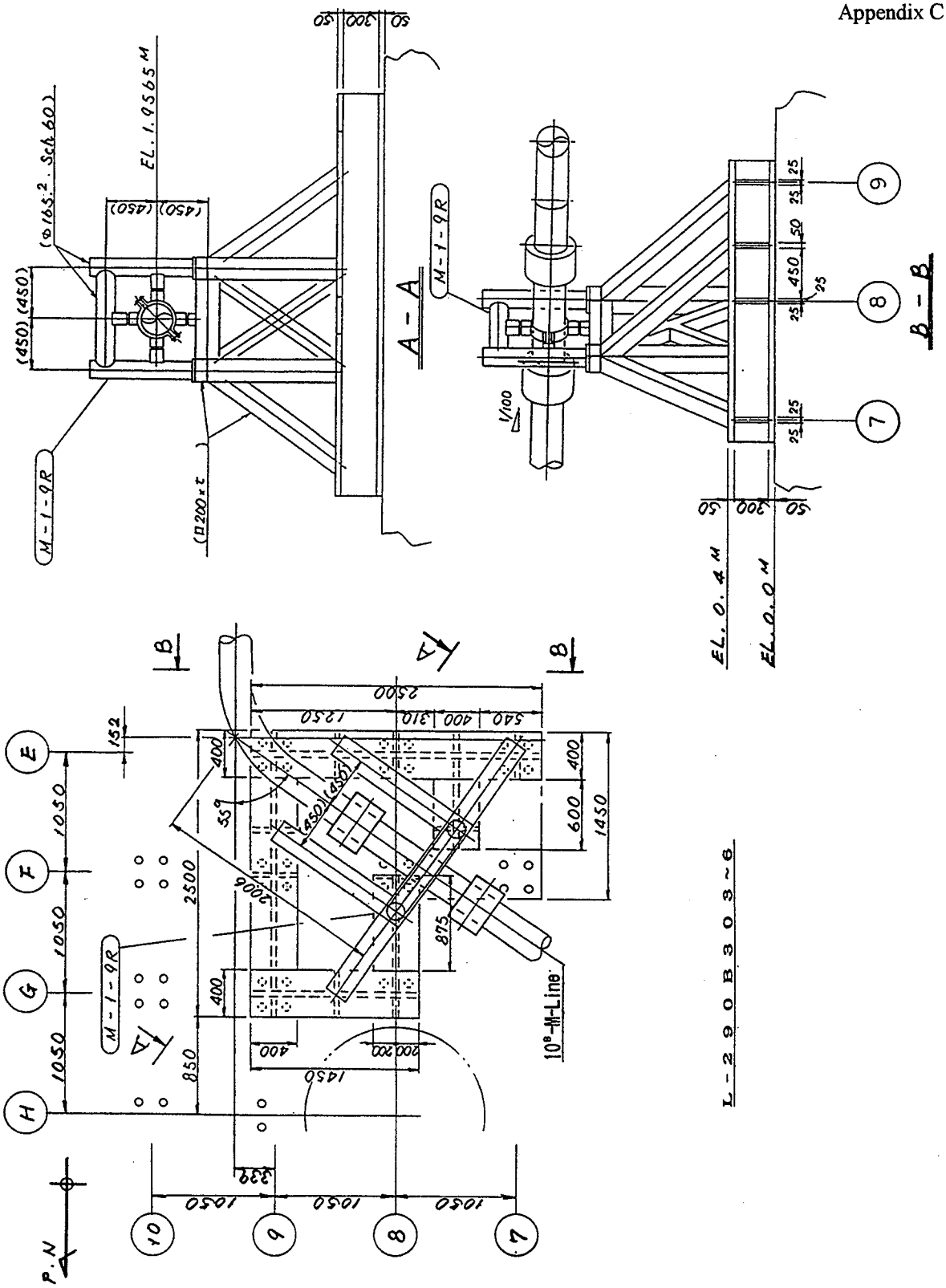

Figure C.7 Schematic Drawing of Support Structures (M-line middle support, Part 2)

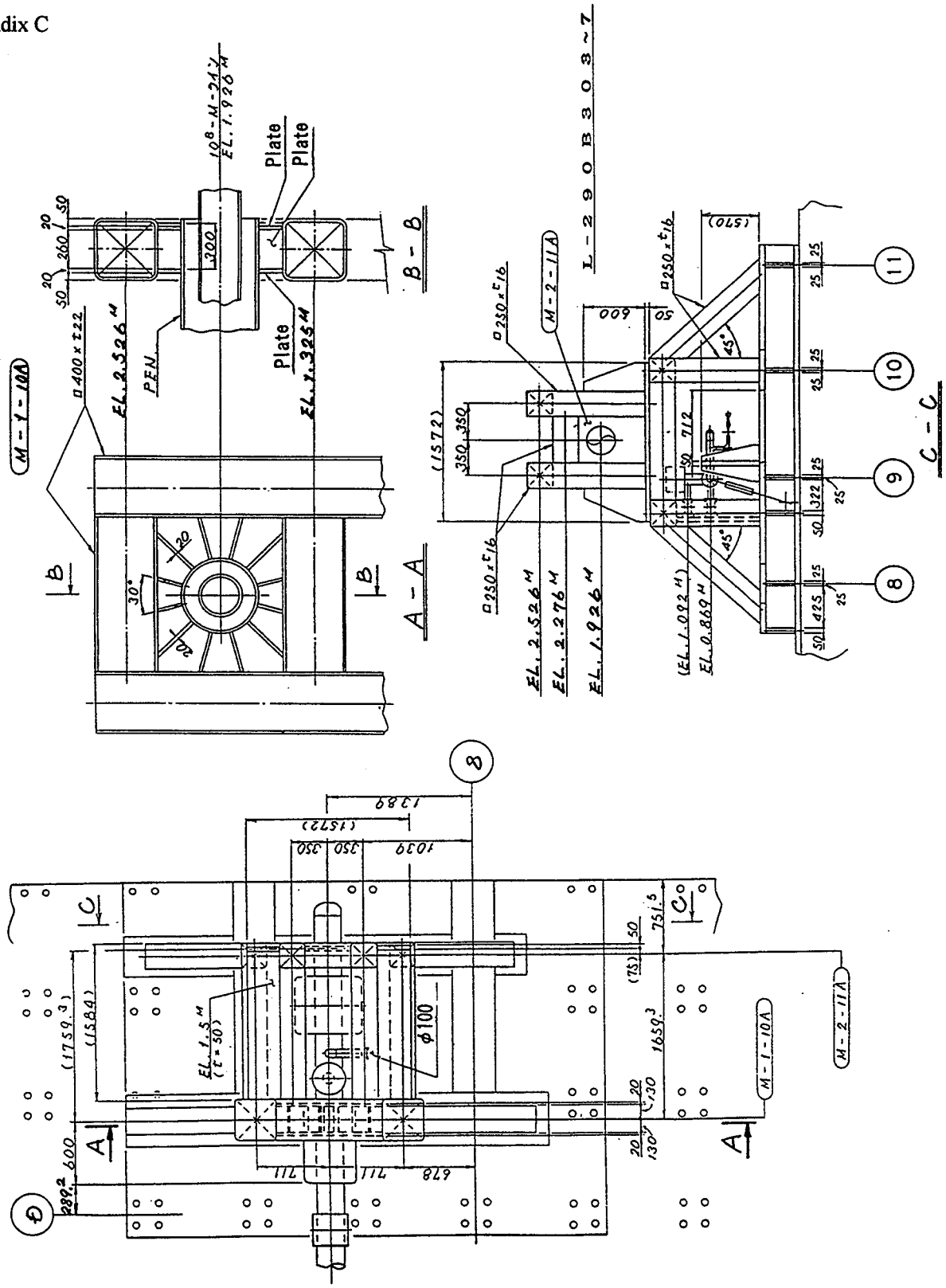

Figure C.8 Schematic Drawing of Support Structure (M-line containment vessel penetration and end support)

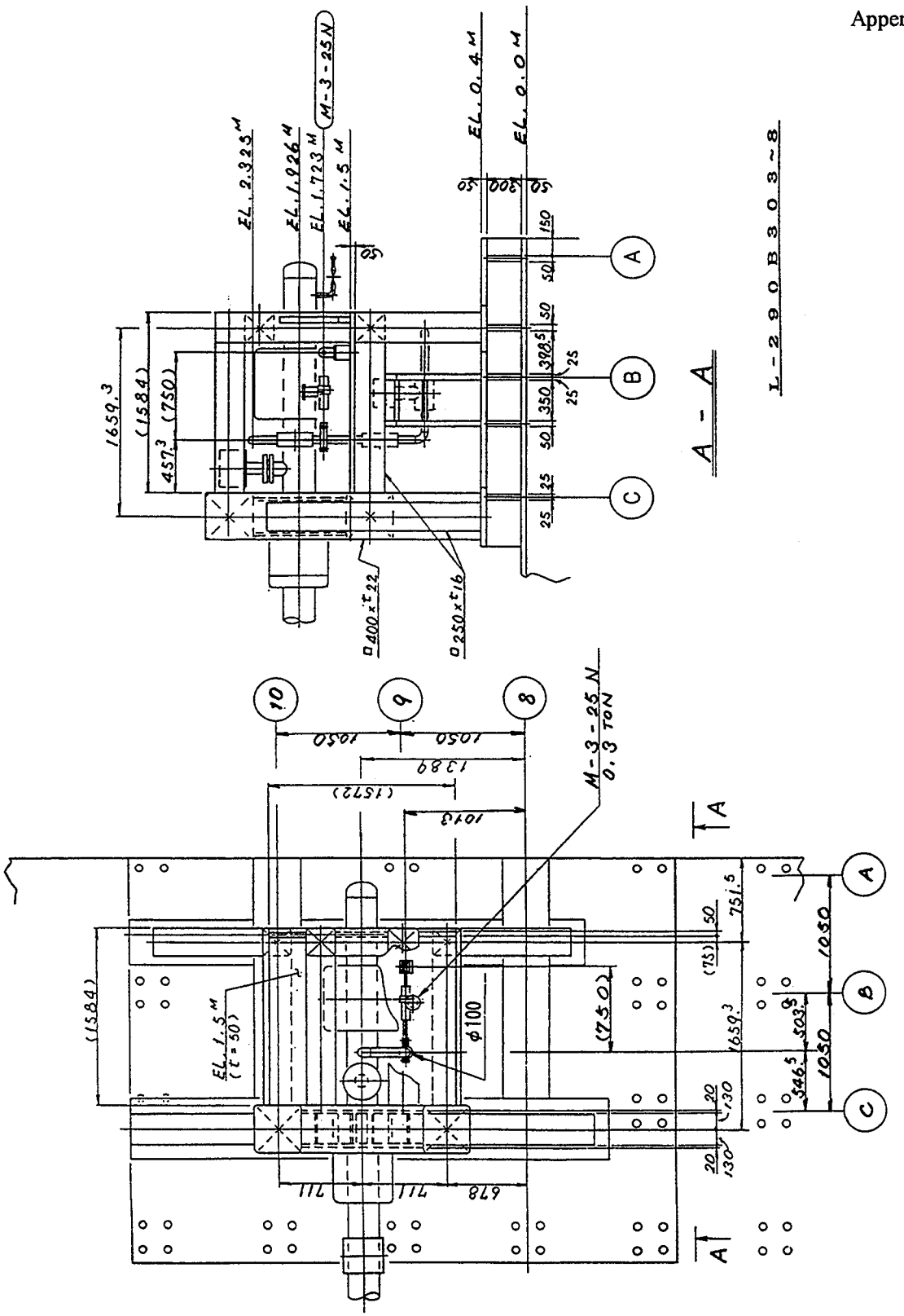

Figure C.9 Schematic Drawing of Support Structure (branch piping snubber of vertical section)

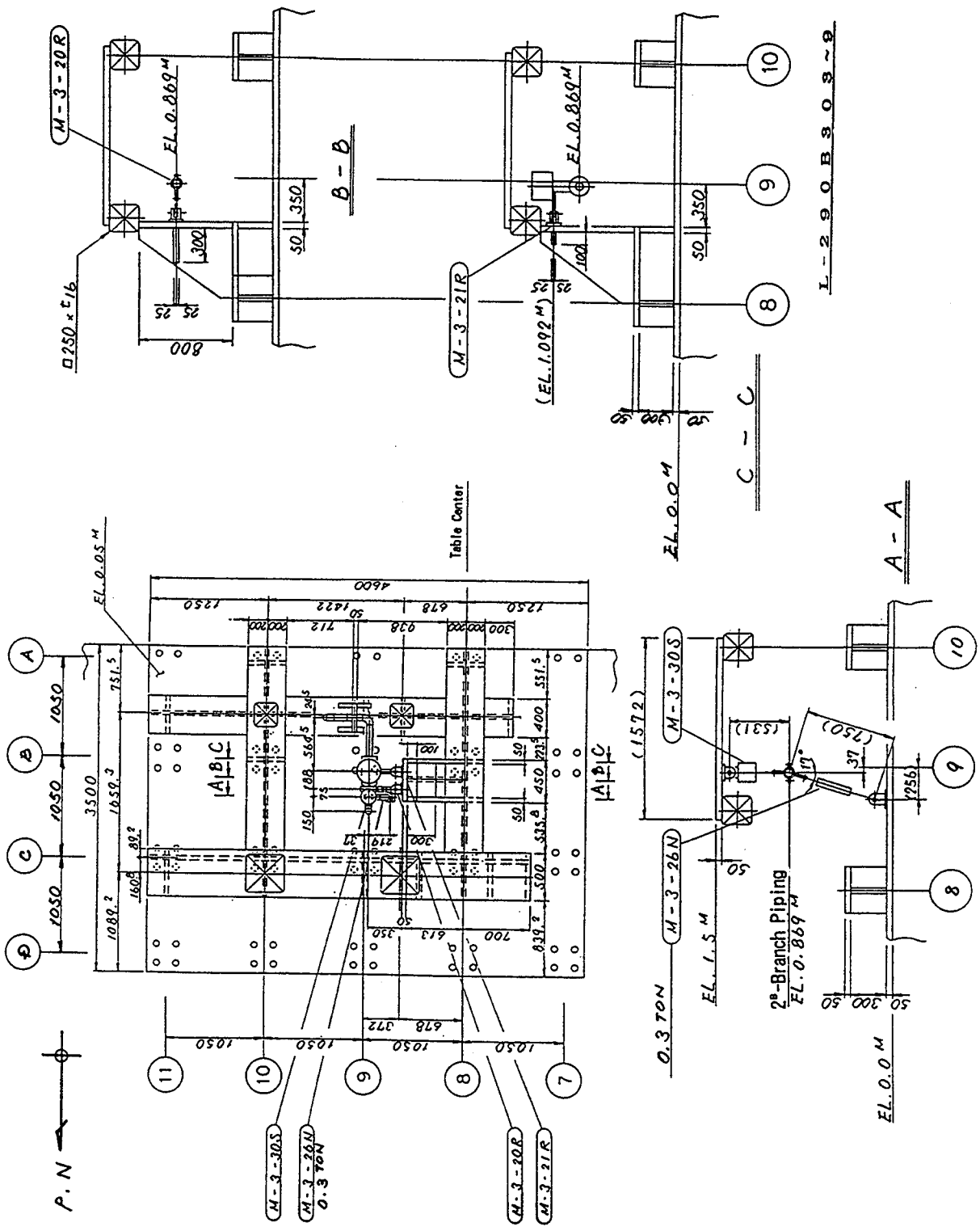

Figure C.10 Schematic Drawing of Support Structure (branch piping support)

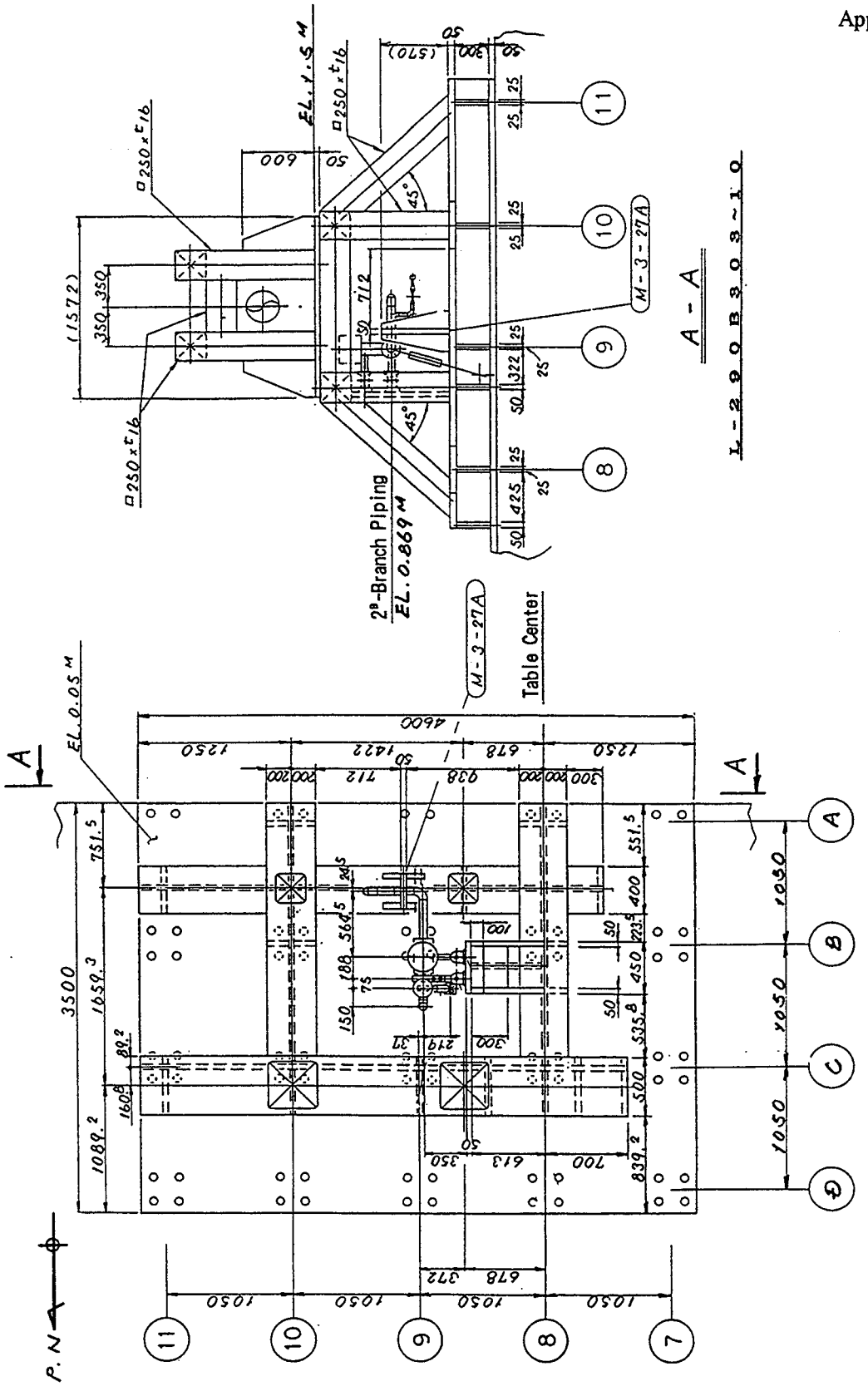

Figure C.11 Schematic Drawing of Support Structure (branch piping end support)

APPENDIX D

INSTRUMENTATION

Table D.1 Sensors List (Conventional Support Test Piping)

Object	Measuring items	Location	Symbols	No. of pt.	Directions	Channels	Total	
MS-line piping	Acceleration	Main run	MA1~4, MA8, MA10, 11	7	3-directions	21	42	141
			MA5,6	2	2-directions	4		
		Branch	MA13	1	3-directions	3		
		Valve	MA12,14,15	3	3-directions	9		
		Support	MA7	1	2-directions	2		
			MA9	1	3-directions	3		
	Displacement	Main run	MD1~7	10	1-direction	10	16	
			MD-8	1	3-directions	3		
		Branch	MD9~11	1	Y-direction	1		
				1	Z-direction	1		
				1	X-direction	1		
	Support load	Main run	MR1~10	10	1-direction	12	16	
		Branch	MR11~14	4	1-direction	4		
	Pipe strain	Straight pipe	MS0,2,2',4,6, 9,10,11,11', 12,13	8	1 axis x 4	32	65	
				2	bending x 2	4		
				1	torsion x 1	1		
		Elbow	MS1,3,5,8,12	2	2 axis x 4	16		
				3	1 axis x 4	12		
	Inner pressure	Straight pipe	MP1,2	2	none	2	2	
FW-line piping	Acceleration	Pipe	FA1~13	13	3-directions	39	39	141
	Displacement	Support	FD2~10	9	1-direction	9	11	
				2	1-direction	2		
	Support load	Support	FR1	8	1-direction	4	13	
			FR2~10	9	1-direction	9		
	Pipe strain	Straight pipe	FS1~15	11	1-axis x 4	44	76	
		Elbow		5	2-axis x 2	20		
		Branch	FS19~22	3	2-axis x 2	12		
	Inner pressure	Straight pipe	FP1,2	2	none	2	2	
Actuator	Acceleration	SG nozzle	AA1,2	2	3-directions	6	13	18
		DSP output	DSP-A	1	none	1		
	Displacement	SG nozzle	AD1X,Y,Z	1	3-directions	3		
		DSP output	DSP-A	1	none	1		
	Support load	MS-line pipe	AS1,2	2	1-direction	2		
Common structure	Acceleration	Vertical 3 location	SA1~3	3	1~2 directions	5	5	

Table D.2 Sensors List (Energy Absorbing Support Test Piping)

Object	Measuring Items	Location	Symbols	No. of Pt.	Directions	Channels	Total	
MS-line piping	Acceleration	Main run	MA1~4,MA8, MA10,11	7	3-directions	21	42	141
			MA5,6	2	2-directions	4		
		Branch	MA13	1	3-directions	3		
		Valve	MA12,14,15	3	3-directions	9		
		Support	MA7	1	2-directions	2		
			MA9	1	3-directions	3		
	Displacement	Support	MD14~17	4	axial	4	12	
		Main run	MD12,13	2	axial	2		
			MD18	1	3-directions	3		
		Branch	MD9~11	1	Y-direction	1		
				1	Z-direction	1		
				1	X-direction	1		
	Support load	Main run	MR8,15~17	4	1-direction	4	8	
		Branch	MR11~14	4	1-direciton	4		
	Pipe strain	Straight pipe	MS0,2,2',4,	8	1-axis x 4	32	74	
		Elbow	6,9,11,11'	1	bending x 1	1		
				1	torsion x 1	1		
			MS1,3,5,	2	2-axes x 12	24		
			8,10,12	4	1-axis x 4	16		
	Inner pressure	Straight pipe	MP1,2	2	none	2	2	
	Temperature	LED	TE1~3	3	none	3	3	
FW-line piping	Acceleration	Pipe	FA1,FA3~13	12	3-directions	36	36	142
	Displacement	Support	FD6,11~15	6	1-direction	6	6	
	Support load	Support	FR6,FR11~15	8	1-direction	4	10	
				6	1-direction	6		
	Pipe strain	Straight pipe	FS1~22	13	1-axis x 4	52	88	
		Elbow		6	2-axes x 2	24		
		Branch		3	2-axes x 2	12		
	Inner pressure	Straight pipe	FP1,2	2	none	2	2	
Actuator	Acceleration	SG nozzle	AA1,2	2	3-directions	6	13	17
		DSP output	DSP-A	1	none	1		
	Displacement	SG nozzle	AD1X,Y,Z	1	3-directions	3		
		DSP output	DSP-D	1	none	1		
	Support load	MS-line pipe	AS1,2	2	1-direction	2		
Common structure	Acceleration	Vertical 3 location	SA1~3	3	1~2 directions	4	4	

Location	Sensor	Direction	Category	Specification	Sensor Type
Main Run	MA 1	X	Common	Accelerometer	AS-CB20 C
		Y	Common	Accelerometer	AS-CB10 C
		Z	Common	Accelerometer	AS-CB10 C
	MA 2	X	Common	Accelerometer	AS-CB20 C
		Y	Common	Accelerometer	AS-CB10 C
		Z	Common	Accelerometer	AS-CB10 C
	MA 3	X	Common	Accelerometer	AS-CB20 C
		Y	Common	Accelerometer	AS-CB10 C
		Z	Common	Accelerometer	AS-CB10 C
	MA 4	X	Common	Accelerometer	AS-CB20 C
		Y	Common	Accelerometer	AS-CB10 C
		Z	Common	Accelerometer	AS-CB10 C
	MA 5	X	Common	Accelerometer	AS-CB10 C
		Y	Common	Accelerometer	AS-CB10 C
		Z	Common	Accelerometer	AS-CB10 C
	MA 6	X	Common	Accelerometer	AS-CB10 C
		Y	Common	Accelerometer	AS-CB10 C
		Z	Common	Accelerometer	AS-CB10 C
	MA 7	X	Common	Accelerometer	AS-CB10 C
		Y	Common	Accelerometer	AS-CB10 C
		Z	Common	Accelerometer	AS-CB10 C
	MA 8	X	Common	Accelerometer	AS-CB 5 C
		Y	Common	Accelerometer	AS-CB 5 C
		Z	Common	Accelerometer	AS-CB 5 C
	MA 9	X	Common	Accelerometer	AS-CB 5 C
		Y	Common	Accelerometer	AS-CB 5 C
		Z	Common	Accelerometer	AS-CB 5 C
	MA 10	X	Common	Accelerometer	AS-CB 5 C
		Y	Common	Accelerometer	AS-CB 5 C
		Z	Common	Accelerometer	AS-CB 5 C
	MA 11	X	Common	Accelerometer	AS-CB 5 C
		Y	Common	Accelerometer	AS-CB 5 C
		Z	Common	Accelerometer	AS-CB 5 C
Branch	MA 12	X	Common	Accelerometer	AS-CB10 C
		Y	Common	Accelerometer	AS-CB10 C
		Z	Common	Accelerometer	AS-CB20 C
Valve	MA 13	X	Common	Accelerometer	AS-CB10 C
		Y	Common	Accelerometer	AS-CB10 C
		Z	Common	Accelerometer	AS-CB 5 C
	MA 14	X	Common	Accelerometer	AS-CB 5 C
		Y	Common	Accelerometer	AS-CB 5 C
		Z	Common	Accelerometer	AS-CB 5 C

Figure D.1 Acceleration Sensing Points on MS-line

Location	Sensor	Direction	Category	Specification	Sensor Type
Main Pipe	MD 1a		Conv.	Disp. Transducer	PU-40 ± 8 mm
	MD 2a		Conv.	Disp. Transducer	PU-40 ± 8 mm
	MD 5a		Conv.	Disp. Transducer	PU-40 ± 8 mm
	MD 6a		Conv.	Disp. Transducer	PU-40 ± 8 mm
	MD 7a	X	Conv.	Disp. Transducer	PU-40 ± 8 mm
Conv. Pipe Support	MD 3b	Z	Conv.	Disp. Transducer	ZAM-W40 ± 10 mm
	MD 4b	Z	Conv.	Disp. Transducer	ZAM-W40 ± 10 mm
	MD 5b		Conv.	Disp. Transducer	ZAM-W40 ± 10 mm
	MD 6b		Conv.	Disp. Transducer	ZAM-W40 ± 10 mm
	MD 7b	X	Conv.	Disp. Transducer	ZAM-W40 ± 10 mm
Main Pipe	MD 8	X	Conv.	Disp. Transducer	ZAM-W40 ± 10 mm
	MD 8	Y	Conv.	Disp. Transducer	ZAM-W40 ± 10 mm
	MD 8	Z	Conv.	Disp. Transducer	ZAM-W40 ± 10 mm
	MD 9	Y	Common	Disp. Transducer	ZAM-W40 ± 10 mm
Branch	MD 10	Z	Common	Disp. Transducer	ZAM-W40 ± 10 mm
	MD 11	X	Common	Disp. Transducer	ZAM-W40 ± 10 mm
Main Pipe	MD 12		EA	Disp. Transducer	ZAM-W100 ± 40 mm
	MD 13		EA	Disp. Transducer	ZAM-W100 ± 40 mm
	MD 14	X	EA	Disp. Transducer	ZAM-W100 ± 40 mm
	MD 18	X	EA	Disp. Transducer	ZAM-W100 ± 40 mm
	MD 18	Y	EA	Disp. Transducer	ZAM-W100 ± 40 mm
	MD 18	Z	EA	Disp. Transducer	ZAM-W100 ± 40 mm
EA Support	MD 15		EA	Disp. Transducer	ZAM-W100 ± 40 mm
	MD 16		EA	Disp. Transducer	ZAM-W100 ± 40 mm
	MD 17		EA	Disp. Transducer	ZAM-W100 ± 40 mm
SG Nozzle	AD 1 X	X	Common	Disp. Transducer	ZAM-W40 ± 10 mm
	AD 1 Y	Y	Common	Disp. Transducer	ZAM-W40 ± 10 mm
	AD 1 Z	Z	Common	Disp. Transducer	ZAM-W40 ± 10 mm

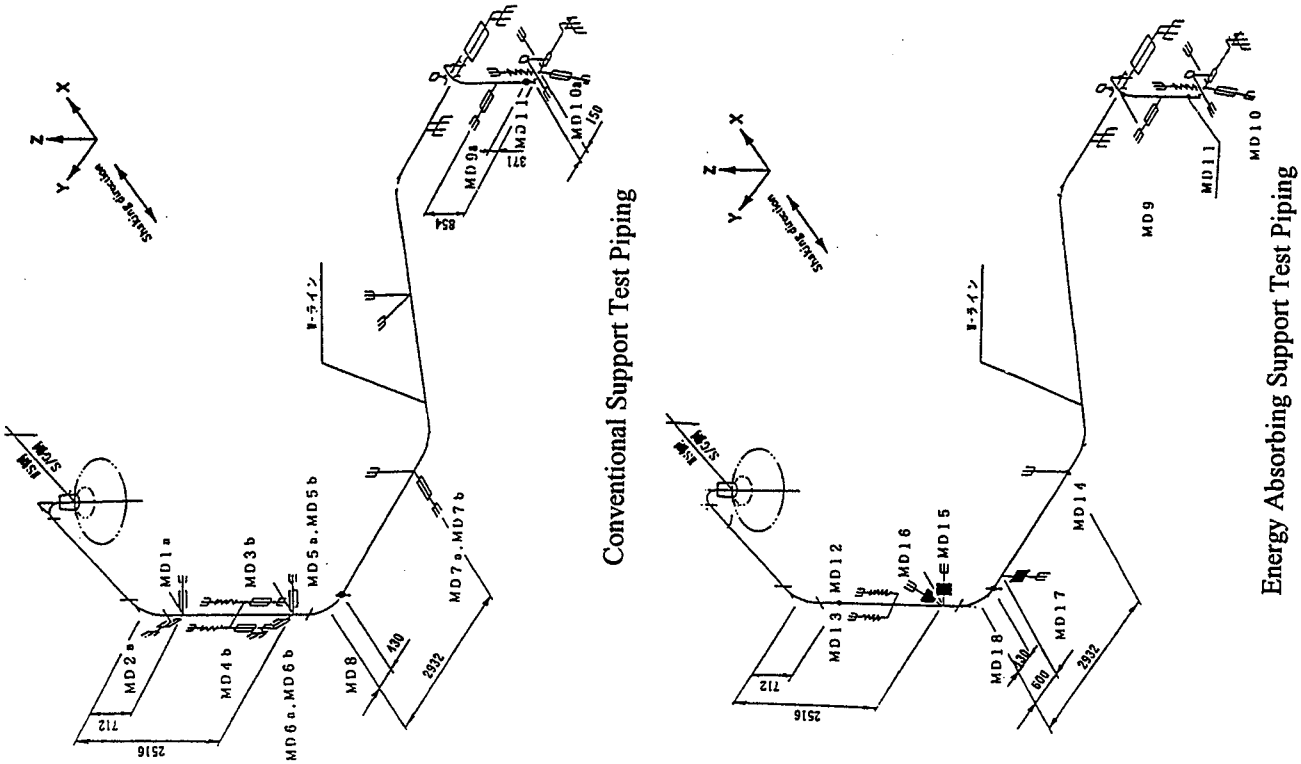

Figure D.2 Displacement Sensing Points on MS-line

Location	Sensor	Direction	Category	Specification	Sensor Type
Main Pipe	MR 1		Conv.	Load Cell	LUK-10TB
	MR 2		Conv.	Load Cell	LUK-10TB
	MR 3		Conv.	Load Cell	LUK-10TB
	MR 4		Conv.	Load Cell	LUK-10TB
	MR 5		Conv.	Load Cell	LUK-10TB
	MR 6		Conv.	Load Cell	LUK-10TB
	MR 7		Conv.	Load Cell	LUK-10TB
	MR 8		Common	Load Cell	Strain Gage
	MR 9		Conv.	Load Cell	Load Cell
	MR 10		Conv.	Load Cell	Load Cell
Branch	MR 11		Common	Load Cell	LUK-500KB
	MR 12		Common	Load Cell	LUK-500KB
	MR 13		Common	Load Cell	Strain Gage
	MR 14		Common	Load Cell	Strain Gage
Main Pipe	MR 1'		EA	Load Cell	LUK-5TB
	MR 2'		EA	Load Cell	LUK-5TB
	MR 3'		EA	Load Cell	LUK-5TB
SG Nozzle	AS 1		Common	Load Cell	LUK-20TB
	AS 2		Common	Load Cell	Strain Gage
Main Pipe	PM 1		Common	Load Cell	PGW-100KD
	PM 2		Common	Load Cell	PGW-100KD

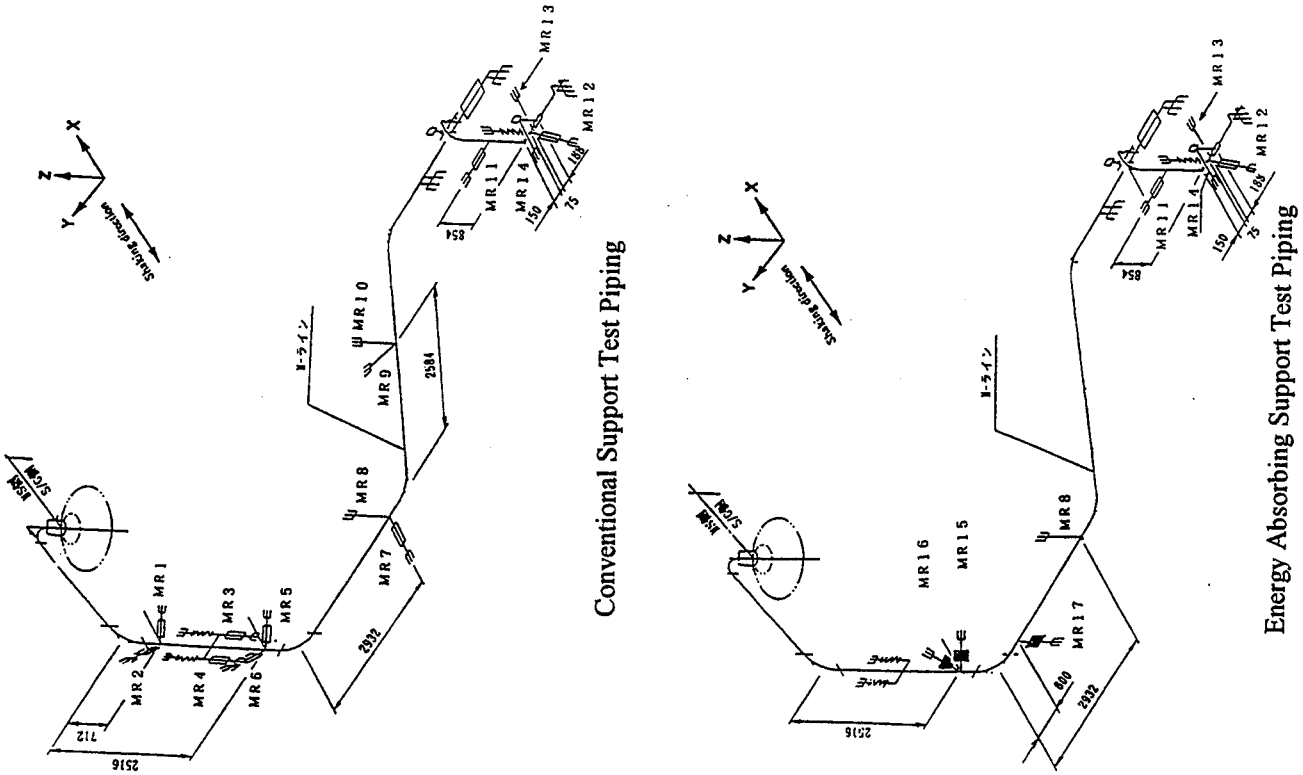

Figure D.3 Support Load Sensing Points on MS-line

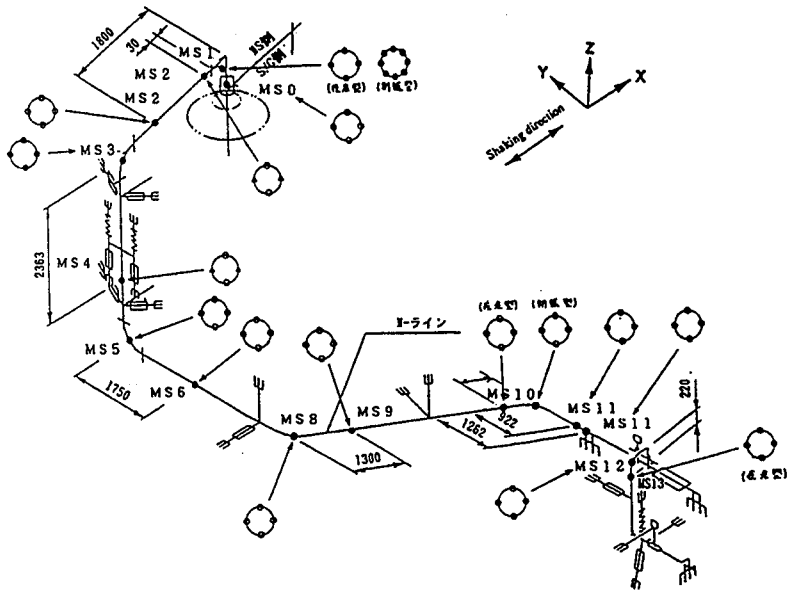

Location	Sensor	Direction	Category	Specification	Sensor Type
Main Pipe	MS 0		Common	Strain Gage	WFCA 1 axis x 4
	MS 1		Common	Strain Gage	WFCA 2 axes x 4
	MS 2		Common	Strain Gage	WFLA 1 axis x 4
	MS 3		Common	Strain Gage	WFCA 2 axes x 4
	MS 4		Common	Strain Gage	WFLA 1 axis x 2 WFLA 3 axes x 2
	MS 5		Common	Strain Gage	WFCA 1 axis x 4
	MS 6		Common	Strain Gage	WFLA 1 axis x 4
	MS 8		Common	Strain Gage	WFCA 1 axis x 4
	MS 9		Common	Strain Gage	WFLA 1 axis x 4
	MS 10		Common	Strain Gage	WFCA 1 axis x 4
	MS 11		Common	Strain Gage	WFLA 1 axis x 4
Branch	MS 12		Common	Strain Gage	WFCA 2 axes x 2
Main Pipe	MS 2′		Common	Strain Gage	WFRA 3 axes x 2 WFLA 1 axis x 2
	MS 11′		Common	Strain Gage	WFLA 1 axis x 4
Branch	MS 13		Conv. Only	Strain Gage	WFLA 1 axis x 4

Figure D.4 Strain Sensing Points on MS-line

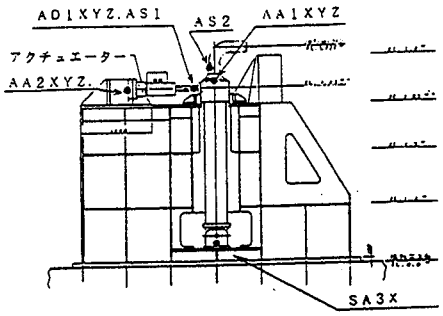

Section view of the common structure

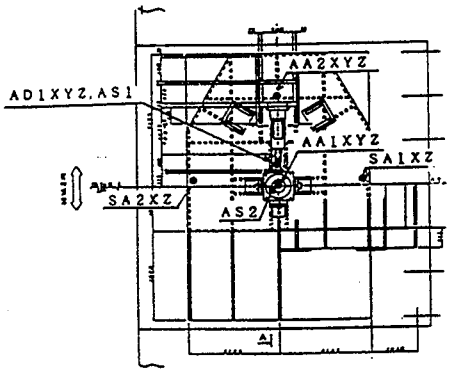

Plan view of the common structure

Location	Sensor	Direction	Category	Specification	Sensor Type
SG Nozzle	AA 1	X	Common	Accelerometer	AS-CB10C
		Y	Common	Accelerometer	AS-CB10C
		Z	Common	Accelerometer	AS-CB10C
	AA 2	X	Common	Accelerometer	AS-CB10C
		Y	Common	Accelerometer	AS-CB10C
		Z	Common	Accelerometer	AS-CB10C
Foundation	SA 1	X	Common	Accelerometer	AS-CB10C
		Z	Common	Accelerometer	AS-CB10C
	SA 2	X	Common	Accelerometer	AS-CB10C
		Z	Common	Accelerometer	AS-CB10C
	SA 3	X	Common	Accelerometer	AS-CB10C

Figure D.5 Sensing for the Actuator, Foundation

Location	Sensor	Direction	Category	Specification	Sensor Type
Anchor	FA 1	X	Common	Accelerometer	AS-101B (10G)
		Y	Common	Accelerometer	AS-101B (10G)
		Z	Common	Accelerometer	AS-101B (10G)
Valve	FA 2	X	Conv.	Accelerometer	AS-101B (10G)
		Y	Conv.	Accelerometer	AS-101B (10G)
		Z	Conv.	Accelerometer	AS-101B (10G)
Main Pipe	FA 3	X	Common	Accelerometer	AS-101B (10G)
		Y	Common	Accelerometer	AS-101B (10G)
		Z	Common	Accelerometer	AS-101B (10G)
Guide	FA 4	X	Common	Accelerometer	AS-101B (10G)
		Y	Common	Accelerometer	AS-101B (10G)
		Z	Common	Accelerometer	AS-101B (10G)
Main Pipe	FA 5	X	Common	Accelerometer	AS-101B (10G)
		Y	Common	Accelerometer	AS-101B (10G)
		Z	Common	Accelerometer	AS-101B (10G)
	FA 6	X	Common	Accelerometer	AS-101B (10G)
		Y	Common	Accelerometer	AS-101B (10G)
		Z	Common	Accelerometer	AS-101B (10G)
Branch	FA 7	X	Common	Accelerometer	AS-101B (10G)
		Y	Common	Accelerometer	AS-101B (10G)
		Z	Common	Accelerometer	AS-101B (10G)
Main Pipe	FA 8	X	Common	Accelerometer	AS-101B (10G)
		Y	Common	Accelerometer	AS-101B (10G)
		Z	Common	Accelerometer	AS-101B (10G)
Branch	FA 9	X	Common	Accelerometer	AS-101B (10G)
		Y	Common	Accelerometer	AS-101B (10G)
		Z	Common	Accelerometer	AS-101B (10G)
Main Pipe	FA 10	X	Common	Accelerometer	AS-101B (10G)
		Y	Common	Accelerometer	AS-101B (10G)
		Z	Common	Accelerometer	AS-101B (10G)
Branch	FA 11	X	Common	Accelerometer	AS-101B (10G)
		Y	Common	Accelerometer	AS-101B (10G)
		Z	Common	Accelerometer	AS-101B (10G)
Branch	FA 12	X	Common	Accelerometer	AS-101B (10G)
		Y	Common	Accelerometer	AS-101B (10G)
		Z	Common	Accelerometer	AS-101B (10G)
	FA 13	X	Common	Accelerometer	AS-101B (10G)
		Y	Common	Accelerometer	AS-101B (10G)
		Z	Common	Accelerometer	AS-101B (10G)
Str Nozzle	AA 2	X	Common	Accelerometer	AS-101B (10G)
		Y	Common	Accelerometer	AS-101B (10G)
		Z	Common	Accelerometer	AS-101B (10G)

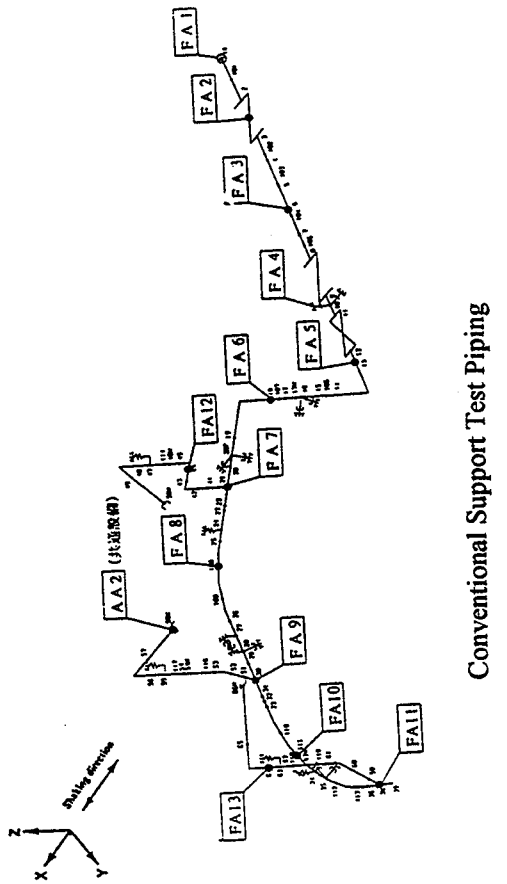

Conventional Support Test Piping

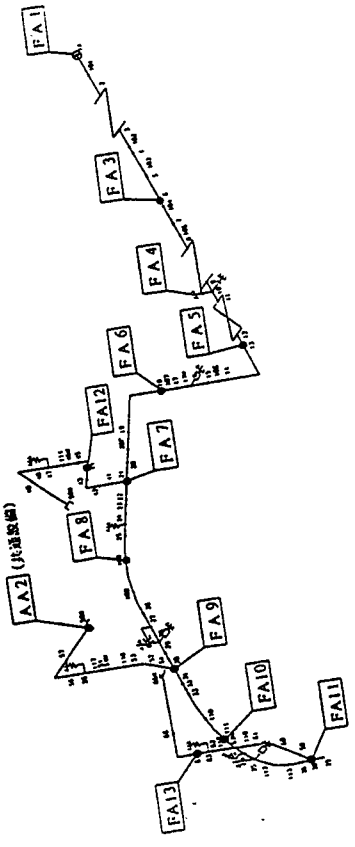

Energy Absorbing Support Test Piping

Figure D.6 Acceleration Sensing Points on FW-line

Location	Sensor	Direction	Category	Specification	Sensor Type
Support	FD 2b	Axial	Conv.	Disp. Transducer	DLT-5A (±5 mm)
	FD 3b	Axial	Conv.	Disp. Transducer	DLT-5A (±5 mm)
	FD 4b	Axial	Conv.	Disp. Transducer	DLT-5A (±5 mm)
	FD 5b	Axial	Conv.	Disp. Transducer	DLT-5A (±5 mm)
	FD 6b	Axial	Common	Disp. Transducer	DLT-5A (±5 mm)
	FD 7a	Axial	Conv.	Disp. Transducer	EX-422 (±5 mm)
	FD 7b	Axial	Conv.	Disp. Transducer	DLT-5A (±5 mm)
	FD 8a	Axial	Conv.	Disp. Transducer	EX-422 (±5 mm)
	FD 8b	Axial	Conv.	Disp. Transducer	DLT-5A (±5 mm)
	FD 9b	Axial	Conv.	Disp. Transducer	DLT-5A (±5 mm)
	FD 10b	Axial	Conv.	Disp. Transducer	DLT-5A (±5 mm)
	FD 11b	Axial	EA	Disp. Transducer	DLT-20A (±20 mm)
	FD 12b	Axial	EA	Disp. Transducer	DLT-20A (±20 mm)
	FD 13b	Axial	EA	Disp. Transducer	DLT-5A (±5 mm)
	FD 14b	Axial	EA	Disp. Transducer	DLT-20A (±20 mm)
	FD 15b	Axial	EA	Disp. Transducer	DLT-5A (±5 mm)

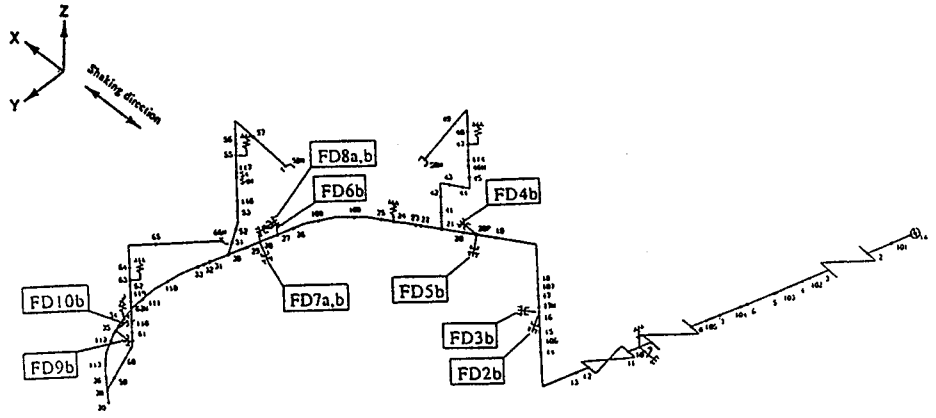

Conventional Support Test Piping

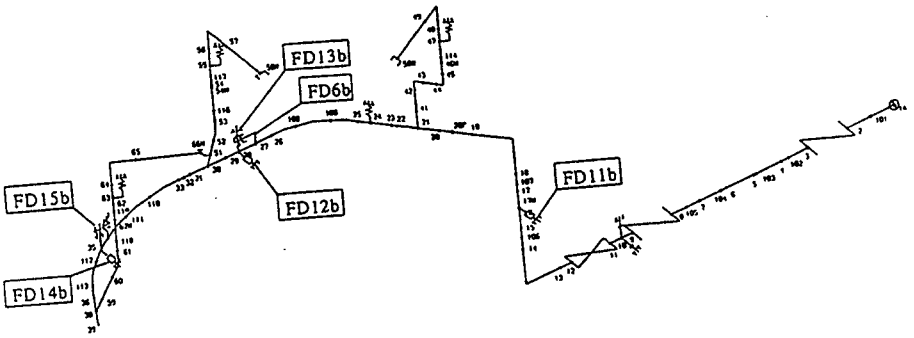

Energy Absorbing Support Test Piping

Figure D.7 Displacement Sensing Points on FW-line

Appendix D

Location	Sensor	Direction	Category	Specification	Sensor Type
Support	FR 1	Z	Common	Strain Gage	KSN
	FR 2	Axial	Conv.	Load Cell	LUK-2TB
	FR 3	Axial	Conv.	Load Cell	LUK-2TB
	FR 4	Axial	Conv.	Load Cell	LUK-2TB
	FR 5	Axial	Conv.	Load Cell	LUK-2TB
	FR 6	Axial	Common	Load Cell	LUK-5TB
	FR 7	Axial	Conv.	Load Cell	LUK-5TB
	FR 8	Axial	Conv.	Load Cell	LUK-5TB
	FR 9	Axial	Conv.	Load Cell	LUK-5TB
	FR 10	Axial	Conv.	Load Cell	LUK-5TB
	FR 11	Axial	EA	Load Cell	LUK-1TB
	FR 12	Axial	EA	Load Cell	LUK-2TB
	FR 13	Axial	EA	Load Cell	LUK-5TB
	FR 14	Axial	EA	Load Cell	LUK-2TB
	FR 15	Axial	EA	Load Cell	LUK-5TB
Main Pipe	FP 1	—	Common	Pressure Gage	PGM-200KE
Branch	FP 1	—	Common	Pressure Gage	PGM-200KE

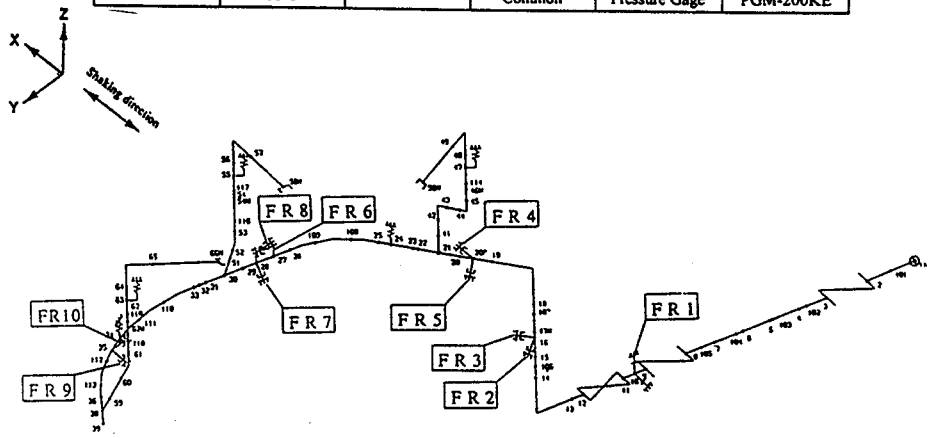

Conventional Support Test Piping

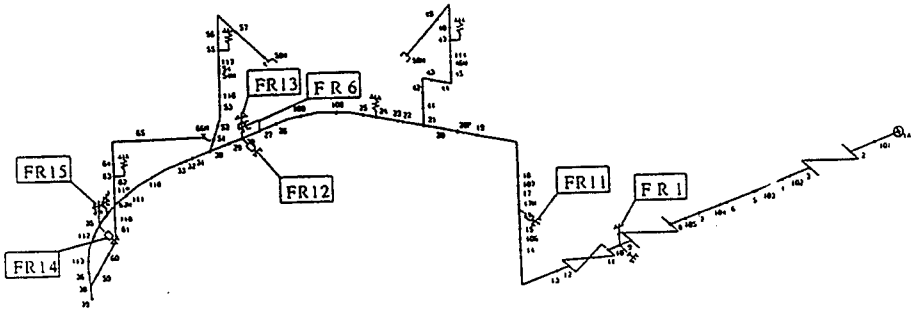

Energy Absorbing Support Test Piping

Figure D.8 Support Load and Internal Pressure Sensing Points on FW-line

Location	Sensor	Direction	Category	Specification	Sensor Type
Straight Run	FS 1	1 axis x 4	Common	Strain Gage	KFG(gage length 5 mm)
Elbow	FS 2	2 axes x 2	Common	Strain Gage	KFG(gage length 5 mm)
	FS 3	2 axes x 2	Common	Strain Gage	KFG(gage length 5 mm)
Branch	FS 4	2 axes x 2	Common	Strain Gage	KFG(gage length 5 mm)
Straight Run	FS 5	1 axis x 4	Common	Strain Gage	KFG(gage length 5 mm)
Branch	FS 6	2 axes x 2	Common	Strain Gage	KFG(gage length 5 mm)
Straight Run	FS 7	1 axis x 4	Common	Strain Gage	KFG(gage length 5 mm)
	FS 8	1 axis x 4	Common	Strain Gage	KFG(gage length 5 mm)
Branch	FS 9	2 axes x 2	Common	Strain Gage	KFG(gage length 5 mm)
Elbow	FS 10	2 axes x 2	Common	Strain Gage	KFG(gage length 5 mm)
	FS 11	2 axes x 2	Common	Strain Gage	KFG(gage length 5 mm)
Straight Run	FS 12	1 axis x 4	Common	Strain Gage	KFG(gage length 5 mm)
Elbow	FS 13	2 axes x 2	Common	Strain Gage	KFG(gage length 5 mm)
Straight Run	FS 14	1 axis x 4	Common	Strain Gage	KFG(gage length 5 mm)
	FS 15	1 axis x 4	Common	Strain Gage	KFG(gage length 5 mm)
	FS 16	1 axis x 4	EA	Strain Gage	KFG(gage length 5 mm)
Elbow	FS 17	2 axes x 2	EA	Strain Gage	KFG(gage length 5 mm)
Straight Run	FS 18	1 axis x 4	EA	Strain Gage	KFG(gage length 5 mm)
	FS 19	1 axis x 4	Common	Strain Gage	KFG(gage length 5 mm)
	FS 20	1 axis x 4	Common	Strain Gage	KFG(gage length 5 mm)
Elbow	FS 21	2 axes x 2	Common	Strain Gage	KFG(gage length 5 mm)
Straight Run	FS 22	1 axis x 4	Common	Strain Gage	KFG(gage length 5 mm)

Figure D.9 Strain Sensing Points on FW-line

APPENDIX E

LIST OF PEAK RESPONSE VALUES AND PLOTS OF SELECTED CHANNELS FOR 3/3 S_2 (F) TEST RUN (RUN NO. 95011107)

Table E.1 List of Recorded Peak Values for F-line with Conventional Supports

	VC-8	VC-9	VC-10	VC-1	VC-2	VC-3	
Test no.	95011203	95011206	95011209	95011103	95011105	95011107	
Targ. accel.	259+52	504+100	763+152	397+66	772+128	1169+194	
Sensor	1/3S1(H+V)	2/3S1(H+V)	3/3S1(H+V)	1/3S2(H+V)	2/3S2(H+V)	3/3S2(H+V)	Unit
FA01X	233	450	692	363	692	1090	GAL
FA01Y	142	175	200	183	200	301	GAL
FA01Z	49	99	158	83	158	249	GAL
FA02X	379	732	1021	822	1328	2052	GAL
FA02Y	204	188	298	243	314	604	GAL
FA02Z	237	245	440	305	474	907	GAL
FA03X	442	885	1177	989	1611	2572	GAL
FA03Y	76	128	102	102	119	170	GAL
FA03Z	323	349	588	409	681	1329	GAL
FA04X	241	474	759	388	767	1181	GAL
FA04Y	113	140	166	157	210	315	GAL
FA04Z	50	100	150	75	125	217	GAL
FA05X	774	1658	1190	1267	1573	2041	GAL
FA05Y	106	155	196	147	204	270	GAL
FA05Z	317	458	590	352	625	1066	GAL
FA06X	735	1073	1289	1012	1696	2025	GAL
FA06Y	968	976	1187	1304	1422	1422	GAL
FA06Z	466	576	796	483	907	1483	GAL
FA07X	614	1204	1561	996	1636	3313	GAL
FA07Y	622	909	829	869	965	1213	GAL
FA07Z	341	357	615	449	640	1164	GAL
FA08X	631	1160	1568	883	1569	3006	GAL
FA08Y	691	959	881	941	1146	1253	GAL
FA08Z	475	585	1023	959	1161	1608	GAL
FA09X	816	1199	1565	1020	1684	2637	GAL
FA09Y	649	943	847	874	1186	1212	GAL
FA09Z	809	1172	1130	1163	1197	1214	GAL
FA010X	1020	1776	1684	1402	2103	2723	GAL
FA010Y	686	944	810	810	997	1086	GAL
FA010Z	472	808	1151	997	945	1108	GAL
FA011X	1434	2164	1988	2005	2450	3045	GAL
FA011Y	838	910	865	1017	1740	1865	GAL
FA011Z	423	634	837	687	969	1163	GAL
FA012X	668	1167	1559	1282	2138	3037	GAL
FA012Y	821	1333	1050	1077	1562	1907	GAL
FA012Z	486	467	587	669	862	1275	GAL
FA013X	1320	2508	2115	1660	2231	3114	GAL
FA013Y	462	853	729	640	1058	1333	GAL
FA013Z	497	826	892	763	952	1235	GAL
FS011	0.3	0.32	0.55	0.37	0.67	1.2	KG/mm2
FS012	0.51	1.02	1.32	1.1	1.75	1.2	KG/mm2
FS013	0.34	0.37	0.53	0.35	0.61	1.18	KG/mm2
FS014	0.51	1.01	1.32	1.14	1.77	2.84	KG/mm2
FS021	0.34	0.59	0.55	0.35	0.75	0.95	KG/mm2
FS022	0.67	0.79	0.89	0.79	0.99	1.32	KG/mm2
FS023	0.34	0.59	0.43	0.49	0.61	0.67	KG/mm2
FS024	0.69	0.77	0.87	0.79	1.01	1.26	KG/mm2
FS031	0.22	0.39	0.31	0.31	0.5	0.53	KG/mm2
FS032	0.57	0.81	0.75	0.68	0.79	0.96	KG/mm2
FS033	0.61	0.81	0.75	0.72	0.75	0.99	KG/mm2
FS034	0.35	0.55	0.46	0.52	0.55	0.75	KG/mm2
FS041	0.18	0.2	0.22	0.22	0.31	0.28	KG/mm2

Table E.1 List of Recorded Peak Values for F-line with Conventional Supports (Cont'd)

	VC-08	VC-09	VC-10	VC-1	VC-2	VC-3	
FS042	0.77	0.81	0.94	0.86	1.23	1.25	KG/mm2
FS043	0.09	0.13	0.15	0.13	0.2	0.24	KG/mm2
FS044	0.31	0.48	0.53	0.55	0.94	0.99	KG/mm2
FS051	0.72	0.74	0.83	0.81	1.03	1.2	KG/mm2
FS052	0.52	0.92	0.81	0.86	0.94	1.53	KG/mm2
FS053	0.88	1.14	1.12	1.12	1.38	1.58	KG/mm2
FS054	0.55	0.72	0.66	0.64	0.72	1.09	KG/mm2
FS061	0.28	0.33	0.29	0.31	0.4	0.44	KG/mm2
FS062	0.57	0.77	0.79	0.81	0.96	1.12	KG/mm2
FS063	0.15	0.18	0.18	0.18	0.26	0.31	KG/mm2
FS064	0.66	0.9	0.9	0.9	1.12	1.42	KG/mm2
FS071	0.39	0.55	0.46	0.52	0.63	0.66	KG/mm2
FS072	0.57	0.9	0.79	0.64	1.01	1.23	KG/mm2
FS073	0.61	0.96	0.86	0.81	0.99	1.18	KG/mm2
FS074	0.81	1.2	1.12	1.01	1.49	1.6	KG/mm2
FS081	0.26	0.39	0.29	0.24	0.33	0.44	KG/mm2
FS082	0.09	0.13	0.11	0.11	0.11	0.15	KG/mm2
FS083	0.22	0.33	0.28	0.26	0.29	0.44	KG/mm2
FS084	0.09	0.15	0.11	0.11	0.15	0.13	KG/mm2
FS091	0.24	0.26	0.28	0.29	0.35	0.4	KG/mm2
FS092	0.61	0.57	0.57	0.61	0.79	0.96	KG/mm2
FS093	0.22	0.31	0.28	0.29	0.33	0.4	KG/mm2
FS094	0.86	1.21	1.18	0.98	1.2	1.6	KG/mm2
FS101	0.29	0.39	0.44	0.42	0.5	0.72	KG/mm2
FS102	0.29	0.44	0.35	0.28	0.44	0.79	KG/mm2
FS103	0.39	0.52	0.57	0.5	0.59	0.9	KG/mm2
FS104	0.24	0.31	0.33	0.28	0.52	0.72	KG/mm2
FS111	0.33	0.57	0.55	0.59	0.86	1.16	KG/mm2
FS112	0.4	0.55	0.81	0.81	1.16	1.27	KG/mm2
FS113	0.59	0.7	1.09	0.86	1.1	1.71	KG/mm2
FS114	0.33	0.46	0.75	0.74	0.9	1.03	KG/mm2
FS121	0.28	0.33	0.37	0.39	0.63	0.66	KG/mm2
FS122	0.49	0.59	0.99	0.99	1.27	1.42	KG/mm2
FS123	0.22	0.33	0.39	0.37	0.59	0.68	KG/mm2
FS124	0.39	0.55	0.68	0.75	0.98	1.03	KG/mm2
FS131	0.35	0.46	0.48	0.42	0.57	0.72	KG/mm2
FS132	0.66	0.81	0.96	0.98	1.33	1.44	KG/mm2
FS133	0.4	0.44	0.55	0.5	0.74	0.86	KG/mm2
FS134	0.63	0.77	0.9	0.96	1.21	1.27	KG/mm2
FS141	0.85	1.03	1.36	1.34	1.8	2.87	KG/mm2
FS142	1.01	1.47	1.77	1.55	1.84	2.3	KG/mm2
FS143	0.72	0.85	1.01	1.09	1.56	2.41	KG/mm2
FS144	0.94	1.44	1.51	1.49	1.91	2.13	KG/mm2
FS151	0.64	0.79	0.99	0.92	0.5	1.23	KG/mm2
FS152	0.59	0.77	0.74	0.72	0.44	1.03	KG/mm2
FS153	0.52	0.64	0.77	0.7	0.59	1.01	KG/mm2
FS154	0.59	0.77	0.85	0.77	0.52	1.14	KG/mm2
FS191	0.61	0.66	0.64	0.7	0.83	1.03	KG/mm2
FS192	0.79	1.1	1.03	0.88	1.14	1.42	KG/mm2
FS193	0.55	0.64	0.59	0.63	0.75	0.99	KG/mm2
FS194	0.81	1.18	1.09	0.99	1.33	1.56	KG/mm2
FS201	0.88	1.05	0.99	0.99	1.31	1.8	KG/mm2
FS202	0.98	1.77	1.42	1.1	1.53	2.01	KG/mm2
FS203	0.83	0.98	0.9	0.94	1.29	1.64	KG/mm2
FS204	0.98	1.84	1.58	1.25	1.69	2.06	KG/mm2

Table E.1 List of Recorded Peak Values for F-line with Conventional Supports (Cont'd)

	VC-08	VC-09	VC-10	VC-1	VC-2	VC-3	
FS211	0.5	0.74	0.66	0.63	0.68	0.79	KG/mm2
FS212	0.92	1.03	1.06	1.2	1.47	1.79	KG/mm2
FS213	0.86	0.98	0.98	0.88	1.14	1.36	KG/mm2
FS214	0.81	0.92	1.01	1.05	1.29	1.6	KG/mm2
FS221	0.88	1.62	1.44	1.2	2.21	2.23	KG/mm2
FS222	1.53	2.63	1.95	1.73	2.1	2.8	KG/mm2
FS223	0.98	1.8	1.69	1.42	2.56	2.52	KG/mm2
FS224	1.56	2.72	2.21	1.9	2.25	2.8	KG/mm2
FR02	184	347	359	322	786	884	KG
FD02b	0.09	0.14	0.16	0.11	0.23	0.32	mm
FR03	475	713	954	528	813	1394	KG
FD03b	0.09	0.2	0.19	0.18	0.26	0.68	mm
FR04	162	417	594	352	708	960	KG
FD04b	0.06	0.12	0.18	0.14	0.22	0.46	mm
FR05	300	539	605	458	1063	1423	KG
FD05b	0.11	0.24	0.33	0.3	0.42	0.71	mm
FR06	1774	2466	2284	276	2673	2453	KG
FD06b	0.41	0.45	0.49	0.46	0.59	0.79	mm
FR07	1095	1634	2317	1544	2345	3518	KG
FD07a	0.42	0.52	0.17	0.52	0.67	0.88	mm
FD07b	0.24	0.27	0.37	0.24	0.35	0.39	mm
FR08	630	1587	1587	1248	1865	2423	KG
FD08a	0.3	0.42	0.5	0.42	0.52	0.63	mm
FD08b	0.11	0.21	0.23	0.17	0.23	0.33	mm
FR09	1156	1975	1957	1651	2365	2732	KG
FD09b	0.24	0.36	0.42	0.46	0.42	0.49	mm
FR10	764	1145	1454	1139	1591	1353	KG
FD10b	0.14	0.31	0.46	0.48	0.54	0.56	mm

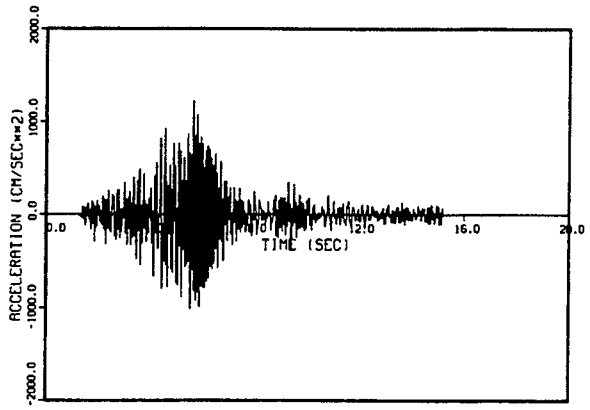

Figure E.1 XOXB

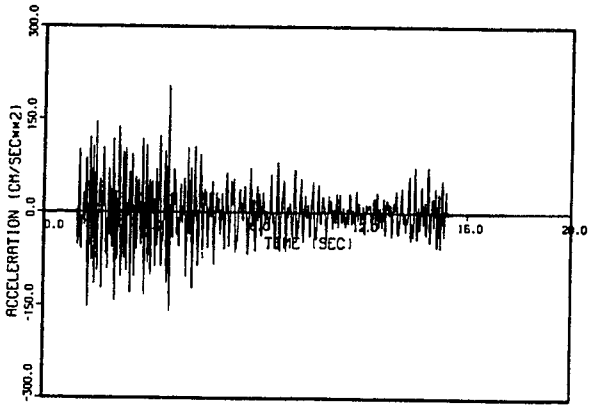

Figure E.2 ZOXB

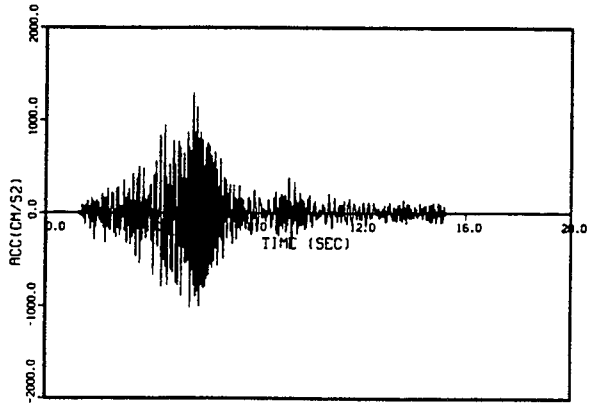

Figure E.3 AA2-X

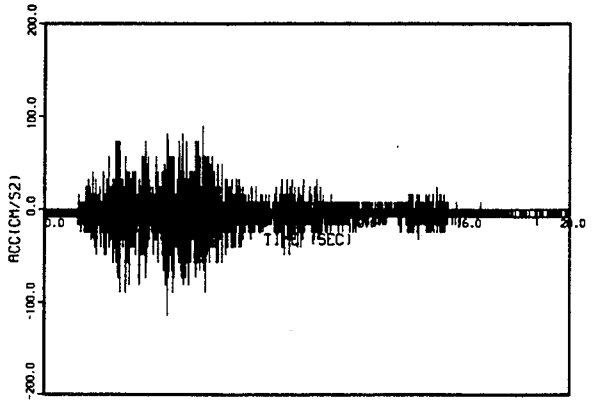

Figure E.4 AA2-Y

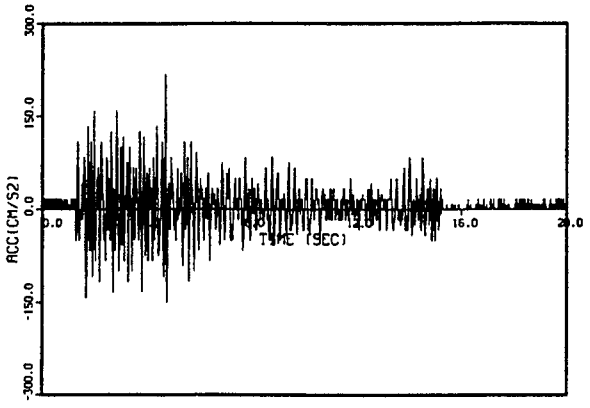

Figure E.5 AA2-Z

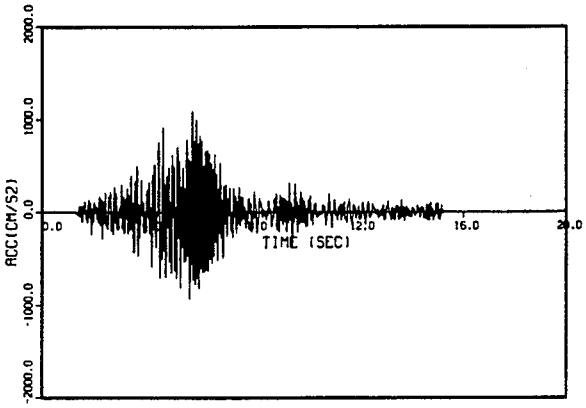

Figure E.6 FA1-X

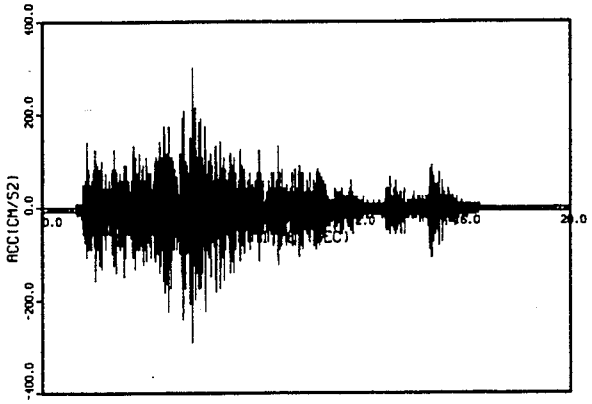

Figure E.7 FA1-Y

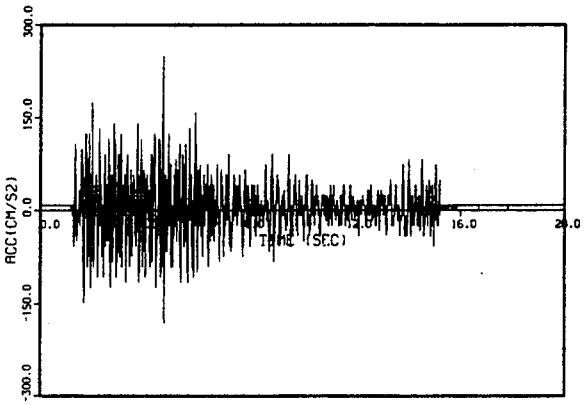

Figure E.8 FA1-Z

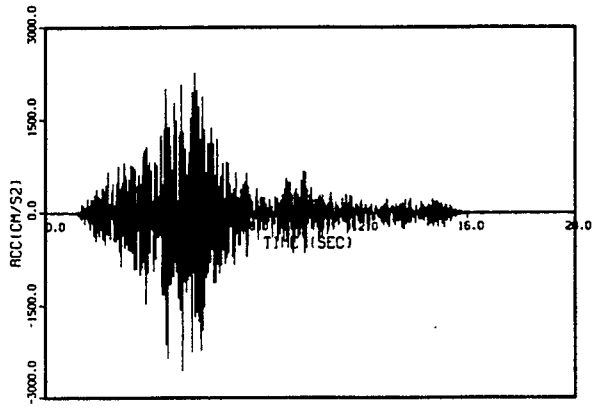

Figure E.9 FA3-X

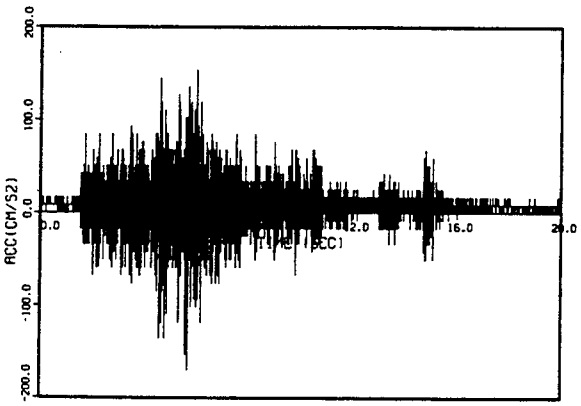

Figure E.10 FA3-Y

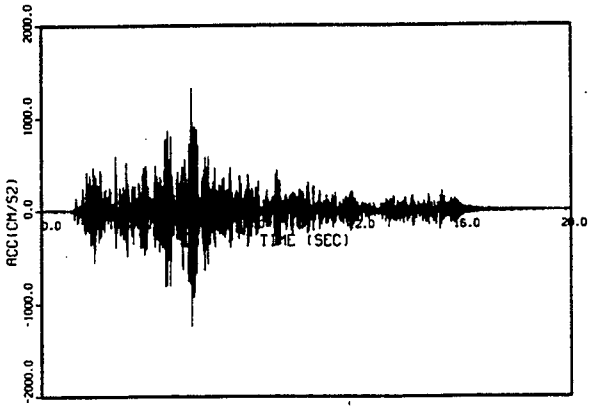

Figure E.11 FA3-Z

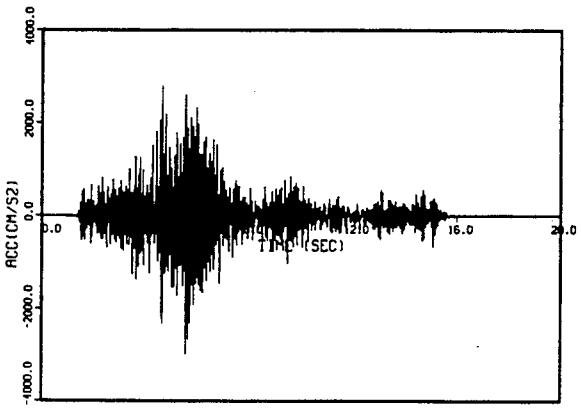

Figure E.12 FA8-X

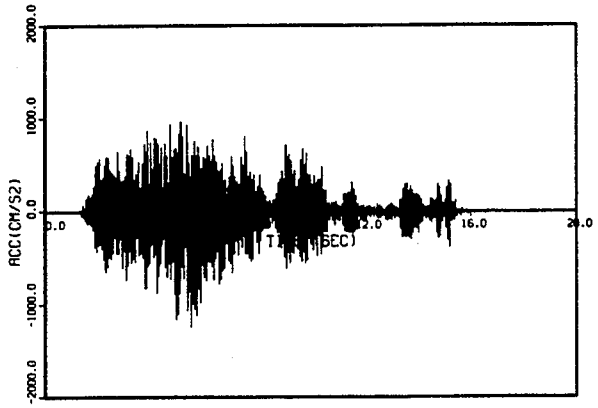

Figure E.13 FA8-Y

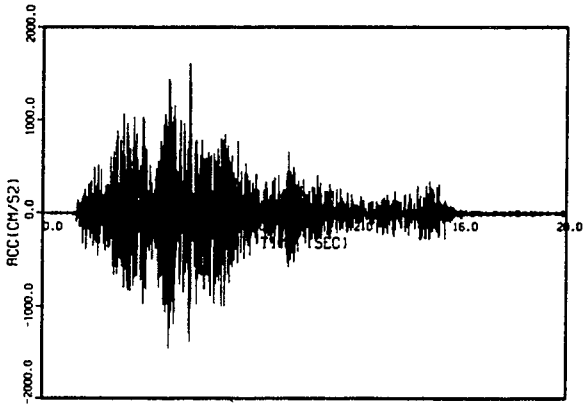

Figure E.14 FA8-Z

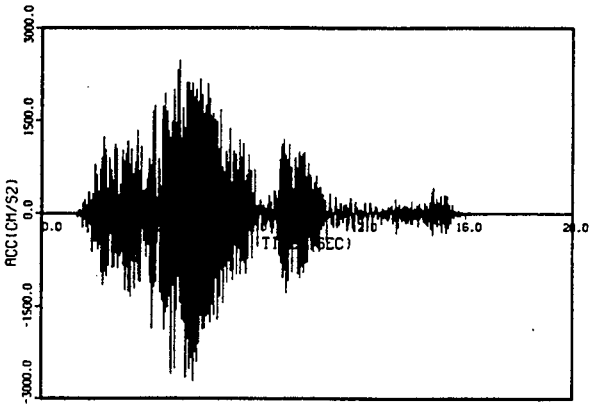

Figure E.15 FA10-X

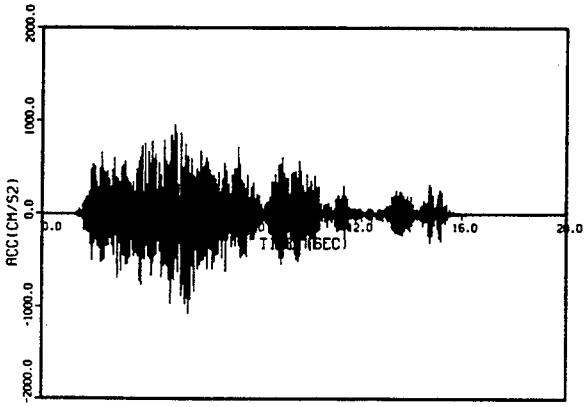

Figure E.16 FA10-Y

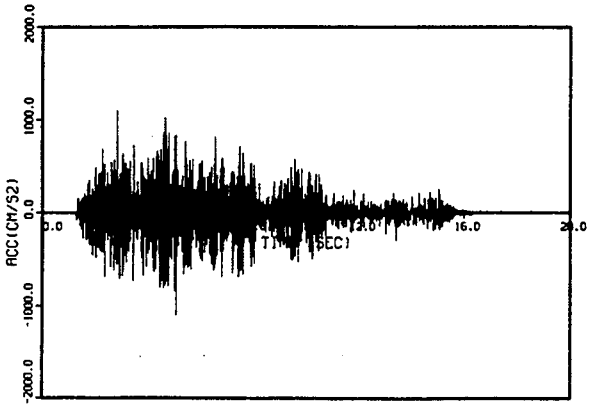

Figure E.17 FA10-Z

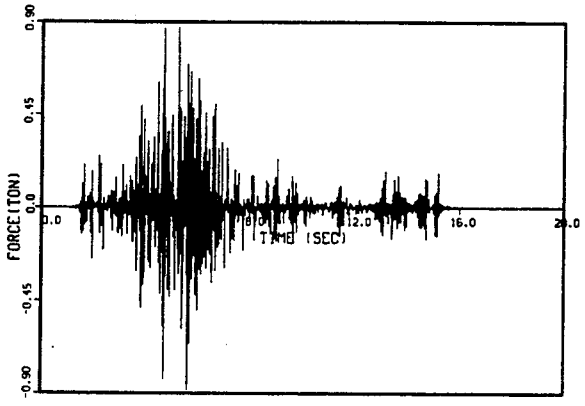

Figure E.18 FR-Z

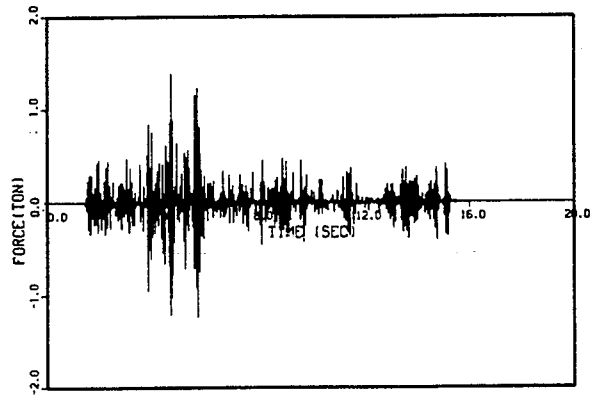

Figure E.19 FR3

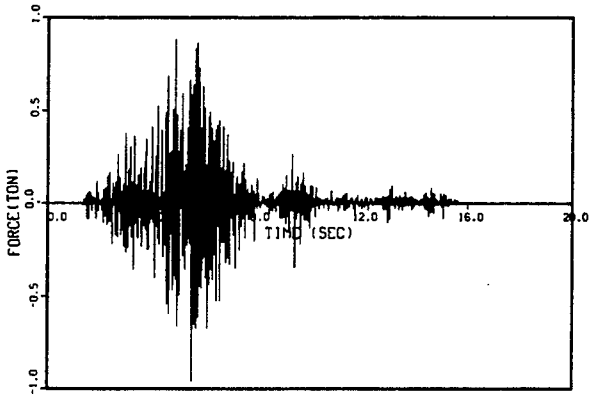

Figure E.20 FR4

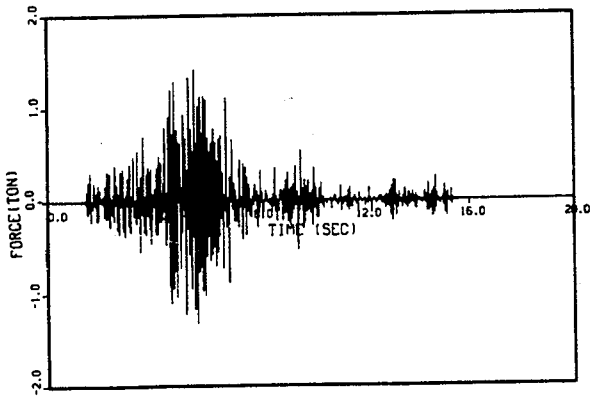

Figure E.21 FR5

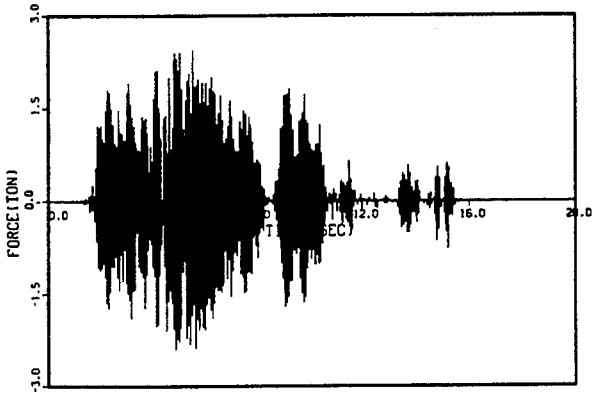

Figure E.22 FR6

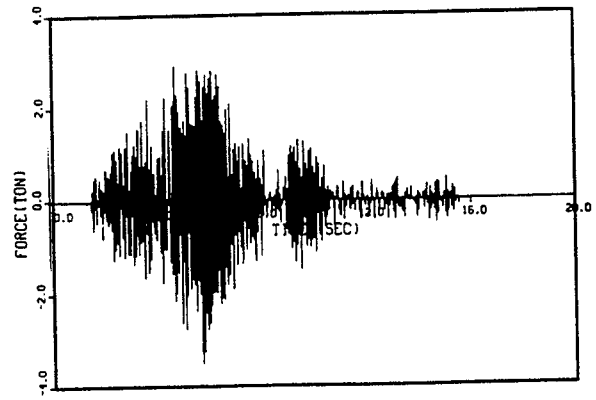

Figure E.23 FR7

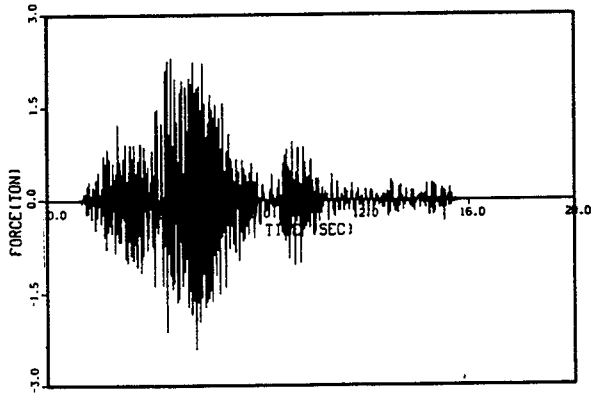

Figure E.24 FR8

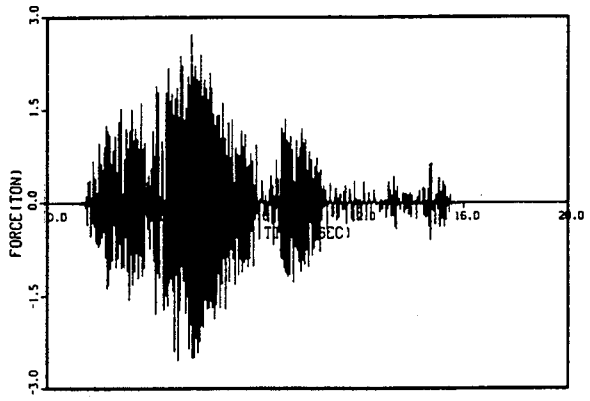

Figure E.25 FR9

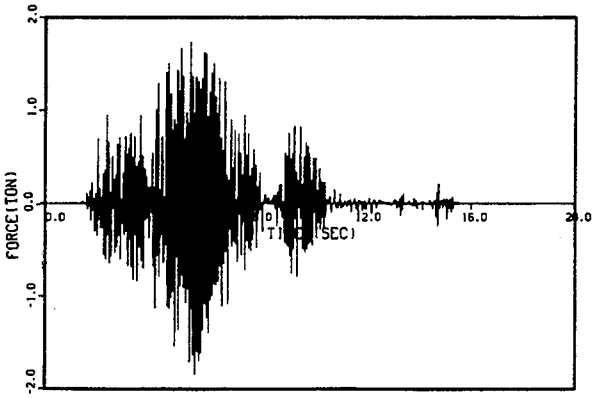

Figure E.26 FR10

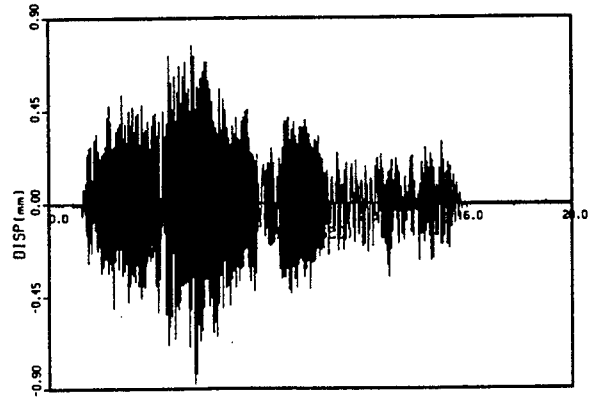

Figure E.27 FD7a

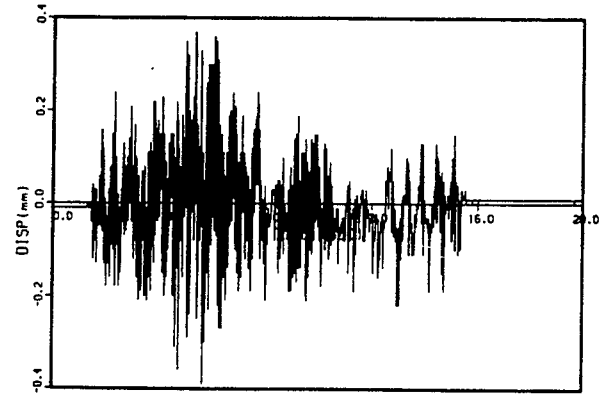

Figure E.28 FD7b

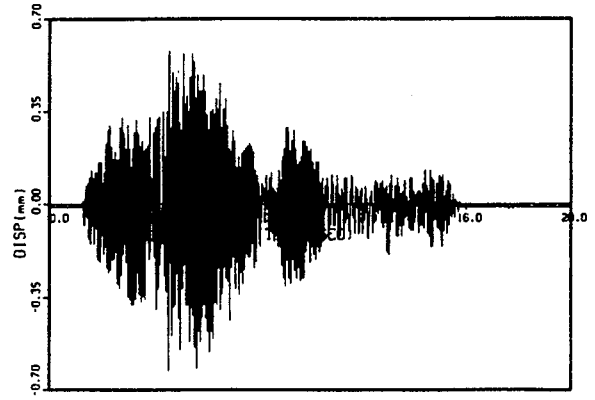

Figure E.29 FD8a

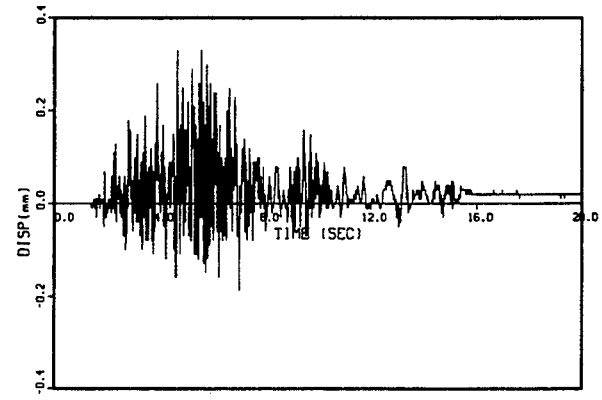

Figure E.30 FD8b

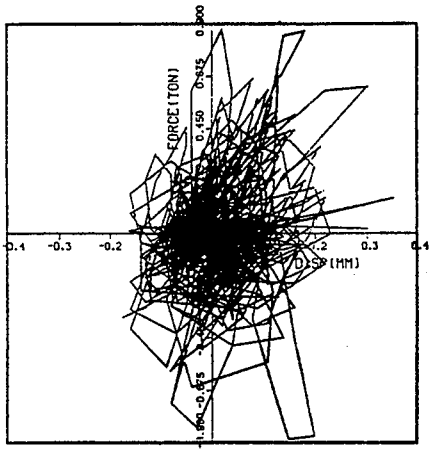

Figure E.31 FD2b-FR2

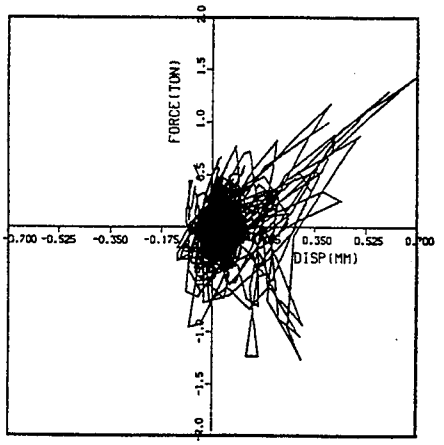

Figure E.32 FD3b-FR3

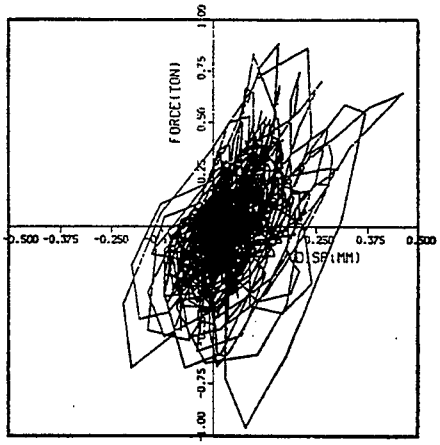

Figure E.33 FD4b-FR4

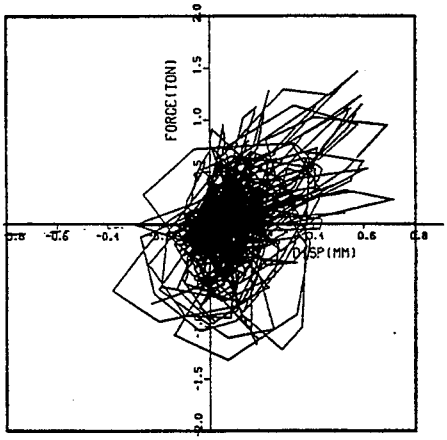

Figure E.34 FD5b-FR5

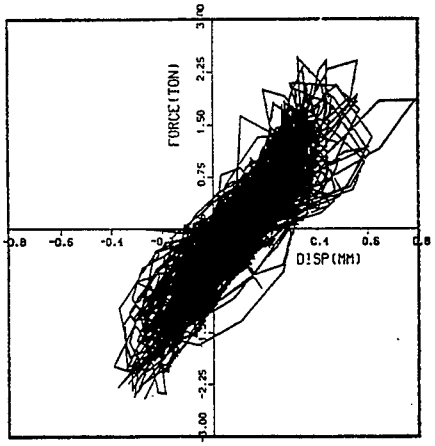

Figure E.35 FD6b-FR6

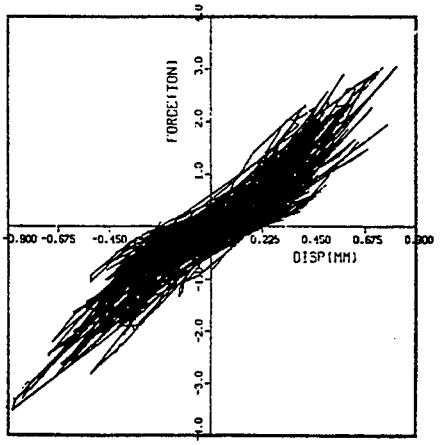

Figure E.36 FD7a-FR7

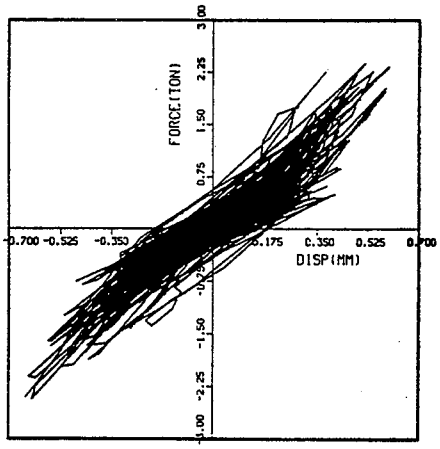

Figure E.37 FD8a-FR8

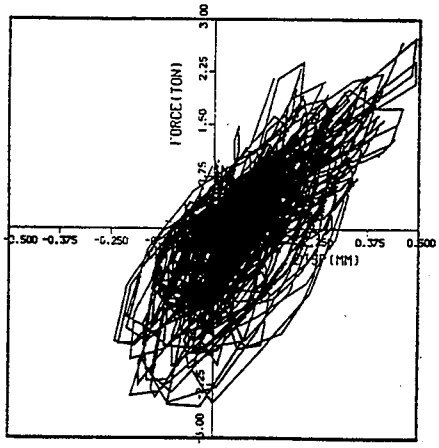

Figure E.38 FD9b-FR9

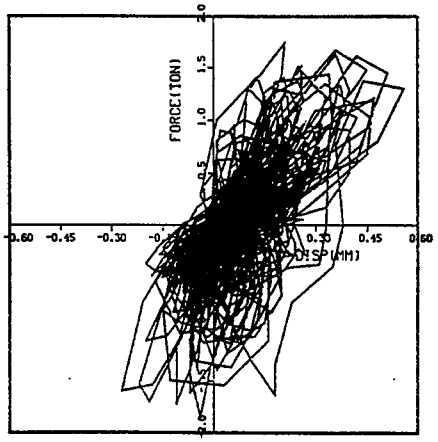

Figure E.39 FD10b-FR10

APPENDIX F

LIST OF PEAK RESPONSE VALUES AND PLOTS OF SELECTED CHANNELS FOR 3/3 S_2 (M) TEST RUN (RUN NO. 94120505)

Table F.1 List of Recorded Peak Values for M-line with Conventional Supports

		VC-04	VC-05	VC-06	VC-11	VC-12	VC-13	
	Targ. accel.	497+113	993+226	1490+340	293+68	570+133	863+202	
	Test no.	941202-03	941202-07	941205-05	941206-03	941206-05	941206-09	
Sensor	S/G CH	1/3S2(H+V)	2/3S2(H+V)	3/3S2(H+V)	1/3S1(H+V)	2/3S1(H+V)	3/3S1(H+V)	Unit
S/GT model	No.	S/G nonl.	S/G nonl.	S/G nonl.	S/G nonl.	S/G nonl.	S/G nonl.	
AA1-X	1-1-2	1771	3430	4938	867	1697	2601	GAL
AA1-Y	1-1-1	107	165	264	66	116	182	GAL
AA1-Z	1-1-3	189	296	395	115	223	272	GAL
AA2-X	1-1-4	562	1076	1654	313	643	988	GAL
AA2-Y	1-1-5	98	156	180	41	74	123	GAL
AA2-Z	1-1-6	143	252	395	93	135	194	GAL
AD1-X	1-1-7	0.93	1.77	2.46	0.57	0.98	1.44	mm
AD1-Y	1-1-8	0.03	0.03	0.06	0.02	0.02	0.03	mm
AD1-Z	1-1-9	0.07	0.14	0.19	0.06	0.09	0.11	mm
AS1	1-1-10	4540	8100	10200	2220	4500	6200	KGF
AS2	1-1-11	4120	7290	9070	2010	4100	5650	GAL
SA2-X	1-1-12	530	1037	1576	294	564	898	GAL
SA2-Z	1-1-13	133	259	393	67	151	217	GAL
SA3-X	1-1-14	523	1023	1547	297	570	883	GAL
DSP-ACC	1-1-15	1093	2111	3129	603	1093	1734	GAL
DSP-DSP	1-2-1	0.79	1.56	2.33	0.46	0.87	1.33	mm
SA1-X	1-2-2	514	1021	1527	285	554	879	GAL
SA1-Z	1-2-3	163	262	417	82	147	205	GAL
MA1-X	3-3-10	2240	4190	5917	1180	2035	3198	GAL
MA1-Y	3-3-11	1549	3308	3987	980	2253	2312	GAL
MA1-Z	3-3-12	916	1470	1689	723	1151	1345	GAL
MA2-X	3-3-13	2203	3699	4735	1200	2203	3042	GAL
MA2-Y	3-3-14	1394	2111	2421	881	1663	1834	GAL
MA2-Z	3-3-15	1007	1728	2070	791	1116	1582	GAL
MA3-X	3-4-1	2275	2840	3720	1993	2458	2957	GAL
MA3-Y	3-4-2	791	1052	1369	617	989	1108	GAL
MA3-Z	3-4-3	883	1285	1614	699	980	1422	GAL
MA4-X	3-4-4	1790	2414	3085	1487	1934	2446	GAL
MA4-Y	3-4-5	409	819	1212	352	582	737	GAL
MA4-Z	3-4-6	753	1186	1445	589	701	987	GAL
MA5-X	3-4-7	1311	2105	2990	1000	1319	1713	GAL
MA5-Y	3-4-8	507	924	1169	474	605	761	GAL
MA6-X	3-4-9	883	1533	1983	742	975	1333	GAL
MA6-Y	3-4-10	630	975	1114	565	631	893	GAL
MA7-X	3-4-11	474	930	1470	263	527	834	GAL
MA7-Z	3-4-12	145	256	406	81	154	210	GAL
MA8-X	3-4-13	985	1611	2111	584	918	1202	GAL
MA8-Y	3-4-14	682	963	1285	578	803	900	GAL
MA8-Z	3-4-15	849	1435	1798	874	1056	1336	GAL
MA9-X	4-1-1	513	951	1423	265	521	811	GAL
MA9-Y	4-1-2	65	98	114	33	66	82	GAL
MA9-Z	4-1-3	136	264	375	68	145	222	GAL
MA10-X	4-1-4	1015	1958	2332	626	967	1211	GAL
MA10-Y	4-1-5	150	285	333	111	198	238	GAL
MA10-Z	4-1-6	461	609	930	362	544	741	GAL
MA11-X	4-1-7	447	941	1435	261	549	850	GAL
MA11-Y	4-1-8	175	247	282	86	150	180	GAL
MA11-Z	4-1-9	118	223	333	72	143	198	GAL
MA12-X	4-1-10	549	1028	1495	292	619	933	GAL
MA-12-Y	4-1-11	153	266	288	92	162	197	GAL
MA12-Z	4-1-12	153	259	409	101	180	255	GAL

Table F.1 List of Recorded Peak Values for M-line with Conventional Supports (Cont'd)

		VC-04	VC-05	VC-06	VC-11	VC-12	VC-13	
MA13-X	4-1-13	633	1472	1694	325	657	989	GAL
MA13-Y	4-1-14	259	435	687	122	290	336	GAL
MA13-Z	4-1-15	266	625	708	167	333	475	GAL
MA14-X	4-2-1	1086	2226	3295	579	1192	1665	GAL
MA14-Y	4-2-2	846	838	1305	419	798	1007	GAL
MA14-Z	4-2-3	158	308	442	134	234	292	GAL
MA15-X	4-2-4	600	1309	2013	272	717	1244	GAL
MA15-Y	4-2-5	329	574	810	165	311	450	GAL
MA15-Z	4-2-6	206	336	639	118	257	366	GAL
MD1a	4-2-7	0.62	1.04	1.35	0.58	0.73	0.89	mm
MD2a	4-2-8	0.82	1.22	1.56	0.51	0.82	1.06	mm
MD3b-Z	4-2-9	0.53	0.74	0.88	0.5	0.61	0.66	mm
MD4b-Z	4-2-10	0.58	0.83	0.94	0.59	0.64	0.7	mm
MD5a	4-2-11	0.57	0.69	0.77	0.55	0.61	0.63	mm
MD5b	4-2-12	0.61	0.66	0.76	0.53	0.64	0.68	mm
MD6a	4-2-13	0.53	0.78	0.85	0.6	0.64		mm
MD6b	4-2-14	0.35	0.5	0.64	0.24	0.38	0.44	mm
MD7a-X	4-2-15	0.3	0.54	0.67	0.26	0.34	0.42	mm
MD7b-X	4-3-1	0.18	0.3	0.31	0.1	0.23	0.25	mm
MD8-X	4-3-2	0.91	1.13	1.28	0.88	1.01	1.04	mm
MD8-Y	4-3-3	0.18	0.44	0.54	0.15	0.25	0.3	mm
MD8-Z	4-3-4	0.41	0.65	0.93	0.36	0.51	0.65	mm
MD9-Y	4-3-5	0.09	0.1	0.14	0.05	0.09	0.1	mm
MD10-Z	4-3-6	0.08	0.15	0.23	0.05	0.14	0.16	mm
MD11-X	4-3-7	0.09	0.23	0.33	0.05	0.1	0.16	mm
MR1 (6T)	4-3-8	1572	3726	5221	909	1863	2972	KGF
MR2 (6T)	4-3-9	1685	4213	6812	373	1653	4188	KGF
MR3 (3T)	4-3-10	631	1082	1465	409	712	999	KGF
MR4 (3T)	4-3-11	590	1080	1412	445	622	1064	KGF
MR5 (10T)	4-3-12	1278	1634	2505	874	1312	1637	KGF
MR6 (10T)	4-3-13	1697	2568	3271	1316	1942	2692	KGF
MR7 (6T)	4-3-14	275	838	1551	180	360	700	KGF
MR8	4-3-15	106	148	430	86	98	128	KGF
MR9a	4-4-1	386	635	1078	326	624	637	KGF
MR9b	4-4-2	471	854	1103	362	443	598	KGF
MR10a	4-4-3	152	271	327	67	122	184	KGF
MR10b	4-4-4	380	566	976	407	563	628	KGF
MR11 (0.3T)	4-4-5	13	17	23	5	14	16	KGF
MR12 (0.3T)	4-4-6	7	18	28	5	9	15	KGF
MR13	4-4-7	21	37	54	14	27	28	KGF
MR14	4-4-8	72	139	213	49	74	130	KGF
MP1	4-4-9	1.1	1.49	1.61	0.78	0.9	1.42	KG/CM2
MP2	4-4-10	1.19	1.38	1.58	0.79	0.99	1.32	KG/CM2
S0-0	4-4-11	0.5	0.76	0.89	0.37	0.52	0.72	KG/mm2
S0-90	4-4-12	0.39	1.04	1.5	0.3	0.56	0.72	KG/mm2
S0-180	4-4-13	0.54	0.8	1.15	0.45	0.56	0.71	KG/mm2
S0-270	4-4-14	0.54	1.3	1.6	0.3	0.69	0.8	KG/mm2
S1-0	4-4-15	0.06	0.11	0.17	0.06	0.07	0.09	KG/mm2
S1-0	5-1-1	0.26	0.67	0.98	0.28	0.33	0.48	KG/mm2
S1-90	5-1-2	0.58	1.47	1.86	0.5	0.74	0.98	KG/mm2
S1-90	5-1-3	0.48	1.13	1.43	0.39	0.52	0.82	KG/mm2
S1-180	5-1-4	0.33	0.82	0.97	0.3	0.41	0.56	KG/mm2
S1-180	5-1-5	0.5	1.24	1.62	0.43	0.59	0.84	KG/mm2
S1-270	5-1-6	0.63	1.3	1.58	0.59	0.69	0.8	KG/mm2
S1-270	5-1-7	0.54	1.37	1.76	0.45	0.61	0.87	KG/mm2
S2-0	5-1-8	0.39	0.76	1.41	0.33	0.35	0.58	KG/mm2
S2-90	5-1-9	0.48	1.1	1.34	0.33	0.58	0.71	KG/mm2

Table F.1 List of Recorded Peak Values for M-line with Conventional Supports (Cont'd)

		VC-04	VC-05	VC-06	VC-11	VC-12	VC-13	
S2-180	5-1-10	0.39	0.76	1.62	0.37	0.43	0.74	KG/mm2
S2-270	5-1-11	0.54	1.28	1.63	0.35	0.69	0.76	KG/mm2
S3-0	5-1-12	0.06	0.07	0.09	0.04	0.04	0.06	KG/mm2
S3-0	5-1-13	0.37	.1	1.41	0.28	0.41	0.59	KG/mm2
S3-90	5-1-14	0.26	0.63	0.87	0.28	0.32	0.41	KG/mm2
S3-90	5-1-15	0.59	1.43	1.99	0.45	0.58	0.97	KG/mm2
S3-180	5-2-1	0.41	0.97	1.41	0.19	0.45	0.78	KG/mm2
S3-180	5-2-2	0.61	1.6	2.3	0.43	0.71	1.06	KG/mm2
S3-270	5-2-3	0.41	0.82	1.13	0.39	0.46	0.56	KG/mm2
S3-270	5-2-4	0.46	1.19	1.63	0.35	0.41	0.71	KG/mm2
S4-0	5-2-5	0.52	1.04	1.37	0.41	0.59	0.85	KG/mm2
S4-90	5-2-6	0.41	0.58	0.74	0.37	0.43	0.63	KG/mm2
S4-180	5-2-7	0.52	0.84	1.28	0.43	0.61	0.8	KG/mm2
S4-270	5-2-8	0.33	0.52	0.67	0.35	0.43	0.54	KG/mm2
S5-0	5-2-9	0.04	0.07	0.07	0.04	0.06	0.07	KG/mm2
S5-90	5-2-10	0.39	0.69	1.02	0.35	0.43	0.63	KG/mm2
S5-180	5-2-11	0.2	0.32	0.41	0.17	0.28	0.26	KG/mm2
S5-270	5-2-12	0.3	0.52	0.78	0.18	0.33	0.45	KG/mm2
S6-0	5-2-13	0.58	0.85	1.05	0.58	0.82	0.85	KG/mm2
S6-90	5-2-14	0.74	1.1	1.52	0.56	0.69	0.85	KG/mm2
S6-180	5-2-15	0.58	0.84	1.06	0.54	0.82	0.84	KG/mm2
S6-270	6-3-1	0.69	1.02	1.41	0.58	0.67	0.87	KG/mm2
S80-	5-3-2	0.37	0.46	0.56	0.3	0.37	0.48	KG/mm2
S8-90	5-3-3	0.32	0.37	0.5	0.28	0.33	0.33	KG/mm2
S8-180	5-3-4	0.24	0.39	0.5	0.24	0.3	0.3	KG/mm2
S8-270	5-3-5	0.54	0.69	0.8	0.39	0.5	0.59	KG/mm2
S9-0	5-3-6	0.32	0.43	0.61	0.37	0.37	0.46	KG/mm2
S9-90	5-3-7	0.3	0.54	0.56	0.3	0.37	0.43	KG/mm2
S9-180	5-3-8	0.3	0.48	0.61	0.45	0.41	0.46	KG/mm2
S9-270	5-3-9	0.35	0.48	0.63	0.39	0.39	0.48	KG/mm2
S11-0	5-3-10	0.17	0.22	0.32	0.15	0.17	0.24	KG/mm2
S11-90	5-3-11	0.28	0.56	0.74	0.2	0.28	0.39	KG/mm2
S11-180	5-3-12	0.15	0.26	0.33	0.09	0.19	0.22	KG/mm2
S11-270	5-3-13	0.3	0.6	0.89	0.2	0.35	0.48	KG/mm2
S12-0	5-3-14	0.19	0.41	0.63	0.15	0.2	0.32	KG/mm2
S12-90	5-3-15	0.13	0.2	0.32	0.09	0.13	0.19	KG/mm2
S12-180	5-4-1	0.45	0.87	1.13	0.24	0.45	0.69	KG/mm2
S12-270	5-4-2	0.13	0.24	0.28	0.13	0.15	0.15	KG/mm2
S2' -0	5-4-3	0.22	0.45	0.48	0.15	0.24	0.37	KG/mm2
S2' -90	5-4-4	0.22	0.32	0.5	0.19	0.26	0.28	KG/mm2
S2' -180	5-4-5	0.54	0.78	0.93	0.35	0.52	0.76	KG/mm2
S2' -270	5-4-6	0.2	0.32	0.46	0.2	0.28	0.32	KG/mm2
S2' NEG	5-4-7	0.19	0.41	0.46	0.12	0.18	0.23	KG/mm2
S11' -0	5-4-8	0.19	0.32	0.46	0.13	0.24	0.33	KG/mm2
S11' -90	5-4-9	0.45	0.93	1.28	0.3	0.52	0.72	KG/mm2
S11' -180	5-4-10	0.22	0.33	0.5	0.15	0.26	0.33	KG/mm2
S11' -270	5-4-11	0.52	1.11	1.47	0.32	0.54	0.78	KG/mm2
S10-0	5-4-12	0.14	0.22	0.28	0.14	0.15	0.2	KG/mm2
S10-90	5-4-13	0.23	0.51	0.61	0.18	0.28	0.36	KG/mm2
S13-180 X	5-4-14	0.21	0.4	0.7	0.14	0.36	0.47	KG/mm2
S13-270 Y	5-4-15	0.11	0.1	0.11	0.06	0.09	0.11	KG/mm2
501X (XO)	6-1-3	509	999	1496	277	564	875	GAL
501Z (ZO)	6-1-4	114	230	345	66	134	189	GAL
PT	6-1-14	59	112	186	33	71	113	GAL
RL	6-1-15	26	51	66	18	32	39	GAL
YW	6-2-1	54	100	154	33	36	91	GAL

Table F.1 List of Recorded Peak Values for M-line with Conventional Supports (Cont'd)

		VC-04	VC-05	VC-06	VC-11	VC-12	VC-13	
ZD2-1	6-2-10	168	318	492	81	176	250	GAL
ZD2-2	6-2-11	137	240	377	75	142	216	GAL
ZD2-3	6-2-12	175	262	357	97	200	272	GAL
ZD2-4	6-2-13	139	264	421	72	150	213	GAL
ZD2-5	6-2-14	125	235	330	74	151	208	GAL
ZD2-6	6-2-15	137	276	418	80	158	225	GAL
ZD2-7	6-3-1	132	235	365	77	158	238	GAL
YD1-W	6-3-2	33	53	88	19	38	59	GAL
YD2-E	6-3-3	41	78	124	24	53	83	GAL
ZD2-10	6-3-4	127	245	367	85	159	235	GAL
ZD2-11	6-3-5	132	262	384	72	144	218	GAL
ZD2-12	6-3-6	133	274	396	85	182	255	GAL
701X (XB)	6-3-11	530	1036	1553	291	573	902	GAL
701Z (XB)	6-3-12	130	259	384	70	133	191	GAL

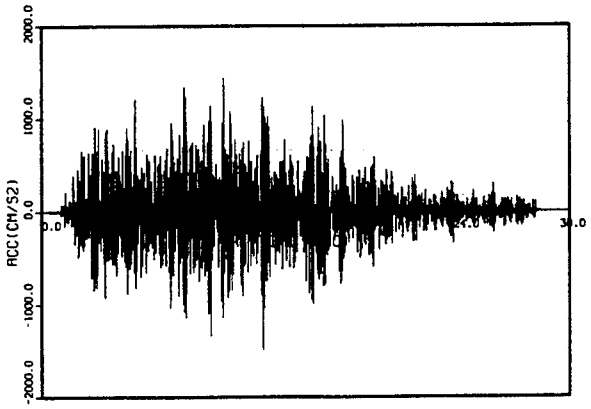

Figure F.1 XOXB

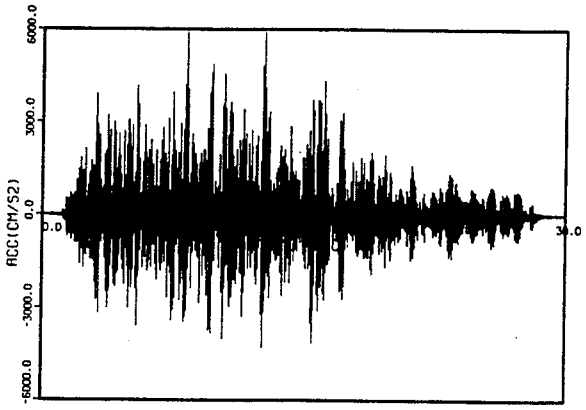

Figure F.2 MA1-X

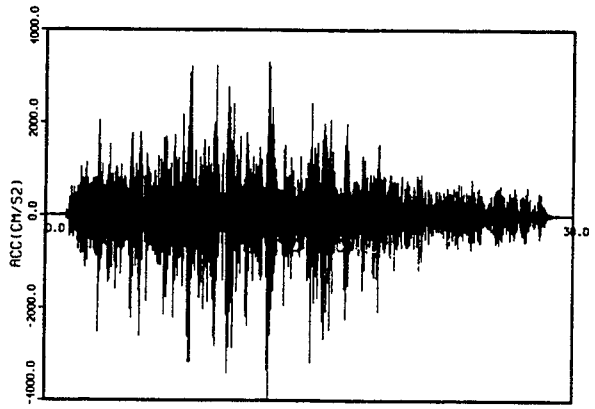

Figure F.3 MA1-Y

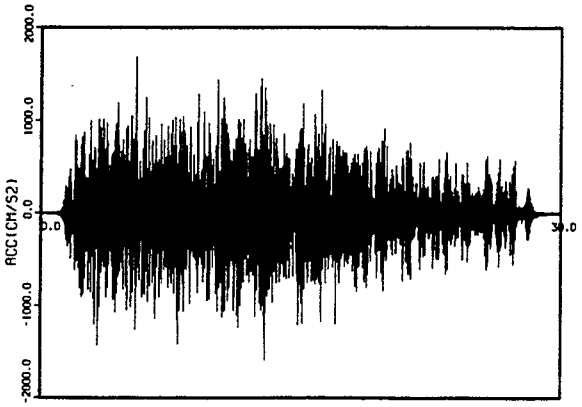

Figure F.4 MA1-Z

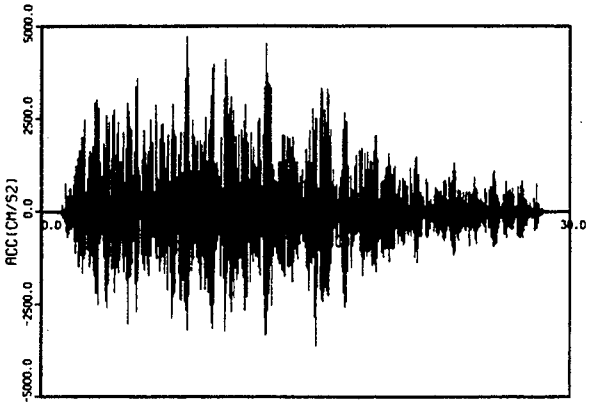

Figure F.5 MA2-X

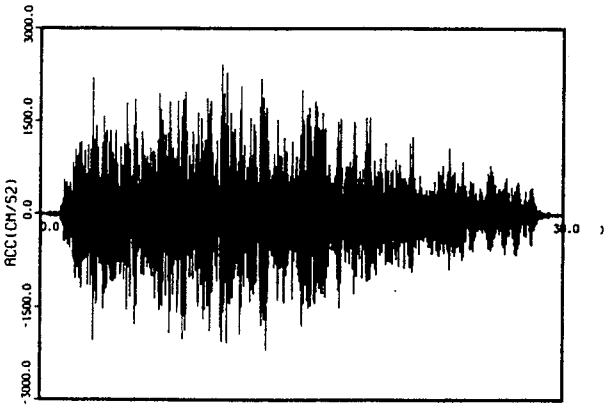

Figure F.6 MA2-Y

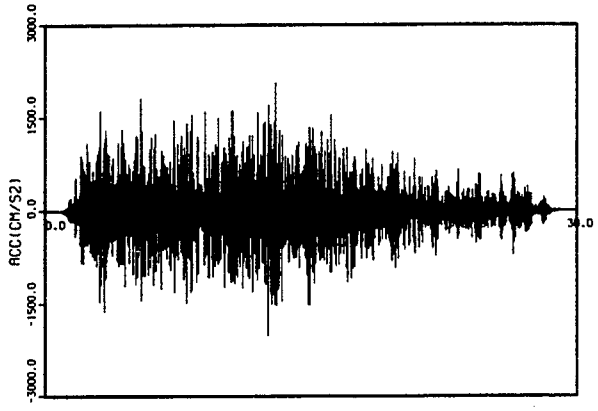

Figure F.7 MA2-Z

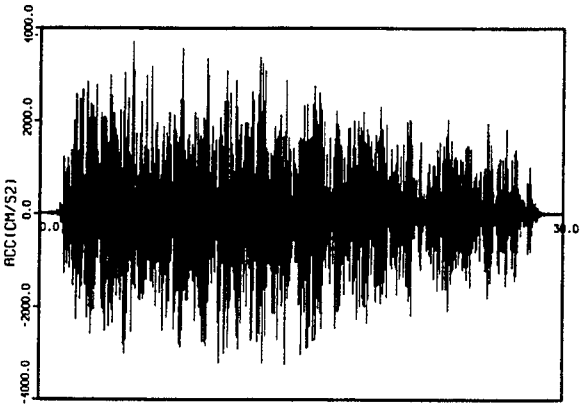

Figure F.8 MA3-X

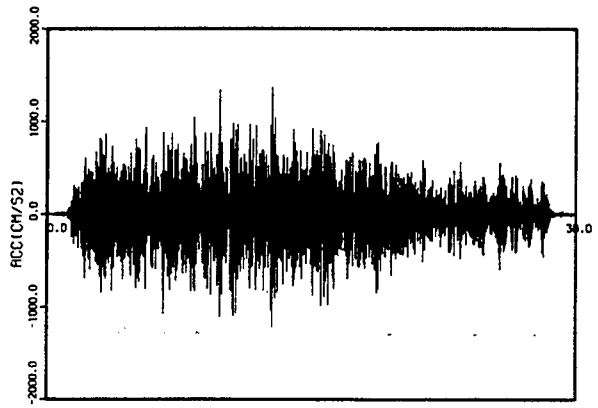

Figure F.9 MA3-Y

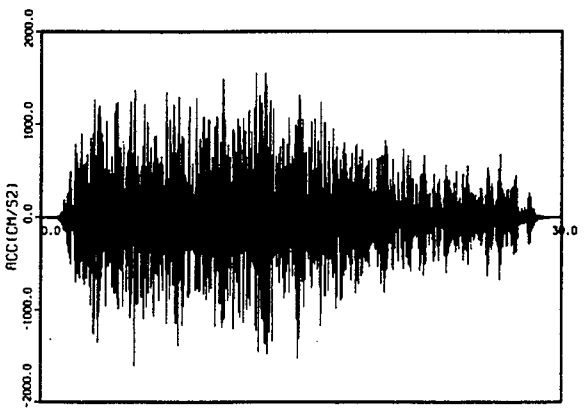

Figure F.10 MA3-Z

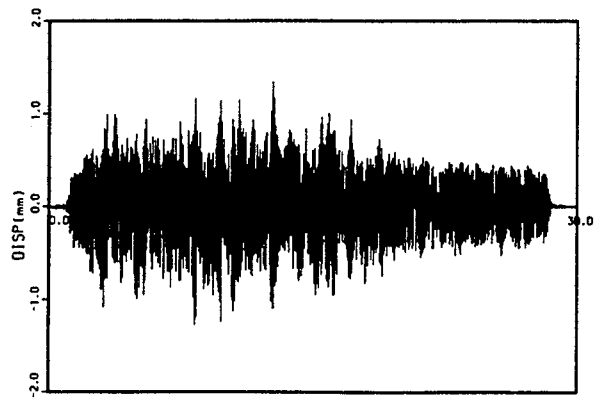

Figure F.11 MD1a

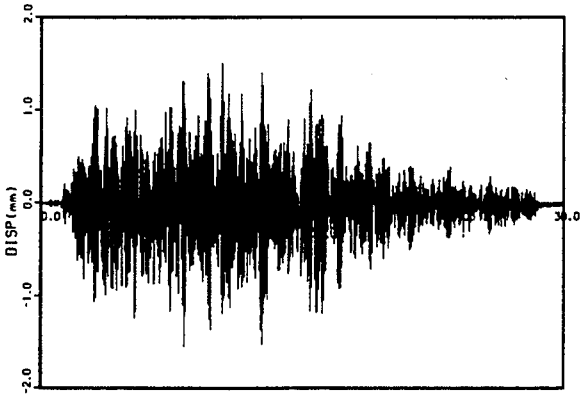

Figure F.12 MD2a

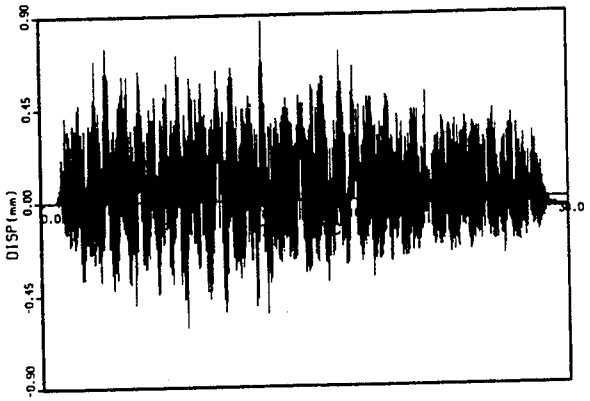

Figure F.13 MD3b

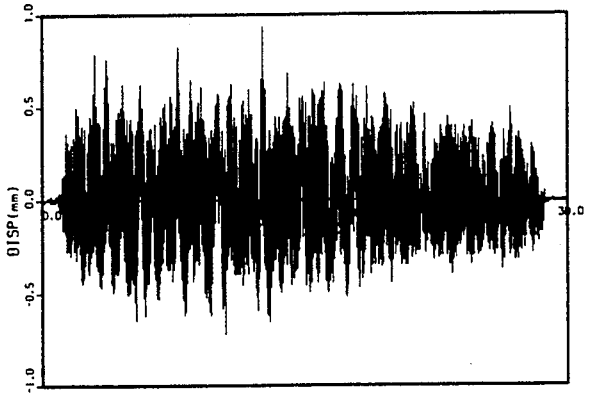

Figure F.14 MD4b

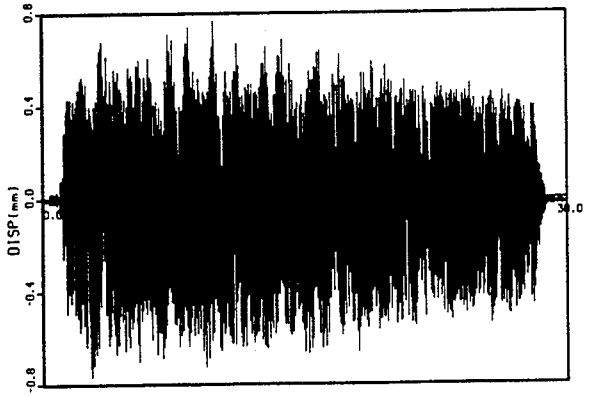

Figure F.15 MD5a

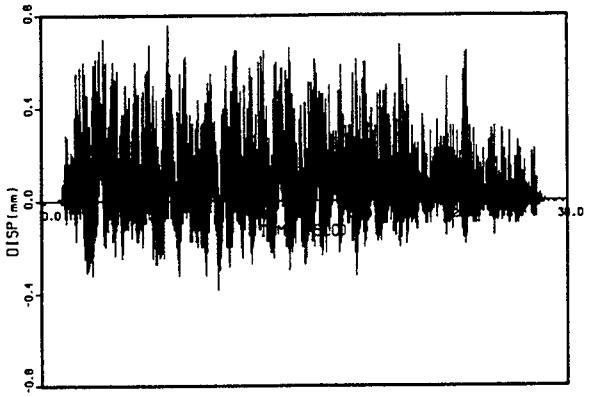

Figure F.16 MD5b

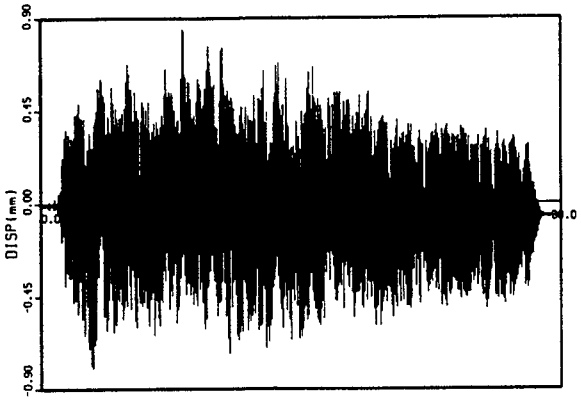

Figure F.17 MD6a

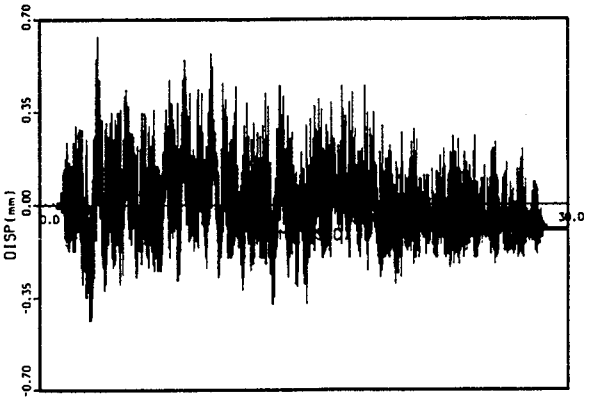

Figure F.18 MD6b

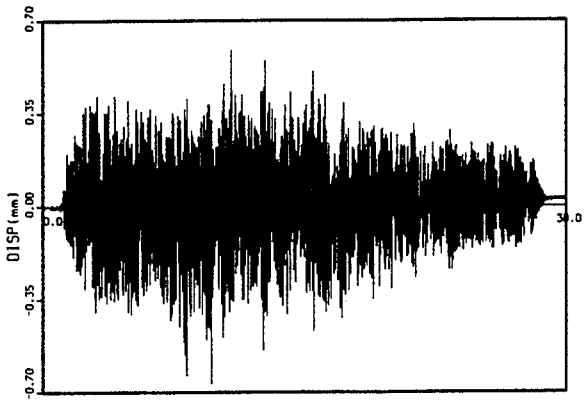

Figure F.19 MD7a

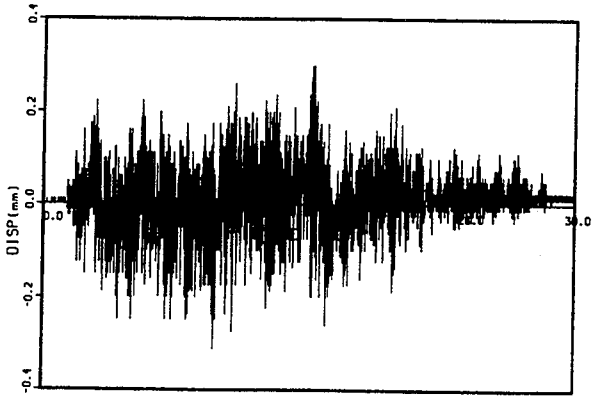

Figure F.20 MD7b

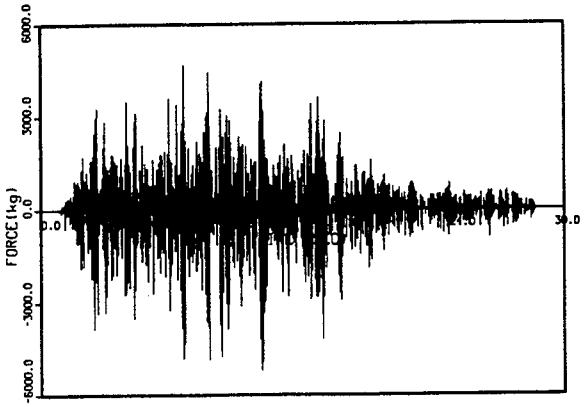

Figure F.21 MR1

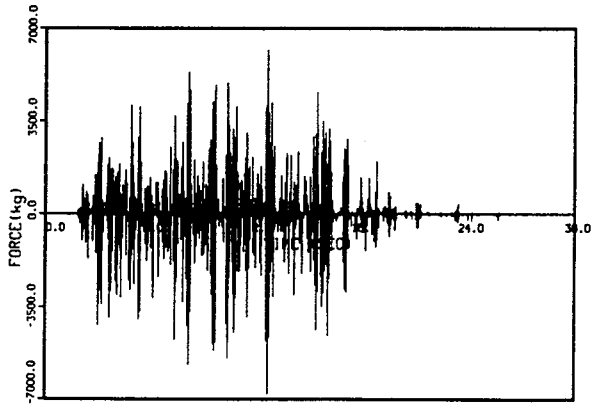

Figure F.22 MR2

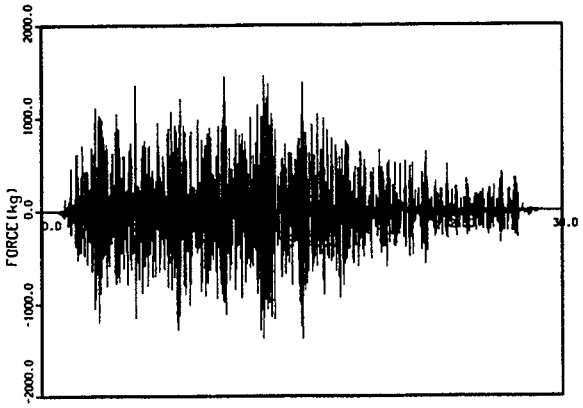

Figure F.23 MR3

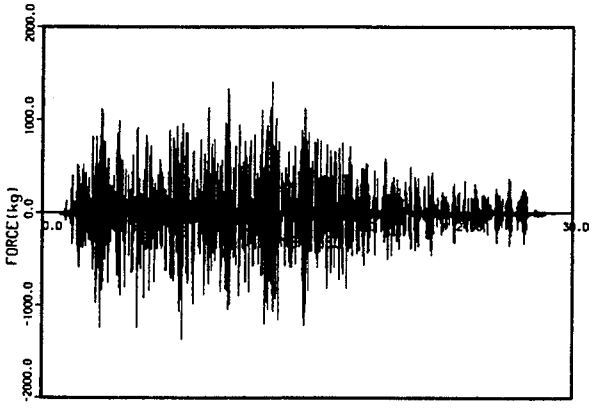

Figure F.24 MR4

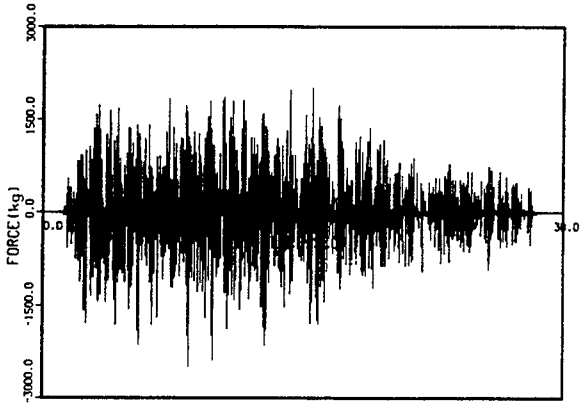

Figure F.25 MR5

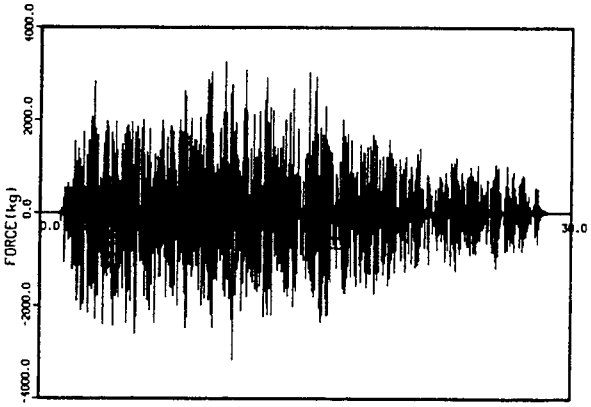

Figure F.26 MR6

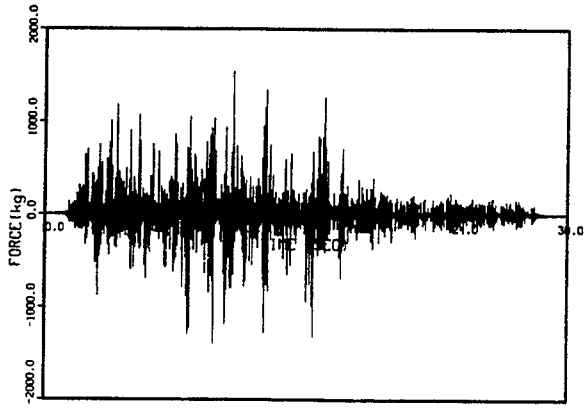

Figure F.27 MR7

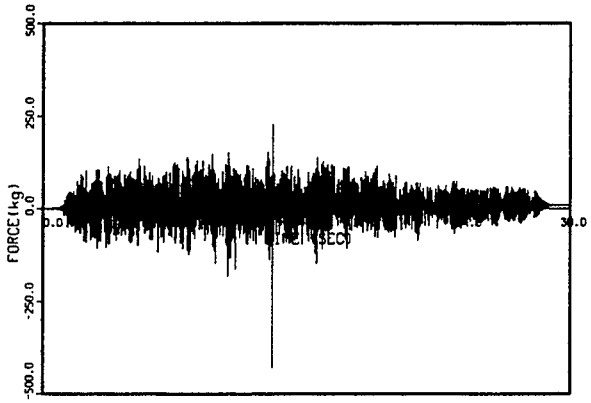

Figure F.28 MR8

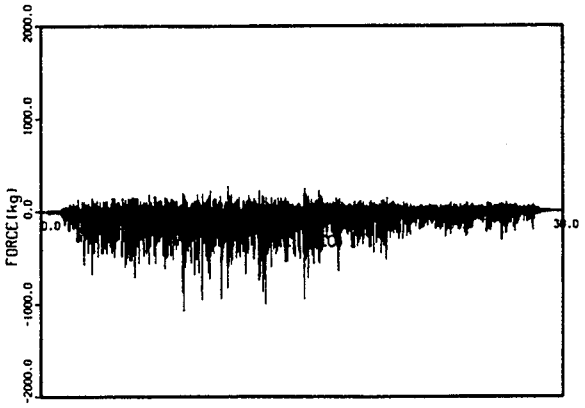

Figure F.29 MR9a

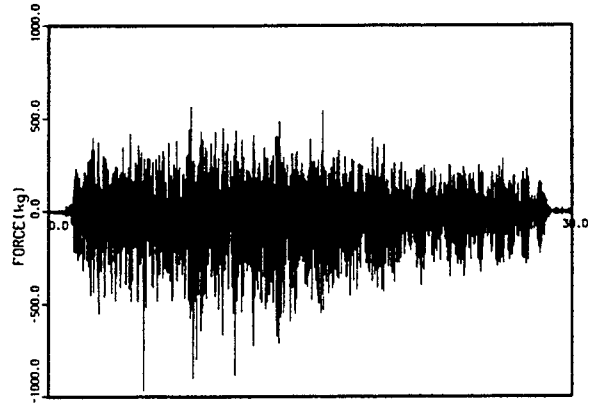

Figure F.30 MR10b

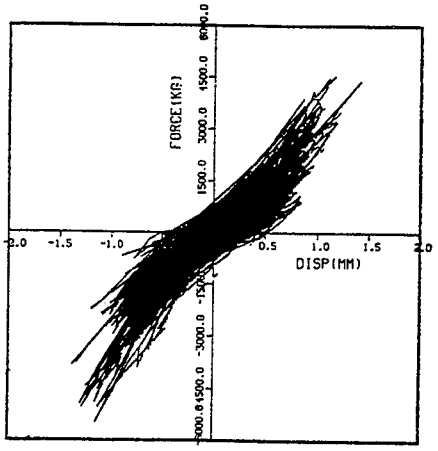

Figure F.31 MD1a-MR1

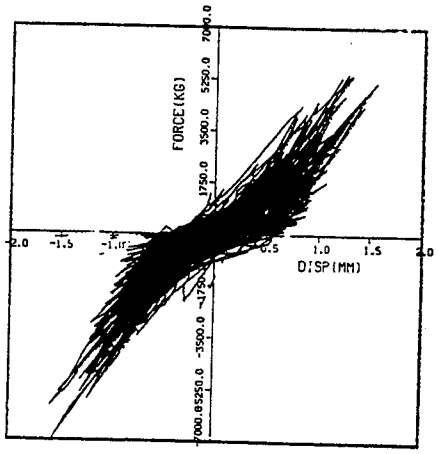

Figure F.32 MD2a-MR2

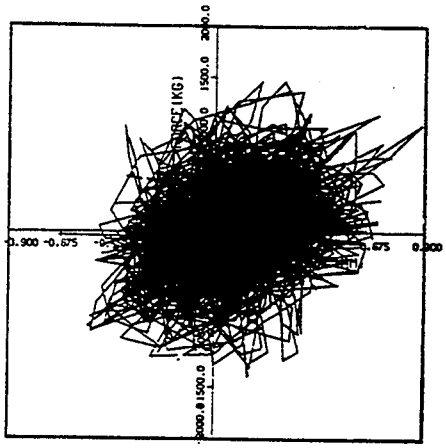

Figure F.33 MD3b-MR3

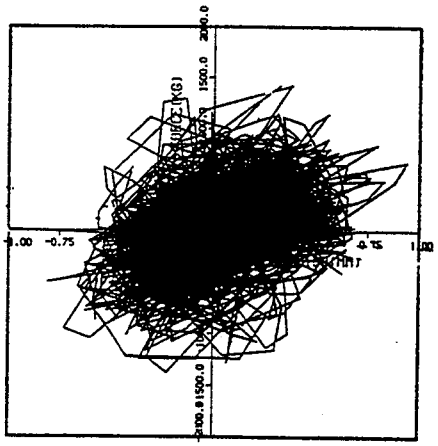

Figure F.34 MD4b-MR4

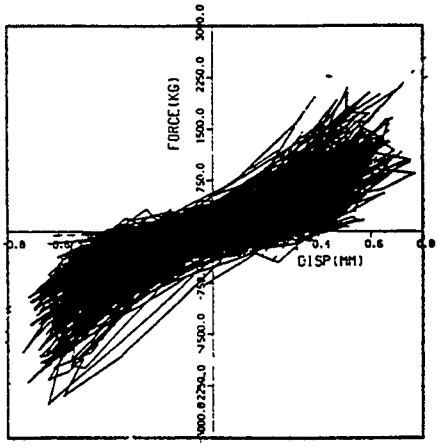

Figure F.35 MD5a-MR5

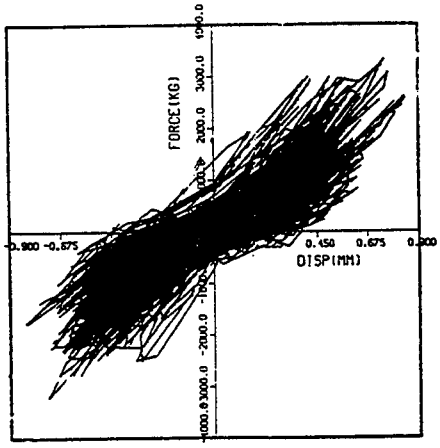

Figure F.36 MD6a-MR6

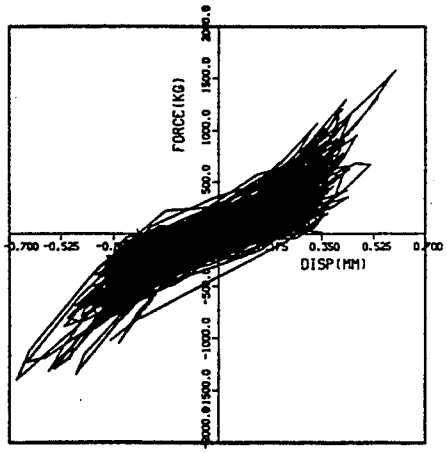

Figure F.37 MD7a-MR7

APPENDIX G

LIST OF PEAK RESPONSE VALUES AND PLOTS OF SELECTED CHANNELS FOR S_2 (A) (F-LINE) TEST RUN (RUN NO. 95051202)

Table G.1 List of Recorded Peak Values for F-line with EAB Supports

Item	1/3S2(A)	2/3S2(A)	3/3S2(A)	1/3S1(A)	2/3S11(A)	3/3S1(A)	
Test no.	DE1-1	DE1-2	DE1-3	DE1-4	DE1-5	DE1-6	
	95051504	95051502	95051202	95042504	95042103	95042106	
Targ. accel.(H+V)	496+113	993+227	1489+340	272+63	543+127	814+190	
Measured(H+V)	513+121	1055+247	1639+392	294+72	580+137	904+213	Unit
FA01X	450	926	1437	259	519	813	GAL
FA01Y	309	493	610	192	384	409	GAL
FA01Z	116	232	341	83	133	191	GAL
FA03X	1545	2225	3015	1008	1686	2261	GAL
FA03Y	221	316	401	128	247	264	GAL
FA03Z	903	1508	1763	732	1133	1431	GAL
FA04X	491	1000	1440	301	595	819	GAL
FA04Y	175	271	315	280	288	385	GAL
FA04Z	125	250	383	83	141	217	GAL
FA05X	1692	2356	2917	1131	1607	2092	GAL
FA05Y	376	475	606	213	417	426	GAL
FA05Z	1083	1727	2229	898	1269	1357	GAL
FA06X	2493	4155	4839	1921	2649	3376	GAL
FA06Y	1995	2744	3216	1355	1902	2147	GAL
FA06Z	1602	2450	3238	1212	1915	2094	GAL
FA07X	2574	3936	5099	1719	2732	3372	GAL
FA07Y	1141	1691	1939	686	1244	1389	GAL
FA07Z	1189	1730	2171	915	1630	1839	GAL
FA08X	2320	3600	4872	1679	2273	2868	GAL
FA08Y	760	1132	1253	708	907	1158	GAL
FA08Z	1599	2212	2897	1334	1956	2359	GAL
FA09X	1335	2254	2977	1199	1624	2322	GAL
FA09Y	857	1324	1540	709	1012	1316	GAL
FA09Z	1340	1644	2378	885	1357	1611	GAL
FA010X	1511	2304	3224	1429	2085	2341	GAL
FA010Y	855	1265	1487	659	1042	1408	GAL
FA010Z	1280	2166	2785	1117	1487	2080	GAL
FA011X	2215	3121	3985	1887	2659	3205	GAL
FA011Y	2097	2918	3677	1615	2142	2731	GAL
FA011Z	2009	2388	2996	1092	1877	2133	GAL
FA012X	2717	4124	5452	1870	2868	3608	GAL
FA012Y	1333	2092	2427	927	1668	1951	GAL
FA012Z	1376	2046	2101	844	1624	2083	GAL
FA013X	1794	2811	3605	1124	1731	2347	GAL
FA013Y	987	1378	1858	613	880	1103	GAL
FA013Z	2179	2565	3243	1124	2025	2351	GAL
AA02X	522	1052	1614	321	627	956	GAL
AA02Y	131	147	254	66	82	132	GAL
AA02Z	143	269	429	76	126	219	GAL
FS011	1.7	2.5	2.9	1.1	1.7	2.2	KG/mm2
FS012	1.9	2.9	4	1.3	2	2.7	KG/mm2
FS013	1.5	2.2	2.6	1.1	1.7	2.2	KG/mm2
FS014	2	3	4.3	1.4	2.2	2.8	KG/mm2
FS021	1.4	2.4	3.3	1	1.6	2	KG/mm2
FS022	1.8	3.4	4.4	1.2	1.9	2.7	KG/mm2
FS023	1.1	1.7	2.5	0.8	1.4	1.7	KG/mm2
FS024	1.9	3.4	4.5	1.2	2	2.7	KG/mm2
FS031	2.6	4.4	5.4	1.9	2.6	3.2	KG/mm2
FS032	2	3	4	1.5	2.3	2.8	KG/mm2
FS033	3.3	5.2	6.9	2.3	3.6	4.5	KG/mm2
FS034	1.1	1.5	2.2	0.7	1.1	1.5	KG/mm2
FS041	1.2	1.9	2.4	0.8	1.1	1.5	KG/mm2

Table G.1 List of Recorded Peak Values for F-line with EAB Supports (Cont'd)

	DE1-1	DE1-2	DE1-3	DE1-4	DE1-5	DE1-6	KG/mm2
FS042	4.8	7.2	9.5	2.9	4.2	5.9	KG/mm2
FS043	0.5	0.7	1	0.3	0.5	0.7	KG/mm2
FS044	1.8	2.7	3.8	1	1.6	2.5	KG/mm2
FS051	1.7	1.6	2.2	0.6	0.9	1.3	KG/mm2
FS052	0.9	1.1	1.6	0.8	1.2	1.4	KG/mm2
FS053	0.9	1.8	2.4	0.7	1	1.3	KG/mm2
FS054	0.9	1.4	1.8	0.6	1	1.5	KG/mm2
FS061	0.4	0.4	0.7	0.3	0.4	0.4	KG/mm2
FS062	2.1	3.6	5	1.7	2.5	3.2	KG/mm2
FS063	0.5	0.9	1.1	0.3	0.5	0.8	KG/mm2
FS064	1.4	2.4	2.9	1.1	1.8	2.6	KG/mm2
FS071	0.9	1.3	2	0.8	1	1.4	KG/mm2
FS072	1.1	2	3	1	1.6	2.3	KG/mm2
FS073	0.9	1.3	1.8	0.7	0.9	1.2	KG/mm2
FS074	1.4	2.3	3.5	1.3	2	2.9	KG/mm2
FS081	0.6	1	1.2	0.4	0.6	0.8	KG/mm2
FS082	0.3	0.4	0.7	0.2	0.3	0.4	KG/mm2
FS083	0.6	1	1.2	0.4	0.6	0.8	KG/mm2
FS084	0.3	0.4	0.6	0.2	0.3	0.4	KG/mm2
FS091	0.7	1.2	2	0.6	0.9	1.2	KG/mm2
FS092	2	3.1	5	1.5	2.5	3.3	KG/mm2
FS093	0.8	1.3	2.2	0.6	0.9	1.1	KG/mm2
FS094	2.8	5.1	8.5	2.4	3.6	4.4	KG/mm2
FS101	1	1.8	2.7	0.7	1.1	1.9	KG/mm2
FS102	2.1	2.9	3.8	1.2	1.8	2.4	KG/mm2
FS103	3	4.3	5.7	1.9	2.8	3.8	KG/mm2
FS104	1.3	1.8	2.4	0.7	1.1	1.4	KG/mm2
FS111	1.6	2.2	2.9	1	1.6	2.2	KG/mm2
FS112	2.3	3.8	5	1.5	2.4	3.5	KG/mm2
FS113	2	3.7	5.9	1.7	2.5	3.5	KG/mm2
FS114	2	3.4	4.6	1.3	2.2	3.1	KG/mm2
FS121	1.1	2.3	3.2	0.8	1.5	1.9	KG/mm2
FS122	1.5	2.6	3.6	1.1	1.9	2.7	KG/mm2
FS123	0.9	2	2.9	0.7	1.3	1.6	KG/mm2
FS124	0.7	1.2	1.8	0.6	0.9	1.2	KG/mm2
FS131	2.7	4.5	5.9	1.8	2.8	3.7	KG/mm2
FS132	3.2	5.3	6.9	2.2	3.7	4.6	KG/mm2
FS133	0.7	1.1	1	0.5	0.7	0.9	KG/mm2
FS134	3.3	5.5	7.1	2.3	3.8	4.6	KG/mm2
FS141	3.4	5.4	8.3	2.3	3.4	5.5	KG/mm2
FS142	3.7	6.4	8.8	2.6	4	6	KG/mm2
FS143	3.6	4.9	6.8	2.2	3.1	4.9	KG/mm2
FS144	4.1	6.8	8.7	2.7	4	5.8	KG/mm2
FS151	2.3	4.2	6	1.7	2.9	4	KG/mm2
FS152	0.9	1.4	1.8	0.7	1.3	1.6	KG/mm2
FS153	2.2	3.9	5.3	1.7	2.6	3.7	KG/mm2
FS154	1.3	2.2	2.7	0.9	1.7	2.4	KG/mm2
FS161	1.1	1.3	1.9	0.9	1.1	1.4	KG/mm2
FS162	0.9	1.3	1.4	0.8	1	1.1	KG/mm2
FS163	1	1.4	1.7	0.7	1.1	1.1	KG/mm2
FS164	0.8	1.4	1.9	0.8	1.1	1.5	KG/mm2
FS171	0.9	1.3	1.7	0.6	0.9	1.2	KG/mm2
FS172	2.8	5.5	8.2	2	3.5	5.4	KG/mm2
FS173	1.6	2.7	4.5	1.4	2.2	2.7	KG/mm2
FS174	2.7	5.5	8.2	2	3.5	5.5	KG/mm2
FS181	3.2	3.8	4.8	2.3	2.6	3.7	KG/mm2

Table G.1 List of Recorded Peak Values for F-line with EAB Supports (Cont'd)

		DE1-1	DE1-2	DE1-3	DE1-4	DE1-5	DE1-6
FS182	1.7	2.4	3.2	1.4	1.9	2.2	KG/mm2
FS183	3.5	4	5.2	2.5	2.9	3.9	KG/mm2
FS184	1.6	2.4	2.5	1.4	1.8	2	KG/mm2
FS191	2.1	3.4	5.7	1.6	2.9	3.5	KG/mm2
FS192	2.5	3.9	6.5	2	2.9	3.7	KG/mm2
FS193	1.6	2.6	4.1	1.2	2.2	2.8	KG/mm2
FS194	2.8	4.9	8.3	2.3	3.5	4.3	KG/mm2
FS201	1.4	2.1	3.1	0.9	1.7	2.1	KG/mm2
FS202	1.5	2.3	2.6	1	1.3	1.9	KG/mm2
FS203	1.8	2.5	3.3	1.1	2	2.8	KG/mm2
FS204	1.8	2.3	3.7	1.2	1.6	2.5	KG/mm2
FS211	1.3	1.9	2.7	0.9	1.2	1.8	KG/mm2
FS212	4	6.9	10.7	3.5	2.5	6.9	KG/mm2
FS213	2.9	4.6	7.3	2.4	3.6	4.4	KG/mm2
FS214	3.6	6.3	9.7	3.2	5	6.3	KG/mm2
FS221	3.9	5.2	6.9	2.5	3.5	5	KG/mm2
FS222	3.2	4.1	6.1	2.1	3.1	4.1	KG/mm2
FS223	4.5	5.8	8.1	2.9	4.1	5.8	KG/mm2
FS224	3	4.1	6.7	2.2	3.2	4.1	KG/mm2
FD06b(snubber)	0.6	0.9	1.1	0.5	0.5	0.7	mm
FD11b(EAB1)	2.3	4.1	5.4	1.5	2.3	3.3	mm
FD12b(EAB2)	2.7	5.3	7.2	1.7	3.3	4.9	mm
FD13b(snubber)	1	1.1	1.3	0.6	0.6	0.9	mm
FD14b(EAB3)	2.9	5.1	8.5	2.1	3.3	4.2	mm
FD15b(snubber)	0.5	0.6	0.8	0.3	0.5	0.6	mm
FR06(snubber)	2360	3908	4663	1844	3108	3952	KG
FR11(EAB1)	565	663	714	478	589	623	KG
FR12(EAB2)	1139	1374	1434	1023	1230	1342	KG
FR13(snubber)	2607	3804	4886	1640	2803	3966	KG
FR14(EAB3)	1058	1318	1453	1003	1213	1264	KG
FR15(snubber)	1954	3096	4374	1342	2104	3403	KG

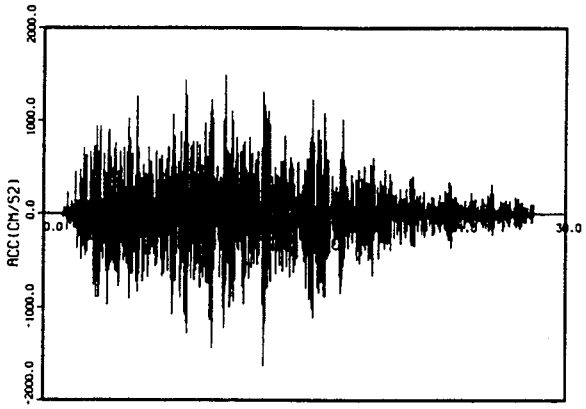

Figure G.1 XOXB

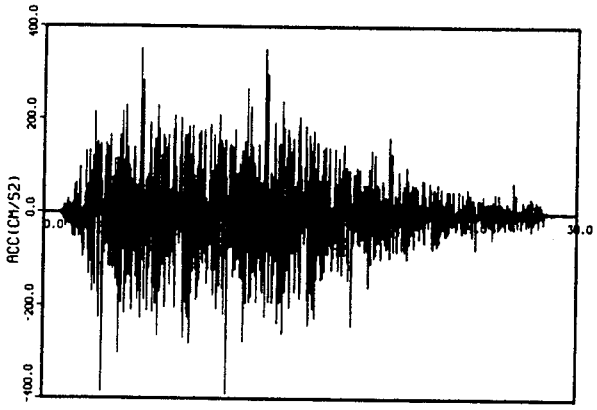

Figure G.2 ZOXB

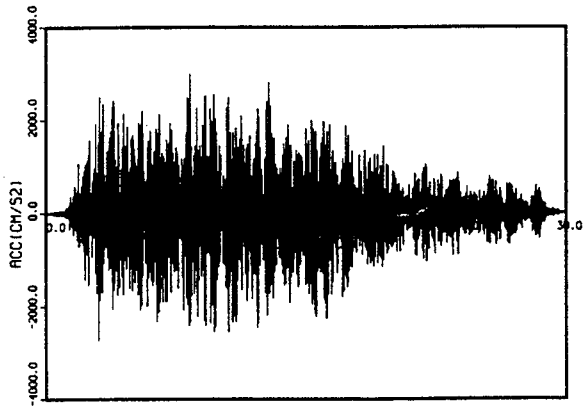

Figure G.3 FA3-X

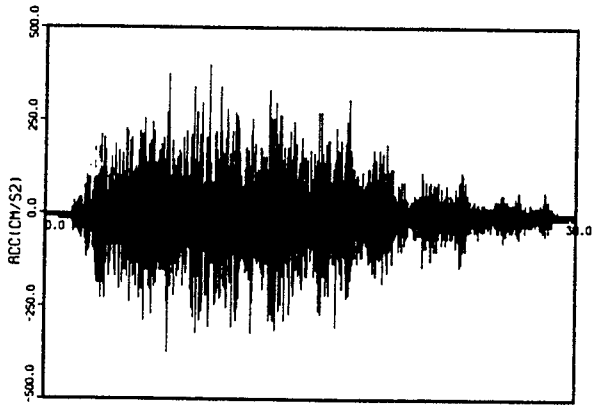

Figure G.4 FA3-Y

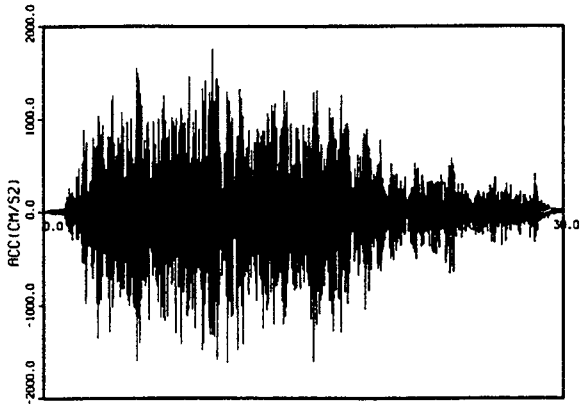

Figure G.5 FA3-Z

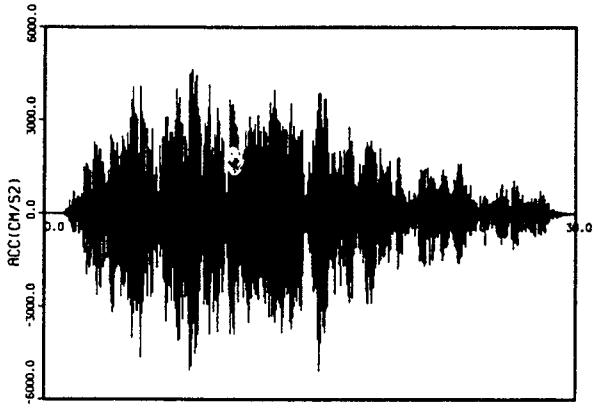

Figure G.6 FA7-X

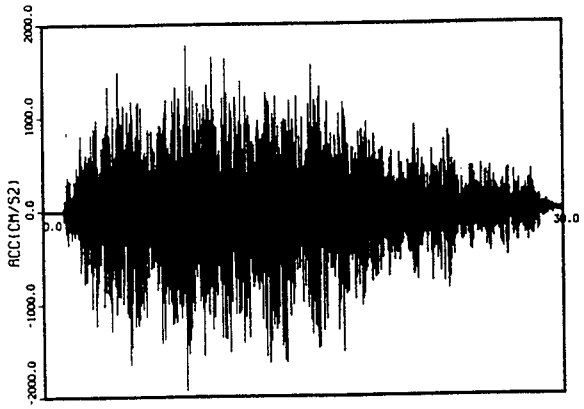

Figure G.7 FA7-Y

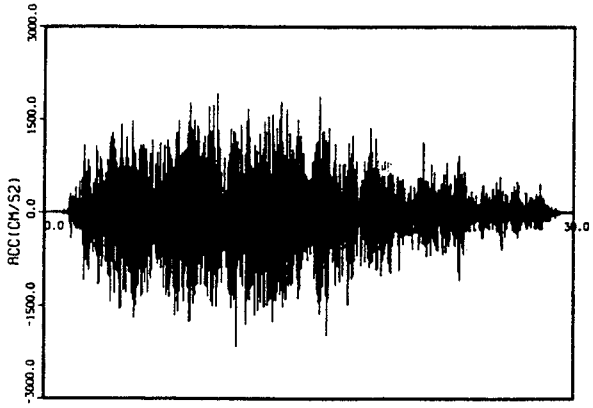

Figure G.8 FA7-Z

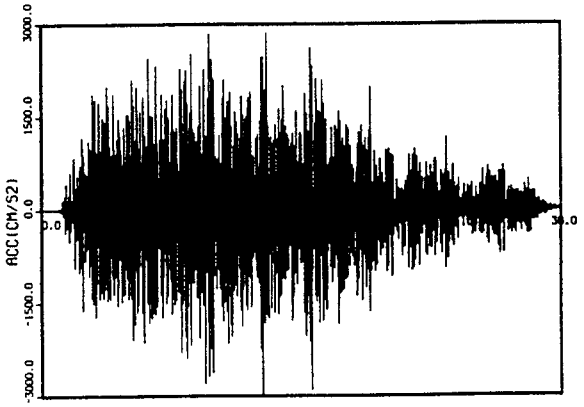

Figure G.9 FA9-X

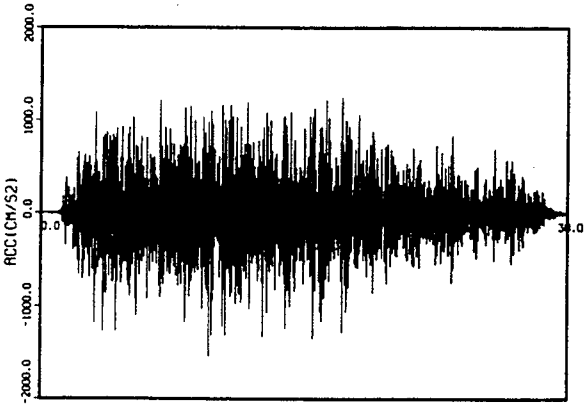

Figure G.10 FA9-Y

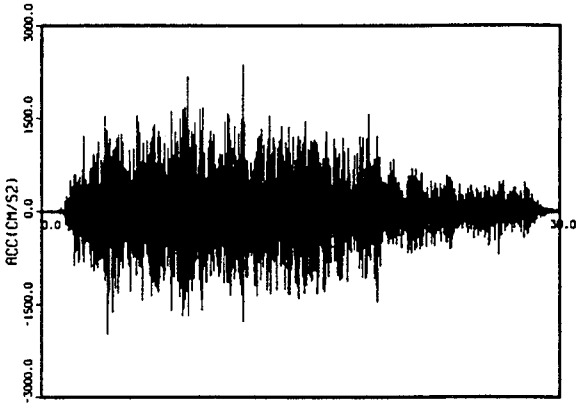

Figure G.11 FA9-Z

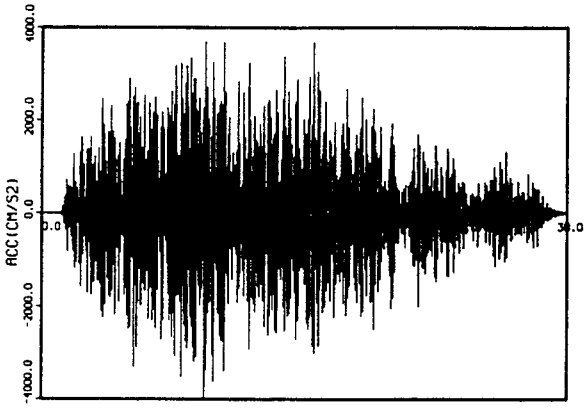

Figure G.12 FA11-X

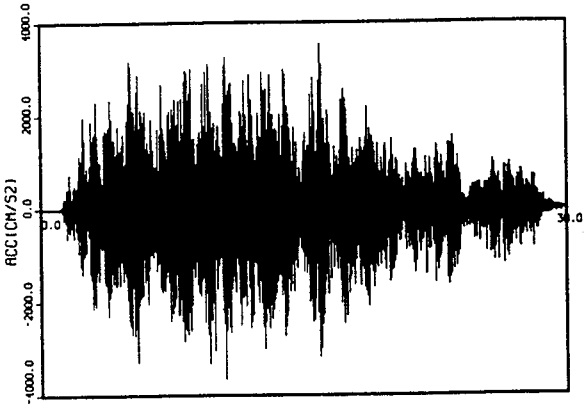

Figure G.13 FA11-Y

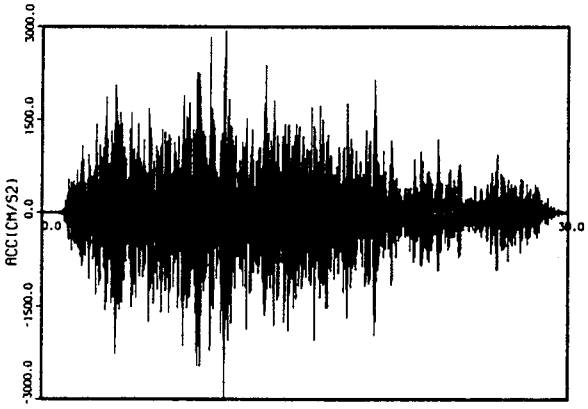

Figure G.14 FA11-Z

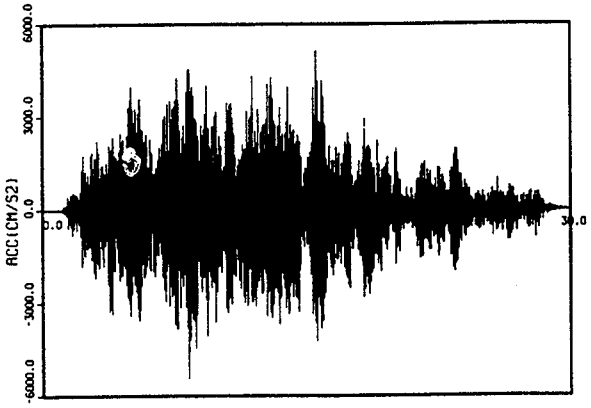

Figure G.15 FA12-X

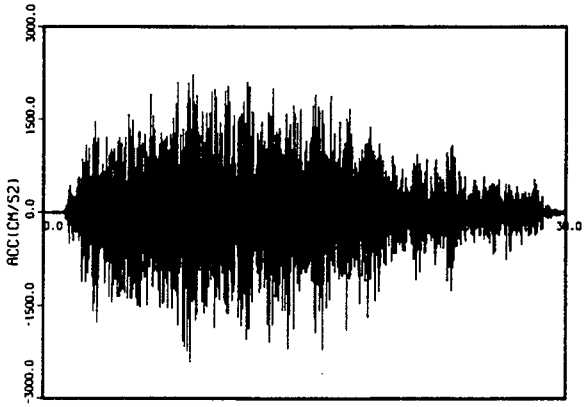

Figure G.16 FA12-Y

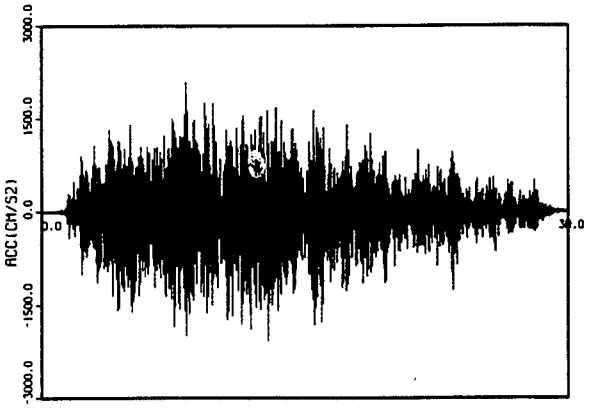

Figure G.17 FA12-Z

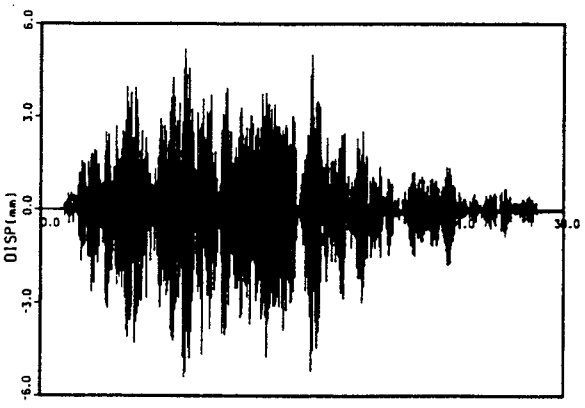

Figure G.18 FD11b

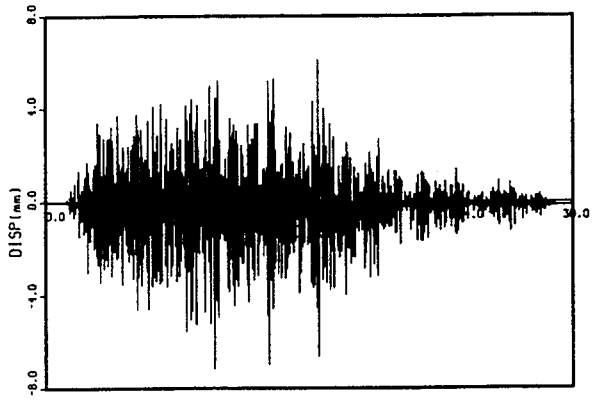

Figure G.19 FD12b

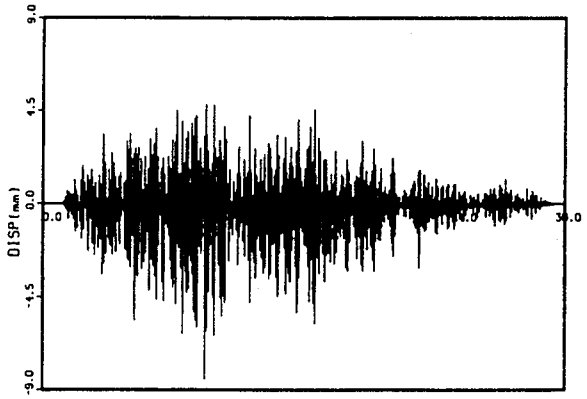

Figure G.20 FD14b

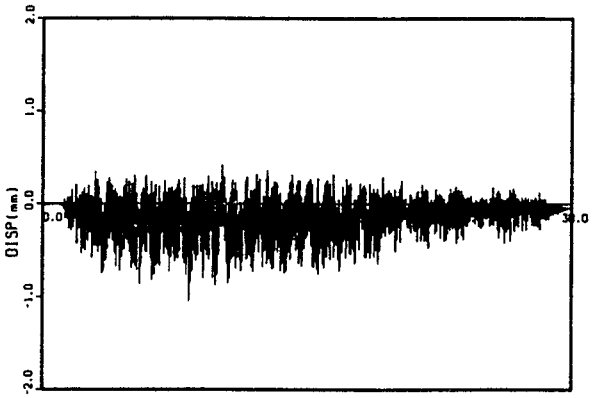

Figure G.21 FD6b

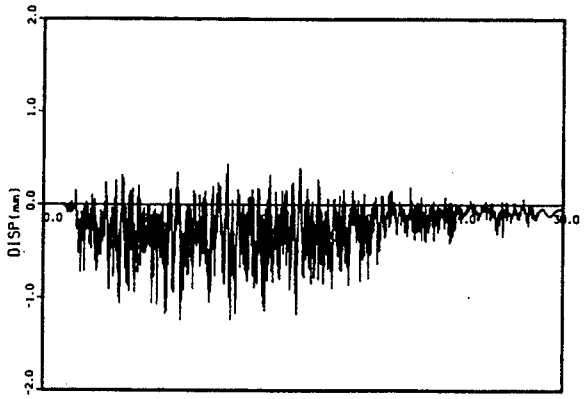

Figure G.22 FD13b

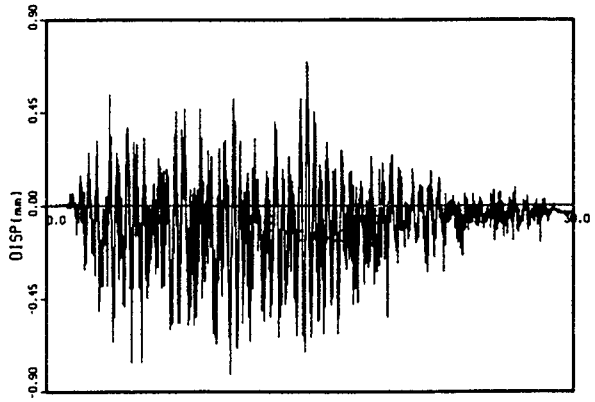

Figure G.23 FD15b

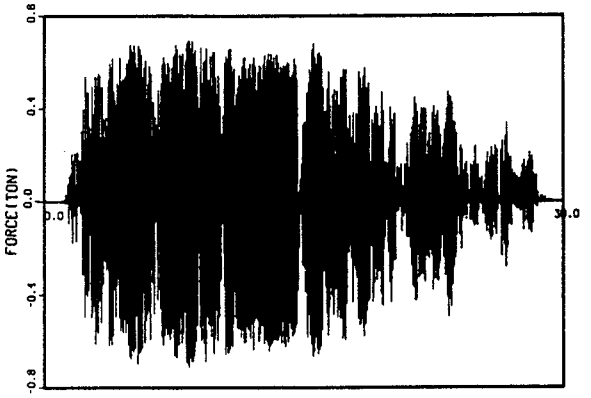

Figure G.24 FR11

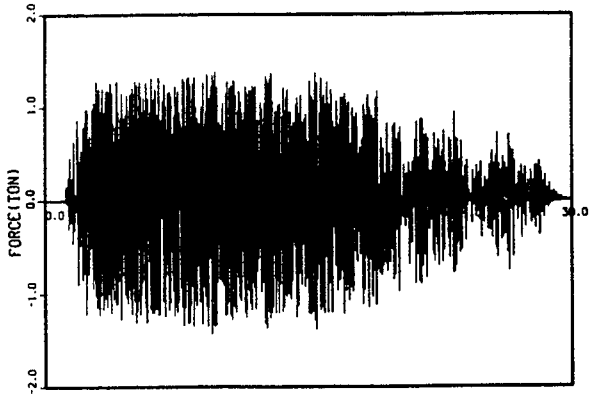

Figure G.25 FR12

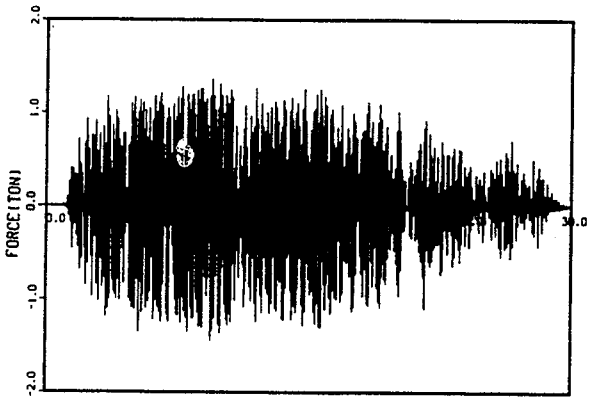

Figure G.26 FR14

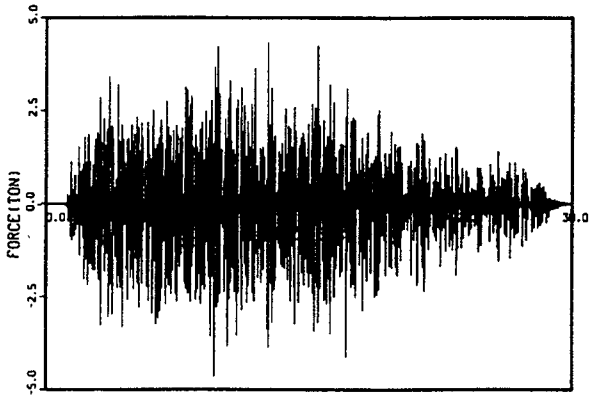

Figure G.27 FR6

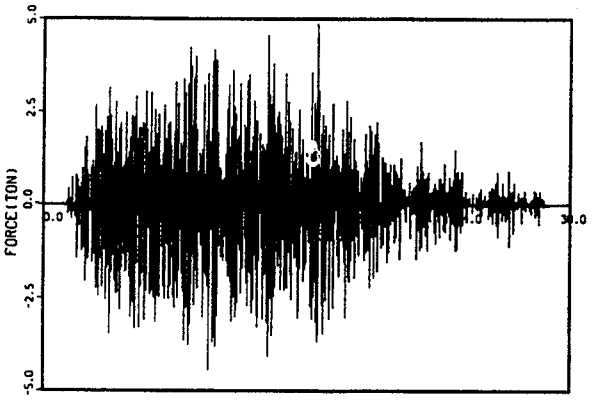

Figure G.28 FR13

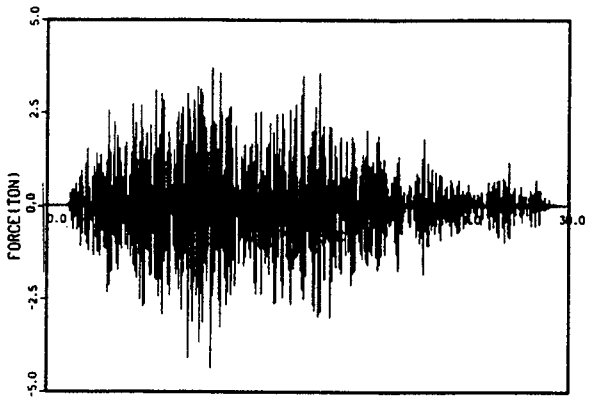

Figure G.29 FR15

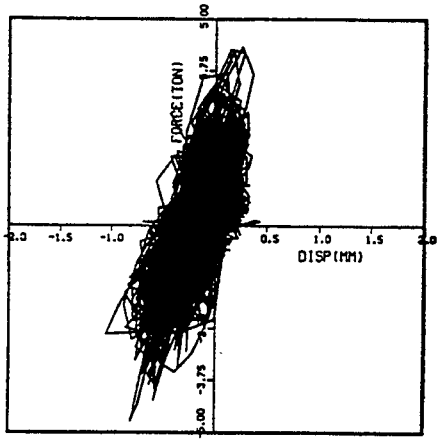

Figure G.30 FD6-FR6

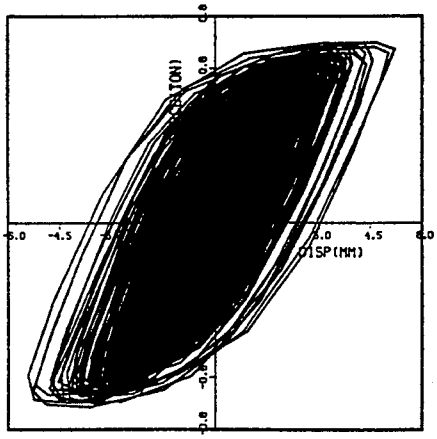

Figure G.31 EAB-1

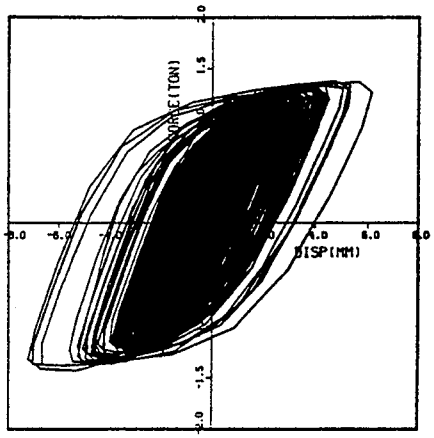

Figure G.32 EAB-2

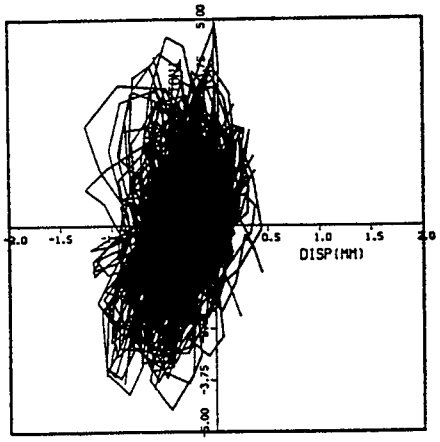

Figure G.33 FD13-FR-13

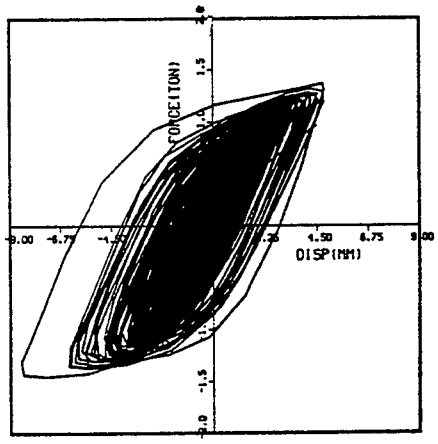

Figure G.34 EAB-3

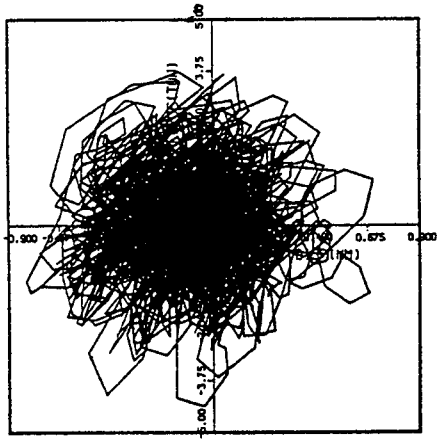

Figure G.35 FD15-FR15

APPENDIX H

LIST OF PEAK RESPONSE VALUES AND PLOTS OF SELECTED CHANNELS FOR 1.2 S_2 (C) (F-LINE) TEST RUN (RUN NO. 95071402)

Table H.1 List of Recorded Peak Values for F-line with EAB Supports under C Waves

Item	2/3S2(1.5T)	2/3S2(1.55T	2/3S2(1.6T)	1.0S2(1.6T)	1.1S2(1.6T)	1.2S2(1.6T)	
	ME-37	ME-38	ME-39	ME-40	ME-41	ME-42	
	95071101	95071102	95071103	95071104	95071105	95071402	
Targ. accel.	993+227	993+227	993+227	1489+340	1638+374	1787+408	
Measured	1056+257	1039+255	1039+250	1524+365	1784+429	1899+468	Unit
FA01X	1022	1013	1022	1515	1818	1931	GAL
FA01Y	351	284	284	343	393	401	GAL
FA01Z	241	250	233	341	399	433	GAL
FA03X	2459	2355	2534	2987	2940	2931	GAL
FA03Y	230	179	205	248	265	265	GAL
FA03Z	963	801	989	971	1210	1244	GAL
FA04X	1096	1139	1182	1648	1855	1898	GAL
FA04Y	228	184	201	236	271	271	GAL
FA04Z	242	242	242	351	409	467	GAL
FA05X	2892	2467	3284	3139	3071	2092	GAL
FA05Y	279	284	270	361	418	410	GAL
FA05Z	952	872	969	917	1181	1313	GAL
FA06X	2363	2077	2294	3112	3627	3671	GAL
FA06Y	2071	1844	2071	2694	3073	3545	GAL
FA06Z	1348	1102	1238	1238	1568	1720	GAL
FA07X	2184	2209	2226	2857	3131	3131	GAL
FA07Y	1340	1101	1253	1413	1812	1764	GAL
FA07Z	1248	1456	1597	1672	1963	1913	GAL
FA08X	2320	2190	2283	3007	3322	3341	GAL
FA08Y	812	795	847	881	993	1184	GAL
FA08Z	2112	2377	2184	2816	2523	2697	GAL
FA09X	2867	2969	3054	4177	4960	4934	GAL
FA09Y	1039	978	1082	986	1013	1177	GAL
FA09Z	2184	2151	2117	2614	2994	3424	GAL
FA010X	4099	4126	4217	5938	7141	7578	GAL
FA010Y	980	953	953	944	971	971	GAL
FA010Z	3929	3671	3301	4427	5063	5682	GAL
FA011X	4447	4665	4723	7392	8751	9892	GAL
FA011Y	2062	1740	1865	2338	3257	3981	GAL
FA011Z	2212	2036	2150	2811	3146	3684	GAL
FA012X	2468	2441	2735	3368	3314	3626	GAL
FA012Y	2057	1863	1722	2004	2534	2181	GAL
FA012Z	1431	1707	1679	1734	2037	1991	GAL
FA013X	2419	2651	2713	3775	4088	3856	GAL
FA013Y	1112	1209	1129	1289	1458	1752	GAL
FA013Z	1352	2625	2566	3355	3973	4059	GAL
AA02X	1044	1036	1044	1534	1783	1912	GAL
AA02Y	99	123	107	123	132	164	GAL
AA02Z	269	236	253	362	429	471	GAL
FS011	1.2	1.1	0.8	1.2	1.4	1.5	KG/mm2
FS012	0.4	0.4	0.4	0.4	0.5	0.6	KG/mm2
FS013	1.4	1.3	1.1	1.5	1.8	2	KG/mm2
FS014	2.6	2.6	2.8	3.3	3.5	3.4	KG/mm2
FS021	2.2	2.4	2.4	3.1	3.5	3.5	KG/mm2
FS022	3.2	3.4	3.5	5	5.9	6.1	KG/mm2
FS023	1.4	1.6	1.6	2	2.1	2	KG/mm2
FS024	2.9	3	3.2	4.6	5.4	5.5	KG/mm2
FS031	3.4	3.4	3	4.6	5.7	5.8	KG/mm2
FS032	3	3.2	3.4	4.9	5.4	5.6	KG/mm2
FS033	3.1	2.9	3.1	4.5	5	5	KG/mm2
FS034	3.1	3.1	3.4	4.6	5.3	5.5	KG/mm2
FS041	1.2	1.1	1.1	1.8	2.1	2.3	KG/mm2

Table H.1 List of Recorded Peak Values for F-line with EAB Supports under C Waves (Cont'd)

	ME-37	ME-38	ME-39	ME-4-	ME-41	ME-42	DE1-6
FS042	4.5	4.2	4.2	6.5	7.6	8	KG/mm2
FS043	0.5	0.5	0.5	0.6	0.7	0.7	KG/mm2
FS044	1.3	1.9	1.4	2.1	2.5	2.4	KG/mm2
FS051	1.7	1.8	1.7	2.5	3.1	3.3	KG/mm2
FS052	1.6	1.5	1.6	1.9	2.5	2.7	KG/mm2
FS053	1.6	1.8	1.6	2.5	3.3	3.5	KG/mm2
FS054	1.2	1.1	1	1.2	2	2.1	KG/mm2
FS061	0.7	0.7	0.7	1	1	1	KG/mm2
FS062	5.3	5.9	6.5	9.1	10.3	10.5	KG/mm2
FS063	1.2	1.1	1.1	1.6	1.9	2	KG/mm2
FS064	3.2	2.9	2.9	4.3	5	5.3	KG/mm2
FS071	1.5	1.7	1.8	2.2	2.6	2.9	KG/mm2
FS072	2.5	2.3	2.3	2.8	3.4	3.4	KG/mm2
FS073	1.3	1.6	1.7	2	2.2	2.3	KG/mm2
FS074	2.9	2.9	2.9	3.3	3.9	3.9	KG/mm2
FS081	1.1	1.2	1.2	1.7	1.8	2	KG/mm2
FS082	0.9	0.9	0.9	1.4	1.7	1.8	KG/mm2
FS083	1.3	1.4	1.5	2	2.3	2.5	KG/mm2
FS084	0.8	0.7	0.7	1.1	1.3	1.5	KG/mm2
FS091	2.3	2.4	2.3	3.8	4.3	4.6	KG/mm2
FS092	5.7	5.6	5.4	8.7	10.6	11.3	KG/mm2
FS093	2.9	3	3.1	4.6	6.5	5.9	KG/mm2
FS094	11.2	11.8	12.2	18	22.3	22.1	KG/mm2
FS101	3.3	3.4	3.6	5.3	6.4	6.6	KG/mm2
FS102	2.2	2	2.1	3.2	3.8	4.1	KG/mm2
FS103	4.3	4	4.1	6.7	7.9	8.4	KG/mm2
FS104	0.9	0.9	0.8	1.1	1.3	1.3	KG/mm2
FS111	2.8	2.7	2.9	4.2	5.1	5.4	KG/mm2
FS112	2.6	3	2.9	4.1	4.6	4.6	KG/mm2
FS113	4.5	5	5.3	7.5	8.5	8.9	KG/mm2
FS114	2.4	2.8	2.7	3.8	4.3	4.3	KG/mm2
FS121	1.7	2	2	3.1	3.3	3.2	KG/mm2
FS122	2.3	2.6	2.6	3.2	3.7	3.8	KG/mm2
FS123	1.9	2.1	2.3	3.4	3.7	3.6	KG/mm2
FS124	1.2	1.1	1.3	1.3	1.4	1.5	KG/mm2
FS131	2.6	2.7	2.7	3.9	4.5	4.5	KG/mm2
FS132	3.5	3.5	3.5	5.2	5.8	5.8	KG/mm2
FS133	0.7	0.8	0.8	0.9	1.1	1.3	KG/mm2
FS134	3.3	3.2	3.1	4.6	5.3	5.4	KG/mm2
FS141	9	9.4	10.4	14.4	16.8	17.5	KG/mm2
FS142	4.7	5.4	5.6	7.7	8.9	9.1	KG/mm2
FS143	7.2	7.4	8.2	11.5	13.6	14.3	KG/mm2
FS144	4.1	3.8	3.9	5.3	6	5.8	KG/mm2
FS151	6.5	7.1	7.8	11.3	12.7	12.8	KG/mm2
FS152	1.7	1.7	1.6	1.8	2.1	2.4	KG/mm2
FS153	5.4	5.9	6.5	9.3	10.3	10.5	KG/mm2
FS154	2.7	2.5	2.6	3.6	4.3	4.6	KG/mm2
FS161	1.4	1.4	1.5	1.8	2.1	2.1	KG/mm2
FS162	1.6	1.5	1.6	1.8	2.2	2.5	KG/mm2
FS163	1.6	1.5	1.6	2.8	2.9	3	KG/mm2
FS164	2.2	2.2	2.1	2.9	3.7	3.8	KG/mm2
FS171	1	1	0.8	1.1	1.3	1.3	KG/mm2
FS172	9.7	10.9	11.5	16.9	19.3	19.8	KG/mm2
FS173	5.7	6.4	6.4	9.6	11.1	11.8	KG/mm2
FS174	9.4	10.6	11.2	16.4	18.7	19.1	KG/mm2
FS181	5.5	4.6	5.1	6.9	7.8	8	KG/mm2

Table H.1 List of Recorded Peak Values for F-line with EAB Supports under C Waves (Cont'd)

	ME-37	ME-38	ME-39	ME-40	ME-41	ME-42	KG/mm2
FS182	3.7	3.7	3.6	5.9	6.5	6.8	KG/mm2
FS183	5.7	5.1	5.4	6.7	7.8	8.9	KG/mm2
FS184	2.8	2.8	2.5	4.2	4.7	4.8	KG/mm2
FS191	6.4	6.4	6.5	20.7	13.5	14	KG/mm2
FS192	8.8	9.4	9.6	14.5	17.1	18	KG/mm2
FS193	4.5	4.6	4.3	7	8.6	9.4	KG/mm2
FS194	10.9	11.5	11.7	17.5	21.2	21.5	KG/mm2
FS201	2	2	2	2.6	3.2	3.1	KG/mm2
FS202	2.8	2.9	3	4.3	4.7	5	KG/mm2
FS203	3.5	3.6	3.6	5.5	6	6.2	KG/mm2
FS204	4.5	5	5	7.6	8.8	9.2	KG/mm2
FS211	2.5	2.5	2.6	3.7	4.4	4.6	KG/mm2
FS212	12.9	13.4	13.6	22.7	26.7	27.8	KG/mm2
FS213	9	9.4	9.6	15.1	17.6	18.8	KG/mm2
FS214	11.7	12.1	12.4	20.7	24.4	25.5	KG/mm2
FS221	8.4	9.1	9.9	15	16.7	16.1	KG/mm2
FS222	7.7	8.3	8.8	12.9	15.2	16.4	KG/mm2
FS223	9.3	9.9	10.9	16.5	18.4	17.8	KG/mm2
FS224	8.6	9.1	9.5	14	16.7	17.8	KG/mm2
FD06b(snubber	1.1	1	1.1	1.2	1.3	1.4	mm
FD11b(EAB1)	2.1	2.3	2.3	3.8	4.4	4.2	mm
FD12b(EAB2)	7.5	8.1	8.3	12.6	13.2	13.4	mm
FD13b(snubber	1.5	1.4	1.4	2	1.8	2	mm
FD14b(EAB3)	9.8	10.1	10.2	16.6	18.9	19.2	mm
FD15b(snubber	0.9	1.2	1.2	1.5	2	2.2	mm
FR06(snubber)	4052	3958	4549	4801	5990	6393	KG
FR11(EAB1)	576	591	602	659	674	706	KG
FR12(EAB2)	1456	1374	1434	1023	1230	1342	KG
FR13(snubber)	4677	5014	5251	7221	7608	7882	KG
FR14(EAB3)	1557	1526	1538	1779	2883	3585	KG
FR15(snubber)	5569	5657	5182	8292	9990	10739	KG

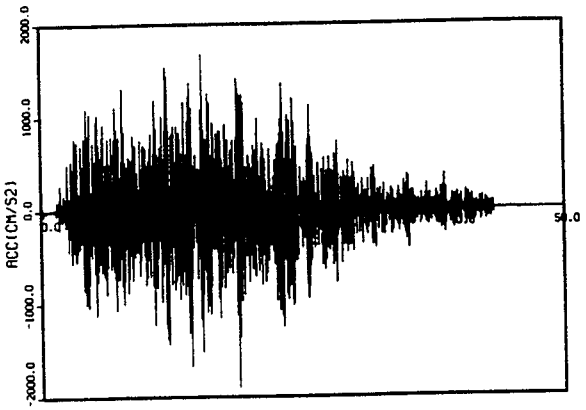

Figure H.1 XO-XB

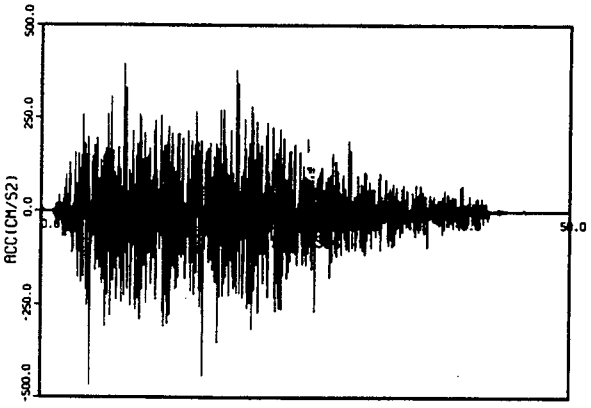

Figure H.2 ZO-XB

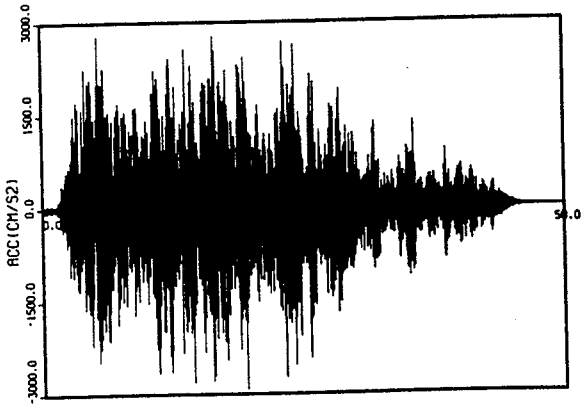

Figure H.3 FA3-X

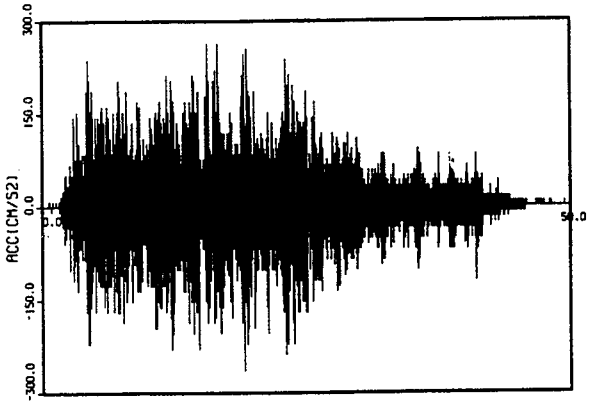

Figure H.4 FA3-Y

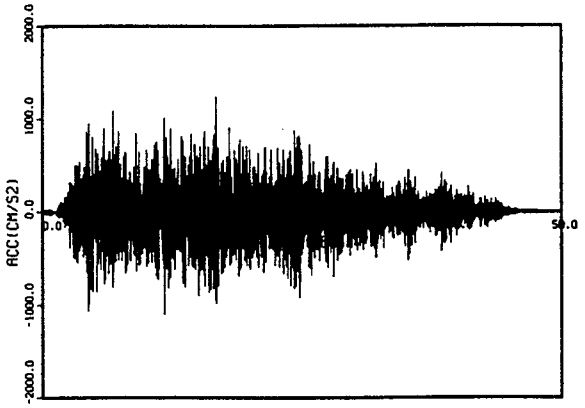

Figure H.5 FA3-Z

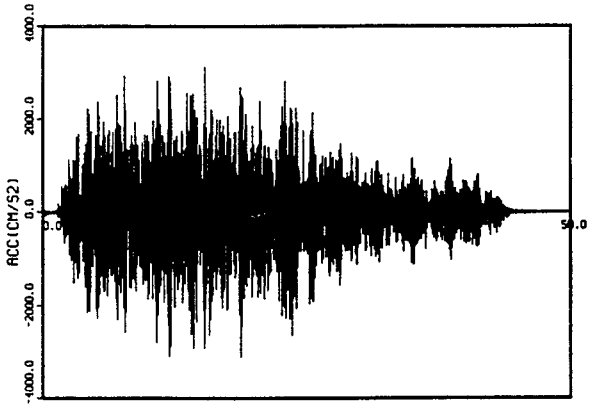

Figure H.6 FA7-X

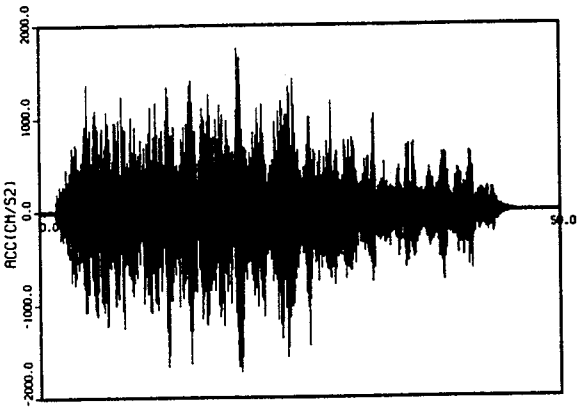

Figure H.7 FA7-Y

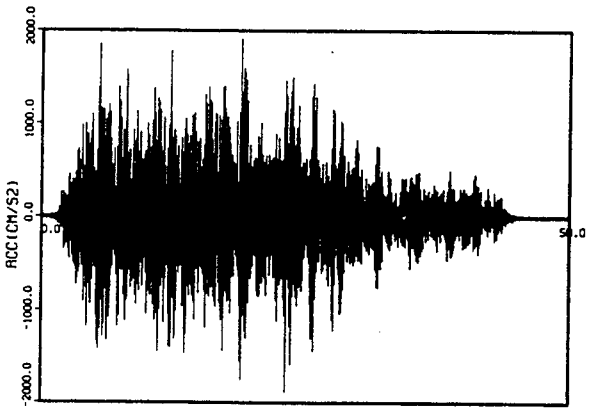

Figure H.8 FA7-Z

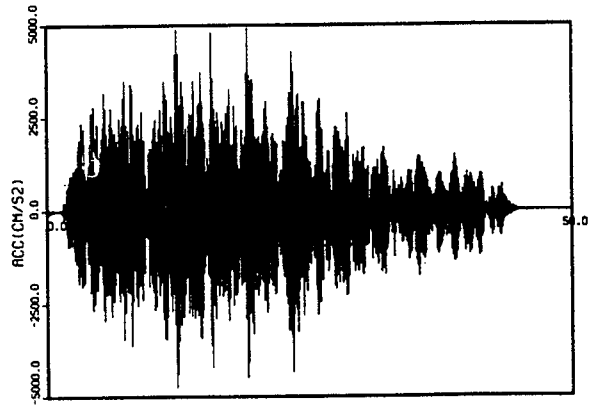

Figure H.9 FA9-X

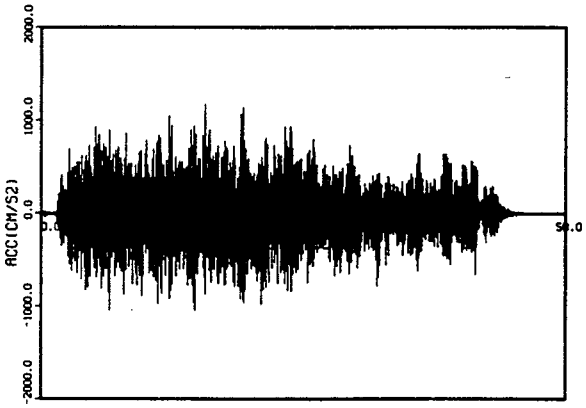

Figure H.10 FA9-Y

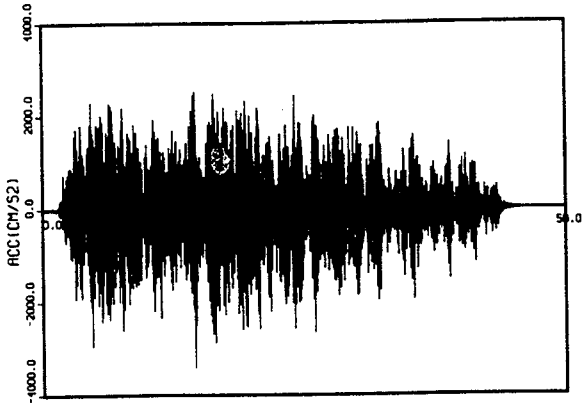

Figure H.11 FA9-Z

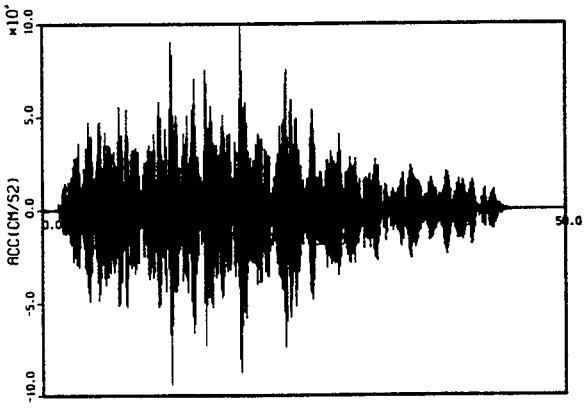

Figure H.12 FA11-X

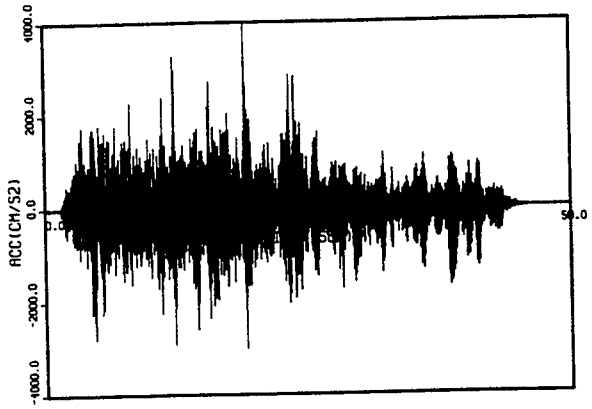

Figure H.13 FA11-Y

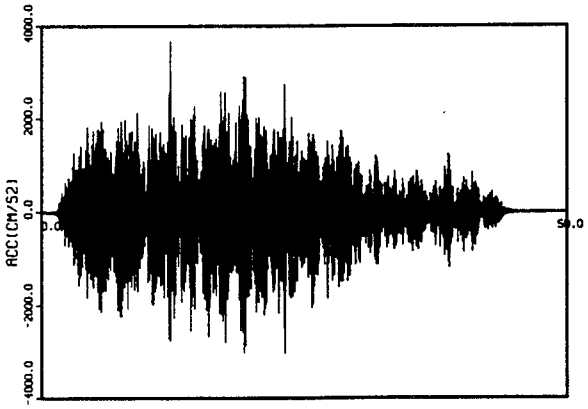

Figure H.14 FA11-Z

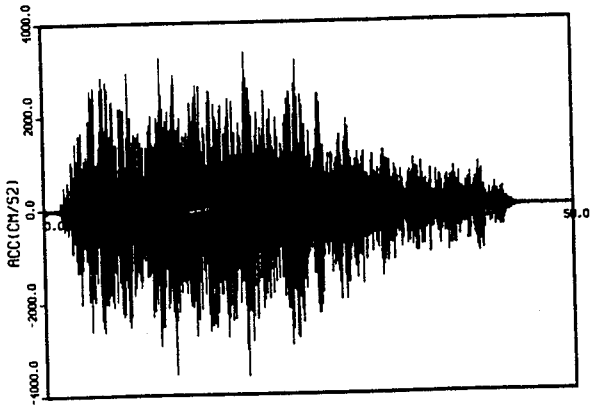

Figure H.15 FA12-X

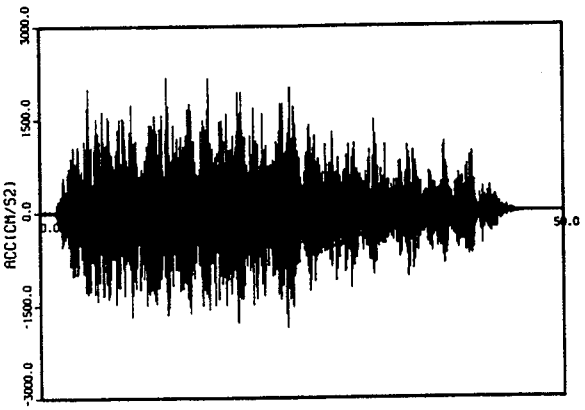

Figure H.16 FA12-Y

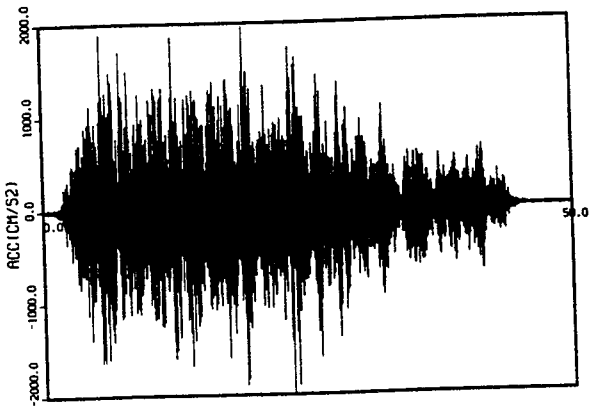

Figure H.17 FA12-Z

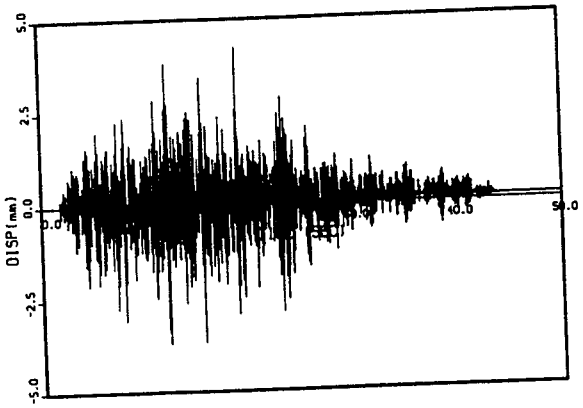

Figure H.18 FD11b

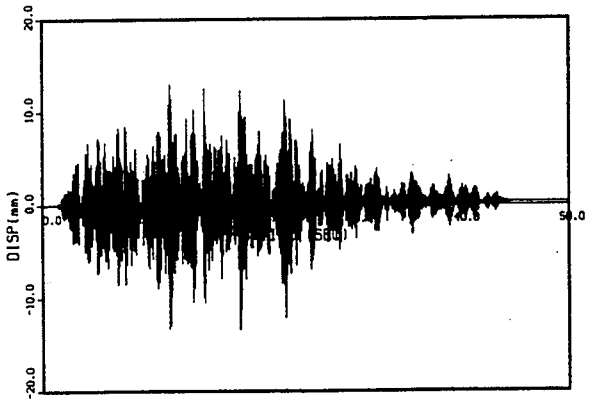

Figure H.19 FD12b

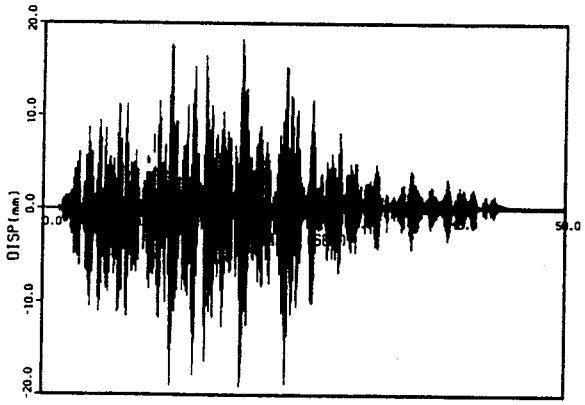

Figure H.20 FD14b

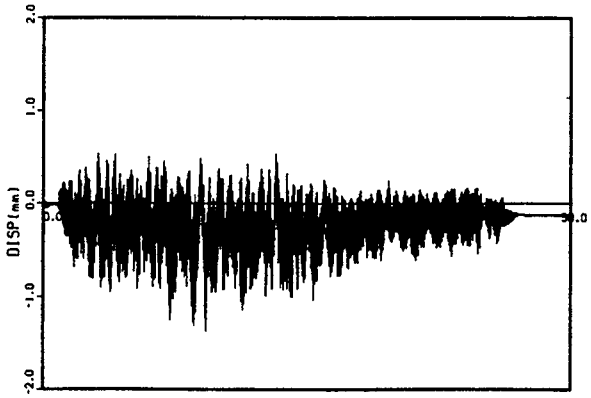

Figure H.21 FD6b

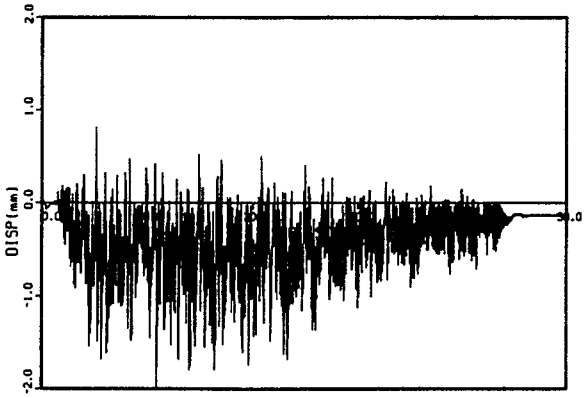

Figure H.22 FD13b

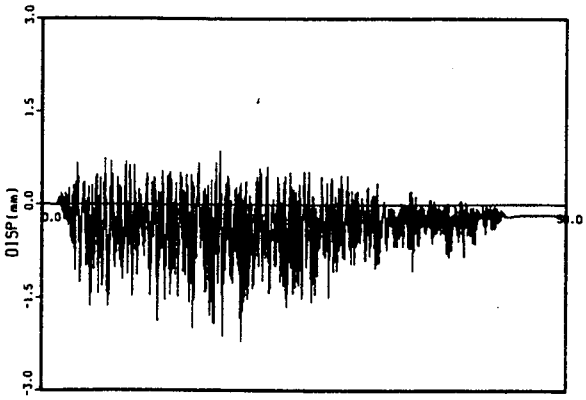

Figure H.23 FD15b

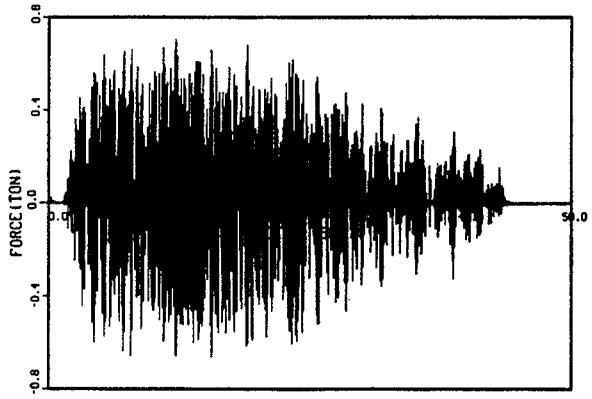

Figure H.24 FR11

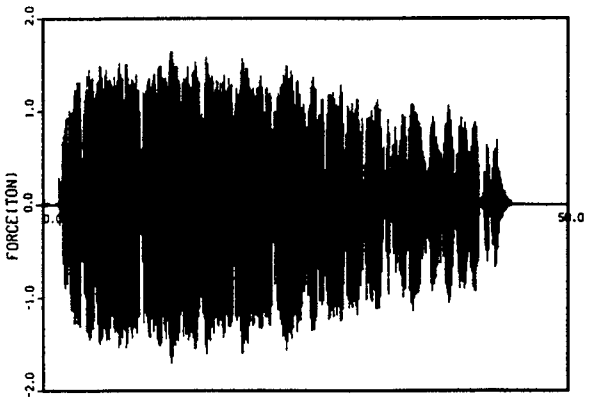

Figure H.25 FR12

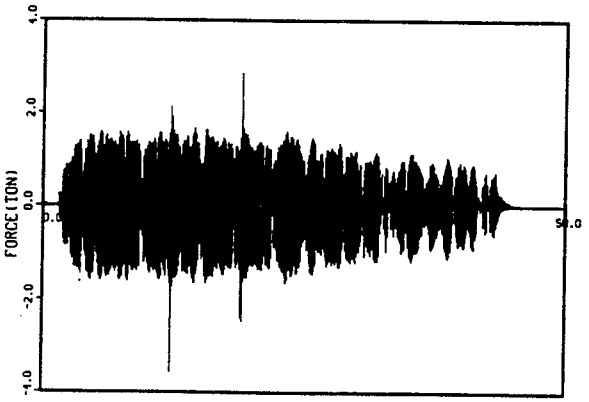

Figure H.26 FR14

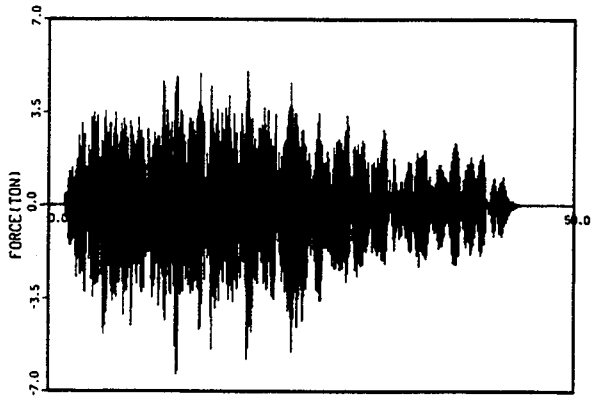

Figure H.27 FR6

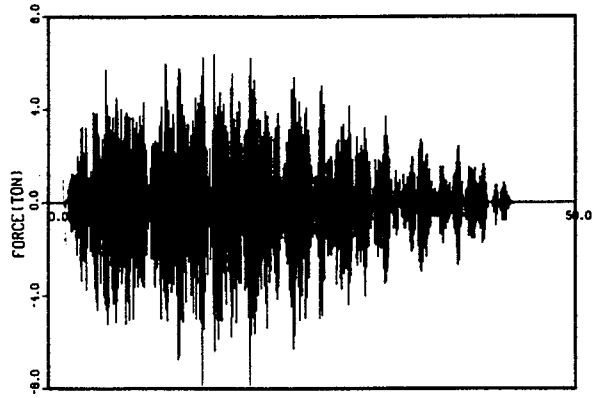

Figure H.28 FR13

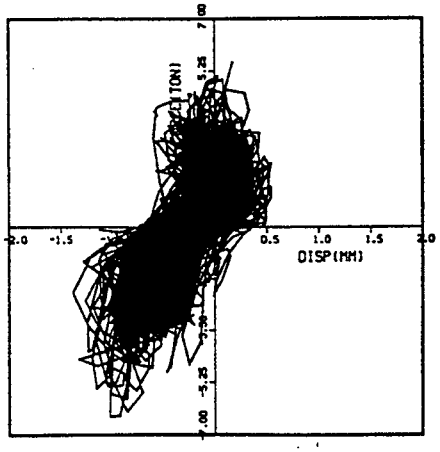

Figure H.29 FD6-FR6

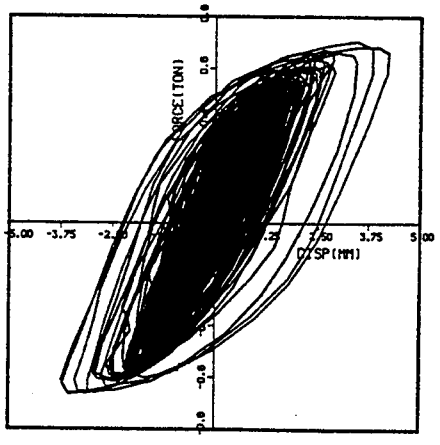

Figure H.30 EAB-1

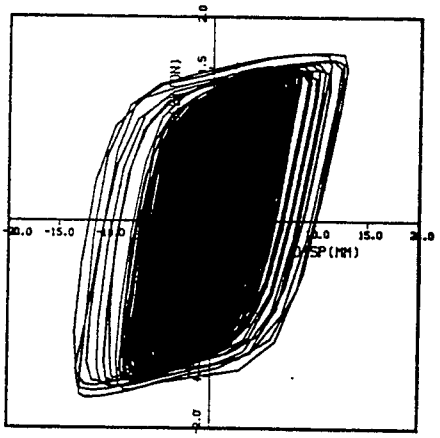

Figure H.31 EAB-2

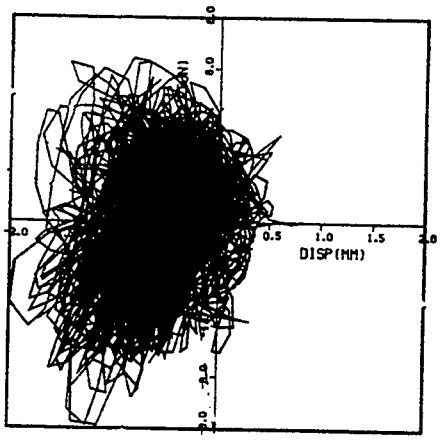

Figure H.32 FD13-FR13

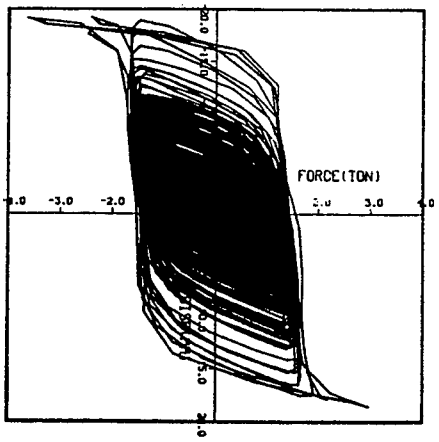

Figure H.33 EAB-3

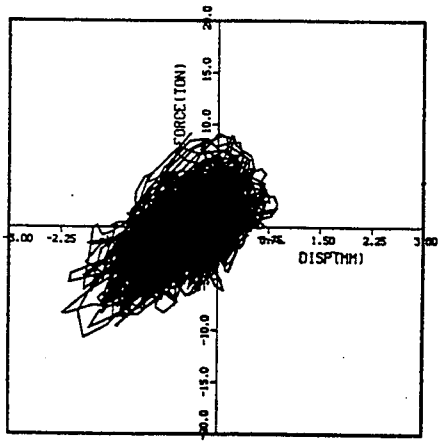

Figure H.34 FD15-FR15

APPENDIX I

LIST OF PEAK RESPONSE VALUES AND PLOTS OF SELECTED CHANNELS FOR S_2 (A) (M-LINE) TEST RUN (RUN NO. 95041909)

Table I.1 List of Recorded Peak Values for M-line with LED Supports Under A Waves

		DE1-4	DE1-5	DE1-6	DE1-1	DE1-2	DE1-3	DE1-3'	DE1-3"	
	Test no.	950425-04	950421-03	950421-06	950419-03	950419-06	950419-09	950424-02	950424-03	
		H+V	H+V	H+V	H+V	H+V	H+V	H+V	H+V	
Sensor	S/G CH	1/3S1(A)	2/3S1(A)	3/3S1(A)	1/3S2(A)	2/3S2(A)	3/3S2(A)	3/3S2(A)	3/3S2(A)	Unit
S/GT model	No.	S/G nonl.	S/G nonl.	S/G nonl.	S/G nonl.	S/G nonl.	S/G nonl.	S/G nonl.	S/G nonl.	
AA1-X	1-1-2	904	1394	1734	1508	2601	4335	4901	4787	GAL
AA1-Y	1-1-1	66	107	148	115	198	322	289	281	GAL
AA1-Z	1-1-3	123	181	247	156	272	445	453	453	GAL
AA2-X	1-1-4	321	626	955	554	1084	1598	1678	1670	GAL
AA2-Y	1-1-5	65	82	131	82	147	197	197	189	GAL
AA2-Z	1-1-6	58	126	218	126	260	404	412	412	GAL
AD1-X	1-1-7	0.46	0.81	1.26	0.98	1.91	2.95	3.25	3.15	mm
AD1-Y	1-1-8	0.05	0.08	0.12	0.08	0.16	0.25	0.26	0.26	mm
AD1-Z	1-1-9	0.05	0.06	0.08	0.06	0.13	0.16	0.22	0.21	mm
AS1	1-1-10	2500	3920	5200	3500	7020	11800	12660	12700	KG
AS2	1-1-11	2300	3600	4810	3210	6400	10820	11510	11590	GAL
SA2-X	1-1-12	302	579	898	539	1078	1617	1706	1706	GAL
SA2-Z	1-1-13	83	158	225	125	284	384	409	401	GAL
SA3-X	1-1-14	296	562	898	539	1047	1594	1664	1688	GAL
DSP-ACC	1-1-15	565	980	1357	1055	2148	3204	3506	3355	GAL
DSP-DSP	1-2-1	0.45	0.75	1.08	0.82	1.65	2.54	2.64	2.62	mm
SA1-X	1-2-2	284	562	886	552	1029	1567	1636	1630	GAL
MA1-X	3-3-10	974	1436	1761	1163	2206	3728	4292	2263	GAL
MA1-Y	3-3-11	996	1666	2454	1490	3769	5486	5444	5034	GAL
MA1-Z	3-3-12	563	806	1092	689	1319	1983	2126	1941	GAL
MA16-X	3-3-13	772	1151	1907	1118	2663	3305	3551	3633	GAL
MA16-Y	3-3-14	1288	2127	2706	2307	4304	7288	8886	8226	GAL
MA16Z	3-3-15	821	1178	1651	1015	1604	2178	2163	2232	GAL
MA17X	3-4-1	1760	2275	2707	2009	2707	4650	4125	4501	GAL
MA17Y	3-4-2	902	1029	1511	736	1519	2208	2050	2073	GAL
MA17Z	3-4-3	859	1204	1558	1004	1654	1927	2000	2192	GAL
MA4-X	3-4-4	1566	2094	2557	2142	2710	3309	3533	3836	GAL
MA4-Y	3-4-5	508	1097	1352	909	1687	2720	2990	2335	GAL
MA4-Z	3-4-6	571	883	1177	813	1315	2017	1895	1974	GAL
MA5-X	3-4-7	1278	1622	1941	1368	2081	2646	2966	3236	GAL
MA5-Y	3-4-8	523	1253	1554	1038	1897	2797	2985	3296	GAL
MA6-X	3-4-9	1225	1316	1650	1166	1716	2133	2141	2383	GAL
MA6-Y	3-4-10	614	1311	1548	1089	2105	2917	3154	3408	GAL
MA7-X	3-4-11	272	514	799	487	957	1470	1563	1532	GAL
MA7-Z	3-4-12	94	137	205	132	265	432	406	402	GAL
MA8-X	3-4-13	717	868	1335	976	1502	2245	2387	2379	GAL
MA8-Y	3-4-14	634	1108	1502	899	1590	2699	2875	2827	GAL
MA8-Z	3-4-15	1113	1724	2260	1691	3274	4891	5172	4636	GAL
MA9-X	4-1-1	827	993	1241	976	1771	2027	2168	2044	GAL
MA9-Y	4-1-2	647	999	1646	1130	1524	2302	2187	2523	GAL
MA9-Z	4-1-3	1425	1989	2782	1971	3397	5010	4404	4498	GAL
MA10-X	4-1-4	869	1032	1218	1072	1714	2015	2169	2283	GAL
MA10-Y	4-1-5	356	459	935	428	1141	1363	1268	1157	GAL
MA10-Z	4-1-6	1284	1968	3392	1869	3598	5501	5064	5171	GAL
MA11-X	4-1-7	274	511	827	489	969	1389	1554	1526	GAL
MA11-Y	4-1-8	200	265	453	230	577	863	786	658	GAL
MA11-Z	4-1-9	80	130	193	118	248	362	400	366	GAL
MA12-X	4-1-10	279	540	889	510	1042	1582	1617	1634	GAL
MA-12-Y	4-1-11	188	275	323	192	503	774	595	511	GAL
MA12-Z	4-1-12	158	202	268	162	346	541	554	527	GAL
MA13-X	4-1-13	609	934	1488	1021	1781	2424	2533	2699	GAL
MA13-Y	4-1-14	214	359	603	458	863	810	879	848	GAL
MA13-Z	4-1-15	200	425	508	400	691	1050	975	1050	GAL

Table I.1 List of Recorded Peak Values for M-line with LED Supports Under A Waves (Cont'd)

		DE1-4	DE1-5	DE1-6	DE1-1	DE1-2	DE1-3	DE1-3'	DE1-3"	
MA14-X	4-2-1	701	964	1384	1349	2051	2577	2875	2805	GAL
MA14-Y	4-2-2	959	1136	1329	983	2828	3578	3328	3239	GAL
MA14-Z	4-2-3	250	292	325	233	425	659	834	851	GAL
MA15-X	4-2-4	812	1395	1784	1538	2553	3538	5910	4022	GAL
MA15-Y	4-2-5	307	552	752	690	1282	1233	1336	1403	GAL
MA15-Z	4-2-6	248	454	559	437	694	833	694	951	GAL
MD12	4-2-7	2.2	3.3	4.65	3.3	6.1	9.2	9.5	9.45	mm
MD13	4-2-8	0.8	1.25	1.85	1.55	2.95	4.1	4.55	4.45	mm
MD15	4-2-11	0.75	1.35	1.8	1.4	2	2.55	2.75	2.8	mm
MD16	4-2-12	1.45	1.95	2.8	2.25	3.5	5.2	5.55	5.65	mm
MD18-X	4-3-2	1.7	2.4	3.10	2.75	3.9	5.5	6	6.05	mm
MD18-Y	4-3-3	1	2.05	2.8	1.6	3.1	4.8	4.75	5	mm
MD18-Z	4-2-13	0.85	1.5	2.2	1.35	2.9	4.55	4.6	4.45	mm
MD17-Z	4-2-14	0.8	1.5	2.25	1.4	2.8	4.5	4.5	4.4	mm
MD14-X	4-2-15	1	1.8	2.4	1.45	2.6	4.25	4.15	4.3	mm
MD9-Y	4-3-5	0.1	0.11	0.13	0.13	0.16	0.21	0.2	0.21	mm
MD10-Z	4-3-6	0.09	0.18	0.23	0.15	0.28	0.39	0.36	0.36	mm
MD11X	4-3-7	0.1	0.26	0.45	0.43	0.8	1.13	0.9	0.98	mm
MD15(1.5T)	4-3-11	524	1049	1253	1110	1397	1603	1628	1623	KG
MD16(1.5T)	4-3-12	1126	1376	1531	1323	1643	1808	1833	1874	KG
MD17(1.0T)	4-3-13	696	861	900	824	937	1011	1003	1000	KG
MR8	4-3-15	145	116	424	62	2397	5907	5912	4536	KG
MR11(0.3T)	4-4-5	15	23	25	25	33	37	35	33	KG
MR12(0.3T)	4-4-6	7	18	28	13	32	65	89	101	KG
MR13	4-4-7	17	40	61	42	55	71	75	78	KG
MR14	4-4-8	73	134	179	124	194	293	296	274	KG
MP1	4-4-9	1.1	1.1	1.36	1.36	1.55	2.58	2.65	2.2	KG/CM2
MP2	4-4-10	1.06	1.19	1.38	1.32	1.91	2.64	2.84	2.37	KG/CM2
TE1	4-2-9	18	17	18	18	18	20	20	20	C
TE2	4-2-10	17	17	18	17	20	25	26	26	C
TE3	4-4-14	18	18	20	18	21	25	24	24	C
S0-0	4-4-11	0.43	0.65	0.93	0.74	1.43	2.34	2.36	2.32	KG/mm2
S0-90	4-4-12	0.41	0.69	1.1	0.67	1.08	1.89	1.93	1.93	KG/mm2
S0-180	4-4-13	0.71	1.24	1.58	1.19	1.75	2.47	2.69	2.58	KG/mm2
S0-270	4-4-14	0.74	1.37	1.91	1.24	2.47	3.68	3.77	3.6	KG/mm2
S1-0 (A)	4-4-15	0.06	0.11	0.15	0.11	0.17	0.26	0.28	0.28	KG/mm2
S1-0 (F)	5-1-1	0.52	0.89	1.32	0.98	1.62	2.55	0.69	2.56	KG/mm2
S1-45 (A)	4-3-8	0.71	1.08	1.52	1.3	1.95	2.68	2.86	2.81	KG/mm2
S1-45 (F)	4-3-9	0.91	1.47	2.16	1.52	3.08	4.55	4.79	4.66	KG/mm2
S1-90	5-1-2	1.71	2.99	4.11	2.92	5.8	8.21	8.47	8.29	KG/mm2
S1-90	5-1-3	1.29	1.93	2.82	2.3	3.62	5.31	5.72	5.65	KG/mm2
S1-135 (A)	4-3-10	1.58	2.45	3.53	2.84	4.7	6.84	7.25	7.26	KG/mm2
S1-135 (F)	4-3-14	1.65	2.97	4.01	2.79	5.24	7.56	7.75	7.73	KG/mm2
S1-180 (A)	5-1-4	0.48	0.74	1.08	0.78	1.41	2.3	2.47	2.3	KG/mm2
S1-180 (F0	5-1-5	0.89	1.39	2.14	1.58	2.68	4.12	4.42	4.22	KG/mm2
S1-225 (A)	4-4-1	0.78	1.49	2.29	1.54	2.77	4.46	4.38	4.22	KG/mm2
S1-225 (F)	4-4-2	1.71	2.98	4	2.79	5.33	7.73	7.95	7.92	KG/mm2
S1-270 (A)	5-1-6	2.08	3.64	5.09	3.55	6.26	9.12	10	9.9	KG/mm2
S1-270 (F)	5-1-7	0.69	1.36	2.04	1.43	2.43	4.05	3.9	3.86	KG/mm2
S1-315 (A)	4-4-3	0.52	0.85	1.26	0.89	1.62	2.64	2.56	2.43	KG/mm2
S1-315 (F)	4-4-4	1.37	2.34	3.2	2.36	4.12	5.87	6.48	5.24	KG/MM2
S2-0	5-1-8	0.41	0.56	0.71	0.59	1.02	1.75	1.78	1.71	KG/mm2
S2-90	5-1-9	0.29	0.36	0.52	0.46	0.72	1.24	1.37	1.21	KG/mm2
S2-180	5-1-10	0.37	0.52	0.71	0.54	0.95	1.73	1.6	1.62	KG/mm2
S2-270	5-1-11	0.22	0.39	0.59	0.33	0.69	1.28	1.23	1.1	KG/mm2
S3-0 (A)	5-1-12	0.09	0.09	-0.15	0.07	0.17	0.35	0.3	0.28	KG/mm2
S3-0 (F)	5-1-13	0.59	0.85	1.19	1.04	1.75	2.82	2.94	2.82	KG/mm2

Table I.1 List of Recorded Peak Values for M-line with LED Supports Under A Waves (Cont'd)

		DE1-4	DE1-5	DE1-6	DE1-1	DE1-2	DE1-3	DE1-3'	DE1-3"	
S3-90 (A)	5-1-14	0.72	1.15	1.65	1.28	2.43	3.44	3.46	3.51	KG/mm2
S3-90 (F)	5-1-15	1.08	1.63	2.34	1.86	3.21	4.89	5.15	5.07	KG/mm2
S3-180 (A)	5-2-1	0.43	0.63	0.87	0.67	1.23	1.92	2.03	2.03	KG/mm2
S3-180 (F)	5-2-2	0.89	1.24	1.76	1.52	2.62	4.27	4.31	4.34	KG/mm2
S3-270 (A)	5-2-3	1.1	1.84	2.71	2.14	3.4	5.48	5.72	5.57	KG/mm2
S3-270 (F)	5-2-4	0.58	0.98	1.43	0.98	1.82	3.23	3.14	2.86	KG/mm2
S4-0	5-2-5	0.43	0.78	0.98	0.82	1.26	1.63	1.5	1.6	KG/mm2
S4-90	5-2-6	0.61	0.95	1.45	0.91	1.97	2.94	2.95	2.9	KG/mm2
S4-180	5-2-7	0.46	0.82	0.97	0.8	1.19	1.88	2.03	1.84	KG/mm2
S4-270	5-2-8	0.48	0.72	1.17	0.63	1.49	2.34	2.21	2.27	KG/mm2
S4-NEJIRI	4-3-1	0.23	0.35	0.49	0.45	0.7	1.15	2.47	1.25	KG/mm2
S5-0	5-2-9	0.13	0.2	0.28	0.2	0.43	0.61	0.59	0.58	KG/mm2
S5-90	5-2-10	0.8	1.39	1.8	1.78	2.6	4.33	4.25	4.38	KG/mm2
S5-180	5-2-11	0.54	0.89	1.34	0.98	2.03	3.05	3.05	3.08	KG/mm2
S5-270	5-2-12	0.5	0.78	1.17	0.85	1.24	1.71	1.62	1.52	KG/mm2
S6-0	5-2-13	0.69	1.13	1.43	1.08	2.45	4.14	4.05	4.16	KG/mm2
S6-90	5-2-14	0.74	1.21	1.39	1.17	1.71	2.32	2.42	2.47	KG/mm2
S6-180	5-2-15	0.2	0.39	0.59	0.41	1.28	2.21	2.16	2.47	KG/mm2
S6-270	5-3-1	0.72	1.1	1.37	1.19	1.71	2.38	2.47	2.42	KG/mm2
S8-0	5-3-2	0.61	0.76	1.04	0.78	1.21	1.54	1.58	1.73	KG/mm2
S8-90	5-3-3	0.39	0.74	0.82	0.67	0.98	1.32	1.24	1.37	KG/mm2
S8-180	5-3-4	0.43	0.56	0.69	0.45	0.8	1.13	1.39	1.47	KG/mm2
S8-270	5-3-5	0.54	1.1	1.47	1.02	1.6	2.01	2.04	2.29	KG/mm2
S9-0	5-3-6	1.19	1.56	2.06	1.56	2.29	3.73	3.34	3.36	KG/mm2
S9-90	5-3-7	0.61	1.19	1.54	1	1.67	2.51	2.36	2.29	KG/mm2
S9-180	5-3-8	1.17	1.6	2.04	1.52	2.27	3.62	3.31	3.27	KG/mm2
S9-270	5-3-9	0.65	1.19	1.54	1.11	1.84	2.66	2.42	0.48	KG/mm2
S11-0	5-3-10	1.28	1.93	2.45	2.01	3.21	4.33	3.85	3.75	KG/mm2
S11-90	5-3-11	0.98	1.28	1.95	1.1	1.86	2.92	2.86	2.81	KG/mm2
S11-180	5-3-12	1.28	1.78	2.29	1.71	2.84	4.12	3.75	3.68	KG/mm2
S11-270	5-3-13	1.1	1.5	2.25	1.26	2.08	3.33	3.07	3.07	KG/mm2
S12-0	5-3-14	0.22	0.39	0.48	0.33	0.71	1	0.87	0.85	KG/mm2
S12-90	5-3-15	0.13	0.22	0.28	0.24	0.35	0.56	0.52	0.54	KG/mm2
S12-180	5-4-1	0.45	0.67	0.97	0.69	1.15	1.76	1.76	1.75	KG/mm2
S12-270	5-4-2	0.11	0.19	0.32	0.24	0.5	0.63	0.54	0.54	KG/mm2
S2' -0	5-4-3	0.32	0.5	0.74	0.46	0.84	1.3	1.39	1.28	KG/mm2
S2' -90	5-4-4	1	1.65	2.32	1.67	2.99	4.66	4.94	4.85	KG/mm2
S2' -180	5-4-5	0.41	0.67	0.91	0.67	1.3	1.97	2.08	2.21	KG/mm2
S2' -270	5-4-6	0.95	1.54	2.21	1.58	2.9	4.44	4.66	4.53	KG/mm2
S2' -NEJIRI	5-4-7	0.26	0.32	0.47	0.34	0.55	0.87	0.9	0.92	KG/mm2
S11' -0	5-4-8	1.71	2.49	3.16	2.55	4.12	5.65	4.96	4.9	KG/mm2
S11' -90	5-4-9	1.34	1.88	2.71	1.54	2.66	4.14	4.05	3.98	KG/mm2
S11' -180	5-4-10	1.78	2.49	3.21	2.43	4.11	5.81	5.09	5.09	KG/mm2
S11' -270	5-4-11	1.37	2.01	2.82	1.69	2.79	4.29	4.29	4.16	KG/mm2
S10-0	5-4-12	0.63	0.91	1.15	0.78	1.28	1.76	1.63	1.67	KG/mm2
S10-90	5-4-13	0.46	1.3	1.34	0.95	1.71	2.19	2.14	2.01	KG/mm2
S10-180	5-4-14	0.58	0.91	1.13	0.91	1.49	2.12	1.82	1.78	KG/mm2
S10-270	5-4-15	0.28	0.63	0.72	0.48	0.76	1.19	1.21	1.11	KG/mm2
MAX. STRESS		2.08	3.64	5.09	3.55	6.26	9.12	10	9.9	KG/mm2
501X (XO)	6-1-3	277	559	867	509	992	1536	1585	1607	GAL
501Z (ZO)	6-1-4	69	126	188	113	230	345	357	360	GAL
PT	6-1-14	34	66	98	57	112	183	193	193	GAL
RL	6-1-15	18	30	39	29	46	61	78	71	GAL
YW	6-2-1	30	53	78	51	95	154	191	193	GAL
ZD2-1	6-2-10	86	159	232	144	308	509	499	509	GAL
ZD2-2	6-2-11	78	135	220	132	259	389	409	396	GAL
ZD2-3	6-2-12	102	178	262	153	245	350	365	367	GAL

Table I.1 List of Recorded Peak Values for M-line with LED Supports Under A Waves (Cont'd)

		D1-4	D1-5	D1-6	D1-1	D1-2	D1-3	D1-3'	D1-3"	
ZD2-4	6-2-13	76	141	215	131	264	414	414	409	GAL
ZD2-5	6-2-14	81	142	200	119	235	345	350	345	GAL
ZD2-6	6-2-15	80	147	205	127	269	406	428	416	GAL
ZD2-7	6-3-1	96	157	230	132	245	379	379	389	GAL
YD1-W	6-3-2	21	35	51	28	51	88	107	110	GAL
YD2-E	6-3-3	24	53	78	42	75	105	137	137	GAL
ZD2-10	6-3-4	81	144	205	123	242	362	404	401	GAL
ZD2-11	6-3-5	76	143	213	118	274	372	396	387	GAL
ZD2-12	6-3-6	80	160	245	125	98	149	379	379	GAL
701X (XB)	6-1-11	294	580	904	538	1043	1597	1661	1685	GAL
701Z (XB)	6-1-12	72	137	213	127	252	396	399	392	GAL

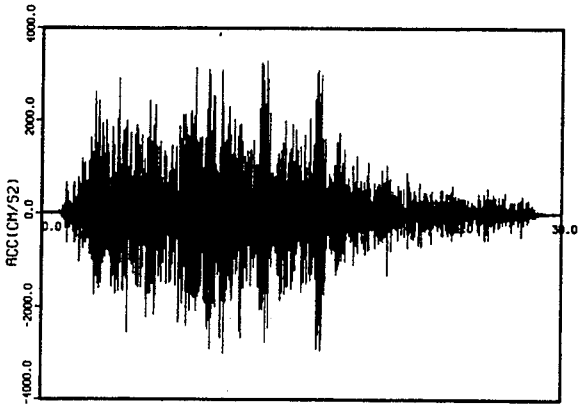

Figure I.1 MA16-X

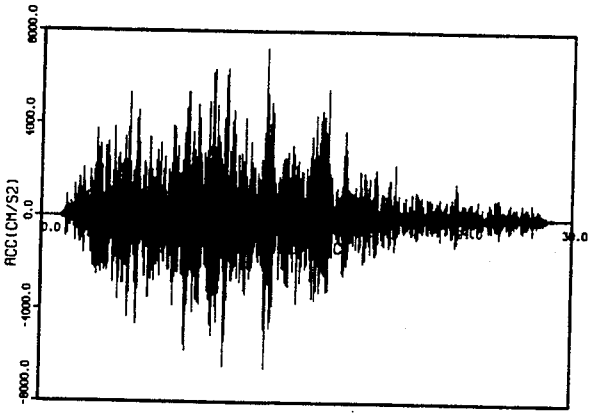

Figure I.2 MA16-Y

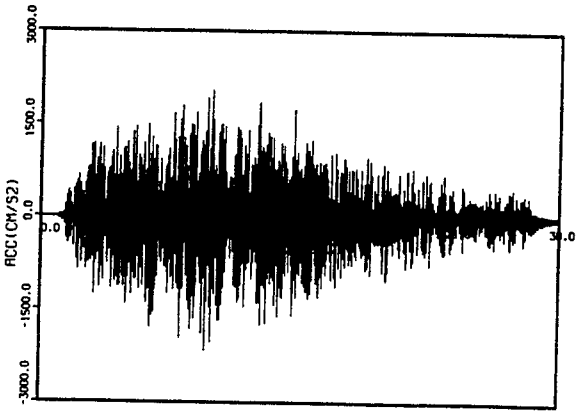

Figure I.3 MA16-Z

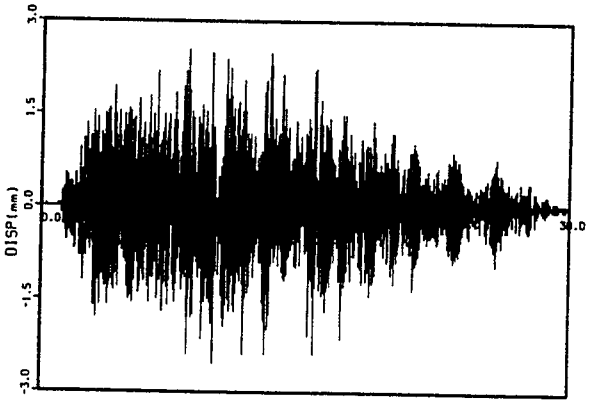

Figure I.4 MD15

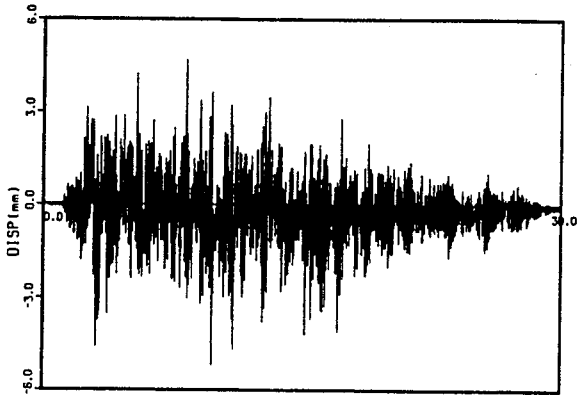

Figure I.5 MD16

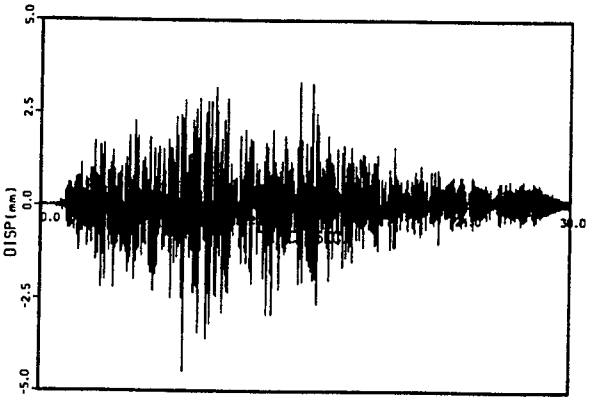

Figure I.6 MD17

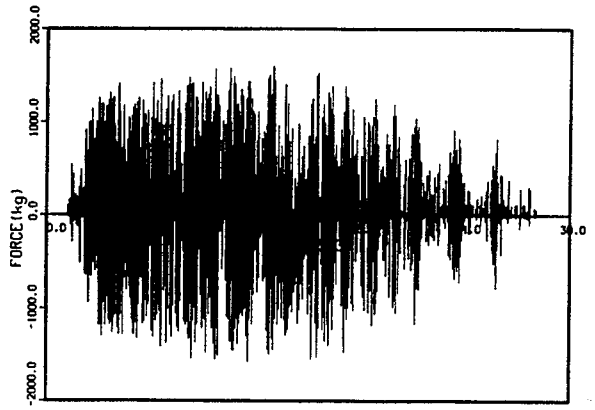

Figure I.7 MR15

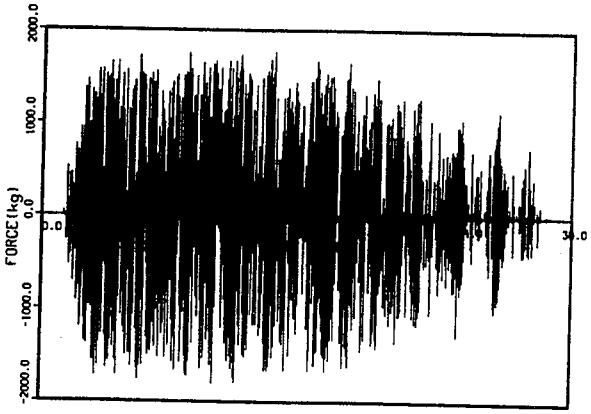

Figure I.8 MR16

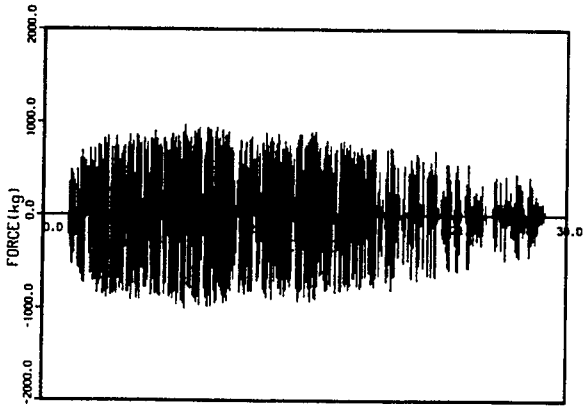

Figure I.9 MR12

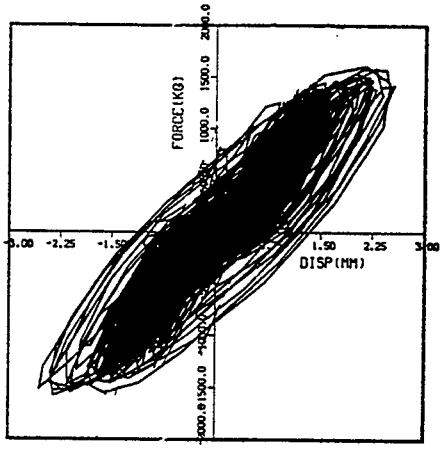

Figure I.10 LED-1

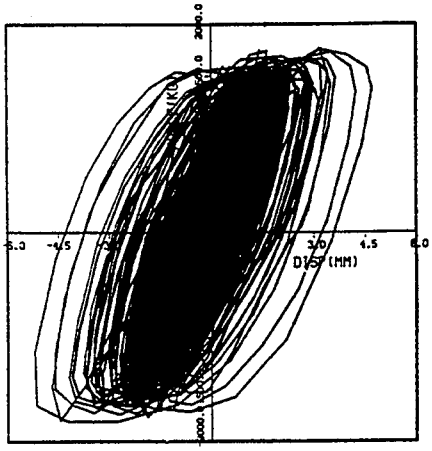

Figure I.11 LED-2

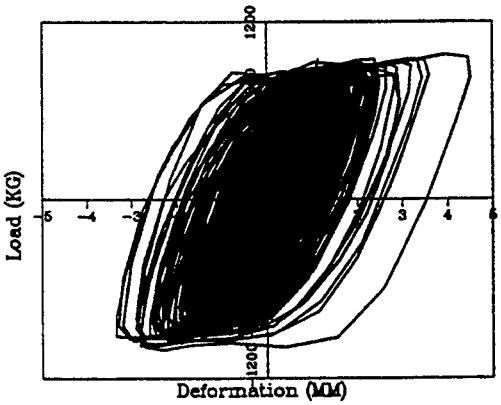

Figure I.12 LED-3

APPENDIX J

LIST OF PEAK RESPONSE VALUES AND PLOTS OF SELECTED CHANNELS FOR TOKACHIOKI (M-LINE) TEST RUN (RUN NO. 95071403)

Table J.1 List of Recorded Peak Values for M-line with LED Supports under Tokachi-Oki Waves

	Test no.	950705-10	950706-06	950707-03	950707-04	950707-05	950707-07	950714-03	
		Tak. 1128ga	Tak. 1504ga	Tak. 1880ga	Tak. 2256ga	Tak. 2444ga	Tak. 2483ga	Tak. 2519ga	
Sensor	S/G CH	H (0.8T)	H (0.8T)	H (0.8T)	H (0.8T)	H (0.8T)	H (0.8T)	H (0.8T)	Unit
AA1-X	1-1-2	1300	1777	2124	2558	2861	2818	2861	GAL
AA1-Y	1-1-1	82	74	82	140	165	165	190	GAL
AA1-Z	1-1-3	41	57	65	98	131	181	255	GAL
AA2-X	1-1-4	1261	1751	2128	2634	2834	2835	2835	GAL
AA2-Y	1-1-5	73	73	90	123	172	180	271	GAL
AA2-Z	1-1-6	25	50	50	75	84	67	75	GAL
AD1-Y	1-1-8	1186	2165	3030	5410	7704	9219	8383	KG
AD1-Z	1-1-9	2194	3409	4316	4809	5024	5145	5431	KG
AS1	1-1-10	800	993	1739	4516	5667	6367	6260	KG
SA2-X	1-1-12	1265	1731	2123	2629	2833	2792	2809	GAL
SA2-Z	1-1-13	50	66	75	83	91	108	108	GAL
SA3-X	1-1-14	1250	1727	2133	2610	2821	2797	2813	GAL
SA1-X	1-2-2	1250	1709	2121	2604	2810	2802	2802	GAL
MA1-X	3-3-10	1624	2206	2411	3660	4412	3916	6037	GAL
MA1-Y	3-3-11	835	1382	1842	2533	3769	3894	5318	GAL
MA1-Z	3-3-12	613	806	865	1260	1689	1857	2487	GAL
MA16-X	3-3-13	1752	2384	2547	3383	3505	4219	4423	GAL
MA16-Y	3-3-14	1282	1664	2071	3009	4373	5245	6166	GAL
MA16Z	3-3-15	798	899	1031	1868	3225	2891	3682	GAL
MA17X	3-4-1	1777	2275	2807	4418	4966	6461	5880	GAL
MA17Y	3-4-2	1076	1717	1749	3095	4377	5113	5857	GAL
MA17Z	3-4-3	795	915	1020	1951	2859	2642	3751	GAL
MA4-X	3-4-4	1966	2493	3053	4348	5323	6091	5915	GAL
MA4-Y	3-4-5	1253	1909	2515	3228	3588	3752	4162	GAL
MA4-Z	3-4-6	597	779	926	1705	2121	2250	2527	GAL
MA5-X	3-4-7	1941	2499	2843	4260	5080	6252	6006	GAL
MA5-Y	3-4-8	1267	1922	2552	3460	3591	3681	4188	GAL
MA6-X	3-4-9	1725	2533	2691	3933	10841	5933	5058	GAL
MA6-Y	3-4-10	1024	1868	2540	3982	11537	3654	4310	GAL
MA7-X	3-4-11	1216	1686	2059	2511	2713	2704	2805	GAL
MA7-Z	3-4-12	34	51	85	94	115	154	222	GAL
MA8-X	3-4-13	1803	2420	2821	3505	3898	4424	5225	GAL
MA8-Y	3-4-14	980	1534	2112	3036	3197	3863	3751	GAL
MA8-Z	3-4-15	956	2111	2713	3027	4487	4990	7432	GAL
MA9-X	4-1-1	1713	2325	3211	3782	4270	4221	4204	GAL
MA9-Y	4-1-2	893	1048	1270	1737	3015	3154	3326	GAL
MA9-Z	4-1-3	1050	1872	2310	2590	3622	3482	5687	GAL
MA10-X	4-1-4	1608	2283	3014	3616	4136	4136	4014	GAL
MA10-Y	4-1-5	412	602	848	1419	1427	1363	1201	GAL
MA10-Z	4-1-6	1004	2355	2800	2882	4792	5056	7790	GAL
MA11-X	4-1-7	1252	1727	2139	2687	2902	2961	2971	GAL
MA11-Y	4-1-8	192	389	624	645	812	846	1449	GAL
MA11-Z	4-1-9	46	75	118	122	181	193	278	GAL
MA12-X	4-1-10	1368	1822	2205	2999	3042	3099	3047	GAL
MA-12-Y	4-1-11	166	328	533	533	665	743	1185	GAL
MA12-Z	4-1-12	57	109	114	202	255	303	351	GAL
MA13-X	4-1-13	2909	2948	3641	3661	3403	4215	3205	GAL
MA13-Y	4-1-14	481	787	603	795	1345	1016	1123	GAL
MA13-Z	4-1-15	675	816	958	1200	1158	1200	1300	GAL
MA14-X	4-2-1	1244	1718	2138	1616	2875	2962	2927	GAL
MA14-Y	4-2-2	221	382	685	685	886	926	1571	GAL
MA14-Z	4-2-3	58	116	125	200	250	350	400	GAL
MA15-X	4-2-4	2646	3986	3942	4709	5206	4882	5012	GAL
MA15-Y	4-2-5	899	1064	1100	1176	1995	1349	1839	GAL
MA15-Z	4-2-6	492	593	766	1039	997	955	1292	GAL

Table J.1 List of Recorded Peak Values for M-line with LED Supports under Tokachi-Oki Waves (Cont'd)

		Tak. 1128ga	Tak. 1504ga	Tak. 1880ga	Tak. 2256ga	Tak. 2444ga	Tak. 2483ga	Tak. 25119ga	
MD12	4-2-7	3.55	5	6.15	10	14.8	14.45	1725	mm
MD13	4-2-8	0.8	1.55	2.95	6.8	9.65	11	10.2	mm
MD15	4-2-11	1.7	2.25	2	2.7	76.85	102.35	4.65	mm
MD16	4-2-12	6.15	10.75	17.3	35	50.85	56.65	54.9	mm
MD18-X	4-3-2	6.05	10	16.20	33	46.5	51.8	50.85	mm
MD18-Y	4-3-3	4.6	8.25	12.8	24	34.5	72	35.95	mm
MD18-Z	4-2-13	1.15	1.6	2.3	8.8	13.5	82.3	15.25	mm
MD17-Z	4-2-14	1.15	1.6	2.25	8.85	13.1	82.2	15.3	mm
MD14-X	4-2-15	5.35	8.3	12.5	23.6	33.85	63.3	65.65	mm
MD9-Y	4-3-5	0.24	0.23	0.25	0.27	0.32	0.3	0.41	mm
MD10-Z	4-3-6	0.31	0.32	0.34	0.36	0.38	0.37	1.98	mm
MD11X	4-3-7	0.33	1.78	1.86	1.91	2.02	2	1730	mm
MD15(1.5T)	4-3-11	1181	1333	1359	1578	1707	1727	1199	KG
MD16(1.5T)	4-3-12	1789	1980	2005	1970	1944	1912	1199	KG
MD17(1.0T)	4-3-13	740	785	875	1165	1262	1307	9998	KG
MR8	4-3-15	226	422	145	4237	9320	12047	4536	KG
MR11(0.3T)	4-4-5	23	25	25	29	34	37	9998	KG
MR12(0.3T)	4-4-6	24	29	38	61	63	73	82	KG
MR13	4-4-7	142	182	207	251	278	248	61	KG
MR14	4-4-8	212	313	371	415	417	410	261	KG
MP1	4-4-9	0.9	1.22	1.16	2.09	2.51	2.06	386	KG/CM2
MP2	4-4-10	0.92	1.51	1.38	2.3	3.16	2.83	3.42	KG/CM2
TE1	4-2-9	26	26	27	28	29	30	4.48	C
TE2	4-2-10	28	36	51	80	102	107	107	C
TE3	4-4-14	26	25	27	31	36	37	40	C
S0-0	4-4-11	1.04	1.45	1.91	3.59	4.07	5.05	5.37	KG/mm2
S0-90	4-4-12	0.8	1.1	1.5	3.01	4.31	4.7	4.59	KG/mm2
S0-180	4-4-13	2.06	2.69	2.97	5.24	6.3	7.15	7.43	KG/mm2
S0-270	4-4-14	1.24	1.45	1.89	2.75	3.59	4.09	3.99	KG/mm2
S1-0 (A)	4-4-15	0.09	0.13	0.17	10.47	0.59	0.59	0.58	KG/mm2
S1-0 (F)	5-1-1	0.84	1.11	1.39	3.34	4.74	5.7	5.18	KG/mm2
S1-45 (A)	4-3-8	1.15	1.56	1.73	3.85	5.76	6.95	6.24	KG/mm2
S1-45 (F)	4-3-9	1.8	2.19	2.88	4.11	5.52	6	6.17	KG/mm2
S1-90	5-1-2	3.46	4.4	5.44	7.6	9.94	10.94	11.29	KG/mm2
S1-90	5-1-3	2.03	2.68	3.05	6.11	9.29	11.46	10.54	KG/mm2
S1-135 (A)	4-3-10	2.27	3.07	3.6	7.32	11.17	14.05	17.93	KG/mm2
S1-135 (F)	4-3-14	3.44	4.46	5.15	7.32	10.2	11.74	11.33	KG/mm2
S1-180 (A)	5-1-4	0.48	0.65	0.89	2.21	3.23	3.86	3.44	KG/mm2
S1-180 (F0	5-1-5	1.21	1.71	2.21	5.13	7.32	8.82	8.04	KG/mm2
S1-225 (A)	4-4-1	1.3	1.73	2.38	4.2	6.15	6.89	7.3	KG/mm2
S1-225 (F)	4-4-2	3.59	4.46	5.29	7.49	10.55	12.13	11.96	KG/mm2
S1-270 (A)	5-1-6	4.33	5.54	6.37	9.57	13.28	16.55	15.84	KG/mm2
S1-270 (F)	5-1-7	1.24	1.63	2.27	3.92	5.95	6.52	6.83	KG/mm2
S1-315 (A)	4-4-3	0.74	0.97	1.36	3.31	4.7	5.18	5.05	KG/mm2
S1-315 (F)	4-4-4	2.58	3.47	3.94	6.47	9.05	11.41	10.74	KG/MM2
S2-0	5-1-8	1.58	2.66	4.11	7.73	10.72	11.43	11.28	KG/mm2
S2-90	5-1-9	0.33	0.72	0.98	1.97	2.97	3.23	3.47	KG/mm2
S2-180	5-1-10	1.45	2.42	3.6	6.76	9.4	10.05	10	KG/mm2
S2-270	5-1-11	0.35	0.63	0.61	1.08	1.67	1.82	1.76	KG/mm2
S3-0 (A)	5-1-12	0.19	0.39	0.59	1.17	1.58	1.67	1.54	KG/mm2
S3-0 (F)	5-1-13	2.6	4.35	6.32	11.78	16.18	17.28	17.11	KG/mm2
S3-90 (A)	5-1-14	1.67	3.16	5.09	10.07	13.75	15.27	14.73	KG/mm2
S3-90 (F)	5-1-15	3.36	5.41	8.23	15.88	21.77	22	20.99	KG/mm2
S3-180 (A)	5-2-1	1.71	2.99	4.29	8.42	11.82	12.39	12.34	KG/mm2
S3-180 (F)	5-2-2	3.86	6.52	9.59	17.95	25.02	26.85	26.94	KG/mm2
S3-270 (A)	5-2-3	2.16	3.2	4.79	7.99	10.92	11.59	11.93	KG/mm2
S3-270 (F)	5-2-4	2.9	4.94	7.67	14.06	19.47	20.44	2.32	KG/mm2

Table J.1 List of Recorded Peak Values for M-line with LED Supports under Tokachi-Oki Waves (Cont'd)

		Tak. 1128ga	Tak. 1504ga	Tak. 1880ga	Tak. 2256ga	Tak. 2444ga	Tak. 2483ga	Tak. 25119ga	
S4-0	5-2-5	0.82	1.21	1.62	3.07	4.5	4.96	4.81	KG/mm2
S4-90	5-2-6	0.67	1.04	1.84	3.98	7.04	7.21	7.69	KG/mm2
S4-180	5-2-7	0.85	1.06	1.19	1.76	2.06	2.27	2.14	KG/mm2
S4-270	5-2-8	0.67	0.93	1.37	3.16	5.61	5.54	6.32	KG/mm2
S4-NEJIRI		0.35	0.46	0.53	0.8	1.1	1.27	1.32	KG/mm2
S5-0	5-2-9	0.2	0.3	0.52	0.76	1.11	1.21	1.15	KG/mm2
S5-90	5-2-10	1.36	2.55	4.33	8.21	12.06	13.67	13.84	KG/mm2
S5-180	5-2-11	1.37	1.75	2.51	3.96	6.11	6.89	6.73	KG/mm2
S5-270	5-2-12	0.95	1.13	1.1	2.27	3.21	3.46	3.94	KG/mm2
S6-0	5-2-13	1.36	1.69	1.71	2.66	3.98	3.72	4.46	KG/mm2
S6-90	5-2-14	1.47	1.93	2.42	3.88	4.74	5.67	4.77	KG/mm2
S6-180	5-2-15	1.1	1.26	1.52	2.27	3.62	3.53	4.31	KG/mm2
S6-270	5-3-1	1.24	1.88	2.43	3.92	4.7	5.55	4.74	KG/mm2
S8-0	5-3-2	0.74	1.3	2.32	4.77	7.34	8.47	8.43	KG/mm2
S8-90	5-3-3	0.78	1.11	1.15	2.03	2.75	3.33	3.34	KG/mm2
S8-180	5-3-4	0.85	1.88	2.84	5.61	8.42	9.6	9.38	KG/mm2
S8-270	5-3-5	1.28	1.93	1.86	3.36	4.74	5.28	5.15	KG/mm2
S9-0	5-3-6	1.08	1.52	2.68	4.61	5.81	7.38	8.3	KG/mm2
S9-90	5-3-7	1.86	2.04	2.16	2.75	3.36	4.51	4.2	KG/mm2
S9-180	5-3-8	1.37	1.82	2.66	5.05	5.74	7.62	7.86	KG/mm2
S9-270	5-3-9	1.62	1.65	1.91	2.58	3.25	4.22	3.81	KG/mm2
S11-0	5-3-10	1.08	1.63	2.27	3.27	3.64	5.11	5.44	KG/mm2
S11-90	5-3-11	3.77	5.2	6.39	8.23	10.81	12.08	11.59	KG/mm2
S11-180	5-3-12	1.1	1.86	2.86	4.12	4.7	6.6	6.82	KG/mm2
S11-270	5-3-13	4.33	6.04	7.36	9.7	12.78	14.42	13.99	KG/mm2
S12-0	5-3-14	1.06	1.08	1.23	1.43	1.75	1.54	1.49	KG/mm2
S12-90	5-3-15	0.3	0.5	0.61	0.48	0.58	0.67	0.78	KG/mm2
S12-180	5-4-1	1.88	1.93	2.4	2.34	3.12	2.95	3.2	KG/mm2
S12-270	5-4-2	0.93	0.95	1	1.17	1.32	1.19	1.17	KG/mm2
S2' -0	5-4-3	0.32	0.48	0.72	2.19	3.38	3.77	3.86	KG/mm2
S2' -90	5-4-4	1.99	2.75	3.57	5.35	7.84	9.4	8.94	KG/mm2
S2' -180	5-4-5	0.61	0.76	1.1	2.66	4.03	4.7	4.33	KG/mm2
S2' -270	5-4-6	2.03	2.77	3.59	5.59	8.03	9.6	9.14	KG/mm2
S2' -NEJIRI	5-4-7	0.21	0.32	0.48	1.72	2.77	3.18	3.15	KG/mm2
S11' -0	5-4-8	1.49	2.16	3.14	4.53	5.03	7.12	7.34	KG/mm2
S11' -90	5-4-9	5.35	7.39	9.07	11.15	14.36	16.01	15.4	KG/mm2
S11' -180	5-4-10	1.45	2.29	3.57	4.96	5.81	8.01	8.6	KG/mm2
S11' -270	5-4-11	5.68	7.91	9.66	11.67	15.25	17.18	16.52	KG/mm2
S10-0	5-4-12	1.11	1.52	2.19	3.88	4.59	5.83	4.87	KG/mm2
S10-90	5-4-13	1.39	2.03	3.14	6.78	9.01	10.76	9.27	KG/mm2
S10-180	5-4-14	0.8	1	1.3	1.84	2.47	2.38	3.03	KG/mm2
S10-270	5-4-15	1	1.52	2.06	4.2	5.78	6.8	6.3	KG/mm2
MAX. STRESS		5.68	7.91	9.66	17.95	25.02	26.85	26.94	KG/mm2
501X (XO)	6-1-3	1264	1734	2119	2606	2810	2805	2864	GAL
501Z (ZO)	6-1-4	19	22	26	34	34	51	49	GAL
PT	6-1-14	56	95	137	120	137	164	166	GAL
RL	6-1-15	17	22	29	36	31	31	49	GAL
YW	6-2-1	83	122	122	124	117	107	132	GAL
ZD2-1	6-2-10	85	124	178	213	218	289	240	GAL
ZD2-2	6-2-11	39	53	66	75	107	115	129	GAL
ZD2-3	6-2-12	93	147	208	213	215	200	240	GAL
ZD2-4	6-2-13	39	61	75	83	83	107	100	GAL
ZD2-5	6-2-14	44	75	98	93	112	107	124	GAL
ZD2-6	6-2-15	53	90	105	115	134	181	191	GAL
ZD2-7	6-3-1	58	110	154	129	142	193	154	GAL
YD1-W	6-3-2	36	63	68	90	93	83	85	GAL
YD2-E	6-3-3	80	115	115	127	124	124	151	GAL

Table J.1 List of Recorded Peak Values for M-line with LED Supports under Tokachi-Oki Waves (Cont'd)

		Tak. 1128ga	Tak. 1504ga	Tak. 1880ga	Tak. 2256ga	Tak. 2444ga	Tak. 2483ga	Tak. 25119ga	
ZD2-10	6-3-4	63	147	147	159	154	218	181	GAL
ZD2-11	6-3-5	39	36	33	53	73	80	95	GAL
ZD2-12	6-3-6	66	120	149	173	183	200	225	GAL
701X (XB)	6-1-11	1259	1722	2129	2633	2829	2800	2824	GAL
701Z (XB)	6-1-12	22	22	29	31	39	36	53	GAL

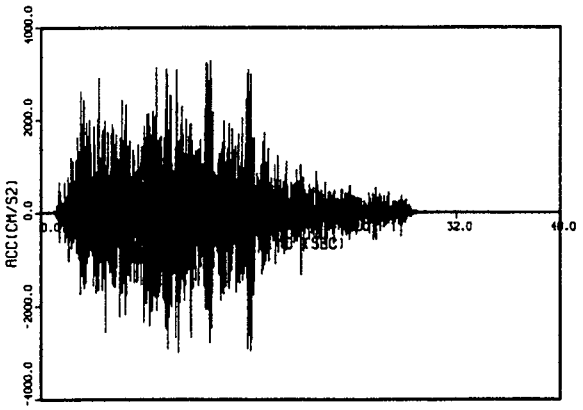

Figure J.1 MA16-X

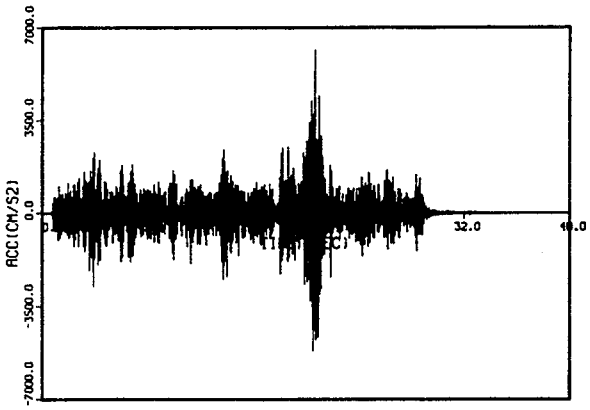

Figure J.2 MA16-Y

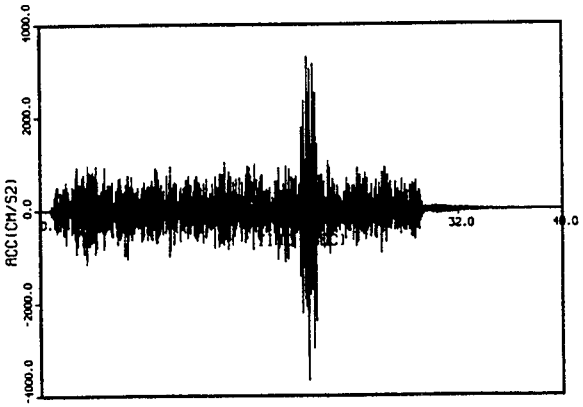

Figure J.3 MA16-Z

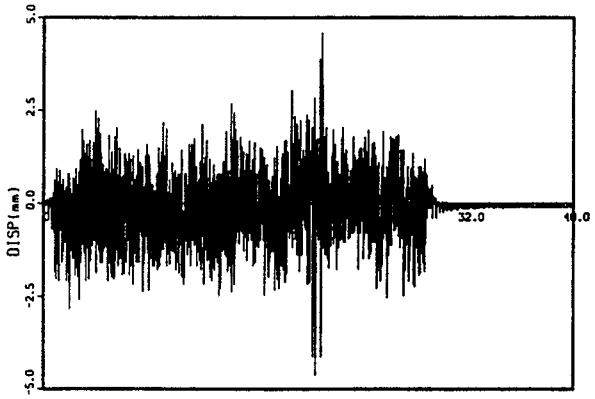

Figure J.4 MD15

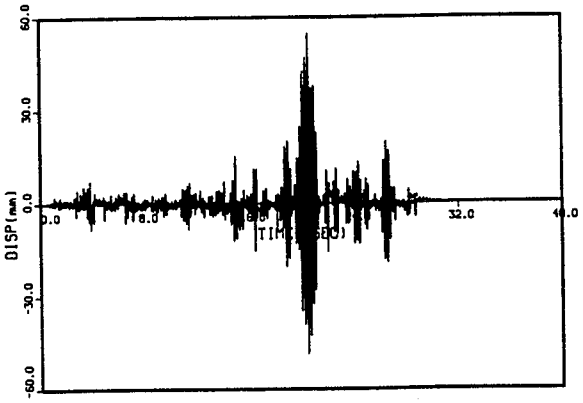

Figure J.5 MD16

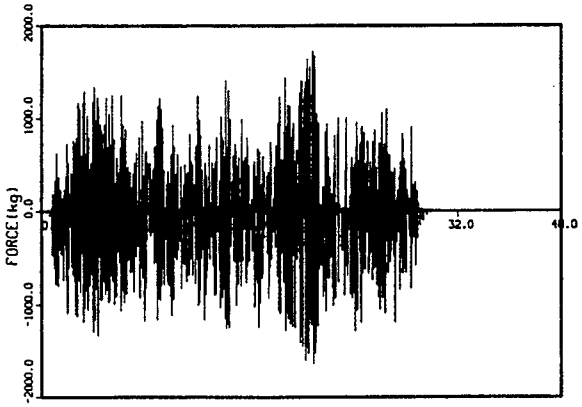

Figure J.6 MR15

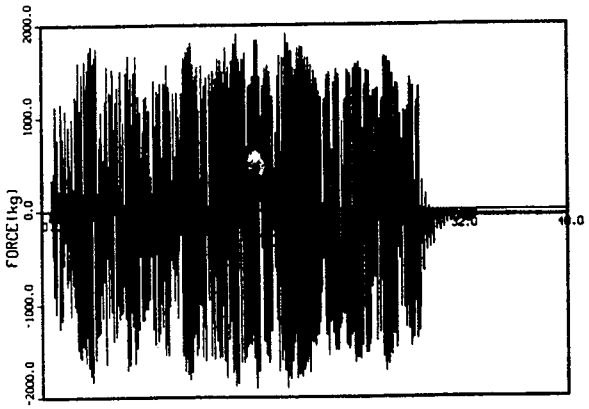

Figure J.7 MR16

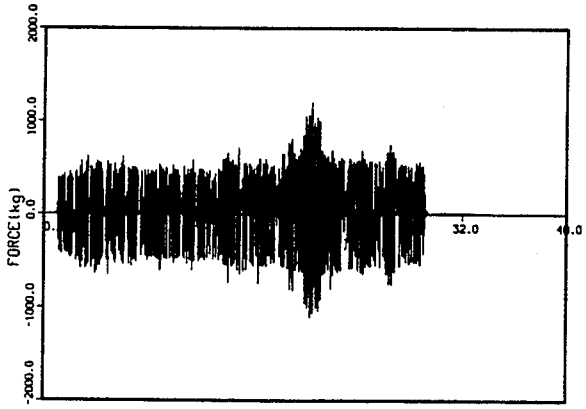

Figure J.8 MR17

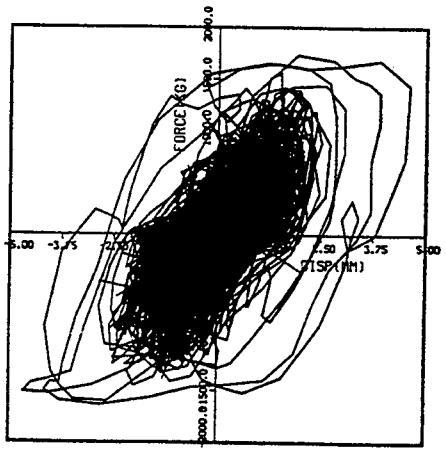

Figure J.9 LED-1

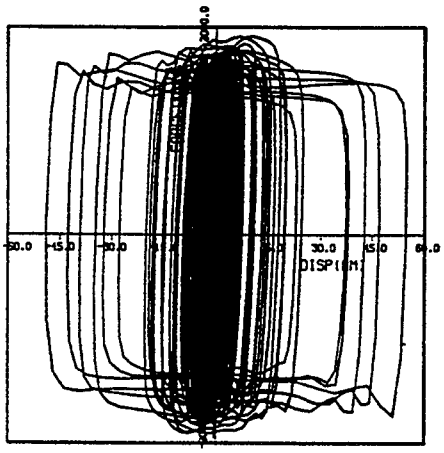

Figure J.10 LED-2

APPENDIX K

PRACTICAL APPLICATION OF EQUIVALENT LINEARIZATION APPROACHES TO NONLINEAR PIPING SYSTEMS[1]

[1]Note: This paper was presented during the ASME/PVP Conference, Honolulu, Hawaii, in 1989.

Practical Application of Equivalent Linearization Approaches to Nonlinear Piping Systems

Young J. Park
Department of Advanced Technology
Brookhaven National Laboratory
Upton, New York 11973

Charles H. Hofmayer
Department of Advanced Technology
Brookhaven National Laboratory
Upton, New York 11973

INTRODUCTION

The use of mechanical energy absorbers as an alternative to conventional hydraulic and mechanical snubbers for piping supports has attracted a wide interest among researchers and practitioners in the nuclear industry (e.g., Ref. [1] and [2]). The basic design concept of energy absorbers (EA) is to dissipate the vibration energy of piping systems through nonlinear hysteretic actions of EA's under design seismic loads. Therefore, some type of nonlinear analysis needs to be performed in the seismic design of piping systems with EA supports.

The equivalent linearization approach (ELA) can be a practical analysis tool for this purpose, particularly when the response spectrum approach (RSA) is also incorporated in the analysis formulations. In this paper, the following ELA/RSA methods are presented and compared to each other regarding their practicality and numerical accuracy:

- Response spectrum approach using the square root of sum of squares (SRSS) approximation (denoted RS in this paper).
- Classical ELA based on modal combinations and linear random vibration theory (denoted CELA in this paper).
- Stochastic ELA based on direct solution of response covariance matrix (denoted SELA in this paper).

New algorithms to convert response spectra to the equivalent power spectral density (PSD) functions are presented for both the above CELA and SELA methods. The numerical accuracy of the three ELA/RSA's are studied through a parametric error analysis. Finally, the practicality of the presented analysis methods is demonstrated in two application examples for piping systems with EA supports.

EQUIVALENT LINEARIZATION APPROACHES

RS Method. According to the classical study by Caughey (1963), the equivalent stiffness, k_{eq} of a hysteretic system is obtained based on the slowly-varying assumption on the nonlinear oscillation, as

$$K_{eq} = \frac{1}{\pi U}\int_0^{2\pi} F(u)\cdot\cos\theta\, d\theta, \quad u = U\cdot\cos\theta \qquad (1)$$

in which, U is the peak displacement amplitude; F(u) is the nonlinear restoring force for the largest hysteresis loop as a function of displacement, u.

For the equivalent modal damping, h_{eq}, the formulation proposed by Tansirikongkol and Pecknold (1980), which is a slight modification of the formulation proposed by Caughey (1963), is used in this study.

$$h_{eq,r} = h_{o,r}\frac{\omega_r}{\omega_{eq,r}} + \frac{\sum_i \epsilon_{ir}^2\cdot S_i}{2M_r\cdot\omega_{eq,r}^2} \qquad (2)$$

$h_{o,r}$ = elastic modal damping
ω_r = frequency for r-th mode
$\omega_{eq,r}$ = equivalent frequency
M_r = modal mass
ϵ_{ir} = modal strain of component-i
S_i = normalized hysteresis area of component-i

$$= \frac{A}{\pi U^2} = \frac{4}{\pi}K_e(1-\alpha)\left(\frac{\mu-1}{\mu^2}\right)\cdots$$

...for bilinear system

A = area of a hysteresis loop
μ = ductility factor of the response

The SRSS approximation is used in the iterative solution scheme, in which the above k_{eq} and h_{eq} are updated, followed by a new eigenvalue analysis of the equivalent linear system.

CELA Method. The method is based on the linear random vibration theory and a modified Kryloff-Bogoliubov equivalent linearization approach. A displacement component, u_i, in a piping system is expressed as,

$$u_i = \sum_r \phi_{ir} q_r + \sum_m \varphi_{im} X_m \qquad (3)$$

in which, q_r is the r-th normal mode response; ϕ_{ir} is the eigenvector of the fixed-based system; X_m is the differential displacement at the m-th fixed degree of freedom; and φ_{im} is the displacement mode due to the m-th differential displacement. Assuming stationality of responses, the covariance for a pair of displacements, u_i and u_j, are obtained as,

$$R_{u_i u_j}(\omega) = \sum_r \sum_s \phi_{ir}\phi_{is} R_{rs} + \sum_m \sum_n \varphi_{im}\varphi_{jm} \bar{R}_{mn} \qquad (4)$$

in which, R_{rs} is the covariance for the r-th and s-th normal mode responses; and $\bar{R}_{mn}$ is the covariance for the m-th and n-th differential displacements.

$$R_{rs} = \sum_k \sum_l C_{kl} \beta_{rk} \beta_{sl} \int_{-\infty}^{\infty} H_r(\omega) H_s(\omega) \sqrt{S_k(\omega) S_l(\omega)}\, d\omega \qquad (5)$$

$$\bar{R}_{mn} = C_{mn} \int_{-\infty}^{\infty} \frac{1}{\omega_4} \sqrt{S_m(\omega) S_n(\omega)}\, d\omega \qquad (6)$$

in which, C_{kl} is the correlation coefficient for the k-th and l-th excitations; β_{rk} is the r-th participation factor for the k-th excitation; $H_r(\omega)$ is the transfer function for the r-th mode; and $S_k(\omega)$ is the k-th PSD function.

The equivalent component stiffness, k_{eq}, and modal damping, h_{eq}, can be defined using the peak distribution functions, $p_1(u, \sigma_e)$ and $p_2(u, \sigma_e)$, as,

$$K_{eq} = \int_0^{\infty} K_{eq}(u) \cdot p_1(u, \sigma_e)\, du \qquad (7)$$

$$h_{eq} = \int_0^{\infty} h_{eq}(u) \cdot p_2(u, \sigma_e)\, du \qquad (8)$$

in which, σ_e is the standard deviation of the strain response. The foregoing eqs. (1) and (2) can be used for the peak response dependent stiffness and damping, $K_{eq}(u)$ and $h_{eq}(u)$.

For the above peak distribution functions, p_1 and p_2, various mathematical models have been suggested in the past (e.g., Refs. [5] and [6]). In this study, the peak distribution functions, p_1 and p_2, are determined in a purely empirical manner based on the observation of the past simulation studies on bilinear hysteretic systems (e.g., Ref. [5] and [7]). The details of the distribution functions are given in an Appendix to this paper.

SELA Method. The method is the direct solution of the response covariance matrix based on the stochastic equivalent linearization approach proposed by Atalik and Utku (1976). This approach may be one of the most popular research topics in this area, and has been applied to hysteretic systems with a relatively small number of degrees of freedom (e.g., Refs. [9] and [10]). According to Wen (1980), the nonlinear restoring force, q, is expressed as,

$$q = \alpha K u + (1 - \alpha) K Z \qquad (9)$$

$$\dot{Z} = f(\dot{u}, Z) \qquad (10)$$

in which u and $\dot{u}$ = the relative displacement and velocity; K = the initial stiffness; α = the postyield stiffness ratio; and Z = the hysteretic component with the unit of displacement. According to Ref. [11], the above hysteretic function, $f(\dot{u}, Z)$, for a bilinear system is expressed as,

$$\dot{Z} = \dot{u} - 0.5\dot{u} H_1(Z) - 0.5 |\dot{u}| H_2(Z) \qquad (11)$$

where

$$H_1(Z) = U(Z - \Delta) + U(-Z - \Delta)$$
$$H_2(Z) = U(Z - \Delta) - U(-Z - \Delta) \qquad (12)$$

in which U(x) = unit step function; and Δ = the yield displacement.

Another class of hysteretic models are obtained by smoothing these functions, $H_1(Z)$ and $H_2(Z)$, as follows:

$$H_1(Z) = \frac{|Z|^n}{\Delta^n}$$
$$H_2(Z) = \frac{Z|Z|^{n-1}}{\Delta^n} \qquad (13)$$

and therefore

$$\dot{Z} = \dot{u} - \frac{0.5}{\Delta^n}\dot{u}|Z|^n - \frac{0.5}{\Delta^n}|\dot{u}|Z|Z|^{n-1} \qquad (14)$$

More detailed description on the practical application of this approach to nonlinear piping systems, including the determination of the maximum response statistics, can be found in Refs. [12], and [13].

RESPONSE SPECTRUM APPROACHES

RS Method. It is one of the significant advantages of this approach that the response spectra can be used directly as the excitation input. However, as the modal damping values change during the iteration according to eq. (2), an interpolation/extrapolation scheme is necessary for converting the response spectral values for an arbitrary damping value, h. In this study, the following empirical formulations are used (Ref. [14]):

$$\frac{S(h)}{S(h=0)} = \frac{1}{1+10h} \quad \text{for } 0.02<h<0.05$$
$$\frac{S(h)}{S(h=0.05)} = \frac{2.25}{1.75+10h} \quad \text{for } 0.05<h<0.2 \qquad (15)$$

CELS Method. Since the method is based on linear random vibration theory, the input response spectra should be converted to an equivalent PSD function. A high accuracy direct conversion method has been developed recently for this purpose (Ref. [15]). The conversion algorithm is summarized below.

The objective here is to obtain an equivalent PSD function, $S_g(\omega)$, given a target acceleration response spectrum, $R_t(\omega, h)$, and a modulating envelope function, I(t), which can be represented by the effective duration, T_e.

The unknown PSD function is discretized at radial frequencies, ω_j, and expressed as the sum of a series of discretized power components, p_j, as,

$$S_g(\omega) = \sum_{j=1}^{m} S(\omega_j)\,\Delta\omega_j\,\delta(\omega_j) = \sum_{j=1}^{m} p_j\,\delta(\omega_j) \qquad (16)$$

in which, $\delta(\omega)$ is the Dirac delta function; and $\Delta\omega_j$ is the incremental radial frequency.

Using the above discretized power components, p_j , the target response spectrum at radial frequencies, ω_k , can be approximated by a superposition of the component response spectra as,

$$R_t^2(\omega_k, h) = \sum_{j=1}^{m} p_j\,R_{k,j}^2(\omega_k, \omega_j, h), \qquad k = 1,n \qquad (17)$$

in which, $R_{k,j}$ represents the peak acceleration response of an SDOF system with a vibration frequency of ω_k , and a viscous damping of h, which is excited by an extremely narrow-banded process whose PSD function is $\delta(\omega_j)$. Using the peak factor approximation by Davenport (1963), $R_{k,j}$ is determined as,

$$R_{k,j}(\omega_k, \omega_j, h) = \left\{\sqrt{2\ln(\nu_j T_e)} + \frac{3.772}{\sqrt{2\ln(\nu_j T_e)}}\right\} \cdot \sqrt{\frac{1+4h^2\chi^2}{(1-\chi^2)^2+4h^2\chi^2}} \qquad (18)$$

in which, $\nu_j = \omega_j/2\pi$, and $\chi = \omega_j/\omega_k$. Given a modulating function, I(t), the equivalent duration, T_e , can be defined as,

$$T_e = \left\{\int_0^t I(t)\,dt\right\} / \max\{I(t)\} \qquad (19)$$

The above power components, p_j , can be obtained by solving a standard least squares problem as,

$$\text{minimize} \quad \sum_{k=1}^{n}\left\{R_t^2(\omega_k,h) - \sum_{j=1}^{m} p_j\,R_{k,j}^2(\omega_k,\omega_j,h)\right\}^2 \qquad (20)$$
$$\text{subject to} \quad p_j \geq 0, \quad j = 1,m$$

Mathematical libraries to solve the above least squares problem is widely available (e.g., IMSL programs). The equivalent PSD function is directly obtained as,

$$S(\omega_j) = p_j/\Delta\omega_j, \quad j = 1,m \qquad (21)$$

The method was applied to response spectra with steep slopes and sharp turning points; one is the Reg. Guide 1.60 spectrum (Ref. [18]), and the other is a Newmark-Hall type spectrum (Ref. [19]). The following modulating function was assumed to determine the effective duration, T_e, of 16.8 sec.

$$\begin{aligned} I(t) &= (t/3)^2 && t<3 \text{ sec.} \\ &= 1.0 && 3<t<16 \text{ sec.} \\ &= e^{-(t-16)/13} && 16<t<20 \text{ sec.} \end{aligned} \qquad (22)$$

To discretize both the PSD and response spectrum functions, 100 frequency points between 0.15Hz and 50Hz, equally spaced on a logarithmic scale, were used (i.e., m = n = 100). The comparisons with the Monte Carlo simulations (500 samples) are shown in Fig. 1 and the obtained PSD functions are shown in Fig. 2. The simulations were performed by using the modulating function of eq. (22) and the PSD functions of Fig. 2. The simulation results slightly overestimate the zero-period acceleration (ZPA) values in both cases. Otherwise,

TABLE 1. CALCULATED COMPONENT PARAMETERS

COMPONENT	REG. 1.60			NEWMARK-HALL		
	f_{gj} (Hz)	h_{gj} (%)	p_j (IN^2/S^3)	f_{gj} (Hz)	h_{gj} (%)	p_j (IN^2/S^3)
1	9.4	29	1120	10.5	20	619
2	6.1	20	81	7.0	20	215
3	4.8	22	51	4.8	20	61
4	3.6	20	26	3.3	20	25
5	2.9	20	9.2	2.2	20	8.4
6	2.3	24	17.2	1.5	18	3.1
7	0.9	20	0.17	0.78	20	0.08

a close match between the target and simulated response spectra can be observed.

It may be fair to point out here that the results presented above are based on the characterization of the earthquake motions by a single damping value, which would not guarantee an equal fit to other damping values. A further study may be necessary for resolving this multiple damping issue.

SELA Method. In this analysis scheme, the input excitation can only be given by shot noise processes (Ref. [9] and [13]). The frequency characteristics of the ground motion are included by means of additional equations of motion, e.g., an additional mass-spring system inserted between the input shot-noise excitations and the structural model, such as the use of the Tajimi-Kanai spectrum. To overcome this limitation, a new analysis scheme is proposed. The method converts an arbitrary response spectrum to a PSD function which represents a linear combination of SDOF response processes (Ref. [13]).

First, consider a seismic acceleration process, $\ddot{x}_j$, which is approximated by a linear combination of mutually independent filtered shot-noise processes, x_j , i.e.,

$$\ddot{x}_g = \sum_{j=1}^{k} \ddot{x}_j \tag{23}$$

The above "component" processes, x_j , represent the displacement responses of SDOF systems subjected to mutually independent shot noise processes, $f_j(t)$.

$$\ddot{x}_j + 2h_{gj}\,\omega_{gj}\,\dot{x}_j + \omega_{gj}^2\,x_j = -f_j(t) \qquad j = 1,k \tag{24}$$

$$E[f_i(t)f_j(t)] = 2\pi p_j\, I(t) \quad \text{for} \quad i = j$$
$$= 0 \quad \text{for} \quad i \neq j \tag{25}$$

in which, h_{gj} and ω_{gj} are the component filter parameters; p_j is the component power intensity; and I(t) is the deterministic modulating function with a unit maximum value (i.e., $I_{max} = 1.0$). In the above, the displacement responses rather than the acceleration responses are used to model the input motions. This is to account for the fact that most response spectra or floor spectra possess a predominantly low-passing frequency characteristic (see Fig. 2).

The power spectrum of the approximated process, $S_{\ddot{x}}(\omega)$, is expressed as,

$$S_{\ddot{x}}(\omega) = \sum_{j=1}^{k} p_j S_j(\omega) \tag{26}$$

where

$$S_j(\omega) = \frac{1}{(\omega^2 - \omega_{gj}^2)^2 + 4h_{gj}^2\omega_{gj}^2\omega^2} \tag{27}$$

Therefore, the corresponding acceleration response spectrum, $\bar{R}_{\ddot{x}}(\omega_0 , h_0)$, for the approximated process is expressed by the following relationship:

$$\bar{R}_{\ddot{x}}^2(\omega_0,h_0) = \sum_{j=1}^{k} p_j R_j^2(\omega_0,h_0) \tag{28}$$

The component power intensities, p_j , are obtained by following the same procedure given in eq. (20), while the filter parameters, $\omega_{g\,j}$ and $h_{g\,j}$, are determined through a sensitivity analysis on the calculated numerical error defined by eq. (20). Therefore, an iterative procedure is necessary to obtain the optimal filter parameters.

The foregoing response spectra were used as application examples. The calculated component power intensities and the filter parameters are tabulated in Table 1, and obtained response spectra and PSD functions are given in Figs. 3 and 4. Since only seven (7) components were used for these examples, the calculated PSD functions are not as smooth as the ones in Fig. 2.

TABLE 2. MAJOR CAUSES OF NUMERICAL ERRORS IN ELA

TYPE OF ELA	CAUSE OF NUMERICAL ERROR
All ELA's	• Inability to reproduce "drift" response due to accumulation of plastic deformation.
RS	• Under/Overshooting detuning effects. • Over estimation of equivalent damping. • Interpolation/Extrapolation of response spectral values to account for damping changes. • SRSS approximation.
CELA	• Conversion from response spectra to PSD functions. • Selection of peak distribution functions to determine k_e and h_e.
SELA	• Error in RSA. • Gaussian assumption on nonlinear response statistics (particularly hysteretic components). • Evaluation of maximum response statistics.

ERROR ANALYSIS

ELA's are subjected to various forms of numerical errors; some are due to the intrinsic deficiencies in the ELA itself, and others are attributed to the unique approximation schemes adopted in an analysis approach. Both qualitative and quantitative evaluations of numerical errors associated with ELA's are necessary for a successful application to practical engineering problems. Table 2 lists major causes of numerical errors that have been identified in the past numerous studies in this area.

The error due to "drifting", or the accumulation of permanent plastic deformation, is one of the most serious numerical errors that is associated with any form of an ELA. However, a past simulation study (Ref. [11]) indicates that this error can be negligible when the postyield stiffness ratio, α (ratio of the postyield stiffness to the initial stiffness), is higher than 0.04 to 0.05, regardless of the other factors such as the level of nonlinearity and the type of hysteretic models.

It is beyond the scope of this paper to single out and quantitatively evaluate each of the items listed in Table 2. Rather, the combined numerical errors associated with the three ELA's are evaluated under structural and loading conditions which can be encountered in a typical seismic analysis.

A simple SDOF system with a bilinear or a smoothed model of eq. (14) (n = 1) is used. The viscous damping is assumed to be 5% and the postyield stiffness ratio is chosen to be 0.05. The foregoing Newmark-Hall type response spectrum is used as the seismic excitation model. As illustrated in Fig. 5, three initial vibration frequencies, 1Hz, 7Hz and 20Hz, are considered. Due to the detuning in the nonlinear responses, the system may move into the peak (20Hz), stay on the top of the peak (7Hz), or move away from the peak (1Hz). For both the CELA and SELA analyses, the foregoing equivalent response spectrum model of Figs. 1(b) and 3(b) are used without any modifications.

The calculated response results are compared with Monte Carlo simulations (MCS), in which the equivalent PSD function in Fig. 2(b) was used to generate 500 samples of acceleration time histories.

The calculated results are summarized in Figs. 6(a) through 6(d), in which the abscisa represents the normalized excitation amplitude (ratio of zero-period acceleration to the yield strength of the SDOF system) and the ordinate represents the calculated peak ductility factor, μ_{max}.

The results for the RS approach indicate that the method tends to underestimate the responses up to a ductility factor of 3 to 4 in all the cases. For the case of f = 7Hz, in which the system stays on the top of the flat spectral peak, the analysis tends to overshoot at the higher nonlinear response range as indicated in Figs. 6(b) and 6(c).

The results from the CELA method slightly underestimate or overestimate the simulation results depending on the relative position of the vibration frequency to the spectral peak. Up to a ductility factor of 6 to 8, the observed numerical errors are not significant in comparison with other methods.

The response results by the SELA method, on the other hand, are unsatisfactory. In all the cases the analysis underestimates the peak response values, particularly for higher frequency cases (see Fig. 6(a)). This probably is attributed to the deficiency in the mathematical model to calculate the maximum response statistics. It should be noted that the numerical errors in the evaluation of variance responses are not significant in the presented cases since the error due to the Gaussian assumption is already accounted for using an error correction scheme from Ref. [11], and the error due to drifting is negligible when the postyield stiffness ratio is higher than 0.04 to 0.05. A further study is necessary to improve the accuracy in estimating the maximum response statistics for the SELA method. Currently, there exist no widely acceptable mathematical models for this purpose.

Among the items in Table 2, the numerical error due to the SRSS approximation in the RS approach is not accounted for in the above error analysis. This is discussed in the following application examples.

APPLICATION EXAMPLES

As examples of the practical application of the ELA's to nonlinear piping systems, two piping systems supported by EA's, as illustrated in Figs. 7 and 8, were analyzed. The outside diameter and wall thickness of the main pipes are 216.3mm and 10.3mm for the Feedwater (F)-line, and 267.4mm and 12.7mm for the Main Steam (M)-line, respectively. These piping systems are the scaled models (scale factor is about 1/2.5) of actual piping in PWR and BWR nuclear power plants, and will be tested using Nuclear Power Engineering Corporation's (NUPEC) large shaking table at Tadotsu

TABLE 3. EQUIVALENT FREQUENCIES AND DAMPING OF M-LINE

MODE	ELASTIC MODEL		RS		CELA	
	Frequency (Hz)	Damping (%)	Frequency (Hz)	Damping (%)	Frequency (Hz)	Damping (%)
1	7.95	2.5	6.32	20.5	6.10	17.7
2	9.65	2.5	7.93	13.9	8.33	7.4
3	11.5	2.5	9.67	11.3	9.98	5.4
4	13.6	2.5	10.7	22.6	11.9	11.3
5	15.4	2.5	11.9	4.1	14.4	3.0

TABLE 4. EQUIVALENT FREQUENCIES AND DAMPING OF F-LINE

MODE	ELASTIC MODEL		RS		CELA	
	Frequency (Hz)	Damping (%)	Frequency (Hz)	Damping (%)	Frequency (Hz)	Damping (%)
1	13.2	2.5	9.43	21.4	9.73	16.5
2	13.9	2.5	11.6	11.5	11.8	7.1
3	17.4	2.5	15.1	8.8	15.6	5.5
4	21.1	2.5	19.4	5.3	19.7	4.3
5	23.6	2.5	22.8	3.3	23.1	2.9

TABLE 5. COMPARISON OF PEAK RESPONSES OF M-LINE

ITEMS	LOCATION	NTH	RS	CELA
Disp. u_x(mm)	Node-150	5.42	5.46	5.64
Accel. A_x (g)	Node-150	3.09	5.64	2.89
EA Deform. (mm)	LED-2	4.98	4.52	4.69
Pipe Stress (kg/mm^2)	Elm.-(3)	3.33	2.42	3.49

TABLE 6. COMPARISON OF PEAK RESPONSES OF F-LINE

ITEMS	LOCATION	NTH	RS	CELA
Disp. u_x(mm)	Node-330	6.11	5.65	5.91
Accel. A_x (g)	Node-330	2.83	3.36	2.79
EA Deform (mm)	EAB-2	6.90	4.68	6.05
Pipe Stress (kg/mm^2)	Elm.-(1)	2.46	2.16	2.25

Engineering Laboratory in Shikoku, Japan.

The piping systems are subjected to horizontal (in the x-direction) and vertical (in the z-direction) acceleration motions as illustrated in Fig. 9, which are the calculated floor responses of a PWR nuclear power plant. The response spectra and the PSD function for the horizontal component are shown in Figs. 10 and 11. The PSD function in Fig. 11 represents an equivalent stationary process with an effective duration, T_e. The effective duration was defined by the time interval in which the power of the accelerogram attains 5% and 95% of the total power. The amplitude of the PSD functions were adjusted to reproduce the peak acceleration values, which were estimated using the Gumbel's type-I distribution function.

In this paper, the foregoing RS approach (based on SRSS approximation) and CELA method (based on linear random vibration theory) are used to compare with conventional nonlinear time history analyses. The application of the SELA method (based on stochastic equivalent linearization) is not attempted herein mainly because the size of the response covariance matrices are excessively large (approximately 1300 x 1300) for these finite element models. In applying the CELA method, the equivalent PSD function in Fig. 11 was directly used (effective duration is 15.7 sec.). In modeling the piping systems, straight and circular curved beam elements were used for the pipes, and axial springs with the smoothed hysteretic model (eq. 14 with n=2) were used to model three EA's for each piping system (i.e., EAB-1, 2, 3 for the F-line an LED-1, 2, 3 for the M-line).

First, a conventional nonlinear time history (NTH) analysis was performed for both the piping systems. An example of the calculated responses of the EA supports is given in Fig. 12. Then, the foregoing RS and CELA analyses were performed; in the analyses, the eigenvalue solutions were updated four (4) times, assuming a cutoff frequency of 50 Hz (i.e., 13 modes for the M-line and 16 modes for F-line were used in the analyses).

The calculated equivalent vibration frequencies and damping for the first 5 modes are tabulated in Tables 3 and 4. A few calculated response results are also compared in Tables 5 and 6. In general, the response results by both the RS and CELA methods correlate reasonably well with the time history analysis results, although the CELA method gives a better agreement than the RS method. Based on a more detailed evaluation of the calculated response results, the SRSS approximation used in the RS method is considered to be a major cause of the observed differences between the RS and CELA analyses.

An example of an acceleration transfer function is shown in Fig. 13 for the F-line. This transfer function was calculated using the CELA method as a ratio of PSD functions.

$$|H(\omega)|^2 = S_R(\omega)/S_g(\omega) \qquad (29)$$

in which, $S_R(\omega)$ and $S_g(\omega)$ are the response and input acceleration PSD functions. There is a significant broad-banded peak at around 10 Hz in the transfer function of Fig. 13. This reflects not only the higher damping values for the lower modes (see Table 4), but also the fact that the first two modes are "merged" into one combined mode.

SUMMARY AND CONCLUSIONS

Three types of equivalent linearization approaches were presented and compared to each other regarding their practicality and numerical accuracy. For a practical application, all the methods were formulated into the response spectrum approach. Two types of conversion schemes were presented to obtain the equivalent PSD functions which were consistent with the prescribed response spectra. The application examples to nonlinear piping systems with energy absorbing supports indicate that the RS method (based on the SRSS approximation) and the CELA method (based on linear random vibration theory) are practical analysis tools for evaluating the seismic response of complex nonlinear piping system with reasonable accuracy. A comparison with the conventional time history analysis results indicates that the CELA method, after some improvements on the definitions of the equivalent component stiffness and the modal damping values, gives a better correlation than the RS method.

ACKNOWLEDGEMENT

The work presented in this paper was performed under the auspices of the U.S. Nuclear Regulatory Commission as a part of a collaborative effort between the USNRC and the Ministry of International Trade and Industry (MITI) of Japan. The authors wish to thank Dr. N. Chokshi for his support and encouragement during the course of this study. The authors also wish to thank N.Tanaka and H.Abe of NUPEC, as well as many other members of the NUPEC, and Mitsubishi and Hitachi staff for providing the information on the piping systems, as well as the permission to use them as numerical examples. Thanks are also due to Prof. Kohei Suzuki of Tokyo Metropolitan University for his detailed review comments.

NOTE

The findings and opinions expressed in this paper are those of the authors, and do not necessarily reflect the views of the U.S. Nuclear Regulatory Commission or Brookhaven National Laboratory.

REFERENCES

[1] Fujita, K., et al., "Study on a Rotary Type Lead Extrusion Damper as a High Damping Support for Nuclear Piping Systems," SMiRT 11, Vol. K, Tokyo, Japan, 1991, pp. 475-479.

[2] Shibata, H., et al., "Development of the Elastic-Plastic Damper and its Application to the Piping System in Nuclear Power Plants," SmiRT 11, Vol. K, Tokyo, Japan, 1991, pp. 487-492.

[3] Caughey, T.K., "Equivalent Linearization Techniques," Journal of the Acoustical Society of America, Vol. 35, Num. 11, November 1963, pp. 1706-1711.

[4] Tansirikongkol, V. and Pecknold, D.A., "Approximate Modal Analysis of Bilinear MDF Systems," Journal of Engineering Division, ASCE, Vol. 106, No. EM2, April 1980, pp. 361-375.

[5] Lutes, L.D., "Stationary Random Response of Bilinear Hysteretic Systems, " Ph.D. Thesis, California Institute of Technology, 1967.

[6] Soda, S. and Tani, S., "Basic Study on Statistical Aseismic Design of Tall Building," Transactions of Architectural Institute of Japan, No. 288, Feb. 1980, pp. 97-105.

[7] Chokshi, N.C. and Lutes, L.D., "Maximum Response Statistics for Yielding Oscillator," Journal of Engineering Mechanics Division, ASCE, Vol. 102, No. EM6, Dec. 1976, pp. 983-996.

[8] Atalik, T.S. and Utku, S., "Stochastic Linearization of Multi-Degree-Of-Freedom Nonlinear Systems," Earthquake Eng. Struct. Dyn., Vol. 4, 1976, pp. 411-420.

[9] Wen, Y.K., "Equivalent Linearization Hysteretic Systems Under Random Excitation," Journal of Applied Mechanics, Vol. 47, No. 1,1980, pp. 150-154.

[10] Park, Y.J., Wen, Y.K., and Ang., A.H-S., "Random Vibration of Hysteretic Systems Under Bi-directional Ground Motions," Earthquake Engineering and Structural Dynamics, Vol. 14, 1986, pp. 543-557.

[11] Park, Y.J., "Equivalent Linearization for Seismic Responses, Part I: Formulation and Error Analysis," Journal of engineering Mechanics, ASCE, Vol. 118, No. 11, Nov. 1992, pp. 2207-2226.

[12] Park, Y.J. and Reich, M., "Nonlinear 3D Piping Analysis Under Stochastic Dynamic Loads," Nuclear Engineering and Design, Vol. 126, 1991, pp. 233-243.

[13] Park, Y.J., "Nonlinear 3-D Piping Analysis Under Stochastic Dynamic Loads: Response Spectrum Approach, " ASME/PVP Conference, Vol. 237-1, New Orleans, June 1992, pp. 217-222.

[14] "Ultimate Strength and Deformation Capacity of Buildings in Seismic Design," Architectural Institute of Japan, 1990.

[15] Park, Y.J., "A New Conversion Method From Response Spectrum to PSD Functions," technical note submitted for possible publication to Journal of Engineering Mechanics, ASCE, 1994.
[16] Davenport, A.G., "Note on the Distribution of the Largest Value of a Random Function with Application to Gust Loading," Proceeding of ICE, Vol. 28, June 1964, pp. 187-196.
[17] International Mathematics and Statistics Libraries, "IMSL-Library Reference Manual," Houston, Texas, 1988.
[18] U.S. Atomic Energy Commission, "Regulatory Guide 1.60," Revision 1, Dec. 1973.
[19] Wiegel, R.L., "Earthquake Engineering," Prentice-Hall, 1970, pp. 403-447.

APPENDIX. PEAK DISTRIBUTION FUNCTIONS

In most of the previous studies, the Rayleigh distribution was used in determining both the equivalent stiffness and damping, i.e., p_1 and p_2 of eqs. (7) and (8). In this study, the use of three different distribution models are recommended for p_1 and p_2, as well as for the maximum response statistics. For determining the equivalent modal damping value in eq. (8), the following Rayleigh distribution is used;

$$p_2(u,\sigma_\epsilon) = \frac{u}{\sigma_\epsilon^2} \exp\left(-\frac{u^2}{2\sigma_\epsilon^2}\right) \qquad (30)$$

Whereas for the equivalent component stiffness in eq. (7), the Gumble type I distribution is used as,

$$p_1(u) = \exp\left[-\exp\left\{-\alpha_u (u - u_u)\right\}\right] \qquad (31)$$

in which, the extreme distribution parameters, u_u and α_u, are determined based on the above Rayleigh distribution as,

$$F(u_u) = \int_0^{u_u} \frac{\lambda}{\sigma_\epsilon^2} \exp\left(-\frac{\lambda^2}{2\sigma_\epsilon^2}\right) d\lambda = 1 - \frac{1}{M_T} \qquad (32)$$

$$\alpha_u = M_T \cdot f(u_u) = \frac{M_T\, u_u}{\sigma_\epsilon^2} \exp\left(-\frac{u_u^2}{2\sigma_\epsilon^2}\right) \qquad (33)$$

in which, M_T is the equivalent mean number of peaks defined as,

$$M_T = \frac{\sigma_{\dot{\epsilon}}}{2\pi\, \sigma_\epsilon} \qquad (34)$$

where, $\sigma_{\dot{\epsilon}}$ is the standard deviation of the 2nd derivative of the strain response.

For evaluating the maximum response statistics, the same Gumble type-I distribution of eq. (31) is used; in which, the parameters α_u and u_u are determined from the mean number of peaks per unit time, $N_T(u)$, as

$$T \cdot N_T(u_u) = 1.0, \quad \alpha_u = -\frac{d}{du}\left\{T \cdot N_T(u)\right\}_{u = u_u} \qquad (35)$$

Based on the Gaussian assumption on the response variables of the equivalent linear system, the following approximate solution is available for $N_T(u)$:

$$N(u) = \frac{\sigma_3(1 - \nu^2)}{4\pi\sigma_2}\left\{1 - erf\,\frac{u}{\sigma_1\sqrt{2(1-\nu^2)}}\right\} \cdot \frac{\sigma_2}{2\pi\sigma_1}\exp\left(-\frac{u^2}{2\sigma_1^2}\right) \qquad (36)$$

$$where,\ \nu = \frac{\sigma_2^2}{\sigma_1\sigma_3},\ \sigma_1^2 = E[\epsilon^2],\ \sigma_2^2 = E\left[\dot{\epsilon}^2\right],\ \sigma_3^2 = E\left[\ddot{\epsilon}^2\right]$$

The selection of the above peak distribution functions is purely empirical and based on the past simulation studies on hysteretic systems (e.g., Refs. [5], [7] and [11]).

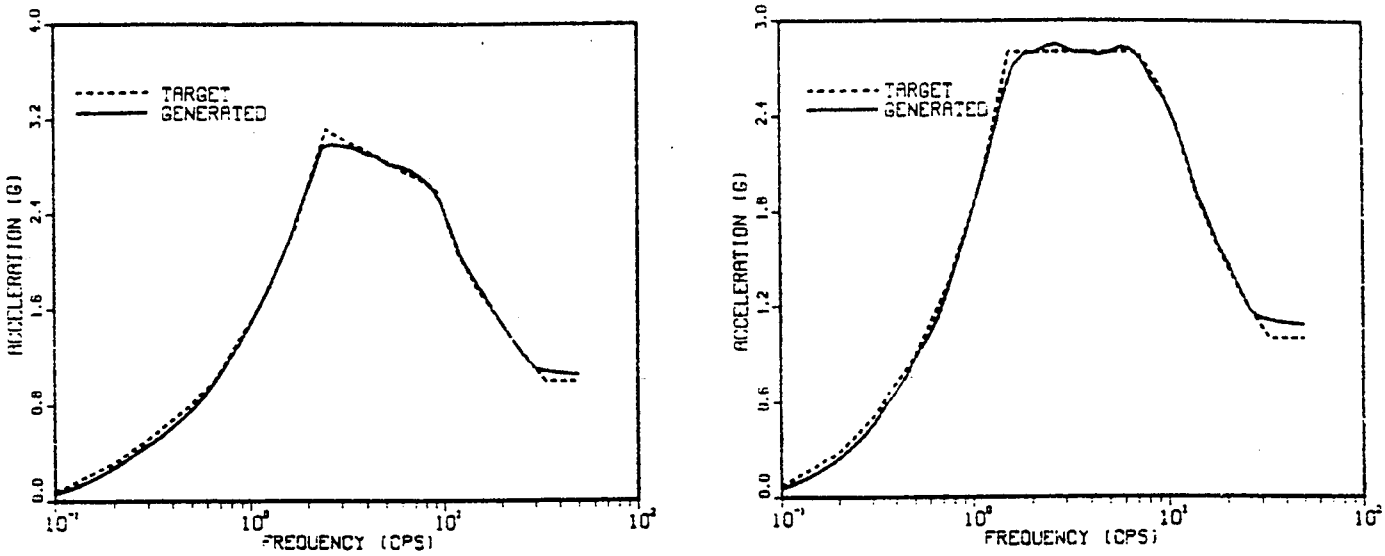

(a) REG 1.60 (b) Newmark-Hall

Fig. 1 Target and Simulated Response Spectra (for CELA)

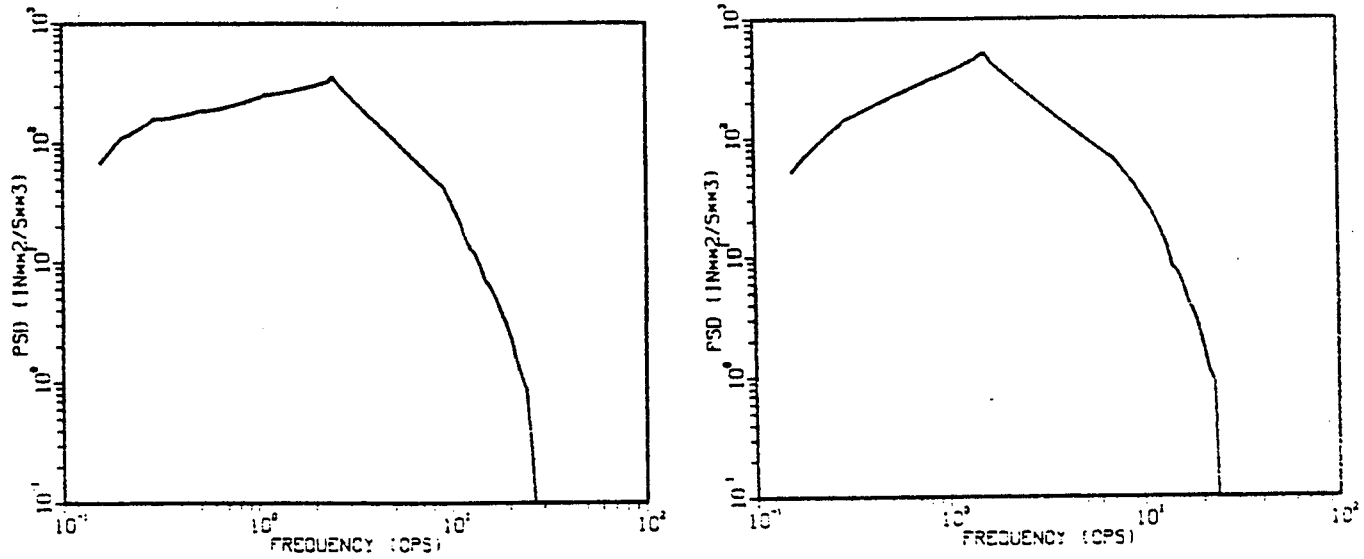

(a) REG 1.60 (b) Newmark-Hall

Fig. 2 Equivalent PSD Functions (for CELA)

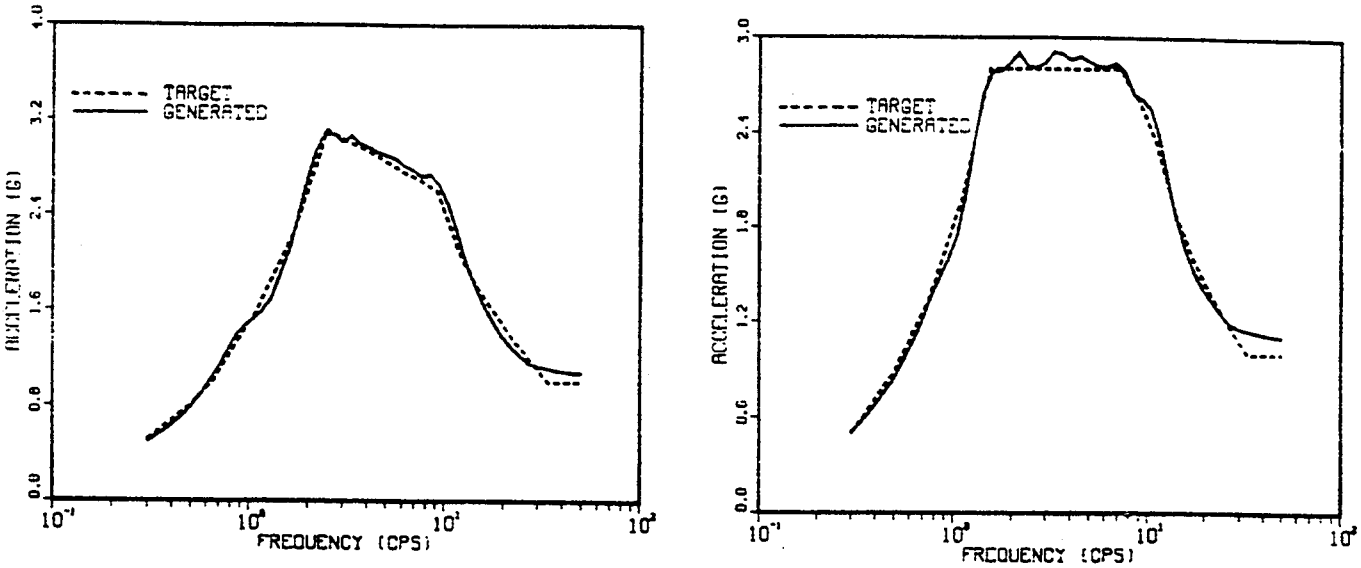

(a) REG 1.60 (b) Newmark-Hall

Fig. 3 Target and Simulated Response Spectra (for SELA)

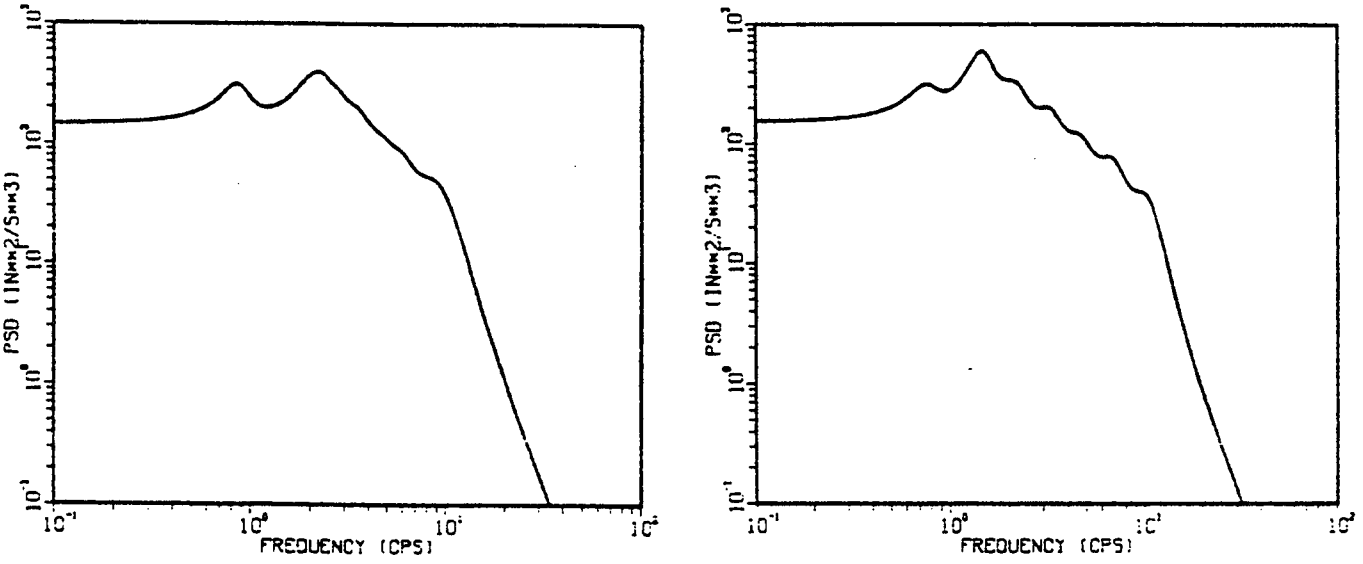

(a) REG 1.60 (b) Newmark-Hall

Fig. 4 Equivalent PSD Functions (for SELA)

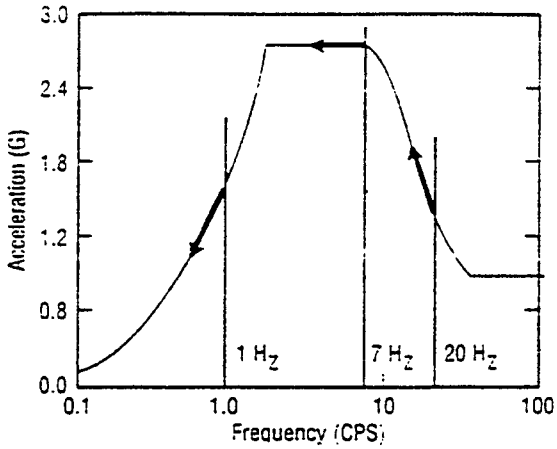

Fig. 5 Newmark-Hall Spectrum and Vibration Frequencies of SDOF

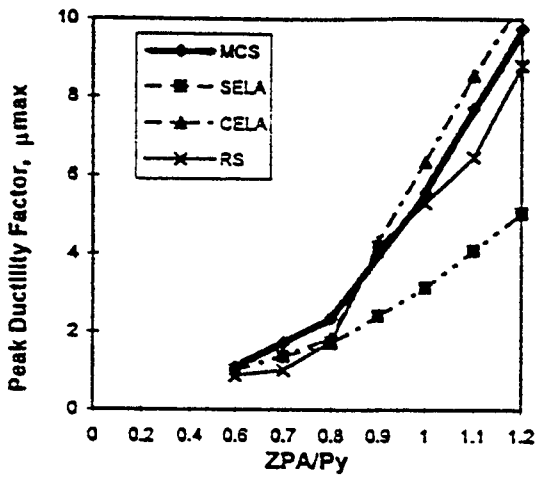

(a) Bilinear model (f = 20 Hz)

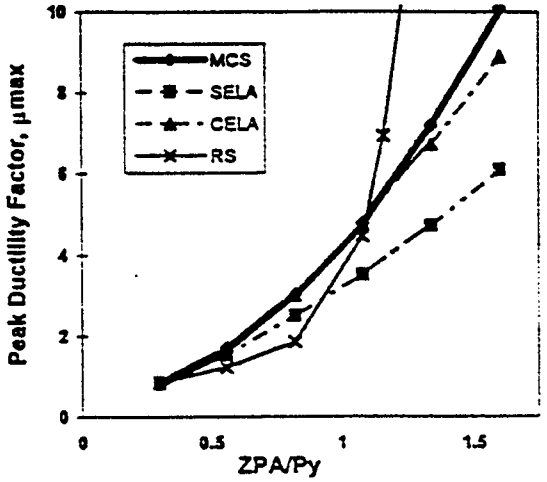

(b) Bilinear Model (f = 7 Hz)

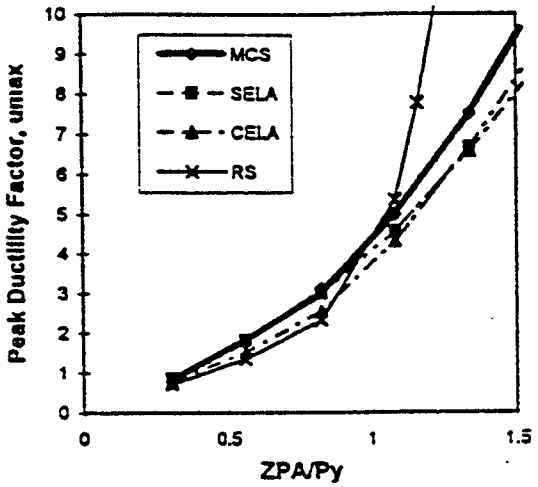

(c) Smoothed Model (f = 7 Hz)

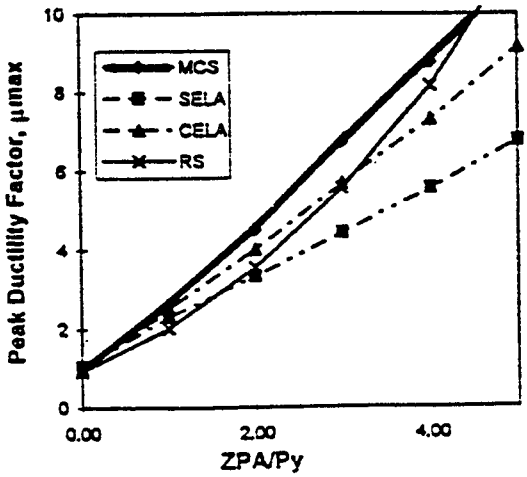

(d) Bilinear Model (f = 1 Hz)

Fig. 6 Comparisons of Nonlinear Responses

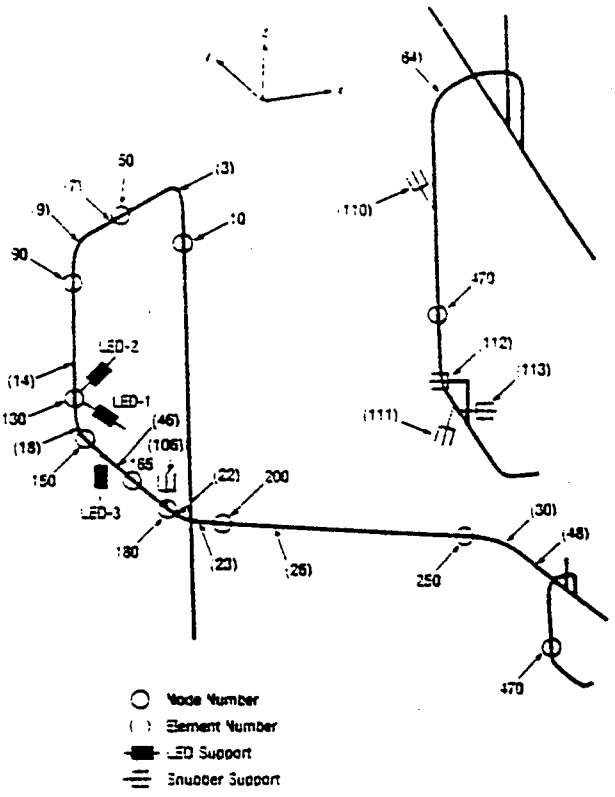

Fig. 7 F.E. Model of Main Steam Line

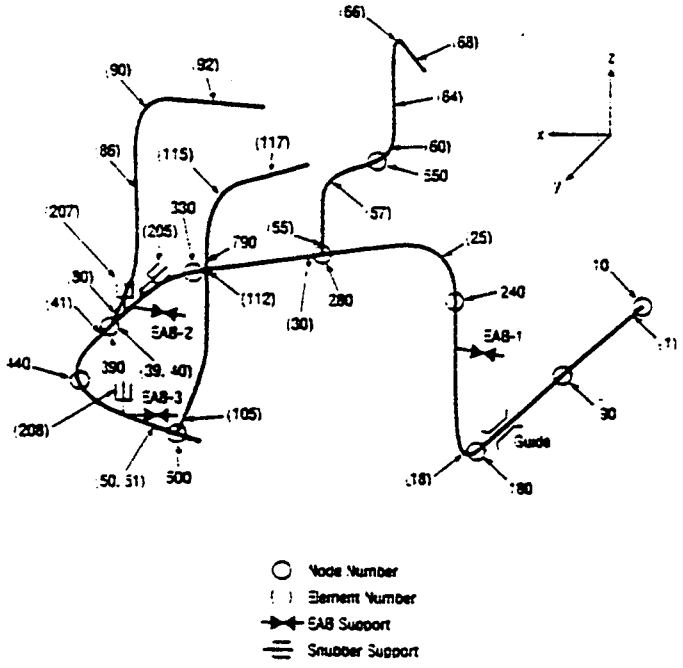

Fig. 8 F.E. Model of Feedwater Line

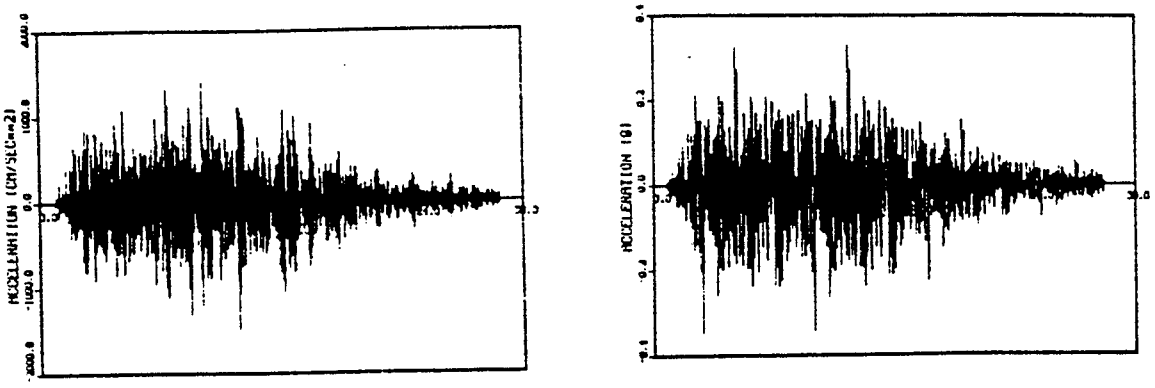

(a) Horizontal (Peak = 1.5 g) (b) Vertical (Peak = 0.35 g)

Fig. 9 Base Motions for Piping Models

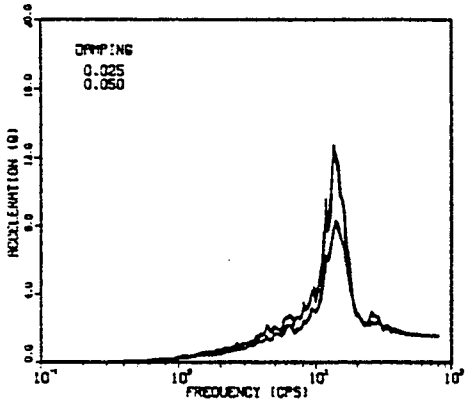

Fig. 10 Response Spectra of Horizontal Motion

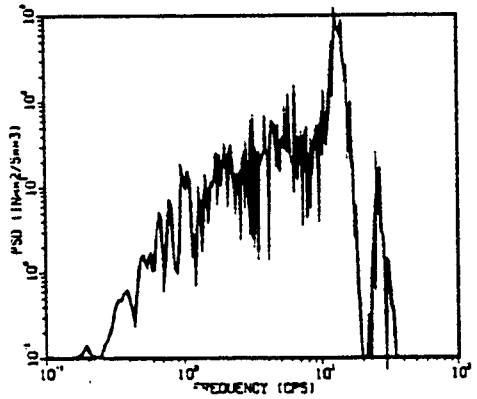

Fig. 11 Equivalent PSD Function of Horizontal Motion

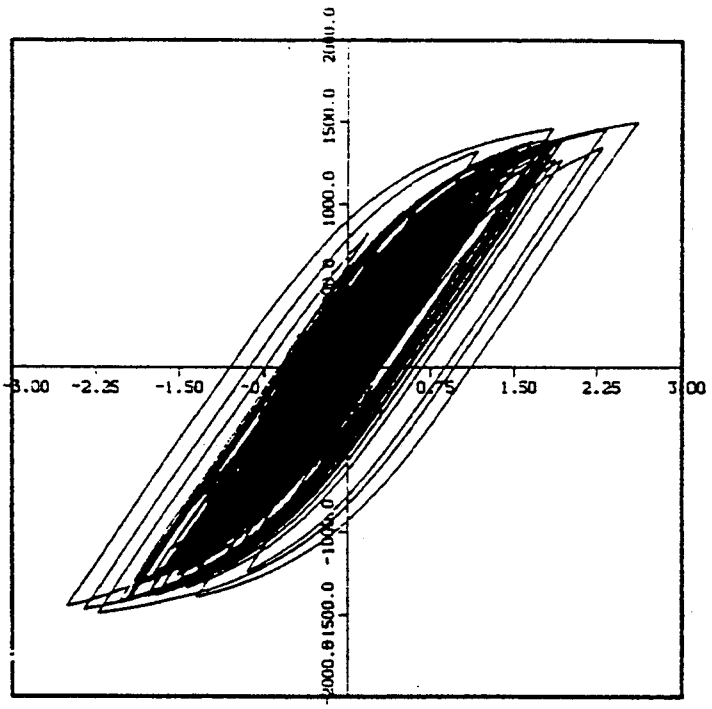

Fig. 12 Example of Hysteretic Response of E.A. Support (LED-1 of M-line)

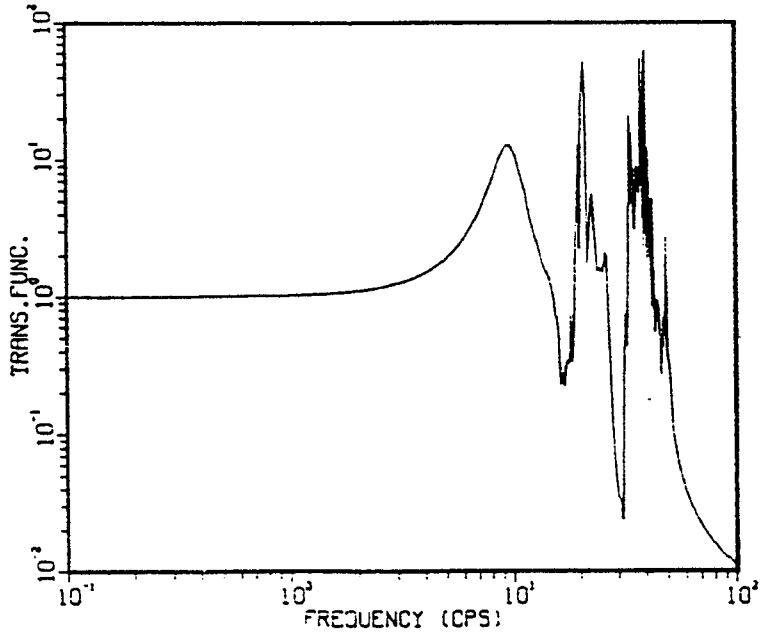

Fig. 13 Example of Acceleration Transfer Function (Node - 390 of F-line)

APPENDIX L[1]

TEST PLAN

[1]Information and data included in this Appendix are offered by NUPEC through their technical report. This information and data are translated, summarized and edited in this Appendix by NRC/BNL.

L.1 Test Facilities

The large-scale shake table at NUPEC's Tadotsu Engineering Laboratory is illustrated in Fig. L.1. The table has dimensions of 15 m x 15 m, and is biaxially controlled (vertical and horizontal) with a maximum loading capacity (total weight of a test model) of 1,000 ton. The maximum excitation capacity is 3,000 ton for the horizontal direction and 3,300 ton for the vertical direction (see Fig. L.2).

The shake table has been used to conduct large scale seismic proving tests of various NPP's components, including steel containment vessels, core internals, the PWR primary coolant system, reactor vessels, emergency diesel generators, control room computer systems, and concrete containment vessels (Ref. L.1).

L.2 Test Model

L.2.1 Piping Systems

As illustrated in Figures L.3 and L.4, the test model consists of the main steam line (M-line) of a typical PWR Plant and the feedwater line (F-line) of a typical BWR Plant. At the end of the M-line, a part of the steam supply pipe for the turbine driven auxiliary feedwater pump (which is called the M-line branch pipe in the report) is also included. The dimensions, properties and internal pressures of the piping are listed in Table L.1. The scale-down factor of the pipe models are 1/2.66 for the M-line and 1/2.3 for the F-line. Table L.2 shows the scaling law used for the test model. Additional weights are attached to the pipes to maintain the scaling law. Detailed information of the test models are given in Appendices A and C of this report. Both the M-line and F-line were filled with water at room temperature and were pressurized to a constant internal pressure during the tests.

L.2.2 Independent Support Motion

For the M-line, the massive steam generator (SG) was not physically modeled. Instead, the SG was replaced by a simple actuated structure corresponding to a mathematical model of the SG as illustrated in Figure L.5. The computer-controlled actuator system simulates the dynamic motions of the SG based on the mathematical model of the SG and sensor readings of the table motions and actuator movements (Ref. L.3). The calculated relative displacement between the SG and the SG-end of the M-line is imposed using a 25-ton hydraulic actuator as illustrated in Figure L.6.

Figure L.7 shows the mathematical model of the SG simulator used during the tests. The natural frequency of this model is about 20 Hz. In addition to the SG-model, a 2 - DOF model, shown in Figure L.8, was also used. The purpose of this system was to reproduce the effect of the prestressed concrete containment vessel (PCCV) at the proper location..

L.2.3 Conventional Pipe Supports

Various pipe supports, including mechanical and hydraulic snubbers, hangers, guide (sliding) supports, and pin supports are installed for both the M-line and F-line. Figure L.9 illustrates the pipe supports for the F-line. The support denoted "FR1" is a guide support (see Figure A.27 in Appendix A). All other supports for the F-line with conventional supports are mechanical snubbers. Figure L.10 illustrates the pipe supports for the M-line. "MR8" is a pin support (see Figure A.14 in Appendix A) while "MR9" and "MR10" are a guide (see Figure A.15).

For both the M-line and F-line, mechanical snubbers are the main pipe supports. Figure L.11 illustrates the various components of the mechanical snubbers used for the MS test (Ref. L.4). The mechanical snubber unit is connected

to the pipe with a clamp, which is tightened by bolts (see Figures A.21 and A.22). When a load is applied to the mechanical snubber, the Load Column is pushed (pulled) in the axial direction. This rotates the Ball Screw through the Ball Nut (the Ball Screw is fixed at its position by Bearings), which in turn rotates the Flywheel. Since the Brake Drum is held to the Flywheel through the Steel Balls by the expansional force in the Return Spring, it also rotates with the Flywheel and the Ball Screw. When the applied load velocity is low, the Brake Drum and the Flywheel rotate together and the snubber unit generates little resistance force and allows free movement (such as for thermal movement). When the applied movement exceeds a certain acceleration level, the Brake Drum and the Flywheel start to rotate at different velocities due to their different inertias. This causes the Steel Ball to push the Brake Drum toward the Brake Shoe. Once a contact is made between the Brake Drum and the Brake Shoe, a friction force is generated, and the Brake Drum and the Flywheel stop rotating, producing a resistant force against the applied load.

Due to gaps between the components of a snubber unit, particularly the gap between the Brake Drum and Brake Shoe, the load-deformation relationship for the snubber is nonlinear as illustrated in Figure L.12. The gaps and tangential stiffnesses, k_t, were provided by the manufacturer, and are listed in Tables L.3 and L.4. During the MS tests, the observed load-deformation behavior was much more complex than that shown in Figure L.12, as described in Appendix M.

L.2.4 Energy Absorbing (EA) Supports

As an alternative to the aforementioned conventional snubbers, the use of mechanical energy absorbers has attracted a wide interest in the nuclear industry (Refs. L.3 and L.5). The basic design concept of energy absorbers (EA) is to dissipate the vibration energy of piping systems through nonlinear hysteretic actions of EA's under design seismic loads. Two types of EA's were used in the MS test program, i.e., EAB (energy absorbing) supports for the F-line and LED (lead extrusion damper) supports for the M-line.

Figures L.13 and L.14 illustrate the EAB support used for the F-line. Figures A.30 and A.34 in Appendix A also show the actual EAB units. As illustrated in Figure L.14, the applied vibration energy is absorbed through the plastic out-of-plane bending of x-shaped steel plates. The steel plates are designed to develop a uniform bending stress along the height under a double-curvature bending deformation. As illustrated in Figure L.16, three (3) EAB supports were attached to the main line of the F-line during the tests.

Figure L.15, as well as Figures A.9 and A.33, show the LED supports. The applied axial movement rotates the octagon-shaped rotor (see Figure A.33), which is surrounded by lead in a chamber. The plastic deformation between the rotor and the lead generates a force resisting the applied load. Figure L.17 shows the location of the three LED supports.

Figures L.18 and L.19 show the hysteretic curves for both the EAB and LED supports obtained from component tests. The hysteresis loops of an EAB support are very similar to those obtained in a typical steel coupon test. The hysteresis loops of a LED support shown in Figure L.19 are more irregular and more complex than those of EAB supports. It is also reported that a significant rate-dependency exists in the load-deformation characteristics of lead extrusion dampers (Ref. L.3).

L.2.5 Instrumentation

A total of 336 channels of measured data were recorded during the tests. The instruments included accelerometers, displacement transducers, strain gages, load cells and pressure gages. The arrangement of various sensors were changed between the tests with conventional supports and the tests with EA supports. A complete description of all the sensors are given in Appendix D of this report.

Tables L.5 through L.8 list and Figures L.20 through L.23 show the selected measurement items used for the correlation studies described in the following chapters. Tables L.5 through L.8 also list the node and element numbers used in the analyses.

L.3 Test Procedures

L.3.1 Input Table Motions

The input table motions were developed from time history analyses of typical PWR and BWR power plants (Ref. L.6), as listed in Table L.9. According to the Japanese seismic design standards for nuclear power plants, two levels of earthquake motions, S_1 and S_2, are used for design analyses. In comparison with the design standards in the U.S., the S_1 motion is somewhat higher than the typical OBE level, and the S_2 motion is approximately equal to the typical SSE level.

As listed in Table L.9, PWR-S_1 and S_2 motions are used for the tests of the M-line with conventional supports, and BWR-S_1 and S_2 for the tests of the F-line with conventional supports. The accelerograms and response spectra are shown in Figures L.24 through L.28. The PCCV wave (also denoted as C/V wave in this report) was obtained from the response of a prestressed concrete pressure vessel, and are used for multiple excitation tests of the M-line with conventional supports.

For the energy absorbing support case, the following waves are used:

A-Wave S_1:	PWR-S_1 motion
A-Wave S_2:	PWR-S_2 motion
B-Wave S_1:	A-Wave S_1 motion with time scale expanded by a factor of 2.72.
B-Wave S_2:	A-Wave S_2 motion with time scale expanded by a factor of 2.72.
Tokachioki:	vertical component of the Hachinohe records from the 1968 Tokachioki earthquake.
C-Wave S_2:	A-Wave S_2 motion with time scale varied for F-line test.

Figure L.29 shows the response spectra for the A-Wave and B-Wave. It should be noted that all the above accelerograms are the "target waves", used as input to the shake table at Tadotsu Lab. The actually recorded table motions are slightly different than the target motions as described later in this report.

L.3.2 Test Runs

A total of about 200 shake table tests were performed at NUPEC's Tadotsu Lab during the MS test program. Most of the test runs are listed in Appendix B of this report along with specifications of table motions and summaries of test conditions.

Table L.10 summarizes the planned test runs for the conventional support case. The seismic proving tests were performed using the design seismic motions; i.e., the PWR-S_1 and S_2 motions for the M-line, and BWR-S_1 and S_2 motions for the F-line. Three (3) levels of table motion amplitude; i.e., amplitude factors of 1/3, 2/3, 3/3, were considered for both the F-line and M-line tests as indicated in Table L.10.

The design confirmation tests were performed for the M-line only. In the first test series, the SG simulator was switched from the original SG model (Figure L.7) to the 2DOF model (Figure L.8) to reproduce the PCCV waves (Figure L.28) at the SG-connection (SG-joint) to the M-line. In the second series, the SG simulator was switched back to the original model (Figure L.7), and the PCCV waves were used as the input table motions.

The design margin (margins) tests were performed for the F-line and M-line separately. The S_2 motions were scaled up by a factor of 1.1, 1.2, and 1.3 for the F-line, and 1.2, 1.3, and 1.5 for the M-line. The objective of the margins tests was to assess the design margin using seismic motions higher than the standard design loads.

Table L.11 summarizes the planned test runs for the EA support case. During the test runs for the conventional support case, a nonlinearity was observed in the computer-controlled actuator system due to small gaps in its hydraulic system. The SG model (Figure L.7) was adjusted slightly during the preliminary tests to compensate for this problem.

In the design confirmation tests - I, both A and B waves were used to prove the effectiveness of the EA supports and the integrity of the piping systems. In addition, the effects of vertical motions were investigated by changing the amplitude of the vertical component, while the horizontal component was held constant.

In the gap test (also referred to as the Design Method Confirmation Test II), the effects of a mechanical gap were investigated with the M-line with EA supports. The independent actuator was removed, and a 1 mm gap was installed at the SG-joint, as illustrated in Figure L.30, to produce impact forces. For comparison purposes, an identical series of tests were performed with the gap closed (independent actuator was not used).

At the last stage of the tests, a large number of margins tests were performed by changing both the amplitude as well as the time scale of the A-wave, B-wave, Tokachioki wave and C-wave, as listed in Table B.5 of Appendix B.

L.4 REFERENCES

L.1 NUPEC, "Proving Tests on the Seismic Reliability for Nuclear Power Plant, Seismic Proving Test of Emergency Diesel Generator System," Nuclear Power Engineering Corporation, 1992.

L.2 NUPEC/MHI, "Verification Test of the Control System for the Multi-Input Wave Simulator," presented during MS Test Program Meeting, June 1994.

L.3 K. Fujita, et al., "Proving Test on the Performance of a Multiple-Excitation Simulator," PVP/ASME, Vol. 312, 1995, pp. 93-100.

L.4 Sanwa Tekki Corporation, "Pipe Hangers and Supports," Cat. No. 948, Sanwa Tekki, 1984.

L.5 H. Shibata, et al., "Development of the Elasto-Plastic Damper with It's Application to the Piping System in Nuclear Power Plants," SMiRT 11, Vol. K, Tokyo, Japan, 1991, pp. 487-492.

L.6 NUPEC, "Seismic Proving Test of Main Steam and Feedwater Systems," presented during MS Test Program Meeting, June 3, 1993.

Table L.1 Piping Parameters

	F-line		M-line	
	Main pipe	**Branch**	**Main pipe**	**Branch**
Size	8B (Sch 60)	5B (Sch 60)	10B (Sch 60)	2B (Sch 40)
O. diameter (mm)	216.3	139.8	267.4	60.5
Thickness (mm)	10.3	8.1	12.7	3.9
Material (*)	SFVC2B	STS410	STS42	STPT38
Minimum yield (*) stress (kg/mm^2)	28/25	25	25	22
Young's modulus (kg/mm^2)	2.1 E+4/1.96 E+4	1.96 E+4	2.05 E+4	
Pressure (psi)	970		1085	

(*) Notification No. 501, Ministry of International Trade and Industry, Japan, 1991.

Table L.2 Scaling Law for MS Seismic Proving Test Model

Physical quantity	**Notation**	**Law of similitude**	**M-line**	**F-line**
Length	ℓ	$\ell_m/\ell_P = 1/N$	1/2.66	1/2.3
Young's modulus	E	$E_m/E_P = 1$	1	1
Strain	ϵ	$\epsilon_m/\epsilon_P = 1$	1	1
Stress	σ	$\sigma_m/\sigma_P = 1$	1	1
Displacement	x	$x_m/x_P = 1$	1/2.66	1/2.3
Force	P	$P_m/P_P = 1/N^2$	1/7.076	1/5.29
Frequency	f	$f_m/f_P = 1/0.7$	1/0.7	1/0.7
Acceleration	α	$\alpha_m/\alpha_P = 1/(0.7^2)/N$	1/1.303	1/1.127
Time	t	$t_m/t_P = 0.7$	0.7	0.7
Weight	w	$w_m/w_P = (0.7^2)/N$	1/5.429	1/4.694
Spring constant	k	$k_m/k_P = 1/N$	1/2.66	1/2.3

Note: Suffix m: model, p: actual plant

Table L.3 F-line Support Properties

Support	Type of support	Capacity (ton)	Component test data		
			K_t (kg/mm)	K_c (kg/mm)	Gap (mm)
FR2	M.S.(*1)	1.0	7333	7333	0.3
FR3	M.S.	3.0	7667	7667	0.3
FR4	M.S.	1.0	4080	4320	0.2
FR5	M.S.	1.0	5010	5500	0.2
FR6	M.S.	6.0	7813	8750	0.3
FR7	M.S.	3.0	6889	7333	0.4
FR8	M.S.	3.0	6667	7111	0.3
FR9	M.S.	3.0	6200	6600	0.3
FR10	M.S.	3.0	7750	8500	0.4
FR13(*2)	M.S.	3.0	7625	8250	0.4
FR15(*2)	M.S.	3.0	7625	8500	0.4

Note (*1): M.S.; Mechanical snubber
(*2): Used during E.A. support tests

Table L.4 M-line Support Properties

Support	Type of support	Capacity (ton)	Component test data	
			$(K_t + K_c)/2$(kg/mm)	Gap (mm)
MR1	M.S.	6.0	6950	0.4
MR2	M.S.	6.0	7650	0.4
MR3	M.S.	3.0	5330	0.4
MR4	M.S.	3.0	4640	0.2
MR5	M.S.	10.0	11100	0.6
MR6	M.S.	10.0	11100	0.6
MR7	H.S. (*1)	6.0	5710	0.3
MR8	Pin support	---	---	---
MR9	Guide	---	---	---
MR10	Guide	---	---	---

Note (*1): H.S.; Hydraulic snubber

Table L.5 Selected Measurement Items for M-line with Conventional Support

Instrumentation I.D.		ISSAC node/element no.	PSAFE2 node number
(Acceleration)			
AA1		N-10	1
MA1		N-50	6
MA2		N-90	10
MA3		N-130	12
MA4		N-150	15
MA5		N-165	42
MA6		N-180	16
MA8		N-200	19
MA10		N-250	21
(Displacement)	(Support load)		
AD1X, Y, Z		N-10	1
MD1a	MR1	101	10
MD2a	MR2	102	10
MD3b	MR3	103	11
MD4b	MR4	104	11
MD5	MR5	105	12
MD6	MR6	106	12
MD7	MR7	107	16
MD8X, Y, Z		N-150	15
MD9	MR11	109	212
MD10	MR12	110	222
MD11		112	261
(Stress)			
MS1		3	4
MS2'		5	5
MS2		7	31
MS3		9	8
MS4		14	33
MS5		17	14
MS6		46	42
MS8		23	18
MS9		25	36
MS10		30	22

Table L.6 Selected Measurement Items for F-line with Conventional Support

Instrumentation I.D.		ISSAC node/element no.	PSAFE2 node number
(Acceleration)			
FA2		N-40	4
FA3		N-90	9
FA5		N-180	18
FA6		N-240	26
FA7		N-280	30
FA8		N-330	35
FA9		N-390	41
FA10		N-440	46
FA11		N-500	52
FA12		N-550	57
FA13		N-790	95
(Displacement)	(Support load)		
—	FR1	N-10	15
FD2b	FR2	201	22
FD3b	FR3	202	22
FD4b	FR4	203	28
FD5b	FR5	204	28
FD6b	FR6	205	38
FD7a, b	FR7	206	39
FD8a, b	FR8	207	39
FD9b	FR9	208	48
FD10b	FR10	209	48
(Stress)			
FS1		1	1
FS2		18	18/19
FS3		25	26/27
FS4		30/55	30
FS5		39	39
FS6		41/80	41
FS7		41	44
FS8		50	50
FS9		51/105	52
FS10		57	55/56
FS11		60	57/58
FS12		64	60
FS13		66	62/63
FS14		68	64
FS15		80	73
FS16		85	78
FS17		90	80/81
FS18		92	92
FS19		105	91
FS20		112	95
FS21		115	98/99
FS22		117	100

Note: For ISSAC models, N-40 indicates a node number and all other numbers represent element numbers.

Table L.7 Selected Measurement Items for M-line with EA Support

Instrument I.D.		ISSAC node/element number	PSAFE2 node number
(Acceleration)			
AA1		N-10	1
MA1		N-50	6
MA16		N-90	10
MA17		N-130	12
MA4		N-150	15
MA5		N-165	35
MA6		N-180	16
MA8		N-200	19
MA10		N-250	21
(Displacement)	(Support force)		
AD1X, Y, Z		N-10	1
MD9	MR11	110	212
MD10	MR12	111	222
MD11		112	261
MD12 (X)		N-90	10
MD13 (Y)		N-90	10
MD14	MR8	106	16
MD15	MR15	LED-1	12
MD16	MR16	LED-2	12
MD17	MR17	LED-3	50
MD18X, Y, Z		N-150	15
(Stress)			
MS1		3	4
MS2		7	31
MS3		9	8
MS4		14	12
MS5		17	14
MS6		47	35
MS10		30	22

Table L.8 Selected Measurement Items for F-line with EA Support

Instrumentation I.D.		ISSAC node/element no.	PSAFE2 node/number
(Acceleration)			
FA3		N-90	6
FA5		N-180	13
FA6		N-240	18
FA7		N-280	21
FA8		N-330	108
FA9		N-390	30
FA10		N-440	111
FA11		N-500	38
FA12		N-550	44
FA13		N-790	119
(Displacement)	(Support load)		
	FR1	N-10	10
FD6b	FR6	205	27
FD11b	FR11	401 (EAB-1)	16
FD12b	FR12	402 (EAB-2)	28
FD13b	FR13	207	28
FD14b	FR14	403 (EAB-3)	112
FD15b	FR15	208	112
(Stress)			
FS1		1	1A
FS2		18	14
FS3		25	19
FS4		30	21
FS5		39	29
FS6		41	30
FS7		43-1	32
FS8		50	113
FS9		51	38
FS10		57	43
FS11		60	45
FS12		64	114
FS13		66	49
FS14		68	50N
FS15		80	51
FS16		86	54N
FS17		90	56
FS18		92	58N
FS19		105	59
FS20		112	119
FS21		115	65
FS22		117	66N

Note: For ISSAC models, N-40 indicates a node number and all other numbers represent element numbers.

Table L.9 List of Input Table Motions

Name	Component	Peak acceleration (g)	Peak velocity (cm/sec)	Duration (sec)
PWR-S_1	Horizontal Vertical	0.83 0.19	18.0 5.8	28.7 28.0
PWR-S_2	Horizontal Vertical	1.50 0.35	29.3 10.1	28.7 28.0
BWR-S_1	Horizontal Vertical	0.73 0.15	18.1 5.3	17.5 17.5
BWR-S_2	Horizontal Vertical	1.13 0.19	19.4 6.0	14.0 14.0
PCCV-S_1	Horizontal	1.14	36.0	29.0
PCCV-S_2	Horizontal	1.40	53.9	29.0

Table L.10 Test Items and Objectives for the Conventional Support Case

Test item	Contents	Objectives
Preliminary test	• Sinusoidal wave test • Random wave test	• Check the controllability of shaking table • Check the independent actuator system • Obtain the vibration characteristics of models
Seismic proving test	• Seismic design motion test using S_1 and S_2 waves (Amplitude scale: 1/3, 2/3, 3/3)	• Prove the seismic integrity of the piping systems
Design method confirmation test (for M-line only)	• Change SG model to 2DOF system (Amplitude scale: 1/6, 1/4, 1/3) • C/V wave test with original SG model (Amplitude scale: 1/3, 2/3, 3/3)	• Obtain M-line response under different combinations of input motions
Marginal test	• S_2 wave test (Amplitude scale: 1.1, 1.2, 1.3 for F-line; 1.2, 1.3, 1.5 for M-line)	• Confirm the seismic design margin

Table L.11 Test Items and Objectives for EA Support Case

Test item	Contents	Objectives
Preliminary test	• Sinusoidal tests • Random wave test • Adjustment of actuator test	• Check the controllability of shaking table • Obtain the vibration characteristics of models • Check the nonlinearity of independent actuator system
Design method confirmation test-I	• A-wave test (scale: 1/3, 2/3, 3/3) • B-wave test (scale: 1/3, 2/3, 3/3) • Repeatability test • Effects of vertical motion test	• Prove seismic integrity of piping system with EA supports • Prove the effectiveness of EA supports • Confirm the nonlinear analysis methods • Investigate the effects of vertical motions
Design method confirmation test-II (gap test)	• Sinesweep test with and without gap • Random wave test with and without gap • A-wave test with and without gap (scale: 1/3, 2/3, 3/3)	• Investigate the effect of gap at SG-joint of M-line
Marginal test	• A-wave test with actuator operated (scale: 1.1, 1.2, 1.3) • B-wave test with actuator operated (scale: 1.1, 1.2, 1.3) • A-wave test with actuator fixed (scale: 1.3 ~ 2.5) • Tokachioki wave test for M-line (amplitude scale: 10 ~ 33) • C-wave test for F-line (scale 2/3 ~ 1.9)	• Obtain the seismic margin of EA supports • Obtain highly plastic responses

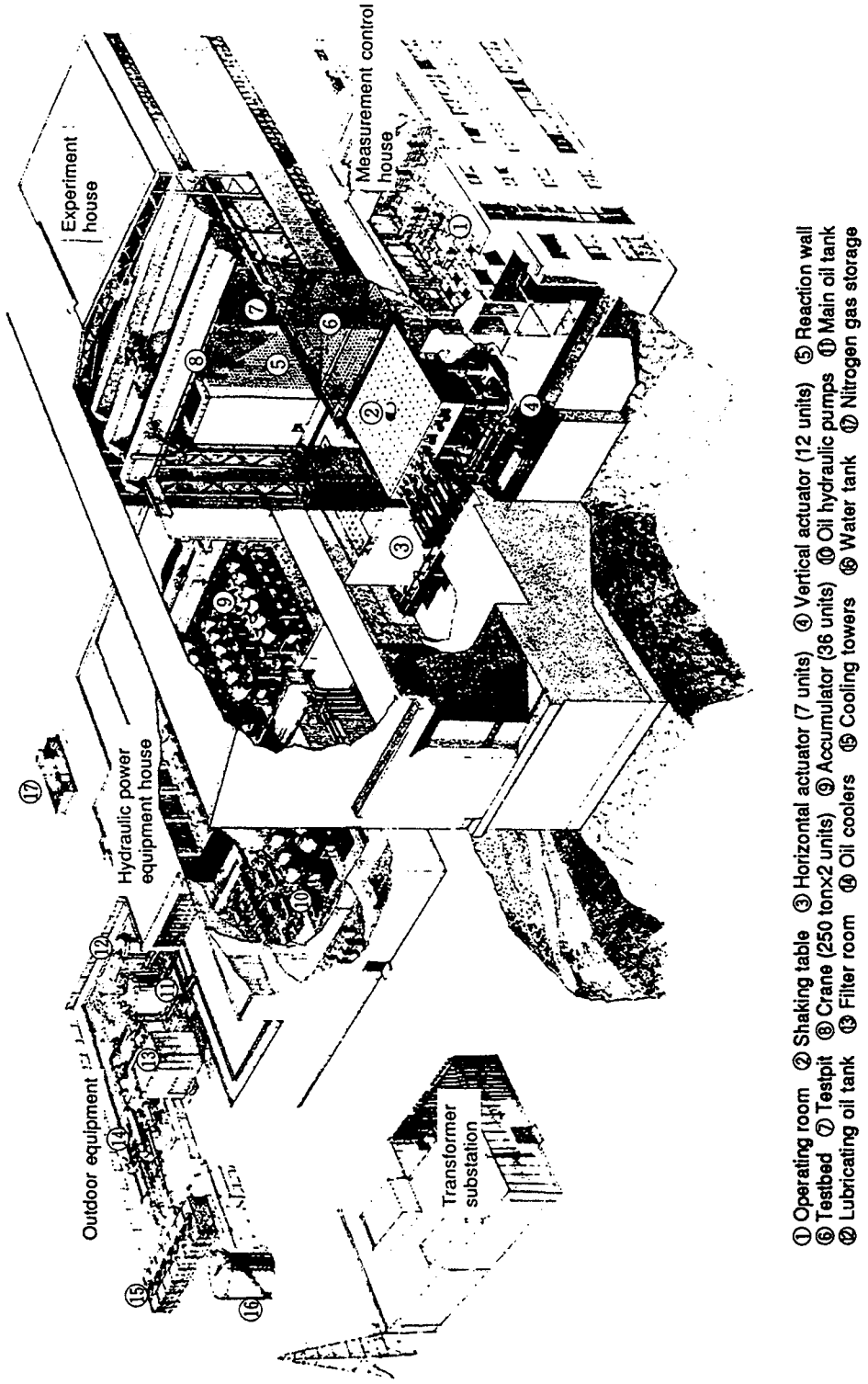

Figure L.1 Test Facilities at Tadotsu Engineering Laboratory (Ref. L.1)

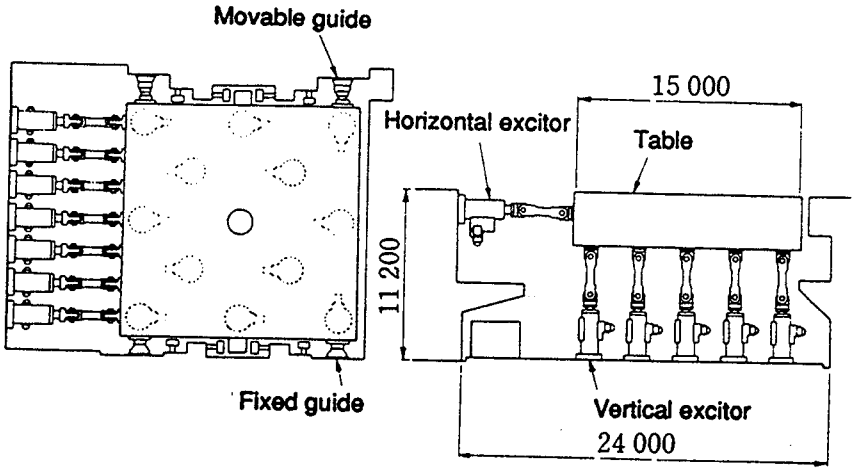

(a) Shaking table

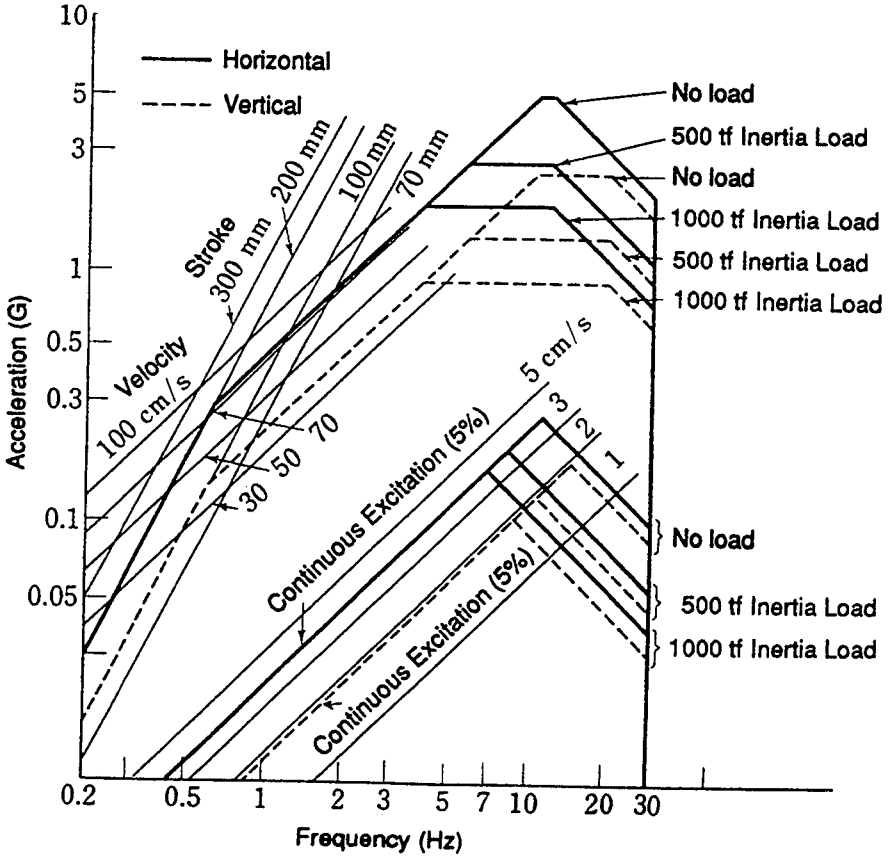

(b) Limit performance

Figure L.2 Shaking Table at Tadotsu Engineering Laboratory (Ref. L.1)

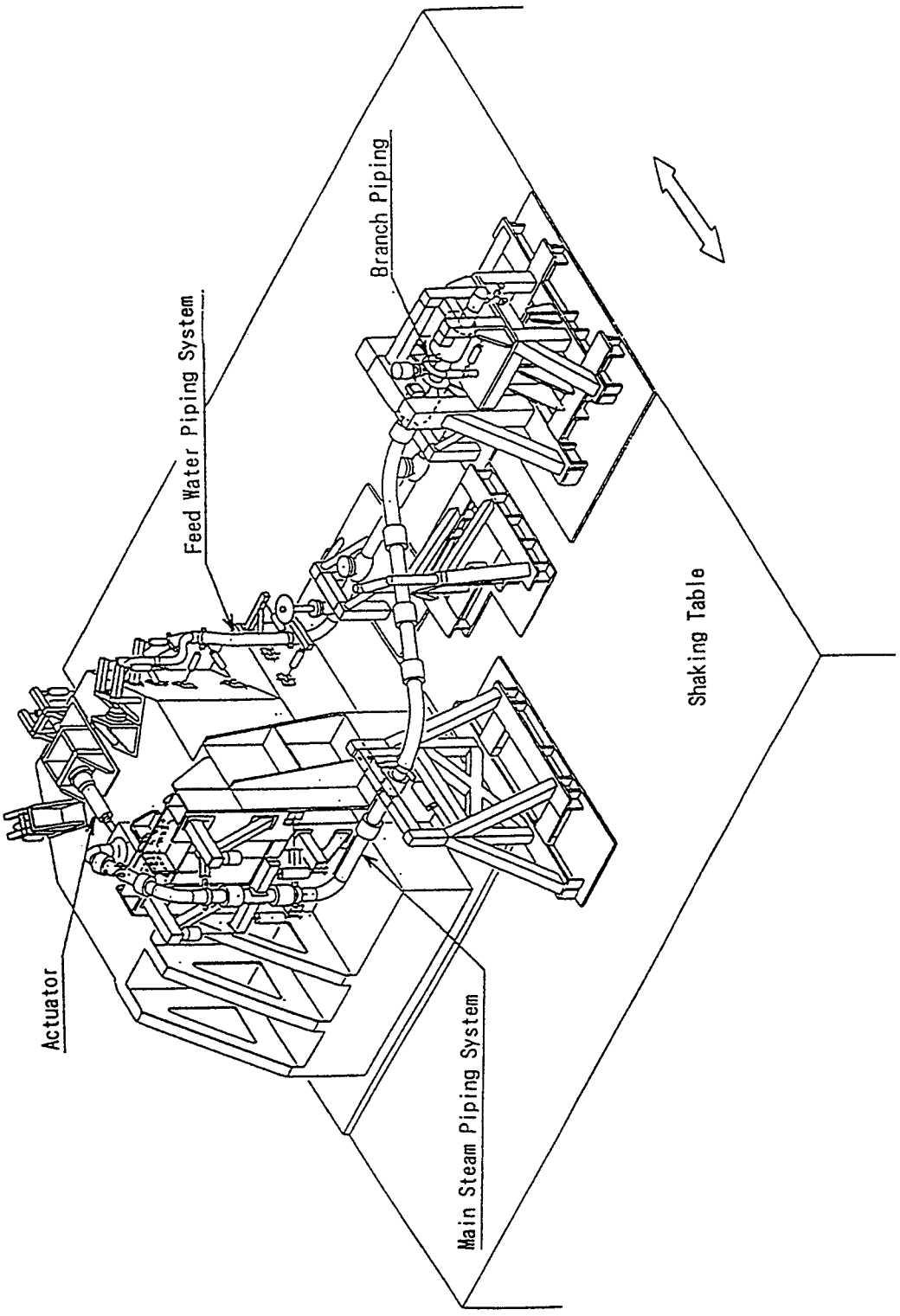

Figure L.3 MS Seismic Proving Test Model

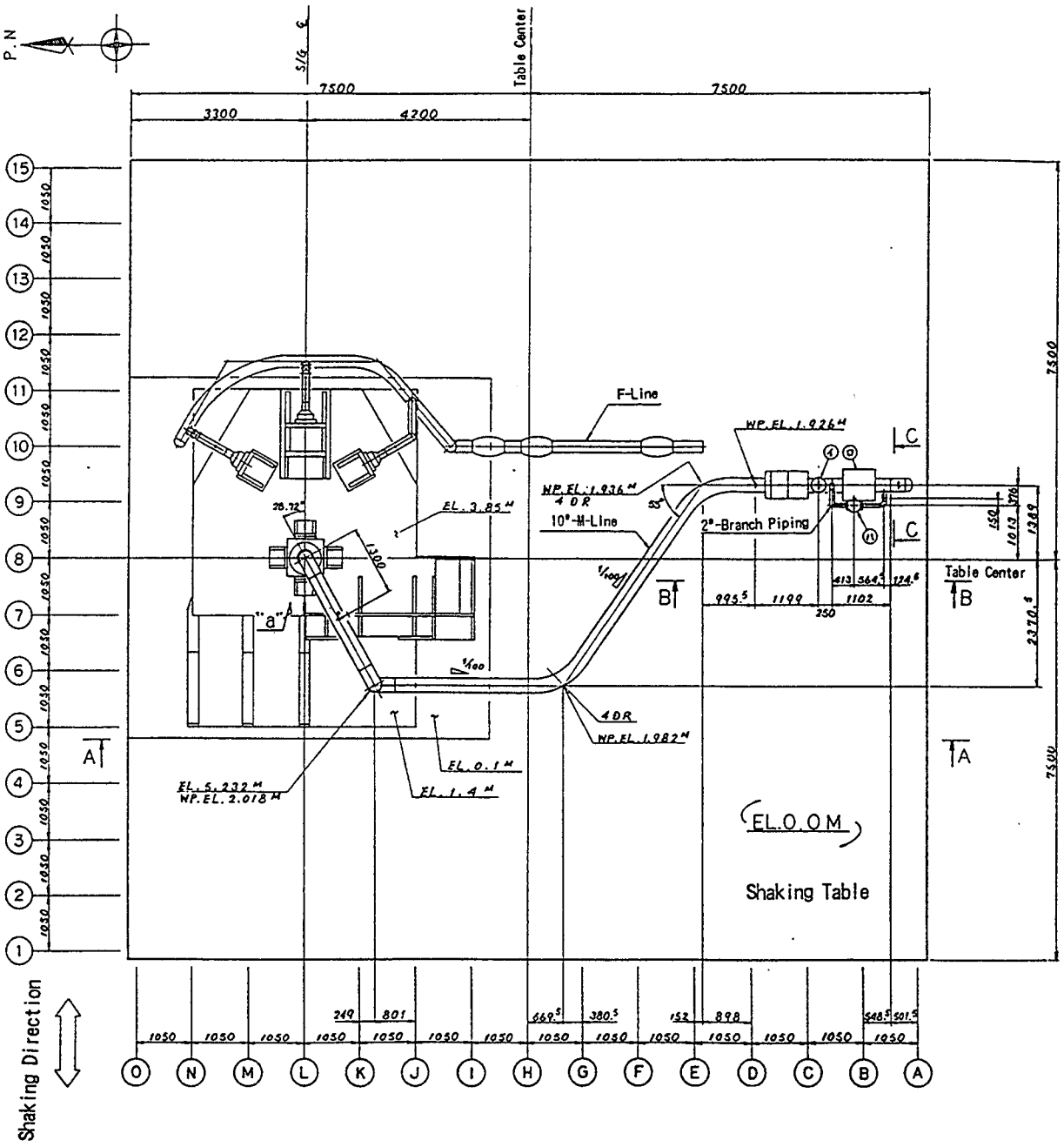

Figure L.4 Plan of MS Seismic Proving Test Model on the Shaking Table

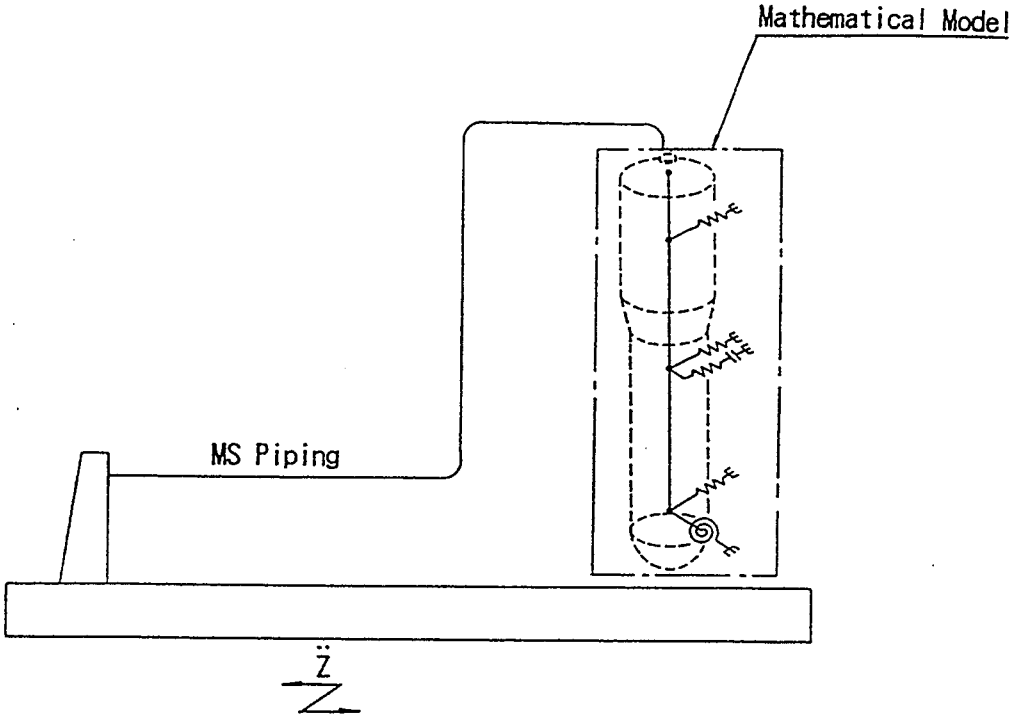

Figure L.5 Concept of Computer-Controlled Actuator System

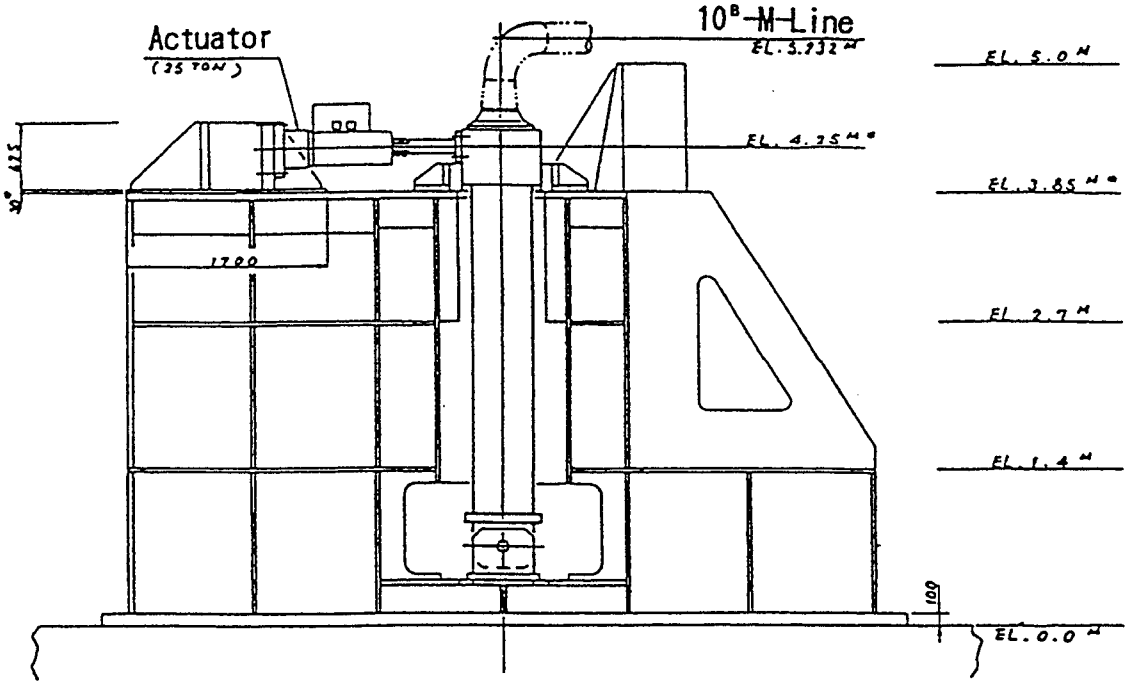

Figure L.6 Detail of Independent Actuator for the M-line

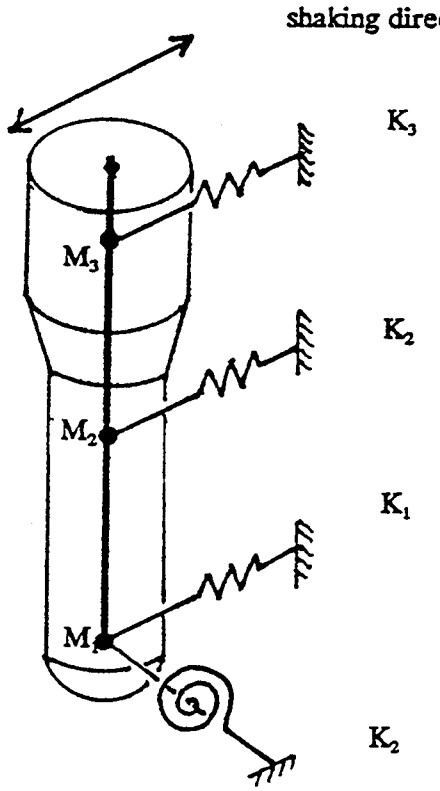

Weight (ton)	
m_1	26.81
m_2	24.18
m_3	32.83

Stiffness	
K_1	2.26×10^5 (kg/mm)
K_2	4.89×10^{11} (kg mm/rad)
K_3	1.32×10^5 (kg/mm)
K_4	3.76×10^4 (kg/mm)

Figure L.7 Mass-spring Model for the SG

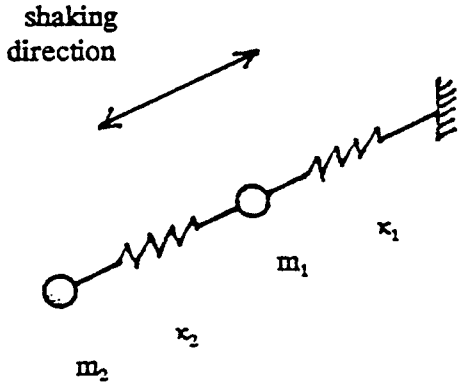

Weight (ton)	
m_1	2.015×10^4
m_2	8.11×10^4

Stiffness	
k_1	5.3×10^6 (kg/mm)
k_2	9.8×10^6 (kg/mm)

Figure L.8 Mass-spring Model for Multiple Excitation Test

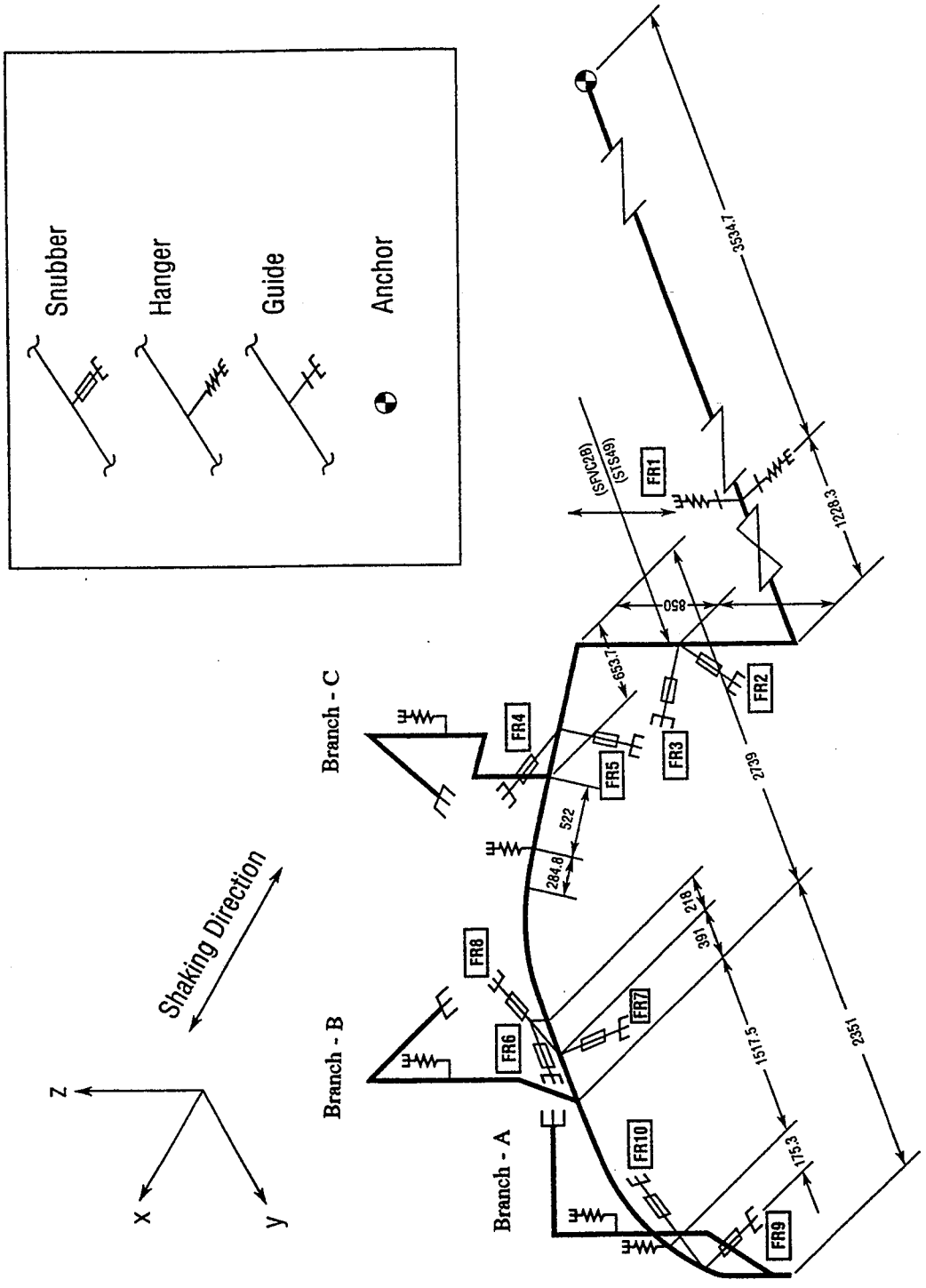

Figure L.9 Pipe Supports of F-line, Conventional Support Case

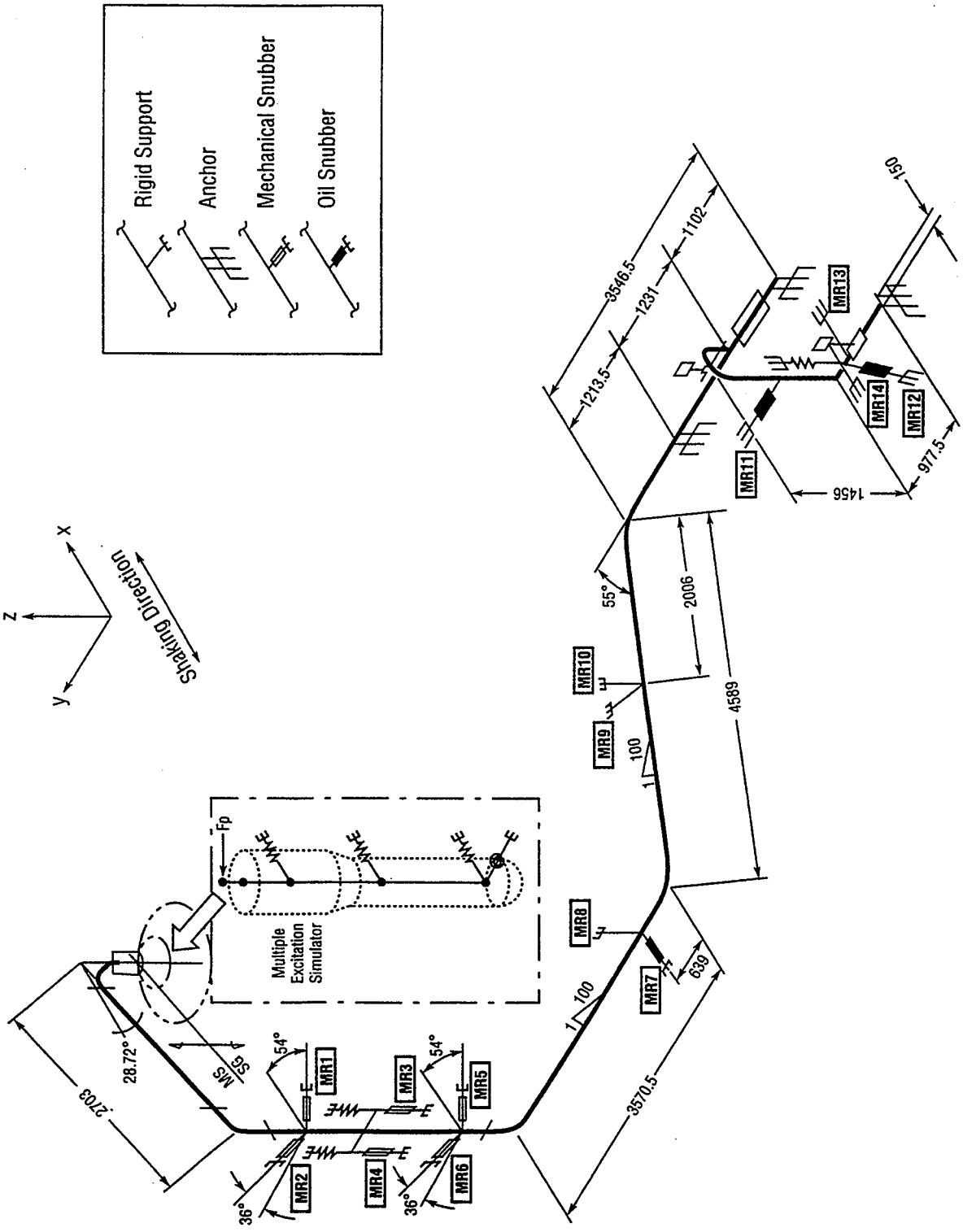

Figure L.10 Pipe Support of M-line, Conventional Support Case

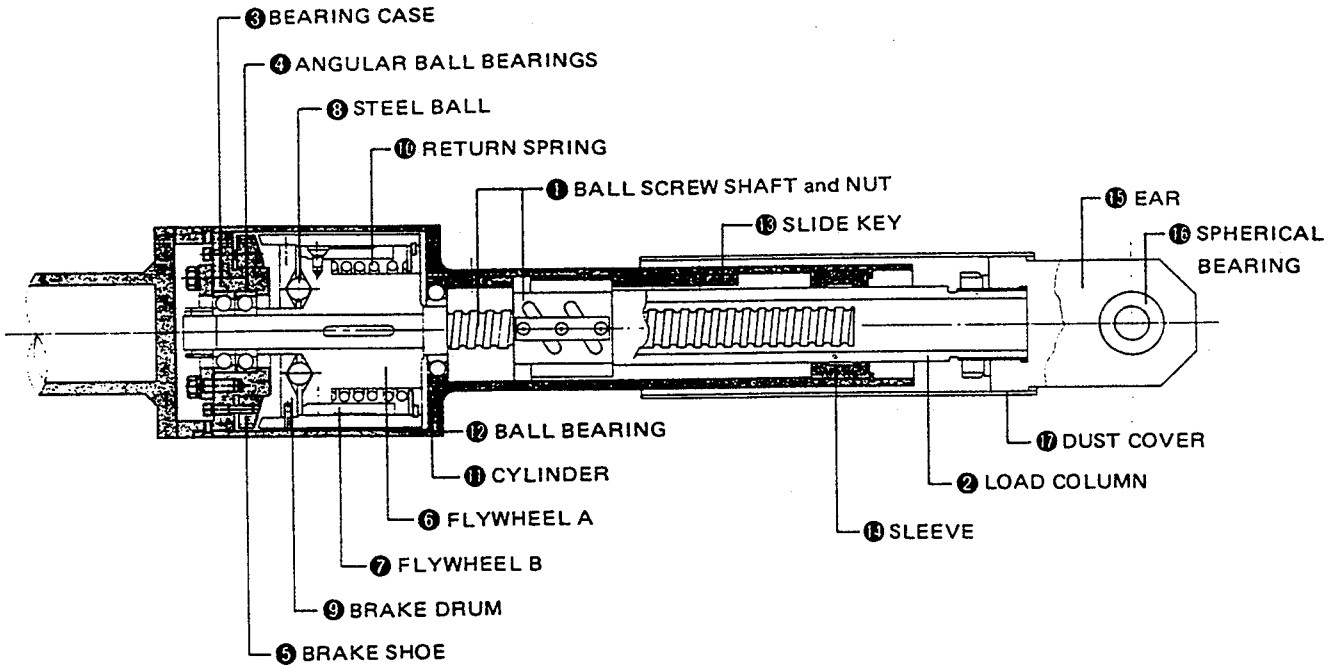

Figure L.11 Mechanical Snubber, Sanwa Tekki (Ref. L.4)

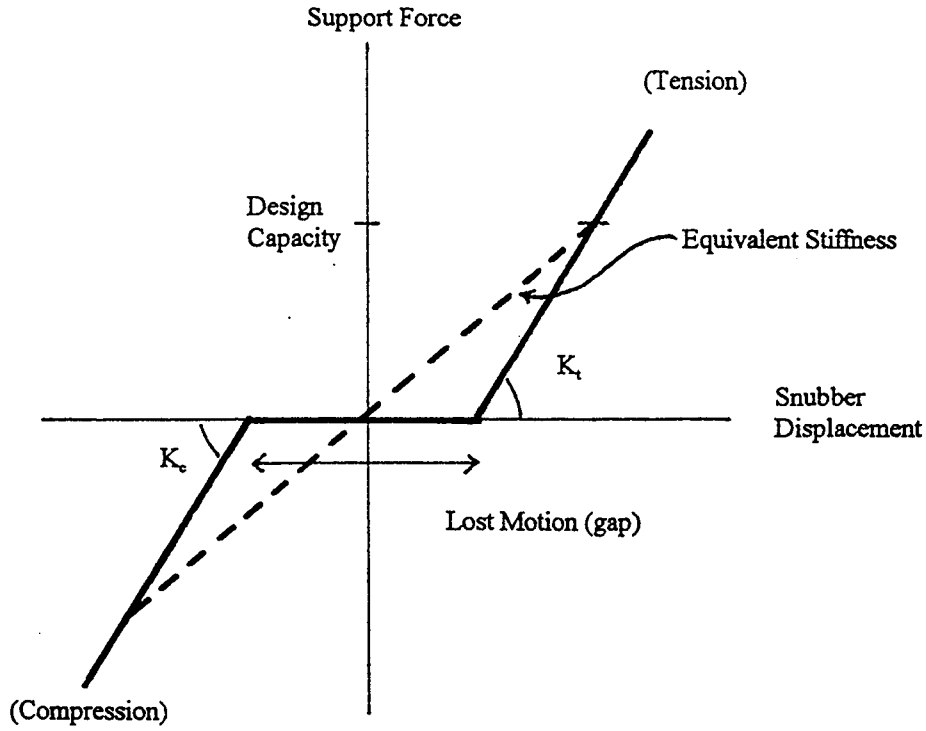

Figure L.12 Idealized Snubber Behavior

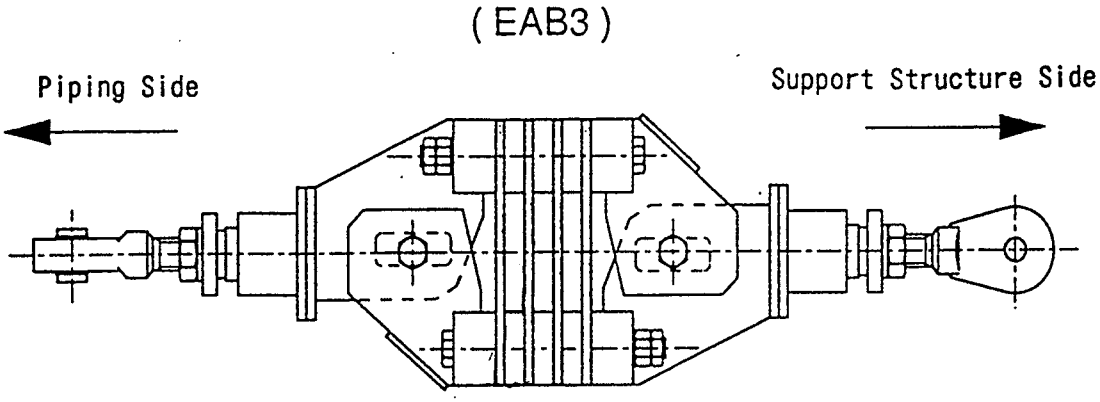

Figure L.13 Energy Absorbing Support (EAB)

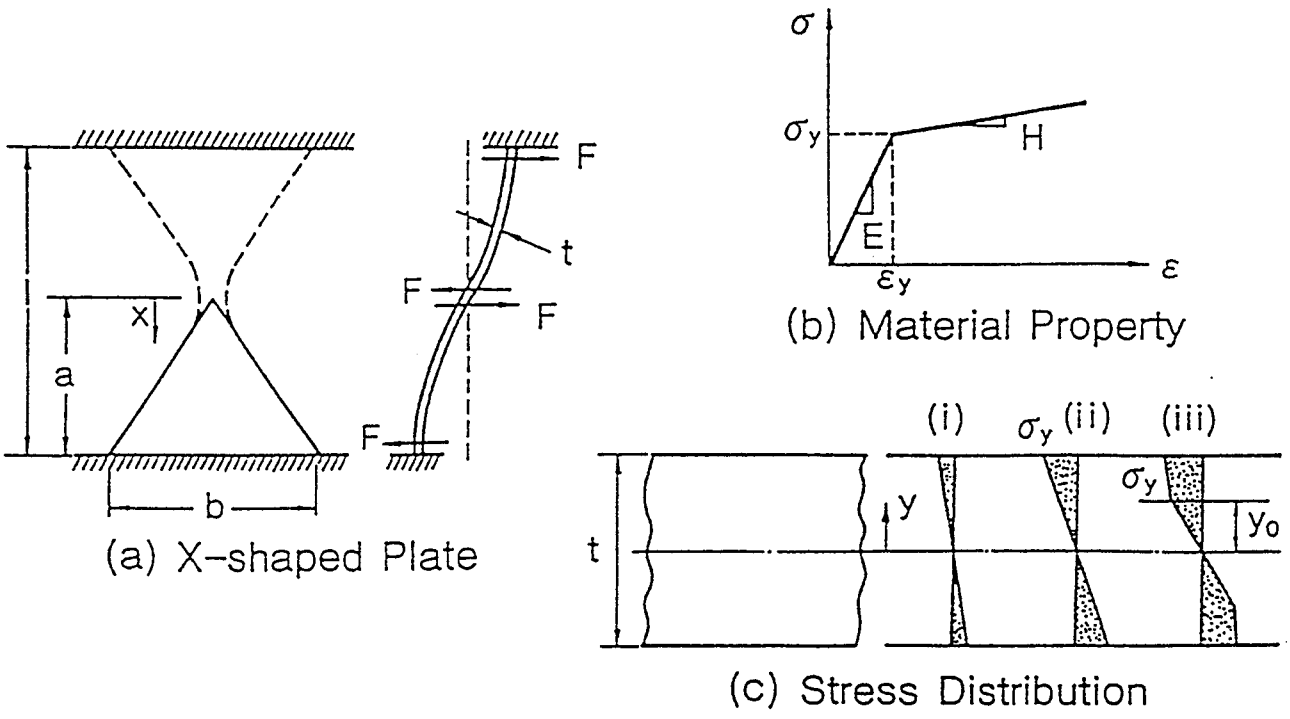

Figure L.14 Mechanical Property of EAB

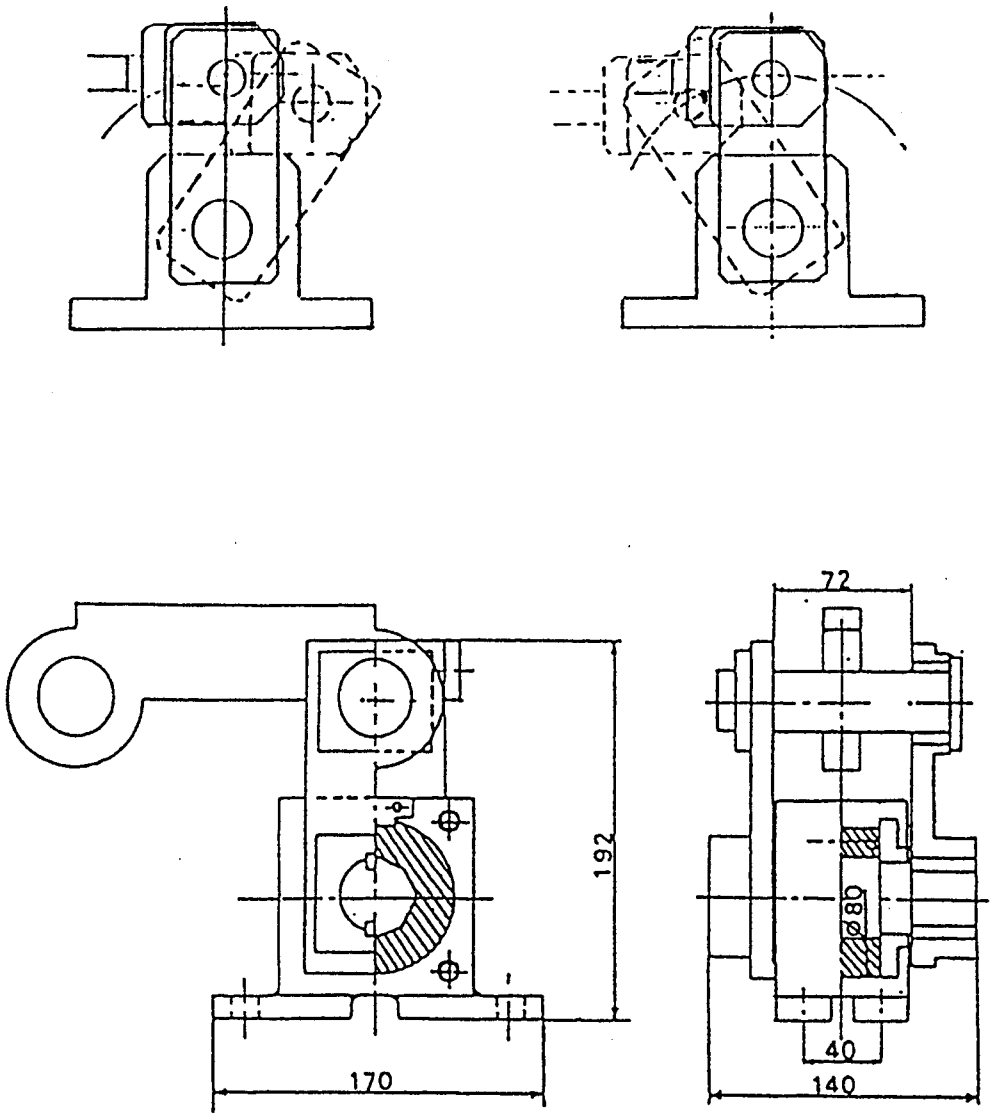

Figure L.15 Lead Extrusion Damper (LED)

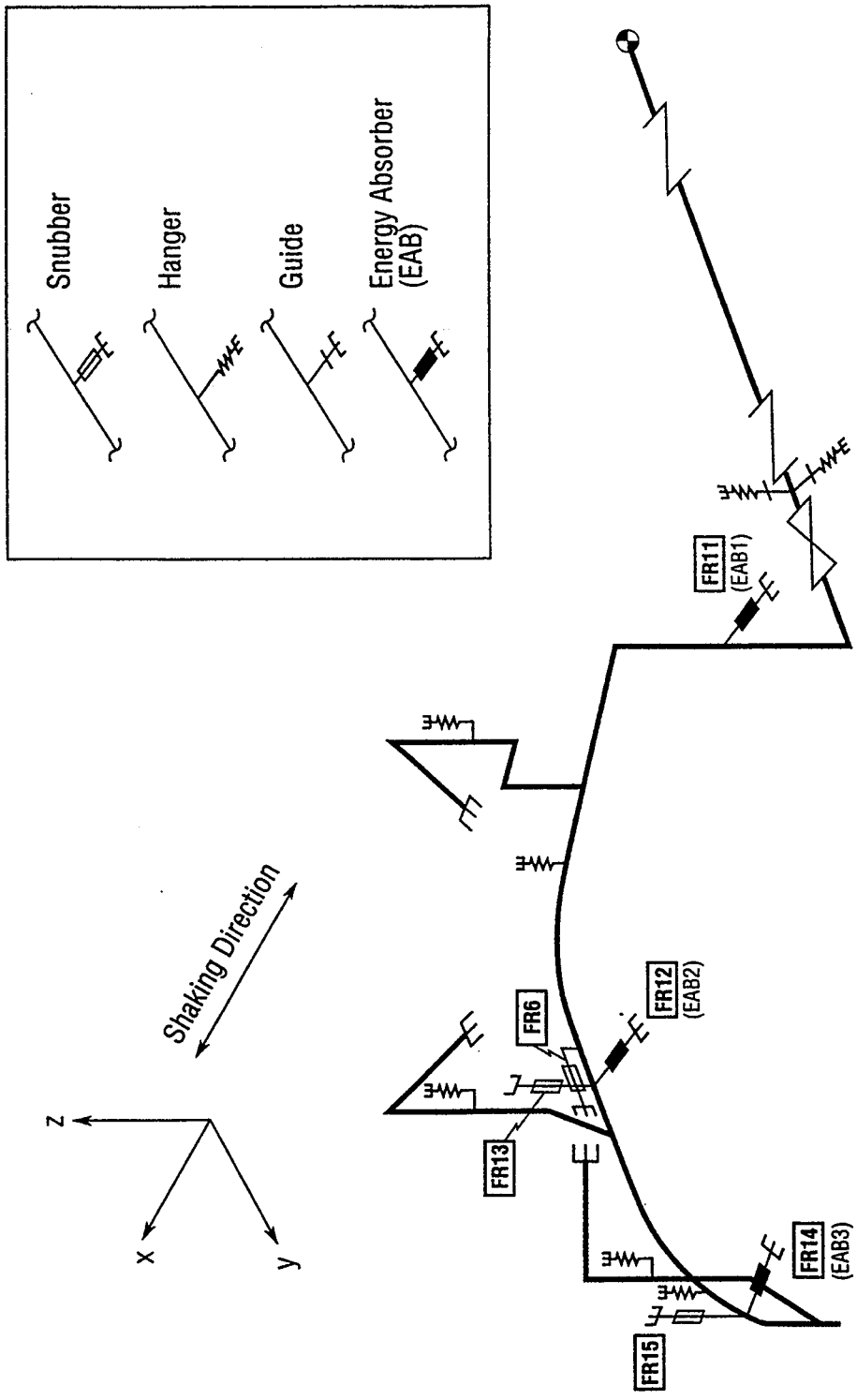

Figure 2.16 Pipe Supports of F-line, EA Support Case

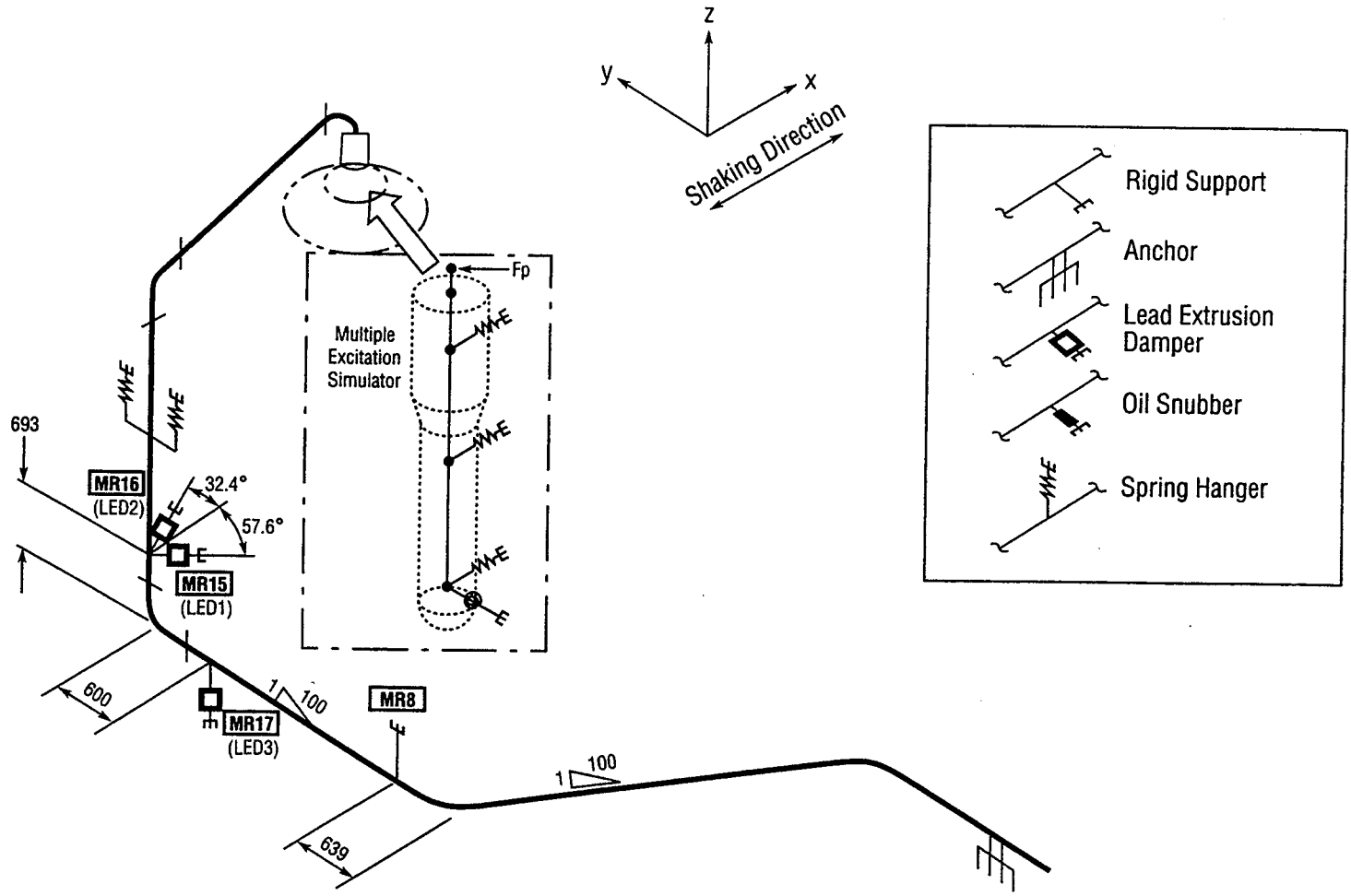

Figure L.17 Pipe Supports of M-line, EA Support Case

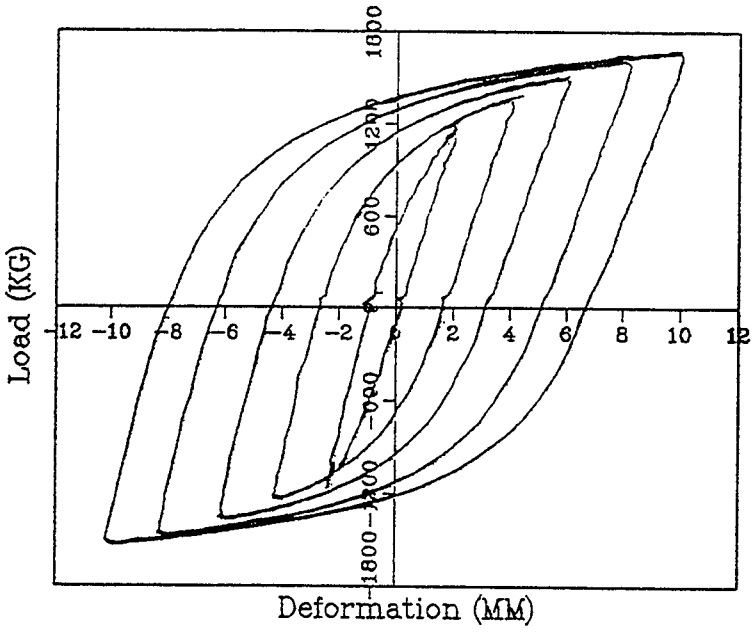

Figure L.18 Component Test Results of EAB Support

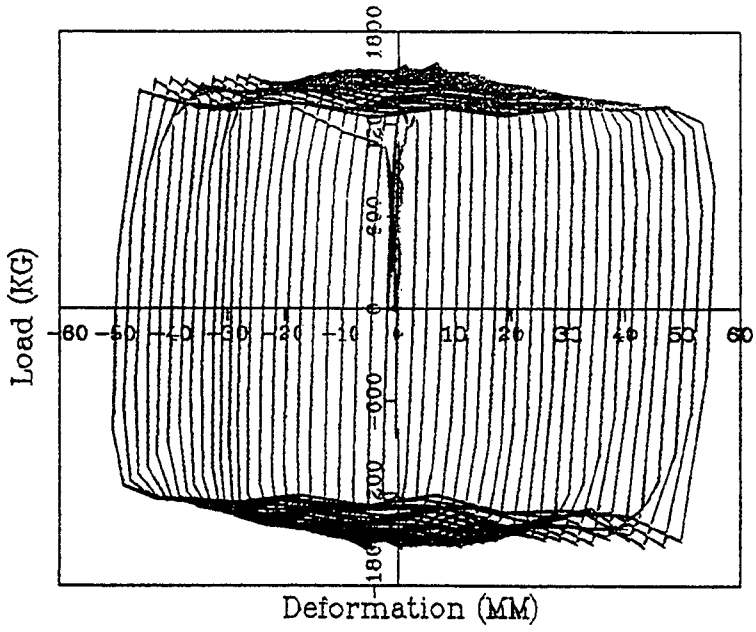

Figure L.19 Component Test Results of LED Support

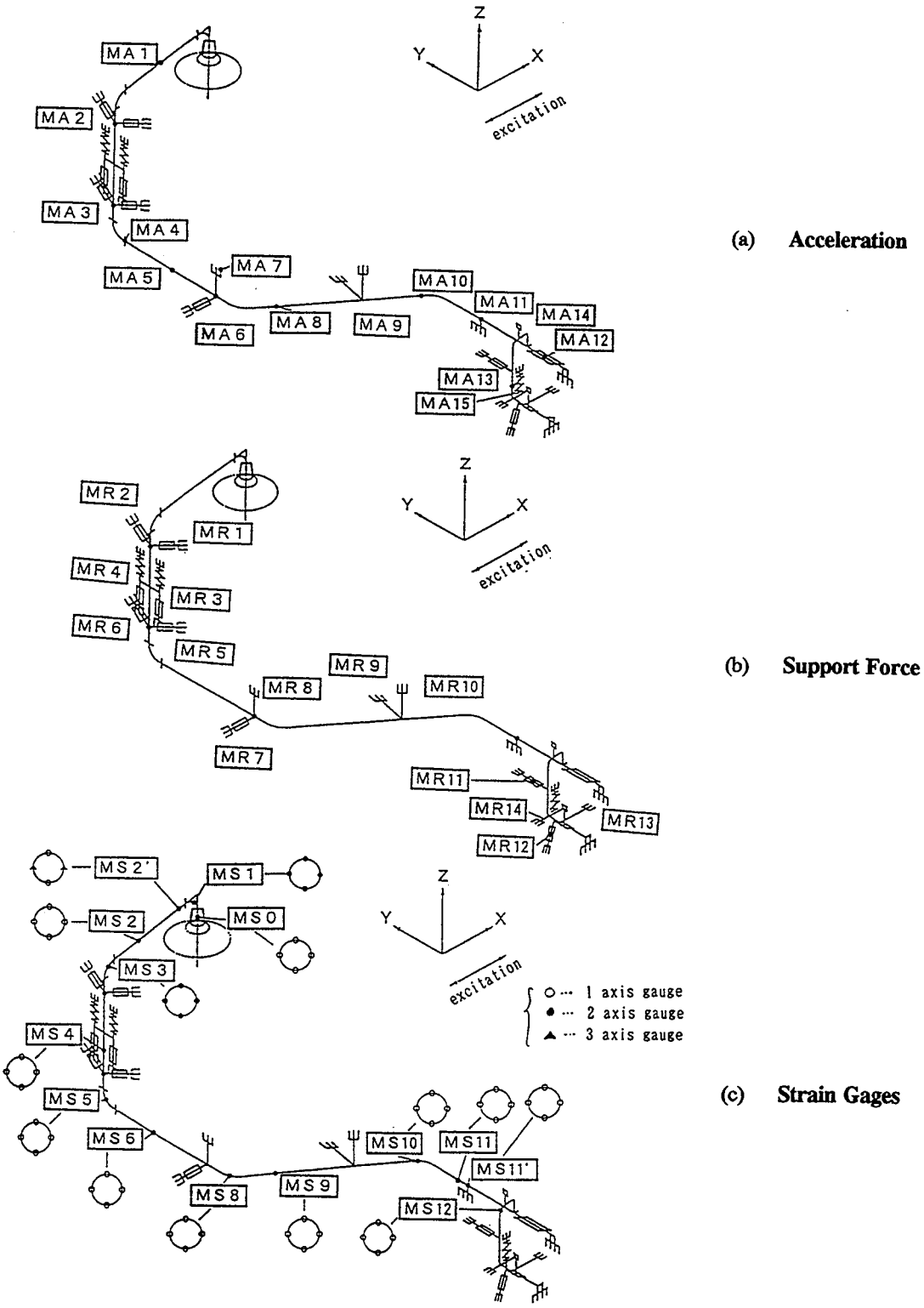

Figure L.20 Instrument for M-line, Conventional Support Case

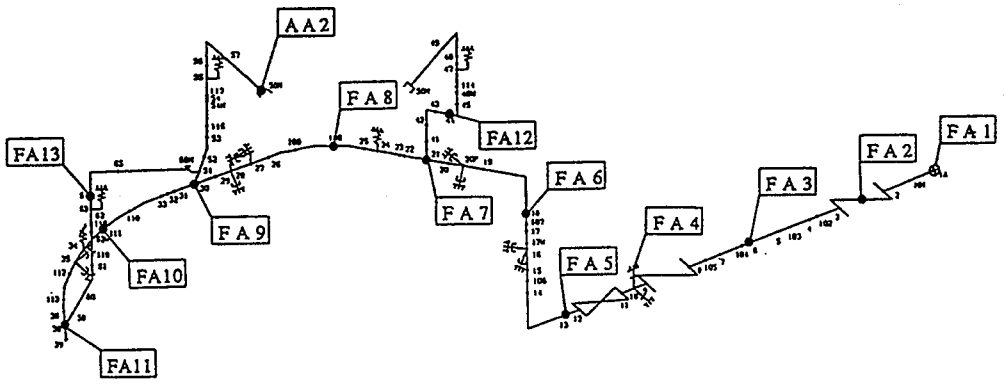

(a) Acceleration

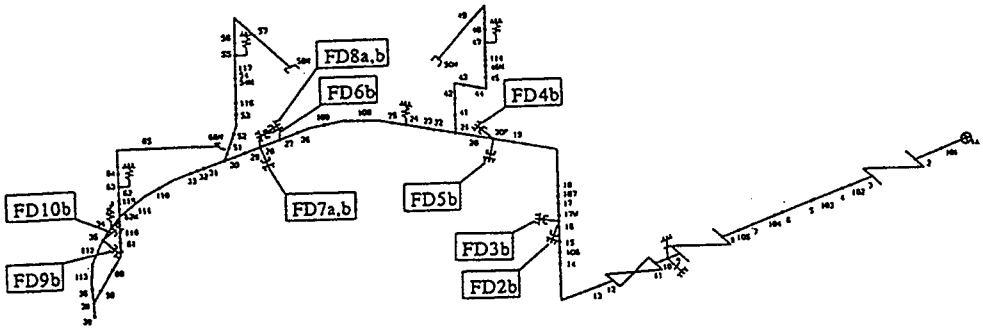

(b) Displacement

Figure L.21 Instrumentation for F-line, Conventional Support Case

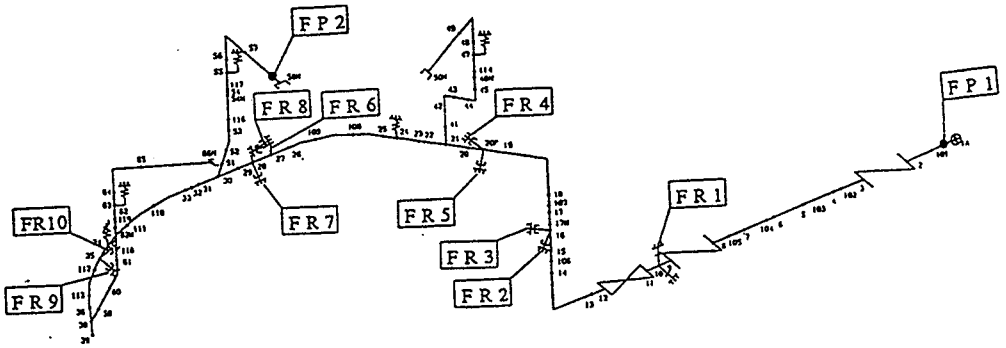

(c) Support Force

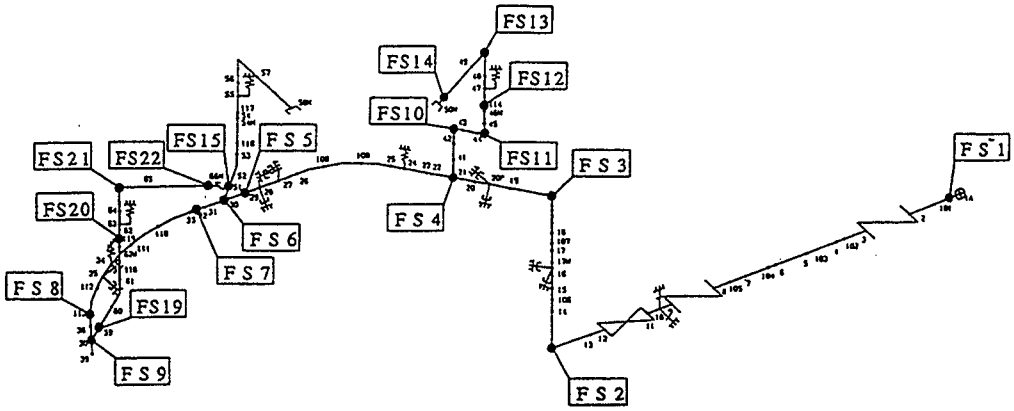

(d) Strain Gages

Figure L.21 Instrumentation for F-line, Conventional Support Case (Cont'd)

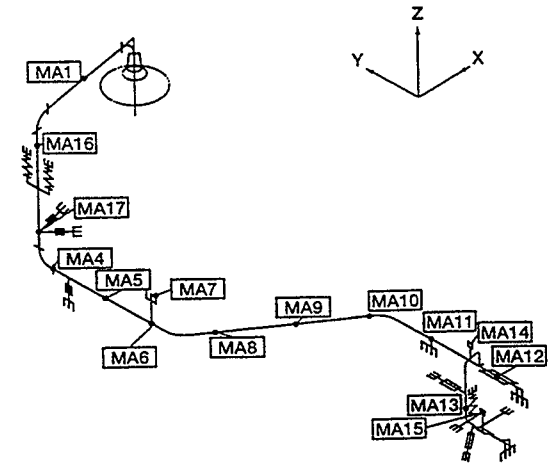

(a) Acceleration

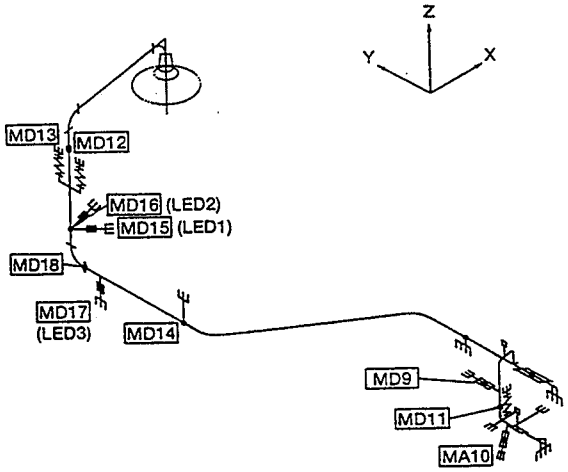

(b) Displacement

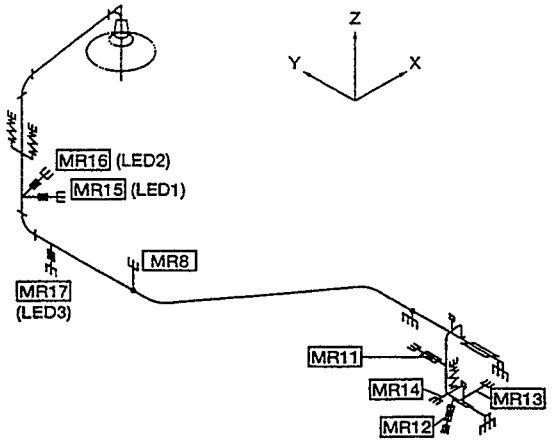

(c) Support Force

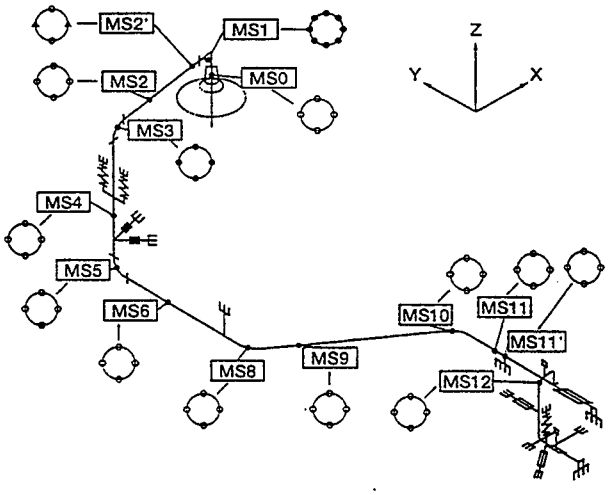

(d) Strain Gages

Figure L.22 Instrument for M-line, EA Support Case

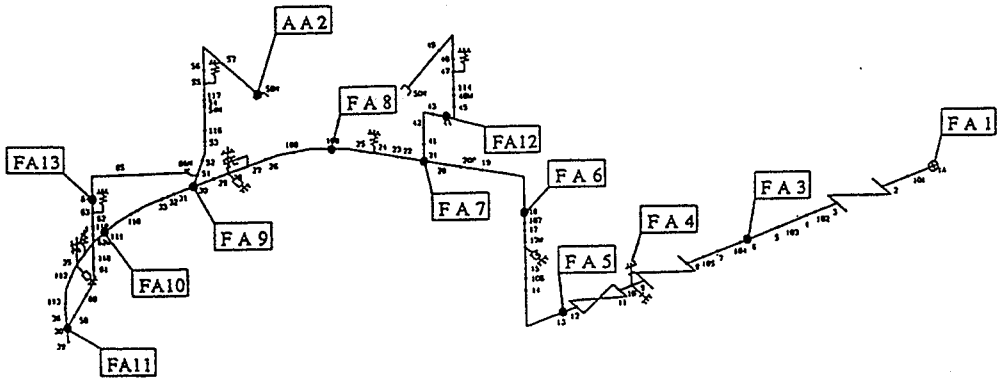

(a) Acceleration

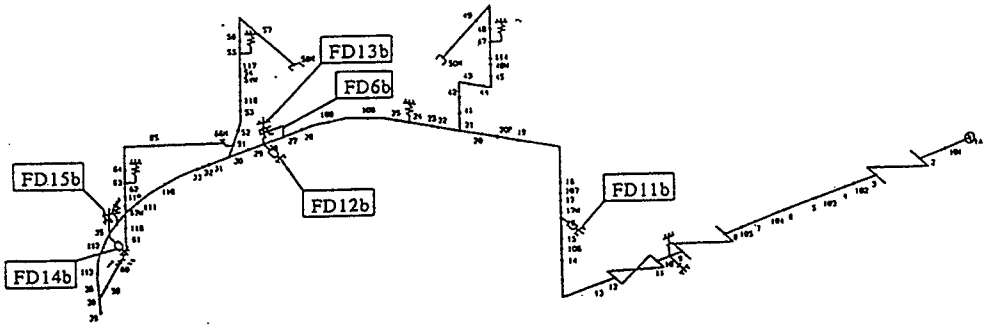

(b) Displacement

Figure L.23 Instrument for F-line, EA Support Case

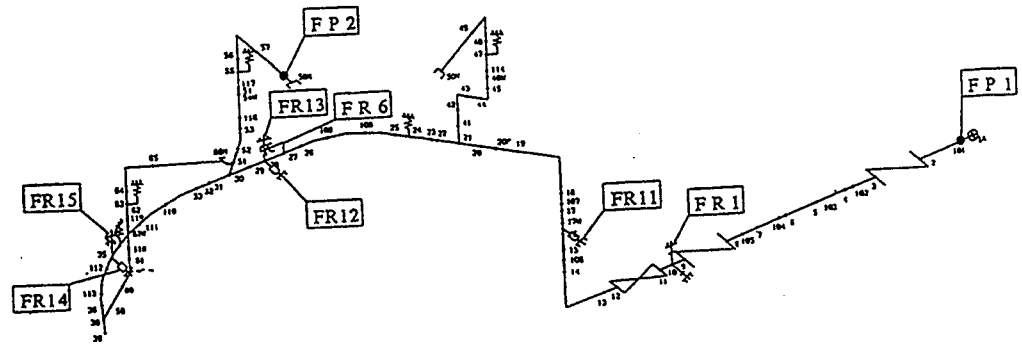

(c) Support Force

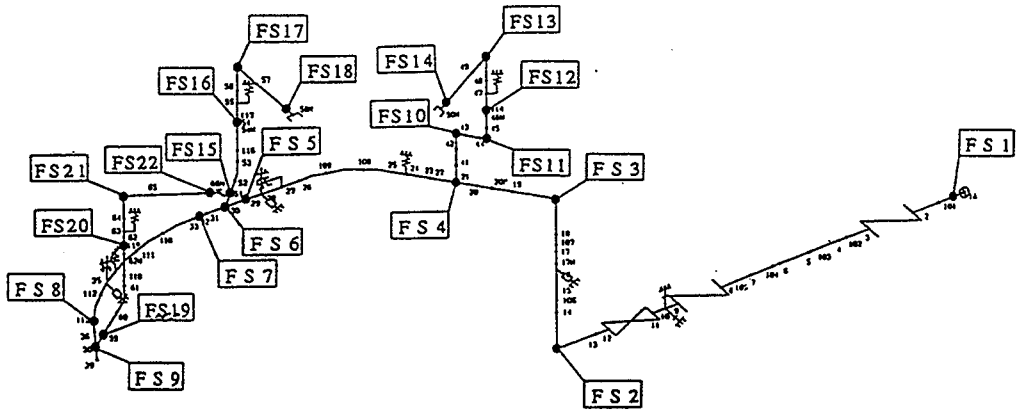

(d) Strain Gages

Figure L.23 Instrument for F-line, EA Support Case (Cont'd)

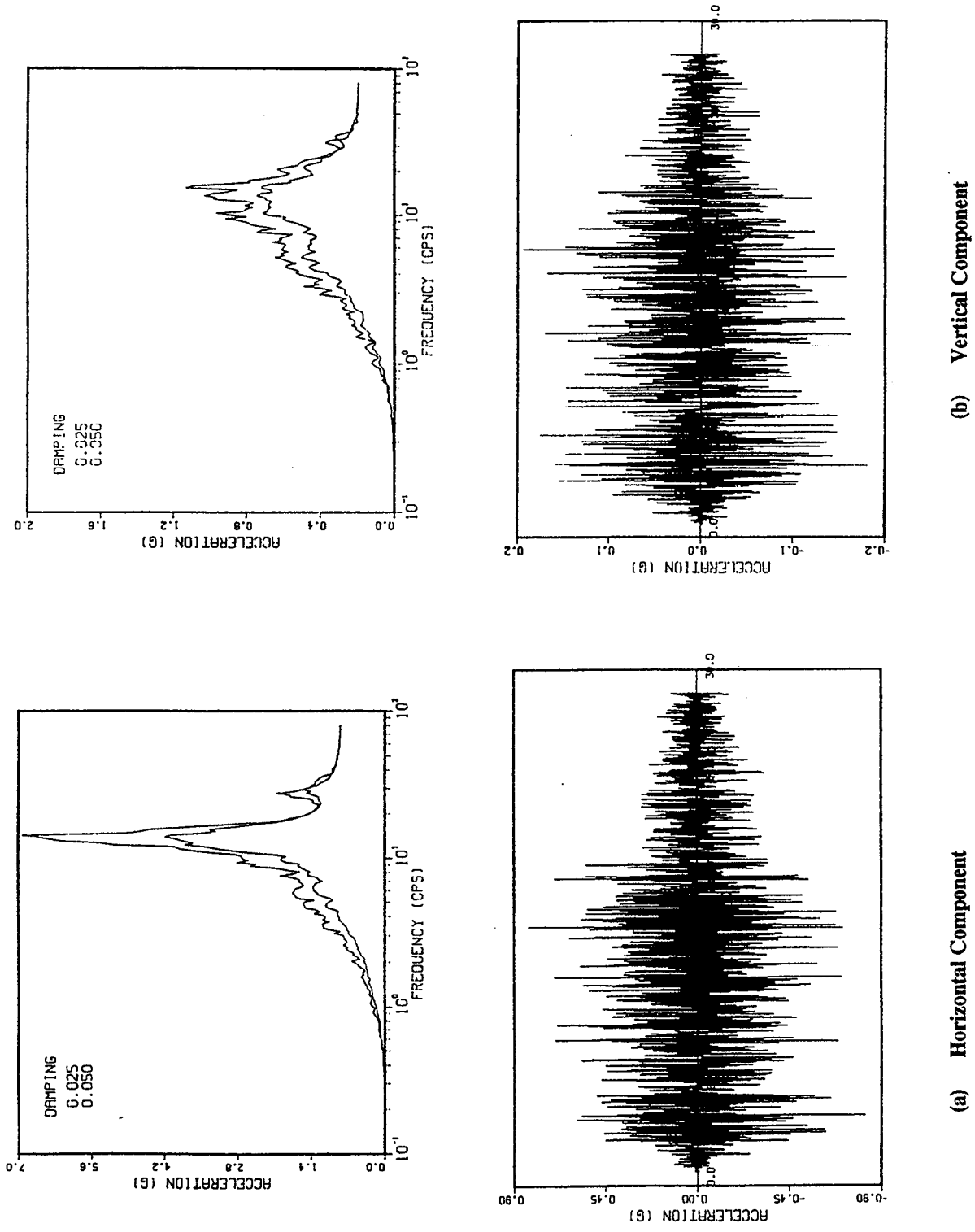

Figure L.24 PWR-S_1 Input Table Motion Accelerograms

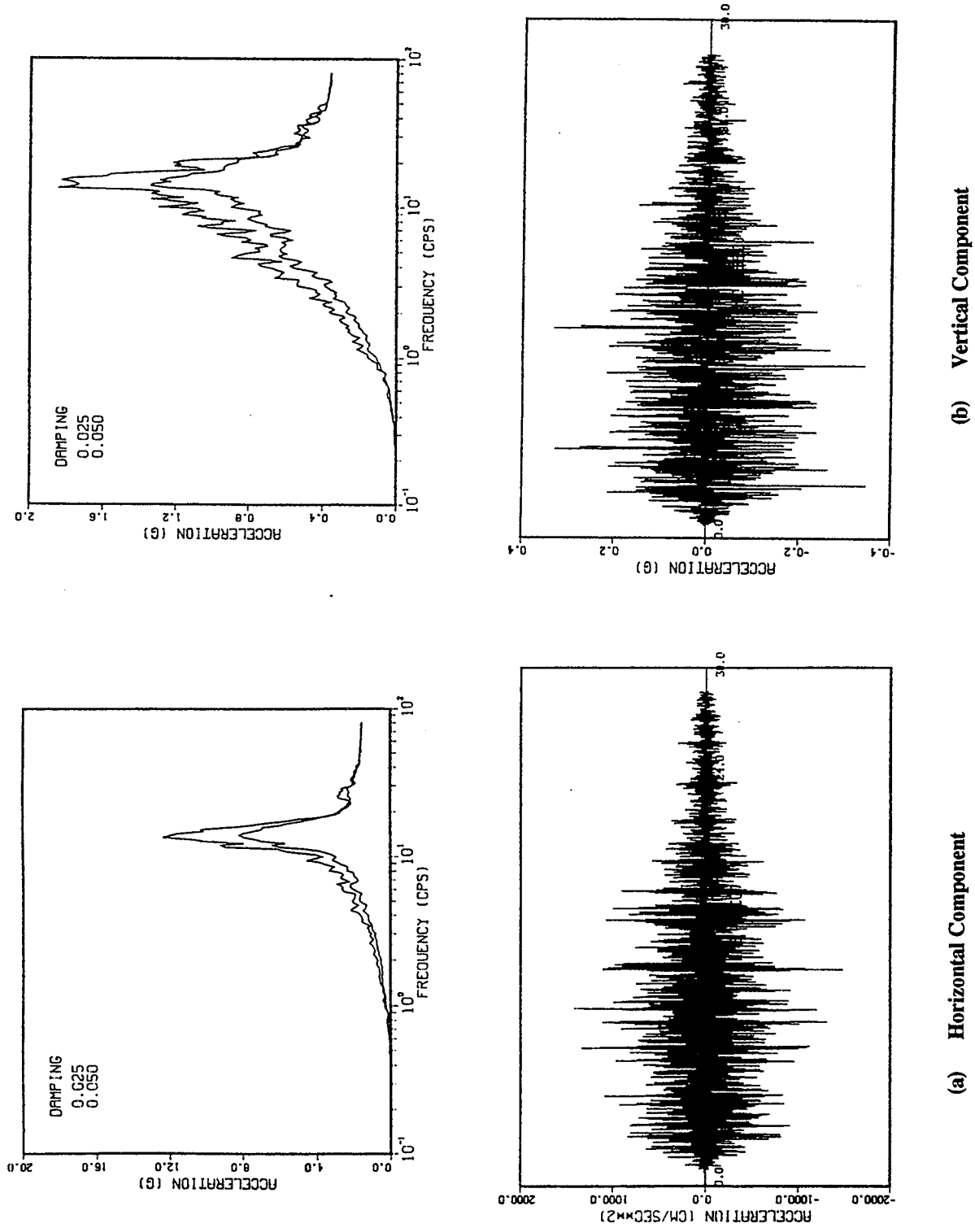

Figure L.25 PWR S_2 Input Table Motion Accelerograms

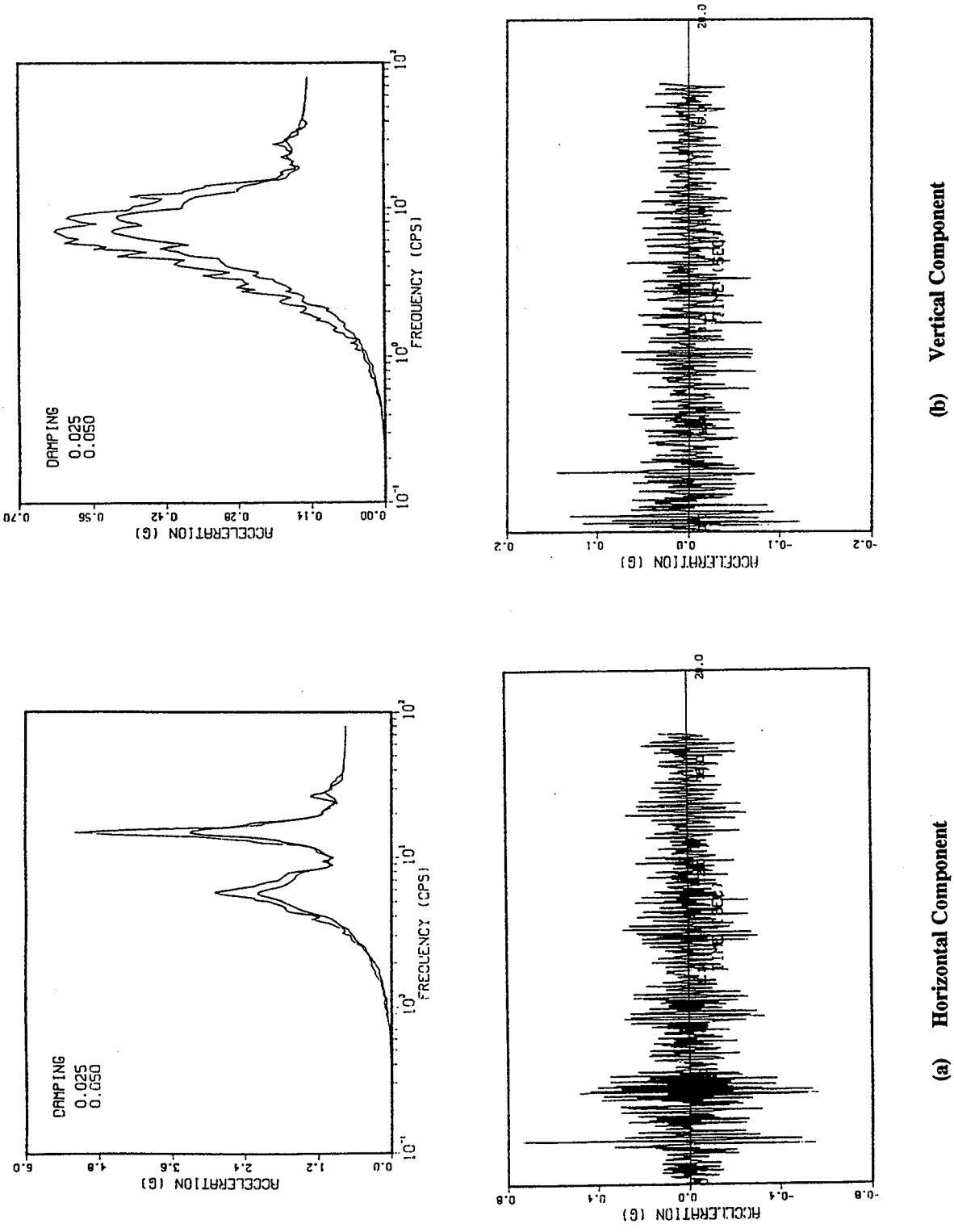

Figure L.26 BWR S_1 Input Table Motion Accelerograms

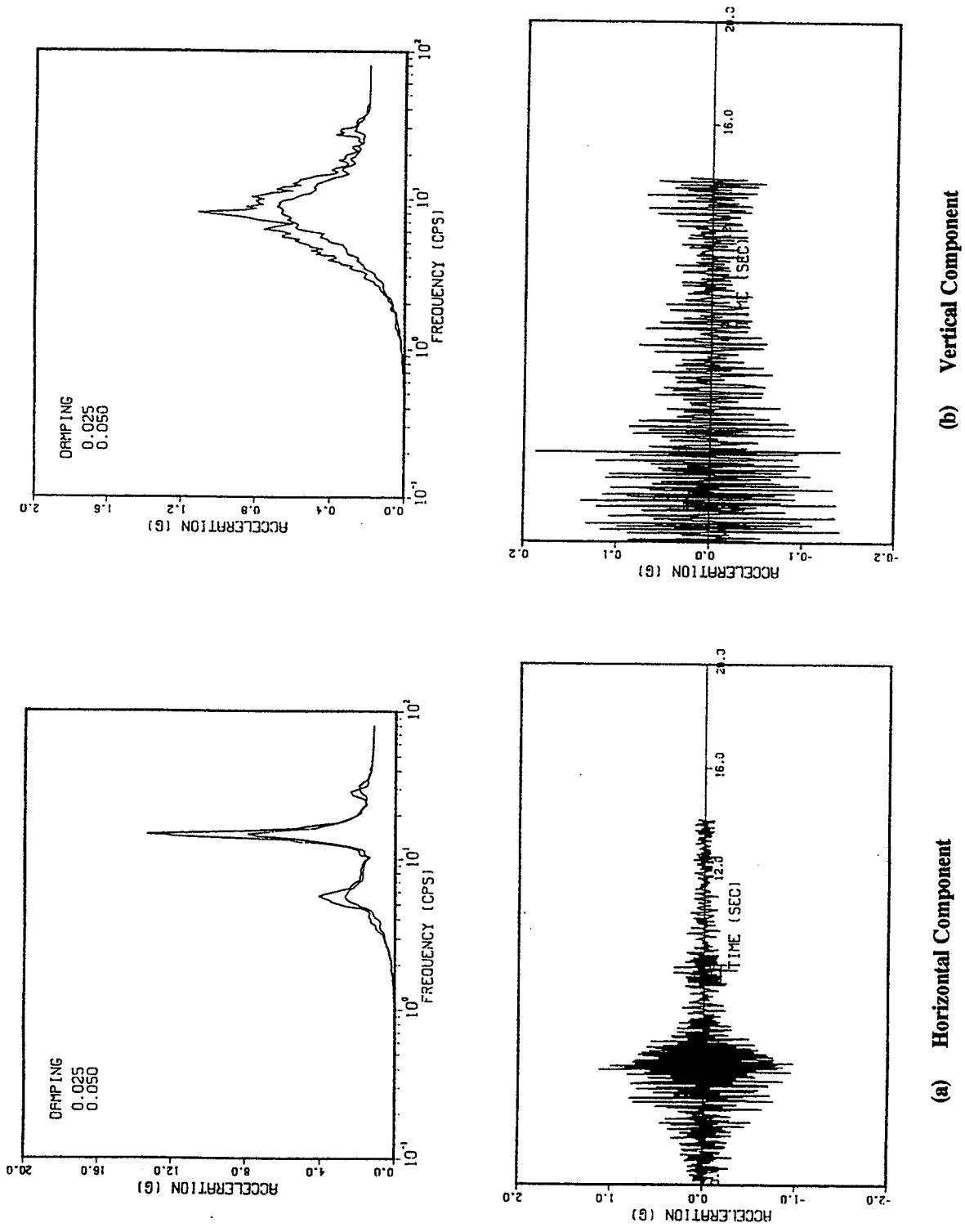

Figure L.27 BWR S_2 Input Table Motion Accelerograms

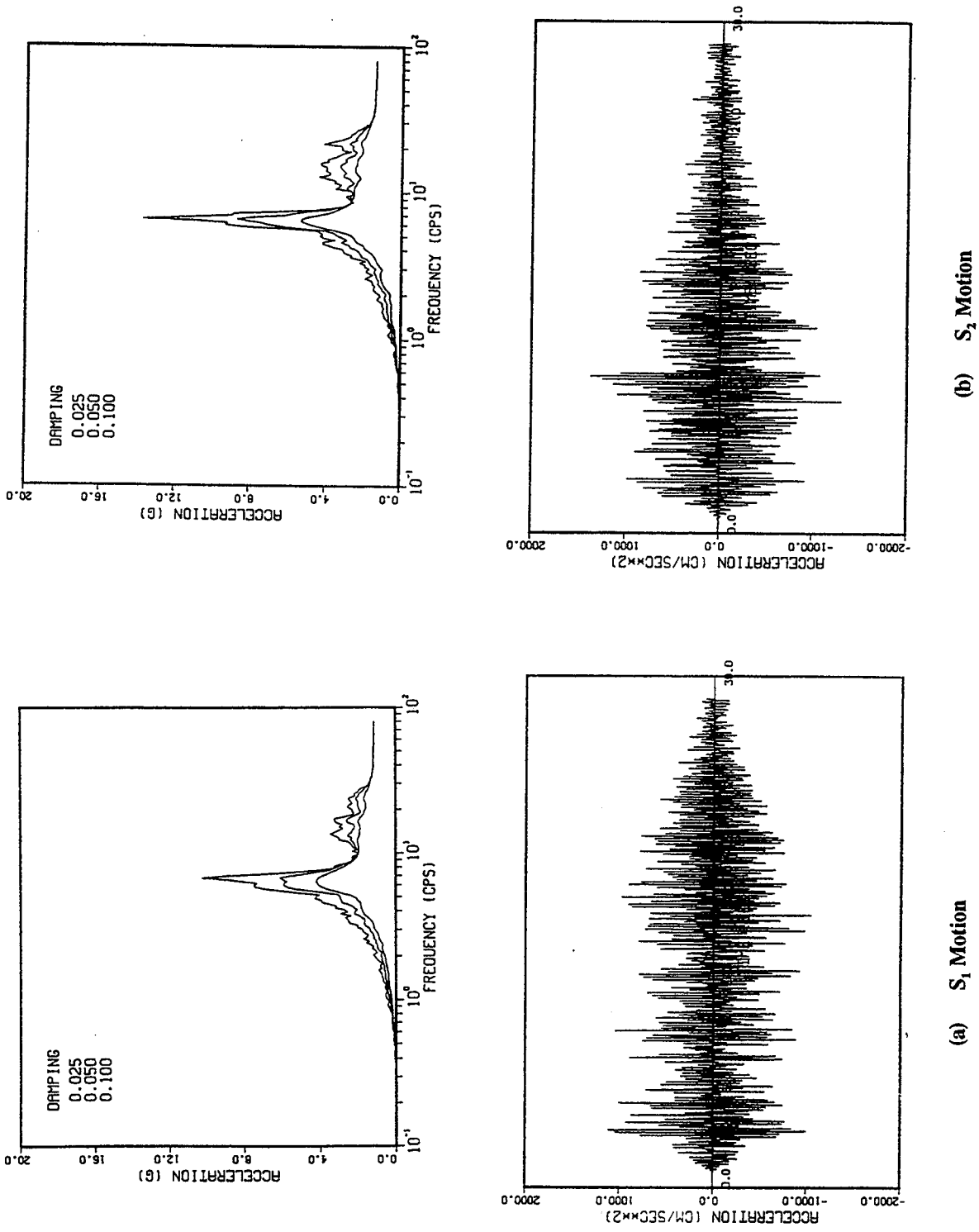

Figure L.28 PCCV Wave Input Table Motion Accelerograms

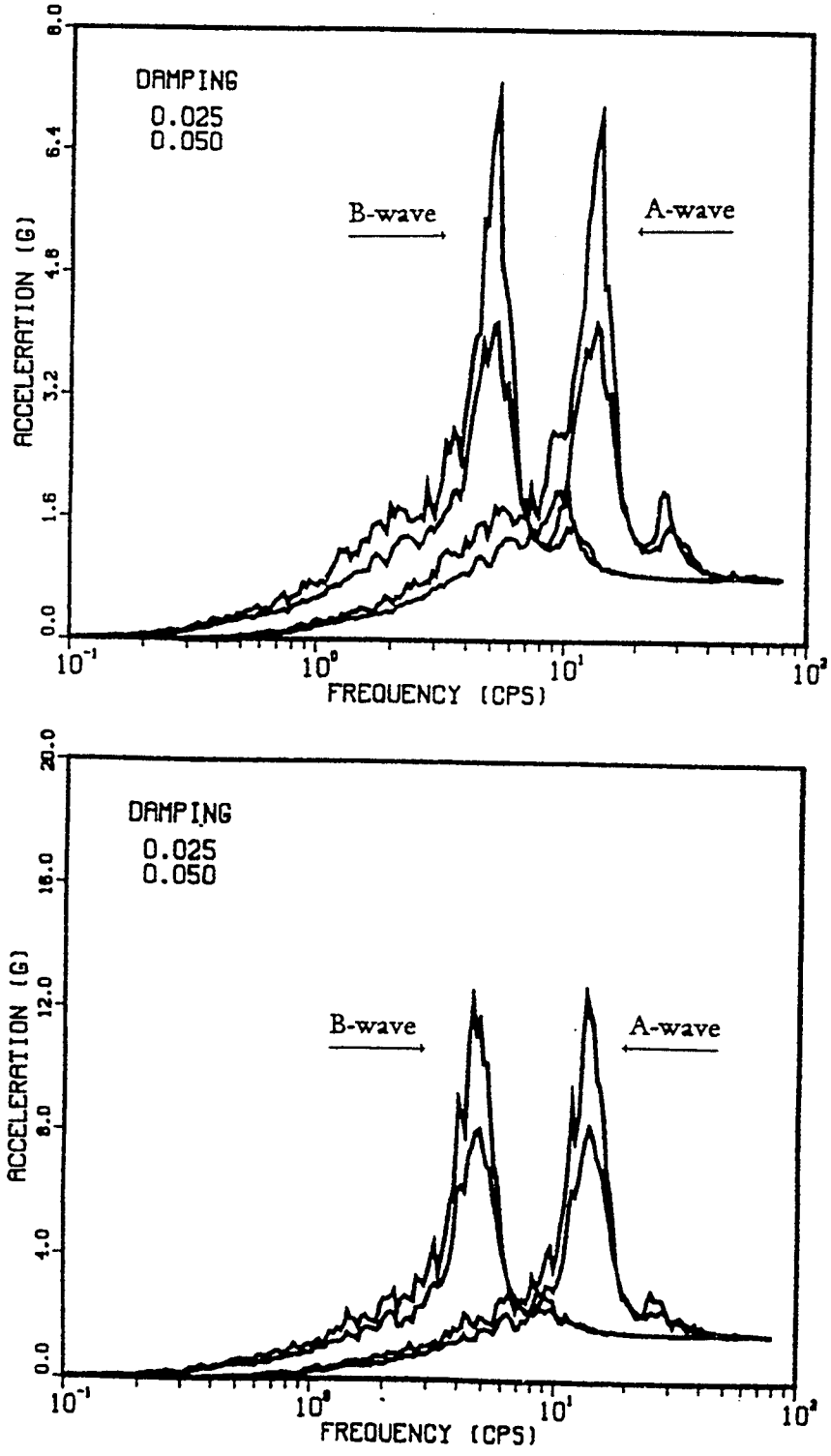

(a) S_1 Motion

(b) S_2 Motion

Figure L.29 Response Spectra of A-Wave and B-Wave

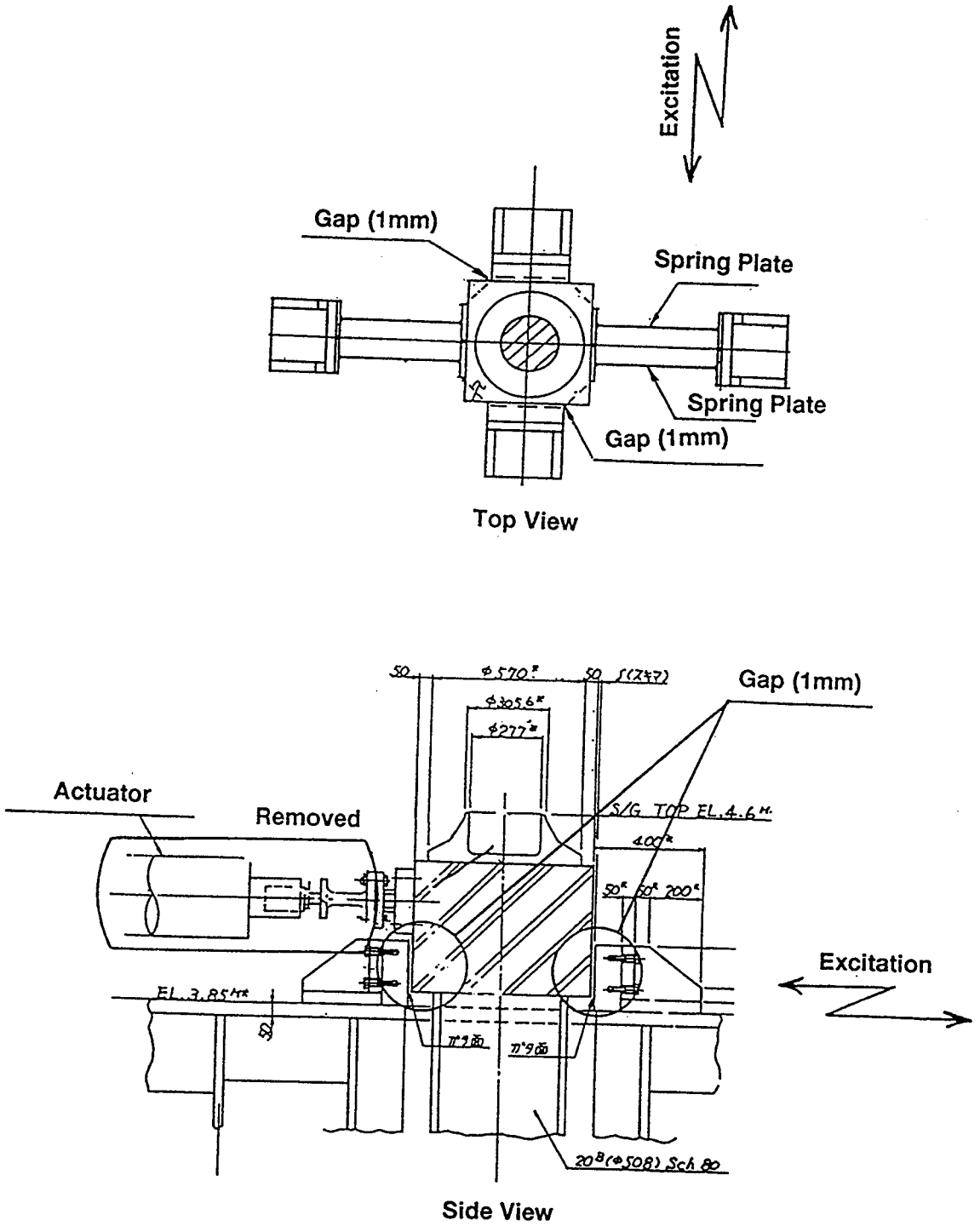

Figure L.30 Detail of Gap Support (Ref. L.8)

APPENDIX M[1]

TEST RESULTS

[1]Information and data included in this Appendix are offered by NUPEC through their technical report. This information and data are translated, summarized and edited in this Appendix by NRC/BNL.

M.1 Shake Table Control

As described in the foregoing chapter, the shake table at the Tadotsu Engineering Laboratory is controlled by two input target motions, i.e., the horizontal (X-direction) and the vertical (Z-direction) input motions. During the MS Test Program, an additional actuator was installed to simulate independent support motions (ISM). Due to the complexity of the test plan and the relatively high-frequency content of the target motions, the accuracy of shaking table control was one of main concerns during the tests.

The measured table motions of a total of six (6) test runs are evaluated as listed in Table M.1. For each test run, a total of five (5) records were used for this evaluation as listed in Table M.2. In the simulation analyses described in Chapter 5 of this report, the measured table motions XOXB, AA1-X, YD2-E and ZOXB are selected to represent the input table motions. The accuracy of the shake table control was evaluated in terms of the peak accelerations and acceleration response spectra. The time histories of some of the table motions listed in Table M.2 can be found in Chapter 5 and Appendices E through J of this report.

M-line Conventional Support Tests. . . . .The peak acceleration values are listed in Table M.3 and the calculated response spectra are shown in Figure M.1 for a test run using the 1.0 S2(M) motions. A damping value of 5% was used for all the calculated response spectra. For the X-direction table motions, the record, XOXB (average of two table motions) compared with the target horizontal motion, XT. The comparison indicates a good agreement with the target motion. However, the spectrum for the independent actuator, AA1-X, shows a spectral peak at around 50 Hz, which was not intended in the test plan. The high frequency motions were caused by higher modes of the SG simulator (see Figure L.7), which was excited by the high frequency motions of the shake table - test model system.

The response spectra for the same set of records as the foregoing X-direction motions were calculated for the vertical motions, Figure M.1 (b).

M-line Multiple Excitation Tests. . . . .In this test series, the SG simulator was switched to the 2-DOF model (Figure L.8) to reproduce the PCCV wave (Figure L.28) at the SG-joint of the M-line. In the tests, only the horizontal motion was considered. In Figure M.2, two spectral peaks can be found for the independent actuator motion of AA1-X. The peak at around 45 Hz was caused by the second mode of the 2-DOF model, and did not exist in the intended PCCV wave motion shown in Figure L.28.

F-line Conventional Support Tests. . . . .The calculated acceleration response spectra are shown in Figure M.3. Since the independent actuator was not activated during the tests, the foregoing high-frequency spectral peak is not observed in the measured table motions. In general, the shake table control was excellent during this series of testing.

B-wave Tests for F- & M-lines with E.A. Supports. . . . .The B-waves were obtained by expanding the time scale of the A-waves, which are identical to the PWR waves shown in Figure M.1, by a factor of 2.72. The comparison of the A and B waves are shown in Figure L.29. The calculated response spectra for the 1.0 S2(B) test run are shown in Figure M.4.

Tokachi-Oki Tests for M-line with LED Supports. . . . .A large number of tests were performed for the M-line with LED supports using the vertical components of the Tokachi-Oki earthquake records by varying both the amplitude and the time scale (see Table B.5 of Appendix B). The response spectra shown in Figure M.5 are from the most severe test run, in which an amplitude factor of 33.5 and a time scale factor of 0.8 were used. In this test series, only the horizontal (X-direction) motions were applied. The table control for this case seems to be excellent.

F-line with EAB Supports using 1.2 S2(C) Wave. . . . .These table motions were obtained by changing the time scale of the A-wave. The response spectra shown in Figure M.6 are for the most severe test run for the F-line, in which an amplitude factor of 1.2 and a time scale factor of 1.6 were used (see Table B.5 of Appendix B). The calculated response spectra indicate excellent table control.

M.2 Test Results of M-line With Conventional Supports

Prior to the earthquake wave tests, preliminary tests were performed to determine the basic dynamic characteristics of the piping system. Table M.4 summarizes the measured frequencies of vibration from the sine sweep tests. Also, measured damping values are tabulated in Table M.5. These results indicate the damping value of the M-line is at least 5% of critical under horizontal excitations.

The test results of the 1.0 S2(M) test run are summarized in Table M.6 and Figures M.7 and M.8. The recorded peak support force of 6.81 tonf for the mechanical snubber MR2 exceeds the rated capacity of 6.0 tonf (see Table L.4). In general, the recorded responses were higher than the values estimated during planning due to the high-frequency components included with independent support motions, as well as due to the gap nonlinearity of the snubbers. The recorded pipe stresses, however, were still much lower than the yield stress of 25 kg/mm^2. (Table L.1)

The hysteretic responses of the snubbers shown in Figure M.8 indicate a complex nonlinearity in snubber behavior. The highly irregular hysteretic response observed for snubbers MR3 and MR4 may be caused by orthogonal (to the snubber axis) forces on the vertically mounted snubbers. Two types of measurements were made to record snubber deformations, i.e., the relative movement of the pipe at the location of the snubber, which is called a-measurements, and the axial deformation of the snubber, which is called b-measurements. As indicated in Table M.6, both types of measurements were made for snubbers MR5, MR6 and MR7. The difference between the two measurements is considered to be caused by slippage in the pipe clamps.

The measured peak responses for several records are plotted as a function of the table motion amplitude for the S1(M) test series in Figure M.9, and for the S2(M) test series in Figure M.10. Due to pipe support nonlinearities in pipe supports, the recorded responses are not proportional to the table motion amplitude.

The test results from the multiple excitation test using the ⅓ S2(M) wave are given in Table M.7 and Figures M.11. In this test, the 2-DOF model shown in Figure L.8 was used for the SG simulator to reproduce the PCCV wave. Although the basic table motion amplitude was only ⅓ of the 1.0 S2(M) test run, larger differential displacements were achieved (e.g., the relative displacement at AA1-X was 3.54 mm compared to 2.46 mm in 1.0 S2(M) test run). As a result, somewhat higher support forces and pipe stresses were measured at several locations as compared with the test results from the 1.0 S2(M) test run tabulated in Table M.6.

M.3 Test Results of F-line with Conventional Supports

The measured frequencies of vibration and damping values from sine sweep tests are tabulated in Tables M.8 and M.9. Due to the hard spring-type nonlinearity of the mechanical snubbers, the frequencies of vibration tend to be greater in the higher amplitude tests, which is considered to be a significant characteristic of the piping system. The damping values, tabulated in Table M.9, indicate that the "elastic" damping value for the fundamental mode is slightly lower than 5%, depending on the excitation amplitude and the direction of excitation.

The test results for the 1.0 S2(F) test run are summarized in Table M.10 and Figures M.12 and M.13. The measured pipe stresses were much lower than the yield stress of 25~28 kg/mm^2 (see Table L.1). The hysteretic behavior of the mechanical snubbers shown in Figure M.13 indicates highly irregular nonlinear characteristics.

The measured peak responses for several parameters are plotted as a function of the table motion amplitude for the S1(F) test series in Figure M.14 and the S2(F) test series in Figure M.15. It can be observed that while the acceleration and pipe stress responses from the 1.0 S2(F) test run are about twice those from the 1.0 S1(F) test run, the support forces from the 1.0 S2(F) test run are not as large in comparison with the 1.0 S1(F) test run. Also, for almost all the measured items, the responses are not proportional to the table motion amplitude. The response amplification factors at higher excitation tend to be reduced, particularly for the pipe stresses and the support forces. A similar trend was also observed in the foregoing M-line test results (see Figures M.9 and M.10).

M.4 Test Results of M-line with LED Supports

As illustrated in Figure L.17, the mechanical snubbers of the M-line were replaced with three (3) LED supports in the main piping and a large number of test runs were performed. The measured vibration frequencies from sine sweep tests at different excitation levels are tabulated in Tables M.11. Due to complex nonlinearity of the LED supports at lower excitation levels, caused mainly by mechanical gaps in the LED supports, no clear tendency can be observed in the measured frequencies (e.g., a possible correlation with excitation level).

The test results from the 1.0 S2(A) test run are given in Table M.12 and Figures M.16 and M.17. Also, several peak response values from the S2(A) wave test series are plotted in Figure M.18 as a function of the table motion amplitude. The responses of the LED supports shown in Figure M.17 indicate stable hysteresis loops of the newly proposed energy absorbing device.

The support forces, plotted in Figure M.18 (d) tend to level off in higher amplitude tests. As a result, the amplification of the pipe stresses tends to be reduced at higher excitation levels as shown in Figure M.18 (b), indicating the effectiveness of the LED supports. Since only three LED supports were installed on the test model, the measured pipe stresses were much higher than those measured in the test cases with conventional supports [e.g., see Figure M.10 (c)].

The same set of test data are given in Table M.13 and Figures M.19 through M.21 for the test series using the B-wave. As the frequency of the table motions was 2.72 times lower than that of the test series using the A-wave, the recorded accelerations were much lower. The responses of the LED supports, shown in Figure M.20, indicate that LED-2 dissipated most of the vibration energy, and the responses of LED-1 and LED-3 were much lower. Under slower vibration loadings (in comparison with the A-wave tests), the hysteresis loops of the LED supports exhibit a pinching behavior, indicating a rate dependent characteristic of the LED supports.

After the ISM tests described above, the SG-joint was fixed to the common support structure and a large number of uniform motion tests were performed mainly for assessing the seismic margin of the LED supports. The most severe test was conducted at the end of the MS Test Program using the Tokachi-Oki earthquake wave (see Figure M.5). The test results are given in Table M.14 and Figures M.22 and M.23. Both LED-2 and LED-3 were subjected to large displacement reversals as shown in Figure M.23 (the hysteretic response of LED-3 was not properly recorded during this test). Under repeated large plastic deformations, the LED support starts to exhibit a strength degradation as well as a negative post-yield stiffness, as shown in the hysteretic responses of LED-2. More complete response results for this test run are given in Appendix J of this report. Referring to the peak response table, Table J.1, the recorded peak temperature for LED-2 was 107.1°C (marks as "TE2"). This large temperature rise may have contributed to the observed strength degradation behavior of LED-2.

The test results for the uniform motion test series using the S2(A) waves are summarized in Figure M.24. These test results were used to verify the nonlinear analysis methods, as described in Chapter 5.

M.5 Test Results of F-line with EAB Supports

As illustrated in Figure L.16, three (3) mechanical snubbers and three (3) EAB supports were installed for this test series. The measured vibration frequencies and damping values at different excitation levels are tabulated in Tables M.15 and M.16. It should be noted that the mechanical snubbers possess a hard spring-type characteristics, i.e., the vibration frequencies tend to increase at higher excitation levels. The EAB supports, on the other hand, are soft spring-type, i.e., the vibration frequencies tend to reduce at higher excitation levels. As the two different pipe support types were combined in the F-line piping system, the measured vibration frequencies listed in Table M.15 indicate no clear tendencies. The damping values, Table M.16, are lower than those for the conventional support case, Table M.9.

The test results for the 1.0 S2(A) wave test run are summarized in Table M.17 and Figures M.25 and M.26. Several peak response values from the S2(A) wave test series are plotted in Figure M.27. The same set of test data for the B-wave test series are given in Table M.18 and Figures M.28 through M.30. The observed hysteretic response of the mechanical snubbers indicates a highly irregular nonlinearity, particularly those in the 1.0 S2(B) test run in Figure M.29. The responses of the EAB supports, on the other hand, are predictable and consistent with the component test results given in the foregoing Figure L.18. The recorded pipe stresses were higher than those for the conventional support cases. However, under an excitation level 2.5 times higher than the design earthquake, the measured pipe stresses were still lower than the yield stress of 25~28 kg/mm^2 [see Figure M.27 (b)]. The peak support forces in mechanical snubbers, FR13 and FR15, found in Figure M.27 (f), were about 2.0 times greater than their design capacity of 4.5 ton (the design capacity is 1.5 times the rated capacity of 3.0 ton). However, no permanent distortion or damage was found on the snubbers after the 2.5 S2(A) test run.

The most severe test wave for the F-line was the 1.2 S2(C) wave, whose response spectra are shown in Figure M.6. The recorded test results are summarized in Table M.19 and Figures M.31 and M.32. The peak displacement response of EAB-3 exceeded the displacement limit of 15 mm, which is the movable length of pins within the slots (see Figure L.13). As a result, the EAB support exhibited a sharp increase in resistant forces as shown in Figure M.32. The peak support force of the mechanical snubber FR15 of 10.74 ton, given in Table M.19, is about 2.4 times higher than the design capacity of 4.5 ton.

M.6 Gap Tests for M-line with LED Supports

The gap tests are described in the previous chapter, and detailed drawing of the artificial gap (± 1.0mm) is shown in Figure L.30. The test results for the 1.0 S2(A) wave test run are summarized in Table M.20 and Figures M.33 and M.34. Significantly higher acceleration values were recorded during the test due to the repeated impacts at the gap location. Actual accelerations, however, are considered to be much higher since the measured records are processed through a low-pass filter which eliminates sharp acceleration pulses. The observed hysteretic responses of LED supports shown in Figure M.34 are somewhat similar to those of the B-wave test in Figure M.20, including the pinching characteristics in the recorded hysteresis loops.

Table M.1 List of Selected Test Runs to Evaluate Table Control

Test Type	Test No.	Table Motion	Test I.D.
M-line Conventional Support	DE1-3	1.0 S2(M)	95041909
M-line Multiple Excitation Test	DC-3	1/3 S2(M)	94120702
F-line Conventional Support	VC-3	1.0 S2(F)	95011107
EA Support B-wave Test	DE1-20	1.0 S2(B)	95042804
M-line EA Support, Marginal Test	ZT-2	Tokachi-Oki	95071403
F-line EA Support, Marginal Test	ZT-1	1.2 S2(C)	95071402

Table M.2 List of Selected Table Motion Channels

Direction	Channel	Type of Record/Sensor Location
X	XT XOXB AA1-X	Target horizontal motion (Input to system) Average of two X-direction table motions Horizontal independent actuator motion
Z	ZT ZOXB	Target vertical motion (input to system) Average of two vertical table motions

Table M.3 List of Peak Acceleration Values for Selected Test Runs

Record Channel	Peak Acceleration Values (g) for Each Test Run					
	1.0 S2(M)	1/3 S2(M)	1.0 S2(F)	1.0 S2(B)	Tokachi-Oki	1.2 S2(C)
XT	1.61	0.55	1.21	1.55	2.62	1.90
XOXB	1.58	0.53	1.25	1.63	2.88	1.94
AA1-X	5.04	2.23	1.58	2.11	2.92	2.08
ZT	0.38	—	0.20	0.33	—	0.44
ZOXB	0.39	—	0.21	0.36	—	0.48

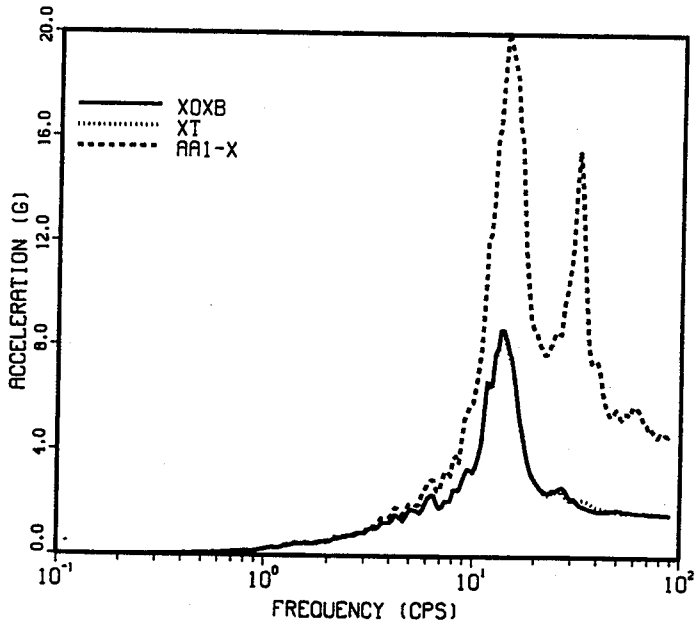

(a) X-direction Motions

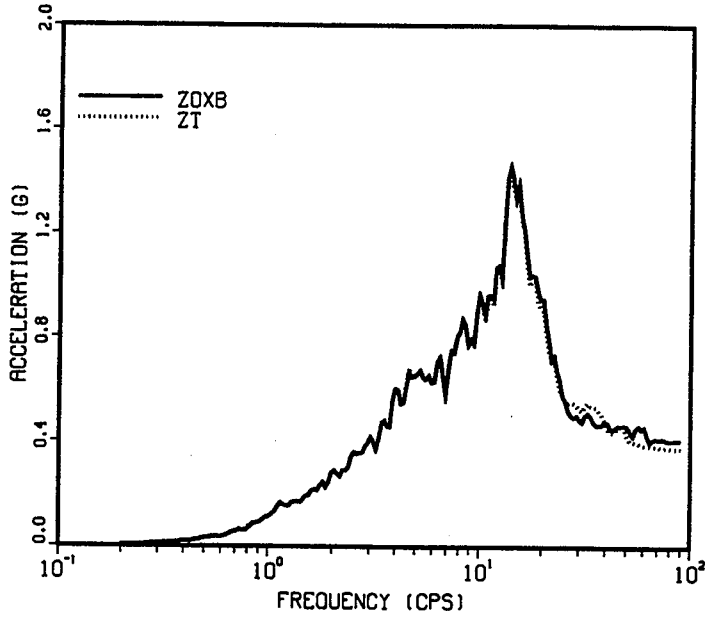

(b) Z-direction Motions

Figure M.1 Acceleration Response Spectra of Recorded Table Motions from 1.0 S2(M) Test Run

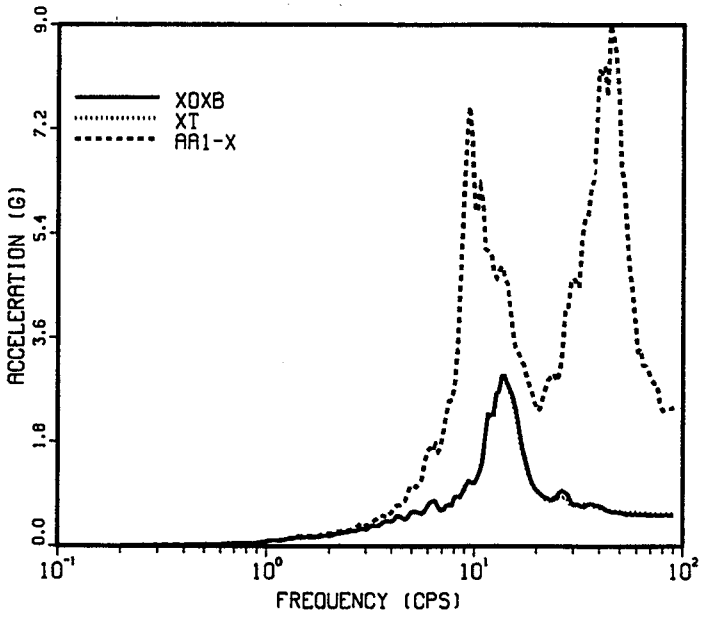

X-direction Motions

Figure M.2 Acceleration Response Spectra of Recorded Table Motions from Multiple Excitation Test Run

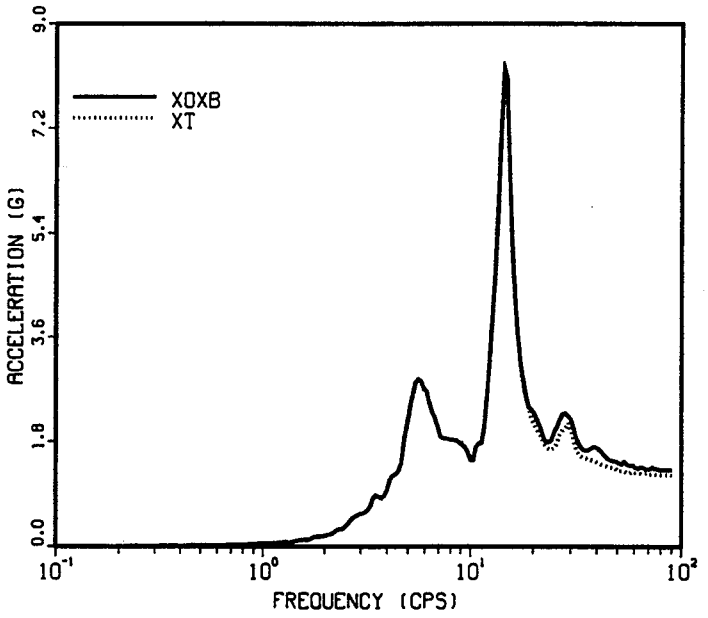

(a) X-direction Motions

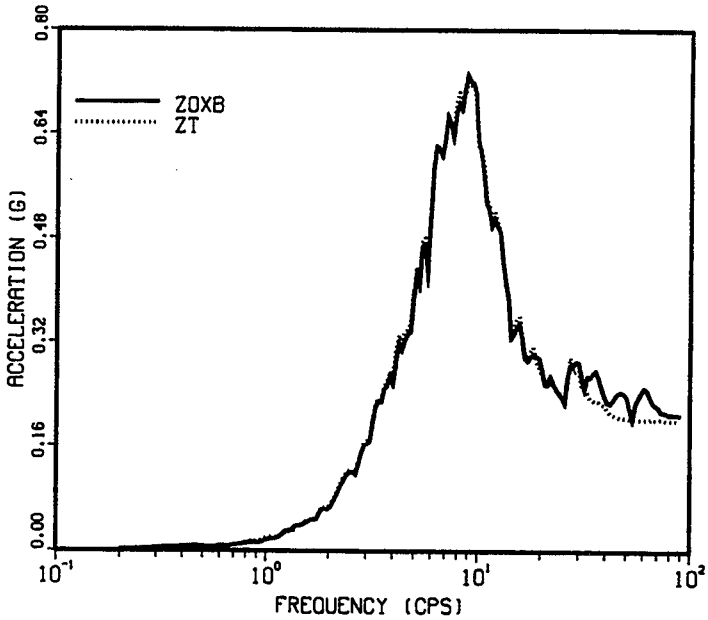

(b) Z-direction Motions

Figure M.3 Acceleration Response Spectra of Recorded Table Motions from 1.0 S2(F) Test Run

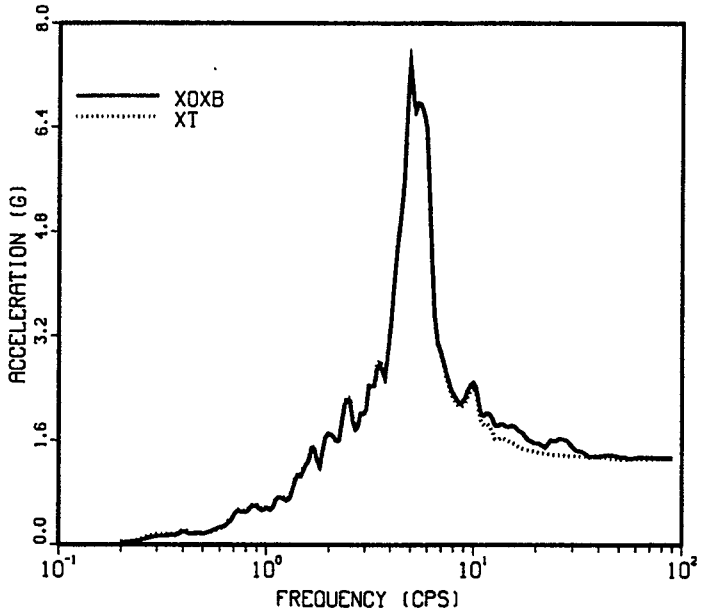

(a) X-direction Motions

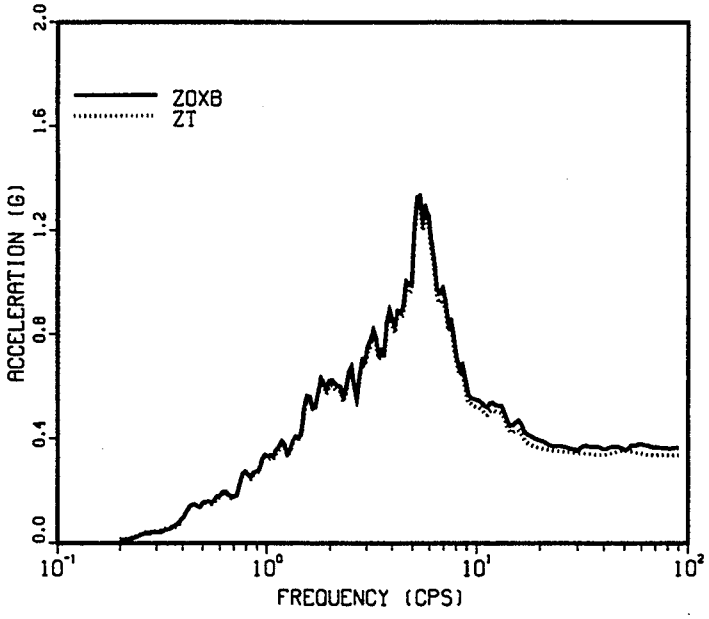

(b) Z-direction Motions

Figure M.4 Acceleration Response Spectra of Recorded Table Motions from 1.0 S2(B) Test Run

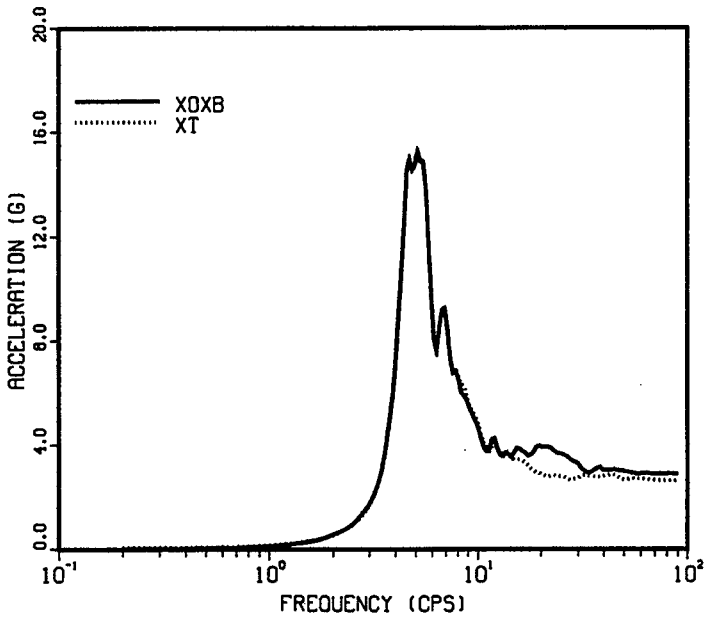

X-direction Motions

Figure M.5 Acceleration Response Spectra of Recorded Table Motions from Tokachi-Oki Test Run

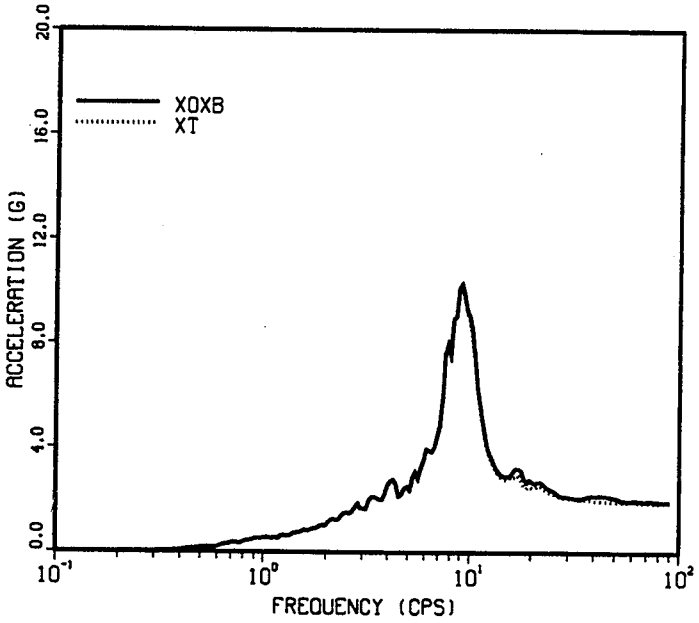

(a) X-direction Motions

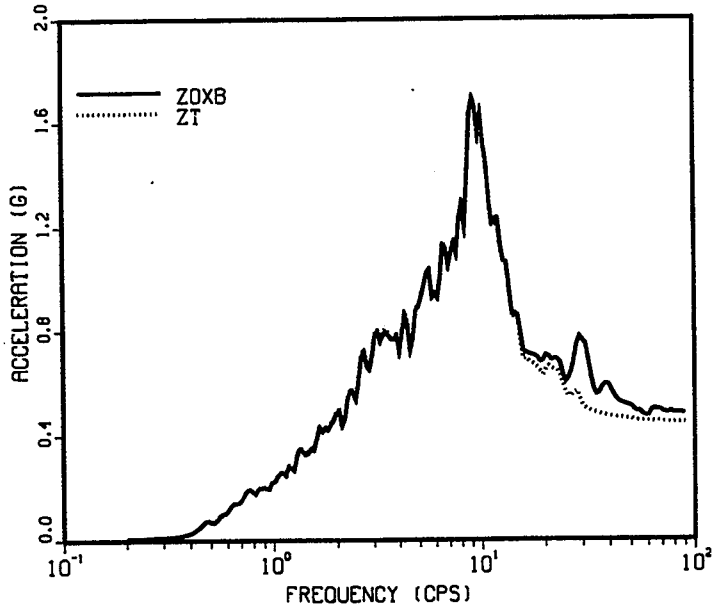

(b) Z-direction Motions

Figure M.6 Acceleration Response Spectra of Recorded Table Motions from 1.0 S2(C) Test Run

Table M.4 Measured Vibration Frequencies of M-line with Conventional Supports

Mode	Frequency (Hz)	Comments
1	20.6	Fundamental Mode of SG-model
2	20.8	Y-direction Piping mode
3	22.6	X-direction Piping mode
4	23.2	Z-direction Piping mode
5	28.0	Branch Piping mode

Note: Obtained from sine sweep tests, 200 gal. for horizontal vibration tests, 130 gal. for vertical vibration tests.

Table M.5 Measured Damping Values of M-line with Conventional Supports

X-direction Fundamental Piping Mode		Z-direction Fundamental Piping Mode	
Input Level (gal.)	Damping (%)	Input Level (gal.)	Damping (%)
50	6.8	30	6.1
100	5.3	60	3.8
150	5.8	90	2.5
175	5.8	110	2.9
200	5.0	130	3.3

Table M.6 Measured Peak Responses of M-line with Conventional Supports, 1.0 S2(M) Test Run

Acceleration (g)			Displacement (mm)			Support Forces (ton)		Pipe Stress (kg/mm²)	
Instrument	**Direction**	**Values**	**Instrument**	**Direction**	**Values**	**Instrument**	**Values**	**Instrument**	**Values**
AA1	X Y Z	5.04 0.27 0.40	AD1	X Y Z	2.46 0.06 0.19	MR1	5.22	MS1	1.86
MA1	X Y Z	6.04 4.07 1.72	MD1a		1.35	MR2	6.81	MS2[1]	0.97
MA2	X Y Z	4.83 2.47 2.11	MD2a		1.56	MR3	1.46	MS2	1.63
MA3	X Y Z	3.80 1.40 1.65	MD3b		0.88	MR4	1.41	MS3	2.30
MA4	X Y Z	3.15 1.24 1.47	MD4b		0.94	MR5	2.51	MS4	1.37
MA5	X Y	3.05 1.19	MD5a (5b)		0.77 (0.76)	MR6	3.27	MS5	1.02
MA6	X Y	2.02 1.14	MD6a (6b)		0.85 (0.64)	MR7	1.55	MS6	1.52
MA8	X Y Z	2.15 1.31 1.83	MD7a (7b)		0.67 (0.31)	MR9	1.10	MS8	0.80
MA10	X Y Z	2.38 0.34 0.95	MD8	X Y Z	1.28 0.54 0.93	MR10	0.97	MS9	0.63

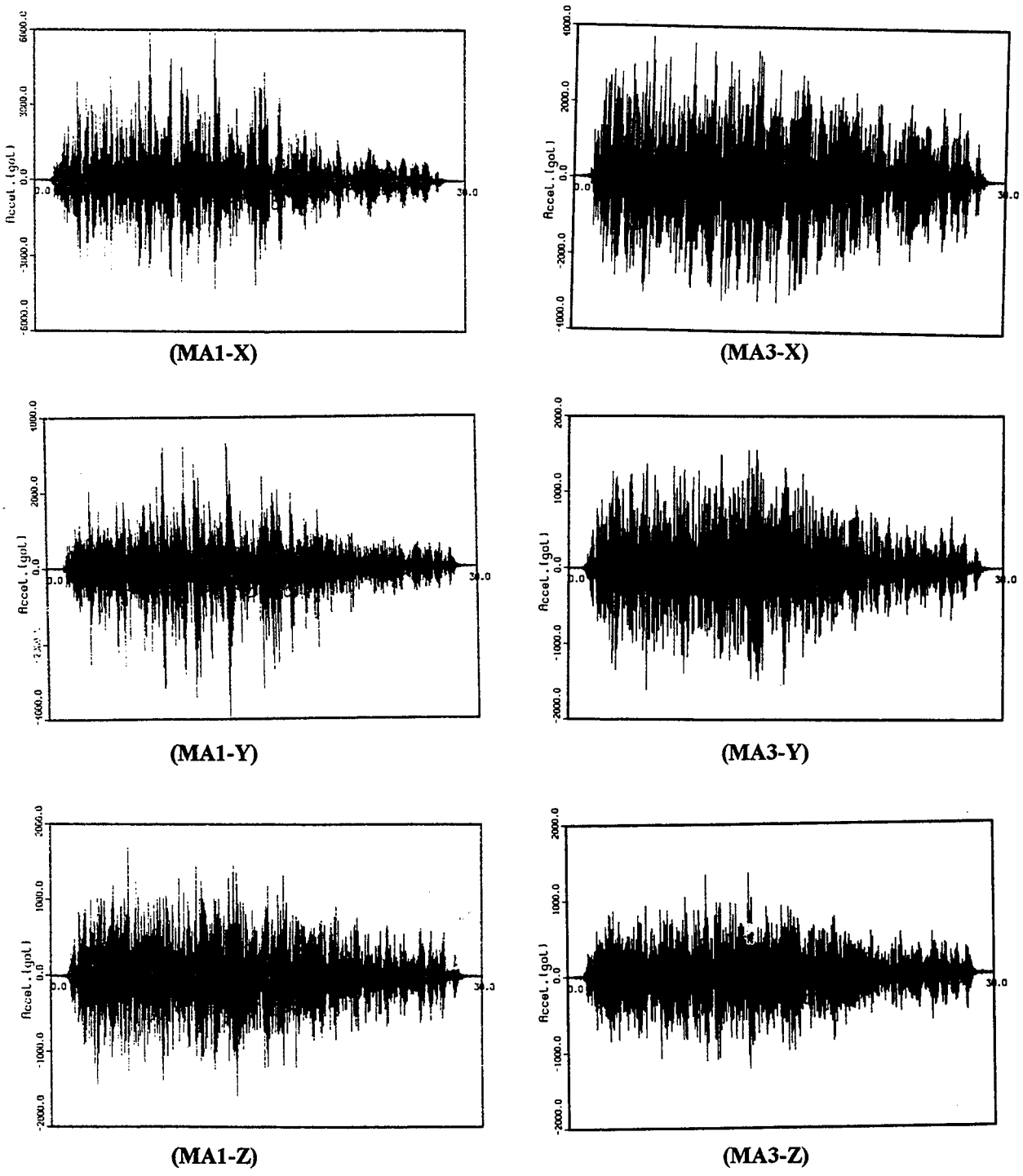

Figure M.7 Acceleration Time Histories of M-line with Conventional Supports, 1.0 S2(M) Test Run

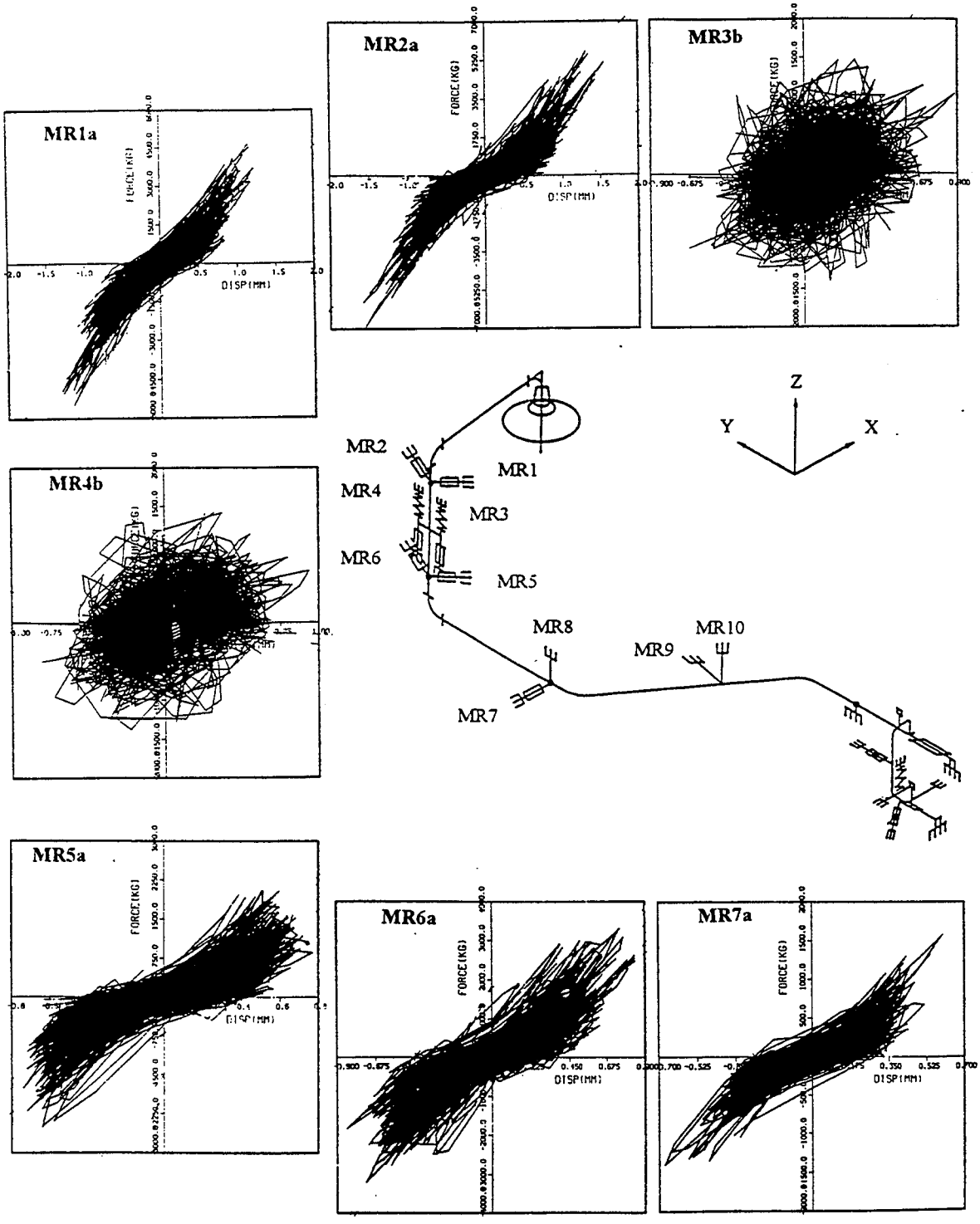

Figure M.8 Hysteretic Responses of Snubbers of M-line with Conventional Supports, 1.0 S2(M) Test Run

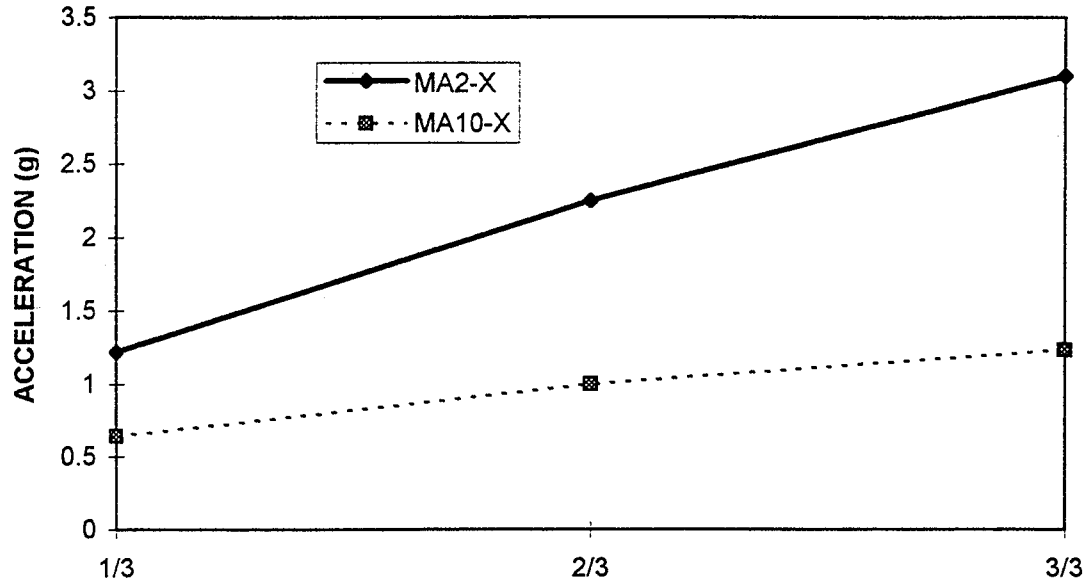

(a) Accelerations

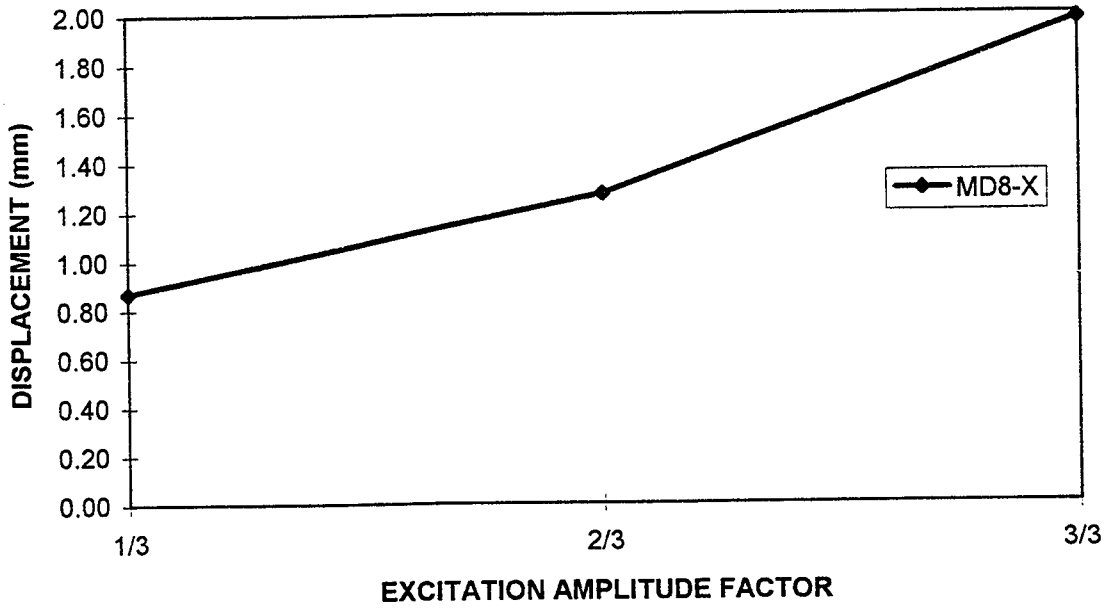

(b) Displacement

Figure M.9 Peak Responses of M-line with Conventional Supports as a Function of Excitation Amplitude, S1(M) Test Series

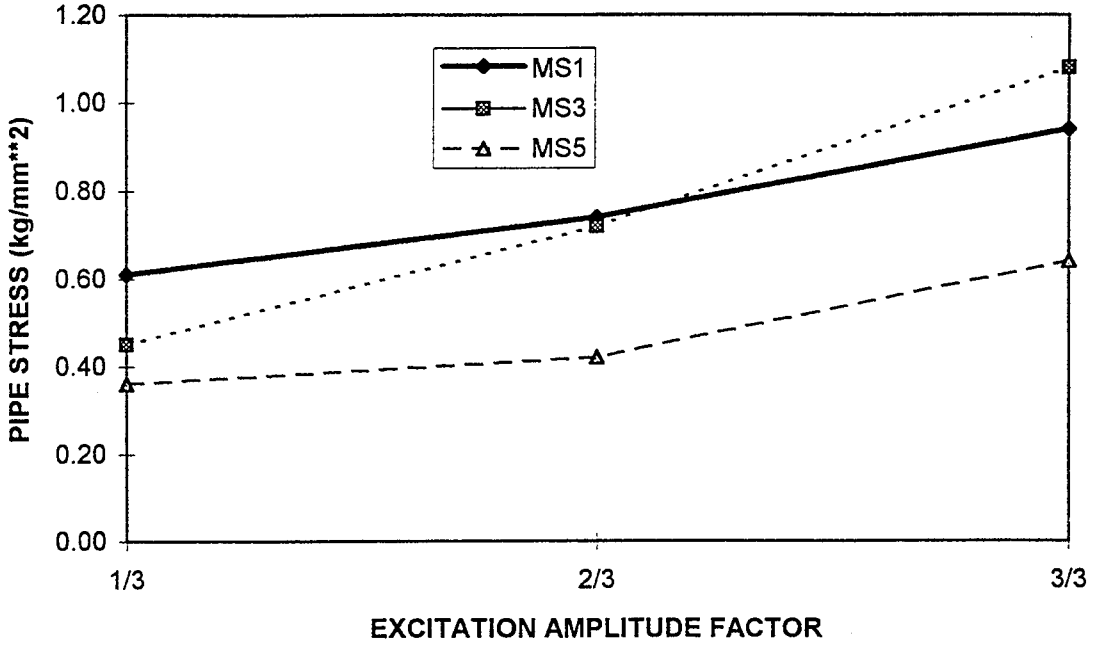

(c) Pipe Stresses

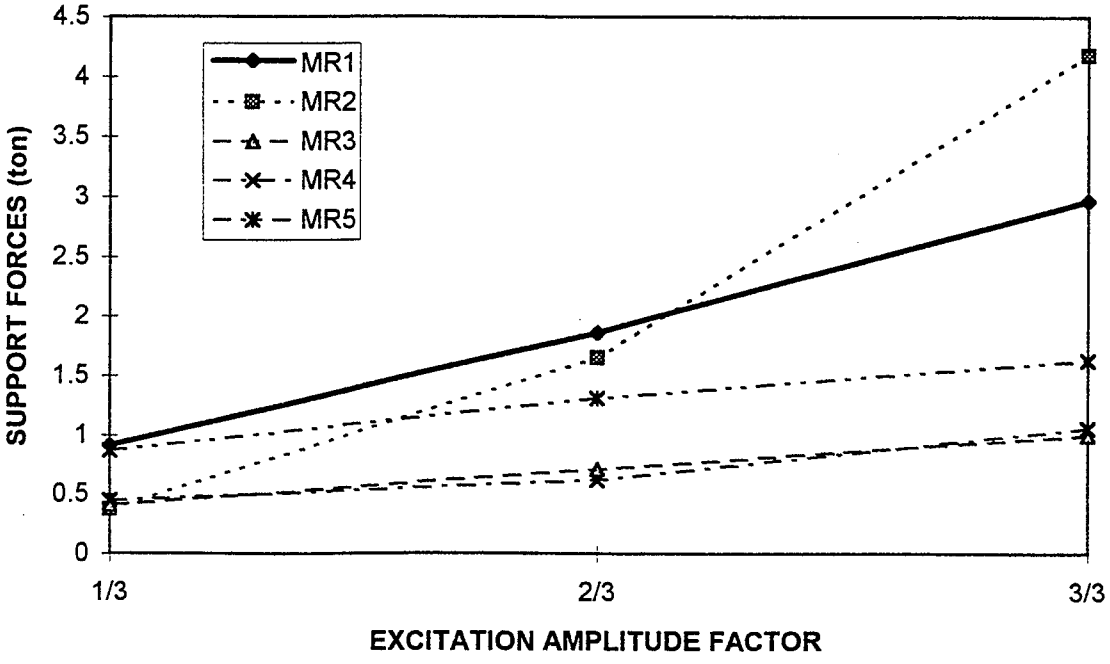

(d) Support Forces

Figure M.9 Peak Responses of M-line with Conventional Supports as a Function of Excitation Amplitude, S1(M) Test Series (Cont'd)

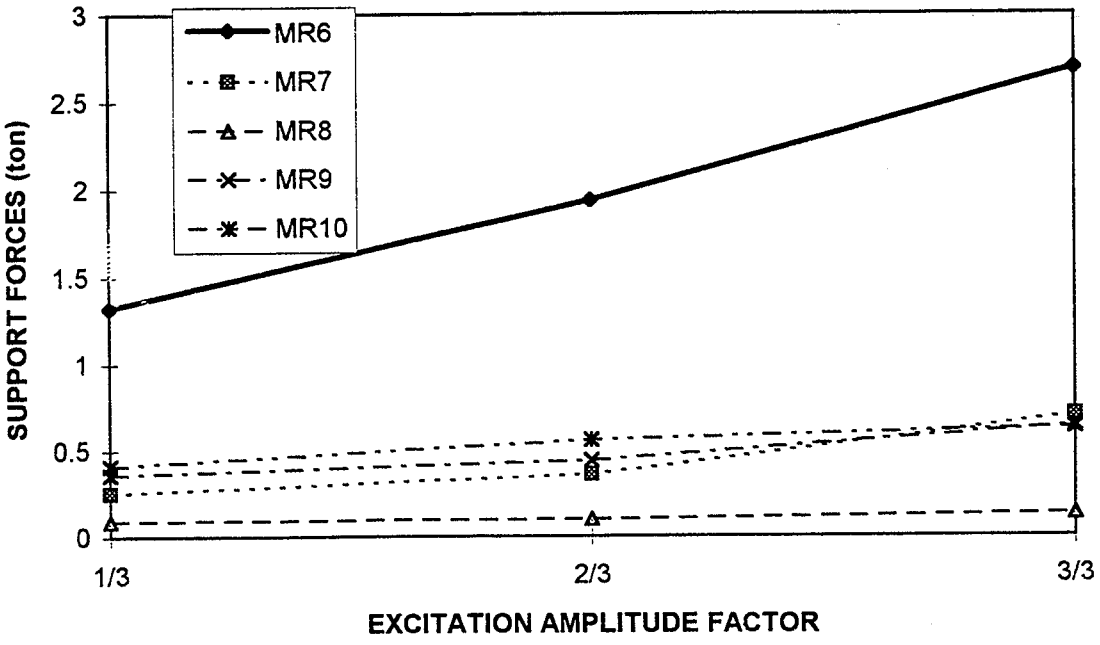

(e) Support Forces

Figure M.9 Peak Responses of M-line with Conventional Supports as a Funciton of Excitation Amplitude, S1(M) Test Series (Cont'd)

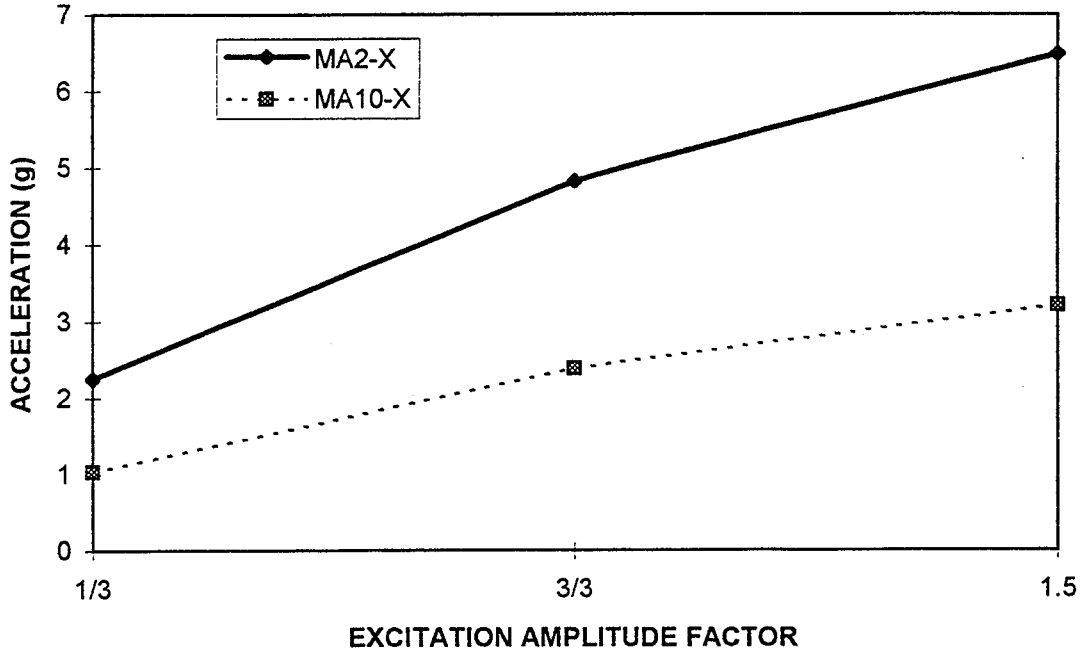

(a) Accelerations

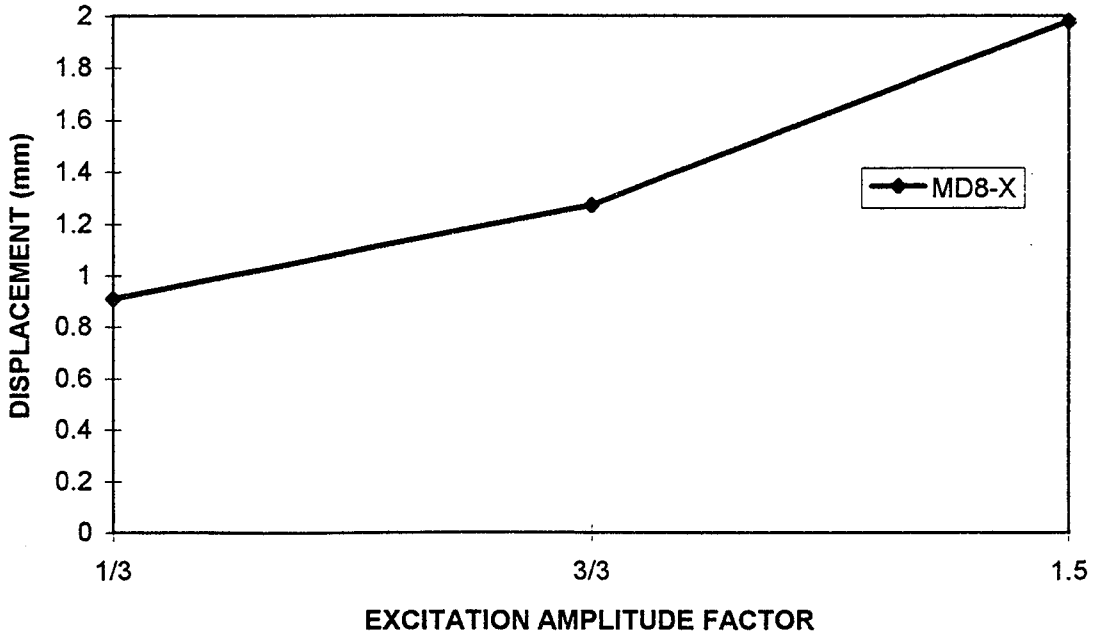

(b) Displacement

Figure M.10 Peak Responses of M-line with Conventional Supports as a Function of Excitation Amplitude, S2(M) Test Series

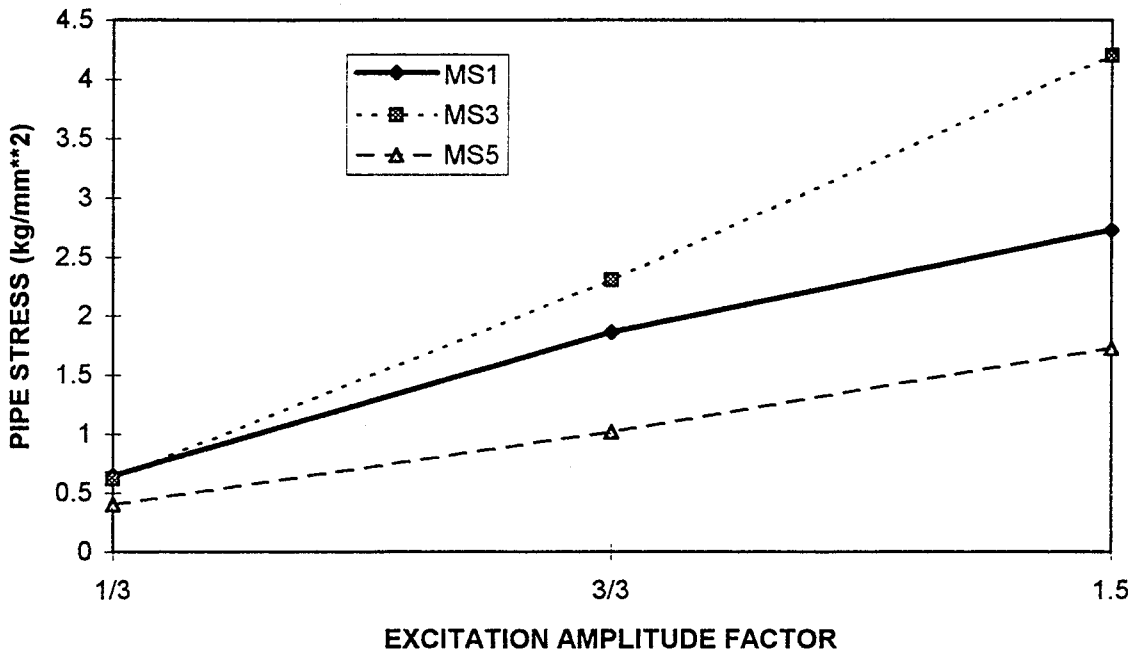

(c) Pipe Stresses

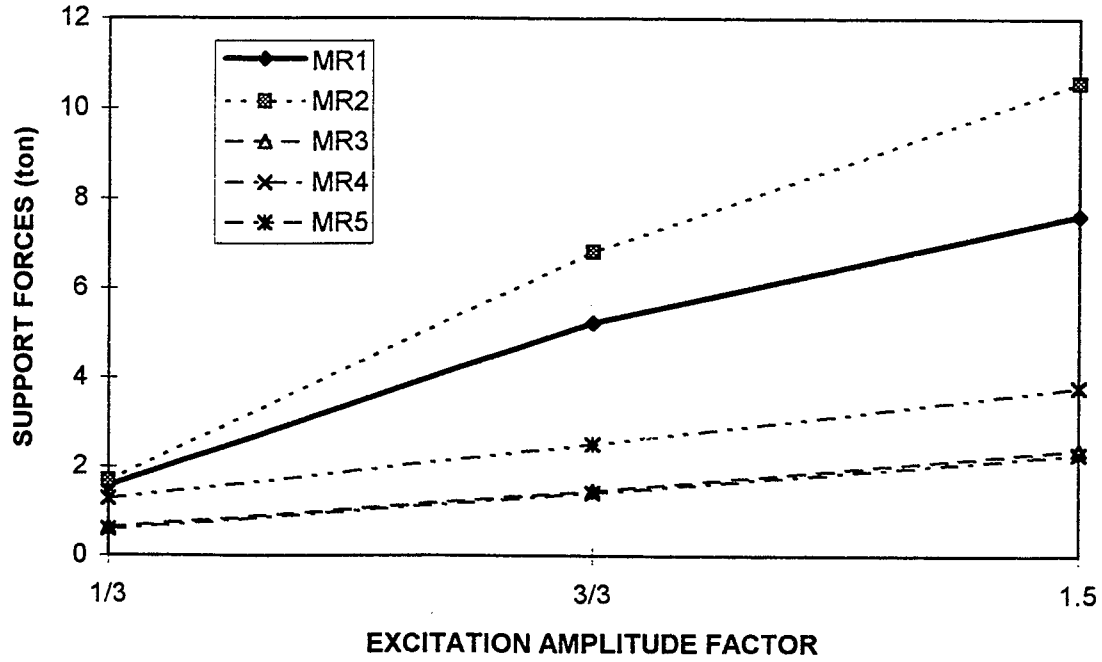

(d) Support Forces

Figure M.10 Peak Responses of M-line with Conventional Supports as a Function of Excitation Amplitude, S2(M) Test Series (Cont'd)

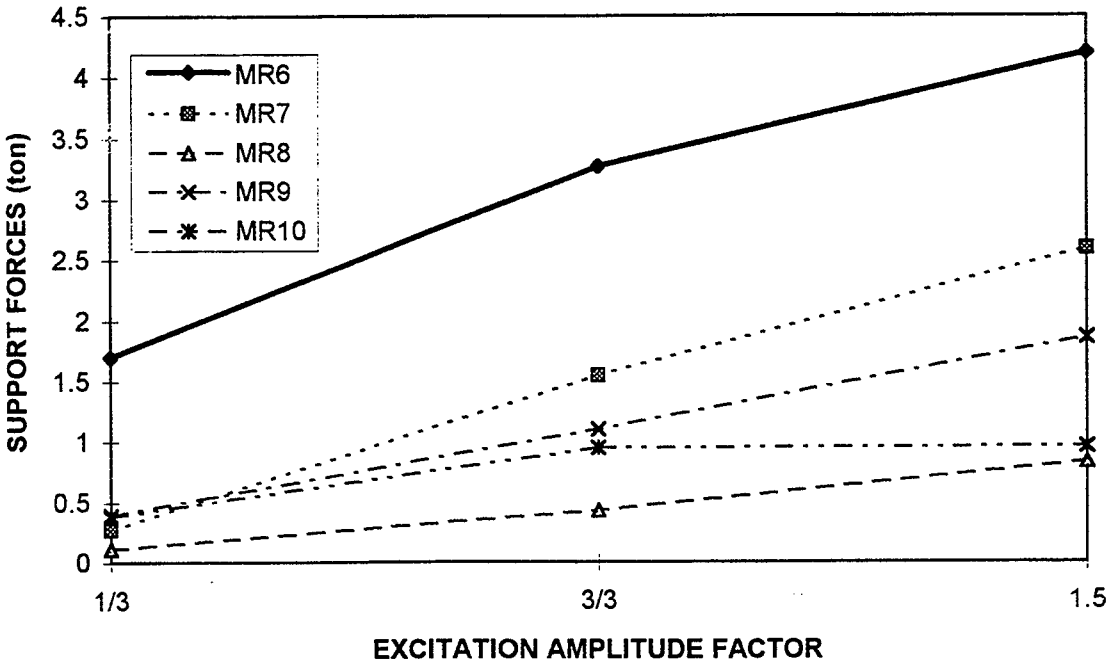

(e) Support Forces

Figure M.10 Peak Responses of M-line with Conventional Supports as a Function of Excitation Amplitude,S2(M) Test Series (Cont'd)

Table M.7 Measured Peak Responses of M-line with Conventional Supports, ⅓ S2(M) Multiple Excitation Test Run

Acceleration (g)			Displacement (mm)			Support Forces (ton)		Pipe Stress (kg/mm^2)	
Instrument	Direction	Values	Instrument	Direction	Values	Instrument	Values	Instrument	Values
AA1	X Y Z	2.23 0.18 0.19	AD1	X Y Z	3.54 0.08 0.27	MR1	6.05	MS1	1.63
MA1	X Y Z	2.43 2.66 1.06	MD1a		1.33	MR2	7.39	MS2'	1.54
MA2	X Y Z	2.01 2.49 1.15	MD2a		1.73	MR3	0.95	MS2	2.18
MA3	X Y Z	2.95 1.38 1.03	MD3b		0.51	MR4	0.67	MS3	3.11
MA4	X Y Z	3.25 0.77 0.64	MD4b		0.55	MR5	2.60	MS4	0.95
MA5	X Y	2.01 0.73	MD5a (5b)		1.00 (0.60)	MR6	2.65	MS5	1.38
MA6	X Y	1.47 0.74	MD6a (6b)		0.85 (0.48)	MR7	1.37	MS6	1.06
MA8	X Y Z	1.06 0.88 1.37	MD7a (7b)		0.51 (0.22)	MR9	0.5	MS8	1.05
MA10	X Y Z	1.02 0.22 0.60	MD8	X Y Z	2.00 0.26 0.45	MR10	0.71	MS9	0.58
								MS10	0.34

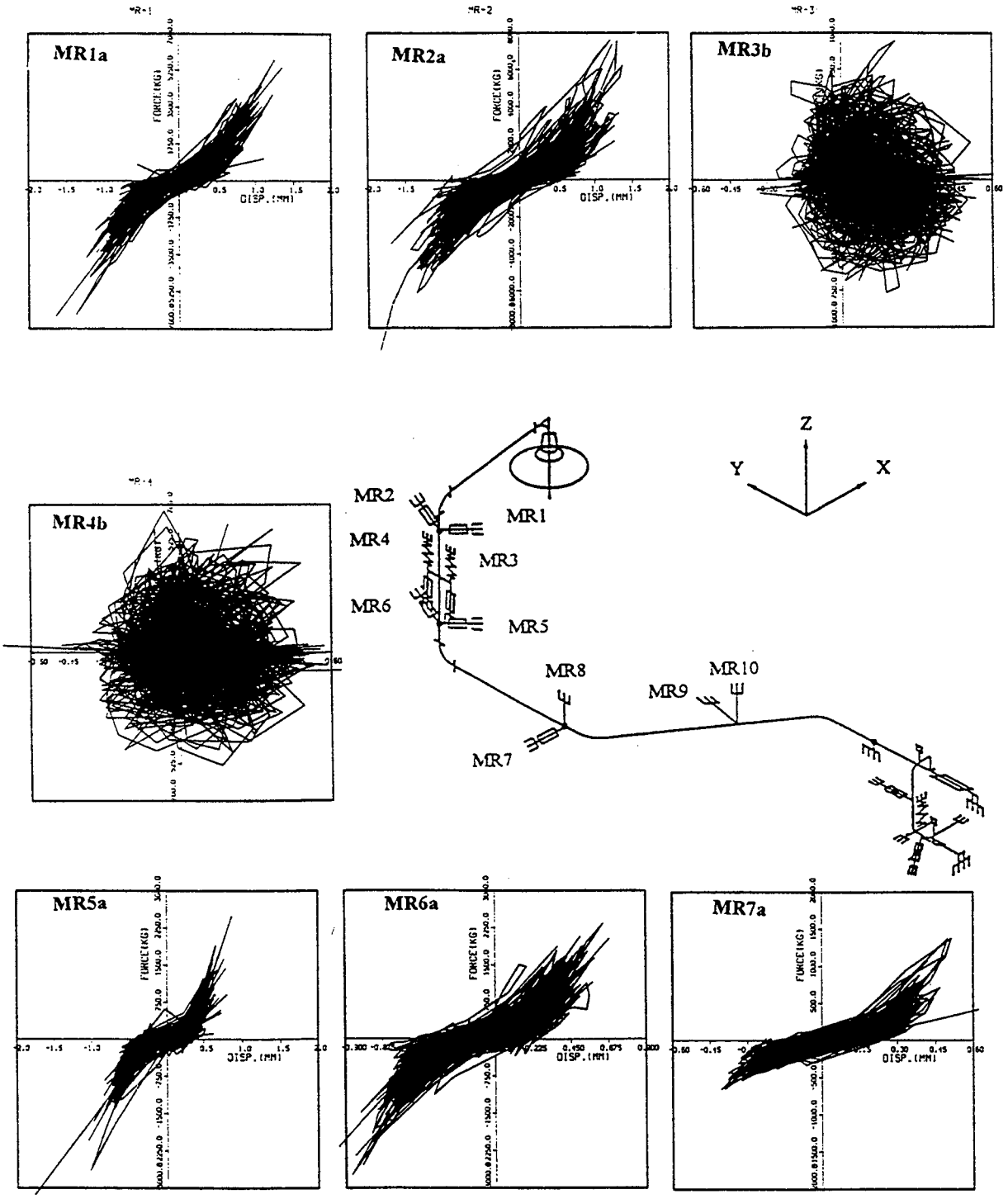

Figure M.11 Hysteretic Responses of Snubbers of M-line with Conventional Supports, 1/3 S2(M) Multiple Excitation Test Run

Table M.8 Measured Vibration Frequencies of F-line with Conventional Supports

Direction of Excitation	Input Level (gal.)	Vibration Modes, Frequencies (Hz)						
		1st	2nd	3rd	4th	5th	6th	7th
Horizontal Vibration	50	13.6	16.0	17.0	-----	-----	-----	25.6
	75	15.6	16.6	20.6	-----	-----	-----	26.2
	100	15.6	16.8	21.6	-----	-----	-----	26.2
	125	16.4	18.6	23.2	-----	-----	26.4	27.8
	150	16.4	21.0	23.4	-----	-----	27.2	28.4
	175	16.6	-----	-----	-----	-----	-----	-----
Vertical Vibration	50	-----	-----	-----	20.2	23.6	-----	24.6
	60	-----	-----	-----	21.8	23.4	-----	25.0
	75	-----	-----	-----	21.6	25.4	26.6	28.2
	90	-----	-----	-----	22.4	25.2	26.8	28.4
	100	-----	-----	-----	22.4	25.8	27.4	28.0

Table M.9 Measured Damping Values of F-line with Conventional Supports

Horizontal Vibration	Input Level (gal.)	50	75	100	125	150	175
	Frequency (Hz)	13.6	15.6	15.6	16.4	16.4	16.6
	Damping (%)	5.9	5.4	4.2	4.0	4.6	4.3
Vertical Vibration	Input Level (gal.)	50	60	75	90	100	
	Frequency (Hz)	20.2	21.8	21.6	22.4	22.4	
	Damping (%)	5.4	3.4	3.2	6.5	7.1	

Table M.10 Measured Peak Responses of F-line with Conventional Supports, 1.0 S2(F) Test Run

Acceleration (g)			Displacement (mm)		Support Forces (ton)		Pipe Stress (kg/mm^2)	
Instrument	Direction	Values	Instrument	Values	Instrument	Values	Instrument	Values
FA2	X Y Z	2.09 0.62 0.93	FD2b	0.32	FR2	0.88	FS1	2.9
							FS2	1.3
FA3	X Y Z	2.63 0.17 1.36	FD3b	0.68	FR3	1.39	FS3	1.0
							FS4	1.3
FA5	X Y Z	2.08 0.28 1.09	FD4b	0.46	FR4	0.96	FS5	1.6
							FS6	1.4
FA6	X Y Z	2.07 1.45 1.51	FD5b	0.71	FR5	1.42	FS7	1.6
							FS8	0.4
FA7	X Y Z	3.38 1.24 1.19	FD6b	0.79	FR6	2.45	FS9	1.6
							FS10	0.9
FA8	X Y Z	3.07 1.28 1.64	FD7a, b	0.88 (0.39)	FR7	3.52	FS11	1.7
							FS12	1.4
FA9	X Y Z	2.69 1.24 1.24	FD8a, b	0.63 (0.33)	FR8	2.42	FS13	1.4
							FS14	2.9
FA10	X Y Z	2.78 1.11 1.13	FD9b	0.49	FR9	2.73	FS15	1.2
							FS19	1.6
FA11	X Y Z	3.11 1.90 1.19	FD10b	0.56	FR10	1.85	FS20	2.1
							FS21	1.8
FA12	X Y Z	3.10 1.95 1.30					FS22	2.8
FA13	X Y Z	3.18 1.36 1.26						

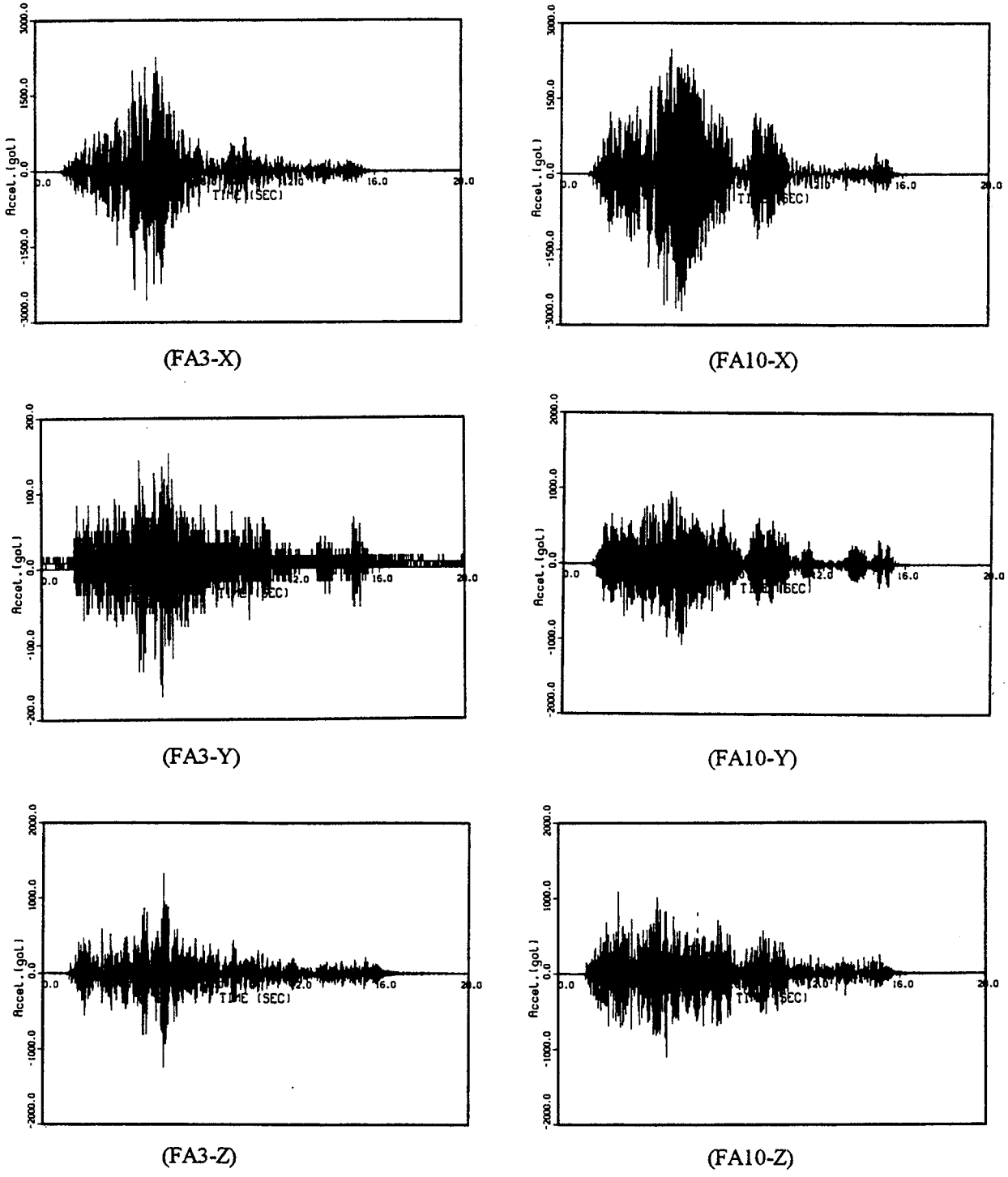

Figure M.12 Acceleration Time Histories of F-line with Conventional Supports, 1.0 S2(F) Test Run

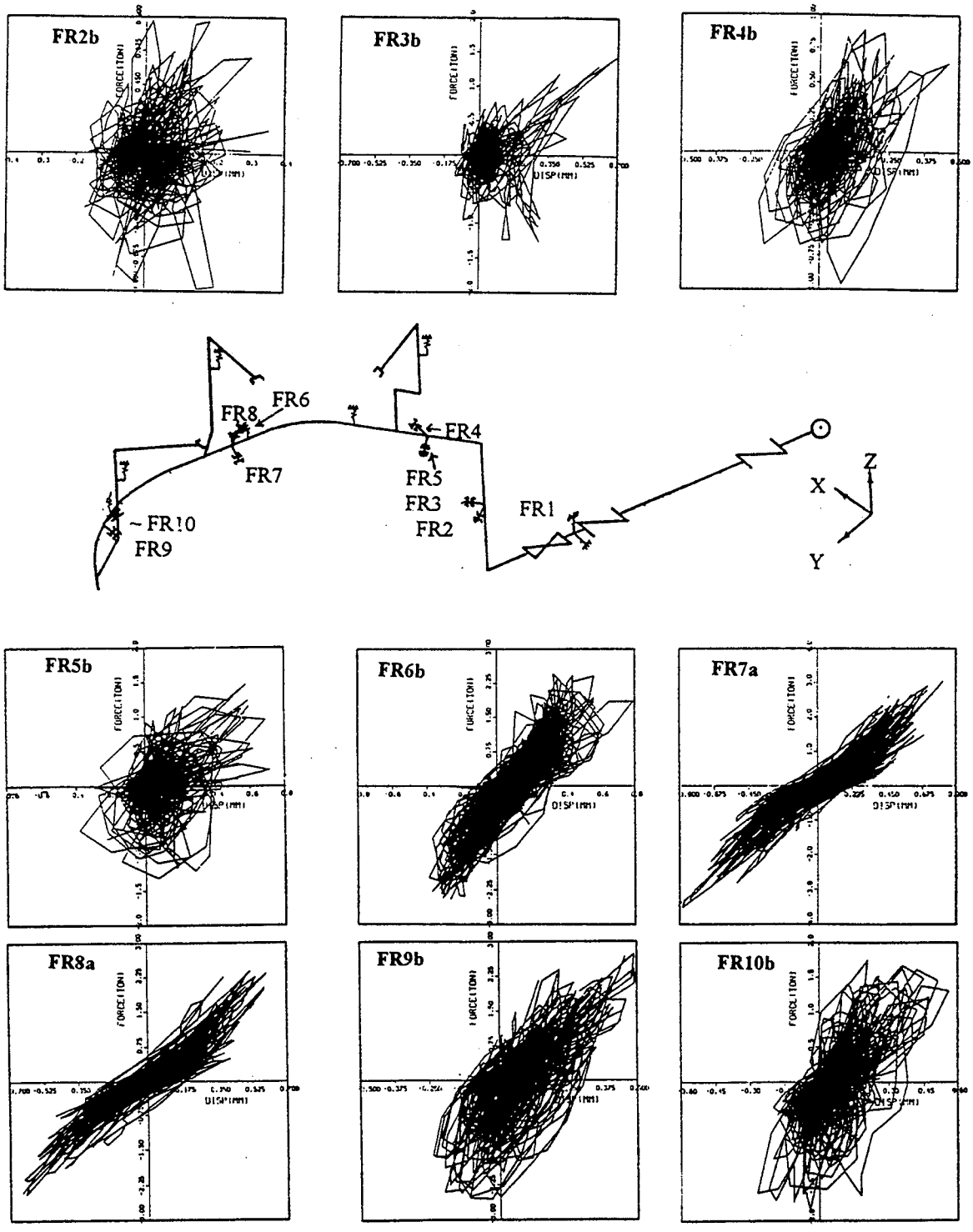

Figure M.13 Hysteretic Responses of Snubbers of F-line with Conventional Supports, 1.0 S2(F) Test Run

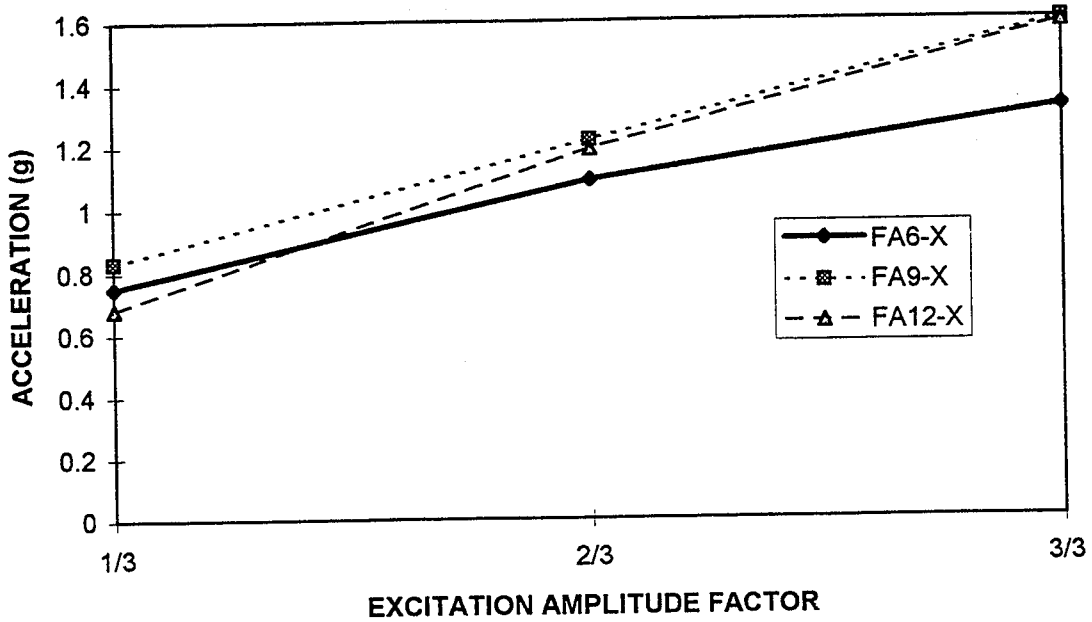

(a) Accelerations

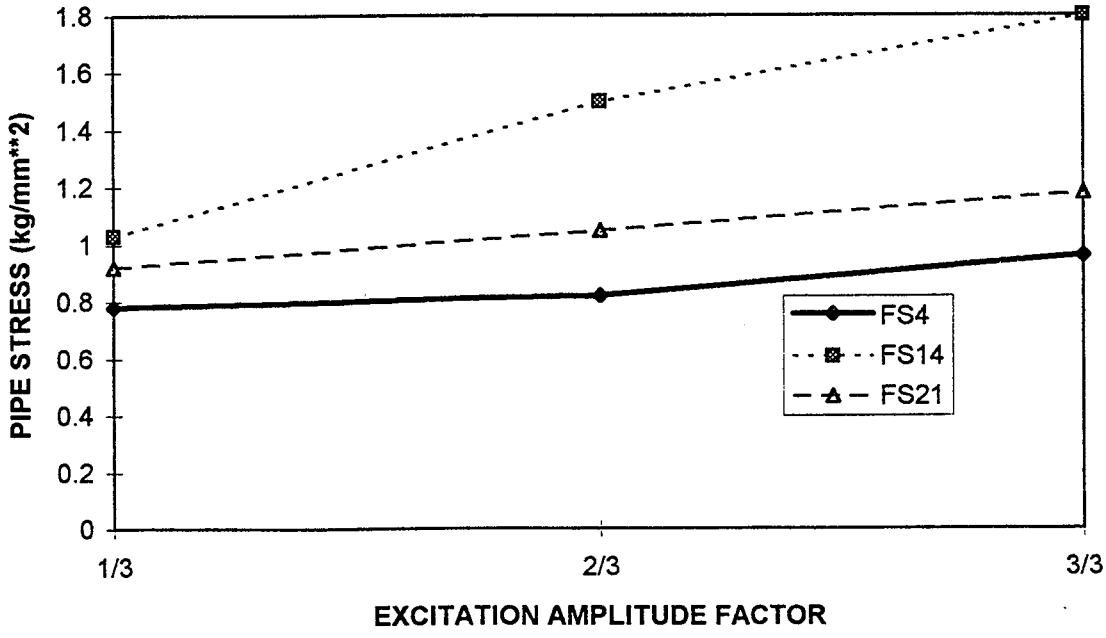

(b) Pipe Stresses

Figure M.14 Peak Responses of F-line with Conventional Supports as a Function of Excitation Amplitude, S1(F) Test Series

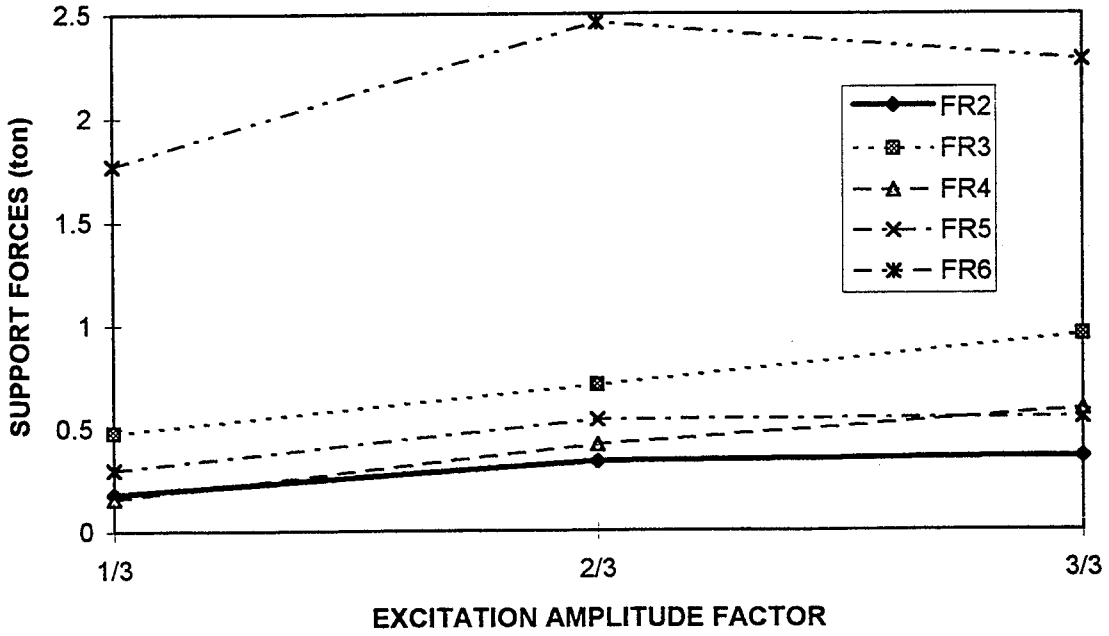

(c) Support Forces

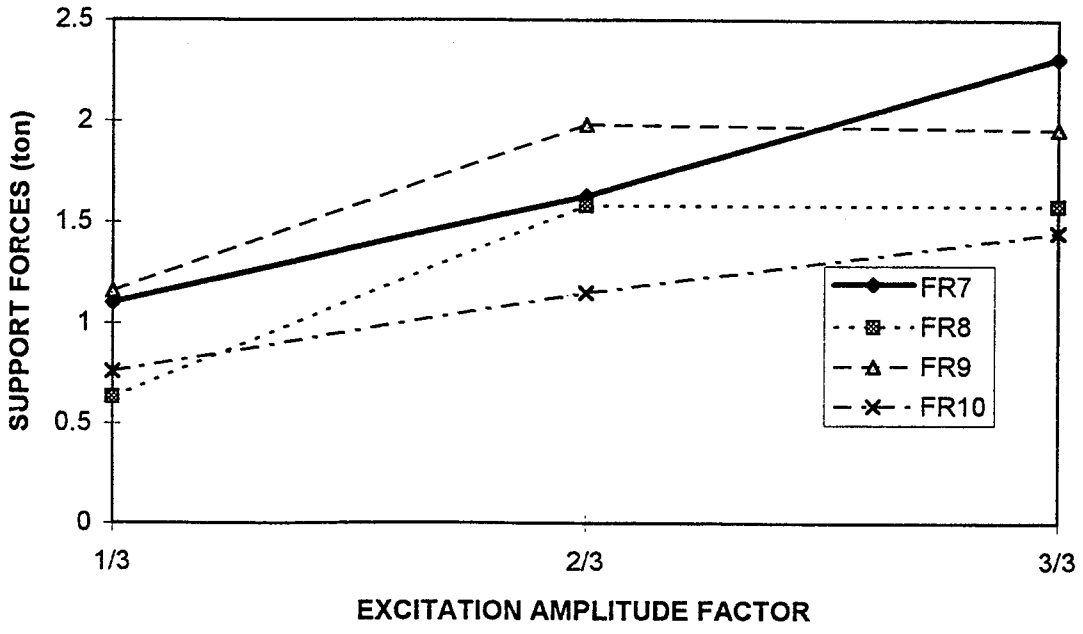

(d) Support Forces (continued)

Figure M.14 Peak Responses of M-line with Conventional Supports as a Function of Excitation Amplitude, S1(F) Test Series (Cont'd)

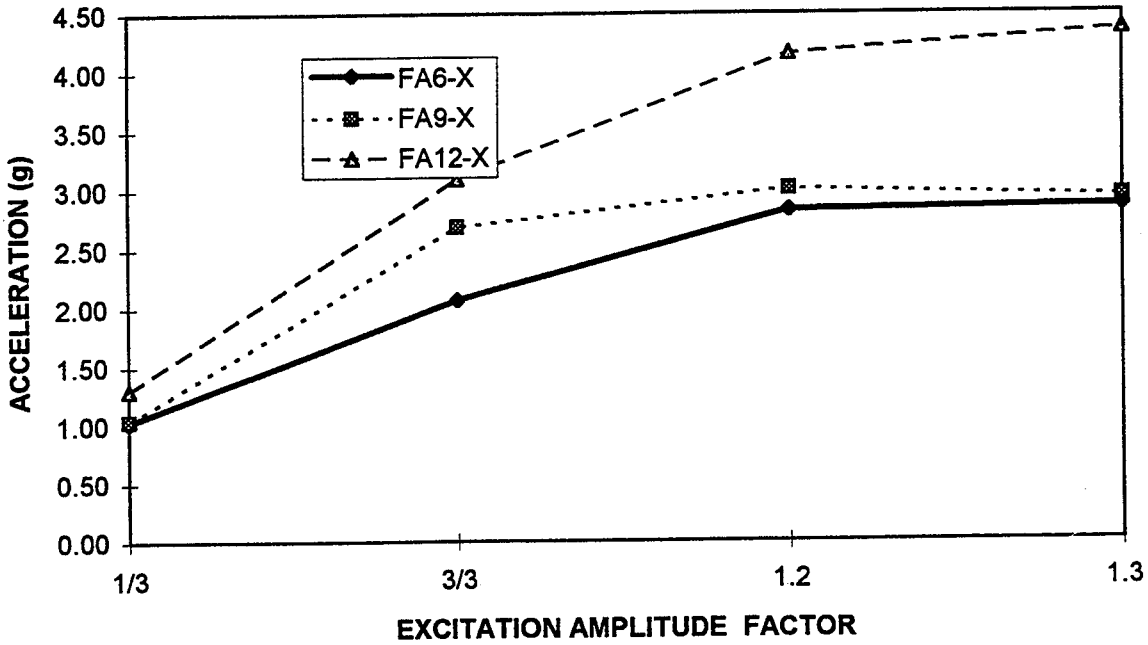

(a) Accelerations

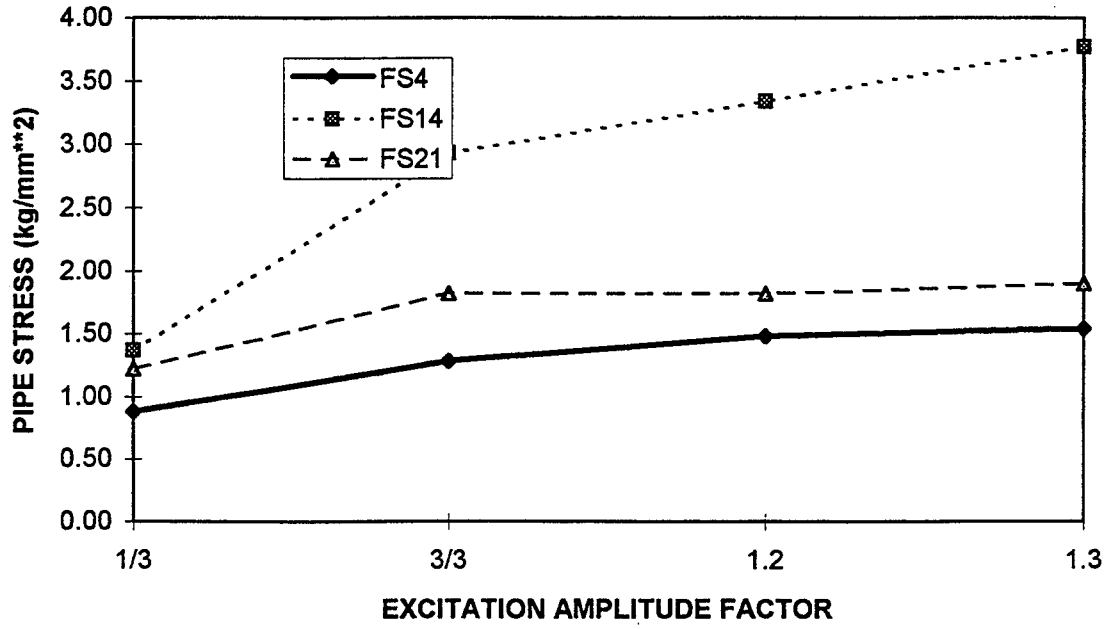

(b) Pipe Stresses

Figure M.15 Peak Responses of F-line with Conventional Supports as a Function of Excitation Amplitude, S2(F) Test Series

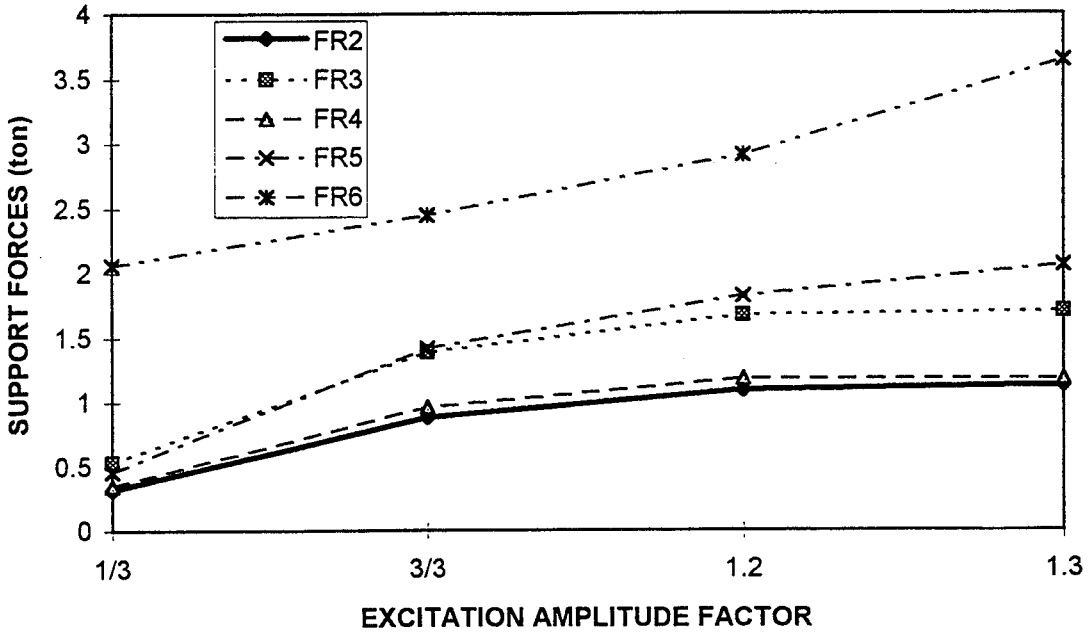

(c) Support Forces

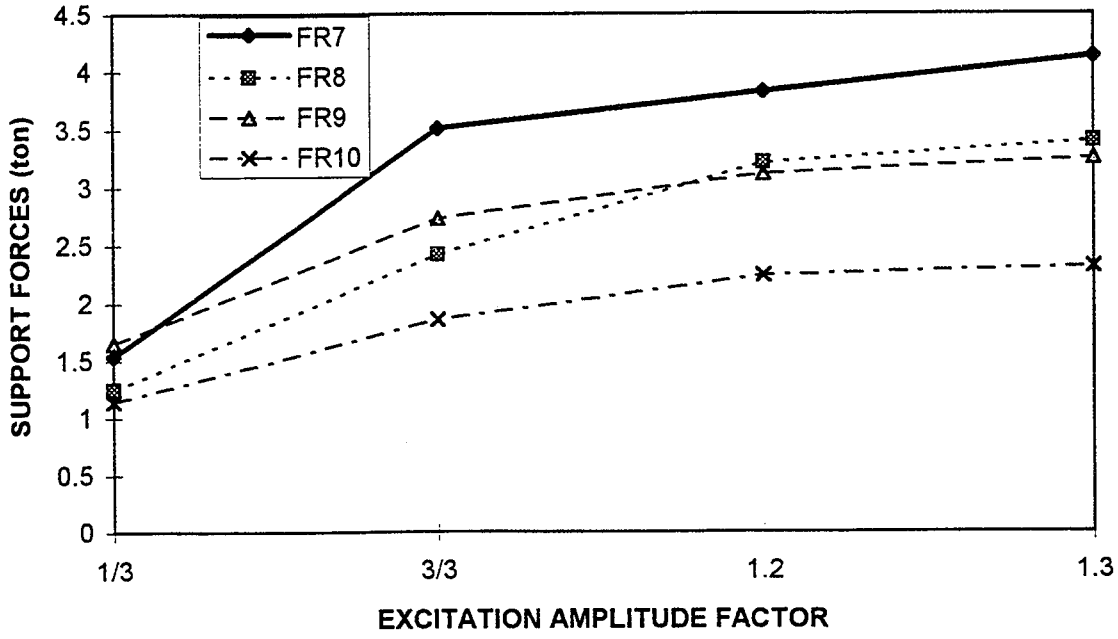

(d) Support Forces (continued)

Figure M.15 Peak Responses of M-line with Conventional Supports as a Function of Excitation Amplitude, S2(F) Test Series (Cont'd)

Table M.11 Measured Vibration Frequencies of M-line with LED Supports

Direction of Excitation	Input Level (gal.)	Vibration Modes, Frequencies (Hz)					
		1st	2nd	3rd	4th	5th	6th
Horizontal Vibration	50	10.2	-----	12.0	14.0	-----	15.8
	100	9.6	-----	12.8	13.8	-----	16.0
	150	9.6	-----	12.6	13.6	-----	15.6
	200	9.8	-----	12.8	14.0	-----	16.0
Vertical Vibration	30	-----	10.4	-----	-----	15.2	-----
	60	-----	11.0	-----	-----	15.0	-----
	90	-----	11.4	-----	-----	14.6	-----
	120	-----	11.6	-----	-----	14.4	-----

Table M.12 Measured Peak Responses of M-line with LED Supports, 1.0 S2(A) Test Run

Acceleration (g)			Displacement (mm)			Support Forces (ton)		Pipe Stress (kg/mm²)	
Instrument	Direction	Values	Instrument	Direction	Values	Instrument	Values	Instrument	Values
AA1	X Y Z	4.42 0.33 0.45	AD1	X Y Z	2.95 0.25 0.19	MR8	5.91	MS1	9.1
MA1	X Y Z	3.80 5.60 2.02	MD15/ LED-1		2.6	MR15/ LED-1	1.60	MS2'	4.7
MA16	X Y Z	3.37 7.44 2.22	MD16/ LED-2		5.2	MR16/ LED-2	1.81	MS2	1.8
MA17	X Y Z	4.74 2.25 1.97	MD17/ LED-3		4.5	MR17/ LED-3	1.01	MS3	5.5
MA4	X Y Z	3.38 2.78 2.06	MD18	X Y Z	5.5 4.8 4.6			MS4	3.0
MA5	X Y	2.70 2.85						MS5	4.3
MA6	X Y	2.18 2.98						MS6	4.1
MA8	X Y Z	2.29 2.75 4.99						MS8	2.0
MA10	X Y Z	2.06 1.39 5.61						MS9	3.7
								MS10	2.2

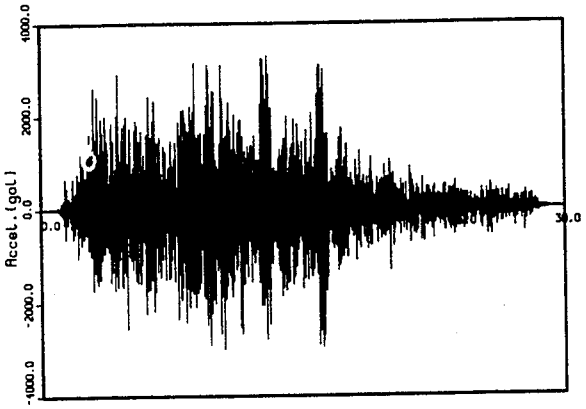

(MA16-X)

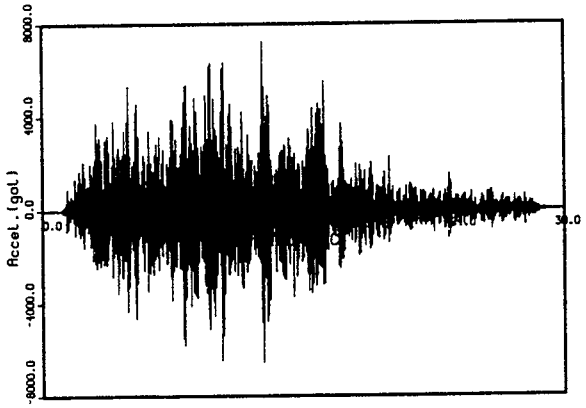

(MA16-Y)

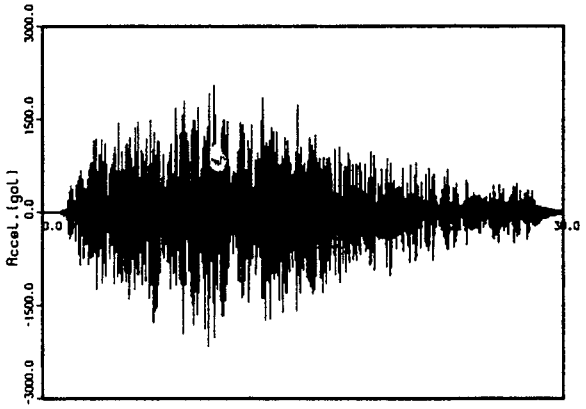

(MA16-Z)

Figure M.16 Acceleration Time Histories of M-line with LED Supports, 1.0 S2(A) Test Run

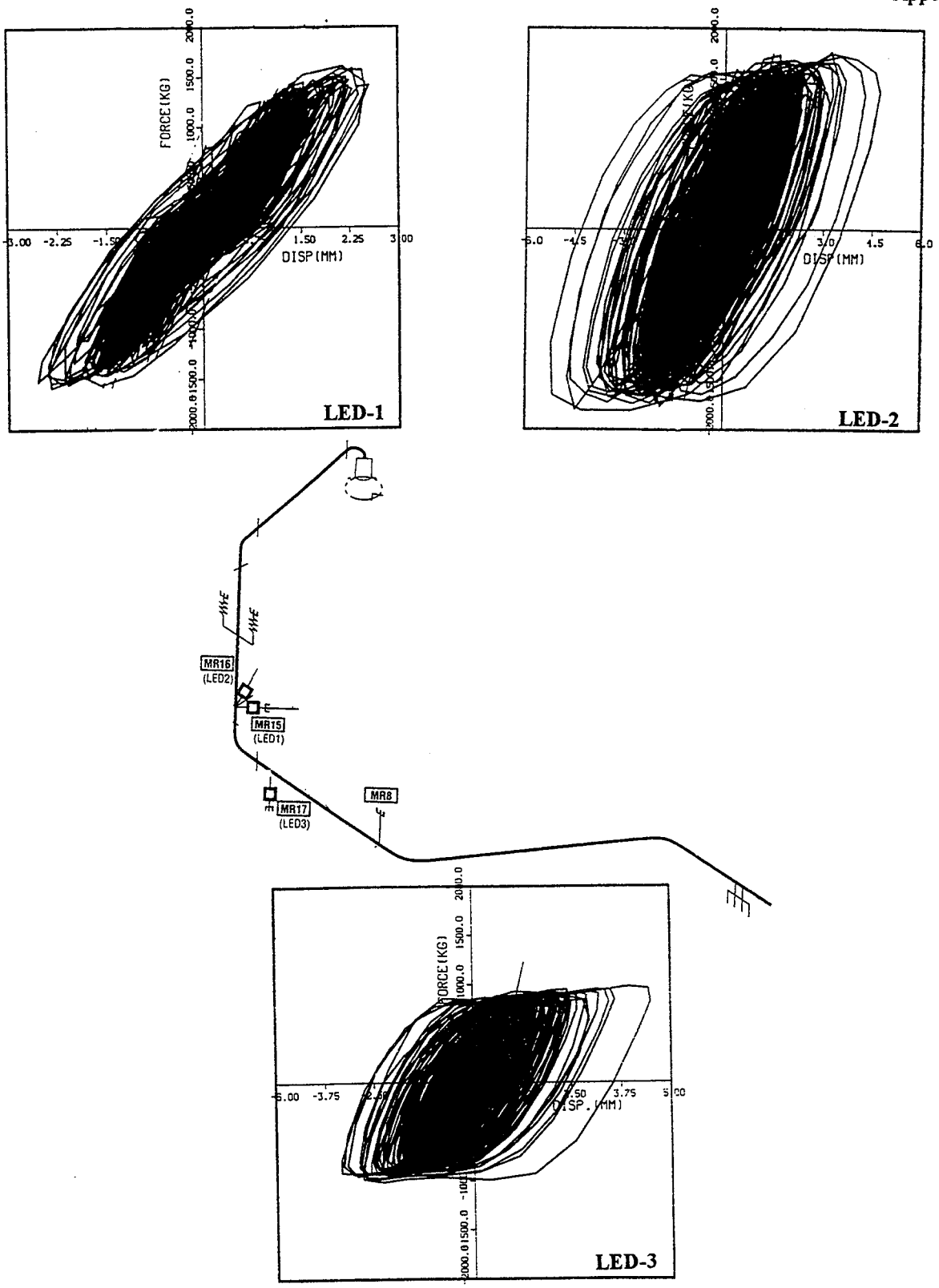

Figure M.17 Hysteretic Responses of M-line with LED Supports, 1.0 S2(A) Test Run

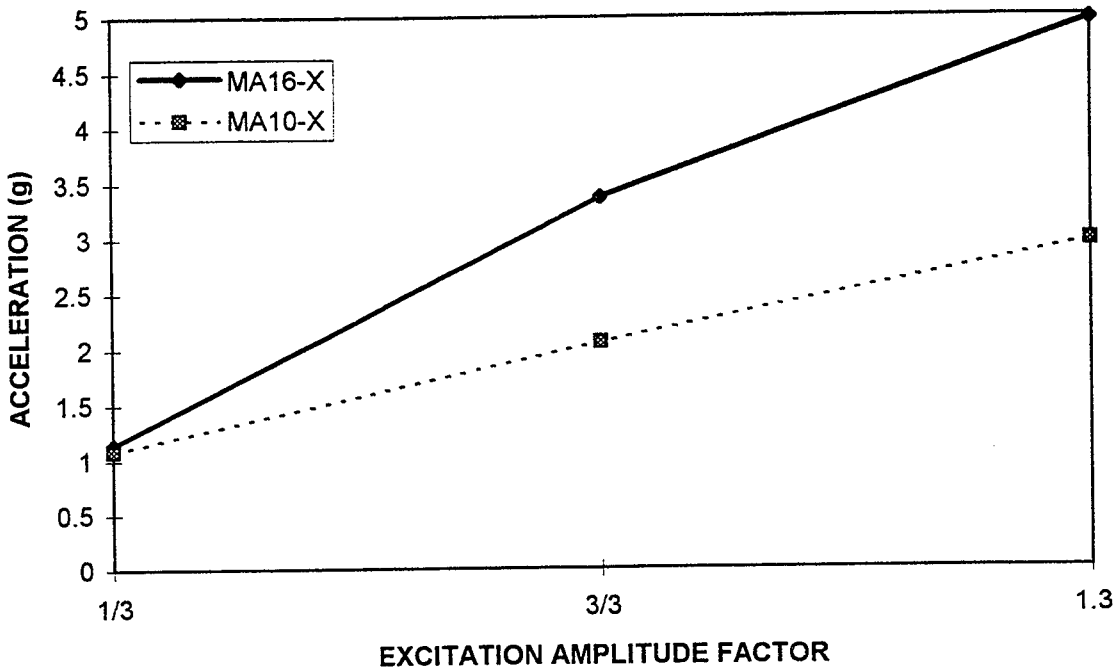

(a) Accelerations

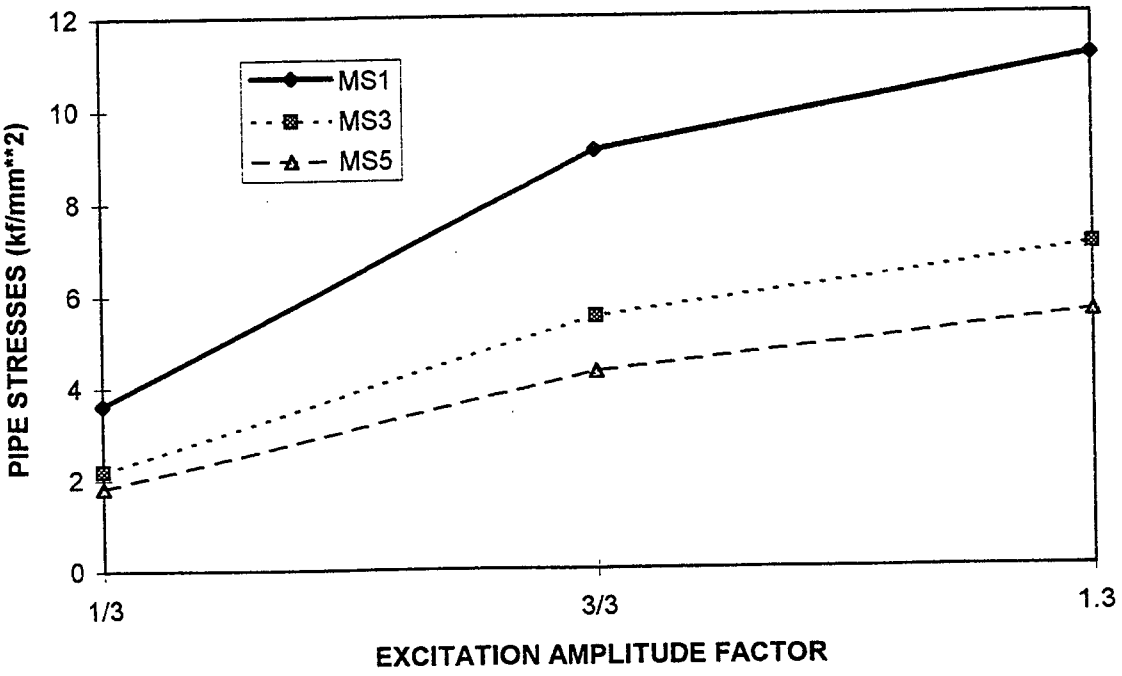

(b) Pipe Stresses

Figure M.18 Peak Responses of M-line with LED Supports as a Function of Excitation Amplitude, S2(A) Test Series

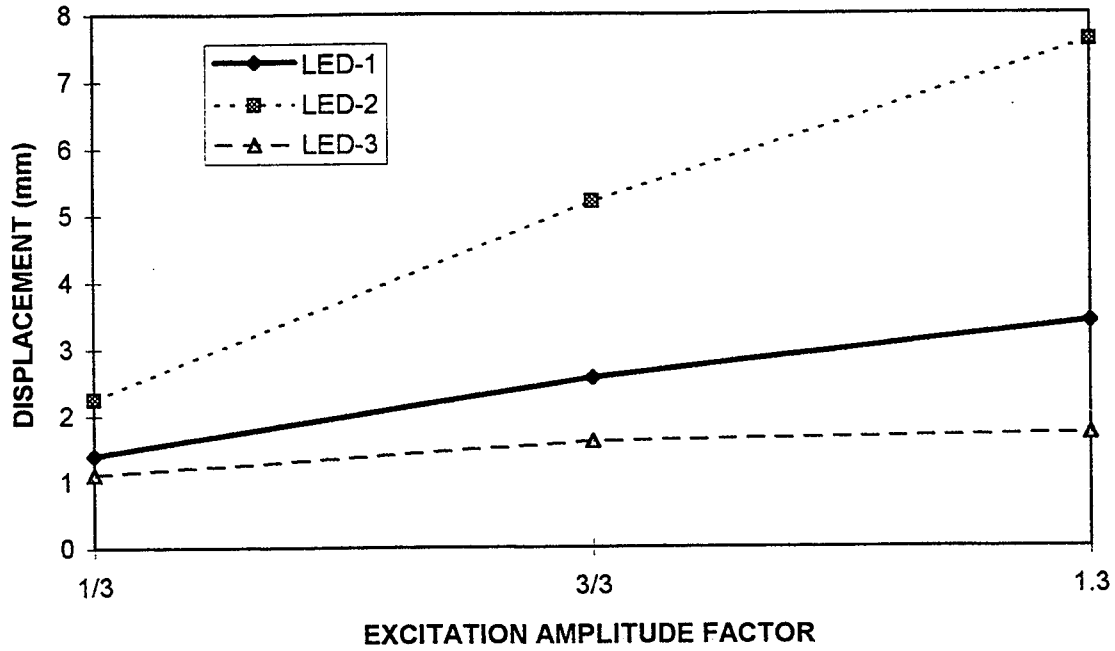

(c) Displacements of LED Supports

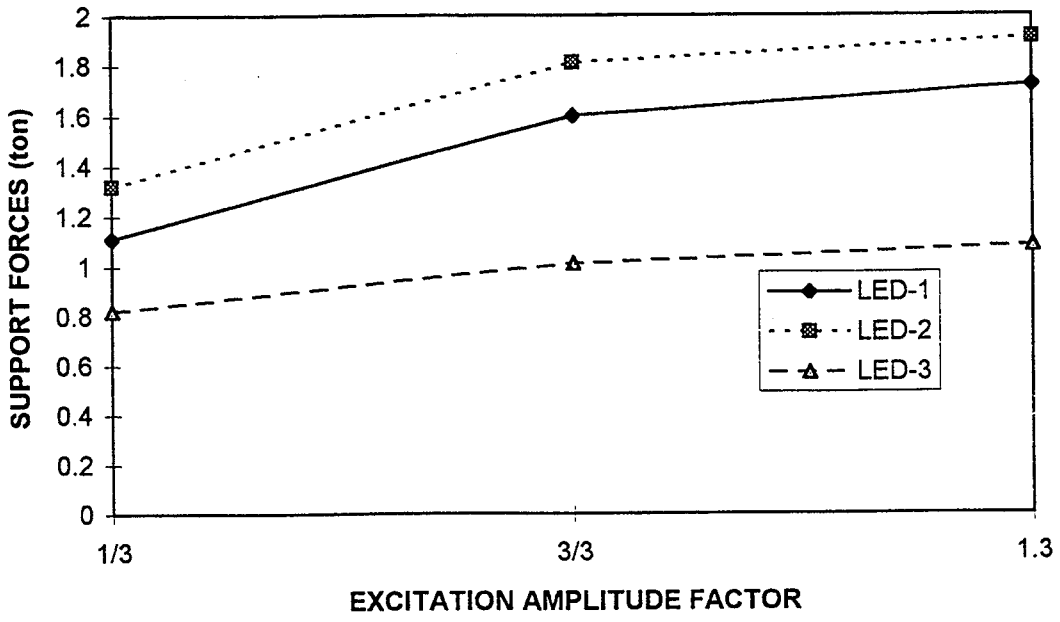

(d) Support Forces

Figure M.18 Peak Responses of M-line with LED Supports as a Function of Excitation Amplitude, S2(A) Test Series (Cont'd)

Table M.13 Measured Peak Responses of M-line with LED Supports, 1.0 S2(B) Test Run

Acceleration (g)			Displacement (mm)			Support Forces (ton)		Pipe Stress (kg/mm²)	
Instrument	Direction	Values	Instrument	Direction	Values	Instrument	Values	Instrument	Values
AA1	X Y Z	2.11 0.10 0.39	AD1	X Y Z	1.91 0.12 0.17	MR8	0.51	MS1	4.85
MA1	X Y Z	2.42 1.21 0.75	MD15/ LED-1		1.20	MR15/ LED-1	1.07	MS2'	2.26
MA16	X Y Z	2.60 2.21 1.07	MD16/ LED-2		8.80	MR16/ LED-2	1.91	MS2	2.24
MA17	X Y Z	2.60 0.97 0.96	MD17/ LED-3		2.00	MR17/ LED-3	0.88	MS3	5.44
MA4	X Y Z	2.50 1.11 0.77	MD18	X Y Z	8.50 6.85 2.00			MS4	1.23
MA5	X Y	2.51 1.08						MS5	2.05
MA6	X Y	2.43 1.13						MS6	2.10
MA8	X Y Z	2.09 0.97 1.18						MS8	1.21
MA10	X Y Z	0.41 1.32 1.66						MS9	1.53
								MS10	1.61

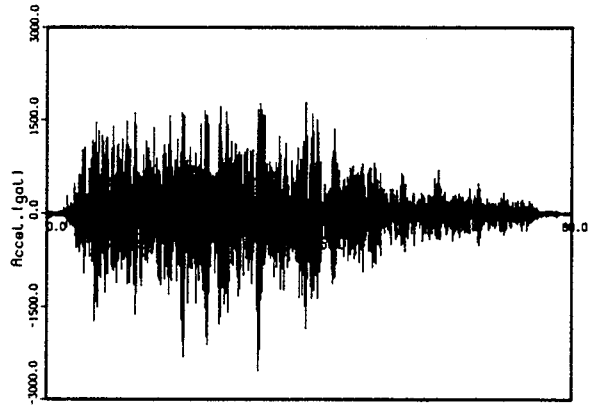

(MA16-X)

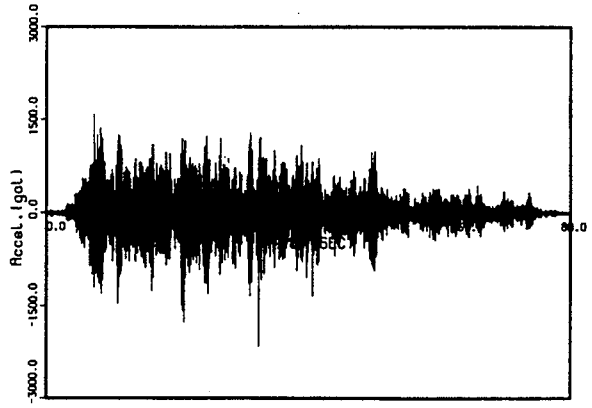

(MA16-Y)

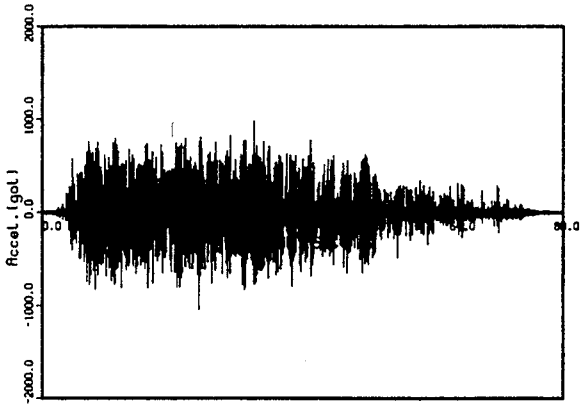

(MA16-Z)

Figure M.19 Acceleration Time Histories of M-line with LED Supports, 1.0 S2(B) Test Run

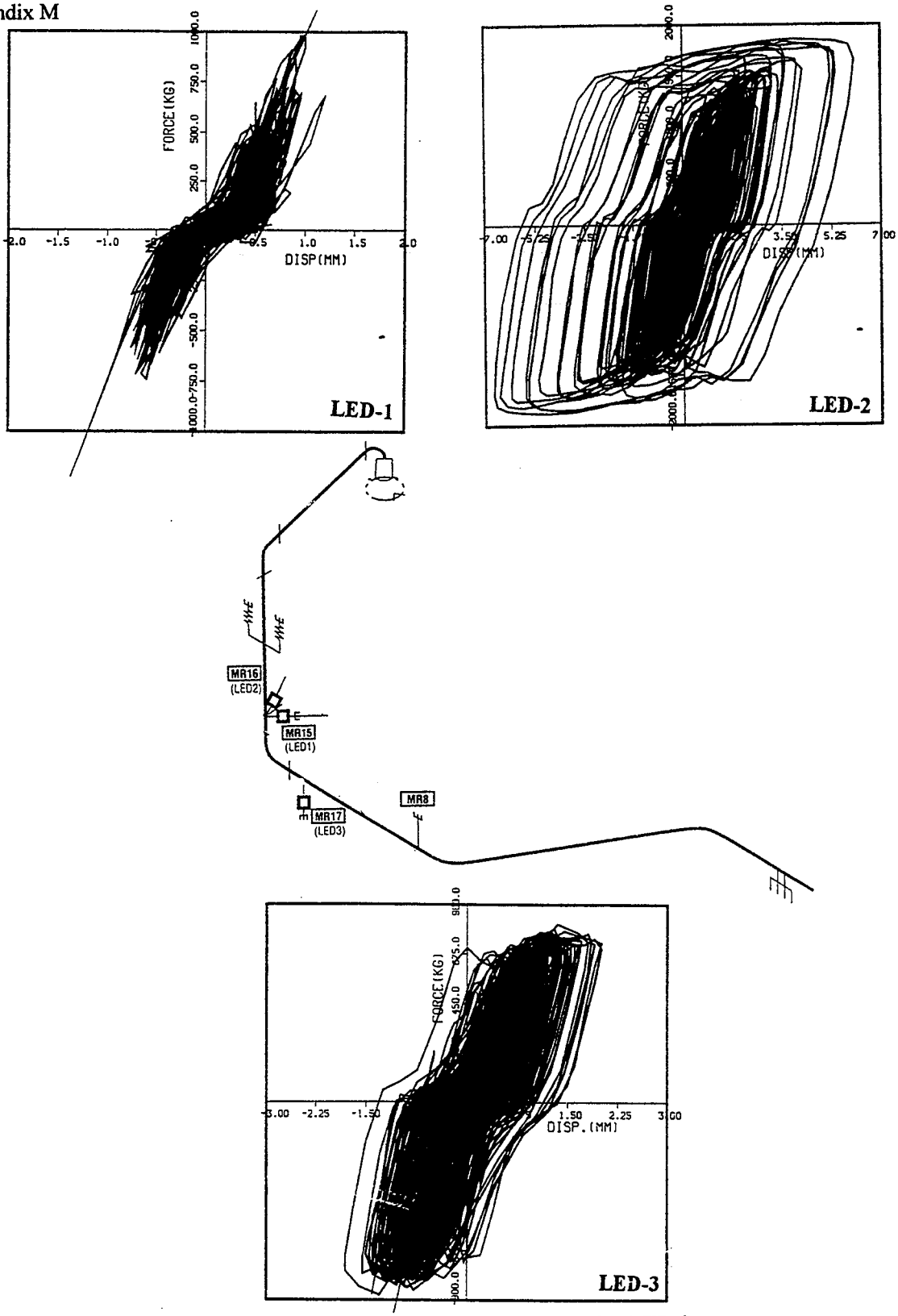

Figure M.20 Hysteretic Responses of M-line with LED Supports, 1.0 S2(B) Test Run

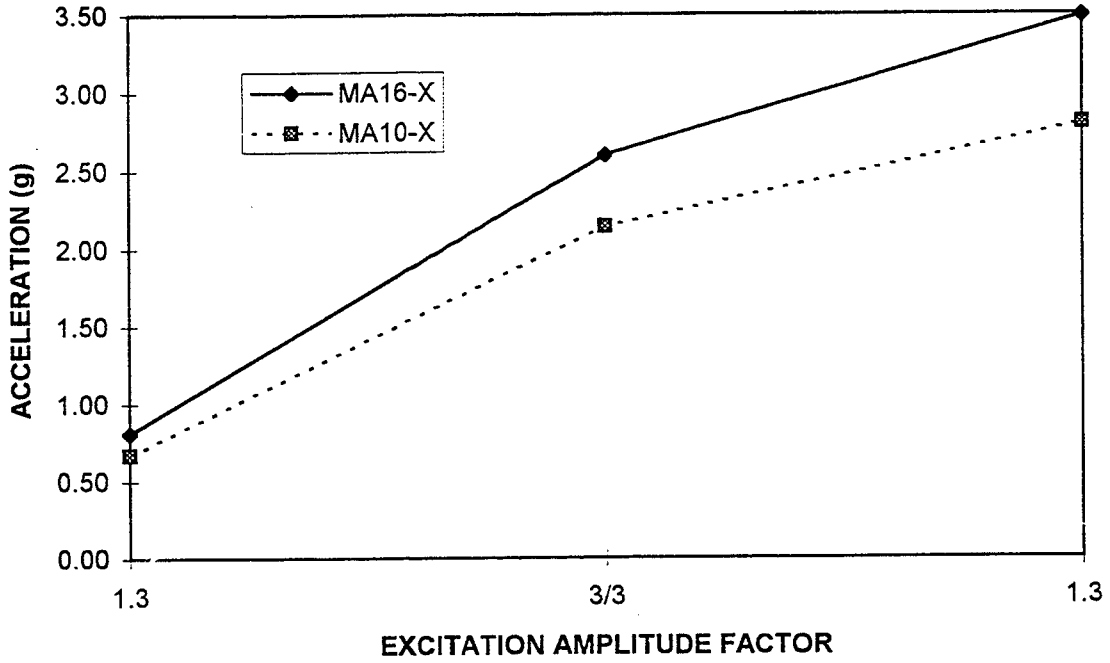

(a) Accelerations

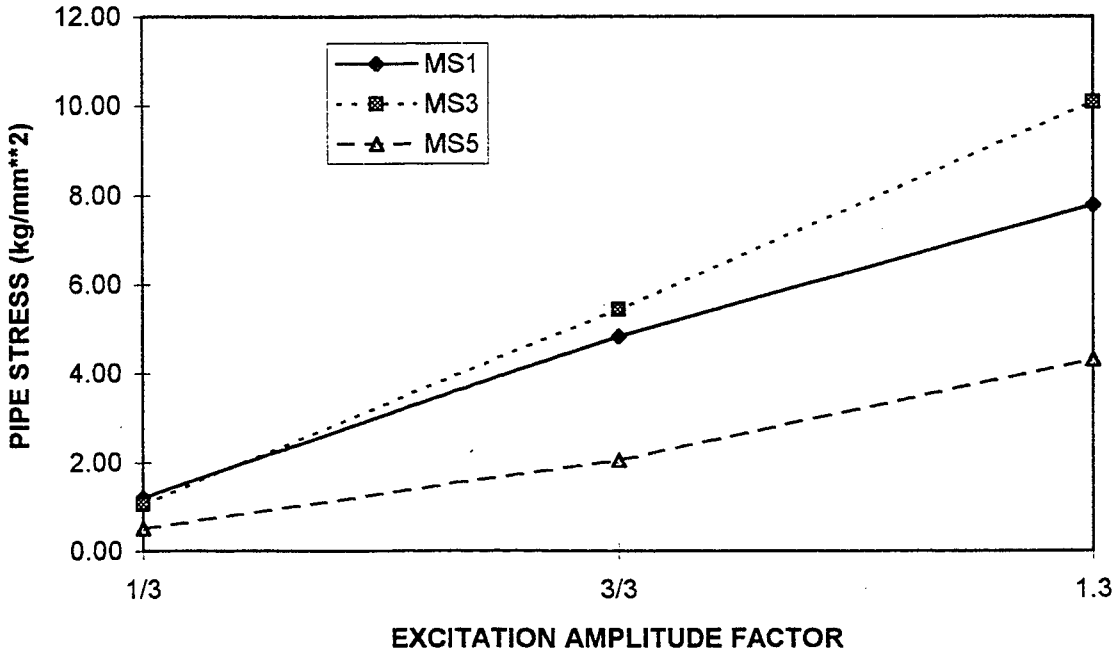

(b) Pipe Stresses

Figure M.21 Peak Responses of M-line with LED Supports as a Function of Excitation Amplitude, S2(B) Test Series

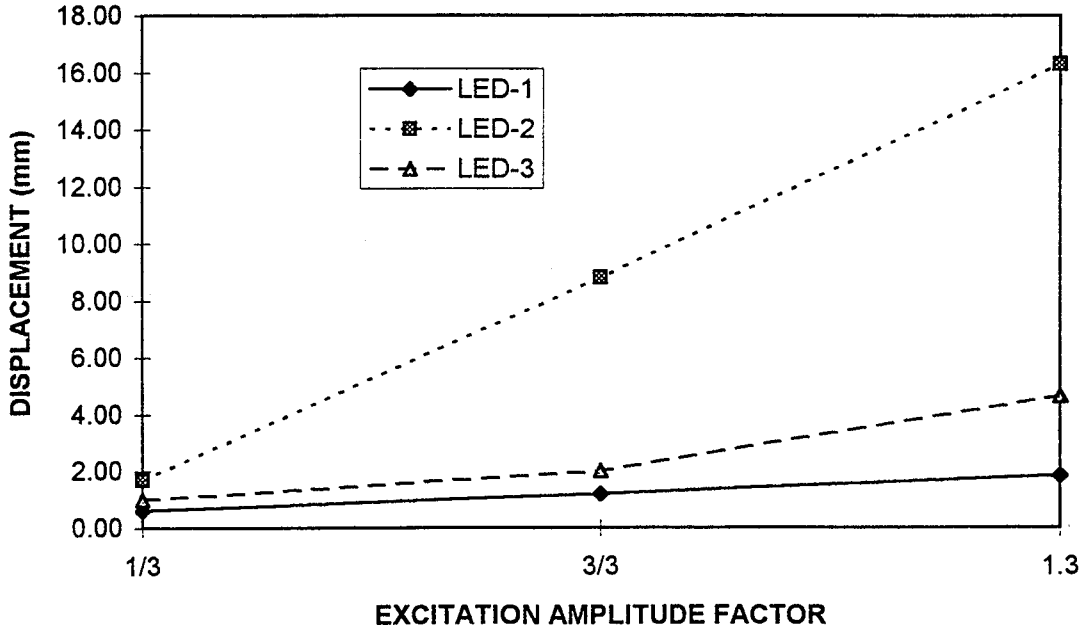

(c) Displacements of LED Supports

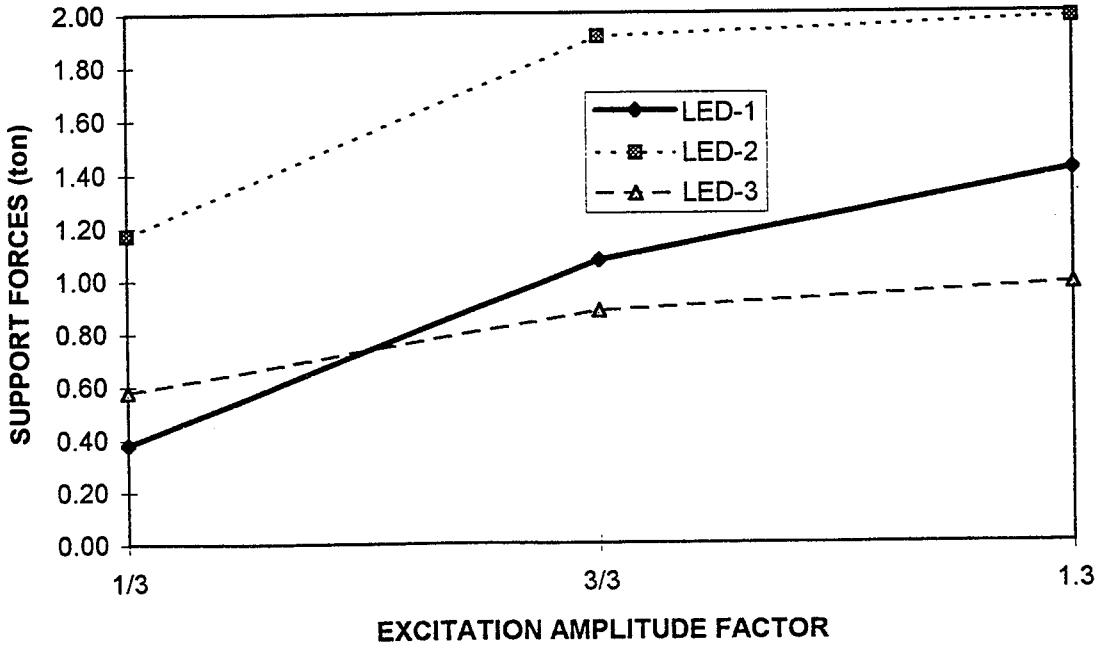

(d) Support Forces

Figure M.21 Peak Responses of M-line with LED Supports as a Function of Excitation Amplitude, S2(B) Test Series (Cont'd)

Table M.14 Measured Peak Responses of M-line with LED Supports without Independent Actuator, Tokachi-Oki Test Run

Acceleration (g)			Displacement (mm)			Support Forces (ton)		Pipe Stress (kg/mm²)	
Instrument	Direction	Values	Instrument	Direction	Values	Instrument	Values	Instrument	Values
MA1	X Y Z	6.16 5.43 2.54	MD12, 13	X Y	17.3 10.2	MR8	1.05	MS1	15.8
MA16	X Y Z	4.51 6.29 3.76	MD15/ LED-1		4.7	MR15/ LED-1	1.73	MS2'	9.1
MA17	X Y Z	6.00 5.98 3.83	MD16/ LED-2		54.9	MR16/ LED-2	1.91	MS2	11.3
MA4	X Y Z	6.04 4.25 2.58	MD17/ LED-3		15.3	MR17/ LED-3	1.20	MS3	26.9
MA5	X Y	6.13 4.27	MD18	X Y Z	50.9 36.0 15.3			MS4	7.7
MA6	X Y	5.16 4.40						MS5	13.8
MA8	X Y	5.33 3.83 7.58					1.20	MS6	4.8
MA10	X Y Z	4.10 2.14 7.95						MS8	9.4
								MS9	8.3
								MS10	9.3

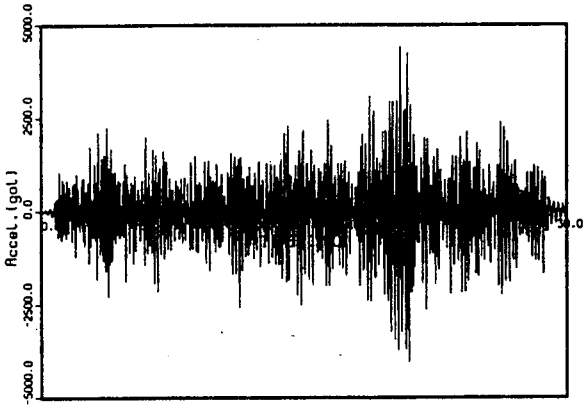

(MA16-X)

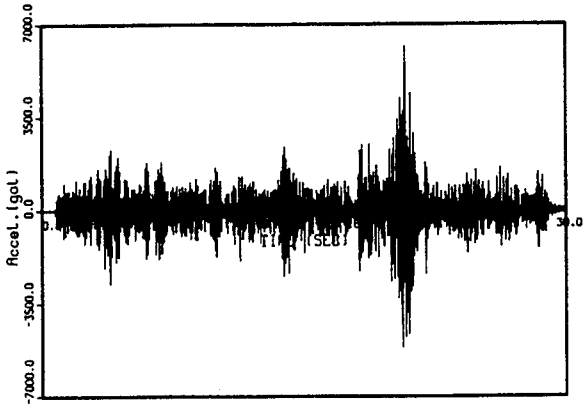

(MA16-Y)

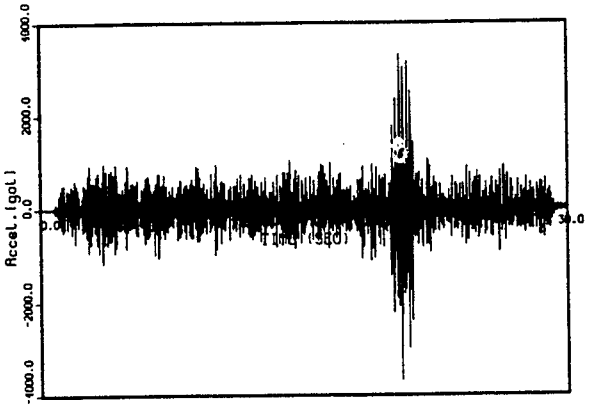

(MA16-Z)

Figure M.22 Acceleration Time Histories of M-line with LED Supports, without Independent Actuator, Tokachi-Oki Test Run

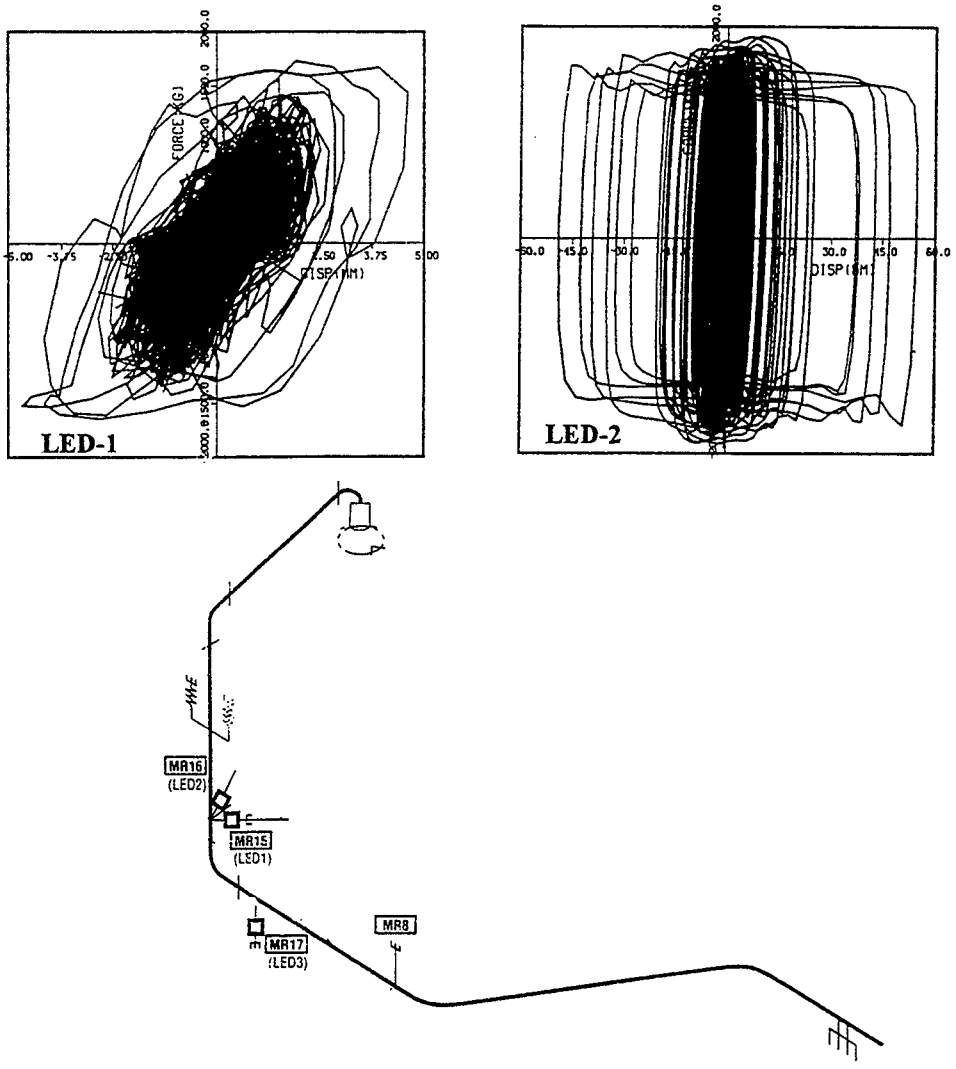

Figure M.23 Hysteretic Responses of M-line with LED Supports without Independent Actuator, Tokachi-Oki Test Run

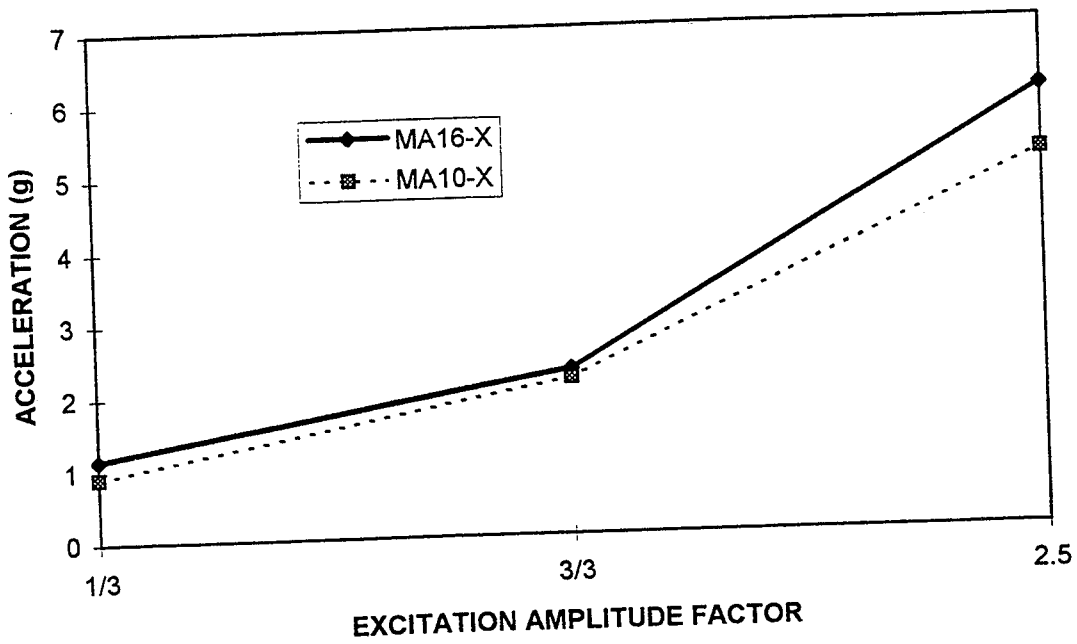

(a) Acceleration

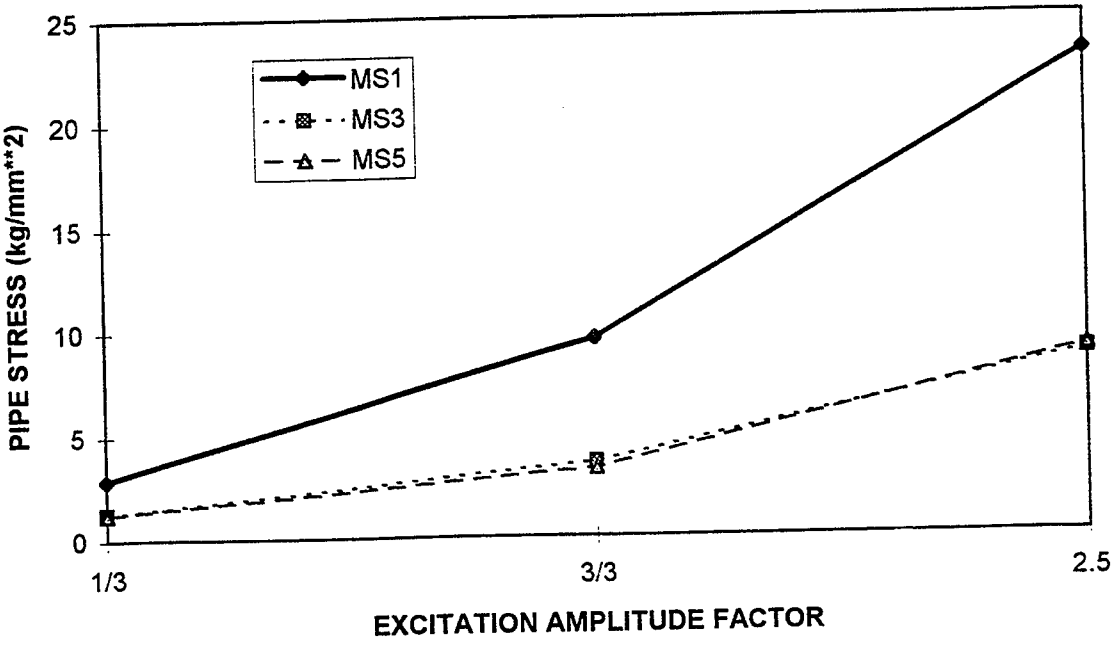

(b) Pipe Stresses

Figure M.24 Peak Responses of M-line with LED Supports without Independent Actuator as a Function of Excitation Amplitude, S2(A) Test Series

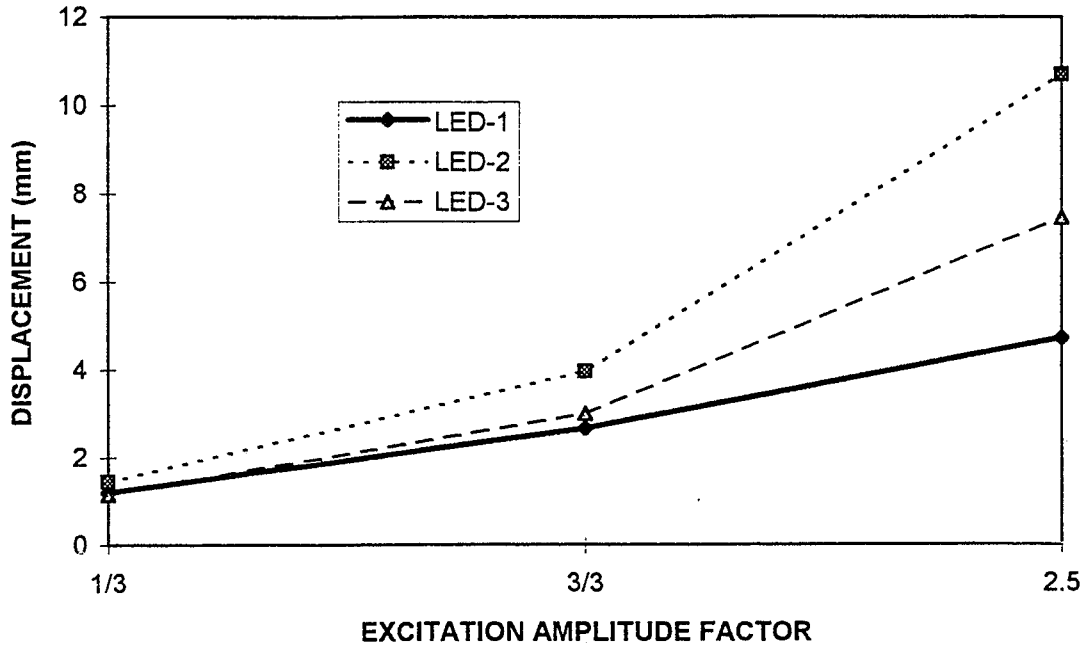

(c) Displacements of LED Supports

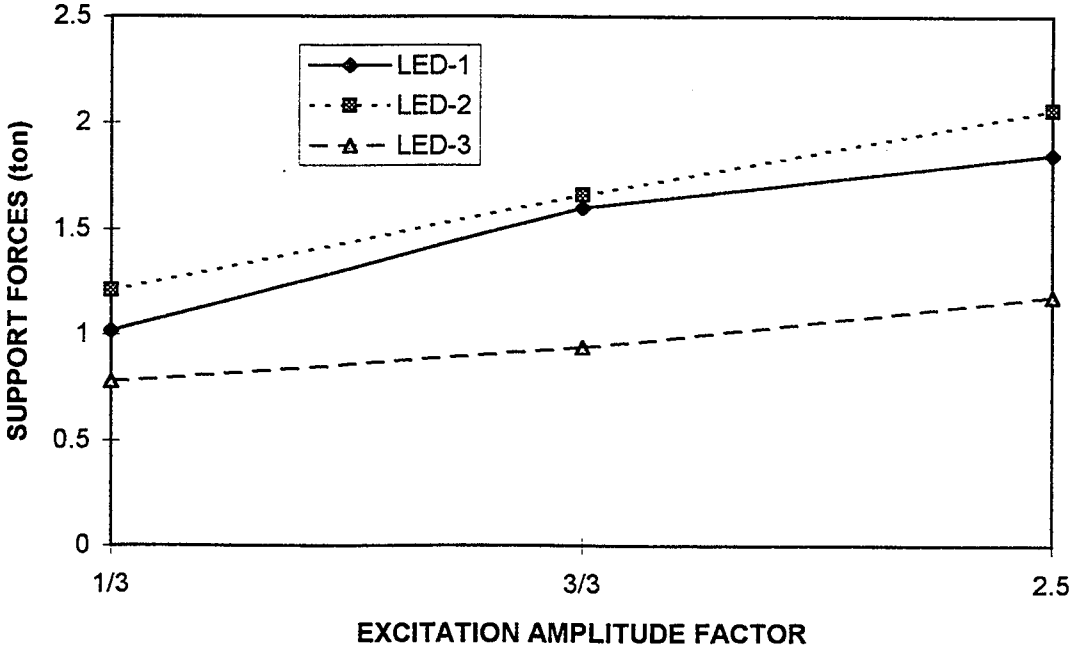

(d) Support Forces

Figure M.24 Peak Responses of M-line with LED Supports without Independent Actuator as a Function of Excitation Amplitude, S2(A) Test Series (Cont'd)

Table M.15 Measured Vibration Frequencies of F-line with EAB Supports

Direction of Excitation	Input Level (gal.)	Vibration Modes, Frequencies (Hz)					
		1st	2nd	3rd	4th	5th	6th
Horizontal Vibration	50 (4~30Hz)	9.8	12.2	13.2	17.6	-----	-----
	100 (4~30Hz)	10.0	13.0	15.4	17.2	-----	-----
	150 (4~30Hz)	10.0	13.0	15.6	17.2	-----	-----
	200 (4~30Hz)	9.8	13.0	15.6	17.4	-----	-----
	250 (5~15Hz)	9.6	12.6	-----	-----	-----	-----
	300 (5~15Hz)	9.4	12.6	-----	-----	-----	-----
Vertical Vibration	30 (4~30Hz)	-----	-----	-----	17.2	22.4	21.6
	60 (4~30Hz)	-----	-----	-----	17.4	23.4	24.6
	90 (4~30Hz)	-----	-----	-----	17.6	23.6	26.0
	120 (4~23Hz)	-----	-----	-----	17.8	-----	-----

Table M.16 Measured Modal Damping Values of F-line with EAB Supports

Direction of Excitation	Input Level (gal.)	Vibration Modes, Modal Damping (%)					
		1st	2nd	3rd	4th	5th	6th
Horizontal Vibration	50	2.7	3.2	2.5	1.9	-----	-----
	100	3.7	2.4	2.0	2.2	-----	-----
	150	6.2	2.4	2.3	2.8	-----	-----
	200	8.2	3.0	2.7	1.5	-----	-----
	250	9.2	3.4	-----	-----	-----	-----
	300	11.7	3.6	-----	-----	-----	-----
Vertical Vibration	30	-----	-----	-----	1.8	2.1	3.6
	60	-----	-----	-----	1.7	3.0	2.9
	90	-----	-----	-----	1.3	1.7	2.6
	120	-----	-----	-----	1.1	-----	-----

Table M.17 Measured Peak Responses of F-line with EAB Supports, 1.0 S2(A) Test Run

Acceleration (g)			Displacement (mm)		Support Forces (ton)		Pipe Stress (kg/mm^2)	
Instrument	Direction	Values	Instrument	Values	Instrument	Values	Instrument	Values
FA3	X Y Z	3.08 0.41 1.80	FD6b	1.05	FR6b	1.66	FS1	4.3
							FS2	4.5
FA5	X Y Z	2.98 0.62 2.28	FD11b/ EAB-1	5.42	FR11b/ EAB-1	0.71	FS3	6.9
							FS4	9.5
FA6	X Y Z	4.94 3.28 3.30	FD12b/ EAB-2	7.20	FR12b/ EAB-2	1.43	FS5	2.4
							FS6	5.0
FA7	X Y Z	5.20 1.98 2.22	FD13b	1.25	FR13b	4.89	FS7	3.5
							FS8	1.2
FA8	X Y Z	4.97 1.28 2.96	FD14b/ EAB-3	8.50	FR14b/ EAB-3	1.45	FS9	8.5
							FS10	5.7
FA9	X Y Z	3.04 1.57 2.43	FD15b	0.82	FR15b	4.37	FS11	5.9
							FS12	3.6
FA10	X Y Z	3.29 1.52 2.84					FS13	7.1
							FS14	8.8
FA11	X Y Z	4.07 3.75 3.06					FS15	6.0
							FS19	8.3
FA12	X Y Z	5.56 2.48 2.14					FS20	3.7
							FS21	10.7
FA13	X Y Z	3.68 1.90 3.31					FS22	8.1

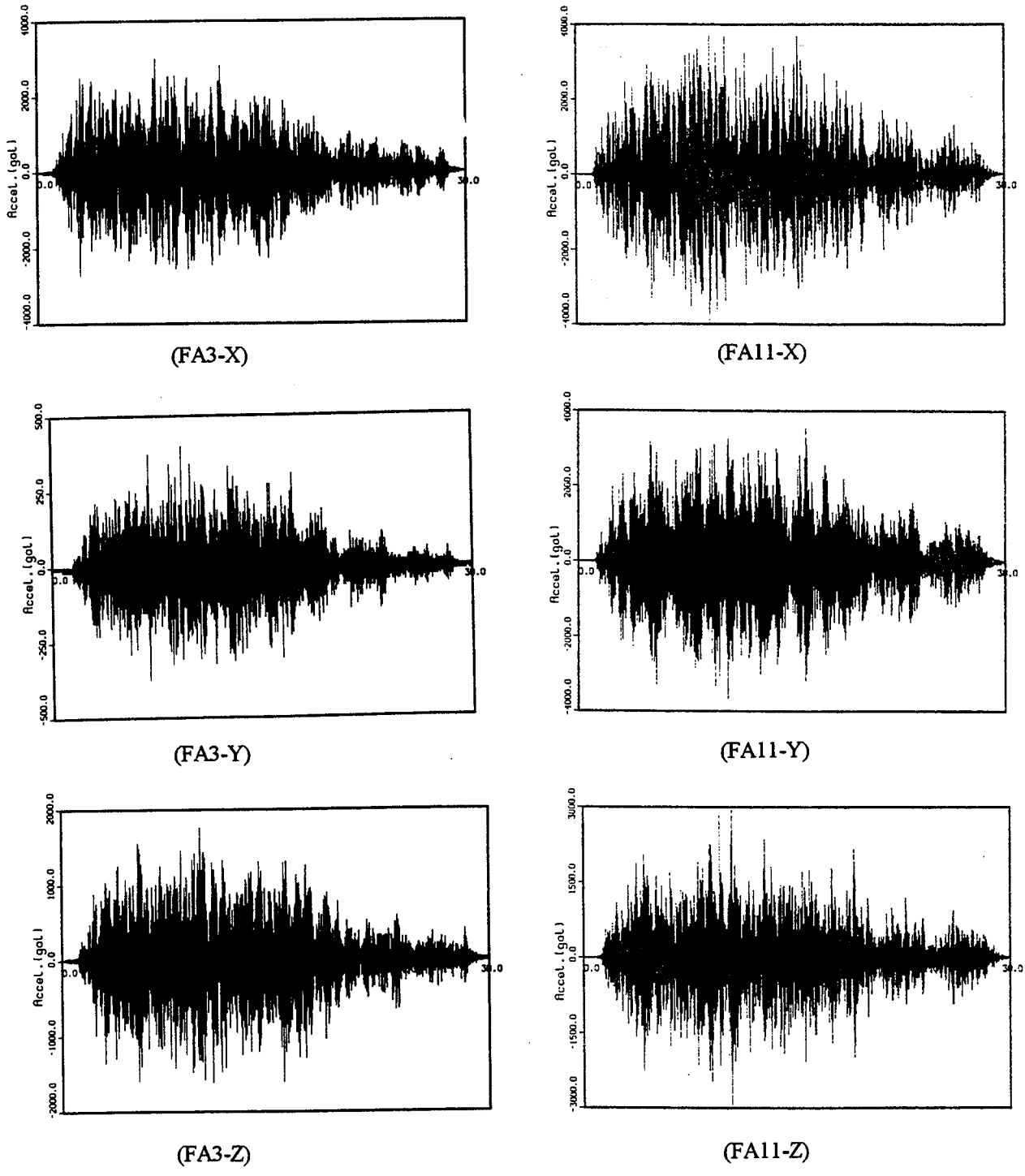

Figure M.25 Acceleration Time Histories of F-line with EAB Supports, 1.0 S2(A) Test Run

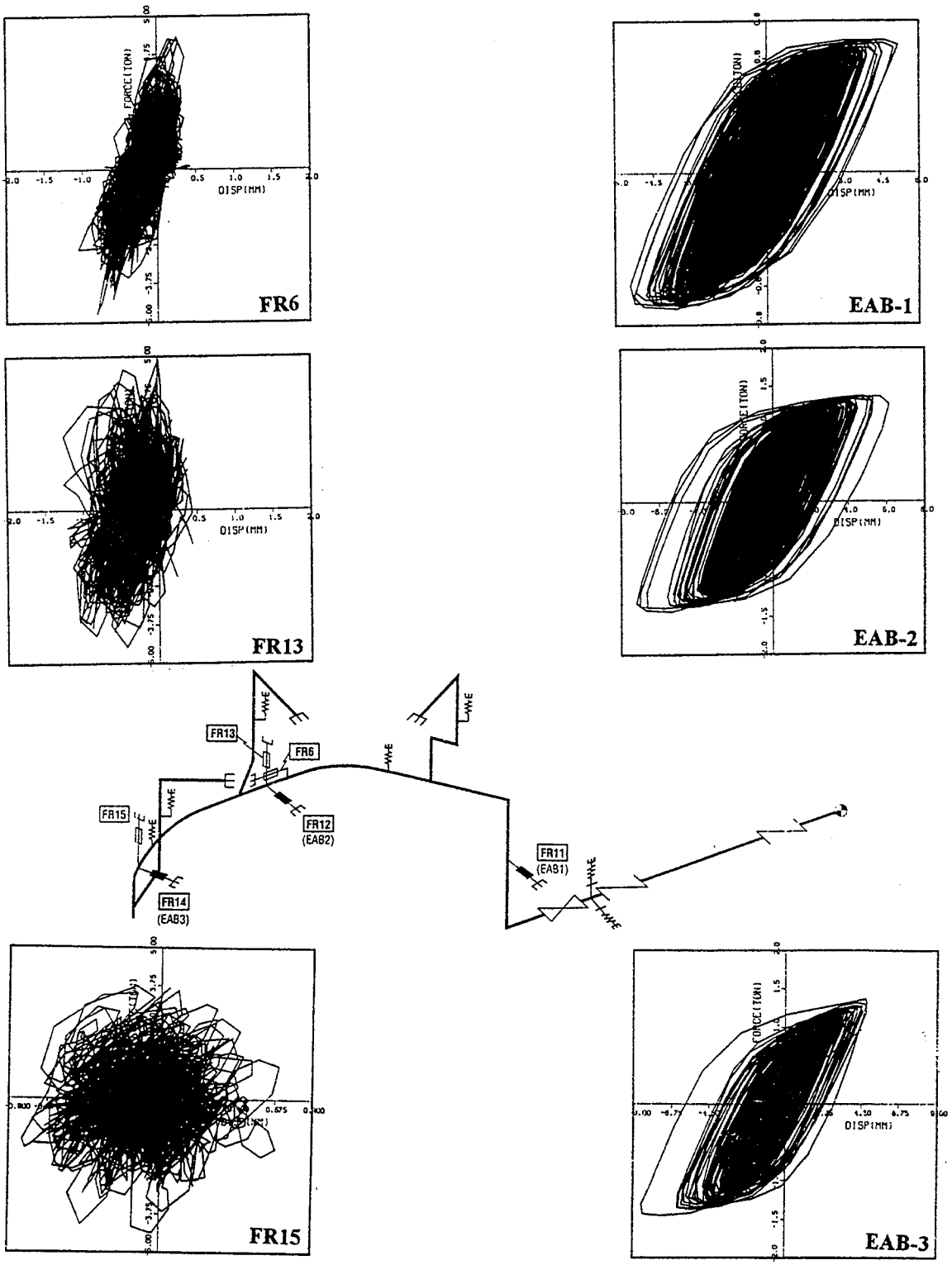

Figure M.26 Hysteretic Responses of F-line with EAB Supports, 1.0 S2(A) Test Run

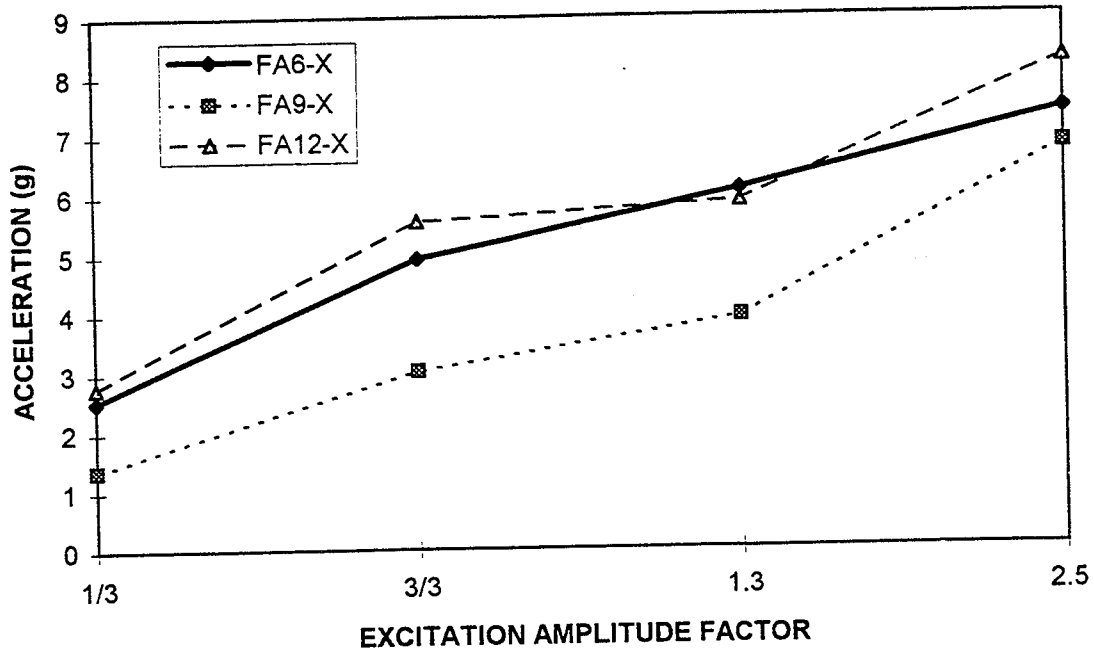

(a) Acceleration

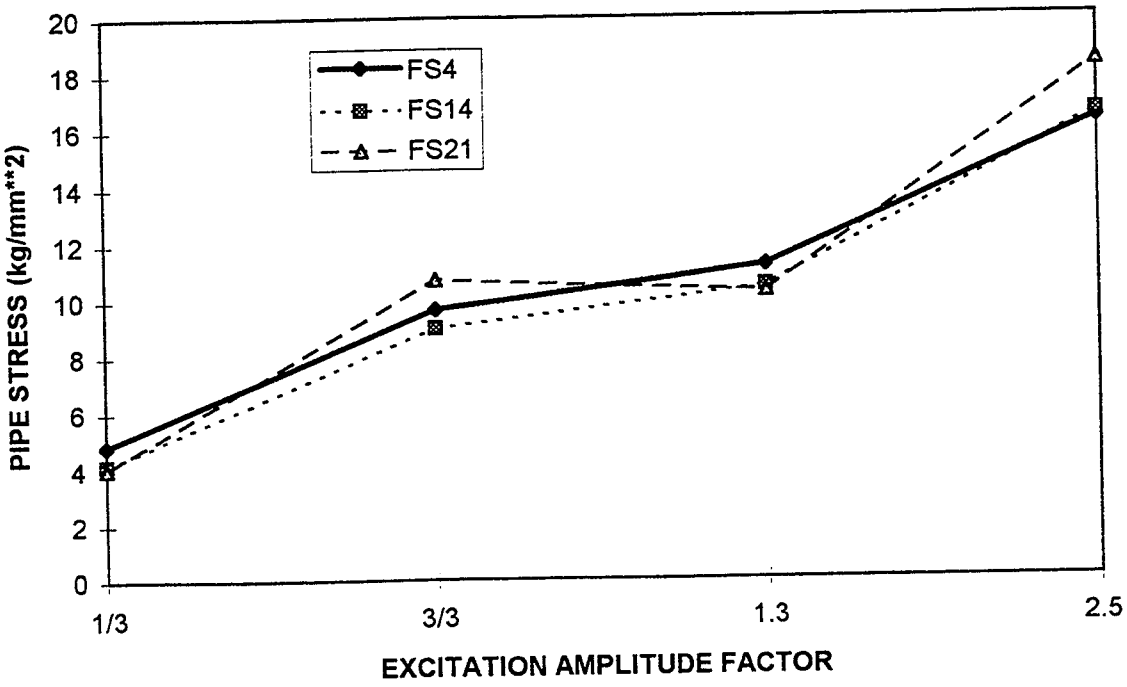

(b) Pipe Stresses

Figure M.27 Peak Responses of F-line with EAB Supports as a Function of Excitation Amplitude, S2(A) Test Series

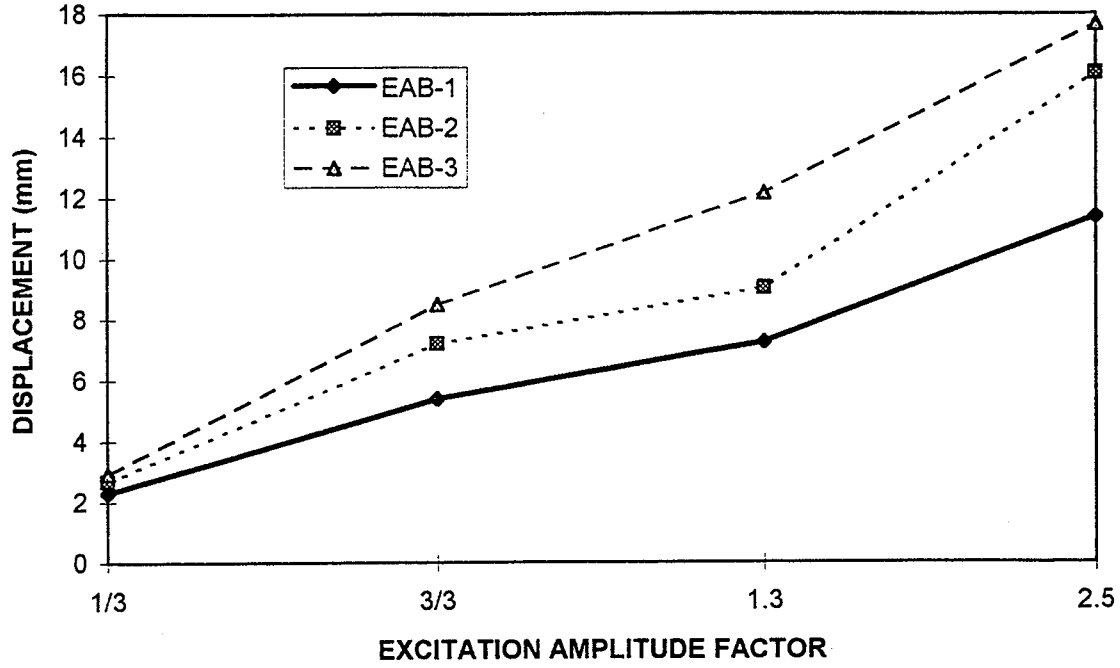

(c) Displacements of EAB Supports

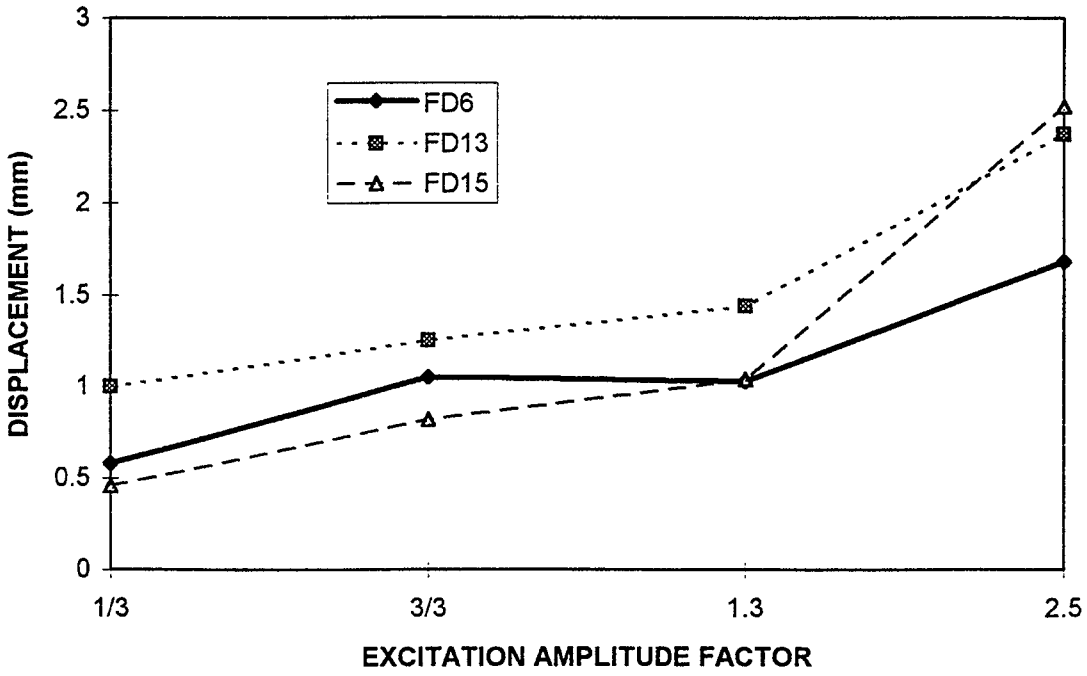

(d) Displacements of Snubbers

Figure M.27 Peak Responses of F-line with EAB Supports as a Function of Excitation Amplitude, S2(A) Test Series (Cont'd)

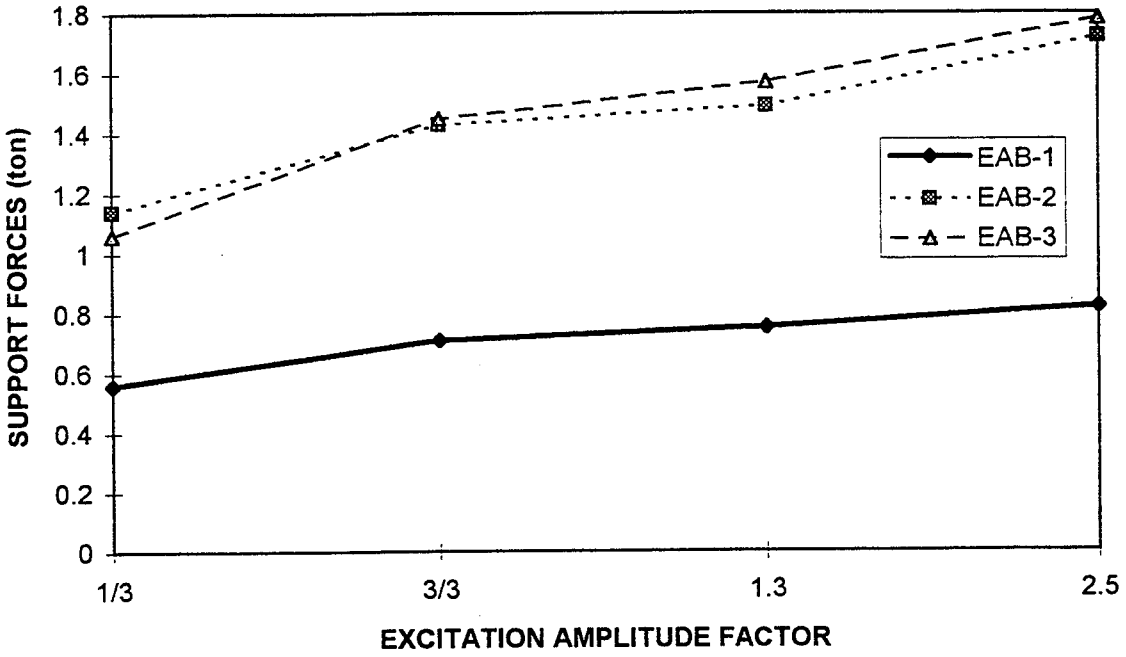

(e) Support Forces of EAB Supports

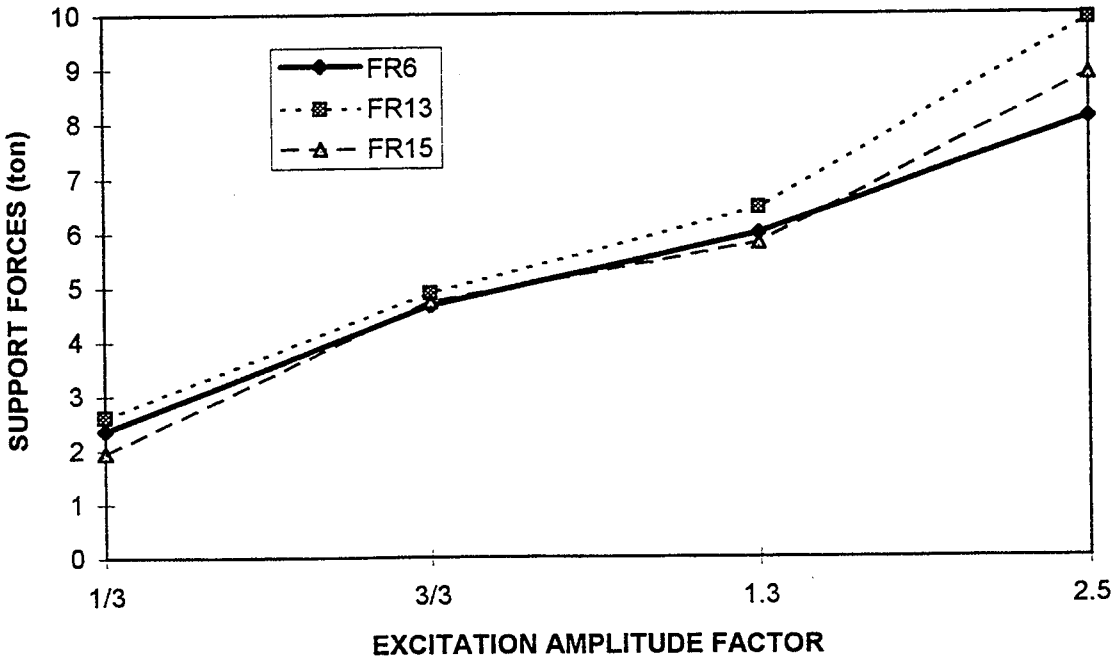

(f) Support Forces of Snubbers

Figure M.27 Peak Responses of F-line with EAB Supports as a Function of Excitation Amplitude, S2(A) Test Series (Cont'd)

Table M.18 Measured Peak Responses of F-line with EAB Supports, 1.0 S2(B) Test Run

Acceleration (g)			Displacement (mm)		Support Forces (ton)		Pipe Stress (kg/mm²)	
Instrument	Direction	Values	Instrument	Values	Instrument	Values	Instrument	Values
FA3	X Y Z	2.03 1.12 0.90	FD6b	0.99	FR6b	3.00	FS1	2.06
							FS2	2.35
FA5	X Y Z	2.16 0.18 0.79	FD11b/ EAB-1	2.64	FR11b/ EAB-1	0.59	FS3	3.25
							FS4	3.15
FA6	X Y Z	2.37 1.21 1.09	FD12b/ EAB-2	5.82	FR12b/ EAB-2	1.41	FS5	1.31
							FS6	4.09
FA7	X Y Z	2.36 0.93 0.96	FD13b	1.65	FR13b	3.68	FS7	1.84
							FS8	1.07
FA8	X Y Z	2.57 0.77 1.41	FD14b/ EAB-3	4.60	FR14b/ EAB-3	1.34	FS9	6.78
							FS10	2.10
FA9	X Y Z	2.42 0.83 1.37	FD15b	1.72	FR15b	2.74	FS11	4.56
							FS12	2.72
FA10	X Y Z	2.69 0.69 1.64					FS13	3.96
							FS14	6.19
FA11	X Y Z	2.74 1.32 1.54					FS15	5.52
							FS19	6.57
FA12	X Y Z	2.41 1.08 1.10					FS20	3.07
							FS21	6.40
FA13	X Y Z	2.54 0.98 1.81					FS22	6.72

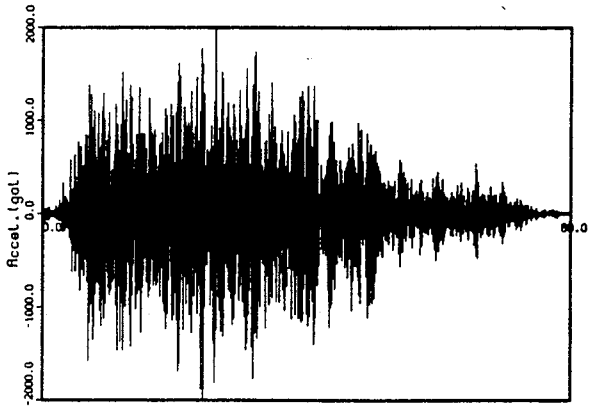

(FA3-X)

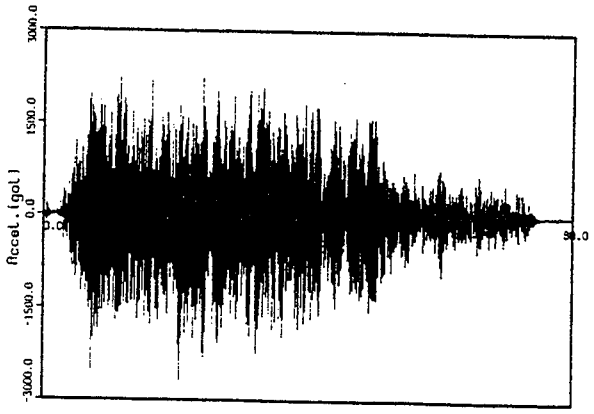

(FA11-X)

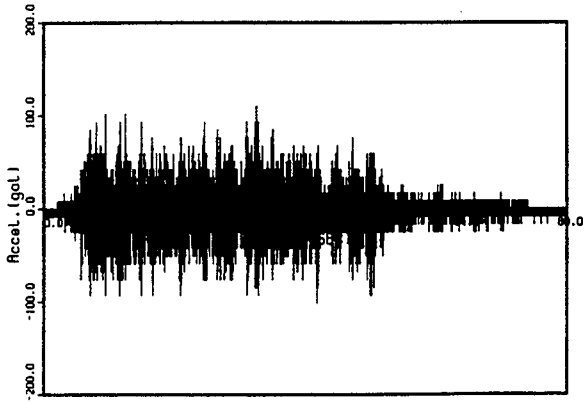

(FA3-Y)

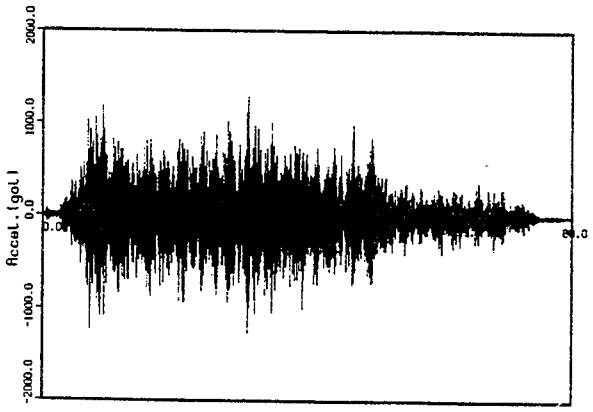

(FA11-Y)

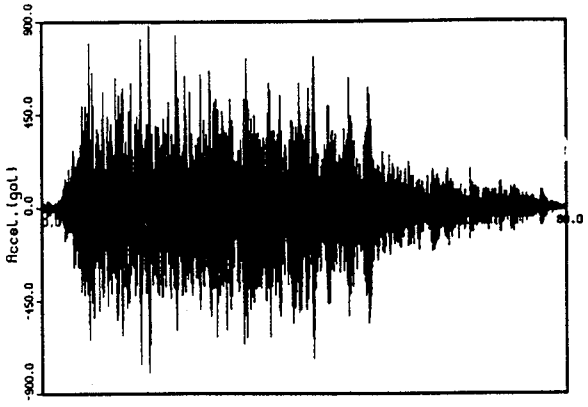

(FA3-Z)

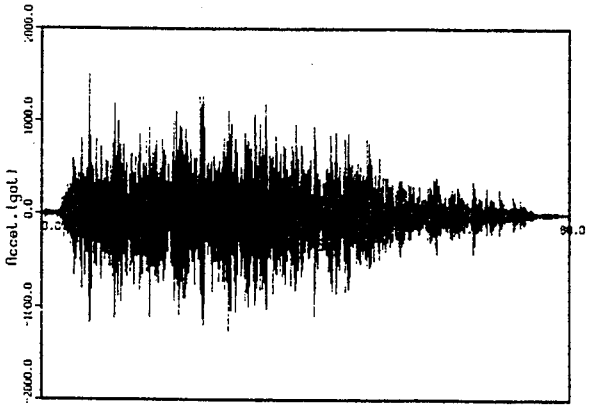

(FA11-Z)

Figure M.28 Acceleration Time Histories of F-line with EAB Supports, 1.0 S2(B) Test Run

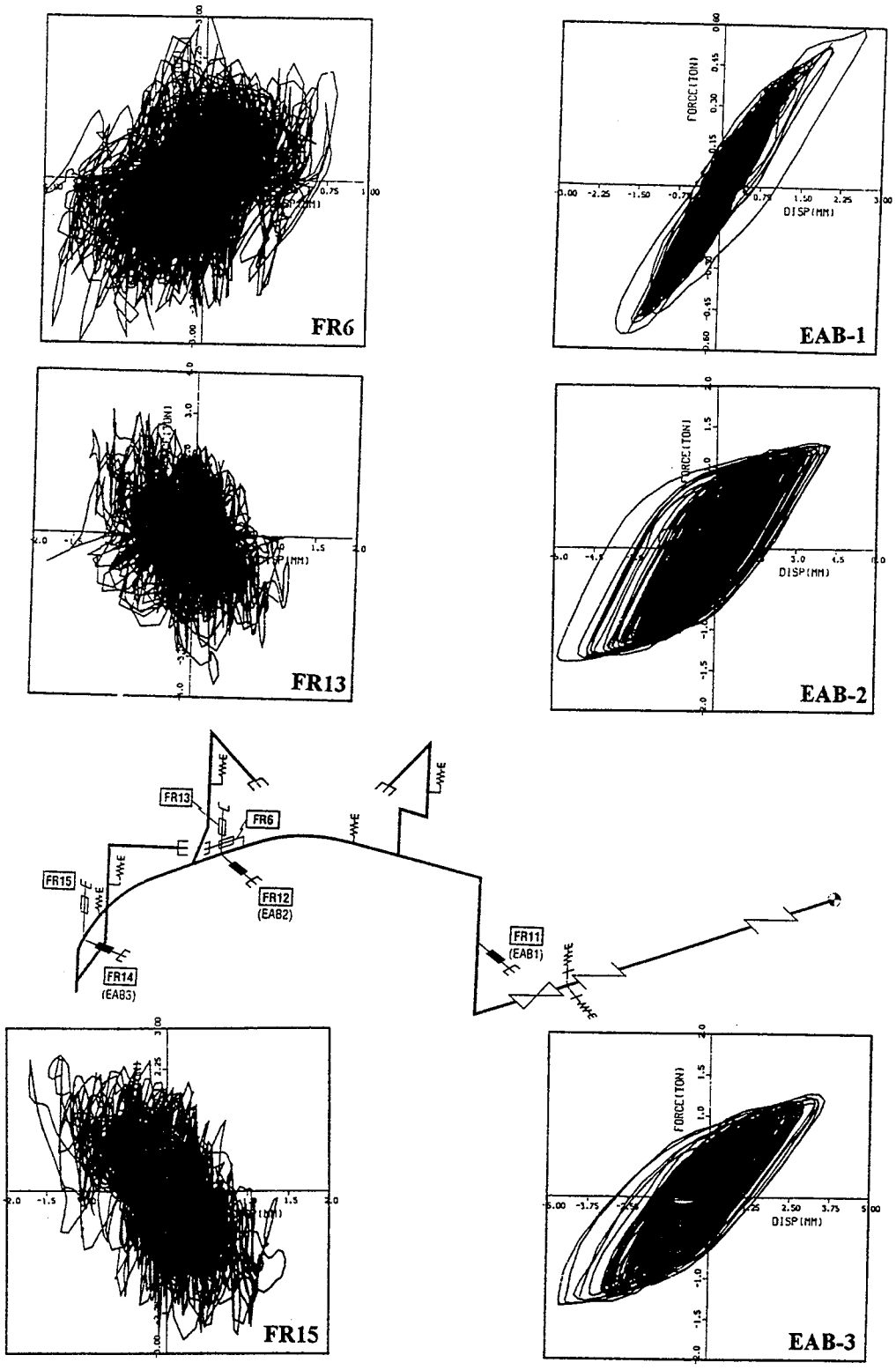

Figure M.29 Hysteretic Responses of F-line with EAB Supports, 1.0 S2(B) Test Run

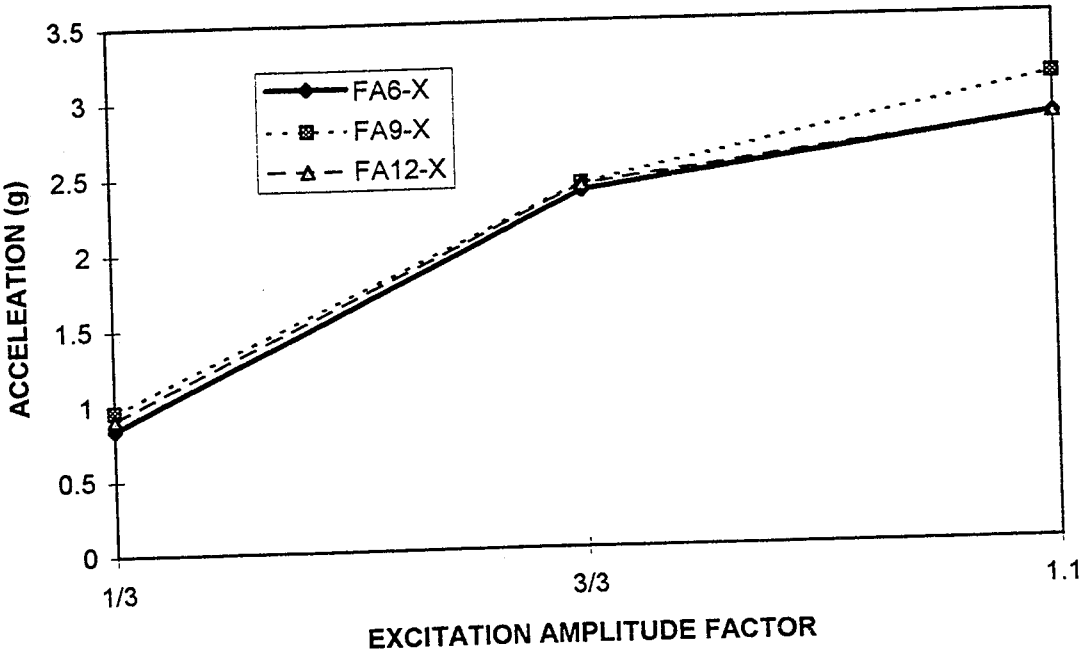

(a) Accelerations

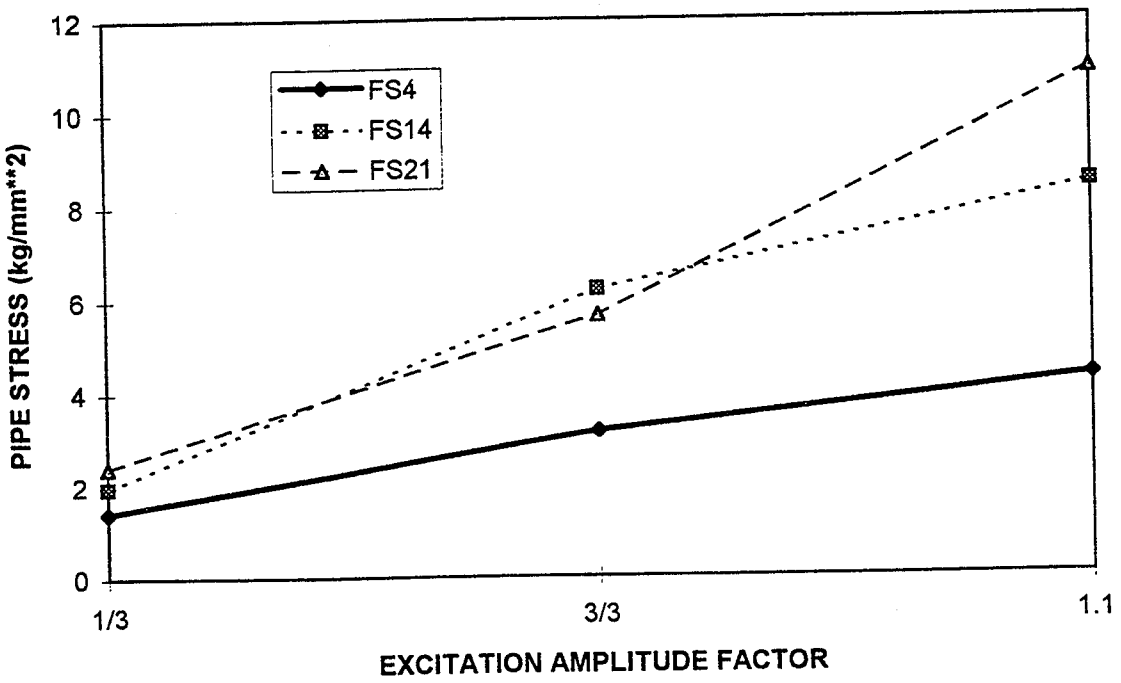

(b) Pipe Stresses

Figure M.30 Peak Responses of F-line with EAB Supports as a Function of Excitation Amplitude, S2(B) Test Series

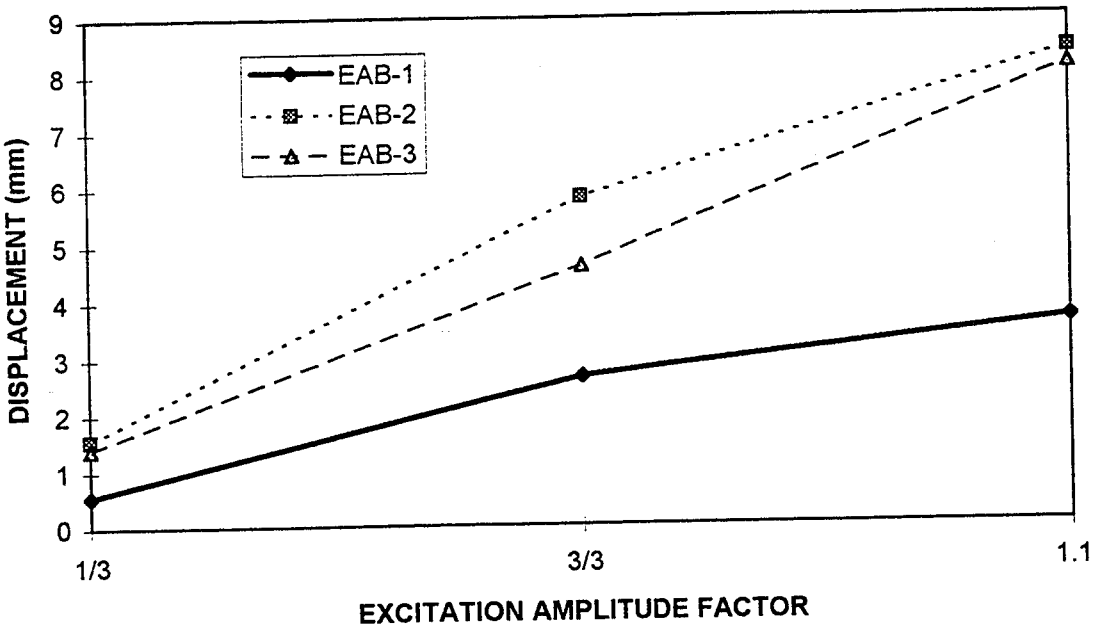

(c) Displacements of EAB Supports

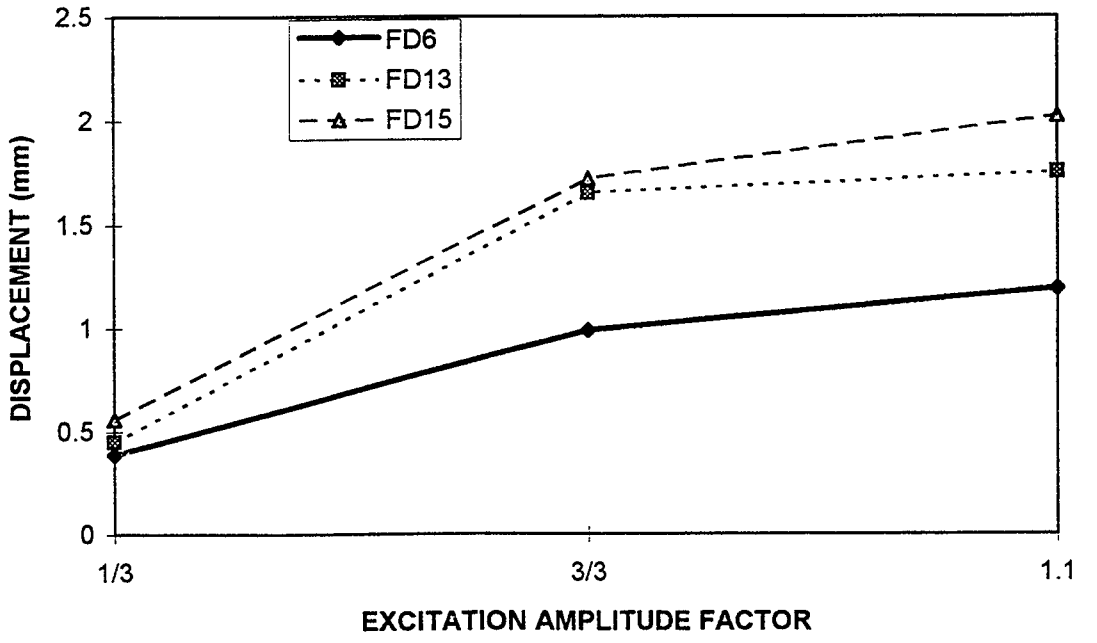

(d) Displacements of Snubbers

Figure M.30 Peak Responses of F-line with EAB Supports as a Function of Excitation Amplitude, S2(B) Test Series (Cont'd)

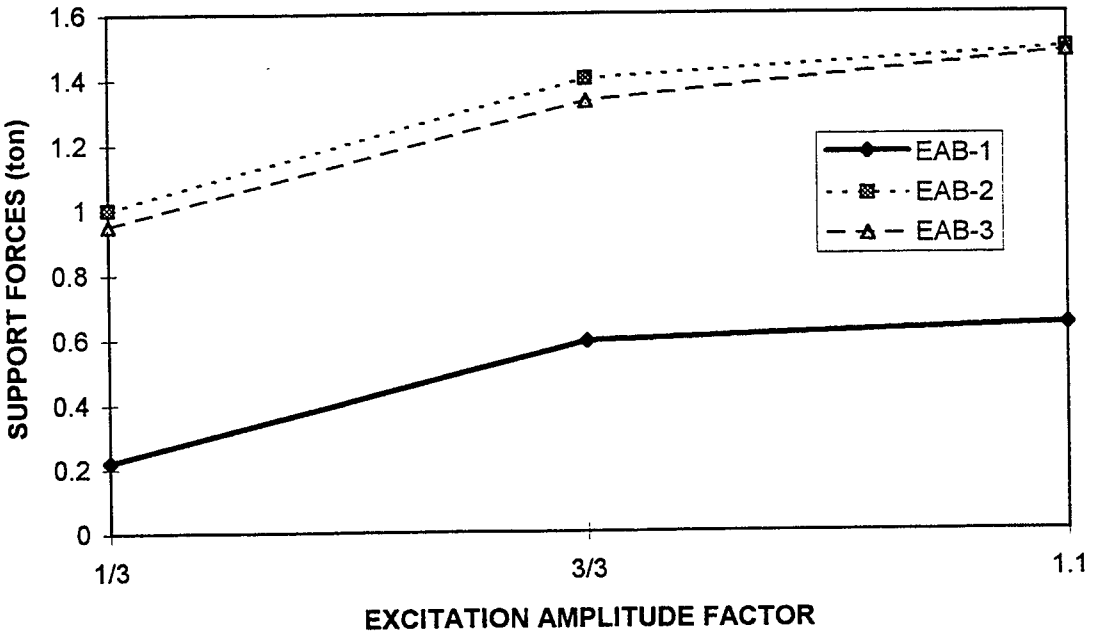

(e) Support Forces of EAB Supports

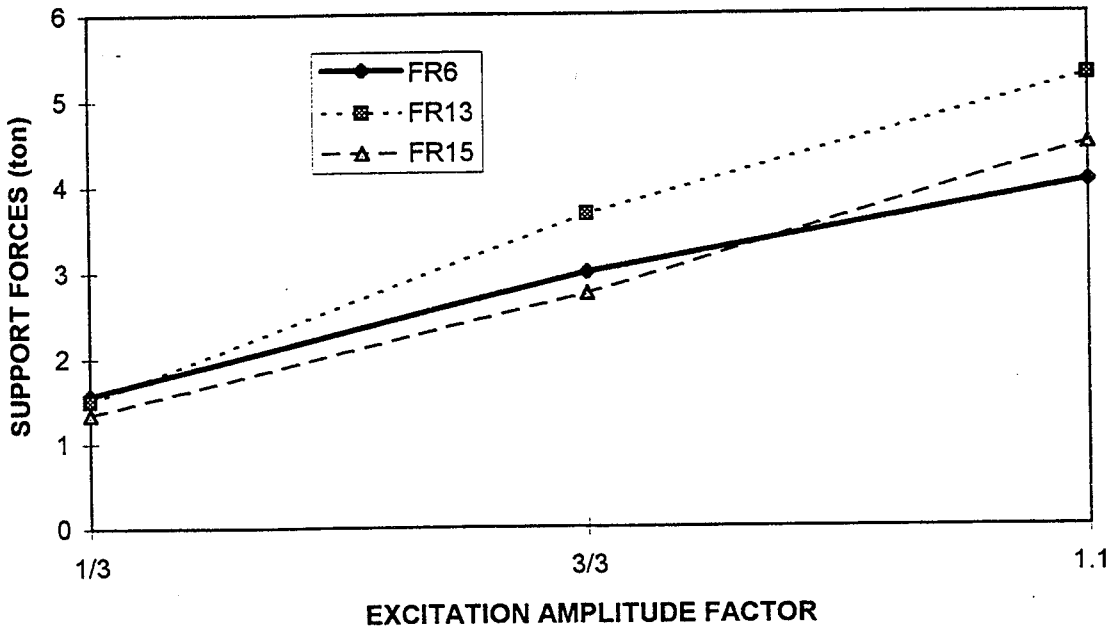

(f) Support Forces of Snubbers

Figure M.30 Peak Responses of F-line with EAB Supports as a Function of Excitation Amplitude, S2(B) Test Results (Cont'd)

Table M.19 Measured Peak Responses of F-line with EAB Supports, 1.2 S2(C) Test Run

Accelerator (g)			Displacement (mm)		Support Forces (ton)		Pipe Stress (kg/mm²)	
Instrument	Direction	Vaiones	Instrument	Values	Instrument	Values	Instrument	Values
FA3	X Y Z	2.99 0.27 1.27	FD6b	1.4	FR6b	6.39	FS1	3.4
							FS2	6.1
FA5	X Y Z	3.13 0.42 1.34	FD11b/ EAB-1	4.2	FR11b/ EAB-1	0.71	FS3	5.8
							FS4	8.0
FA6	X Y Z	3.75 3.62 1.76	FD12b/ EAB-2	13.4	FR12b/ EAB-2	1.71	FS5	3.5
							FS6	10.5
FA7	X Y Z	3.19 1.80 1.95	FD13b	2.0	FR13b	7.88	FS7	3.9
							FS8	2.5
FA8	X Y Z	3.41 1.21 2.75	FD14b/ EAB-3	19.2	FR14b/ EAB-3	3.59	FS9	22.1
							FS10	8.4
FA9	X Y Z	5.03 1.20 3.49	FD15b	2.2	FR15b	10.74	FS11	8.9
							FS12	3.8
FA10	X Y Z	7.73 0.99 5.80					FS13	5.8
							FS14	17.5
FA11	X Y Z	10.09 4.06 3.76					FS15	12.8
							FS19	21.5
FA12	X Y Z	3.70 2.23 2.03					FS20	9.2
							FS21	27.8
FA13	X Y Z	3.93 1.79 4.14					FS22	17.8

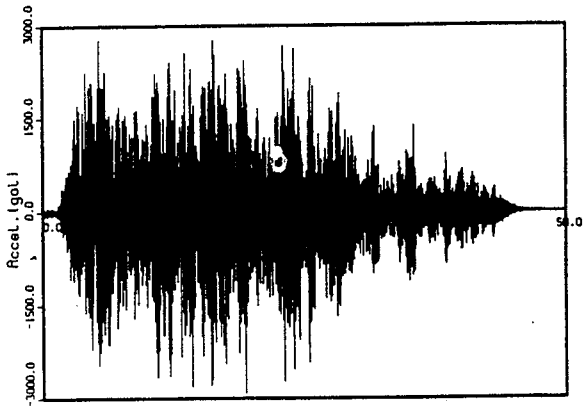

(FA3-X)

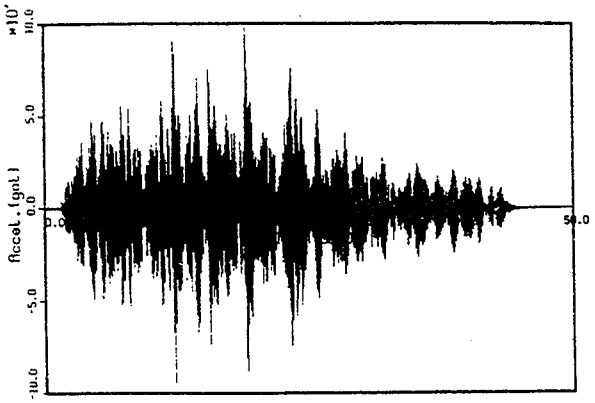

(FA11-X)

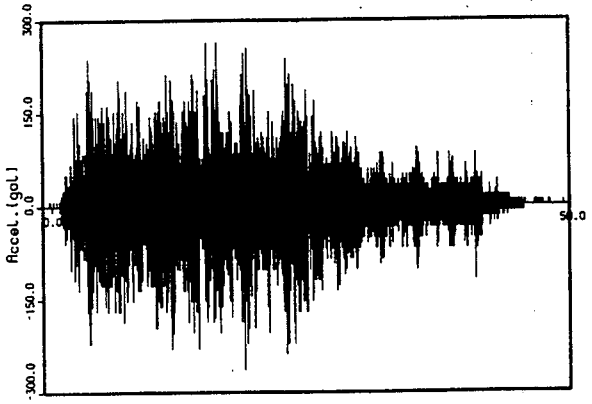

(FA3-Y)

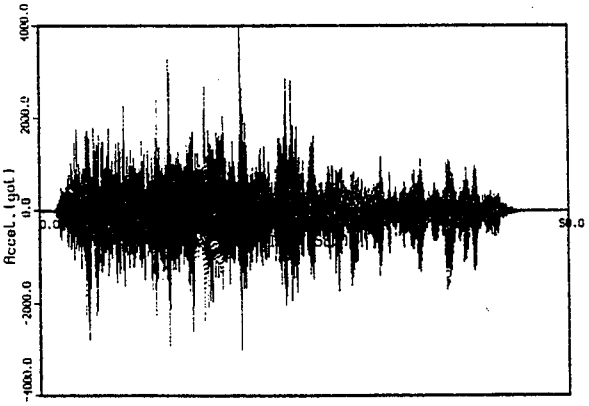

(FA11-Y)

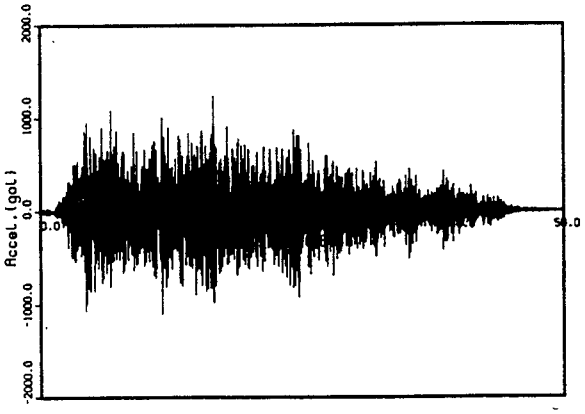

(FA3-Z)

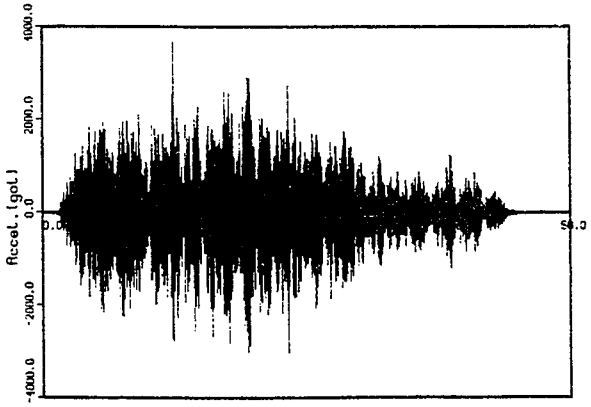

(FA11-Z)

Figure M.31 Acceleration Time Histories of F-line with EAB Supports, 1.2 S2(C) Test Run

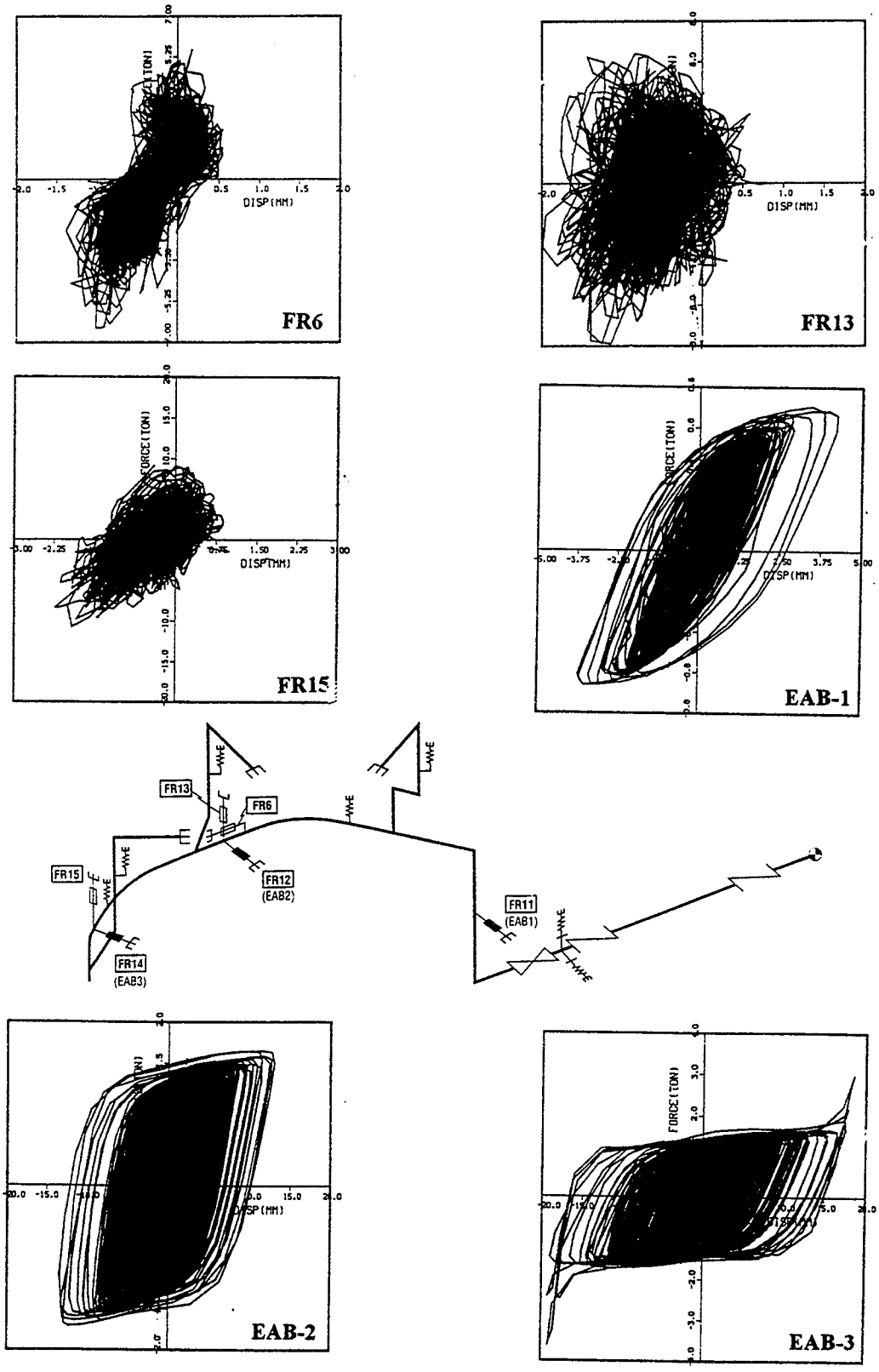

Figure M.32 Hysteretic Responses of F-line with EAB Supports, 1.2 S2(C) Test Run

Table M.20 Measured Peak Responses of M-line for Gap Test, 1.0 S2(A) Test Run

Acceleration (g)			Displacement (mm)			Support Forces (ton)		Pipe Stress (kg/mm²)	
Instrument	Direction	Values	Instrument	Direction	Values	Instrument	Values	Instrument	Values
AA1	X Y Z	9.85 20.13 4.42	AD1	X Y Z	1.61 0.34 0.26	MR8	0.19	MS1	7.35
MA1	X Y Z	8.45 10.50 11.61	MD15/ LED-1		2.40	MR15/ LED-1	1.44	MS2'	3.90
MA16	X Y Z	11.41 19.57 6.92	MD16/ LED-2		4.50	MR16/ LED-2	1.74	MS2	2.45
MA17	X Y Z	9.25 9.14 8.87	MD17/ LED-3		4.15	MR17/ LED-3	1.03	MS3	4.08
MA4	X Y Z	8.02 5.01 6.24	MD18	X Y Z	4.85 4.60 4.15			MS4	3.22
MA5	X Y	7.25 4.29						MS5	3.94
MA6	X Y	11.12 4.36						MS6	3.53
MA8	X Y Z	6.01 6.43 8.96						MS8	2.75
MA10	X Y Z	5.10 4.73 9.05						MS9	2.60
								MS10	2.82

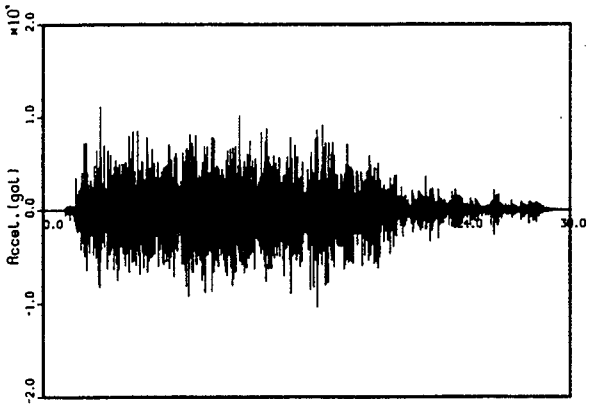

(MA16-X)

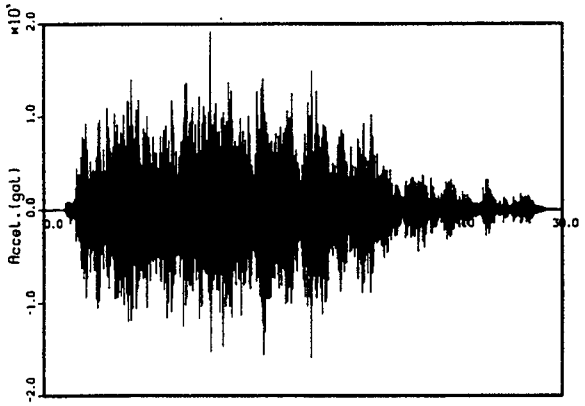

(MA16-Y)

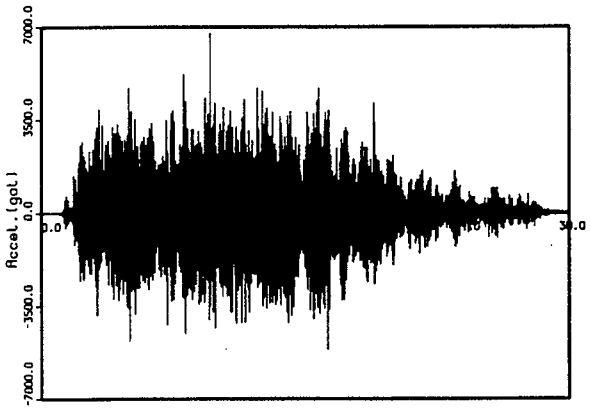

(MA16-Z)

Figure M.33 Acceleration Time Histories of M-line for Gap Test, 1.0 S2(A) Test Run

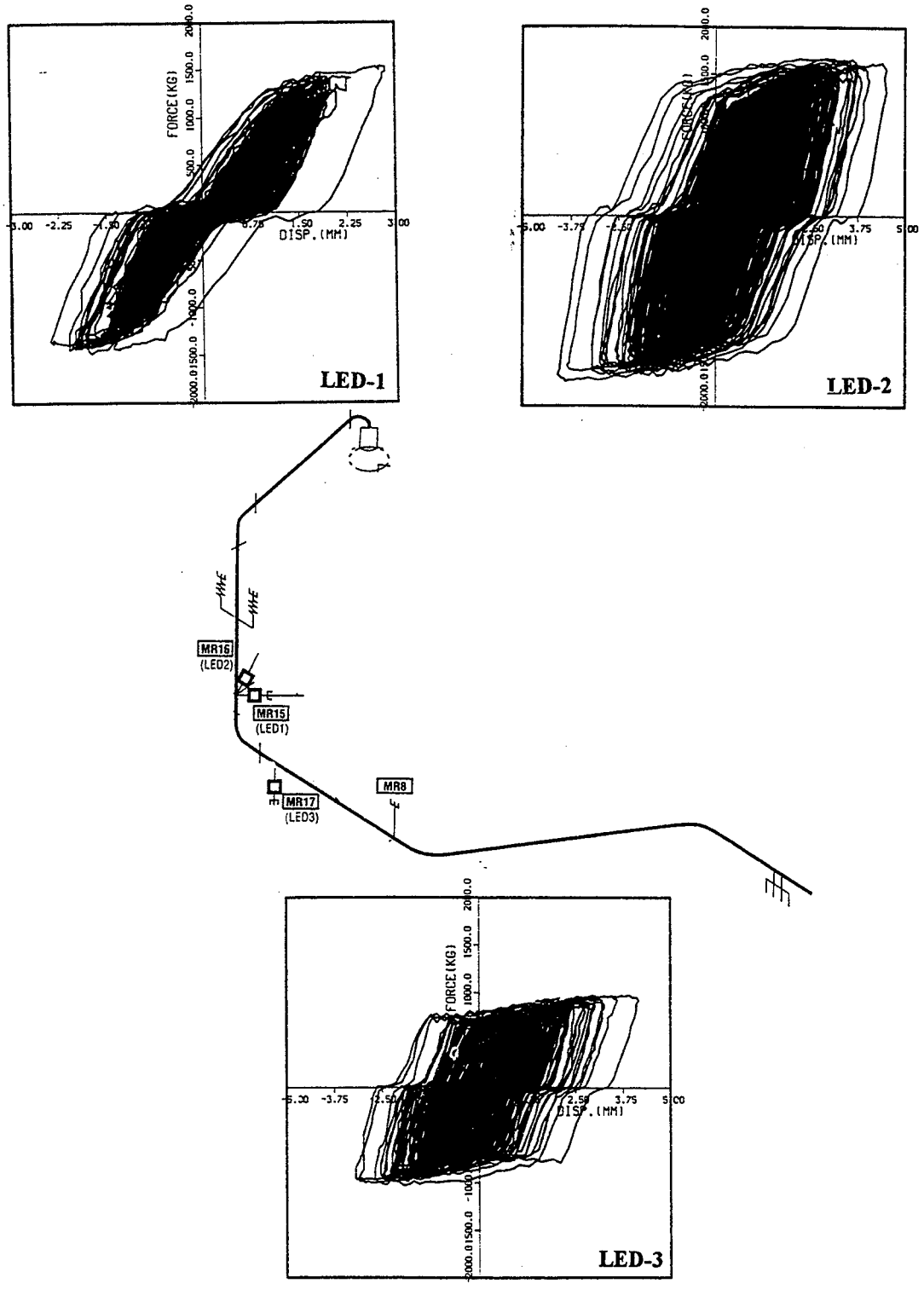

Figure M.34 Hysteretic Responses of M-line for Gap Test, 1.0 S2(A) Test Run

NRC FORM 335 (2-89) NRCM 1102, 3201, 3202

U.S. NUCLEAR REGULATORY COMMISSION

BIBLIOGRAPHIC DATA SHEET

(See instructions on the reverse)

1. REPORT NUMBER (Assigned by NRC, Add Vol., Supp., Rev., and Addendum Numbers, if any.)

NUREG/CR-6559
BNL-NUREG-52532

2. TITLE AND SUBTITLE

Large-Scale Vibration Tests of Main Steam and Feedwater Piping Systems With Conventional and Energy-Absorbing Supports

3. DATE REPORT PUBLISHED

MONTH	YEAR
August	1998

4. FIN OR GRANT NUMBER

W6081

5. AUTHOR(S)

Y. J. Park, G. DeGrassi, P. Bezler, and C. H. Hofmayer

6. TYPE OF REPORT

7. PERIOD COVERED *(Inclusive Dates)*

8. PERFORMING ORGANIZATION - NAME AND ADDRESS *(If NRC, provide Division, Office or Region, U.S. Nuclear Regulatory Commission, and mailing address; if contractor, provide name and mailing address.)*

Department of Advanced Technology
Brookhaven National Laboratory
Upton, NY 11973-5000

9. SPONSORING ORGANIZATION - NAME AND ADDRESS *(If NRC, type "Same as above"; if contractor, provide NRC Division, Office or Region, U.S. Nuclear Regulatory Commission, and mailing address.)*

Division of Engineering Technology
Office of Nuclear Regulatory Research
U.S. Nuclear Regulatory Commission
Washington, D.C. 20555-0001

10. SUPPLEMENTARY NOTES

N. C. Chokshi, NRC Project Manager

11. ABSTRACT *(200 words or less)*

As part of collaborative efforts between the United States and Japan, the U.S. Nuclear Regulatory Commission (USNRC) and Brookhaven National Laboratory (BNL) participated in the Seismic Proving Test program of main steam and feedwater systems (MS) conducted by the Nuclear Power Engineering Corporation (NUPEC) for the Ministry of International Trade and Industry (MITI) of Japan. Scaled models of main steam piping for a typical PWR plant and feedwater piping for a BWR plant were fabricated by NUPEC and subjected to a large number of earthquake motions at NUPEC's Tadotsu Engineering Laboratory. Initially, the piping systems were supported by conventional snubbers and subjected to design level earthquakes as well as excitations beyond the design level. Then the snubbers were replaced by energy absorbing devices, and tests at various excitation levels up to the deformation limits of the energy absorbers were performed. This report describes the evaluation of the test results and BNL's post-test analyses.

12. KEY WORDS/DESCRIPTORS *(List words or phrases that will assist researchers in locating the report.)*

Seismic testing; Nuclear piping; Energy absorbers; Shaking table tests; Dynamic analysis; Earthquake motions

13. AVAILABILITY STATEMENT

unlimited

14. SECURITY CLASSIFICATION

(This Page) unclassified

(This Report) unclassified

15. NUMBER OF PAGES

16. PRICE

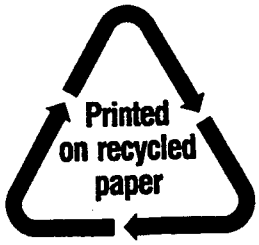

Federal Recycling Program